Catalytically-active Inclusion Bodies and Ferritin-based aggregates for Biotechnology

Inaugural dissertation

for the attainment of the title of doctor
in the Faculty of Mathematics and Natural Sciences
at the Heinrich Heine University Düsseldorf

presented by

Gizem Ölçücü

from Bakırköy

Jülich, October 2022

from the institute for Molecular Enzyme Technology
at the Heinrich Heine University Düsseldorf

Published by permission of the
Faculty of Mathematics and Natural Sciences at
Heinrich Heine University Düsseldorf

Supervisor: Prof. Dr. Karl-Erich Jaeger
Co-supervisor: Prof. Dr. Martina Pohl

Date of the oral examination: 25.01.2023

Dedicated to Nezahat Dizici

Table of Contents

I. Conference Contributions

Ölçücü, Gizem*, Küsters, Kira, Oldiges, Marco, Jaeger, Karl-Erich, and Ulrich Krauss. Catalytically-active Inclusion Bodies (CatIBs) and Ferritin-based Immobilizates for Biotechnology. *CLIB Competence Center Biotechnology (CKB) Final Symposium*. Düsseldorf, Germany. **2021**. (Poster presentation).

Ölçücü, Gizem*. Catalytically-active Inclusion Bodies (CatIBs) and Ferritin-based Immobilizates for Biotechnology. *CLIB Competence Center Biotechnology (CKB) Symposium WP2: Raw Materials*. Online. **2021**. (Oral presentation).

Ölçücü, Gizem*. Catalytically-active Inclusion Bodies (CatIBs) and Ferritin-based Immobilizates for Biotechnology. *CLIB Competence Center Biotechnology (CKB) Symposium WP1: Resource efficiency*. Online. **2020**. (Oral presentation).

Ölçücü, Gizem*, Jaeger, Karl-Erich, and Ulrich Krauss. *CLIB Competence Center Biotechnology (CKB) Symposium*. Düsseldorf, Germany. **2019**. (Poster presentation).

Fejzagić, Alexander V.*, Friedrichs, Teresa, **Ölçücü, Gizem**, Dibble, Claire, Wäscher, Martin, Krauss, Ulrich, Classen, Thomas, Pohl, Martina, Jaeger, Karl-Erich, and Jörg Pietruska. Flow chemistry. *CLIB Competence Center Biotechnology (CKB) Symposium*. Düsseldorf, Germany. **2019**. (Oral presentation).

Ölçücü, Gizem. *1st Japan-Germany-Switzerland Workshop for Enzyme Technology and Bioprocess Development*. Toyama, Japan. **2019**. (Participation).

Ölçücü, Gizem*. Catalytically-active Inclusion Bodies (CatIBs) and Ferritin-based Immobilizates for Biotechnology. *CLIB Competence Center Biotechnology (CKB) Symposium WP1: Resource efficiency*. Jülich, Germany. **2019**. (Oral presentation).

Ölçücü, Gizem*. Catalytically-active Inclusion Bodies (CatIBs) and Ferritin-based Immobilizates for Biotechnology. *CLIB Competence Center Biotechnology (CKB) Symposium WP2: Raw Materials*. **2019**. (Oral presentation).

* presenting author

II. List of Publications

Jäger, Vera D., Lamm, Robin, Küsters, Kira, **Ölçücü, Gizem**, Oldiges, Marco, Jaeger, Karl-Erich, Büchs, Jochen, and Ulrich Krauss. "Catalytically-active inclusion bodies for biotechnology -general concepts, optimization, and application". Applied Microbiology and Biotechnology 104.17 (2020), pp. 7313-7329.

Ölçücü, Gizem, Klaus, Oliver, Jaeger, Karl-Erich, Drepper, Thomas, and Ulrich Krauss. "Emerging Solutions for in vivo Biocatalyst Immobilization: Tailor-Made Catalysts for Industrial Biocatalysis". ACS Sustainable Chemistry & Engineering. 9 (2021), pp. 8919-8945.

Küsters, Kira, Pohl, Martina, Krauss, Ulrich, **Ölçücü, Gizem**, Albert, Sandor, Jaeger, Karl-Erich, Wiechert, Wolfgang, and Marco Oldiges. "Construction and comprehensive characterization of an EcLDCc-CatIB set-varying linkers and aggregation inducing tags". Microbial Cell Factories 20.49 (2021).

Ölçücü, Gizem, Baumer, Benedikt, Küsters, Kira, Möllenhoff, Kathrin, Oldiges, Marco, Pietruszka, Jörg, Jaeger, Karl-Erich, and Ulrich Krauss. "Catalytically Active Inclusion Bodies-Benchmarking and Application in Flow Chemistry". ACS Synthetic Biology 11 (2022), pp. 1881-1896.

Ölçücü, Gizem, Jaeger, Karl-Erich, and Ulrich Krauss. *Design, Production, and Characterization of Catalytically Active Inclusion Bodies*. Ed. by Julian Kopp and Oliver Spadiut. Vol. 2617. Methods in Molecular Biology. Springer US, 2023, pp. 49–74.

Ölçücü, Gizem, Krauss, Ulrich, Jaeger, Karl-Erich and Jörg Pietruszka. "Carrier-Free Enzyme Immobilizates for Flow Chemistry". Chemie Ingenieur Technik 95 (2023), pp. 531-542.

Ölçücü, Gizem, Wollenhaupt, Bastian, Kohlheyer, Dietrich, Jaeger, Karl-Erich and Ulrich Krauss. "Generation of Magnetic Protein Aggregates by Supramolecular Assembly of Ferritin Cages". Biomacromolecules. (in preparation).

III. Abbreviations

***p*-NPB** para-nitrophenyl butyrate

6-APA 6-aminopenicillanic acid

ADH alcohol dehydrogenase

ASU asymmetric unit

AtHNL hydroxynitrile lyase from *Arabidopsis thaliana*

ATP adenosine triphosphate

BFD benzoylformate decarboxylase

BFP blue fluorescent protein

Bfr bacterioferritin

BsLA lipase A from *Bacillus subtilis*

CatIBs catalytically-active inclusion bodies

CatMPAs catalytically-active magnetic protein aggregates

CBD_{cell} cellulose-binding domain from *Cellulomonas fimi*

CCE crude cell extract

CLEAs cross-linked enzyme aggregates

DAP 1,3-diaminopropane

DLS dynamic light scattering

Dps mini-ferritin

DTT dithiothreitol

EcftnA ferritin A from *E. coli*

EcftnA H34L+T64I double mutant of EcftnA with increased magnetism

EcLDC lysine decarboxylase from *E. coli*

ee enantiomeric excess

ELPs elastin-like peptides

FLLEX flow liquid-liquid extraction

FMDV foot and mouth disease virus

FtMt mitochondrial ferritin

fur ferric uptake regulator

GDH glucose dehydrogenase

GFP green fluorescent protein

HbHNL hydroxynitrile lyase from *Hevea brasiliensis*

HCA_3 hydroxycarboxylic acid receptor 3

HuFtnH H-chain of human ferritin

IBs inclusion bodies

IPTG isopropyl β-D-1-thiogalactopyranoside

LbADH alcohol dehydrogenase from *Levilactobacillus brevis*

LLPS liquid-liquid phase separation

MeHNL hydroxynitrile lyase from *Manihot esculenta*

MenD 2-succinyl-5-enol-pyruvyl-6-hydroxy-3-cyclohexene-1-carboxylate synthase

MPAs magnetic protein aggregates

MRI magnetic resonance imaging

MtSEOF sieve element occlusion by forisome from *Medicago truncatula*

NADPH nicotinamide adenine dinucleotide phosphate

Ni-NTA nickel-nitrilotriacetic acid

PCR polymerase chain reaction

PDB protein data bank

PfBAL benzaldehyde lyase from *Pseudomonas fluorescens*

PHA polyhydroxyalkanoate

PhaA acetyl-CoA acetyltransferase

PhaB acetoacetyl-CoA reductase

PhaC polyhydroxybutyrate synthase

PHB polyhydroxybutyrate

PhoC acid phosphatase from *Enterobacter aerogenes*

PoxB pyruvate oxidase from *Paenibacillus polymyxa* E681

PRM proline-rich motif

RADH alcohol dehydrogenase from *Ralstonia sp.*

Rfp1 red fluorescent protein 1

SH3 SRC homology 3 domain

STY space time yield

TEM transmission electron microscopy

VLPs virus-like particles

YFP yellow fluorescent protein

IV. List of Figures

V. List of Tables

VI. Abstract

In the last decades, pollution, deforestation and global warming caused by human influence have prompted the urgent search for greener industrial processes that minimize further harm to our environment. To this end, green processes utilizing biocatalysts emerged as a viable alternative to classical chemical catalyst driven processes in chemical industries. Enzymes as renewable catalysts, can be produced sustainably, and offer additional benefits from the performance standpoint due to their excellent selectivities and high efficiencies. In industry, enzymes are commonly used in immobilized form, i.e. achieved by binding or adsorbing enzymes to various carriers to allow their reuse and recycling. Widespread incorporation of enzymes within the chemical industry, however, remains largely limited due to their high production costs, as well as drawbacks of current immobilization strategies, such as the necessity of laborious and expensive preparation steps.

In the last years, so-called *in vivo* enzyme immobilization strategies that forego the use of carriers and combine enzyme overproduction and immobilization of enzymes in a single step have started to emerge. Within this framework, catalytically-active inclusion bodies (CatIBs), where target proteins are rationally localized within intracellular proteinaceous aggregates called inclusion bodies (IBs), serve as a promising alternative for enzyme immobilization. Relying on the fusion of genes encoding a CatIB inducing tag and the target gene, followed by overexpression of the gene fusion in a suitable host under the right conditions, CatIBs of the target protein can be easily produced and recovered from the cell lysate, and can be directly used for catalysis. The CatIB strategy is cheap, simple, and widely applicable, evidenced by the numerous proteins of varying complexity being successfully immobilized as CatIBs to date.

In this PhD thesis, the CatIB strategy was extended by the utilization of three short, synthetic peptide tags as CatIB inducing elements, namely 18AWT, L6KD and GFIL8. Various fusion strategies were implemented, which included variation of the fusion terminus as well as linker iterations, in order to provide an in depth understanding of the design principles that are imperative for the production of highly active and stable CatIBs. The targets for immobilization included industrially relevant enzymes such as alcohol dehydrogenase from *Ralstonia sp.* (RADH) and lipase A from *Bacillus subtilis* (BsLA), as well as the red fluorescent protein mCherry. Superior properties displayed by certain BsLA and RADH CatIBs were demonstrated, as their very high activity and production yields ensured that these CatIBs perform significantly better, even when compared to

soluble enzymes. Furthermore, the excellent stability of CatIBs allowed their use in flow chemistry for the first time. Characterization of numerous CatIB producers revealed that the industrially relevant properties of CatIBs are highly dependent on the utilization of the optimal CatIB tag at the optimal terminus, which is variable depending on the target protein.

In addition, a novel *in vivo* immobilization strategy was established to generate magnetic protein aggregates (MPAs), based on a fusion protein consisting of the yellow fluorescent protein citrine, and the iron storage protein ferritin. Ferritin variants, including a mutant with increased magnetic properties, were generated and tested to produce MPAs with the most desirable properties. To this end, the gene fusions were overexpressed in *Escherichia coli* and the immobilizates could be obtained from the cell lysate via centrifugation in a similar manner to CatIBs. The lysates containing MPAs were shown to be magnetic, evidenced by their attraction to permanent neodymium magnets, and this property enabled their purification using magnetic columns. Furthermore, catalytically-active magnetic protein aggregates (CatMPAs) could be generated by employing a biological bait-prey strategy to immobilize RADH, by post-translationally linking RADH to MPAs.

Lastly, the rapidly growing field of *in vivo* enzyme immobilization necessitated an overview over the state-of-the-art, therefore several literature reviews as well as a book chapter were prepared and included within the framework of this PhD thesis. These encompassed an overview over various alternative *in vivo* immobilization methods, the flow chemistry applications of immobilized enzymes, and strategies, advantages, drawbacks, applications and complete wet lab methodology related to the production and characterization of CatIBs.

In conclusion, the use of green biocatalysts obtained with optimized *in vivo* immobilization protocols is crucial for the widespread acceptance of biocatalysis in synthetic chemistry and industry. Therefore, the development of new immobilization methods and the improvement of existing ones, as achieved here as part of this PhD thesis, is expected to provide numerous benefits for the next generation of industry, economy, and the environment alike.

VII. Zusammenfassung

In den letzten Jahrzehnten haben Umweltverschmutzung, Abholzung der Wälder und die durch den Menschen verursachte globale Erwärmung dazu geführt, nach umweltfreundlicheren Verfahren zu suchen, die unsere Umwelt so wenig wie möglich belasten. In der chemischen Industrie haben sich hierbei Prozesse unter Verwendung von Biokatalysatoren als praktikable, umweltfreundliche Alternative zu klassischen von chemischen Katalysatoren getriebenen Prozessen herausgestellt. Enzyme als erneuerbare Katalysatoren können nachhaltig produziert werden und besitzen zudem eine herausragende Selektivität und hohen Effizienz. In der Industrie werden Enzyme häufig in immobilisierter Form verwendet. Dies geschieht z.B. durch Bindung oder Adsorption an verschiedene Träger, wodurch die Wiederverwertung der Katalysatoren möglich wird. Der breite Einsatz von Enzymen in der chemischen Industrie ist jedoch aufgrund ihrer aufwendigen und kostenintensiven Produktion und Immobilisierung, nach wie vor stark eingeschränkt.

In den letzten Jahren wurden sogenannte *in vivo* Enzym-Immobilisierungsstrategien entwickelt, die ohne Träger auskommen und Enzymproduktion und Immobilisierung in einem einzigen Schritt ermöglichen. Hierbei sind insbesondere katalytisch aktive Einschlusskörper (Englisch: catalytically active inclusion bodies; CatIBs), bei denen Zielproteine rational in intrazellulären Proteinaggregaten, den sogenannten Inclusion Bodies (IBs), eingelagert werden, eine vielversprechende Alternative für die Immobilisierung von Enzymen. Durch die Fusion von Genen, die für einen CatIB-induzierenden Tag und das Zielgen kodieren, und die anschließende Überexpression dieser Genfusionen in einem geeigneten Wirt unter den richtigen Bedingungen, können CatIBs des Zielproteins leicht hergestellt und aus dem Zelllysat gewonnen und direkt zur Katalyse verwendet werden. Die CatIB-Strategie ist billig, einfach und weithin anwendbar, wie die große Zahl an Zielproteinen unterschiedlicher Komplexität zeigt, die bisher erfolgreich als CatIBs immobilisiert wurden.

In dieser Doktorarbeit wurde die CatIB-Strategie durch die Verwendung von drei kurzen, synthetischen Peptid-Tags als CatIB-Tags, nämlich 18AWT, L6KD und GFIL8, erweitert. Es wurden verschiedene Fusionsstrategien implementiert, die sowohl Variationen des Fusionsterminus als auch Iterationen des Linkers beinhalteten, um ein besseres Verständnis der Designprinzipien zu erlangen, die für die Produktion von hochaktiven und stabilen CatIBs unerlässlich sind. Zu den Zielproteinen gehörten industriell relevante Enzyme wie die Alkoholdehydrogenase aus *Ralstonia* sp. (RADH) und die Lipase A aus

Bacillus subtilis (BsLA) sowie das rot fluoreszierende Protein mCherry. Für einige RADH und BsLA CatIB Varianten konnten, im Vergleich zu den entsprechenden gereinigten, löslichen Enzymen, herausragende Eigenschaften wie hohe Aktivitäten und Produktionsausbeuten nachgewiesen werden. Darüber hinaus ermöglichte die hohe Stabilität der CatIBs zum ersten Mal eine Verwendung in der Flusschemie. Die Charakterisierung zahlreicher CatIB-Produzenten zeigte, dass die industriell relevanten Eigenschaften von CatIBs in hohem Maße von der Verwendung des optimalen CatIB-Tags am optimalen Terminus abhängen, der sich jedoch je nach Zielprotein unterscheiden kann.

Darüber hinaus wurde eine neue *in vivo* Immobilisierungsstrategie zur Gewinnung magnetischer Proteinaggregate (MPAs) entwickelt, die auf einem Fusionsprotein des gelb fluoreszierenden Proteins Citrin und dem Eisenspeicherprotein Ferritin basiert. Ferritin-Varianten, einschließlich einer Mutante mit verbesserten magnetischen Eigenschaften, wurden erzeugt und getestet, um MPAs mit geeigneten Eigenschaften herzustellen. Zu diesem Zweck wurden die entsprechenden Genfusionen in *Escherichia coli* überexprimiert wobei die Immobilisate direkt aus dem Zelllysat durch Zentrifugation auf ähnliche Weise wie CatIBs gewonnen werden konnten. Aufgrund ihrer magnetischen Eigenschaften, belegt durch Lokalisierungsexperimente mit Neodym-Permanentmagneten, konnten die MPAs mit Hilfe magnetischer Säulenmaterialien gereinigt werden. Darüber hinaus konnten katalytisch aktive, magnetische Proteinaggregate (Englisch: catalytically-active magnetic protein aggregates; CatMPAs) des Enzyms RADH durch Anwendung einer biologischen Bait-Prey-Strategie erzeugt werden, wobei RADH posttranslational kovalent an MPAs gebunden wurde.

Schließlich erforderte das schnell wachsende Feld der *in vivo* Enzymimmobilisierung einen Überblick über den aktuellen Stand der Technik. Daher wurden im Rahmen dieser Doktorarbeit mehrere Übersichtsartikel sowie ein Buchkapitel verfasst. Diese Arbeiten umfassten einen Überblick über verschiedene *in vivo* Immobilisierungsmethoden, die Anwendungen von immobilisierten Enzymen in der Flusschemie, sowie einen Überblick über Strategien, Vorteile, Nachteile, Anwendungen sowie eine vollständige Methodensammlung zur Produktion und Charakterisierung von CatIBs.

Abschließend lässt sich sagen, dass die Verwendung grüner Biokatalysatoren, die mit optimierten *in vivo* Immobilisierungsstrategien gewonnen wurden, für die breite Akzeptanz der Biokatalyse in der synthetischen Chemie und der Industrie entscheidend ist. Hierbei bietet die Entwicklung neuer und die Verbesserung bestehender Immobilisierungsmethoden, wie sie hier im Rahmen dieser Doktorarbeit durchgeführt wurden, viele Vorteile für die nächste Generation der Industrie, die Wirtschaft und die Umwelt gleichermaßen.

1. Introduction

1.1. History of biocatalysis: From ancient usage to modern milestones

Our species has a long history when it comes to reaping the benefits of biotechnology. Defined loosely as the "manipulation of living organisms, systems and processes for the benefit of society, environment and industry" [1], biotechnology has been unknowingly used by humankind since antiquity. Despite being largely limited to fermentative technology until 1800s (**Figure 1.1**), all around the globe, humankind has exploited microorganisms and by extension, enzymes for their survival for thousands of years, *i.e.* to make fermented foods and beverages which could be consumed safely or stored for longer periods of time. The earliest indication of intentional utilization of biotechnology points towards the Raqefet Cave in modern-day Israel, where, approximately 13,000 years ago, the semi-sedentary people living in this region are suggested to have used fermentation techniques for beer brewing [2]. Similarly, evidence of fermentation to make a beverage using rice, honey, and fruits can be found in China, dating back 9,000 years [3]. Around the same time frame, substantial amounts of fish were being fermented for long term storage purposes on the east coast of Sweden [4]. In Anatolia, around the region of the Sea of Marmara, milk was being extensively processed for storage as early as 6500 BC [5], and in northern Europe, cheese production had already started as early as 6000 BC [6]. In Northern Greece red wine was being produced as early as 4300 BC [7], and although the preparation of flatbread that likely excluded the utilization of yeast existed prior to this date [8], the earliest definitive proof of yeast being used for bread-making purposes dates back approximately 2,500 years, where leavened bread samples were recovered from Egypt [9].

The number of such examples showing the ancient use of microorganisms can be extended even further, though the underlying indication of the evidence is clear; despite lacking the advanced biotechnology knowledge that we possess today, our ancestors have exploited and relied on biocatalysis for their survival for a very long time. In fact, the use of fermentation predates one of the most significant discoveries in the history of our species such as the invention of writing (ca. 3200 BC, **Figure 1.1**) by thousands of years [10]. Interestingly, there is evidence that our evolutionary adaptations toward metabolizing fermented food sources date back much further than the development of fermentative techniques. As the first enzyme involved in the metabolism of

ethanol found in naturally fermenting fruits [11], an ancestral alcohol dehydrogenase enzyme revived from hominids was shown to acquire a mutation that greatly enhanced its catalytic activity towards the alcohol 10 million years ago, roughly parallel to the adaptation to an increasingly terrestrial life [12]. Along the same lines, a recent study revealed that humans have an increased sensitivity towards the metabolites of lactic acid bacteria, which in turn activate hydroxycarboxylic acid receptor 3 (HCA_3) that regulates immune functions and energy homeostasis [13]. As HCA_3 is functionally present only in hominids, this finding suggests that ingesting foods fermented by lactic acid bacteria may have provided a positive selective pressure to maintain the function of this unique receptor. Regardless, it appears that fermentation may have played a role in the evolutionary adaptations of humans as well.

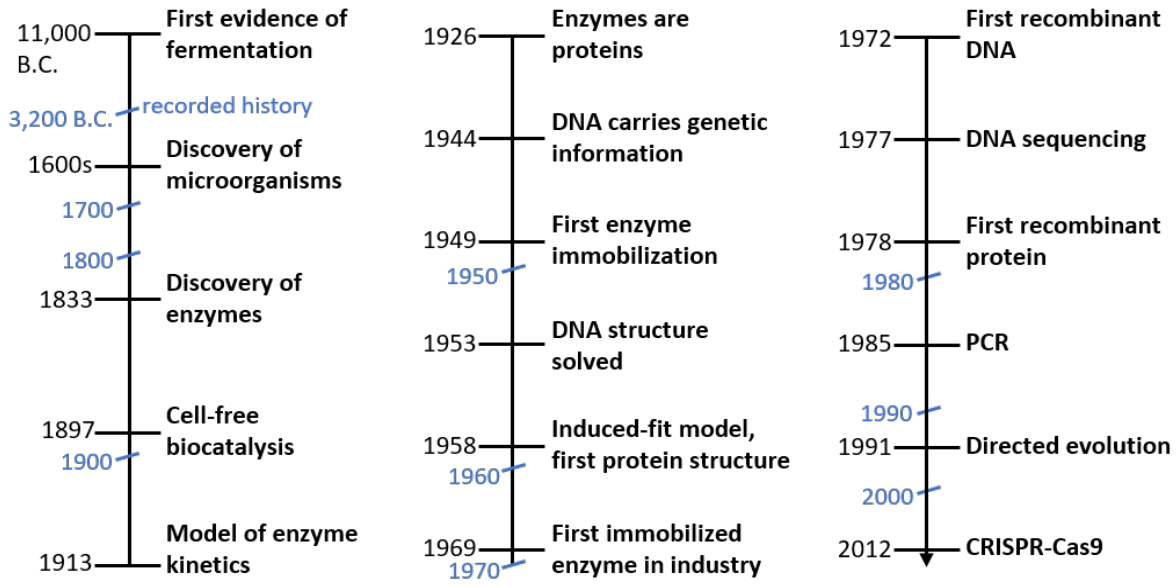

Figure 1.1. Chronological representation of milestones related to biocatalysis from ancient use to modern breakthroughs.

The modern history of biotechnology on the other hand, is rather recent; it begins with the discovery of the first enzyme in the early 1800s by Anselme Payen and Jean-François Persoz [14, 15] (**Figure 1.1**). Payen and Persoz made the important discovery that an aqueous extract of malt that they prepared contained a heat-sensitive *component* which could convert starch into sugar. Naming this previously unknown *component* diastase, they published their findings in 1833. Shortly after this discovery, its presence was detected in other cereals, saliva, and animal pancreas, and today we know that "diastase" is not a single enzyme but rather a cocktail of amylases [16, 17]. Two years after this discovery, Jöns J. Berzelius put forth the concept of catalysis, and later that of biocatalysis

[18]. Despite the initial description of microorganisms by Antoni van Leeuwenhoek and Robert Hooke in 1600s [19], almost 200 years later, it was still not known that yeast was a living organism, and the process of fermentation was thought to be a purely chemical one [20].

Owing to the improvements in microscopy, the studies conducted on beer and wine revealed yeasts as living organisms that are able to reproduce, paving the way for Louis Pasteur's work that established the principle of alcoholic fermentation by yeast cells [20, 21, 18]. As the study of enzymes was deeply intertwined with the study of fermentation, the word *ferment* was being used to refer both to enzymes and the activity of yeasts at this time point, until finally, Wilhelm F. Kühne coined the term ***enzyme*** for biological catalysts in 1878, almost 50 years after their initial discovery [22, 21]. There was also interest in the commercial use of enzymes at the time, as the very first companies that focused on supplying enzyme preparations such as rennet for cheese production had emerged, though the supply was limited to fermentative applications for bread and beer making [23].

The late 1800s marked the beginning of a time with a rapid increase in important discoveries related to biocatalysis, starting with the "lock and key" model of enzyme specificity by Emil Fischer, and the discovery of cell-free biocatalysis, where Eduard Buchner demonstrated fermentation of sugar into carbon dioxide and ethanol using yeast extract free of living cells, which lead to a Nobel Prize in Chemistry [18, 24]. It was soon followed by the discovery of the first cofactors, and the mathematical model of enzyme kinetics was established by Leonor Michaelis and Maud L. Menten in 1913 [17, 18]. In 1926, the first crystallization of an enzyme was achieved by James B. Sumner, confirming that enzymes are indeed proteins. The field of molecular biology was similarly developing at a rapid pace as evidenced by groundbreaking milestones, such as the Avery–MacLeod–McCarty experiment that established DNA as the carrier of genetic information in 1944, almost a century after the first description of DNA as "nuclein" by Friedrich Miescher [25]. In 1953, James Watson and Francis Crick elucidated the 3D structure of DNA based on the X-ray diffraction images by Rosalind Franklin and Maurice Wilkins [26, 17]. Five years later, the 3D structure of myoglobin was solved based on X-ray crystallography, which was soon followed by the structures of hemoglobin and lysozyme [27, 17]. At the same time, Daniel E. Koshland proposed the induced-fit model to explain the conformational changes of the proteins upon substrate binding, as opposed to the earlier "lock and key" hypothesis [28].

In 1949, the very first enzyme immobilization technologies, which were based on

the covalent binding of enzymes on activated cellulose supports had started to emerge, allowing biocatalysts to be reused and paving the way for their industrial application [23, 29] (**Figure 1.1**). By the end of 1960s, industry's interest in biocatalysis and immobilization was growing, and this era saw the first industrial scale uses of immobilized enzymes, namely amino acid acylases to produce amino acids and penicillin amidase to produce 6-aminopenicillanic acid (6-APA), a precursor of different penicillins [17, 23, 30]. Similarly, the glucose isomerase enzyme used in high fructose corn syrup production was immobilized in 1970s, driven by the high costs associated with the initial use of the enzyme in its free form. This time period also saw important advancements in DNA sequencing [31, 32] along with the first recombinant DNA technologies [33]. The synthesis of short synthetic DNAs by Kjell Kleppe in 1971 [34] paved the way for the invention of the polymerase chain reaction (PCR) by Kary Mullis in 1985 [35], which in turn allowed a faster development and commercialization of enzymes. In 1990s, directed evolution approaches were invented and applied to tailor biocatalysts for specific applications, initially through random mutagenesis followed by high-throughput screening methods, and later via generation of smarter libraries through to the advancements in bioinformatics and sequencing technologies [36]. For her pioneering work on directed evolution of enzymes, Frances H. Arnold received a Nobel prize in Chemistry in 2018. The development of the CRISPR/Cas9 gene editing technique, for which Jennifer A. Doudna and Emmanuelle Charpentier received the 2020 Nobel prize in Chemistry, represents the most recent breakthrough in molecular biology, with huge application potential for industrial strain engineering [37].

Thanks to all these breakthrough technologies, today enzymes are used in a wide range of sectors such as food, feed, pharmaceutical, textile and cosmetic industries. The global demand for enzymes is currently at $6.4 billion, which is expected to reach $8.7 billion by 2026 [38, 39]. The gross majority of all enzymes produced on an industrial scale are hydrolases (nearly 75%) such as proteases and lipases, which are predominantly used in food and detergent industries [40, 38]. Carbohydrases that catalyze the synthesis or the breakdown of carbohydrates, such as amylases and cellulases, are often employed in food, textile and paper industries, among other sectors. In food, chemical and pharmaceutical industries, enzymes are often used in an immobilized form [41]. For efficiency and scale-up considerations, approximately 90% of the industrial enzymes are produced heterologously, in engineered bacterial or fungal hosts along with yeasts, irrespective of the origin of the genes encoding these enzymes [42, 43]. Protein engineering is applied to modify industrial enzymes to obtain a desired property (e.g. broadened substrate specificity, stability, etc.), and successful implementation of immobilization meth-

ods have enabled the continuous, cost efficient use of such enzymes on an industrial scale [41, 44]. Today, numerous methods to immobilize enzymes exist, and depending on the method of choice, immobilization can confer additional benefits to the enzyme, but also incurs additional costs [41]. In summary, advancements in molecular biology and biotechnology, and importantly, the discovery and developments in enzyme immobilization, allowed the efficient utilization of biocatalysts in numerous industrial sectors.

1.2. Immobilization of Enzymes

In recent years, the negative impact of industrial processes on our environment became increasingly apparent, which lead to environmentally-friendly processes with smaller ecological footprints to gain increasingly more attention. In this sense, using enzymes as biologically derived, green (bio)catalysts has an obvious advantage when compared to conventional chemical catalysts. Enzymes are renewable, possess lower environmental (and physiological) toxicity, are associated with less waste generation, and their use generally requires less energy due to mild operation conditions [45, 46, 47]. Furthermore, microorganisms that overproduce such enzymes can be cultivated using renewable feedstocks, making the entire process more sustainable [45, 48, 42]. Using enzymes instead of chemical catalysts offers big advantages from a performance standpoint as well; enzymes can catalyze reactions with high chemo-, stereo- and regioselectivity with great efficiencies, typically introducing a 10^6 to 10^{12} fold increase in reaction rate compared to the uncatalyzed reaction [49, 50, 47].

Despite such desirable properties, enzymes are still underutilized in the industry due to several factors, such as their low tolerance to harsh process conditions like high temperature or extreme pH values [51, 46]. Through protein engineering, enzymes can be rendered more tolerant towards various process parameters [52]. Another important factor that hinders the widespread use of enzymes is due to economic concerns. For cofactor dependent enzymes, expensive cofactors such as nicotinamide adenine dinucleotide phosphate (NADPH) or adenosine triphosphate (ATP) can be a major issue, which can be partially remedied by the use of efficient cofactor recycling systems. The price of enzymes on the other hand, is highly variable and can range from a few cents per kilogram for efficient processes, such as those employing hydratases or isomerases, to hundreds of euros per kilogram, i.e. for cytochrome P450 applications [52, 53].

A vital parameter that enables the cost efficient use of enzymes is immobilization; biocatalysts that are physically fixed in (or restricted to) a certain space that allows

their recovery from the reaction system, while retaining their catalytic activity [45, 54]. Immobilization can not only improve the efficiency of the process by allowing the easy recovery and recycling of enzymes but can also bestow the immobilized enzyme with desired properties such as increased catalytic activity, stability, or broadened tolerance towards certain process parameters [53, 46]. Moreover, co-immobilization by confining multiple enzymes in the same space for cascade reactions is an attractive possibility, as co-immobilization often benefits from an increased initial reaction rate due to enzymes being in close proximity [55, 56]. Since immobilization is often crucial for industrial enzymes, the development of novel immobilization techniques and improvement of the existing ones with regard to cost efficiency, ease of application, and enhancements to catalyst properties is vital for application. Furthermore, advancements in immobilization have the potential to elevate more biocatalysts to the industrial enzyme category by overcoming the limitations of enzymes and building on their advantages, thereby pushing the industry towards green practices by providing an economic incentive.

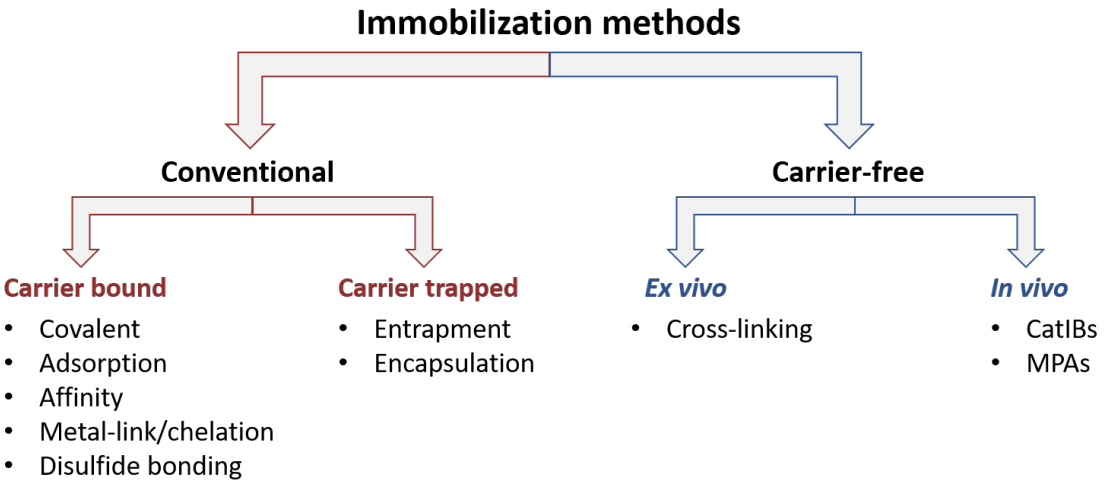

Figure 1.2. Overview of immobilization methods.

Immobilization methods can be divided into two groups; conventional methods that utilize carriers (left), and carrier-free methods (right). The conventional immobilization methods include techniques relying on the binding of the enzymes to carriers, such as covalent attachment, adsorption, affinity binding, chelation/metal-link immobilization, and disulfide bonding, or confinement of enzymes within carriers, such as entrapment and encapsulation. Carrier-free immobilization methods can be divided into two groups, *ex vivo* techniques where the production and immobilization of the enzyme constitute two separate steps (as in cross-linking), and *in vivo* methods where immobilization takes place during enzyme production (such as for CatIBs and MPAs). CatIBs: Catalytically-active inclusion bodies, MPAs: Magnetic protein aggregates.

Immobilization methods can be roughly divided into two categories (**Figure 1.2**): **I.** conventional, *ex vivo* immobilization approaches using carriers, which is based on either

carrier binding or confinement of enzymes in/on suitable materials, and **II.** more recent, carrier-free immobilization techniques which include *in vivo* approaches often based on bioconjugation that combine enzyme overproduction and immobilization in one step. The properties displayed by the immobilized enzyme highly depend on the mode of immobilization, and therefore, strengths, drawbacks, as well as application areas of each approach will be discussed in more detail in the following chapters.

1.2.1. Conventional Immobilization Methods

1.2.1.1. Immobilization via Carrier Binding

One of the most commonly used immobilization methods is the immobilization of enzymes via carrier binding (see **Table 1.1** for an overview of currently used conventional immobilization methods), where enzymes are either covalently attached to or adsorbed onto organic or inorganic support materials [46, 54, 57]. Depending on the mode of attachment, this method can be regarded as reversible or irreversible. For a biocatalyst that is covalently bound to the carrier, the immobilization is irreversible, as separation of the enzyme from the support would diminish the activity of the enzyme [54]. The irreversible nature of covalent binding might be desirable depending on the application, for instance for processes where the presence of the enzyme is not desired in the final product. Subsequently, the method prevents enzyme leakage which is advantageous, however, when the enzyme activity starts to decay over time, it is necessary to discard the entire support material together with the immobilized enzyme, which can render the approach quite expensive. Typically, covalent attachment is achieved by the utilization of cross-linking reagents such as glutaraldehyde or epichlorohydrin, which functionalizes the surface of the support material and serves as a linker, facilitating the formation of Schiff bases with side chain amino groups of the enzyme and the functional groups of the support matrix [46, 54, 58]. Thus, highly stable ether, thioether, amide, or carbamate bonds are generated between cysteine, lysine, histidine, aspartic, and glutamic acid residues of the enzyme and the support material.

Covalent attachment is generally regarded as a harsh method that often requires chemical activation steps capable of denaturing enzymes. In addition, cross-linking might happen via residues at or close to the active site of the enzyme, resulting in a significant loss of activity [46, 54]. When multiple reactive groups on the surface of the enzyme are involved in support attachment (as in multipoint covalent immobilization), the activity of the enzyme is usually decreased due to the impaired flexibility of the enzyme, though

Table 1.1. Enzymes immobilized by conventional methods and their applications.

Immobilization Method	Enzyme	Carrier	Application Area
Covalent binding	Lipase	Magnetic nanoparticles	Biodiesel industry [59]
	Horseradish peroxidase	Reduced graphene oxide	Bioremediation [60]
	Catalase	Carbon nanotubes	Food industry [61]
	Xylanase	Alginate beads	Food, paper industry [62]
	Penicillin amidase*	Epoxy	Pharmaceutical industry [63]
	β-galactosidase*	Synthetic polymers	Food industry [63]
Ionic binding	Lipase*	Synthetic polymers	Food industry [63]
	β-galactosidase*	Synthetic polymers	Food industry [63]
Adsorption	α-amylase	ZrO_2	Food industry [64]
	Catalase	Electrospun nanofibers	Food industry, bioremediation [65]
	Lipase*	Resin	Pharmaceutical and biodiesel industry [63, 66]
	Lipase*	Synthetic polymers	Bulk chemicals [63]
	Lipase*	Silica	Food industry [63]
	D-glucose isomerase*	Silica	Food industry [63]
	Xylose isomerase*	Silica	Food industry [41]
Entrapment	Pectinase	Calcium alginate hydrogel	Food, detergent industry [67]
	Rennin	Tubular cellulose / starch gel	Food industry [68]
	Laccase	Single-walled nanotube	Food industry [69]
Encapsulation	Peroxidase	Gelatin hydrogel	Food industry, bioremediation [70]
	Glucose oxidase	Polymer-resin composite	Food industry, bioremediation [71]

Enzymes marked with an asterisk (*) refer to actual use cases, whereas the remaining examples refer to literature-listed potential application areas.

this reduction in enzyme mobility can also provide a positive effect on stability, as this effect is thought to suppress unfolding at the same time [72]. Still, it is possible to regulate the covalent immobilization in a site-directed way by employing a system called PRECISE (protein residue-explicit covalent immobilization for stability enhancement) based on click chemistry, which enables rational assignment of the amino acid residues to be involved in covalent binding [73]. This in turn generates enzyme immobilizates displaying improved activity compared to undirected covalent immobilization, by ensuring that the active site of the enzyme is protected from unwanted covalent attachments. The support matrices themselves can also have a large impact on immobilization success and the properties of the immobilized enzyme. Materials commonly used as carriers include silica and inorganic oxides such as titanium or aluminum oxide, which are preferred due the presence of surface hydroxyl groups that facilitate enzyme binding, carbon based supports such as activated charcoal, and organic materials like chitosan [57, 54]. Likewise, new and unconventional materials that include functionalized magnetic nanoparticles that can be easily recovered, single or multi-walled carbon nanotubes that enhance electron transfer and are thus beneficial for immobilization of enzymes such as oxidoreductases, and electrospun nanofibers which minimize mass transport limitations have gained popularity as unique carriers in recent years [46, 57, 74, 75].

An alternative to the covalent attachment of enzymes to support matrices is the non-covalent adsorption to the carrier, which results in more weakly bound and hence reversibly immobilized biocatalysts [54]. Due to the low binding strength, the active site of the enzyme is generally unobstructed which is beneficial for the activity of the immobilizate [76]. Adsorption can hereby occur via Van der Waal's forces, hydrophobic, or ionic interactions [50, 54]. The method is simple, gentle, and relatively cheap, yet, is prone to enzyme leakage and can still suffer from the hindrance of the active site along with diffusional limitations. Additionally, due to the weakness of attachment, usually the amount of enzyme that can be immobilized is much lower compared to covalent binding, which can be overcome to a certain degree by employing surface modified carrier materials that support adsorption [76]. A large variety of organic and inorganic support matrices are available for immobilization via adsorption, where chitosan, cellulose, alginate, silica, various metal oxides or ion-exchange or epoxy resins being commonly used to this end, in addition to newer materials such as graphene oxide, electrospun nanofibers, magnetic nanoparticles, and metal-organic frameworks with extremely high surface areas and porosity [76, 50, 57, 77, 45]. Among the properties exhibited by these carriers, inertness, surface area, porosity, thermal stability, mechanical strength, cost, and availability are important parameters for their selection, and as there is no universal carrier

material for all enzyme applications, these properties must be carefully considered depending on the process at hand.

In addition to the two main methods described above which are commonly used for carrier binding, additional approaches that utilize alternative binding strategies exist. Affinity binding is a technique that allows the linkage of the enzyme to a carrier matrix by utilizing the affinity between two complementary biomolecules. [54, 78]. It relies on the attachment of an affinity tag, i.e. an antibody, to a selected site on the enzyme, and the attachment of a complementary affinity ligand to the matrix, which enables strong binding between the enzyme and the support. Binding via affinity tags might be of covalent (as in HaloTag system[79]) or ionic nature. For instance, it is possible to immobilize a His-tagged enzyme onto a support material displaying surface metal ions such as Ni^{2+}, Cu^{2+} or Fe^{3+} via ionic affinity binding [54]. HaloTag based immobilization on the other hand is based on the formation of covalent bonds, where the gene encoding the 33 kDa HaloTag is fused to that of the target enzyme, with the HaloTag facilitating the covalent binding to a HaloTag ligand when both moieties come in close proximity [80]. The HaloTag is derived from an engineered haloalkane dehalogenase enzyme from *Rhodococcus rhodochrous*, where a point mutation prevents the hydrolysis of an alkyl-enzyme intermediate which is formed during the interaction, therefore ensuring the formation of a stable adduct. Irrespective of the mode of binding, the affinity binding method offers very high selectivity and enables direct immobilization from the crude cell extract [79]. However, the main disadvantage is the high costs of such affinity matrices rendering the method quite expensive [54].

Chelation or metal-link immobilization can likewise generate enzyme immobilizates. Metal-link immobilization is achieved by precipitating salts of titanium and zirconium onto the surface of the carrier matrix, which link the enzyme to the support material [54, 78]. The method is simple and capable of producing immobilizates that display relatively high activities, yet suffer from variable operational stability and low reproducibility. Chelators can be immobilized on solid supports via covalent binding in order to control the formation of adsorption sites and improve reproducibility. As the immobilized proteins can be eluted by using competing soluble ligands that would replace the retained enzymes or by altering reaction conditions that would result in the release of the enzyme from the support, the method is reversible, and the support matrix can be regenerated via chelators for the next application. Finally, it is possible to immobilize enzymes by thiol-disulfide exchange reactions, where a disulfide bond is formed between the exposed, nonessential thiol groups of the biocatalyst and the thiol-reactive groups of the support matrix [81]. Despite the covalent nature of the bond, the method is reversible as

the covalent bond be broken by applying a suitable reagent such as dithiothreitol (DTT) under mild conditions and is applicable to enzymes that do not contain thiol groups by means of chemical or genetic modification.

Table 1.2. General advantages and drawbacks of immobilization methods.

Immobilization Method	Advantages	Disadvantages
Covalent binding	No leakage, simple, selective application	Low activity, matrix or enzyme regeneration not possible, low enzyme loading
Adsorption	Simple, low cost, matrix or enzyme regeneration possible	High leakage, nonspecific adsorption issues
Affinity binding	Very high selectivity, site specific immobilization	High cost
Metal-link/ Chelation	Simple, low activity loss	Low reproducibility
Entrapment	Widely applicable, minimal activity loss	High leakage, mass transfer limitations
Encapsulation	High enzyme loading, low leakage	Mass transfer limitations
CLEAs	Widely applicable, low leakage, no carrier	Optimization required based on target, variable loss of activity
CatIBs	Simple, cheap, no carrier, no additional immobilization steps	Optimization required based on target, variable loss of activity

Constructed using the information in references [78, 82, 83, 84, 85].

In conclusion, a wide range of immobilization strategies that rely on carrier binding exists, and depending on the application, the nature of the carrier, and the mode of binding to such carriers, these strategies can confer certain benefits to the immobilized biocatalyst or suffer from certain drawbacks (**Table 1.2**). Re-usability of the carrier, along with costs and ease of application vary depending on the method of choice, yet all of these strategies require additional steps to bind the enzymes to the matrix and may require modifications on the target enzyme to render them applicable. Furthermore, activity losses due to immobilization can be severe (i.e. in undirected covalent attachment), and therefore usually require additional considerations for optimal integration.

1.2.1.2. Immobilization via Entrapment or Encapsulation in a Carrier

As outlined in the previous section, biocatalysts can be immobilized on the surface of carrier materials reversibly or irreversibly, via binding of the enzyme to the carrier. Carriers can also be used to confine enzymes without the involvement of bonds. This is achieved by entrapment or encapsulation of enzymes within the 3D matrix of carrier materials [86]. In this mode, the carrier allows low-molecular-weight molecules such as substrate(s) and product(s) to pass through, while retaining the enzyme [78, 87]. Entrapment is a simple method that is widely used for immobilization, and polymer gels that are synthetic or organic of nature, such as gels of agarose, gelatin, calcium alginate, polyacrylamide, and chitosan based hydrogels are commonly used for this purpose [46, 86]. To achieve entrapment, the target enzyme is mixed together with a suitable polymer solution prior to polymerization, and the mixture can be shaped into a desired form, for instance by extrusion [87]. The method is widely applied for the immobilization of whole cells in addition to free enzymes, however, care must be taken in such applications when gels that are toxic of nature, such as polyacrylamide gels, are used [86]. Organic polymer gels are nontoxic and therefore more suitable for this purpose, but often suffer from low mechanical stability, which can be partially remedied by using cross-linking agents.

Moreover, enzymes can be entrapped in hollow, semi-permeable membranes of nylon, cellulose or polysulfone in an approach called fiber entrapment [87, 54]. Solid supports such as activated carbon or porous ceramics can also be used to immobilize enzymes via this mode. Finally, microencapsulation can be utilized, where hollow, microscopic spheres containing the target enzyme are entrapped within a membrane. Along these lines, liposomes, which are artificial vesicles of spherical shape derived from lipid bilayers of phospholipids or cholesterol, are used to entrap biocatalysts within their core [88]. This is achieved by taking advantage of the property of phospholipids to spontaneously assume a "closed" form when they are hydrated in aqueous solutions due to hydrophobic effects. In addition to biocatalysis, liposomes have found applications in medicine where they are used for the encapsulation of drugs, as well as for biodiagnostic applications. All of the above-mentioned modes of encapsulation and entrapment are generally prone to enzyme leakage, lack of control over the microenvironment the enzyme is trapped in, and most importantly, significant mass transfer limitations **Table 1.2)** contributing to low activities observed with this method [87, 86, 78]. The effects on stability can also be variable [87, 46, 54]. In conclusion, entrapment and encapsulation-based immobilization methods have several severe drawbacks impacting the activity of the immobilizate, while still having found wide application in industry. The application

examples and carriers used for immobilization using encapsulation or entrapment are given in **Table 1.1)**.

1.2.2. Carrier-free Immobilization Methods

1.2.2.1. Cross-linking based Immobilization

Cross-linked enzyme aggregates (CLEAs) are carrier-free immobilizates that show marked differences from those obtained via conventional immobilization methods described in the previous chapters. The technology is based on iterations of an earlier method called cross-linked enzymes (CLEs) which were discovered more than 50 years ago [85]. CLEs were generated by mixing an aqueous solution of glutaraldehyde with the enzyme preparation which cross-links the reactive amine groups on the surface of the protein. Despite enabling successful immobilization, this method proved difficult in terms of handling, impaired the activity of the enzymes dramatically, hindered their stability, and was not reproducible. The strategy that subsequently built upon CLEs was the generation of cross-linked enzyme crystals (CLECs), which emerged in the 1990s. CLECs were generated by batch crystallization of enzymes, followed by cross-linking via glutaraldehyde [89]. The CLEC method could generate immobilizates of controllable size by modifying various parameters of the crystallization process (i.e. temperature, pH, mixing speed), giving rise to enzyme crystals of 1-100 µm [89, 82]. Batch crystallization of the enzymes allowed for uniform particle formation, and the ability to control the size of the formed crystals allowed tailoring of the process for a desired application, for instance, generating crystals of 5 µm or smaller in size is desirable for detergent and personal care product applications, whereas larger crystal sizes are preferred for biocatalytic applications due to ease of filtration [89]. Additionally, CLECs were much more stable compared to CLEs and had better activity retention [85]. The method was deemed applicable for a wide range of enzymes and was commercialized soon after its development [90], however, due to the time consuming and difficult nature of crystallization, purification, and high costs, CLECs had severe limitations, which prompted the development of CLEAs [85].

CLEAs can be generated by precipitating enzymes out of a solution, followed by cross-linking to lock enzymes in an insoluble form, which allows their retention via centrifugation, filtration or decantation [85, 45, 50]. CLEAs can be prepared from purified enzymes or directly from the crude cell extract in an appropriate buffer, where the enzyme of interest is precipitated by the addition of polyethylene glycol or saturated salt

solutions such as ammonium sulfate [85, 58]. The precipitated enzyme retains its 3D structure, and therefore activity, in the process. Upon recovery of the enzyme aggregates, they are transferred into a solution of cross-linking agent (commonly glutaraldehyde) under constant agitation, which renders the aggregates permanently insoluble, therefore rendering the CLEA strategy an irreversible immobilization method [85, 58, 54]. Cross-linkage by glutaraldehyde is achieved in the same way as described for CLEs, where the free amino groups of lysine residues at the enzyme surface react with those of neighboring enzymes, and the precise nature of cross-linking depends on the pH of the solution. Depending on the enzyme targeted for immobilization, the success of the method is variable or unstable CLEAs may form, due to the localization of lysine residues being different for each target [85]. Furthermore, for certain targets such as nitrilases, the method was shown to generate immobilizates that possess extremely low activities or are completely devoid of activity, postulated to be due to the cross-linking of residues at the active site [90]. This undesirable effect can be partially overcome by switching to a cross-linker with a larger size (i.e. bulky polyaldehydes) which are less likely to reach the active site of the enzyme and form unintended linkages that affect the activity of the immobilizate. In addition to the selection of cross-linkers, it is often necessary to adjust and optimize other process parameters such as temperature, pH, precipitants, and the ratio of cross-linker to the enzyme in order to generate CLEAs, some of which can be automated [85]. Despite the above-mentioned drawbacks, CLEAs also offer several advantages and the process has been applied to numerous targets, most of which are hydrolases [85, 90].

The most obvious advantage of the CLEA strategy is that the method does not rely on carriers, which makes it relatively simple and cost-effective (see **Table 1.2** , [85]). CLEAs are often suitable for use with organic solvents and have high productivities, and unless the active site of the enzyme is disturbed via unintended linkages, can retain relatively high activities. As the particle size is a factor that impacts diffusion, tailoring the process parameters may help generate CLEAs of smaller size which favor optimal reaction rates, though this change comes at the expense of ease of handling due to filtration difficulties that would arise with small particle sizes. Additionally, different CLEA concepts exist, such as combi-CLEAs consisting of multiple enzymes allowing cascade reactions, or multipurpose CLEAs (multi-CLEAs) that contain several different enzymes involved in various non-cascade reactions [85, 50]. A bio-imprinting approach has also been used in combination with CLEAs to enhance certain properties of the target enzymes such as substrate specificity or activity, where imprinted-CLEAs are generated [50, 91]. For instance, a conformational change was introduced to a lipase by the sup-

plementation of additives such as surfactants or crown ethers, which favor a more active conformation, and this conformational change was made permanent via cross-linking to generate hyperactive CLEAs [92]. Depending on the aim, it is also possible to include carriers in this method, for instance, by generating silica-CLEA composites, or magnetic mCLEAs by an additional cross-linking step to attach CLEAs to magnetic nanoparticles to allow magnetic separation.

Lastly, a recent immobilization strategy that generates immobilizates called spherezymes can also be classified as a non-conventional approach for enzyme immobilization. Immobilization via the spherezyme strategy involves cross-linking of enzyme molecules immobilized on the surface of hydrophobic solvent droplets, and has so far only been applied to lipases [50]. The method relies on the self-immobilization of lipases via a water-in-oil emulsion, where the aqueous solution containing lipases is supplemented by hydrophobic solvents [93]. Lipases then migrate to the phase boundary where the hydrophobic active site surface (exposed due to lid opening) self-orients towards the hydrophobic layer where the enzymes are cross-linked in this orientation, giving rise to spherezymes. Notably, spherezymes of *Pseudomonas fluorescens* lipase were generated within a microfluidic chip, where the cross-linker and mineral oil were pumped into the chambers, and the soluble lipase was supplied via aqueous droplets, generating spherezymes which were used to hydrolyze *p*-nitrophenol butyrate as a model substrate [94].

In conclusion, both the generation of CLEAs and spherezymes are facile methods, capable of producing enzyme immobilizates without requiring carrier materials or purification, though the application of spherezymes is severely limited, i.e. as it relies on lipase-specific structural features for immobilization. While drastically different from conventional immobilization techniques, these methods are not true *in vivo* approaches (unlike catalytically-active inclusion bodies, see next chapter), as they require additional steps to yield the enzyme in an immobilized form upon release from the cell. Furthermore, the CLEA method is subject to variable degrees of activity loss in addition to requiring optimizations for each target. Nonetheless, the generation of CLEAs represents a method that is widely applicable to many enzymes of commercial interest.

1.2.2.2. Catalytically-active Inclusion Bodies

In the last years, the production of catalytically-active inclusion bodies (CatIBs) has emerged as a promising, fully *in vivo* method for enzyme immobilization [95, 84, 96, 97, 98]. The method is based on the on-demand generation of inclusion bodies (IBs) of

protein(s) of interest in bacterial cells. Conventional IBs are produced in the cytoplasm due to strong overproduction of recombinant proteins which lead to aggregation and subsequent deposition of the un- or misfolded protein aggregates into IBs [99]. Despite the long-held traditional perception as inactive cellular waste, such IBs can retain a variable degree of activity, which was documented since the 1980s [100]. Physically, IBs and hence also CatIBs, are dense particles that are insoluble in aqueous and organic solutions, with a size ranging between 50-800 nm, and they can be easily detected via phase contrast microscopy as they appear as refractive particles at the cell poles, and via transmission electron microscopy where they appear as electrodense, dark areas [99, 101, 102]. The presence of IBs has been shown in yeasts and mammalian cells (called aggresomes for the latter), in addition to bacteria [103]. Despite their usual localization at the cell poles, the occurrence of IBs in the periplasmic space has also been reported, where an aggregation-prone double mutant of a maltose-binding protein (which localizes to the periplasm) gave rise to the formation of periplasmic IBs when fused to a target protein [104].

IBs have a complex composition as they can contain amyloid-like structures to a variable degree, depending on expression conditions and the properties of the heterologously produced protein [105, 106]. CatIBs share the same physical properties as conventional IBs, however, unlike natural IBs, they are generated rationally via the genetic fusion of an aggregation inducing element to either the 5' or 3' end of a target gene, which allows for the aggregation of the fusion protein during heterologous overexpression of the gene fusion within the cell (**Figure 1.3**). Furthermore, the CatIB method relies on the physical properties of IBs to allow easy preparation of the target proteins. Since CatIBs are insoluble particles, they are easily retained upon centrifugation of the crude cell extract, which results in the supernatant containing soluble proteins and the pellet which contains CatIBs.

As mentioned above, aggregation inducing elements (also called CatIB tags) are the driving force of successful CatIB formation in cells. CatIB tags can be artificial, synthetic peptides that are only a few (8-20) amino acids in length, protein domains of moderate (42-172 residues) length, and even entire proteins of almost 600 residues in length [103]. The choice of CatIB tag and its fusion site has a profound impact on the properties of the resulting CatIBs. Examples of such CatIB tags, their applications, and their properties will be introduced in the upcoming subchapters in detail. In addition, peptide linkers which are typically between 12-25 residues, with flexible or rigid structures (i.e. flexible glycine-serine or rigid proline-threonine linkers) can be included between the CatIB tag and the target, and these linkers can affect the activity of the CatIB immobilizate [107,

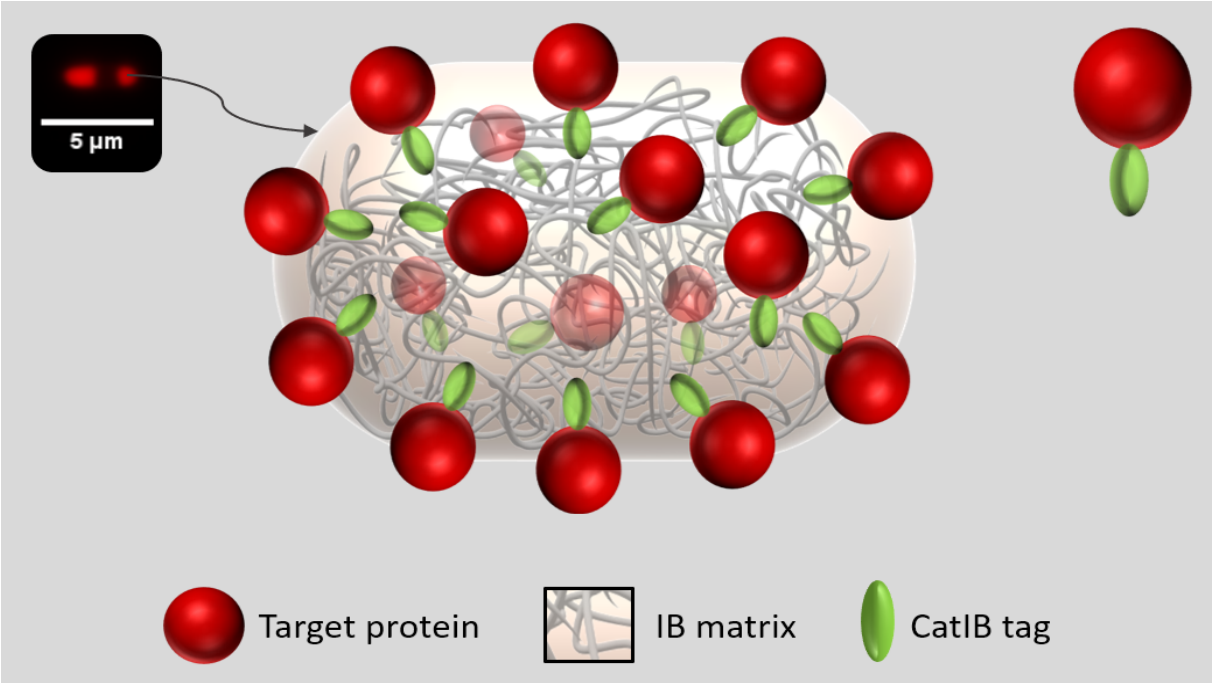

Figure 1.3. Visual representation of catalytically-active inclusion bodies.

Genetic fusion of the target gene with a CatIB tag results in the production of a fusion protein (upper right corner) composed of the target protein (red spheres) fused to a CatIB tag (green ellipses). The natively folded (and hence active) fusion protein is incorporated into the inclusion body (IB) matrix, formed by the aggregated fusion protein. Upper left: Fluorescence microscopy image depicting *E. coli* cells producing GFIL8-mCherry CatIBs, where CatIBs are localized at the cell poles. Adapted with permission from [103]. Copyright © 2021 American Chemical Society.

108]. Additional factors that have a large influence on CatIB formation and properties are expression and cultivation conditions, where a low temperature during expression favors CatIB formation, and strong inducers promote high CatIB yields [84].

The CatIB method is widely applicable, as evidenced by the successful generation of CatIBs for numerous proteins and enzymes with varying degrees of complexity in the last years, including but not limited to reporter proteins such as red fluorescent protein mCherry, yellow fluorescent protein (YFP) and green fluorescent protein (GFP), monomeric enzymes such as lipase and β-glycosidase, dimeric enzymes such as a hydroxynitrile lyase and 2-succinyl-5-enol-pyruvyl-6-hydroxy-3-cyclohexene-1-carboxylate synthase (MenD), tetrameric, cofactor dependent enzymes such as benzaldehyde lyase and alcohol dehydrogenase, and even a cofactor dependent dodecameric enzyme L-lysine decarboxylase [104, 108, 109, 110, 111, 112, 113, 114, 115]. Furthermore, CatIBs can be magnetized *ex vivo* by iron oxide particles to allow for an even easier separation and recycling [116], and synthetic cascade reactions have been realized using CatIBs of

benzyaldehyde lyase and alcohol dehydrogenase [117]. Despite their increasing popularity, CatIBs have not found industrial application, yet remain promising candidates for application due to their high purity, stability, ease of production, handling, and recycling, along with high activities (see **Table 1.2**, [84, 95, 103]). However, there is no universal CatIB tag that can immobilize every target protein, and usually optimizations are required to implement the method successfully. For example, if the structure of the target protein does not allow the identification of an unsuitable fusion terminus, both N- and C- terminal fusions should ideally be tested. In addition, linkers could be varied or excluded altogether to tune the CatIB formation efficiency or the activity of the target protein [108]. Nevertheless, the CatIB method is cost-efficient, simple, and does not require carrier materials as it combines production and purification of the enzyme immobilizate in one step due to its *in vivo* nature, and further excludes laborious chromatographic purification steps. Therefore, CatIBs represent a promising, fully biological method for enzyme immobilization. Due to the ever-accumulating knowledge regarding CatIBs in recent years, a review paper providing a comprehensive overview of the field (**Section 2.4**), as well as a book chapter covering design, production, and handling of CatIBs (**Section 2.5**) have been prepared and published as part of the here presented work. The tables that provide an overview of all CatIB tags and target proteins are listed in **Section 2.4**, **Table 1**, and further in **Section 2.6**, **Table 1**.

1.2.2.2.1. Protein domains as CatIB tags

As outlined in the previous chapter, the fusion of suitable CatIB tags to a given immobilization target is the driving force of CatIB formation in bacterial cells. For this purpose, aggregation prone protein domains represent the most commonly used group of CatIB tags, which were fused to numerous proteins by different groups in the past years [84, 96, 97, 98, 103, 118]. For instance, TdoT (tetramerization domain of the cell-surface protein tetrabrachion) is a coiled-coil domain with a size of 53 amino acids that has been widely employed for CatIB formation (**Figure 1.4**). The TdoT tag originates from the archaeon *Staphylothermus marinus*, and was originally used as a fusion partner for enzymes including MenD, lipase A from *Bacillus subtilis* (BsLA) and hydroxynitrile lyase from *Arabidopsis thaliana* (AtHNL), with the intention of increasing the stability of these enzymes via increasing their oligomerization state [109]. In addition to stabilizing target proteins and increasing their tolerance towards low pH values, the tag led to successful CatIB formation for the targets, where the enzymatic activity was detected predominantly (over 76%) in the insoluble CatIB fraction for the resulting immobilizates. The recyclability of MenD and AtHNL CatIBs in aqueous and micro-aqueous organic solvent

based reaction systems were demonstrated, respectively. The TdoT tag was later used to generate CatIBs of YFP, mCherry, an alcohol dehydrogenase, a benzaldehyde lyase, a lysine decarboxylase, and a benzoylformate decarboxylase [108, 117, 119, 110]. For the reporter proteins mCherry and YFP, low to medium-high CatIB formation efficiencies of 32% and 65% were reported, respectively [108, 117]. The stability and recyclability of the TdoT CatIBs were also demonstrated for lysine decarboxylase from *E. coli* (EcLDC), along with very high conversion rates (87-100%) [110]. Furthermore, TdoT CatIBs of alcohol dehydrogenase from *Ralstonia sp.* (RADH) and benzaldehyde lyase from *Pseudomonas fluorescens* (PfBAL) displayed over 68% of the total enzymatic activity of the corresponding crude cell extracts, and the corresponding Co-CatIBs, where both enzymes are co-localized within CatIBs were further used in two-step cascade reaction for the production of (1R,2R)-1-phenylpropane-1,2-diol (PPD), which is a precursor of the calcium channel blocker diltiazem [108, 117]. Furthermore, tuning the CatIB formation efficiencies by removal of the flexible linker between the TdoT tag and target protein was demonstrated for mCherry and YFP CatIBs. Recently, two new, unique coiled-coil domains named NSPdoT and HVdoT were identified (from rotavirus and human vasodilator-stimulated phosphoprotein, respectively), and used to generate AtHNL CatIBs [120]. An increased tolerance towards low pH and high temperature for the NSPdoT and HVdoT CatIBs was demonstrated, similar to TdoT CatIBs.

The 172 amino acid long, dimeric, coiled-coil domain 3HAMP, which is part of the oxygen sensor protein Aer2 from *Pseudomonas aeruginosa*, has also been employed as a CatIB tag (**Figure 1.4**). 3HAMP CatIBs were generated with mCherry, YFP, RADH, PfBAL, EcLDC, benzoylformate decarboxylase and alcohol dehydrogenase from *Levilactobacillus brevis* (LbADH) as targets [108, 117]. Notably, morphological differences were reported for 3HAMP CatIBs of PfBAL when compared to TdoT CatIBs, which appeared as "diffuse" particles rather than well defined, compact CatIBs formed by TdoT. A one-on-one comparison between CatIBs produced using these two tags also revealed differences in yields, protein and lipid contents, as well as activity variations for the same enzyme, where 3HAMP CatIBs showed lower yields, contained less protein, had a higher lipid content and were almost 20 times more active when compared to their TdoT counterparts. In addition, the recyclability and stability of 3HAMP CatIBs in a biphasic reaction system were also demonstrated.

The point mutant of the aggregation prone human Aβ-amyloid peptide (Aβ(F19D), **Figure 1.4**), which consists of 42 residues, was similarly used as a "pull-down" tag for CatIB formation [115]. The hydrophobic Aβ-amyloid peptide is a cleavage product of the β-amyloid precursor protein and is the main constituent of extracellular plaque de-

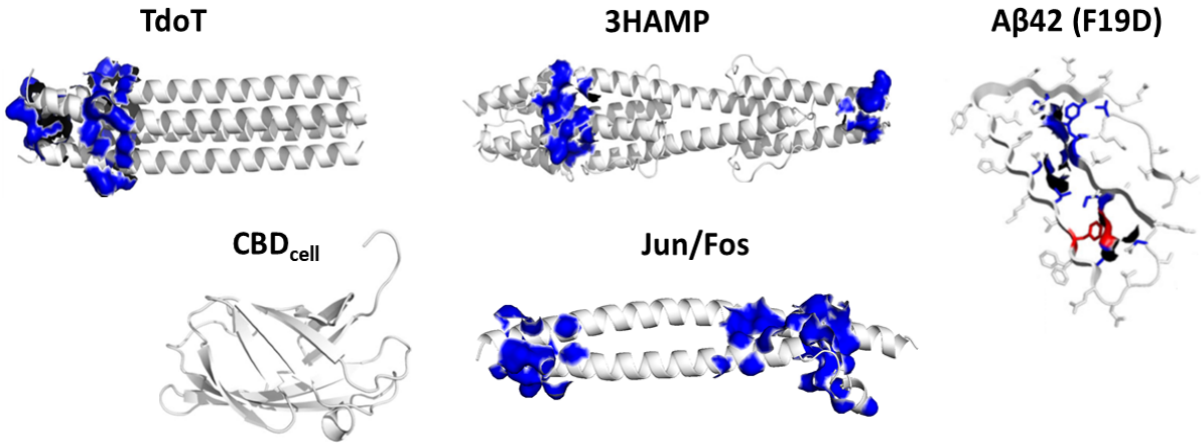

Figure 1.4. Models depicting a few examples of protein domains used as CatIB inducing tags.

Cartoon or stick representations of the structures are depicted in gray, and the hydrophobic surface patches are shown in blue. TdoT: tetramerization domain of the cell-surface protein tetrabrachion from *S. marinus* (protein data bank (PDB) ID: 1FE6). 3HAMP: part of the oxygen sensor protein Aer2 from *P. aeruginosa* (PDB ID: 3LNR). Aβ(F19D): Aβ-amyloid peptide from *Homo sapiens*, shown as a monomer with the F19D substitution in red (PDB ID: 5OQV). CBD_{cell}: Cellulose binding domain from *C. fimi* (PDB ID: 1EXG). Jun/Fos: bZIP domains of leucine zippers Jun and Fos from *Homo sapiens* (PDB ID: 5VPA). The hydrophobic patch analyses were performed by Ulrich Krauss as described by Jäger *et al.*[84]. Images of TdoT, 3HAMP, Aβ(F19D) and CBD_{cell} are adapted from [84]. Reproduced under the terms of the Creative Commons CC BY license. Copyright © 2020 [84].

posits within the brains of Alzheimer's patients which is one of the characteristics of the disease [121]. Nevertheless, Aβ(F19D) peptide was used to generate blue fluorescent protein (BFP) CatIBs in *E. coli* [115]. Similarly, the cellulose-binding domain from *Cellulomonas fimi* (CBD_{cell}), which is 108 residues in length (**Figure 1.4**), and from *Clostridium cellulovorans* (156 residues) were used to generate CatIBs of several enzymes including β-glucuronidase, β-glycosidase, polyphosphate kinase PPK3, D-sialic acid aldolase, UDP–glucose pyrophosphorylase, D-amino acid oxidase, as well as reporter proteins GFP and DsRed [122, 123, 124, 111, 116]. Notably, enzyme activity was detected almost entirely in the insoluble fraction (above 90%) for β-glucuronidase, β-glycosidase, D-amino acid oxidase and D-sialic acid aldolase CatIBs.

Recently, more protein domains have been shown to promote CatIB formation. For instance, bZIP domains of Jun (62 residues) and Fos (93 residues) leucine zippers (**Figure 1.4**) were also used to form CatIBs of a GFP variant [125]. As leucine zipper domains consist of amphipathic α-helices that can form a dimer, the fusion of two complementary domains to a target gives rise to a coiled-coil which was employed as a pull-

down tag. Interestingly, different Jun and Fos fusion strategies which included fusion of both domains to N- and C-terminus of the target (for Jun and Fos, respectively), and co-production of N-terminally Jun tagged target, together with N-terminally Fos tagged target were both shown to be successful to drive CatIB formation. Similarly, an α-helical CHAD domain of a short-chain polyphosphatase from *E. coli*, as well as SACS2 CHAD from *Saccharolobus solfataricus* were fused to a small peptide derived from the polyphosphatase, as well as turbo GFP [126]. Both triple-fusions yielded CatIBs, albeit with varying efficiencies. Quite recently, the SpyTag/SpyCatcher pair was used to generate CatIBs of GFP and an octameric leucine dehydrogenase[127]. Conventionally, the SpyTag/SpyCatcher pair (14 and 116 residues, respectively) are used to link different proteins post-translationally via the interaction of the pair, which were originally generated by splitting a bacterial adhesin domain that is capable of spontaneous, intramolecular isopeptide bond formation [128]. In contrast to this conventional use, fusion of SpyTag/SpyCatcher to the leucine dehydrogenase, also yielded CatIBs with high CatIB formation efficiencies of 85% [127]. The corresponding SpyTag/SpyCatcher CatIBs were further cross-linked via glutaraldehyde to generate CLEA-CatIBs, which displayed remarkable thermal stability, stability in organic solvents and were recyclable, showing enhanced performance compared to CLEAs.

In conclusion, various protein domains including coiled-coil or aggregation prone domains have been used to immobilize numerous proteins via the CatIB strategy in the last years. The TdoT tag appears as the most widely employed CatIB tag thus far, yet has been overwhelmingly used in N-terminal fusions (except for EcLDC), leaving room for investigating the possibility of enhancing CatIB formation efficiencies or CatIB activities by varying the fusion terminus of the tag. Along the same lines, as the improvement in CatIB formation efficiencies were previously reported for some of the above described CatIBs upon altering the linker separating the CatIB tag and the target, it would be worthwhile to investigate if such a strategy could be applied to different CatIBs in order to generate immobilizates that display more desirable properties. These questions have therefore been investigated within the scope of this thesis (**Section 1.3**, **Section 2.1** and**Section 2.2**).

1.2.2.2.2. Short peptides as CatIB tags

Short CatIB tags can be classified as peptides up to 20 residues in length with different physical properties, which can be α-helical in structure (such as 18AWT), fully hydrophobic (GFIL8) or possess surfactant-like (L6KD) properties[103], (**Figure 1.5**). For

instance, the self-assembling, surfactant-like peptide tag L6KD (with an amino acid sequence of LLLLLLKD) and its variants (L6K2 and DKL6) are only 8 amino acids in length, and consist of a hydrophobic "tail" and a hydrophilic "head" [112]. These peptides are completely artificial and designed to mimic surfactants, and were shown to be capable of self-assembly in aqueous solutions [112, 129]. L6KD and its two variants were used to generate CatIBs of amadoriase II (from *Aspergillus fumigatus*) in *E. coli* [112]. L6KD was also succesfully employed for the generation of GFP, BsLA, and β-xylosidase (from *Aequorea victoria*, *Bacillus subtilis and Bacillus pumilus*, respectively) CatIBs with high efficiencies, resulting in more than 60% of the enzymatic activity detected in the insoluble (CatIB) fraction for these targets. The structure of CatIBs generated by the surfactant-like peptide L6KD was examined by proteinase K digestion and binding assays with amyloid-specific dyes such as thioflavin T and Congo red, revealing the presence of amyloid-like fibrils for the CatIBs generated by the L6KD tag.

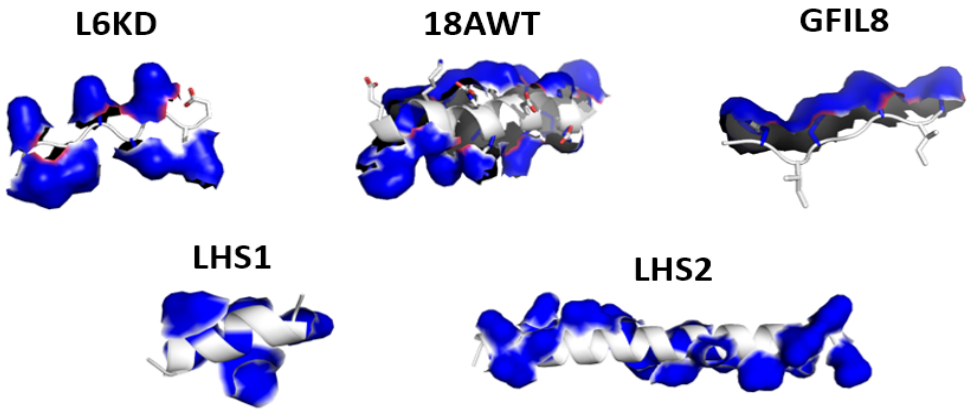

Figure 1.5. Models depicting a few examples of short artificial peptides and their variants commonly used as CatIB-inducing tags.

Cartoon or stick representations of the structures are shown in gray, and the hydrophobic surface patches are shown in blue. L6KD, 18AWT, GFIL8 and LHS1 represent short artificial peptide tags, where the LHS2 is the lengthier variant of the latter peptide. The structures of L6KD, 18AWT, and GFIL8 were modeled taking into account the known secondary structure [84]. The LHS2 structure was predicted and modelled using AlphaFold [130] and LHS1 was modeled by truncation the LHS2 structure. The hydrophobic patch analyses were performed by Ulrich Krauss as described by Jäger *et al.*[84]. Depicted structures for L6KD, 18AWT, and GFIL8 are modified from [84]. Reproduced under the terms of the Creative Commons CC BY license. Copyright © 2020 [84].

An amphipathic, α-helical peptide of 18 residues in length, called 18AWT (sequence: EWLKAFYEKVLEKLKELF) has also been shown to promote CatIB formation [113], (**Figure 1.5**). The 18AWT peptide was designed to resemble the short apolipopro-

tein A-I mimetic peptide sequence of Apolipoprotein E4, which is involved in lipoprotein metabolism in mammals with certain variants associated with various diseases including Alzheimer's [113, 131]. The 18AWT peptide was subsequently shown to be membrane associated, and was further engineered in an attempt to increase its amphipathicity by altering its ion pairs in a rational manner, where the lysines in the 18AWT peptide were sequentially substituted with glutamic acids (and vice versa) [113]. This resulted in the generation of several peptide variants including 18Arev, where the ion pairs were completely reversed, and BsLA as well as GFP CatIBs generated by 18Arev as a CatIB tag yielded cytoplasmic CatIBs, in contrast to the lipid associated 18AWT CatIBs. Furthermore, morphology investigations on 18AWT and 18Arev CatIBs hinted at a difference with respect to L6KD CatIBs, revealing that CatIBs of 18AWT and its variants are devoid of amyloids. In addition, the CatIBs of lipid-associated 18AWT and variants displayed lower activities compared to variants such as 18Arev that were not lipid associated.

The fully hydrophobic peptide GFIL8, possessing a length of 8 residues (sequence: GFILGFIL) and its double-length variant GFIL16 were used to generate GFP, BsLA, amadoriase II and Ulp1 protease CatIBs [114, 132], (**Figure 1.5**). The GFIL8 peptide was originally derived from the tetrapeptide GFIL, which was synthesized due to its postulated self-assembling and hydrogelation properties, and the tetrapeptide was shown to have a stable structure at physiological pH, with a tendency to form antiparallel β-sheet structures at pH values above 8.5 [133]. Nevertheless, the GFIL8 tag derived from the tetrapeptide was shown to form "typical" CatIBs, i.e. unlike the lipid-associated CatIBs formed by 18AWT, and resulted in enzyme immobilizates that displayed nearly 85% of the enzymatic activity in the insoluble fraction for lipase A, and over 66% for amadoriase II [114]. Furthermore, GFIL8 CatIBs of the Ulp1 protease was shown to be stable, resistant to degradation, and possessed approximately 40% of the activity when compared to its soluble counterpart derived from the crude cell extract [132].

EAK16 is another synthetic peptide employed as a CatIB tag, it consists of 16 amino acids and possesses a β-sheet structure, where opposingly charged glutamic acid and lysine residues are sandwiched between alanines [134]. The EAK16 peptide is derived from zuotin, a Z-DNA binding protein from *Saccharomyces cerevisiae* [135], and was further engineered to increase its hydrophobicity, which gave rise to the ELK16 peptide (sequence: $\text{LELELKLK})_2$) [134]. ELK16 was used as a CatIB tag and resulted in the successful generation of amadoriase II, β-xylosidase, GFP and tyrosine phenol-lyase CatIBs [136, 134]. Similar to L6KD CatIBs, Fourier-transform infrared spectroscopy analyses performed on ELK16 CatIBs hinted at the presence of amyloid-like structures. Additionally, elastin-like peptides (ELPs), which typically had been used for soluble expression *in*

vivo, followed by the temperature/salt concentration dependent, reversible aggregation of their fusion partners *in vitro* [137] were also used as CatIB inducing tags [138]. Quite recently, a 10-residue-long, aggregation prone peptide tag named LHS1 (sequence: LH-SAKIVVIG) was derived by combining and modifying two short sequences present at the N- and C- terminus of a short-chain polyphosphatase from *E. coli* [126]. Notably, the LHS1 tag was limited in its ability to pull-down turbo GFP. The lengthier variant of the LHS1 tag was generated in the same study and named LHS2 (32 residues, sequence $((LHS)_3AKIVVIG)_2$), and while not being "short" *per se*, the tag had a higher efficiency when shifting the fluorescence of the highly soluble target turbo GFP into the insoluble cell fraction.

In summary, there are numerous short peptides that have successfully been applied as CatIB tags, which can bestow CatIBs with unique properties depending on the employed tag. Furthermore, the inclusion of an intein (such as self-cleaving Mxe GyrA) between the target protein and the CatIB tag can facilitate the release of the target into the soluble fraction, therefore allowing column-free purification of the target, demonstrated earlier with some of these tags [114, 139]. However, it should be noted that the peptide tags described above in detail, namely 18AWT, L6KD, and GFIL8, have been overwhelmingly used in C-terminal fusions, and were generally applied to a limited number of target proteins, promoting future studies to test their applicability range. Nevertheless, the use of such short, self-assembling peptides with unique properties can prove to be advantageous in terms of cost-effectiveness and convenient synthesis of the genetic construct, whereas their effectiveness in "pulling-down" highly soluble, large, and difficult to immobilize targets needs investigation. These issues, namely the general applicability of the 18AWT, L6KD, and GFIL8 tags to more complex protein targets and investigation of their ability in pulling down highly soluble target proteins, have been investigated within the scope of the here presented PhD thesis (**Section 1.3**, **Section 2.1**).

1.2.2.2.3. Proteins as CatIB tags

To generate CatIBs, also complete aggregation prone proteins can be used as CatIB tags, where their genes are fused to those of the target proteins. To this end, the VP1 capsid protein from the foot and mouth disease virus (FMDV), which has a size of 209 residues, 396 amino acid long, defective folding mutant of maltose binding protein MalE31 from *E. coli*, (**Figure 1.6**), and 574 amino acid long pyruvate oxidase from *Paenibacillus polymyxa* E681 (PoxB) are all examples for aggregation-prone proteins that have been used as pull-down tags for CatIB formation [104, 115, 140]. FMDV VP1 was

used as a CatIB tag with GFP and β-galactosidase as targets, where the latter enzyme displayed almost half of the total enzymatic activity in the insoluble fraction[115]. Interestingly, MalE31 fusions with β-lactamase and alkaline phosphatase from *E. coli* as targets gave rise to periplasmic CatIBs, due to the tendency of natural MalE31 to be translocated to the periplasm. This indicates that the translocation process was not hampered by the fusion of the protein to different targets when the signal sequence for translocation was included in the constructs. Furthermore, the enzymatic activity of the targets was predominantly detected in the insoluble fraction (95%) for both targets [104]. PoxB was also employed as a CatIB tag, with GFP, α-amylase and β-lactamase as targets for immobilization, where α-amylase displayed 77% and β-lactamase displayed over 95% of the total activity in the CatIB fraction for the targets [140].

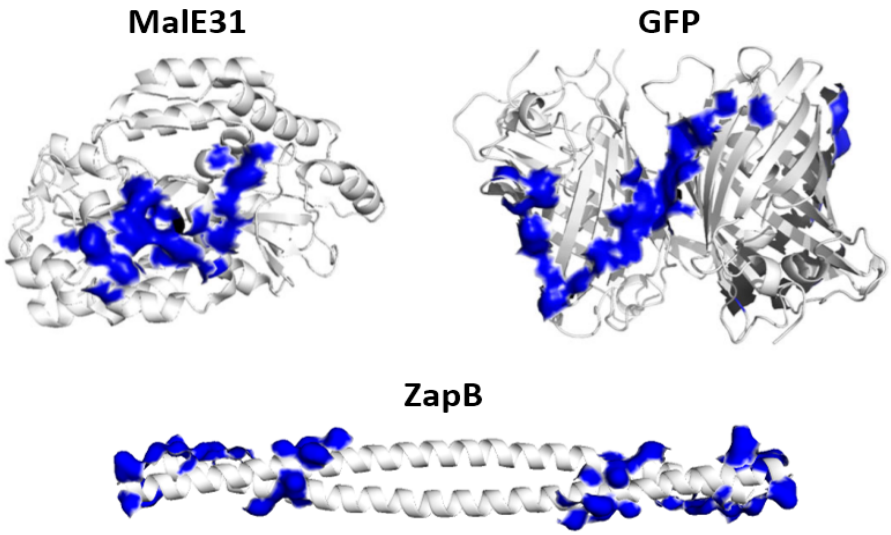

Figure 1.6. Models depicting a few examples of full-length proteins used as CatIB inducing tags.

Cartoon representations of the structures are shown in gray, and the hydrophobic surface patches are shown in blue. MalE31: defective folding mutant of maltose binding protein from *E. coli* (PDB ID: 1LAX). GFP: Green fluorescent protein from *A. victoria* (PDB ID: 1GFL). ZapB: cell division protein from *E. coli* (PDB ID: 2JEE). The hydrophobic patch analyses were performed by Ulrich Krauss as described by Jäger *et al.*[84]. Depicted structures for MalE31 and GFP are modified from [84]. Reproduced under the terms of the Creative Commons CC BY license. Copyright © 2020 [84].

Recently, the small cell division protein ZapB of 81 amino acids from *E. coli* (**Figure 1.6**) has been added to the toolbox of proteins successfully used as CatIB inducing tags, where the high propensity of ZapB to form a dimeric coiled-coil structure as a pull-down tag, rather than its aggregation tendency, served as the driving force in fluorescent CatIB

formation [141]. The coiled-coil propensity of the protein was estimated to be higher than for the coil-coil domains TdoT and 3HAMP, and the fusion of ZapB successfully shifted the target proteins into the insoluble fraction for mCherry and GFP as estimated by SDS-PAGE analyses (with 55% and 95%, respectively). The study also demonstrated the effect of different CatIB inducing tags on the activity, where the intensity of GFP fluorescence was found to be two times higher for ZapB CatIBs compared to the corresponding Aβ42 CatIBs, with the authors suggesting that tags with a high β-sheet propensity that generate amyloid-like structures can result in CatIBs with reduced activities (or fluorescence), owing to their tendencies to aggregate rapidly. Interestingly, GFP itself (238 residues, (**Figure 1.6**) had been previously employed as an aggregation inducing protein tag to generate CatIBs of acid phosphatase from *Enterobacter aerogenes* (PhoC), where GFP also retained its fluorescence [107]. The study revealed that variation of linkers between GFP as a CatIB tag and PhoC as the target has a large impact on the activity of the immobilizate, where the rigid (sequence: $(AAAKE)_5$) linker lead to an increase of activity for the target as well as fluorescence of the tag when compared to the flexible (sequence: $(GGGS)_5$) linker. The effect of intradomain linkers on CatIB properties represents another research question that has been explored in more detail within the scope of this thesis (**Section 1.3**, **Section 2.2**). In summary, several full-length proteins have been employed as CatIB tags, where also the native function of the protein used as the CatIB tag was retained in addition to the activity of target protein.

1.2.2.3. Other carrier-free immobilization methods

Apart from the CatIB strategy, various other *in vivo* immobilization techniques have been developed (**Figure 1.7**), which combine heterologous protein production and immobilization in one step. Such *in vivo* immobilization methods have also been reviewed as part of this PhD thesis (**Section 1.3**, **Section 2.6**).

For instance, conventional, inactive IBs can be used as a proteinaceous support material for enzyme immobilization where target proteins can be displayed on the surface of the IB particles (**Figure 1.7, A**). In the IB display approach, a peptide or protein domain that interacts with a specific partner peptide or protein domain (i.e. via dimerization to form a coiled-coil) is fused to a target protein. The corresponding interaction partner is similarly fused to a protein that drives IB formation. Upon co-production, protein immobilizates are generated where the target protein localizes to the surface of the IB matrix through the interaction of the interacting protein partners. To this end, leucine zipper domains fused to a cellulose binding domain known to generate IBs, and

red fluorescent protein 1 (Rfp1) as target protein, formed IBs decorated with Rfp1 [142]. Similarly, a galactose oxidase, an alcohol dehydrogenase (ADH), and a formate dehydrogenase were displayed on polyhydroxybutyrate synthase (PhaC) IBs using E- and K-coils [143], to facilitate a cascade reaction using the ADH and formate dehydrogenase for the production of (*S*)-4-chloro-α-methylbenzyl alcohol [144, 145].

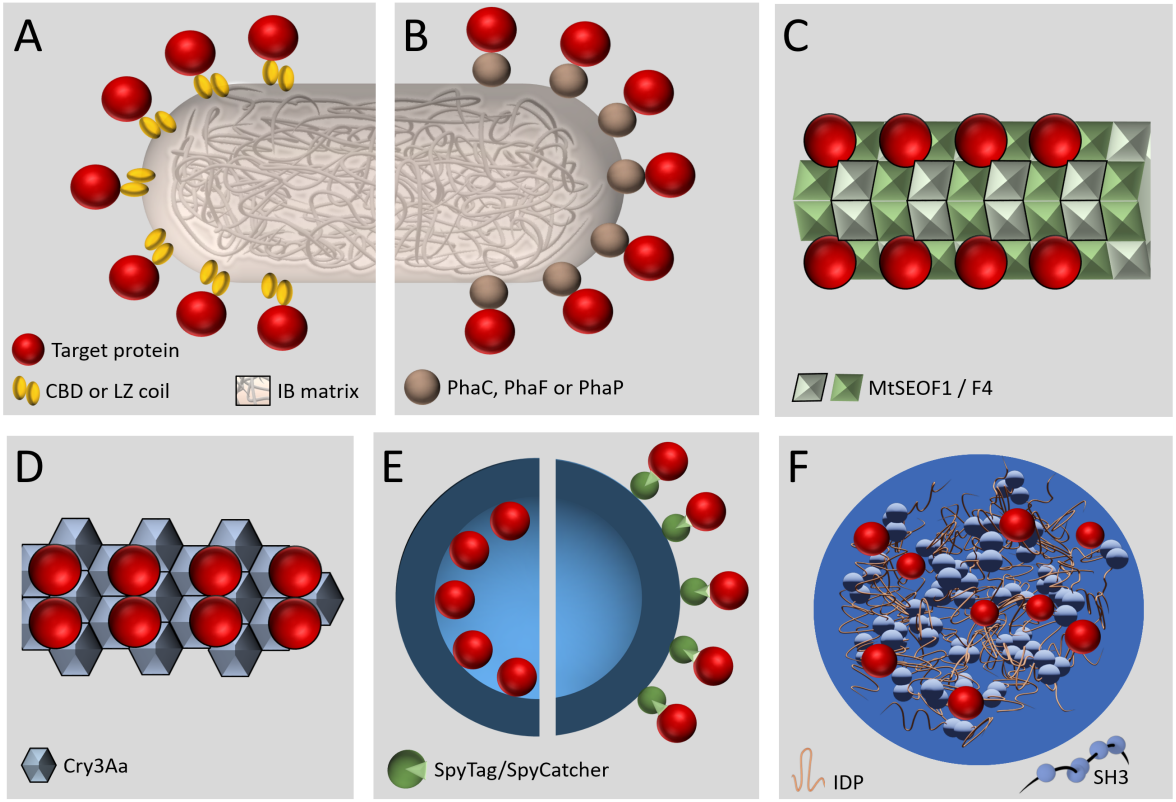

Figure 1.7. Visual representation of selected *in vivo* immobilization methods.

(A) Inclusion body display. **(B)** PHA granules. **(C)** Forizymes. **(D)** Cry3Aa crystals. **(E)** Virus-like particles showing target protein directly linked to (left) or displayed onto (right) capsid proteins. **(F)** Liquid-liquid phase separation. CBD: cellulose binding domain. LZ: leucine zipper. IB: inclusion body. PhaC: polyhydroxybutyrate synthase. PhaF, PhaP: polyhydroxyalkanoate granule-associated proteins. MtSEOF1 and MtSEOF4: sieve element occlusion by forisome (SEOF) subunits, Cry3Aa: crystal-forming protein from B. *thuringiensis*. IDP: intrinsically disordered protein. SH3: SRC homology 3 domain. Adapted with permission from [103]. Copyright © 2021 American Chemical Society.

Polyhydroxyalkanoate (PHA) granules are biopolymers composed of (*R*)-3-hydroxy fatty acids of various length and include polyhydroxybutyrate (PHB) which is formed by various bacteria [103]. PHB synthesis takes place by the joint action of three enzymes, acetyl-CoA acetyltransferase (PhaA), acetoacetyl-CoA reductase (PhaB) and PHA synthase (PhaC), where the latter was shown to accumulate as IBs when expressed in *E. coli*

[146, 145], as outlined above for the IB display approach. In PHA granule based immobilization, PhaC is utilized in a different manner, as the granules produced by the action of this enzyme also involve the localization of PhaC to the surface of the biopolymer, where it can serve as an anchor to display target proteins (**Figure 1.7, B**). This property was exploited via the fusion of GFP to PhaC, where PHA granules displaying fluorescence were generated [147, 148]. The same principle can be extended to other proteins that are present at the surface of the PHA granules (such as the phasins PhaF or PhaP), which was applied to display enzymes including P450-BM3 monooxygenase, β- galactosidase and lysine decarboxylase onto PHA granules [149, 150, 151].

Forizymes are functionalized plant mechanoprotein complexes (called forisomes), which undergo conformational changes in a calcium concentration dependent manner [103]. When the genes encoding certain forisome subunits (sieve element occlusion by forisome from *Medicago truncatula* (MtSEOF), such as MtSEOF1-4) are fused to a target gene, the fusion generates the artificial, functionalized forizyme with a tubular shape and a size ranging from 10 × 1 µm to 55 × 5 µm, located roughly in the middle of the host cell (**Figure 1.7, C**) [152, 103]. As of now, there is only one study that generated forizymes, where the authors immobilized a blue fluorescent protein, a YFP variant, a glucose-6-phosphate dehydrogenase, and a hexokinase within forizyme immobilizates produced in *Saccharomyces cerevisiae* [153].

Another *in vivo* immobilization approach utilizes protein crystals which are formed naturally by Cry3Aa protein of *Bacillus thuringiensis*, and is achieved by molecular biological fusion of target genes to the gene encoding Cry3Aa (**Figure 1.7, D**) [103]. The approach was used to successfully entrap GFP, mCherry, peptide deformylase, BsLA, and dieselzyme 4 (a mutant of *Proteus mirabilis* lipase) within the Cry3Aa crystals [154, 155, 156]. Very recently, the Cry3Aa approach was combined with the SpyTag/SpyCatcher strategy to co-immobilize three enzymes of the menaquinone biosynthesis pathway, including MenD[157].

Virus-like particles (VLPs) are formed by multiprotein complexes that contain viral capsid proteins with self-assembling properties, and can be used to entrap target proteins, or act as a scaffold for surface display in combination with SpyTag/SpyCatcher system (**Figure 1.7, E**) [103]. For example, VLP P22 is the capsid protein of *Salmonella typhimurium* bacteriophage P22, and consists of the coat protein and the scaffolding protein, where the latter localizes to the interior of the capsid protein shell [158]. This property can be exploited to entrap target proteins within VLPs by fusing the gene encoding the target protein to that of the scaffolding protein and co-expressing the gene fusion

together with the coat protein gene. Notably, a cascade reaction with β-glucosidase, galactokinase, and glucokinase from *Pyrococcus furiosus* was realized within VLPs [159].

Lastly, membraneless organelles or liquid-protein condensates that are formed by liquid-liquid phase separation (LLPS) can also be used to localize proteins of interest (**Figure 1.7, F**) [103]. LLPS can be induced via the multivalent interactions of proteins containing certain domains such as e.g. SRC homology 3 domain (SH3) and its proline-rich motif (PRM) ligand, which was utilized for co-immobilization of two proteins by fusing mCherry to SH3, and a GFP variant to the ligand [160]. This strategy was further extended, where 16 repeats of the intrinsically disordered regions of a consensus sequence of MaSp1 protein, which was shown to be sufficient in triggering cellular compartmentalization, was used to immobilize GFP, mCherry, as well as an aminotransferase and a decarboxylase via LLPS in *E. coli*, where the two enzymes were used in a cascade reaction to produce 1,3-diaminopropane (DAP) [161].

In conclusion, new *in vivo* approaches based on the genetic fusion of target genes to those of self-crystallizing proteins, biopolymers, or even intrinsically disordered protein domains that self compartmentalize have started to emerge rapidly in the recent years. Application of these methods to more targets could prove to be beneficial for elucidating the applicability range, benefits, as well as potential drawbacks of these approaches.

1.2.2.4. Magnetic Protein Aggregates (MPAs)

Magnetic protein aggregates (MPAs) represent a new approach to generate *in vivo* protein immobilizates, and the method was developed as part of the here presented PhD thesis as an alternative method for enzyme immobilization (**Section 1.3**, **Section 2.3**). The strategy is based on ferritin, which is a non-heme iron storage protein that is found in all kingdoms of life [162]. Ferritin consists of 24 α-helical subunits which form a spherical, hollow shell that can store up to 4500 iron molecules (**Figure 1.8**) [163, 164, 162]. The iron storage process starts with the entry of soluble, ferrous iron (Fe^{2+}) ions via 8 hydrophilic channels (0.2–0.5 nm) that are present on the 3-fold axis of the protein shell [164, 162, 165, 166]. Ferroxidation takes place by the oxidation of ferritin bound Fe^{2+} by O_2 to form oxo-bridged iron intermediates, which later form ferric (Fe^{3+}) iron ions. The Fe^{3+} ions then migrate to the hollow core of the protein and are stored in the form of ferrihydrite crystals. The mechanism of iron release from ferritin is not fully understood, however, strong chelators of Fe^{3+} and reducing agents are known to extract iron from the hydrophilic channels with varying rates, where the process is slow for strong

chelators. Under physiological conditions, the iron recycling process is thought to be achieved via the lysosomal degradation of ferritin.

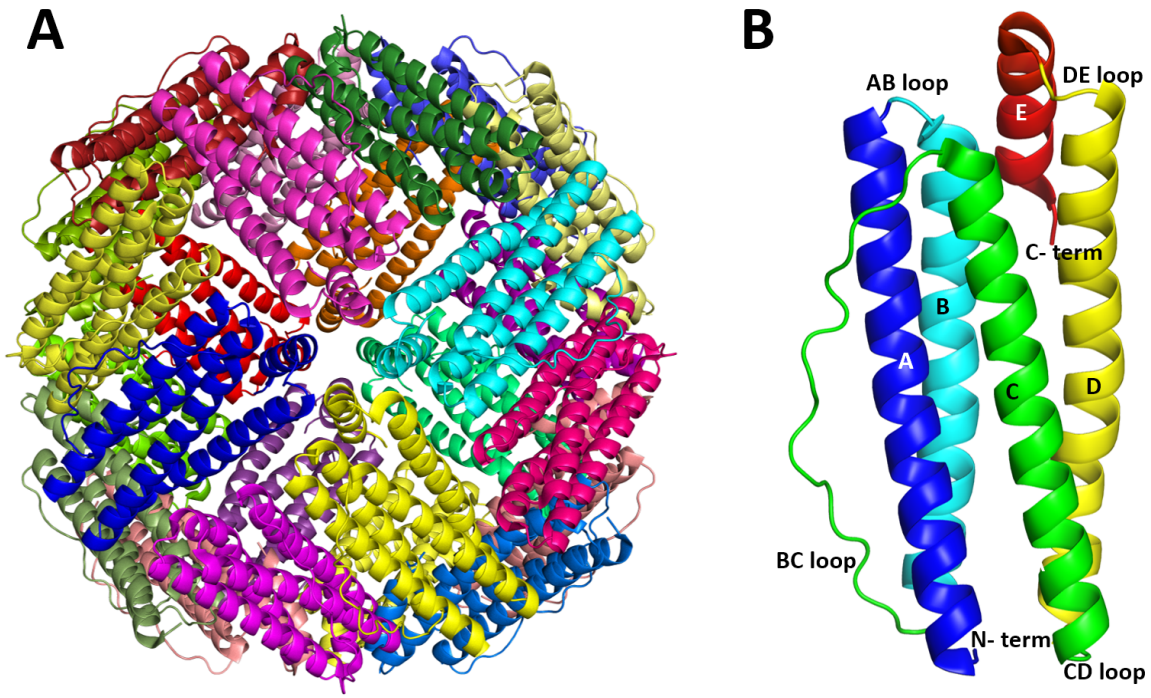

Figure 1.8. Non-heme ferritin from *E. coli* (EcftnA).

(A) 3D structure of EcftnA (PDB ID: 1EUM). **(B)** Cartoon representation depicting a single EcftnA subunit. Each EcftnA subunit consists of two sets of antiparallel α-helices (AB and CD) and a short C-terminal E helix. Each helix is connected either via short (AB, CD, and DE) or long (BC) loops [167].

Across the kingdoms of life, different types of ferritins exist, yet all ferritins possess a ferroxidase center which is present in the central region of ferritin subunits [164, 162]. For instance, animal ferritins are generally heteropolymers, consisting of two subunit types (heavy and light chain, H- and L-chain respectively), where the H-chain possesses the ferroxidase activity and the L-chain facilitates mineralization [162]. In mammals, the H- and L-chains assemble in varying ratios depending on tissue type. For example, heart and brain tissues have H-chain rich ferritins that possess higher ferroxidase activity, whereas spleen and liver contain L-chain rich ferritins that incorporate more iron and are more stable [165]. Interestingly, mitochondrial ferritin (FtMt) is also present in mammals, where FtMt is translocated to the organelle to assume its functional form by forming a homopolymer at this site and is involved in protection against oxidative stress in certain cell types. Plant ferritins are also heteropolymers, however, both subunits are of the H-chain type [168]. In contrast, bacterial and archaeal ferritins are homopolymers,

where the 24meric protein is of H-chain type, despite displaying low sequence identity when compared to H-chain ferritins of eukaryotes.

The main role of ferritins in nature is to protect the cell from oxidative damage in addition to acting as an iron storage unit, however, additional functions such as regulation of translation, microtubule binding, and chemokine receptor signaling have been attributed to ferritins [162, 168, 164, 165]. The products of aerobic metabolism such as superoxide and hydrogen peroxide form highly reactive and toxic hydroxyl radicals upon interaction with free Fe^{2+} ions under oxidizing conditions, therefore the regulation of intracellular iron levels is extremely important for cell vitality. *E. coli* expresses two ferritins, *ftnA* and *ftnB*, where the product of the former gene (FtnA) is the main constituent for iron storage and responsible for up to 50% of the iron found within the cells, and the latter encodes a ferritin-like protein, which has atypical residues at its ferroxidase center with a less clear role in iron storage [169, 170]. FtnB might have a major role in iron-sulfur cluster synthesis in *E. coli*, and it was shown to be involved in iron-sulfur cluster repair in *Salmonella enterica* sv. Typhimurium [171, 172].

In addition to ferritins, other iron binding proteins exist in bacteria, such as bacterioferritin (Bfr), which possesses 24 subunits similar to ferritin. Unlike ferritin however, Bfr contains up to 12 heme groups, which are generally of protoporphyrin IX form. Exceptions to typical Bfr are those of *Desulfovibrio desulfuricans* and *Pseudomonas aeruginosa*, where the former organism has a novel heme, and the latter possesses a unique Bfr which is a heteropolymer composed of one Ftn and one Bfr subunit [164, 173]. Another type of iron storage protein found in bacteria is mini-ferritin (Dps), which is a homo 12mer induced in the stationary phase of cell growth [164, 162]. Dps from *E. coli* has a higher affinity towards H_2O_2 compared to O_2, indicating that this protein is employed in protection against DNA damage due to redox oxidative stress. Dps proteins can store approximately 500 iron atoms per Dps molecule, and hence possess a much smaller capacity for iron storage as compared to ferritin.

Ferritins possess a number of interesting physicochemical properties, facilitating their application in biotechnology, life sciences, and biomedicine. For instance, iron-loaded ferritin can be used as a contrast agent in magnetic resonance imaging (MRI), or ferritin cages can be used as a nanoreactor for the production of quantum dots, which are fluorescent semiconductor nanocrystals typically comprised of group IIB-VIA or IIA-VA atoms such as CdS, ZnSe, and GaAs, with applications ranging from solar cells, LEDs and DNA hybridization to biosensors [162, 174]. Quantum dots can also be rendered biocompatible via encapsulation by the ferritin cages, which prevents the leakage of toxic

ions, and the approach additionally offers high thermostability and metal ion scavenging abilities to the entrapped nanocrystals. The encapsulation ability and the described benefits are bestowed by the unique properties of the ferritin cage, which possesses a well-defined and highly stable structure at physiological pH, capable of self-assembly following disassembly at highly acidic or alkaline conditions. Therefore, ferritin cages can also be used for the entrapment of drugs such as cisplatin within the ferritin cavity, allowing the protein to be used as a cancer drug delivery platform. Moreover, the outer shell of ferritin can be modified to allow its use as a multivalent scaffold or to yield desired properties, i.e. by incorporation of long alkyl chains to yield fully hydrophobic nanoparticles that are completely soluble in organic solvents [162, 175]. Furthermore, ferritin is capable of mineralizing compounds other than iron, such as phosphate, manganese, cadmium sulfide, cobalt, nickel, silver, palladium, and zinc selenide, and was utilized for bioremediatation to remove phosphate from seawater and industrial waste [162, 166]. Similar to semiconductor synthesis described for the quantum dots, ferritin can also be used to produce carbon nanotubes, silicon-based nanodisks, and various hybrid materials such as gold nanoclusters [176], as its inner cavity is capable of mineralizing different compounds also serves as an ideal, spatially restricted reaction chamber for the synthesis of such nanomaterials [177, 166, 162, 174]. The ferritin cage has been used in vaccine development as well, where hemagglutinin from the influenza virus was fused to the ferritin cage, followed by immunization in mice [178].

Recently, proof-of-concept demonstrations for enzyme immobilization using ferritin started to emerge as well. For instance, a ferritin from the archaeon *Archaeoglobus fulgidus* was used to encapsulate GFP together with several enzymes that were fused to GFP [179]. This was achieved by exploiting the uniquely large cavities of this archaeal ferritin, as well as its ability to reversibly disassemble at neutral pH, which allowed the positively supercharged GFP to be encapsulated within the ferritin cage upon mixing crude cell extracts containing ferritin with protein fusions. Along the same lines, a β-glucosidase variant was displayed onto ferritin cages by the K-coil/E-coil approach, where the individual E- and K- coils, rich in lysine and glutamic acid residues that can form heterooligomeric coiled-coils, were fused to the target enzyme and ferritin, respectively [180]. This was achieved *ex vivo* in multiple steps, where the E-coil tagged ferritin was precipitated by ammonium sulfate and purified via size exclusion chromatography, followed by iron loading, density gradient purification of iron-loaded ferritin, binding of ferritin to nickel-nitrilotriacetic acid (Ni-NTA) column and incubation with K-coil tagged β-glucosidase to link the proteins together, which were finally eluted from the column.

The immobilization strategy developed as part of this PhD thesis is based on generating gene fusions that encode the iron storage protein ferritin, and a YFP variant citrine from *Aequorea victoria* [181, 182], which was shown to form fluorescent protein aggregates when overexpressed in *E. coli* cells. These ferritin-based aggregates are released from the cells upon lysis and can be obtained from the crude cell extract via centrifugation as they are predominantly present in the insoluble fraction, similar to Cat-IBs (**Section 1.2.2.2**). Despite the superparamagnetism of iron-loaded ferritin [183], the magnetic properties of such citrine-ferritin fusions have not been described in the literature. Therefore, the possibility of producing magnetic protein aggregates (MPAs) using a solely *in vivo*-based approach was investigated within this thesis. To this end, various citrine-ferritin fusions have been investigated and their potential for immobilization was explored via post-translational attachment to a target enzyme (**Section 2.3**).

1.3. Aim and Scope of the Thesis

Enzyme immobilization serves a vital function for the use of biocatalysts in biotechnology. Studies directed towards improving the shortcomings of available methods, as well as the development of new immobilization techniques, are very important steps for fostering the acceptance and application of enzymes in synthetic chemistry and biotechnology. Therefore, the here presented PhD thesis expands the current knowledge on catalytically-active inclusion bodies (CatIBs) by comprehensive characterization of CatIBs generated by natural and artificial tags, as well as linker iterations, and further investigates their applicability for biocatalysis via flow chemistry. In addition, this work describes the development of a novel method for the generation of fully biologically produced, magnetic protein aggregates (MPAs) as a new *in vivo* immobilization technique.

The aims of this PhD thesis are therefore:

I. Characterization and benchmarking CatIBs of industrially relevant enzymes and challenging targets with regard to important process parameters, such as residual activity, yield, and purity, as well as the first evaluation of CatIBs in flow chemistry (**Section 2.1**).

II. Exploration of the role of intra-domain linkers with regard to important CatIB properties, and properties of CatIBs generated by various linker combinations from a pragmatic standpoint (**Section 2.2**).

III. Development of a new *in vivo* immobilization method to generate purer, easier-to-purify immobilizates by producing self-immobilizing proteins that exhibit magnetism (MPAs), as well as proof-of-concept application of the method for the immobilization of enzymes (**Section 2.3**).

IV. Offering a collection of know-how on strategies to generate CatIBs by assessing parameters deemed important for CatIB generation, as well as summarizing the current knowledge in the field (**Section 2.4**).

V. Putting the ever-expanding toolbox of *in vivo* immobilization methods into a broader perspective by providing a comprehensive literature review of the existing methods, where each method is assessed critically and comparatively (**Section 2.5**).

VI. Sharing the technical knowledge related to wet lab methods necessary to generate CatIBs from construct design principles to characterization methods including activity analyses, by providing a step-by-step laboratory manual (**Section 2.6**).

VII. Providing an up-to-date review on *in vivo* immobilization methods from the perspective of flow chemistry (**Section 2.7**).

2. Results

2.1. Publication 1. Catalytically-Active Inclusion Bodies - Benchmarking and Application in Flow Chemistry

Gizem Ölçücü, Benedikt Baumer, Kira Küsters, Kathrin Möllenhoff, Marco Oldiges, Jörg Pietruszka, Karl-Erich Jaeger, and Ulrich Krauss*

*corresponding author

ACS Synthetic Biology 11 (2022), pp. 1881-1896.

https://pubs.acs.org/doi/10.1021/acssynbio.2c00035

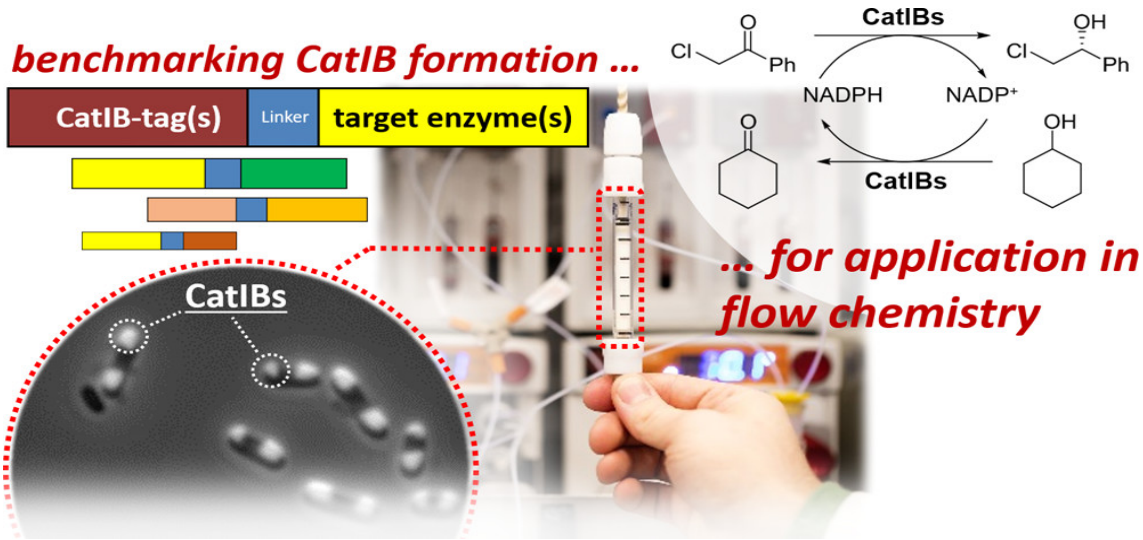

Author Contributions: U.K., K.-E.J., and J.P. conceived and designed the study. G.O., supervised by U.K., generated all constructs, prepared CatIBs, and performed activity/fluorescence assays for CatIB benchmarking and all other experiments unless mentioned otherwise. B.B., supervised by J.P., performed the flow synthesis experiments, and K.K. and M.O. conceived and performed the automated microscopy analyses. K.M. performed all statistical analyses. The manuscript was written through contributions of all authors. All authors have given approval to the final version of the manuscript.

ACS SyntheticBiology

pubs.acs.org/synthbio

Research Article

Catalytically Active Inclusion Bodies—Benchmarking and Application in Flow Chemistry

Gizem Ölçücü, Benedikt Baumer, Kira Küsters, Kathrin Möllenhoff, Marco Oldiges, Jörg Pietruszka, Karl-Erich Jaeger, and Ulrich Krauss*

Cite This: *ACS Synth. Biol.* 2022, 11, 1881−1896

Read Online

ACCESS | Metrics & More | Article Recommendations | Supporting Information

ABSTRACT: In industries, enzymes are often immobilized to obtain stable preparations that can be utilized in batch and flow processes. In contrast to traditional immobilization methods that rely on carrier binding, various immobilization strategies have been recently presented that enable the simultaneous production and in vivo immobilization of enzymes. Catalytically active inclusion bodies (CatIBs) are a promising example for such in vivo enzyme immobilizates. CatIB formation is commonly induced by fusion of aggregation-inducing tags, and numerous tags, ranging from small synthetic peptides to protein domains or whole proteins, have been successfully used. However, since these systems have been characterized by different groups employing different methods, a direct comparison remains difficult, which prompted us to benchmark different CatIB-formation-inducing tags and fusion strategies. Our study highlights that important CatIB properties like yield, activity, and stability are strongly influenced by tag selection and fusion strategy. Optimization enabled us to obtain alcohol dehydrogenase CatIBs with superior activity and stability, which were subsequently applied for the first time in a flow synthesis approach. Our study highlights the potential of CatIB-based immobilizates, while at the same time demonstrating the robust use of CatIBs in flow chemistry.

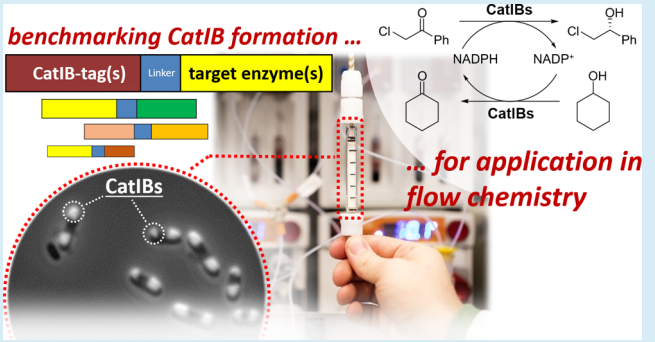

KEYWORDS: *inclusion bodies, enzyme immobilization, biocatalysis, protein engineering, flow chemistry*

Immobilization fulfills a key role in realizing the full potential of enzymes for industrial applications. As green catalysts with a broad application potential, the superior performance parameters ascribed to enzymes, such as efficiency, high selectivity, and catalytic activity,[1,2] are often overshadowed by their limitation to operate under mild conditions and the high costs associated with their use.[3] Therefore, generating enzyme immobilizates that can be effectively recycled and reused, which display improved stability and increased tolerance toward harsh process conditions, is an important step toward sustainable bioprocesses. In recent years, immobilized enzymes have become attractive catalysts for use in flow chemistry.[4,5] Flow chemistry involves a chemical reaction run in a continuous flow stream, often using immobilized catalysts in a packed-bed column or plug flow reactor. Reactive components are mixed in a mixing device and then pumped through the reactor containing the catalyst. This mode of operation provides major advantages such as faster reactions, cleaner products, safer reactions, and easy scale-up.[6] Considering that packed-bed reactors are often used as reactors in flow chemistry applications, enzymes must withstand these conditions and retain high volumetric activities and operational stability.[7−9] Recently, immobilization of target enzymes by covalent linkage to Spy or Halo tags has proven useful for flow chemical applications;[10−15] however, covalent immobilization strategies often suffer from a loss of activity, greatly affecting the overall enzymatic performance.

Generally, improved performance of the immobilized biocatalyst results from the confinement of the enzyme molecules within or at the surface of a support or carrier material. Among the different methods developed for enzyme immobilization,[10−12] recently developed in vivo immobilization strategies (summarized in refs 12−14), relying on modular construction principles harnessed in synthetic biology, are particularly attractive as they often combine enzyme overproduction and immobilization in one step, thereby reducing costs and labor. These methods include the entrapment of target proteins in *Bacillus thuringiensis* Cry3Aa protein crystals, virus-like particles, polyhydroxyalkanoate granules, forizymes,

Received: January 21, 2022
Published: May 2, 2022

protein condensates generated by liquid−liquid phase separation, or catalytically active inclusion bodies (CatIBs).[13] Among these strategies, the generation of catalytically active inclusion bodies (CatIBs), also called active inclusion bodies,[15−20] has been developed as a facile method for producing enzyme immobilizates without the need of chromatographic purification or time-consuming immobilization steps. In contrast to the conventional view of inclusion bodies (IBs) as unfolded and hence inactive waste material accumulating due to strong overexpression of heterologous genes, for example, in *Escherichia coli*, some naturally occurring proteins that accumulate as IBs as well as artificially generated CatIBs have been shown to retain a variable degree of (catalytic) activity.[21,22] Successfully applied to numerous proteins and enzymes to date, the CatIB strategy is based on the use of coiled-coil domains,[21,23−26] aggregation-prone domains/proteins,[27−31] or synthetic peptides[26,32−34] as "pull-down" tags, where the genes or gene fragments encoding such tags are fused to either the 5′ or 3′ end of the gene encoding the target enzyme. Overexpression of such a gene fusion in a suitable bacterial host under the right CatIB-formation-inducing conditions[20] allows the sequestration of the natively folded target fusion protein within CatIBs, with the supporting matrix or carrier being formed by the un- or misfolded fraction of the overproduced fusion protein. CatIBs, like IBs, are composed of 80−95% of the heterologous expressed protein[35] and can be obtained easily after cell lysis with centrifugation, allowing for easy and cost-efficient preparation. Numerous reports of successful immobilization via the CatIB approach using a number of CatIB-inducing tags and target proteins have been described; however, a rational prediction of best suited tags or fusion sites for CatIB formation is still not possible. Most studies reported in the literature generate CatIBs via fusing the CatIB-inducing tag to a target protein from a single terminus. The activities reported for CatIBs usually compare the insoluble (CatIB) fraction solely to the crude cell extract (CCE), but not to the purified soluble protein[30−34,36,37] which can lead to an overestimation of the activity of the enzyme immobilizate due to the overestimation of the protein concentration of the soluble reference protein in the CCE. Contrarily, a high degree of misfolded target protein within CatIBs might result in an underestimation of the CatIB activity. Additionally, a quantitative assessment of CatIB residual activities (specific activity of lyophilized CatIBs relative to the specific activity of the corresponding soluble purified enzyme) and stabilities has only rarely been reported.[23,24,38,39] Such data would be useful to estimate the effectiveness of CatIB formation and application, especially when the high cost associated with the production and use of enzymes is considered.[40]

In summary, a comprehensive benchmarking study, where different CatIB-formation-inducing tags and fusion strategies are compared with regard to key performance parameters is lacking at present. To address this issue, we here performed a benchmarking study of a number of widely employed CatIB-formation-inducing tags. The key performance parameters studied here were as follows:

(i) CatIB-formation efficiency, defined as the amount of activity/fluorescence of the washed CatIB-containing pellet fractions relative to the activity/fluorescence of the crude cell extract obtained by cell lysis.

(ii) Residual activity and stability of the lyophilized CatIB immobilizate relative to the corresponding soluble purified enzyme. These parameters should ideally be determined from initial rate velocities of the CatIBs expressed as specific activity (U/mg protein) or turnover number (k_{cat} s^{-1})[25] to allow for a fair comparison. Note that CatIB immobilizates, albeit being relatively pure, can contain other proteinaceous impurities,[41] which likely results in an underestimation of their residual activities.

(iii) Biomass specific activity yields, calculated by multiplying the specific activity of CatIBs (in U/mg CatIBs) by the yields (in mg CatIBs/g wet cells), can therefore be defined as the "catalytic activity per gram wet cells". This parameter allows for the quantitative comparison of different CatIBs considering their specific activity and production yields and taking different expression levels and different degrees of stability into consideration.

Using these parameters, CatIB formation was assessed for 24 constructs bearing short, self-assembling artificial peptide tags 18AWT,[33] L6KD,[32] GFIL8,[34] or the coiled-coil domain TdoT[42] from *Staphylothermus marinus*. To broadly evaluate the potential of the different tags for CatIB formation, a set of three different target proteins and enzymes of variable complexity were used as targets.

The presented comprehensive analyses allowed the determination of the most versatile CatIB-inducing element(s), while at the same time providing further insights into CatIB formation. To demonstrate application, CatIBs were utilized in a flow chemistry approach for the conversion of ketones to the corresponding alcohols using cyclohexanone and *ω*-chloroacetophenone as model substrates. Our study highlights the potential of CatIB-based immobilizates, which combine high activities and stabilities with ease of preparation and hence low cost, while at the same time demonstrating robust use of CatIBs in flow chemistry for the first time.

RESULTS AND DISCUSSION

Fusion Strategy, Tag, and Target Selection. Among the more widely used tags for inducing CatIB formation,[21,23−26,32−34,36,43−45] we chose 18AWT, L6KD, GFIL8, and TdoT, which were genetically fused to the 5′ or 3′ end of the genes encoding red fluorescent protein mCherry[46] from *Discosoma striata*, alcohol dehydrogenase[47] from *Ralstonia* sp. (RADH), and lipase A[48] from *Bacillus subtilis* (BsLA) as target proteins, thereby generating fusion proteins with either N- or C-terminally fused tag (Figure 1). This fusion strategy, relying on modular construction principles, allows the facile exchange of the genes encoding the CatIB-inducing tag together with the linker, along with the target proteins, by including restriction endonuclease recognition sites between these elements.

The three synthetic peptide tags (18AWT, L6KD, GFIL8) were selected primarily based on their small size (0.9−2.3 kDa, 8−18 residues), which is expected to reduce the impact of the tag on proper folding and hence the activity of the target within CatIBs. In addition, high CatIB-formation efficiencies were reported previously for all of the selected synthetic peptide tags.[32−34] Due to these reasons, we excluded larger proteins and protein domains such as cellulose binding domains[28] or the foot-and-mouth disease virus (FMDV) capsid protein VP1[30] from our benchmarking study. The TdoT tag (5.7 kDa, 53 residues) was selected as, previously widely employed, reference construct.[21,23−26,45]

The fluorescent reporter protein mCherry[46] and industrially relevant lipase BsLA[48] were selected for immobilization due to

https://doi.org/10.1021/acssynbio.2c00035
ACS Synth. Biol. 2022, 11, 1881−1896

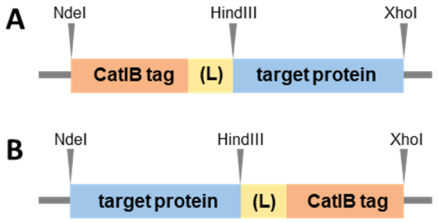

Figure 1. Schematic illustration of the fusion strategy for the constructs generated in this study. The strategy allows the exchange of the genes encoding CatIB-inducing tag together with its linker (if present), and the target protein using the depicted restriction endonucleases. CatIB tag refers to synthetic peptide tags 18AWT, L6KD, GFIL8, or the coiled-coil protein domain TdoT. For TdoT constructs containing a linker, (L) refers to the flexible $(GGGS)_3$ linker. For mCherry-TdoT construct that lacks a linker polypeptide, the target gene and the tag are separated by lysine−leucine, encoded by the *Hin*dIII site. For 18AWT-, L6KD-, or GFIL8-bearing constructs, (L) refers to the linker polypeptide with the amino acid sequence PTPPTTPTPPTTPTPTP, abbreviated as (PT) in text. (A) Illustration of the N-terminal CatIB-inducing tag harboring constructs. (B) Illustration of the C-terminal CatIB-inducing tag harboring constructs. All constructs generated and used in this study are listed in Table S1.

being rather small monomeric targets, in addition to their earlier use in studies generating CatIBs[21,23,25,32−34] to provide a better basis for comparison. The tetrameric alcohol dehydrogenase RADH was selected as a more complex target based on earlier success in generating RADH CatIBs using the much larger TdoT and 3HAMP tags,[21,25] to investigate the capabilities of CatIB-inducing elements as small as eight residues to immobilize a rather large and complex multimeric enzyme.[47] The selection for the target proteins was additionally aimed toward improving the low residual activities reported for TdoT CatIBs (2% for RADH as target enzyme),[25] low CatIB formation efficiency for mCherry (4−32% depending on the linker)[21] and moderate stabilities[44] previously reported for CatIBs of these targets. Note that, mCherry, BsLA and RADH control constructs that lacked a fused aggregation tag were previously shown to be produced predominately in soluble form, and fusion of TdoT as a CatIB-tag promoted production of the corresponding fusion proteins as CatIBs.[23,25,44]

Short, Synthetic Peptides Enable Efficient CatIB Formation. The primary factor that determines the success of a CatIB-based immobilization strategy is the ability of a given tag to induce CatIB formation. CatIB/IB formation can easily be observed by microscopy, where CatIBs/IBs are detected as refractile particles accumulating at the cell poles during heterologous overexpression of the fusion protein.[41,49] The use of fluorescent reporters as target hereby aids in determining proper folding of the fusion protein within the CatIB particles, providing the first hint toward CatIB-formation success. Therefore, to qualitatively assess the success of CatIB formation, microscopic analyses were conducted with *E. coli* BL21(DE3) strains overproducing target protein fusions consisting of mCherry, BsLA and RADH, tagged either N- or C-terminally with the synthetic, CatIB-formation-inducing peptides 18AWT, L6KD and GFIL8. As reference constructs, all targets were fused N-terminally with the coiled-coil domain TdoT[42] from *S. marinus*, which was previously shown to induce CatIB formation for the three targets.[21,23,25] Constructs with the TdoT tag at the C-terminus were also generated and included in the analysis. To provide a better one-on-one comparison, the newly generated C-terminal TdoT-bearing RADH and BsLA constructs harbored a flexible $(GGGS)_3$ linker, whereas mCherry-TdoT construct did not contain a linker, similar to their N-terminal TdoT-bearing counterparts previously studied.[21,23,25] Likewise, all N- and C-terminal 18AWT, L6KD, and GFIL8 harboring constructs contained a PT linker for consistency with previous studies[32−34] (see Table S1 for an overview of all constructs).

For rapid screening purposes, we employed automated microscopy,[50] on live cells overproducing the different fusion constructs. All TdoT reference strains showed sustained IB/CatIB formation (Figure 2A−C, rightmost panels), in agreement with the literature.[21,23,25] This clearly proves the applicability of the automated microscopy method for rapid detection of IB/CatIB formation. The strains overproducing mCherry fusion constructs with N-terminally fused 18AWT, L6KD, and GFIL8 tags yielded fluorescent inclusion bodies (Figure 2A). In contrast, the corresponding strains producing the C-terminally tagged mCherry fusions (with the exception of the mCherry-18AWT producing strain) displayed a uniform fluorescence throughout the cells (Figure 2D), indicative of a lack of IB/CatIB formation. For the mCherry-18AWT producing strain, the majority of the cells (64%) displayed uniform fluorescence similar to the remaining C-terminally tagged mCherry constructs, but inclusion bodies could be detected in the remaining 36% of the cells that were analyzed (Figure 2D, leftmost panel, additional images in Figure S1). Strains producing BsLA and RADH fusions revealed the successful generation of IBs/CatIBs for all constructs bearing either of the three short synthetic tags, independent of the fusion terminus (Figure 2B,C,E,F), with the RADH fusion constructs with N- and C- terminally fused L6KD tag, and with the N-terminal GFIL8 tag showing especially prominent IBs/CatIBs.

Next, CatIB-formation efficiencies[13,20] were determined to obtain quantitative insight into CatIB formation. For this, all CatIB-producing strains were cultivated under identical conditions, cells lysed and the resulting crude cell extract (CCE) fractionated to obtain soluble and insoluble protein fractions. The latter were further washed with lysis buffer (50 mM sodium phosphate buffer, 100 mM NaCl, pH 8.0) to obtain the final CatIB-containing pellets. CatIB-formation efficiencies are hereby defined as the amount of activity/fluorescence of the washed pellet fractions (P2) relative to the activity/fluorescence of their crude cell extracts (CCEs; set to 100%) after cell lysis. The corresponding values are shown in Figure 3. Note that the same data for the washed pellet fraction (P2) along with the corresponding data for of all other fractions can be found in Figure S2 and numerical values for CatIB formation efficiencies are further listed in Table S2.

Irrespective of the fusion site or the employed tag, all mCherry constructs except for the internal control (TdoT-mCherry) displayed lower CatIB formation efficiencies compared to BsLA and RADH constructs (Figure 3A). The TdoT-mCherry construct, displayed the highest CatIB formation efficiency (22%), which was significantly higher than the remaining mCherry constructs ($p < 0.0001$). The values observed here for the N-terminal 18AWT/L6KD/GFIL8 tagged mCherry fusions are in contrast to clear CatIB/IB formation as observed microscopically for all of these constructs (Figure 2A). This might in part be explained by the low stability of the corresponding CatIBs, which readily become solubilized during washing steps and/or low expression yields

https://doi.org/10.1021/acssynbio.2c00035
ACS Synth. Biol. 2022, 11, 1881−1896

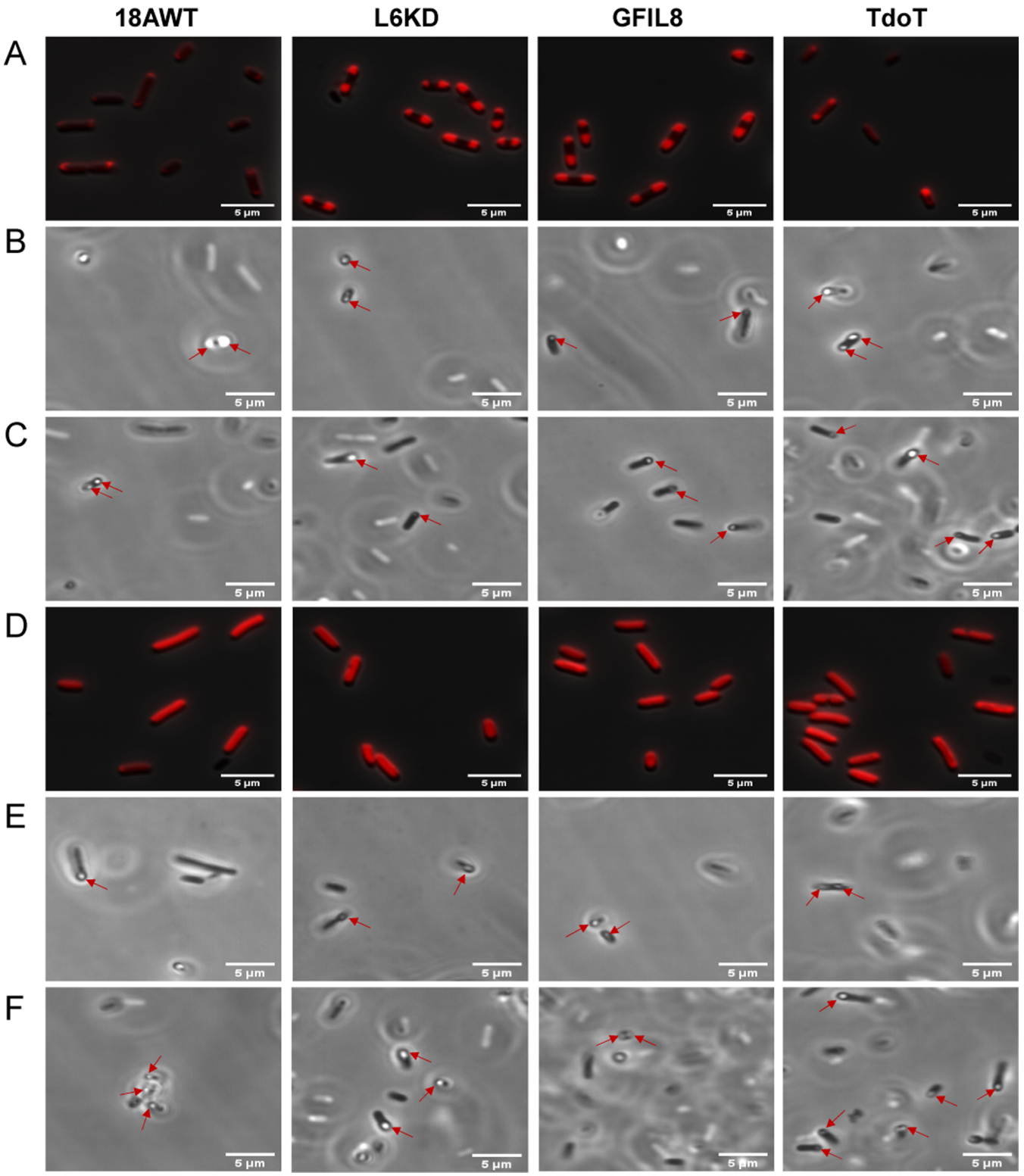

Figure 2. Microscopy analyses for the rapid identification of CatIB/IB formation. Microscopic images of *E. coli* BL21(DE3) cells overproducing target protein-tag fusions, with either N-terminal (A−C) or C-terminal (D−F) CatIB-inducing tags. All cultivations were performed as described in the Methods section. CatIBs in the phase contrast images (B, C, E, F) are marked with red arrows. (A) N-terminal tag-bearing mCherry strains. From left to right: 18AWT-PT-mCherry, L6KD-PT-mCherry, GFIL8-PT-mCherry, and TdoT-mCherry. (B) N-terminal tag-bearing BsLA strains. Left to right: 18AWT-PT-BsLA, L6KD-PT-BsLA, GFIL8-PT-BsLA, and TdoT-L-BsLA. (C) N-terminal tag-bearing RADH strains. Left to right: 18AWT-PT-RADH, L6KD-PT-RADH, GFIL8-PT-RADH, and TdoT-L-RADH. (D) C-terminal tag harboring mCherry strains. From left to right: mCherry-PT-18AWT, mCherry-PT-L6KD, mCherry-PT-GFIL8, and mCherry-TdoT. (E) C-terminal tag harboring BsLA strains. From left to right: BsLA-PT-18AWT, BsLA-PT-L6KD, BsLA-PT-GFIL8, and BsLA-L-TdoT. (F) C-terminal tag harboring RADH strains. From left to right: RADH-PT-18AWT, RADH-PT-L6KD, RADH-PT-GFIL8, and RADH-L-TdoT.

https://doi.org/10.1021/acssynbio.2c00035
ACS Synth. Biol. 2022, 11, 1881−1896

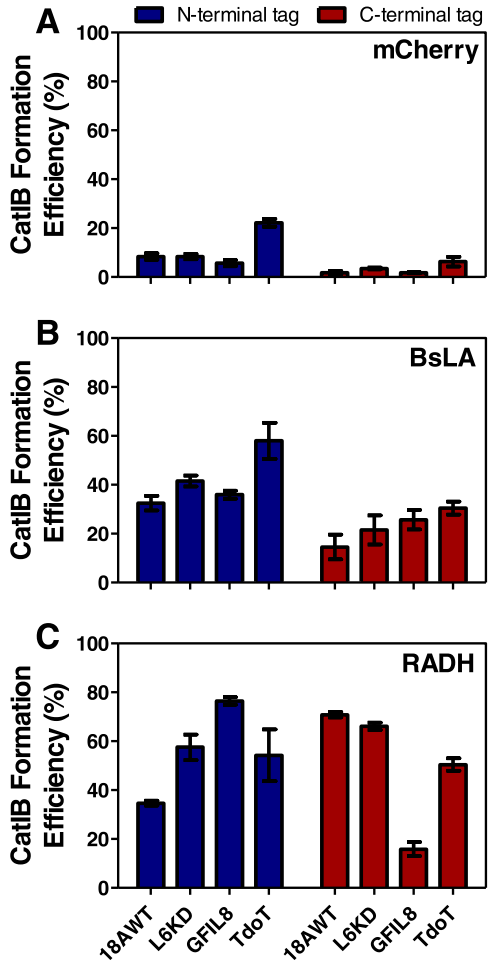

Figure 3. Quantitative assessment of CatIB formation. CatIB-formation efficiencies of mCherry (A), BsLA (B), and RADH (C) constructs harboring either N-terminal (blue) or C-terminal (red) CatIB-formation-inducing tags 18AWT, L6KD, GFIL8, and TdoT. CatIB formation efficiencies correspond to the activity (or for mCherry, fluorescence) detected in the washed pellet fractions in comparison to the activity/fluorescence of the crude cell extracts (set to 100%) for the individual constructs. BsLA activity was determined via initial rate activity assay by photometrically detecting the formation of *p*-nitrophenolate (*p*-NP) formed by hydrolysis of *p*-nitrophenyl butyrate (*p*-NPB) as substrate. RADH activity was determined using a discontinuous assay by photometrically monitoring the consumption of the cofactor reduced nicotinamide adenine dinucleotide phosphate (NADPH) at six time points as the enzyme catalyzes the conversion of cyclohexanone to cyclohexanol. Error bars represent the standard error of the mean derived from at least three biological replicates.

for some of the constructs, as evidenced by sodium dodecyl sulfate-polyacrylamide gel electrophoresis (SDS-PAGE) analyses (Figure S3), showing either moderate expression (for 18AWT), an mCherry band in the wash fraction (for L6KD), or a thinner mCherry band in the washed pellet fraction compared to unwashed pellet fraction (for GFIL8). For highly soluble and therefore difficult to immobilize protein targets such as mCherry,[21] this suggests that the shorter synthetic peptide tags are less efficient in pulling them down compared to larger tags such as TdoT. It should also be noted that, for TdoT-mCherry, earlier studies reported an improvement of CatIB formation efficiency upon the deletion of the linker region,[21] and since all 18AWT, L6KD or GFIL8 constructs generated in this study included a PT linker, deletion of the linker could likewise aid in improving the low CatIB formation efficiencies for these constructs. Indeed, the importance of the intradomain linkers on CatIB formation and the properties of CatIBs were shown in recent studies.[26] While not being within the scope of this benchmarking study, investigation of such an approach to improve CatIB-formation efficiencies for highly soluble constructs could prove to be a worthwhile effort in the future.

For BsLA, on average N-terminal fusion of the different tags resulted in higher CatIB-formation efficiencies (p = 0.0007) compared to C-terminal fusions (Figure 3B). Fusion of the TdoT tag to the N-terminus of BsLA yielded significantly higher CatIB-formation efficiency (58%; in line with previous observations that reported a high CatIB-formation efficiency for this construct[23]) compared to the remaining BsLA constructs (p = 0.0001; N-terminal L6KD-BsLA fusion). High CatIB formation efficiency observed for TdoT-BsLA was followed by constructs with N-terminally fused L6KD (42%), GFIL8 (36%), and 18AWT (33%) tags. The TdoT-tagged construct similarly yielded the highest CatIB formation efficiency among the C-terminally tagged fusions (30%). However, differences between the C-terminal BsLA fusions did not reach statistical significance. It should be noted here, that higher CatIB-formation efficiencies have previously been reported for identically constructed BsLA fusion constructs.[32−34] Differences in cultivation and expression conditions, handling of the resulting immobilizates, and the parameters governing the activity assays, likely account for the variance observed here. Indeed, the growth medium, temperature during cultivation and expression, the strength and manner of induction, method of cell lysis, and the preparation procedure of CatIBs are known to have a profound impact on the activity profile and stability.[20,27,51−53] As, analyzing all constructs under identical conditions and therefore using the methodology previously established for the TdoT-harboring reference constructs[21,25] was imperative for our benchmarking purposes, an additional adaptation of the above-mentioned parameters was not performed.

The strains overproducing RADH fusions (Figure 3C) showed significantly higher CatIB-formation efficiencies than all other constructs (p < 0.0001). The construct bearing an N-terminal GFIL8 tag yielded the highest CatIB-formation efficiency (76%), which was followed by the C-terminal 18AWT (71%), C-terminal L6KD (66%) and N-terminal L6KD constructs (58%), whereas no statistically significant difference was found between these constructs. However, the N-terminal GFIL8-RADH fusion performed significantly better than all of the remaining RADH constructs (highest p = 0.049; N-terminal TdoT-RADH fusion with 54% CatIB formation efficiency). Moreover, despite yielding the highest CatIB formation efficiency when fused N-terminally, the presence of the GFIL8 tag at the C-terminus resulted in a CatIB-formation efficiency of only 16%, with the difference being highly statistically significant (p < 0.0001). Therefore, the same tag can yield very different results when fused to the opposite termini, highlighting the necessity of testing different fusion sites for improving the success of immobilization. In addition to CatIB formation efficiency and SDS-PAGE analyses (Figure S3), a purity assessment was performed for all constructs (Table S3), where the two of the best RADH CatIBs highlighted above (N-terminal GFIL8 and C-terminal 18AWT tagged constructs) were of high purity (above 56%; see the Methods section for details). In conclusion, the small synthetic peptides 18AWT, L6KD, and GFIL8 are sufficient to

https://doi.org/10.1021/acssynbio.2c00035
ACS Synth. Biol. 2022, 11, 1881−1896

effectively induce CatIB formation for all target proteins tested here, when present at the optimal terminus. Thus, the employed tag as well as the fusion terminus should always be varied when designing constructs for CatIB-formation.

Short Synthetic Tags and Selection of the Proper Fusion Terminus Enables the Production of CatIBs with High Residual Activity. To allow comparative analyses and easy storage of all CatIBs, we prepared sufficient quantities in lyophilized form as described previously.[21] This mode of preparation at the same time provides CatIBs in a formulation suitable for long-term storage, e.g., for use in industry. We next determined the residual enzyme activity of the BsLA and RADH CatIBs, defined as the specific activity of lyophilized CatIBs relative to the specific activity of the corresponding soluble, purified enzyme (set to 100%) (Figure 4). For CatIBs,

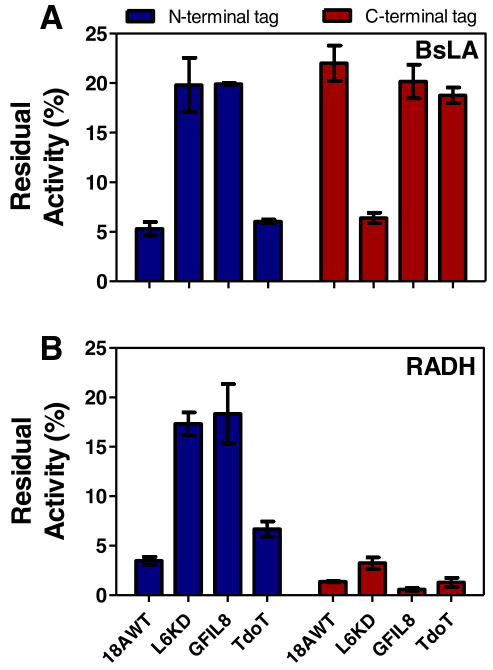

Figure 4. CatIB-activity assessment. Residual activities of BsLA (A) and RADH (B) CatIBs after lyophilization, compared to the activity of soluble, purified BsLA and RADH, which were set to 100%. N-terminal 18AWT-, L6KD-, GFIL8-, and TdoT-bearing constructs are shown in blue, whereas C-terminally tagged constructs are shown in red. Error bars represent the standard error of the mean derived from at least three biological replicates for the constructs generated in this study. The numerical values used to generate the activity data depicted in this figure can be found in Table S2.

protein contents of the lyophilizates (given in Table S4, calculated using theoretical extinction coefficients in Table S5) were used to determine the specific activities that were then compared to their soluble, purified counterparts. Note that, due to technical difficulties in quantitatively comparing the fluorescence of soluble mCherry and turbid mCherry CatIB samples, we did not attempt to quantify the residual fluorescence of the mCherry CatIBs, but still carried out all other characterization steps such as SDS-PAGE analyses, yield and protein content determination (see below).

In general, BsLA CatIBs showed high residual activities, with the constructs bearing C-terminal 18AWT, GFIL8, and TdoT as well as N-terminal L6KD and GFIL8 tags showing at least 19% of the activity relative to the soluble, purified BsLA (Figure 4A). Moreover, these constructs all showed significantly higher residual activities than the remaining BsLA constructs (highest $p = 0.002$; C-terminal TdoT against C-terminal L6KD). GFIL8-BsLA CatIBs demonstrated superior residual activities independent of the fusion terminus, and performed essentially identical to the N-terminal L6KD construct (20% of soluble BsLA activity). The residual activity of the N-terminal TdoT-bearing "internal control" construct[23] was not determined in previous studies, but displayed only 6% of the activity of the purified enzyme in the study presented here, similar to constructs with C-terminal L6KD (6%) and N-terminal 18AWT (5%) tags. Fusion of the TdoT tag to the C-terminus of BsLA instead improved the residual activity by more than 3-fold ($p = 0.002$), reaching levels on par with the other best-performing CatIBs formed by fusion of the synthetic peptide tags. Taken together, and with the exception of C-terminal L6KD and N-terminal 18AWT harboring constructs, significantly higher residual activity (near 4-fold improvement) could be obtained for the BsLA fusion constructs bearing the small artificial peptide tags ($p < 0.001$) compared to the previously described control construct.

For RADH CatIBs (Figure 4B), constructs with the N-terminal tags displayed on average significantly higher residual activities compared to their C-terminally fused counterparts ($p < 0.001$). N-terminal GFIL8 and L6KD harboring RADH CatIBs showed the highest activities with 18 and 17% of the purified soluble RADH, respectively. This corresponds to an approximately 3-fold improvement in residual activity compared to the N-terminal TdoT reference construct (7% of the soluble RADH activity; GFIL8: $p = 0.013$ and L6KD: $p = 0.037$). In contrast, CatIBs generated by tag fusion to the C-terminus of RADH displayed low residual activities, corresponding to less than 4% of the soluble RADH activity (Figure 4B). Here, the C-terminal TdoT-bearing RADH construct was not an exception, displaying only 1% of the activity to that of the soluble, purified RADH. These results indicate that C-terminal tag fusions are not feasible for RADH, and the presence of an N-terminal L6KD or GFIL8 tag can boost the residual RADH activity significantly compared to the fusion of a coiled-coil tag such as TdoT.

In fact, the fusion of synthetic peptides from the optimal terminus (with the exception of 18AWT fused to the N-terminus RADH) resulted in CatIBs displaying significantly higher catalytic activities as shown above, compared to corresponding N-terminal TdoT CatIBs, which suggests that shorter tags might indeed have less impact on proper folding of the target within CatIBs, thus yielding immobilizates displaying higher activities. Here it should also be noted that, among the constructs generated in this study, one TdoT construct (BsLA-L-TdoT) displayed residual activities within the range of the best-performing constructs harboring the synthetic peptide tags (lowest $p = 0.88$, against C-terminal 18AWT), which could indicate that, for certain cases, the size of the CatIB-inducing tag might be less relevant when the optimal fusion site for a specific tag is exploited.

In summary, the best-performing tag and fusion site are target-dependent, and should therefore always be identified by testing to obtain CatIB immobilizates with high activities.

CatIB Yields Are Influenced by Tag and Fusion Site. In addition to catalytic activities, the yield of CatIBs (i.e., the amount of dry CatIBs obtainable from each construct, per given amount of cells) is an important factor for assessing the overall potential of the enzyme immobilizates for industrial applica-

https://doi.org/10.1021/acssynbio.2c00035
ACS Synth. Biol. 2022, 11, 1881−1896

tions. To this end, the lyophilized CatIBs, which were obtained following a process of cell lysis, washing of the resulting CatIBs, and freeze drying, were carefully weighed and used in yield calculations (see Table S4 for both CatIB and protein yields for all constructs). Since for application purposes, a construct that generates moderately active CatIBs in very high amounts could prove more useful than a construct generating highly active CatIBs albeit in extremely low amounts (and vice versa), "biomass specific activity yields" were calculated for all constructs to provide a better one-on-one comparison. Biomass specific activity yields were calculated by multiplying the activity of CatIBs (in U/mg CatIBs) by the yields (in mg CatIBs/g wet cells), and can therefore be defined as the "catalytic activity per gram wet cells" (see Figure 5).

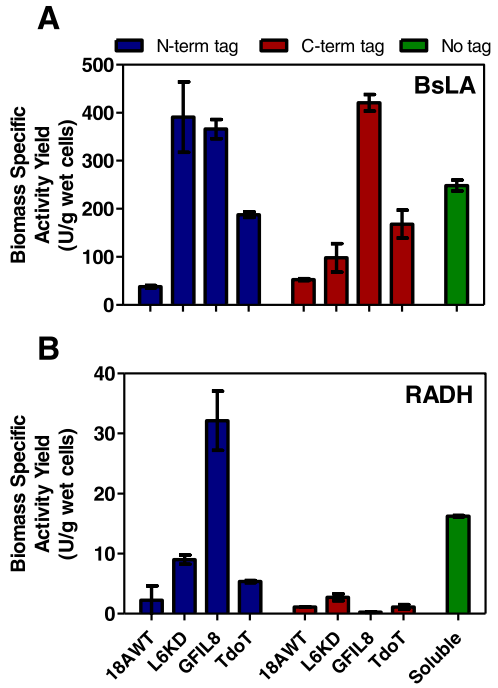

Figure 5. CatIB and soluble enzyme yield evaluation. Biomass specific activity yields of BsLA (A) and RADH (B) CatIBs and the respective soluble enzymes. The values depicted are calculated by multiplying the specific activities of lyophilized CatIBs (U/mg lyophilizate) by yields (mg CatIBs/g wet cells), and for the case of soluble enzymes, specific activities of the soluble, purified enzymes (U/mg enzyme) by yields (mg enzyme/g wet cells). Error bars represent the standard error of the mean derived from at least three biological replicates for the constructs generated in this study. See Table S4 for the numerical values depicted in the figure, as well as yields for all constructs.

For BsLA (Figure 5A), CatIBs formed by N-terminal fusion of L6KD as well as GFIL8 CatIBs bearing the tag at either the N- or C-terminus, yielded the best-performing CatIBs among all BsLA constructs. High biomass specific activity yields hereby result from their high specific activity complemented by high production yields (Table S4). By contrast, and despite displaying activities comparable to that of GFIL8 constructs (Figure 4A), the CatIBs obtained from the C-terminal TdoT-bearing BsLA construct, yielded less than half of the amount of lyophilizate produced by the GFIL8 constructs (Table S4), and consequently shows a significantly lower biomass specific activity yield (N-terminal GFIL8 fusion: $p = 0.026$; C-terminal GFIL8 fusion: $p = 0.003$). The impact of production yields on the overall application potential of the CatIBs can be seen even more clearly for the RADH CatIBs (Figure 5B), where the CatIBs obtained from the N-terminal GFIL8 harboring construct that proved to generate the highest amount of CatIBs (11 g lyophilizate/100 g wet cells, Table S4) among all tested constructs, combined with a high residual activity, results in a significantly higher biomass specific activity yield compared to the remaining RADH constructs ($p < 0.001$). Importantly, the constructs highlighted above for their high biomass specific activity yields (namely, the BsLA constructs harboring GFIL8 from either terminus and the RADH construct harboring the N-terminal GFIL8 tag) showed significantly higher biomass specific activity yields compared to their soluble, purified BsLA and RADH counterparts (Figure 5A,B, green bars) (highest $p = 0.034$; N-terminal GFIL8-RADH fusion), highlighting the application potential of the CatIBs approach, i.e., when CatIB production is suitably optimized.

In conclusion, CatIB yields (both in terms of obtainable amount and activity) are highly dependent on the fused tag and fusion site, and the proper exploitation of the method can yield immobilizates with superior performance. Biomass specific activity yields could therefore prove to be a simple to determine, yet very useful parameter for selecting the best-performing CatIB producers for application.

Lyophilized CatIBs of BsLA and RADH Are Highly Stable. Apart from activity and yields, the stability of an enzyme immobilizate is a decisive parameter for its usefulness. We therefore determined the stability of the freeze-dried BsLA and RADH CatIBs by incubating the corresponding CatIB suspensions in sodium phosphate buffer for 5 days at room temperature and performing activity assays on each day. As a reference, the corresponding soluble purified enzymes were used, which were overproduced under identical conditions, column purified, and either stored frozen in lyophilized form until the stability test or used directly for analysis upon fresh preparation and purification (for details, see the Methods section). All BsLA CatIBs showed superior stability (Figure 6A,B). Here, the CatIBs obtained from the construct containing an N-terminal 18AWT tag showed 90% of the initial activity after 5 days of incubation, followed by 88% for the TdoT-harboring construct and 86% for L6KD and GFIL8 constructs. Similarly, C-terminally tagged constructs showed minimal activity loss during the 5-day incubation, where 88% of the initial BsLA activity was retained by CatIBs formed from using the GFIL8 tag, 85% for L6KD, 84% for 18AWT, and 81% for the TdoT construct. In contrast, the activity of the soluble BsLA decreased to 23% of its initial value within the same time frame. A similar trend was observed for all N-terminal tag-bearing RADH constructs (Figure 6C), where 96, 94, 88, and 87% of the initial enzyme activity was retained for 5 days for GFIL8, TdoT, L6KD, and 18AWT CatIBs, respectively. In contrast, soluble RADH retained only 31% of its initial activity. Interestingly, all RADH CatIBs that were obtained by C-terminal tag fusion, which previously displayed rather low residual activities (Figure 4B, red bars), also showed lower stability (Figure 6D). Overall, CatIBs obtained via the TdoT fusion were the most stable among the C-terminal tag fusions, retaining 45% of their original activity at day 5 and thereby still outperforming the soluble RADH in terms of stability. In summary, with the exception of RADH CatIBs formed by C-terminal tag fusion, which also displayed low residual activities, most CatIBs showed high stability compared to the soluble

https://doi.org/10.1021/acssynbio.2c00035
ACS Synth. Biol. 2022, 11, 1881−1896

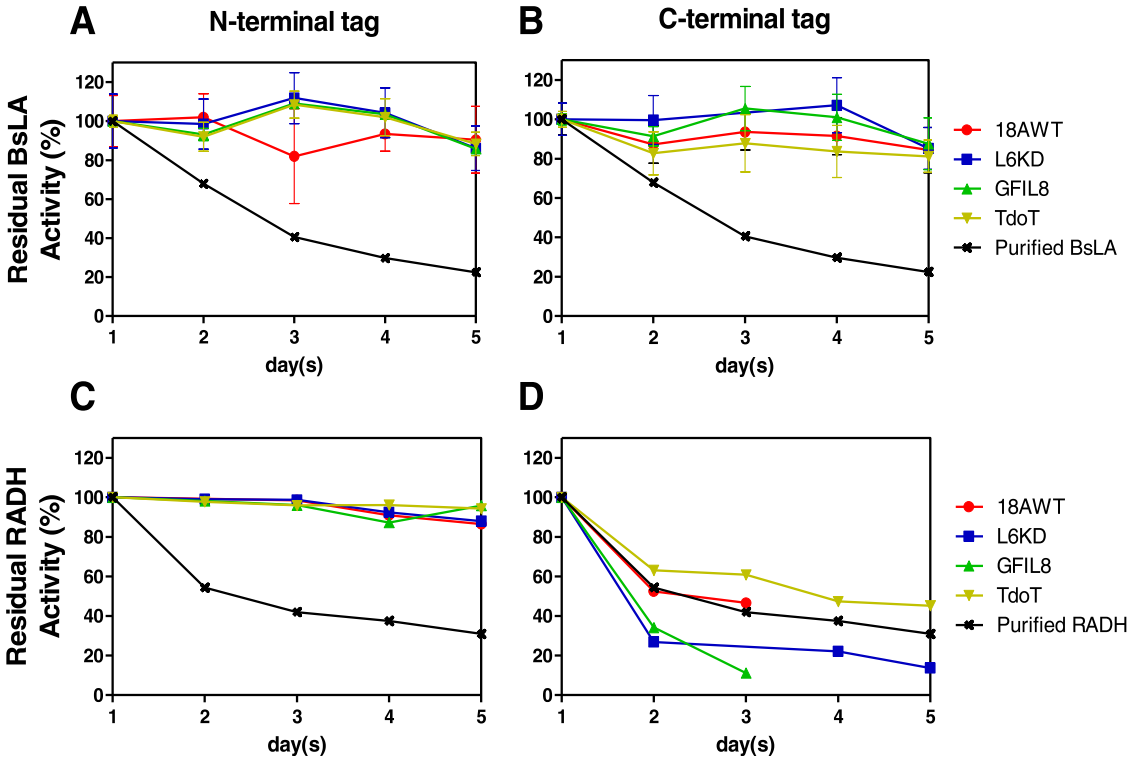

Figure 6. CatIB stability evaluation. Stability of lyophilized BsLA (A, B) and RADH (C, D) CatIBs over 5 days, relative to their corresponding activities detected at day 1 (set to 100%). Stability data of purified BsLA and RADH are shown as black lines in their respective panels. (A) BsLA constructs with N-terminal 18AWT, L6KD, GFIL8, and TdoT tags. (B) BsLA constructs with C-terminal 18AWT, L6KD, GFIL8, and TdoT tags. (C) RADH constructs with N-terminal 18AWT, L6KD, GFIL8, and TdoT tags. (D) RADH constructs with C-terminal 18AWT, L6KD, GFIL8, and TdoT tags. For C-terminal 18AWT and GFIL8 constructs of RADH, the measurements were stopped on day 3 due to low activities. Unless stated otherwise, the values were obtained from at least three biological replicates. Values depicted are mean and standard error of the mean (see Table S2 for the numerical values and details from the stability data at the end of the measurements for all constructs).

purified enzymes, highlighting the application potential of CatIB immobilizates.

Flow Chemistry Application of Best-Performing RADH CatIBs. The highest activity and stability were observed for N-terminal GFIL8 harboring RADH CatIBs; therefore, this construct was selected as a catalyst for flow synthesis. As previously shown, a closed-loop cofactor regeneration system in continuous flow synthesis can be used for biocatalytic redox reactions using oxidoreductases and substoichiometric amounts of $NADP^+$; hence, we herein report the application of CatIBs in this mode.[54] Since the usage of RADH for the asymmetric transformation of various bulky-bulky and small-bulky ketones to the corresponding alcohols in high yields and enantioselectivities was postulated earlier,[55] we used cyclohexanone (**1a**) as well as ω-chloroacetophenone (**1b**) as model substrates.

Batch Synthesis. To test CatIBs in synthesis, some batch experiments were performed first. Two batches with ω-chloroacetophenone (**1b**) as substrate were prepared: one with cyclohexanol, and a second one with 2-propanol as cosubstrate. The results of the reaction are shown in Scheme 1 (for more results, see Tables S9 and S10). For 2-propanol, nearly no conversion was observed after 96 h, which is in line with studies showing the relative reaction rate being low with this alcohol.[55] However, with cyclohexanol, a turnover of >99% and a yield of 88% after 96 h were achieved (Scheme 1), thereby confirming the proof of concept. It is worth noting that *ee* decreases from 98% after 24 h to 88% after 96 h (see Tables S9 and S10).

Scheme 1. Asymmetric Reduction of Ketone 1b to Alcohol 2b in Batch Comparing Cyclohexanol and 2-Propanol as Cosubstrates[a]

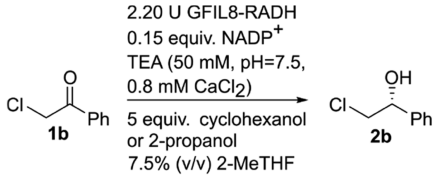

[a]Conversion and enantiomeric excess (ee) were determined using thin-layer chromatography (TLC) and gas chromatography (GC). ee could not be determined due to low conversion.

Preparation of Packed-Bed Reactor. The application of CatIBs in flow synthesis proved challenging due to the small particle size of these bionanomaterials.[20] This favors washout from the column and subsequently leads to clogging of the flow liquid−liquid extraction (FLLEX) membrane, which is essential for the closed-loop system. Accordingly, CatIBs must be physically trapped, which was carried out using silica, which is known to be largely inert toward enzymes, inside an Omnifit column.[56,57] Initially, CatIBs were sandwiched between two layers of silica; however, this strategy did not prove to be effective, as it led to clogging and to a sharp increase of counterpressure after just 1 min and 45 s (see Figure S5) as the

https://doi.org/10.1021/acssynbio.2c00035
ACS Synth. Biol. 2022, 11, 1881−1896

CatIBs were strongly compressed and became rock-solid. The simple solution to this problem was to directly mix the CatIBs with silica in a ratio of 1:2.5% (w/w CatIBs/silica) to prevent compression. In this way, CatIBs were rendered applicable for flow synthesis (for preparation procedure, see the Methods section and Table S7 and Figure S6).

Simple Flow-Through. The initial flow experiments were done in simple flow-through with stoichiometric amounts of cofactor NADPH. Cyclohexanone (**1a**) and ω-chloroacetophenone (**1b**) were tested as model substrates for the reduction to the corresponding alcohols **2a** and **2b** (Scheme 2).

Scheme 2. Schematic Representation of the Reactor Setup and the Reactions Utilizing GFIL8-RADH CatIBs[a]

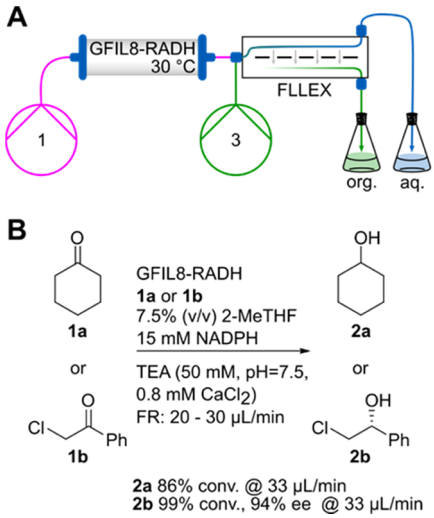

[a](A) Schematic representation of the simple flow-through system using phase separation technique by Asia FLLEX system. As biocatalyst, RADH CatIBs bearing N-terminal GFIL8 tag was used. Color code: magenta, mixed phase of aqueous and organic components (pump 1 and after column); green, organic extraction solvent; blue, aqueous phase after extraction. (B) Reaction scheme of GFIL8-RADH-catalyzed reduction of ketones **1a** and **1b** to alcohols **2a** and **2b**.

A mixture of ketones **1a** or **1b** (15 mM) with 7.5% (v/v) 2-MeTHF, 15 mM NADPH in TEA buffer were pumped (pump 1, Scheme 2A) through a common Omnifit column (size: 5 × 50 mm^2; for immobilization procedure, see the Methods section and Table S7 and Figure S6) filled with CatIBs. Extraction was carried out using diisopropyl ether as solvent (pump 3, Scheme 2A) with the Asia FLLEX system. For the enzyme-catalyzed reduction of cyclohexanone (**1a**) to cyclohexanol (**2a**), a turnover of 86% over 120 min (collection quantified every 20 min) was achieved at a flow rate (FR) of 33 μL/min (Scheme 2). Lowering the flow rate to 20 μL/min did not result in higher turnover (85% over 120 min; for more results, see Table S8). Furthermore, attention should also be paid to asymmetric reduction of ω-chloroacetophenone (**1b**) yielding (*R*)-2-chloro-1-phenylethanol-1-ol (**2b**). At a given flow rate of 33 μL/min, a full conversion >99% with 94% ee over 120 min was achieved (collection every 20 min; see Table S11). At this point, it should be mentioned that for ketone **1b**, the addition of 2-MeTHF was absolutely essential; otherwise, crystallization in the tubes was observed. As outlined above, we show here for the first time that CatIBs can be successfully used in flow synthesis.

Closed-Loop Cofactor Regeneration. After establishing the simple flow-through mode, a closed-loop cofactor regeneration system consisting of three Asia pumps was tested. Pump 1 (Figure 7, blue) was used for the aqueous cofactor

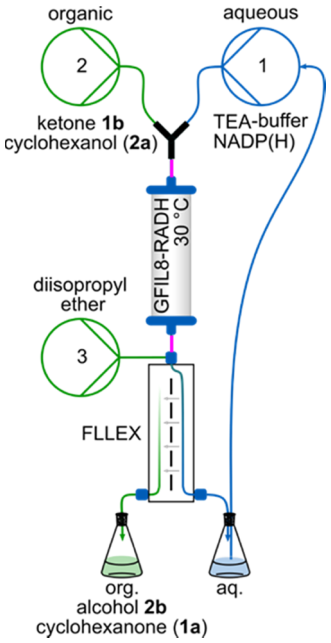

Figure 7. Closed-loop cofactor regeneration setup using phase separation technique by Asia FLLEX system. As a biocatalyst, CatIBs of RADH harboring N-terminal GFIL8 tag were used. Color code: green, organic substrate and cosubstrate containing layer; blue, aqueous cofactor and buffer containing layer; magenta, mixed aqueous/organic layer.

containing stream with TEA buffer. Pump 2 (Figure 7, green) delivered the substrate dissolved in cosubstrate and served as cosolvent at the same time. Both streams were connected through a *y*-piece and the mixed stream (Figure 7, magenta) was pumped over the prepared catalyst cartridge. Pump 3 introduced diisopropyl ether as an extraction solvent by phase separation through the FLLEX system. The product could be collected and the aqueous layer could be reintroduced into the system. A schematic representation of the system is shown in Figure 7.[54]

First, reaction conditions for the reduction of ketone **1b** were determined using cyclohexanol as cosolvent and cosubstrate for cofactor regeneration (for the procedure, see Table S12). The reaction is presented in Scheme 3A. Collection of the product occurred over 360 min in 60-min steps, and conversion as well as ee were determined using gas chromatography (to follow the exact reaction course, see Table S12). For a concentration of 10 mM substrate, an average turnover of 75% was observed. The increase of ee to 99% is in good agreement for this substrate using soluble enzyme[55] and superior compared to the simple flow-through (94%, Tables S11 and S12). We attribute this to the absence of 2-MeTHF. Increasing the concentration to 12.5 and 15 mM resulted in average conversions of 70 and 57%, respectively (see Table S12). Lowering the amount of $NADP^+$ to substoichiometric 2 mM resulted in a remarkable increase in turnover for 15 mM substrate concentration to 69%, and clearly demonstrates how efficient the CatIBs perform, since they must reduce the substrate and also rapidly regenerate the cofactor (for more information, see Table S12). Here, a slight decrease

https://doi.org/10.1021/acssynbio.2c00035
ACS Synth. Biol. 2022, 11, 1881−1896

Scheme 3. Reaction Scheme and Conversion in the Closed-Loop Cofactor Regeneration Mode Using GFIL8-RADH CatIBs[a]

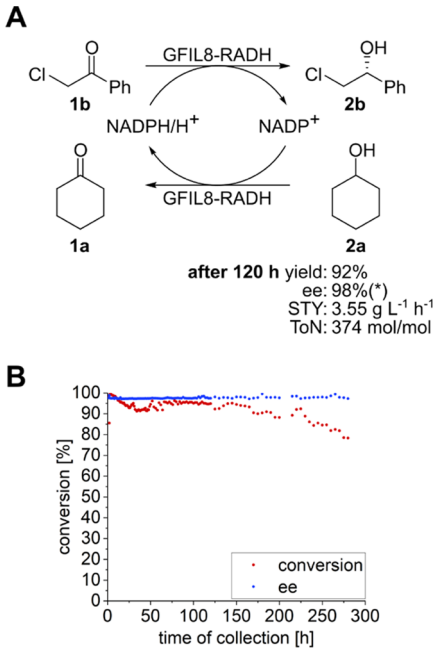

[a](A) Reaction scheme of GFIL8-RADH catalyzed asymmetric reduction of ω-chloroacetophenone **1b** to the corresponding alcohol **2b**. Cofactor regeneration occurs through oxidation of cyclohexanol **2a** reducing $NADP^+$ to NADPH by the very same enzyme. STY: space-time-yield, ToN: turnover number (for NADP(H)). (B) Continuous synthesis of alcohol **2b** over 280 h using a column filled with 38 U RADH and substoichiometric amounts of $NADP^+$ (2.00 mM). Color code: conversion is depicted in red, and ee is depicted in blue.

in ee to 98% was observed. These conditions were then used for the subsequent synthesis of alcohol **2b** in continuous mode. Therefore, the reactor and thus the amount of enzyme was increased by a factor of 2.5 to enable almost complete conversion and to ensure greater long-term stability of the column (see the Methods section). Remarkably, after 120 h of continuous production, a yield of 92% with 98% ee was achieved, resulting in a space-time yield (STY) of 3.55 g/(L × h) and a turnover for the cofactor (ToN) of 374 mol/mol (Scheme 3A). The production was followed for another 160 h, and only a moderate decrease in conversion to 78% with the same *ee* was observed, thus proving the stability and reliability of the CatIBs (Scheme 3B).

CONCLUSIONS

The study presented here employed a benchmarking strategy to provide a comprehensive assessment of catalytically active inclusion bodies (CatIBs) as in vivo produced protein immobilizates. Among the tested fusion tags for inducing CatIB formation, utilizing GFIL8 or L6KD tags instead of TdoT proved generally beneficial, as these tags gave rise to CatIBs with enhanced residual activities (more than 3-fold higher activity compared to TdoT CatIBs). In addition, when considering protein yields and activity, the corresponding CatIBs even outperformed their soluble purified enzyme counterparts with regard to biomass specific activity yields. However, for targets that are difficult to "pull-down," the effectiveness of the short peptides 18AWT, L6KD, and GFIL8 appeared to be limited, as replacing the larger TdoT tag with these shorter peptides did not improve the CatIB-formation efficiencies. Note that further studies, apart from tag and fusion site variation, could also include iteration of different linker variants, which were shown to have an impact on CatIB-formation efficiency and CatIB properties.[21,26,58] This, however, would increase the number of variants exponentially and is beyond the scope of the present study. In the future, the use of automated cloning and CatIB characterization methods might help to address such issues.

The here presented benchmarking study further enabled the production of highly stable and active CatIBs for application as enzyme immobilizates in continuous flow chemistry, e.g., suitable for the synthesis of valuable compounds, e.g., active pharmaceutical ingredients (APIs).[2,7] To this end, the application of CatIB immobilizates in flow chemistry was demonstrated in this study for the first time, and excellent turnover rates and ee values were obtained in both simple flow-through and continuous production reactions in a closed-loop cofactor regeneration mode. Additionally, long-term stability of the CatIBs (over 280 h) was demonstrated, suggesting a great potential for future synthetic applications.

In summary, CatIBs display superior stabilities, are relatively easy to obtain without the need for chromatographic purification or additional immobilization steps during production, and can even boost the catalytic activities of the enzymes via employing the best possible tag/terminus combination. CatIBs can thus be regarded as stable and highly active immobilizates that can be produced solely by biological means, thus yielding renewable, bio-based immobilizates, making them promising candidates for a variety of industrial applications.

METHODS

Cloning. For the generation of mCherry fusion harboring 18AWT, L6KD, and GFIL8 tags, synthetic genes harboring 5′-*Nde*I and 3′-*Xho*I sites, and a *Hin*dIII site flanked by the genes encoding mCherry and the PT linker were synthesized for both N- and C-terminal tag-bearing constructs (Invitrogen GeneArt Gene Synthesis, Thermo Fisher Scientific). The plasmids containing the synthetic gene fusions were hydrolyzed using *Nde*I and *Xho*I, and ligated with a similarly digested pET28a vector (Merck, Darmstadt, Germany). The resulting expression plasmids containing the respective mCherry gene fusions were used for the fusion of the corresponding RADH and BsLA encoding genes. The gene encoding RADH was amplified via polymerase chain reaction (PCR) using suitable oligonucleotides containing 5′-*Hin*dIII and 3′-*Xho*I sites (for generating constructs with N-terminally fused tags) or 5′-*Nde*I and 3′-*Hin*dIII sites (for generating constructs with C-terminally fused tags), using 3HAMP-L-RADH construct[21] as a template. The gene encoding BsLA was similarly amplified via PCR using TdoT-L-BsLA construct[23] for the generation of C-terminally tagged BsLA constructs. The BsLA-PT-GFIL8 strain created in this study was used as a template for generating N-terminally tagged BsLA fusions, using primers with 5′-*Hin*dIII and 3′-*Xho*I sites. The plasmid pEcFbFP-L-TdoT[59] served as a template for the amplification of the genes encoding $(GGGS)_3$ linker and TdoT, using appropriate oligonucleotides harboring 5′-*Hin*dIII and 3′-*Xho*I sites to allow the generation of C-terminal TdoT gene fusions. N-terminal tag-bearing BsLA constructs, along with the C-terminal TdoT-bearing BsLA and RADH constructs were generated via In-Fusion Cloning, according to kit

https://doi.org/10.1021/acssynbio.2c00035
ACS Synth. Biol. 2022, 11, 1881−1896

instructions (Clontech Laboratories, Inc., Takara Bio, Saint-Germain-en-Laye, France). The remaining constructs (C-terminal 18AWT-, L6KD-, and GFIL8-bearing BsLA constructs and all RADH constructs except for C-terminal TdoT-harboring construct) were generated by cloning the appropriately hydrolyzed PCR products into the similarly digested pET28a vectors containing either of the 18AWT/L6KD/GFIL8 tags and the PT linker created as described above, by exchanging the *mcherry* gene with either *bsla* or *radh*. Here, to obtain RADH and BsLA constructs with C-terminally fused 18AWT/L6KD/GFIL8 tags, the PCR products of *bsla* and *radh* flanked by 5′-*Nde*I and 3′-*Hin*dIII sites were digested with these restriction endonucleases and ligated to the similarly digested, C-terminal tag-bearing mCherry constructs. N-terminal 18AWT/L6KD/GFIL8 harboring RADH constructs were likewise generated by ligating the appropriately digested PCR product of *radh* flanked by 5′-*Hin*dIII and 3′-*Xho*I sites to the digested N-terminal tag-bearing mCherry construct, by replacing the *mcherry* with *radh*. All PCR primers used in the study are listed in Table S6. All constructs were verified by sequencing (Seqlab GmbH, Göttingen, Germany).

Strains, Media, and Cultivation Conditions. *E. coli* DH5α was used as a cloning host for the generation of all plasmids used in the study. Heterologous expression of the gene fusions was performed using *E. coli* BL21(DE3). Lysogeny broth (LB)[60] medium was employed for the cultivation of strains during the cloning procedure, and for the precultures of the expression strains. For the expression, autoinduction (AI) medium[61] consisting of terrific broth (12 g/L casein-hydrolysate, 24 g/L yeast extract, 2.2 g/L KH_2PO_4, 9.4 g/L K_2HPO_4, and 5 g/L glycerol at pH 7.2) supplemented with 0.5 g/L glucose and 2 g/L lactose was used. For automated microscopy experiments, the expression strains were cultivated in 48-well FlowerPlates (m2p-labs GmbH, Baesweiler, Germany) in M9-AI medium in a BioLector (m2p-labs GmbH, Baesweiler, Germany). M9-AI medium was prepared by mixing sterile stock solutions to yield a final concentration of 5 g/L $(NH_4)_2SO_4$, 3 g/L K_2HPO_4, 6.8 g/L Na_2HPO_4, 0.5 g/L NaCl, 2 g/L NH_4Cl, 0.2 g/L $MgSO_4{\cdot}7H_2O$, 1.5 mg/L $CaCl_2{\cdot}5H_2O$, 15 mg/L $FeSO_4$, 0.2 g/L $Na_3C_6H_5O_7{\cdot}2H_2O$, 10 mg/L thiamine, 0.75 mg/L $AlCl_3{\cdot}6H_2O$, 0.6 mg/L $CoCl_2{\cdot}6H_2O$, 2.5 mg/L $CuSO_4{\cdot}5H_2O$, 0.5 mg/L H_3Bo_3, 17.1 mg/L $MnSO_4{\cdot}H_2O$, 3 mg/L $Na_2MoO_4{\cdot}2H_2O$, 1.7 mg/L $NiCl_2{\cdot}6H_2$, 15 mg/L $ZnSO_4{\cdot}7H_2O$, 5 g/L glycerol, 0.5 g/L glucose and 2 g/L lactose. LB precultures, for CatIB production, were cultivated at 37 °C at 130 rpm for 12−18 h. Expression cultures were inoculated from the LB precultures at a starting OD_{600} of 0.05, and the cells were initially cultivated at 37 °C for 3 h at 130 rpm (1000 rpm for FlowerPlates), after which the temperature was decreased to 15 °C and the expression carried out for 69 h under the same shaking conditions. A filling volume of 10% was used for all shake flask cultivations. All cultures were supplemented with 50 μg/mL kanamycin for plasmid maintenance.

Preparation of CatIBs and Soluble Enzymes. Expression cultures were harvested via centrifugation (7500*g*, 30 min, 4 °C). The cells were resuspended (10% w/v) in lysis buffer (50 mM sodium phosphate buffer, 100 mM NaCl, pH 8.0) and lysed at 1000−1500 bar with three passes through an Emulsiflex-C5 high-pressure homogenizer (Avestin Europe GmbH, Mannheim, Germany) under cooling. Crude cell extract (CCE) was centrifuged (15 000*g*, 30 min, 4 °C) to obtain the supernatant (S1) and the unwashed pellet fractions (P1). The pellet fraction was resuspended in Milli-Q water (1:1 w/w) centrifuged a second time (15 000*g*, 30 min, 4 °C) to obtain the washed, CatIB-containing pellet fraction (P2) along with the supernatant of the wash step (S2). The washed CatIBs were resuspended (1:1 w/w) in Milli-Q ultrapure water, frozen at −80 °C, and subsequently lyophilized (Christ ALPHA 1-3 LD Plus, Martin Christ Gefriertrocknungsanlagen GmbH, Osterode, Germany). After lyophilization, the CatIBs were ground into a fine powder using glazed mortars and pestles, flushed with argon, and stored at −20 °C. Soluble RADH was prepared, lyophilized, and stored as described previously.[25] For the production of the soluble BsLA control, *E. coli* BL21(DE3) carrying pHis6-L-BsLA as expression plasmid, encoding a 6× His-tagged BsLA protein (with N-terminal linker polypeptide)[23] was cultivated, harvested and lysed as described earlier for the corresponding CatIBs. Soluble BsLA was purified by metal ion affinity chromatography using Ni-NTA Superflow column (Qiagen, Hilden, Germany) with equilibration buffer (50 mM NaPi, pH 8.0, 300 mM NaCl, 10 mM imidazole), washing buffer (50 mM NaPi, pH 8.0, 300mM NaCl, 20 mM imidazole) and elution buffer (50 mM NaPi, pH 8.0, 300 mM NaCl, 250 mM imidazole). For desalting, a Sephadex-G25 column (GE Healthcare, Little Chalfont, U.K.) was used and the protein was eluted in 10 mM glycine at pH 10. Purified soluble BsLA was frozen rapidly using liquid nitrogen and stored at −20 °C.

Cell Fractionation for Determining Relative Activity/Fluorescence and CatIB-Formation Efficiencies. To determine the activity/fluorescence distribution of the constructs, crude cell extracts (CCEs) were prepared as described above and fractionated as described previously.[25] Briefly, the CCEs were diluted in lysis buffer (50 mM sodium phosphate buffer, 100 mM NaCl, pH 8.0) in a suitable amount. Half of the diluted CCE samples were centrifuged (7697*g*, 2 min, room temperature) resulting in the supernatant (S1), and CatIB-containing, unwashed pellet (P1) fractions. P1 was resuspended in lysis buffer (1:1 v/v) for the washing step, and centrifuged (7697*g*, 2 min, room temperature), giving rise to the supernatant of the wash step (S2) and the washed pellet containing CatIBs (P2). P2 was resuspended again in lysis buffer (1:1 v/v). The activity/fluorescence of the CCE, S1, and P2 (in some cases, additionally P1) fractions was measured to determine the distribution of activity/fluorescence among each fraction. To quantify the CatIB formation efficiencies, the activity/fluorescence measured in the P2 fraction (washed CatIBs) was expressed relative to the total activity/fluorescence of the crude cell extract, which was set to 100%.

Fluorescence Spectrophotometry. mCherry fluorescence of crude cell extract, supernatant, and pellet fractions was measured in black Nunc 96-Well MicroWell polypropylene plates (ThermoFisher Nunc, Waltham) as described elsewhere,[25] in quadruples of 100 μL sample, per each fraction. A TECAN infinite M1000 PRO fluorescence MTP reader (TECAN, Männedorf, Switzerland) was used for the measurements (λ_{ex} 587 nm, λ_{em} 610 nm, bandwidth 5 nm, *z*-position 18.909 μm, enhancement 120, flash number 25, flash frequency 400 Hz). To ensure proper suspension of mCherry in the insoluble fractions, a shaking step of 5−10 s was implemented (654 rpm, amplitude 2 mm) prior to measurements.

Determination of RADH Activity. RADH activity was measured by a discontinuous photometric assay[21] using cyclohexanone as substrate, by monitoring the consumption of NADPH determined photometrically at six time points, in a 5-min assay. The total reaction volume was 1750 μL and

https://doi.org/10.1021/acssynbio.2c00035
ACS Synth. Biol. 2022, 11, 1881−1896

contained 0.4 mM NADPH and 100 mM cyclohexanone in TEA buffer (50 mM triethanolamine, 0.8 mM $CaCl_2$, pH 7.5). Initially, a 1.4 mL reaction mixture containing 0.5 mM NADPH and 125 mM cyclohexanone in TEA buffer was prepared and incubated at 30 °C for 5 min. RADH containing samples, which were either cell fractions suitably diluted in sodium phosphate buffer (50 mM sodium phosphate buffer, 100 mM NaCl, pH 8.0), or 0.5−1 mg/mL lyophilized RADH CatIBs in sodium phosphate buffer, or 5 μg/mL soluble, purified RADH in sodium phosphate buffer, were similarly incubated at 30 °C for 5 min. After the preheating step, the reaction was started by mixing 350 μL of the RADH containing samples thoroughly with 1.4 mL of the reaction mixture, where a 250 μL sample was taken immediately after starting the reaction and diluted 1:3 in methanol to stop the reaction. The remainder of the reaction mixture was incubated at 30 °C for 5 min under constant agitation at 1000 rpm, sampled every minute, and the reaction was stopped in the same manner. When measuring cell fractions displaying low activities, the assay was extended to 10 min to increase the sensitivity, in which case the reaction mixture was sampled once every 2 min instead of every minute. The samples were centrifuged (7697*g*, 5 min, room temperature), transferred to disposable cuvettes and absorption spectra were measured from 280 to 500 nm (Cary 60 UV−Vis Spectrophotometer, Agilent, Santa Clara). All RADH activity measurements for the generated constructs were performed with at least three biological replicates. For stability investigations, the RADH CatIBs and soluble, purified RADH were incubated at room temperature for 5 days, with the samples tested for RADH activity each day. RADH activity was calculated using the molar extinction coefficient of NADPH, determined under the assay conditions[25] ($\varepsilon_{340\ nm}$ = 1.975 mM^{-1} cm^{-1}). One unit (U) of enzyme activity was defined as the amount of enzyme that led to the conversion of 1 mmol NADPH to $NADP^+$ per minute, under the given reaction conditions. Specific RADH activities were calculated as U/mg CatIBs (using the initial weight of CatIBs in assay), and as U/mg protein (derived from the calculated protein content of CatIBs in assay; see the Determination of Protein Concentration of CatIBs, SDS-PAGE, and Purity Analyses section).

Determination of BsLA Activity. The activity of BsLA was measured in a continuous photometric assay using *p*-nitrophenyl butyrate (*p*-NPB) as substrate and detecting the rate of *p*-nitrophenolate (*p*-NP) formation based on the increase in absorption at 410 nm.[23] The reactions were performed in disposable cuvettes with a volume of 1 mL that contained 0.8 mM *p*-NPB in sodium phosphate buffer (50 mM sodium phosphate buffer, 100 mM NaCl, pH 7.0) at 25 °C. The reaction mixture was prepared using a stock solution of 16 mM *p*-NPB in acetonitrile, which was preincubated at 25 °C for 5 min. BsLA-containing samples, cell fractions diluted in sodium phosphate buffer (50 mM sodium phosphate buffer, 100 mM NaCl, pH 7.0), 0.5 mg/mL lyophilized CatIBs in lysis buffer, or 17.8 μg/mL purified soluble BsLA (in glycine, pH 10), were incubated to 25 °C in disposable cuvettes in a temperature-controlled spectrophotometer (Cary 60 UV−Vis Spectrophotometer, Agilent, Santa Clara). The reaction mixture (950 μL) was added to 50 μL of the BsLA-containing sample to ensure rapid mixing and start of the measurement. The absorption at 410 nm was followed for 1 min at the constant temperature of 25 °C. For each reaction mixture, a blank control reaction was run that contained 50 μL of sodium phosphate buffer without enzyme, and the rate of the control reaction was subtracted from the enzyme-containing reactions. All measurements were performed in triplicates or quadruples of at least three biological replicates. For stability investigations, BsLA CatIBs and purified, soluble BsLA were incubated at room temperature for 5 days and the assay was repeated each day as described above. BsLA activity was calculated using the molar extinction coefficient of *p*-NP determined under the assay conditions (ε_{410nm} = 8.367 mM^{-1} cm^{-1}). 1 U was defined as the amount of enzyme that leads to the release of 1 mmol *p*-NP per minute, under the reaction conditions. Specific BsLA activities were calculated in U/mg CatIBs (using the initial weight of lyophilized CatIBs in assay) and as U/mg (using the calculated protein content of CatIBs in assay; see the Determination of Protein Concentration of CatIBs, SDS-PAGE, and Purity Analyses section).

Determination of Protein Concentration of CatIBs, SDS-PAGE, and Purity Analyses. The protein content of CatIBs was determined by measuring the absorption of CatIBs dissolved in 6 M guanidine-hydrochloride at 280 nm.[21,23,25] The molar extinction coefficients of the constructs were calculated via the ProtParam tool.[62] The theoretical extinction coefficients and molecular weights of all of the constructs generated and used in this study are listed in Table S5. For SDS gel analyses, either NuPAGE 4−12% Bis−Tris protein gels with MES SDS running buffer (50 mM MES, 50 mM TRIS, 0.1% SDS, 1 mM ethylenediaminetetraacetic acid (EDTA), pH 7.3) or 5−12% acrylamide gels in electrophoresis buffer (25 mM Tris, 192 mM glycine, 0.1% SDS) were used. For SDS-PAGE, the protein concentration of the supernatant fraction (S1) was determined using the Bradford assay[63] with bovine serum albumin (0.01−0.1 mg/mL) as standard. The cell fractions were boiled at 100 °C for 3 min prior to loading, and the volume required to load 10 μg of protein for the S1 fraction served as the loading volume for the remaining crude cell extract (CCE), supernatant from the wash (S2) and pellet (P1 and P2) fractions. All gels contained 3 μL of PageRuler Prestained Protein Ladder (Thermo Fisher Nunc, Waltham). The purity of the different CatIB preparations was assessed densitometrically by analyzing the corresponding SDS-PAGE gels using the Fiji software.[64] The entire P2 lanes, containing the target protein bands of all constructs were converted to a peak representation and the density of the bands was analyzed. The background was subtracted. The areas under each density peak were calculated, and the area under the curve for each target protein was compared to the area under the curve for its subsequent P2 lane for each target (set to 100%) to derive the purity values listed in Table S3.

Microscopic Analyses. Live cells of mCherry expression strains were analyzed for CatIB formation using an inverted Nikon Eclipse Ti microscope (Nikon GmbH, Düsseldorf, Germany) equipped with a Plan Apo λ 100× Oil Ph3 DM objective (Nikon GmbH, Düsseldorf, Germany), Nikon DS-Qi2 camera (Nikon GmbH, Düsseldorf, Germany), SOLA light engine (Lumencor) for fluorescence excitation, and a fluorescence filter for mCherry with an excitation bandwidth of 540−580 nm, a dichroic mirror of 562 nm and an emission bandwidth of 580−641 nm (AHF Analysentechnik, Tübingen, Germany). Fluorescence and camera exposure times were 200 ms for ph3 and 50 ms for the mCherry filter at 10% lamp intensity. Cells were cultivated in AI medium for 69 h as described above. A volume of approximately 1 mL (corresponding to an OD_{600} of 10) was sampled from the expression cultures and centrifuged (7697*g*, 1 min, room temperature),

https://doi.org/10.1021/acssynbio.2c00035
ACS Synth. Biol. 2022, 11, 1881−1896

and resuspended in the same volume of lysis buffer (50 mM sodium phosphate buffer, 100 mM NaCl, pH 8.0). Microscopy samples were appropriately diluted in lysis buffer before imaging and immediately applied to the poly-(dimethylsiloxane)-based microfluidic chips via a syringe, where the single cells were retained within the chip chambers with dimensions ranging from 58.4 μm × 58.9 μm × 1 μm to 59.3 μm × 99.1 μm × 1 μm. Analysis of the microscopy images was performed using Fiji.[64]

Automated Microscopy. For automated microscopy, the CatIB strains were cultivated in a BioLector as explained above. The BioLector was integrated into a liquid handling system (Freedom Evo, Tecan, Männedorf, Switzerland). After 72 h of cultivation, the CatIB-producing cells were harvested from each well of the FlowerPlate. The samples were stored in a deep well plate at 4 °C on the robotic deck until automated microscopy was performed. For image acquisition, a self-built injection station[50] was used. The station was connected via 70 cm perfluoroalkoxy (PFA) tubing (inner diameter: 0.8 mm; outer diameter: 1.6 mm, VWR, Darmstadt, Germany) to a flow chamber (height: 20 μm, length: 58.5 mm, width: 800 μm, microfluidic ChipShop, Jena, Germany). The chamber was fixed on an inverted Nikon Eclipse Ti microscope (Nikon GmbH, Düsseldorf, Germany) equipped with a CFI Plan Apo Lambda 100× Oil objective (Nikon GmbH, Düsseldorf, Germany). The microscope was placed next to the liquid handling platform. Each sample (300 μL) followed by 400 μL of H_2O was injected into the injection station with a velocity of 1 μL/s. After the injection of 600 μL, the flow was set to zero to allow image acquisition. A 1 μL pulse with a velocity of 1 μL/s with a 4 min delay was performed three times to flush in new cells. A total of 500 images were taken of each sample in the flow chamber with a Thorlab camera DCC154M-GL (Thorlabs, Inc., Newton, New Jersey). Analysis of the microscopy images was performed using Fiji.[64]

Flow Chemistry—Column Packing. Silica gel was used as a solid phase to physically trap the RADH CatIBs in a 5 × 50 mm^2 Omnifit column. For the continuous production of alcohol **2b**, a 5 × 150 mm^2 Omnifit column was used to ensure full conversion and longer stability. Both columns were first covered with a layer of silica (approx. 2 mm high) and then rinsed from the opposite side with buffer to solidify the silica. CatIBs and silica (1:2.5% m/m) were mixed, filled on top of the column, and the rinsing step was repeated. Another layer of silica was then carefully added and slightly compressed upon insertion of the column stamp to avoid flushing out the CatIBs. The column was rinsed again before use. Further details are described in Figure S5 and Table S7.

Syrris Asia Flow Devices. Syringe pump: The different channels were equipped with yellow syringes (50.0/100 μL). Software: As software, the Asia Manager PC Software (version 1.71) was used and flow rates were set in the pump settings. Automated collector: As an automated collector for product collection, a Gilson FC 203B was used. Collection occurred in device-controlled manual time mode. Flow liquid−liquid extraction (FLLEX): The FLLEX module was equipped with Merck FHLP02500 poly(tetrafluoroethylene) (PTFE) membranes without polyethylene support. System pressure was set to 3.00 bar, and the cross-membrane pressure (CMP) for diisopropyl ether was set to 50.0 mbar.

Batch Synthesis. In a 50 mL flask, a suspension of 2.20/4.40 U GFIL8-RADH CatIBs in 9.9 mL TEA buffer (50 mM, pH 7.5, 0.8 mM $CaCl_2$) was prepared. $NADP^+$ (0.15 equiv, 17.7 mg, 23 μmol) and cyclohexanol (**2a**, 5.00 equiv, 75.1 mg, 0.75 mmol) or 2-propanol (5.00 equiv, 45.1 mg, 0.75 mmol) were added. Then, ω-chloroacetophenone (**1b**, 23.2 mg, 0.15 mmol) was dissolved in 750 μL of 2-MeTHF and added to the enzyme solution, resulting in a 15 mM solution. After 24/48/72 h or 24/96 h, an aliquot (~300 μL) was taken, extracted with methyl *tert*-butyl ether (MTBE) and conversion was checked using TLC. Further, conversion and ee were analyzed by gas chromatography (GC) with chiral stationary phase. After completion, the mixture was filtered through a pad of celite and the aqueous layer was extracted four times with ethyl acetate. Organic layers were collected, combined, and washed once with brine. The solution was dried over magnesium sulfate, and the solvent was removed in vacuo. The product **2b** was then isolated and purified by flash column chromatography (PE/EtOAc 97:3). Alcohol **2b** was isolated as pale yellow oil in 88% yield (20.6 mg, 0.13 mmol), and 86% ee (for details, see Tables S9 and S10).

Synthesis in Flow with Closed-Loop Continuous Regeneration System: (*R*)-2-Chloro-1-phenylethan-1-ol (2b). Channel 1 (solution 1, aqueous): 4 mL total volume: 2 mM $NADPNa_2$ was dissolved in TEA buffer (50 mM, pH 7.5, 0.8 mM $CaCl_2$). Channel 2 (solution 2, organic): Substrate (508 mg, 3.28 mmol) was dissolved in cyclohexanol to result in a 150 mM solution. Due to the flow rate ratio between channels 1 and 2, the actual concentration in the reactor is 15 mM. Channel 3 (extraction, organic): Extraction was done in FLLEX with diisopropyl ether. Channels 1 and 2 of Syrris Asia syringe pump were filled with prepared solutions 1 and 2. An Omnifit column (5 × 150 mm^2) with 137.5 mg/30.3 U of GFIL8-RADH CatIBs as a catalyst was used as a reactor (cartridge was filled as described above and according to Figures S5 and S6 and Table S7). The flow rates were set to: channel 1, 30.0 μL/min; channel 2, 3.00 μL/min; and channel 3, 33.0 μL/min. The product was collected with an autosampler in 60-min steps and the aqueous layer was recycled into the initial vial. Conversions were tracked over time by GC utilizing a chiral stationary phase. After the substrate vial 1 was empty, it was filled with cyclohexanol (**1b**) and the system was rinsed for 90 min. The contents of all vials were combined and dried with magnesium sulfate. The solvent was reduced in vacuo. The substrate/product mixture was separated via flash column chromatography (PE/EtOAc 97:3). The product **2b** was obtained after 120 h as a pale yellow oil in a yield of 92% (469 mg, 2.99 mmol) and 98% ee (Scheme 3). ^{1}H NMR (600 MHz, $CDCl_3$): δ = 7.34−7.29 (m, 4H, Ar-H), 7.28−7.23 (m, 1H, H-5), 4.83 (dd, $^3J_{1,1'}$ = 8.9 and 3.4 Hz, 1H, H-1), 3.68 (dd, $^2J_{1'\text{-vic}}$ = 11.3, $^3J_{1',1}$ = 3.4 Hz, 1H, H-1′), 3.58 (dd, $^2J_{1'\text{-vic}}$ = 11.3, $^3J_{1',1}$ = 8.9 Hz, 1H, H-1′). ^{13}C NMR (151 MHz, $CDCl_3$): δ = 140.03 (C-2), 128.85 (C-4), 128.61 (C-5), 126.17 (C-3), 74.22 (C-1), 52.45 (C-1′). IR (attenuated total reflection (ATR), film): $\tilde{\nu}$ = 3546, 3385 (OH), 1494, 1454, 1427, 1248, 1199, 1085, 1062, 1011, 916, 870, 825, 766, 721, 696, 613, 544, 521. R_f = 0.25 (PE/EtOAc 9:1). GC: column: FS Hydrodex βTBDAc, Macherey & Nagel (25 m × 0.25 mm). Retention time: t_R = 11.5 min (*R* enantiomer), 12.4 min (*S* enantiomer). Carrier gas: H_2, 0.6 bar. Solvent: MTBE. Method: 60 °C−15 min, 5 °C/min to 150 °C−5 min.

Statistical Analysis. All data were analyzed using R version 4.1.2. Means were compared using one- and two-sided *t*-tests. When more than two means were compared, Tukey's multiple comparisons of means test were applied. *P*-values below 0.05 were considered significant.

https://doi.org/10.1021/acssynbio.2c00035
ACS Synth. Biol. 2022, 11, 1881−1896

■ ASSOCIATED CONTENT

Supporting Information

The Supporting Information is available free of charge at https://pubs.acs.org/doi/10.1021/acssynbio.2c00035.

Overview of constructs; oligonucleotides used in this study; additional benchmarking data: supporting microscopy analyses; relative fluorescence and activity, CatIB formation efficiencies, SDS-PAGE analyses, protein content, biomass specific activity yields, extinction coefficients, and molecular weights of all constructs; automated microscopy setup; additional flow synthesis information: data and pictorial representation of the columns; reduction of cyclohexanone in simple flow-through mode; GC chromatograms of cyclohexanol and cyclohexanone; additional data on batch cofactor regeneration and the influence of the employed CatIB concentration; asymmetric reduction of ω-chloroacetophenone in simple flow-through mode; screening for preliminary reactions conditions; NMR analyses of the products; GC chromatograms of ω-chloroacetophenone and (*R*)-2-chloro-1-phenylethan-1-ol; and supporting references (PDF)

■ AUTHOR INFORMATION

Corresponding Author

Ulrich Krauss − *Institute of Molecular Enzyme Technology, Heinrich Heine University Düsseldorf, Forschungszentrum Jülich GmbH, D-52425 Jülich, Germany; IBG-1: Biotechnology, Institute of Bio- and Geosciences, Forschungszentrum Jülich GmbH, D-52425 Jülich, Germany;* orcid.org/0000-0003-2219-7388; Phone: +49 2461-61-2939; Email: u.krauss@fz-juelich.de

Authors

Gizem Ölçücü − *Institute of Molecular Enzyme Technology, Heinrich Heine University Düsseldorf, Forschungszentrum Jülich GmbH, D-52425 Jülich, Germany; IBG-1: Biotechnology, Institute of Bio- and Geosciences, Forschungszentrum Jülich GmbH, D-52425 Jülich, Germany*

Benedikt Baumer − *Institute of Biorganic Chemistry, Heinrich Heine University Düsseldorf, Forschungszentrum Jülich GmbH, D-52425 Jülich, Germany;* orcid.org/0000-0003-1916-3777

Kira Küsters − *IBG-1: Biotechnology, Institute of Bio- and Geosciences, Forschungszentrum Jülich GmbH, D-52425 Jülich, Germany*

Kathrin Möllenhoff − *Mathematical Institute, Heinrich Heine University Düsseldorf, 40225 Düsseldorf, Germany*

Marco Oldiges − *IBG-1: Biotechnology, Institute of Bio- and Geosciences, Forschungszentrum Jülich GmbH, D-52425 Jülich, Germany; Institute of Biotechnology, RWTH Aachen University, D-52074 Aachen, Germany*

Jörg Pietruszka − *Institute of Biorganic Chemistry, Heinrich Heine University Düsseldorf, Forschungszentrum Jülich GmbH, D-52425 Jülich, Germany; IBG-1: Biotechnology, Institute of Bio- and Geosciences, Forschungszentrum Jülich GmbH, D-52425 Jülich, Germany;* orcid.org/0000-0002-9819-889X

Karl-Erich Jaeger − *Institute of Molecular Enzyme Technology, Heinrich Heine University Düsseldorf, Forschungszentrum Jülich GmbH, D-52425 Jülich, Germany; IBG-1: Biotechnology, Institute of Bio- and Geosciences, Forschungszentrum Jülich GmbH, D-52425 Jülich, Germany;* orcid.org/0000-0002-6036-0708

Complete contact information is available at: https://pubs.acs.org/10.1021/acssynbio.2c00035

Author Contributions

U.K., K.-E.J., and J.P. conceived and designed the study. G.O., supervised by U.K., generated all constructs, prepared CatIBs, and performed activity/fluorescence assays for CatIB benchmarking and all other experiments unless mentioned otherwise. B.B., supervised by J.P., performed the flow synthesis experiments, and K.K. and M.O. conceived and performed the automated microscopy analyses. K.M. performed all statistical analyses. The manuscript was written through contributions of all authors. All authors have given approval to the final version of the manuscript.

Notes

The authors declare no competing financial interest.

■ ACKNOWLEDGMENTS

The authors thank Bastian Wollenhaupt from the micro scale bioengineering working group (IBG-1, Forschungszentrum Jülich) for imaging of mCherry strains using fluorescence microscopy, Nadiia Pozhydaieva (HHU, Düsseldorf) for her skillful assistance in cloning of the BsLA strains with C-terminal tags, and Justyna Kulig (IBG-1, Forschungszentrum Jülich) for kindly providing the purified, soluble RADH sample. The authors also thank Esther Knieps-Grünhagen (IMET HHU, Düsseldorf, Forschungszentrum Jülich) for the purification of soluble BsLA. The research was financially supported by the CLIB Competence Centre Biotechnology (CKB) funded by the European Regional Development Fund ERDF (34.EFRE 0300096 and 34.EFRE 0300097).

■ REFERENCES

(1) Badenhorst, C. P. S.; Bornscheuer, U. T. Getting Momentum: From Biocatalysis to Advanced Synthetic Biology. *Trends Biochem. Sci.* **2018**, *43*, 180−198.

(2) Santi, M.; Sancineto, L.; Nascimento, V.; Braun Azeredo, J.; Orozco, E. V. M.; Andrade, L. H.; Gröger, H.; Santi, C. Flow Biocatalysis: A Challenging Alternative for the Synthesis of APIs and Natural Compounds. *Int. J. Mol. Sci.* **2021**, *22*, No. 990.

(3) Singh, R.; Kumar, M.; Mittal, A.; Mehta, P. K. Microbial enzymes: industrial progress in 21st century. *3 Biotech* **2016**, *6*, No. 174.

(4) Homaei, A. A.; Sariri, R.; Vianello, F.; Stevanato, R. Enzyme immobilization: an update. *J. Chem. Biol.* **2013**, *6*, 185−205.

(5) Benítez-Mateos, A. I.; Contente, M. L.; Roura Padrosa, D.; Paradisi, F. Flow biocatalysis 101: design, development and applications. *React. Chem. Eng.* **2021**, *6*, 599−611.

(6) De Santis, P.; Meyer, L.-E.; Kara, S. The rise of continuous flow biocatalysis − fundamentals, very recent developments and future perspectives. *React. Chem. Eng.* **2020**, *5*, 2155−2184.

(7) Peñafiel, I.; Cosgrove, S. C. Biocatalysis in Flow for Drug Discovery. In *Flow Chemistry in Drug Discovery. Topics in Medicinal Chemistry*; Alcazar, J. et al., Eds.; Springer, 2021.

(8) Thompson, M. P.; Peñafiel, I.; Cosgrove, S. C.; Turner, N. J. Biocatalysis Using Immobilized Enzymes in Continuous Flow for the Synthesis of Fine Chemicals. *Org. Process Res. Dev.* **2019**, *23*, 9−18.

(9) Romero-Fernández, M.; Paradisi, F. Protein immobilization technology for flow biocatalysis. *Curr. Opin. Chem. Biol.* **2020**, *55*, 1−8.

(10) Wahab, R. A.; Elias, N.; Abdullah, F.; Ghoshal, S. K. On the taught new tricks of enzymes immobilization: An all-inclusive overview. *React. Funct. Polym.* **2020**, *152*, No. 104613.

(11) Datta, S.; Christena, L. R.; Rajaram, Y. R. Enzyme immobilization: an overview on techniques and support materials. *3 Biotech* **2013**, *3*, 1−9.
(12) Rehm, F. B.; Chen, S.; Rehm, B. H. Enzyme Engineering for In Situ Immobilization. *Molecules* **2016**, *21*, No. 1370.
(13) Ölçücü, G.; Klaus, O.; Jaeger, K.-E.; Drepper, T.; Krauss, U. Emerging Solutions for in Vivo Biocatalyst Immobilization: Tailor-Made Catalysts for Industrial Biocatalysis. *ACS Sustainable Chem. Eng.* **2021**, *9*, 8919−8945.
(14) Rehm, F. B. H.; Chen, S.; Rehm, B. H. A. Bioengineering toward direct production of immobilized enzymes: A paradigm shift in biocatalyst design. *Bioengineered* **2018**, *9*, 6−11.
(15) Krauss, U.; Jäger, V. D.; Diener, M.; Pohl, M.; Jaeger, K.-E. Catalytically-active inclusion bodies-Carrier-free protein immobilizates for application in biotechnology and biomedicine. *J. Biotechnol.* **2017**, *258*, 136−147.
(16) García-Fruitós, E.; Vazquez, E.; Diez-Gil, C.; Corchero, J. L.; Seras-Franzoso, J.; Ratera, I.; Veciana, J.; Villaverde, A. Bacterial inclusion bodies: making gold from waste. *Trends Biotechnol.* **2012**, *30*, 65−70.
(17) de Marco, A.; Ferrer-Miralles, N.; Garcia-Fruitos, E.; Mitraki, A.; Peternel, S.; Rinas, U.; Trujillo-Roldan, M. A.; Valdez-Cruz, N. A.; Vazquez, E.; Villaverde, A. Bacterial inclusion bodies are industrially exploitable amyloids. *FEMS Microbiol. Rev.* **2019**, *43*, 53−72.
(18) Köszagová, R. Inclusion Bodies in Biotechnology. *J. Microbiol., Biotechnol. Food Sci.* **2020**, *9*, 1191−1196.
(19) Slouka, C.; Kopp, J.; Spadiut, O.; Herwig, C. Perspectives of inclusion bodies for bio-based products: curse or blessing? *Appl. Microbiol. Biotechnol.* **2019**, *103*, 1143−1153.
(20) Jäger, V. D.; Lamm, R.; Küsters, K.; Ölçücü, G.; Oldiges, M.; Jaeger, K.-E.; Büchs, J.; Krauss, U. Catalytically-active inclusion bodies for biotechnology-general concepts, optimization, and application. *Appl. Microbiol. Biotechnol.* **2020**, *104*, 7313−7329.
(21) Jäger, V. D.; Kloss, R.; Grünberger, A.; Seide, S.; Hahn, D.; Karmainski, T.; Piqueray, M.; Embruch, J.; Longerich, S.; Mackfeld, U.; Jaeger, K.-E.; Wiechert, W.; Pohl, M.; Krauss, U. Tailoring the properties of (catalytically)-active inclusion bodies. *Microb. Cell Fact.* **2019**, *18*, No. 33.
(22) Worrall, D. M.; Goss, N. H. The formation of biologically active beta-galactosidase inclusion bodies in *Escherichia coli*. *Aust. J. Biotechnol.* **1989**, *3*, 28−32.
(23) Diener, M.; Kopka, B.; Pohl, M.; Jaeger, K.-E.; Krauss, U. Fusion of a Coiled-Coil Domain Facilitates the High-Level Production of Catalytically Active Enzyme Inclusion Bodies. *ChemCatChem* **2016**, *8*, 142−152.
(24) Kloss, R.; Limberg, M. H.; Mackfeld, U.; Hahn, D.; Grünberger, A.; Jäger, V. D.; Krauss, U.; Oldiges, M.; Pohl, M. Catalytically active inclusion bodies of L-lysine decarboxylase from *E. coli* for 1,5-diaminopentane production. *Sci. Rep.* **2018**, *8*, No. 5856.
(25) Jäger, V. D.; Lamm, R.; Kloss, R.; Kaganovitch, E.; Grünberger, A.; Pohl, M.; Büchs, J.; Jaeger, K.-E.; Krauss, U. A Synthetic Reaction Cascade Implemented by Colocalization of Two Proteins within Catalytically Active Inclusion Bodies. *ACS Synth. Biol.* **2018**, *7*, 2282−2295.
(26) Küsters, K.; Pohl, M.; Krauss, U.; Ölçücü, G.; Albert, S.; Jaeger, K.-E.; Wiechert, W.; Oldiges, M. Construction and comprehensive characterization of an EcLDCc-CatIB set-varying linkers and aggregation inducing tags. *Microb. Cell Fact.* **2021**, *20*, No. 49.
(27) Arié, J.-P.; Miot, M.; Sassoon, N.; Betton, J. M. Formation of active inclusion bodies in the periplasm of *Escherichia coli*. *Mol. Microbiol.* **2006**, *62*, 427−437.
(28) Choi, S.-L.; Lee, S. J.; Ha, J.-S.; Song, J. J.; Rhee, Y. H.; Lee, S.-G. Generation of catalytic protein particles in *Escherichia coli* cells using the cellulose-binding domain from *Cellulomonas fimi* as a fusion partner. *Biotechnol. Bioprocess Eng.* **2011**, *16*, 1173−1179.
(29) Park, S. Y.; Park, S. H.; Choi, S. K. Active inclusion body formation using *Paenibacillus polymyxa* PoxB as a fusion partner in *Escherichia coli*. *Anal. Biochem.* **2012**, *426*, 63−65.
(30) García-Fruitós, E.; Gonzalez-Montalban, N.; Morell, M.; Vera, A.; Ferraz, R. M.; Aris, A.; Ventura, S.; Villaverde, A. Aggregation as bacterial inclusion bodies does not imply inactivation of enzymes and fluorescent proteins. *Microb. Cell Fact.* **2005**, *4*, No. 27.
(31) Nahalka, J.; Nidetzky, B. Fusion to a pull-down domain: a novel approach of producing *Trigonopsis variabilis* D-amino acid oxidase as insoluble enzyme aggregates. *Biotechnol. Bioeng.* **2007**, *97*, 454−461.
(32) Zhou, B.; Xing, L.; Wu, W.; Zhang, X. E.; Lin, Z. Small surfactant-like peptides can drive soluble proteins into active aggregates. *Microb. Cell Fact.* **2012**, *11*, No. 10.
(33) Lin, Z.; Zhou, B.; Wu, W.; Xing, L.; Zhao, Q. Self-assembling amphipathic alpha-helical peptides induce the formation of active protein aggregates in vivo. *Faraday Discuss.* **2013**, *166*, 243−256.
(34) Wang, X.; Zhou, B.; Hu, W.; Zhao, Q.; Lin, Z. Formation of active inclusion bodies induced by hydrophobic self-assembling peptide GFIL8. *Microb. Cell Fact.* **2015**, *14*, No. 88.
(35) Ramón, A.; Senorale-Pose, M.; Marin, M. Inclusion bodies: not that bad. *Front. Microbiol.* **2014**, *5*, No. 56.
(36) Jiang, L.; Xiao, W.; Zhou, X.; Wang, W.; Fan, J. Comparative study of the insoluble and soluble Ulp1 protease constructs as Carrier free and dependent protein immobilizates. *J. Biosci. Bioeng.* **2019**, *127*, 23−29.
(37) Wu, W.; Xing, L.; Zhou, B.; Lin, Z. Active protein aggregates induced by terminally attached self-assembling peptide ELK16 in *Escherichia coli*. *Microb. Cell Fact.* **2011**, *10*, No. 9.
(38) Nahalka, J. Physiological aggregation of maltodextrin phosphorylase from *Pyrococcus furiosus* and its application in a process of batch starch degradation to alpha-D-glucose-1-phosphate. *J. Ind. Microbiol. Biotechnol.* **2008**, *35*, 219−223.
(39) Gifre-Renom, L.; Cano-Garrido, O.; Fabregas, F.; Roca-Pinilla, R.; Seras-Franzoso, J.; Ferrer-Miralles, N.; Villaverde, A.; Bach, A.; Devant, M.; Aris, A.; Garcia-Fruitos, E. A new approach to obtain pure and active proteins from *Lactococcus lactis* protein aggregates. *Sci. Rep.* **2018**, *8*, No. 13917.
(40) Tufvesson, P.; Lima-Ramos, J.; Nordblad, M.; Woodley, J. M. Guidelines and cost analysis for catalyst production in biocatalytic processes. *Org. Process Res. Dev.* **2011**, *15*, 266−274.
(41) Rinas, U.; Garcia-Fruitos, E.; Corchero, J. L.; Vazquez, E.; Seras-Franzoso, J.; Villaverde, A. Bacterial Inclusion Bodies: Discovering Their Better Half. *Trends Biochem. Sci.* **2017**, *42*, 726−737.
(42) Stetefeld, J.; Jenny, M.; Schulthess, T.; Landwehr, R.; Engel, J.; Kammerer, R. A. Crystal structure of a naturally occurring parallel right-handed coiled coil tetramer. *Nat. Struct. Biol.* **2000**, *7*, 772−776.
(43) Han, H.; Zeng, W.; Zhang, G.; Zhou, J. Active tyrosine phenol-lyase aggregates induced by terminally attached functional peptides in *Escherichia coli*. *J. Ind. Microbiol. Biotechnol.* **2020**, *47*, 563−571.
(44) Jäger, V. D.; Piqueray, M.; Seide, S.; Pohl, M.; Wiechert, W.; Jaeger, K.-E.; Krauss, U. An Enzymatic 2-Step Cofactor and Co-Product Recycling Cascade towards a Chiral 1,2-Diol. Part II: Catalytically Active Inclusion Bodies. *Adv. Synth. Catal.* **2019**, *361*, 2616−2626.
(45) Kloss, R.; Karmainski, T.; Jäger, V. D.; Hahn, D.; Grünberger, A.; Baumgart, M.; Krauss, U.; Jaeger, K.-E.; Wiechert, W.; Pohl, M. Tailor-made catalytically active inclusion bodies for different applications in biocatalysis. *Catal. Sci. Technol.* **2018**, *8*, 5816−5826.
(46) Shaner, N. C.; Campbell, R. E.; Steinbach, P. A.; Giepmans, B. N.; Palmer, A. E.; Tsien, R. Y. Improved monomeric red, orange and yellow fluorescent proteins derived from Discosoma sp. red fluorescent protein. *Nat. Biotechnol.* **2004**, *22*, 1567−1572.
(47) Man, H.; Kędziora, K.; Kulig, J.; Frank, A.; Lavandera, I.; Gotor-Fernández, V.; Rother, D.; Hart, S.; Turkenburg, J. P.; Grogan, G. Structures of Alcohol Dehydrogenases from Ralstonia and Sphingobium spp. Reveal the Molecular Basis for Their Recognition of 'Bulky−Bulky' Ketones. *Top. Catal.* **2014**, *57*, 356−365.
(48) van Pouderoyen, G.; Eggert, T.; Jaeger, K. E.; Dijkstra, B. W. The crystal structure of *Bacillus subtilis* lipase: a minimal alpha/beta hydrolase fold enzyme. *J. Mol. Biol.* **2001**, *309*, 215−226.
(49) Carrió, M.; Cubarsi, R.; Villaverde, A. Fine architecture of bacterial inclusion bodies. *FEBS Lett.* **2000**, *471*, 7−11.

https://doi.org/10.1021/acssynbio.2c00035
ACS Synth. Biol. 2022, 11, 1881−1896

(50) Jansen, R.; Küsters, K.; Morschett, H.; Wiechert, W.; Oldiges, M. A fully automated pipeline for the dynamic at-line morphology analysis of microscale Aspergillus cultivation. *Fungal Biol. Biotechnol.* **2021**, *8*, No. 2.
(51) Doglia, S. M.; Ami, D.; Natalello, A.; Gatti-Lafranconi, P.; Lotti, M. Fourier transform infrared spectroscopy analysis of the conformational quality of recombinant proteins within inclusion bodies. *Biotechnol. J.* **2008**, *3*, 193−201.
(52) Peternel, Š.; Grdadolnik, J.; Gaberc-Porekar, V.; Komel, R. Engineering inclusion bodies for non denaturing extraction of functional proteins. *Microb. Cell Fact.* **2008**, *7*, No. 34.
(53) Lamm, R.; Jäger, V. D.; Heyman, B.; Berg, C.; Curten, C.; Krauss, U.; Jaeger, K.-E.; Büchs, J. Detailed small-scale characterization and scale-up of active YFP inclusion body production with *Escherichia coli* induced by a tetrameric coiled coil domain. *J. Biosci. Bioeng.* **2020**, *129*, 730−740.
(54) Baumer, B.; Classen, T.; Pohl, M.; Pietruszka, J. Efficient Nicotinamide Adenine Dinucleotide Phosphate [NADP(H)] Recycling in Closed-Loop Continuous Flow Biocatalysis. *Adv. Synth. Catal.* **2020**, *362*, 2894−2901.
(55) Lavandera, I.; Kern, A.; Ferreira-Silva, B.; Glieder, A.; de Wildeman, S.; Kroutil, W. Stereoselective bioreduction of bulky-bulky ketones by a novel ADH from Ralstonia sp. *J. Org. Chem.* **2008**, *73*, 6003−6005.
(56) Ronda, L. B. S.; Bruno, S.; Campanini, B.; Mozzarelli, A.; Abbruzzetti, S.; Viappiani, C.; Cupane, A.; Levantino, M.; Bettati, S. Immobilization of Proteins in Silica Gel: Biochemical and Biophysical Properties. *Curr. Org. Chem.* **2015**, *19*, 1653−1668.
(57) Cellesi, F.; Tirelli, N. Sol−gel synthesis at neutral pH in W/O microemulsion: A method for enzyme nanoencapsulation in silica gel nanoparticles. *Colloids Surf., A* **2006**, *288*, 52−61.
(58) Huang, Z.; Zhang, C.; Chen, S.; Ye, F.; Xing, X. H. Active inclusion bodies of acid phosphatase PhoC: aggregation induced by GFP fusion and activities modulated by linker flexibility. *Microb. Cell Fact.* **2013**, *12*, No. 25.
(59) Longerich, S. *Funktionell aktive Proteinaggregate zur Realisierung einer Enzymkaskade in katalytisch-aktiven Inclusion Bodies*, Master Thesis; Heinrich Heine University Düsseldorf: Düsseldorf, 2017; p 75.
(60) Bertani, G. Studies on lysogenesis. I. The mode of phage liberation by lysogenic *Escherichia coli*. *J. Bacteriol.* **1951**, *62*, 293−300.
(61) Studier, F. W. Protein production by auto-induction in high density shaking cultures. *Protein Expression Purif.* **2005**, *41*, 207−234.
(62) Gasteiger, E. H. C.; Gattiker, A.; Duvaud, S. E.; Wilkins, M. R.; Appel, R. D.; Bairoch, A. Protein Identification and Analysis tools on the ExPASy Server. In *The Proteomics Protocols Handbook*, Walker, J. M., Ed.; Humana Press: Totowa, 2005; pp 571−607.
(63) Bradford, M. M. A rapid and sensitive method for the quantitation of microgram quantities of protein utilizing the principle of protein-dye binding. *Anal. Biochem.* **1976**, *72*, 248−254.
(64) Schneider, C. A.; Rasband, W. S.; Eliceiri, K. W. NIH Image to ImageJ: 25 years of image analysis. *Nat. Methods* **2012**, *9*, 671−675.

2.1.1. Publication 1. Supporting Information

Gizem Ölçücü, Benedikt Baumer, Kira Küsters, Kathrin Möllenhoff, Marco Oldiges, Jörg Pietruszka, Karl-Erich Jaeger, and Ulrich Krauss*

*corresponding author

ACS Synthetic Biology 11 (2022), pp. 1881-1896. Reprinted with permission from [184]. https://pubs.acs.org/doi/10.1021/acssynbio.2c00035

Catalytically-Active Inclusion Bodies – Benchmarking and Application in Flow Chemistry

Gizem Ölçücü[†,‡], Benedikt Baumer[$], Kira Küsters[‡], Kathrin Möllenhoff[⊥], Marco Oldiges[‡,#], Jörg Pietruszka[$,‡], Karl-Erich Jaeger[†,‡] and Ulrich Krauss[†,‡,*]

[†]Institute of Molecular Enzyme Technology, Heinrich Heine University Düsseldorf, Forschungszentrum Jülich GmbH, Wilhelm Johnen Strasse, D-52425 Jülich, Germany

[$]Institute of Biorganic Chemistry, Heinrich Heine University Düsseldorf, Forschungszentrum Jülich GmbH, Wilhelm Johnen Strasse, D-52425 Jülich, Germany

[‡]Institute of Bio- and Geosciences IBG-1: Biotechnology, Wilhelm Johnen Strasse, Forschungszentrum Jülich GmbH, D-52425 Jülich, Germany

[⊥] Mathematical Institute, Heinrich Heine University Düsseldorf, Universitätsstrasse 1, 40225, Düsseldorf, Germany

[#]Institute of Biotechnology, RWTH Aachen University, Worringer Weg 3, D-52074 Aachen, Germany

*Corresponding author. E-mail: u.krauss@fz-juelich.de. Phone: +49 2461-61-2939.

Supporting Information

Abbreviations

ADH	Alcohol dehydrogenase
CatIBs	Catalytically active inclusion bodies
ee	Enantiomeric excess
EtOAc	Ethyl acetate
FLLEX	Flow Liquid Liquid Extraction
GC	Gas chromatography
MTBE	Methyl tert-butyl ether
PE	Petrol ether
RADH	*Ralstonia sp*.ADH
U	Units

Table S1. List of the constructs used in the study.

Construct name	
Soluble BsLA*,[1] Soluble RADH*,[2]	
N-terminally tagged	**C-terminally tagged**
18AWT-PT-mCherry L6KD-PT-mCherry GFIL8-PT-mCherry TdoT-mCherry*,[3]	mCherry-PT-18AWT mCherry-PT-L6KD mCherry-PT-GFIL8 mCherry-TdoT
18AWT-PT-BsLA L6KD-PT-BsLA GFIL8-PT-BsLA TdoT-L-BsLA*,[1]	BsLA-PT-18AWT BsLA-PT-L6KD BsLA-PT-GFIL8 BsLA-L-TdoT
18AWT-PT-RADH L6KD-PT-RADH GFIL8-PT-RADH TdoT-L-RADH*,[4]	RADH-PT-18AWT RADH-PT-L6KD RADH-PT-GFIL8 RADH-L-TdoT

All constructs harboring the synthetic tags 18AWT, L6KD or GFIL8 at either terminus contained the linker polypeptide with the amino acid sequence PTPPTTPTPPTTPTPTP, abbreviated as (PT). The mCherry constructs bearing the TdoT tag did not contain a linker. RADH and BsLA strains harboring the TdoT tag at either terminus contained a linker polypeptide with the amino acid sequence $(GGGS)_3$, abbreviated as (L). 21 of the strains listed in the table, namely N- and C-terminal synthetic tag bearing strains (18AWT-PT-mCherry, L6KD-PT-mCherry, GFIL8-PT-mCherry, mCherry-PT-18AWT, mCherry-PT-L6KD, mCherry-PT-GFIL8, 18AWT-PT-BsLA, L6KD-PT-BsLA, GFIL8-PT-BsLA, BsLA-PT-18AWT, BsLA-PT-L6KD, BsLA-PT-GFIL8, 18AWT-PT-RADH, L6KD-PT-RADH, GFIL8-PT-RADH, RADH-PT-18AWT, RADH-PT-L6KD and RADH-PT-GFIL8), and C-terminal TdoT bearing strains (mCherry-TdoT, BsLA-L-TdoT and and RADH-L-TdoT) were generated in this study. The remaining strains marked with an asterisk (*), namely the soluble enzyme controls, or reference constructs harboring the N-terminal TdoT tag for positive CatIB formation were generated elsewhere and referenced accordingly.

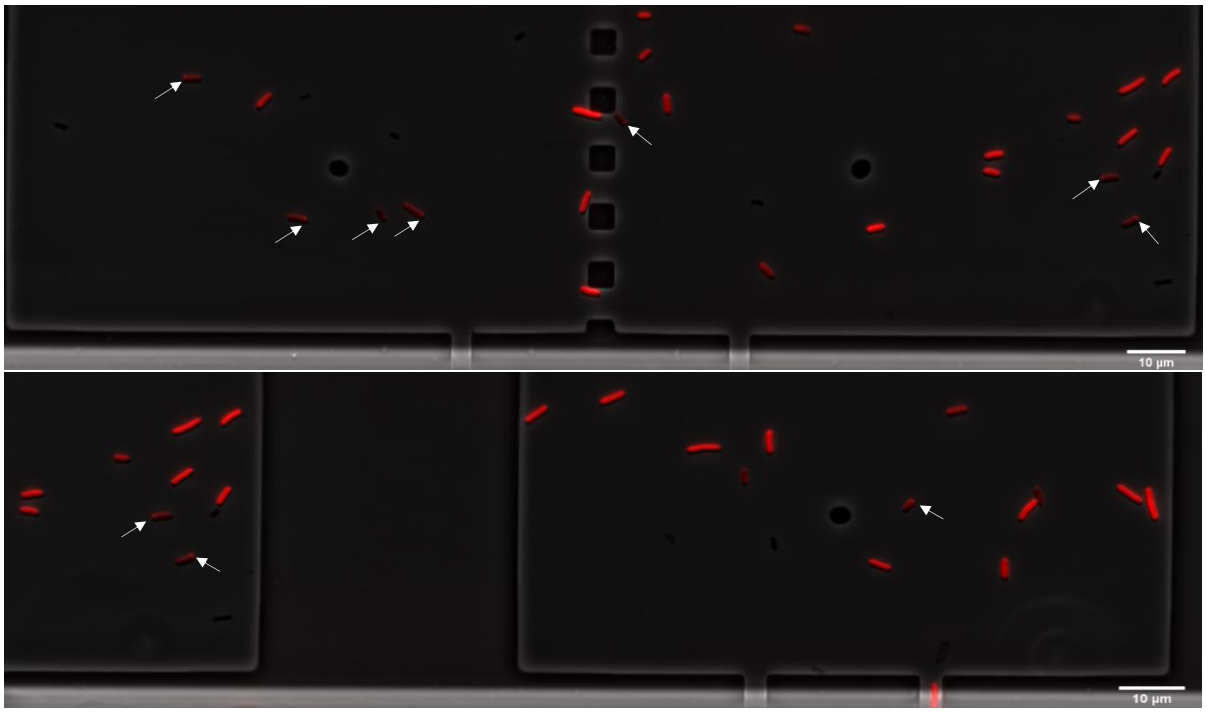

Figure S1. Fluorescence microscopy image examples of *E. coli* BL21(DE3) cells overproducing the mCherry-PT-18AWT fusion protein. Cells displaying either fluorescent CatIB formation (marked with white arrows) or uniform fluorescence can be seen.

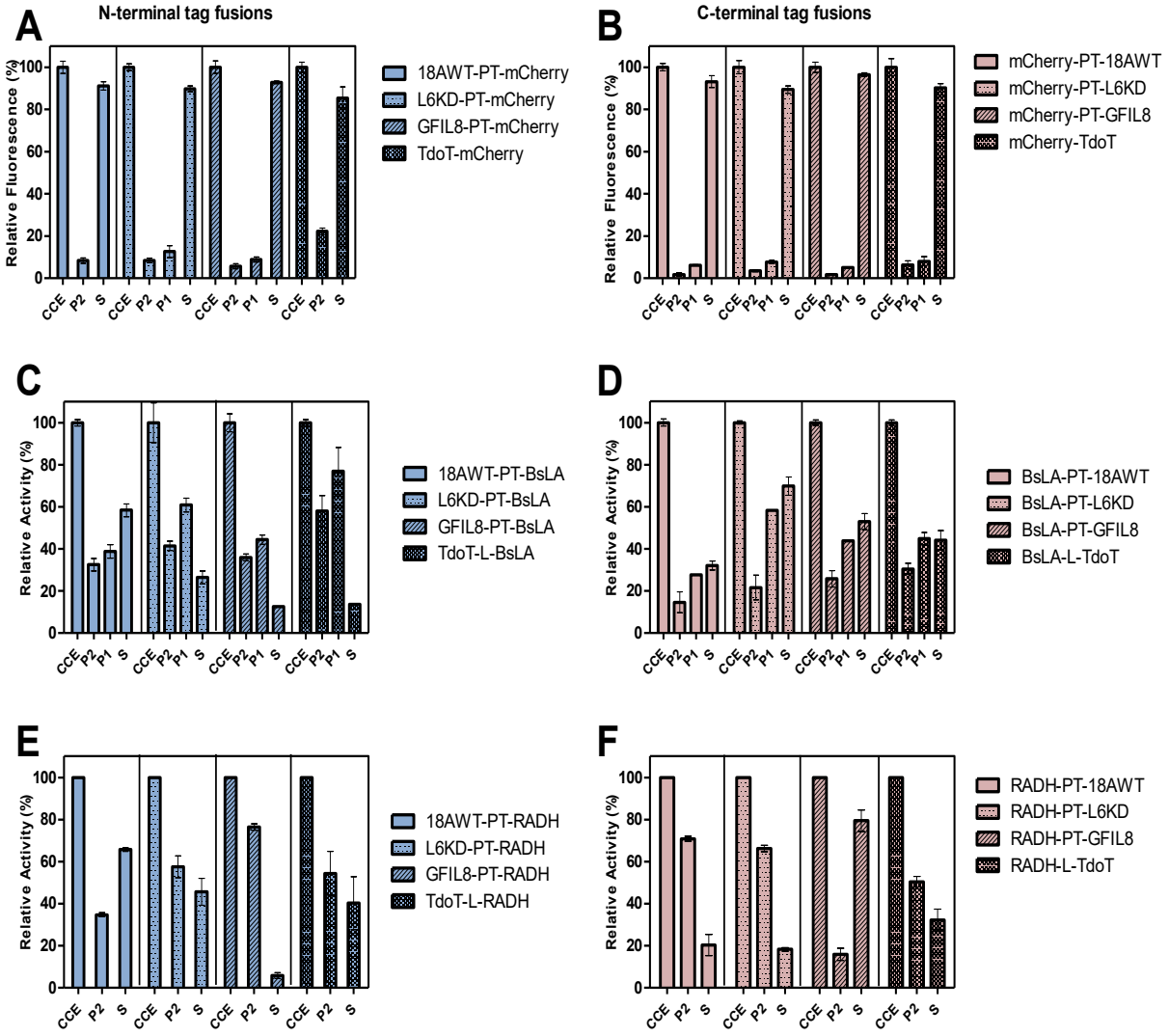

Figure S2. Relative fluorescence/activity of all cell fractions for the constructs evaluated in this study. CCE: crude cell extract. P2: washed pellet (CatIB fraction). P1: unwashed pellet. S: Supernatant. **(A)** Fluorescence distribution of N-terminal tag bearing mCherry constructs. **(B)** Fluorescence distribution of C-terminal tag bearing mCherry constructs. **(C)** Activity distribution of N-terminal tag bearing BsLA constructs. **(D)** Activity distribution of C-terminal tag bearing BsLA constructs. **(E)** Activity distribution of N-terminal tag bearing RADH constructs. **(F)** Activity distribution of C-terminal tag bearing RADH constructs.

Table S2. CatIB formation efficiencies of all mCherry, BsLA and RADH constructs, along with residual activity and stability data for lyophilized CatIBs of BsLA and RADH.

Constructs	CatIB formation efficiency[1] (%)		Residual activity[2] (%)		Activity remaining after 5 days[3] (%)	
	Mean	SE	Mean	SE	Mean	SE
mCherry						
18AWT-PT-mCherry	8.4	1.3	na	na	na	na
L6KD-PT-mCherry	8.4	1.1	na	na	na	na
GFIL8-PT-mCherry	5.7	1.3	na	na	na	na
TdoT-mCherry	22.2	1.6	na	na	na	na
mCherry-PT-18AWT	1.8	0.7	na	na	na	na
mCherry-PT-L6KD	3.5	0.3	na	na	na	na
mCherry-PT-GFIL8	1.8	0.2	na	na	na	na
mCherry-TdoT	6.3	1.9	na	na	na	na
BsLA						
18AWT-PT-BsLA	32.5	3.0	5.3	0.7	90.4	17.1
L6KD-PT-BsLA	41.5	2.3	19.8	2.7	86.1	11.5
GFIL8-PT-BsLA	36.0	1.7	19.9	0.1	85.8	1.8
TdoT-L-BsLA	58.0	7.4	6.1	0.2	88.3	6.0
BsLA-PT-18AWT	14.6	5.0	22.0	1.8	84.3	11.5
BsLA-PT-L6KD	21.5	5.9	6.4	0.5	85.2	10.6
BsLA-PT-GFIL8	25.7	4.0	20.2	1.7	87.6	13.1
BsLA-L-TdoT	30.4	2.7	18.8	0.8	81.2	8.2
RADH						
18AWT-PT-RADH	34.6	1.0	3.5	0.4	86.5 (1)	na
L6KD-PT-RADH	57.5	5.2	17.3	1.1	88.0 (1)	na
GFIL8-PT-RADH	76.4	1.5	18.3	3.0	95.8 (1)	na
TdoT-L-RADH	54.2	10.6	6.7 (2)	0.8	94.3 (1)	na
RADH-PT-18AWT	70.8	1.1	1.4	0.1	46.6* (1)	na
RADH-PT-L6KD	66.2	1.5	3.2	0.6	13.7 (1)	na
RADH-PT-GFIL8	15.8	2.9	0.6	0.1	11.2* (1)	na
RADH-L-TdoT	50.4	2.5	1.3	0.5	45.2 (1)	na

SE refers to standard error of the mean. Unless stated otherwise, the values were obtained from at least three biological replicates with three technical replicates each. For the cases where a different number of replicates were tested, the number of replicates is indicated within parentheses. **1:** Activity (or fluorescence) of the washed pellet fraction (P2) relative to the activity/fluorescence of the corresponding crude cell extract (set to 100%). **2:** Activity of the lyophilized CatIBs relative to the activity of the corresponding soluble purified enzyme (set to 100%). **3:** Activity of the lyophilized CatIBs after 5 days relative to the activity of the corresponding CatIBs measured on day 1. RADH CatIBs displaying low residual activities are marked with an asterisk (*), where the activity measurements were discontinued after day 3, and therefore the values listed in the table for the marked constructs refer to the activity remaining at day 3 instead.

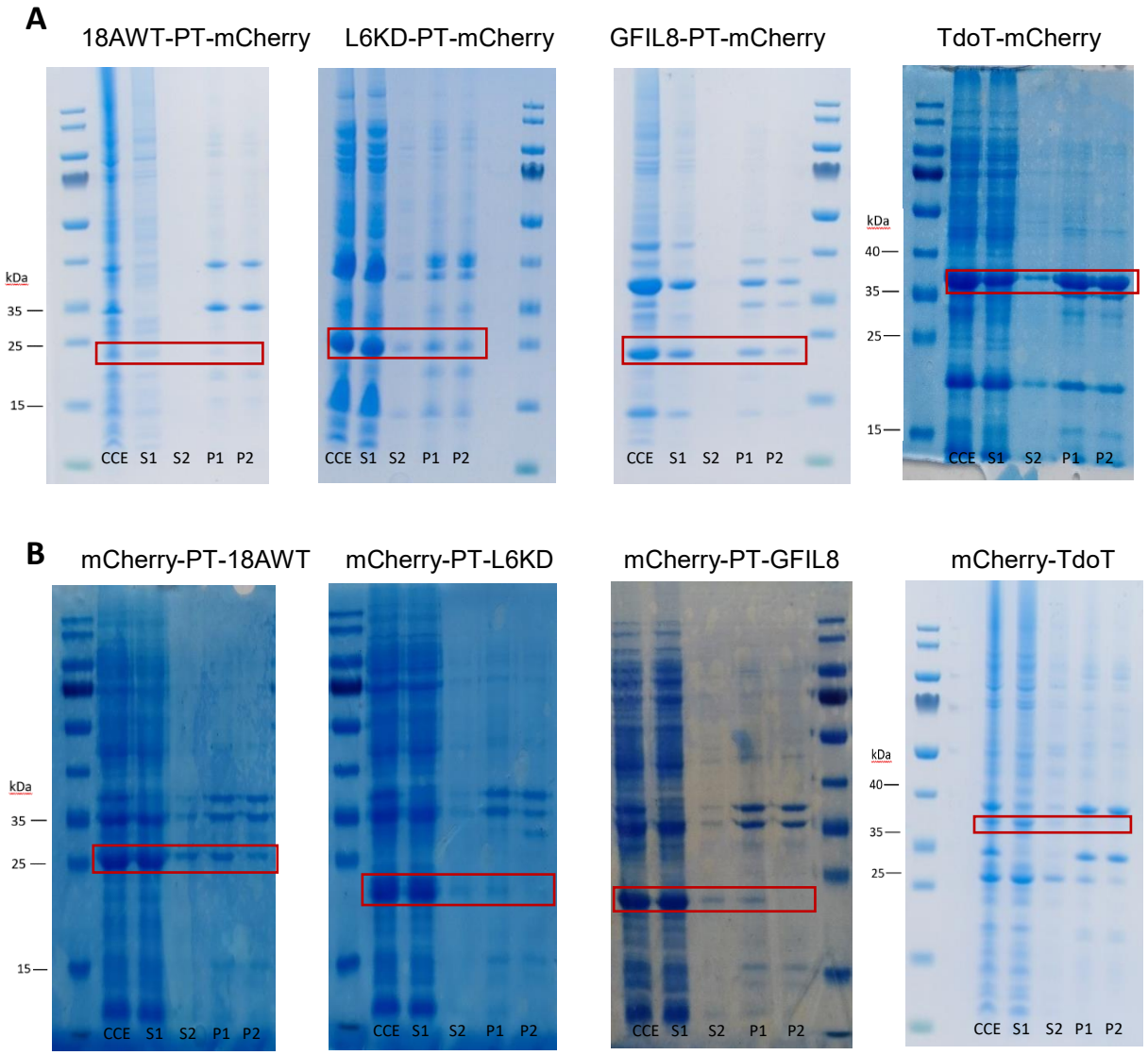

Figure S3. SDS-PAGE analyses of cell fractions of the constructs analyzed in the study producing the CatIB inducing tag-protein fusions. Fusion proteins in all fractions are highlighted using red rectangles. CCE: crude cell extract. S1: supernatant. S2: supernatant of the wash step. P1: unwashed pellet. P2: washed pellet (CatIB fraction). Protein content of the S1 fraction was determined with Bradford assay. For all constructs, the volume required to contain 10 µg protein for the S1 fraction was determined, and the same sample volume was used for the remaining CCE, S2, P1 and P2 fractions. **(A)** N-terminally tagged mCherry constructs, from left to right: 18AWT-PT-mCherry (31.1 kDa), L6KD-PT-mCherry (29.7 kDa), GFIL8-PT-mCherry (29.6 kDa), TdoT-mCherry (32.7 kDa). **(B)** C-terminally tagged mCherry constructs, from left to right: mCherry-PT-18AWT (31.1 kDa), mCherry-PT-L6KD (29.7 kDa), mCherry-PT-GFIL8 (29.6 kDa), mCherry-TdoT (32.7 kDa). **(C)** N-terminally tagged BsLA constructs, from left to right: 18AWT-PT-BsLA (23.6 kDa), L6KD-PT-BsLA (22.4 kDa), GFIL8-PT-BsLA (22.3 kDa),TdoT-L-BsLA (26.2 kDa). **(D)** C-terminally tagged BsLA constructs, from left to right: BsLA-PT-18AWT (23.6 kDa), BsLA-PT-L6KD (22.4 kDa), BsLA-PT-GFIL8 (22.3 kDa), BsLA-L-TdoT (26.2 kDa). **(E)** N-terminally tagged RADH constructs, from left to right: 18AWT-PT-RADH (31 kDa), L6KD-PT-RADH (29.6 kDa), GFIL8-PT-RADH (29.6 kDa), TdoT-L-RADH (34.2 kDa). **(F)** C-terminally tagged RADH constructs, from left to right: RADH-PT-18AWT (31 kDa), RADH-PT-L6KD (29.6 kDa), RADH-PT-GFIL8 (29.6 kDa), RADH-L-TdoT (34.2 kDa).

Figure S3 (continued)

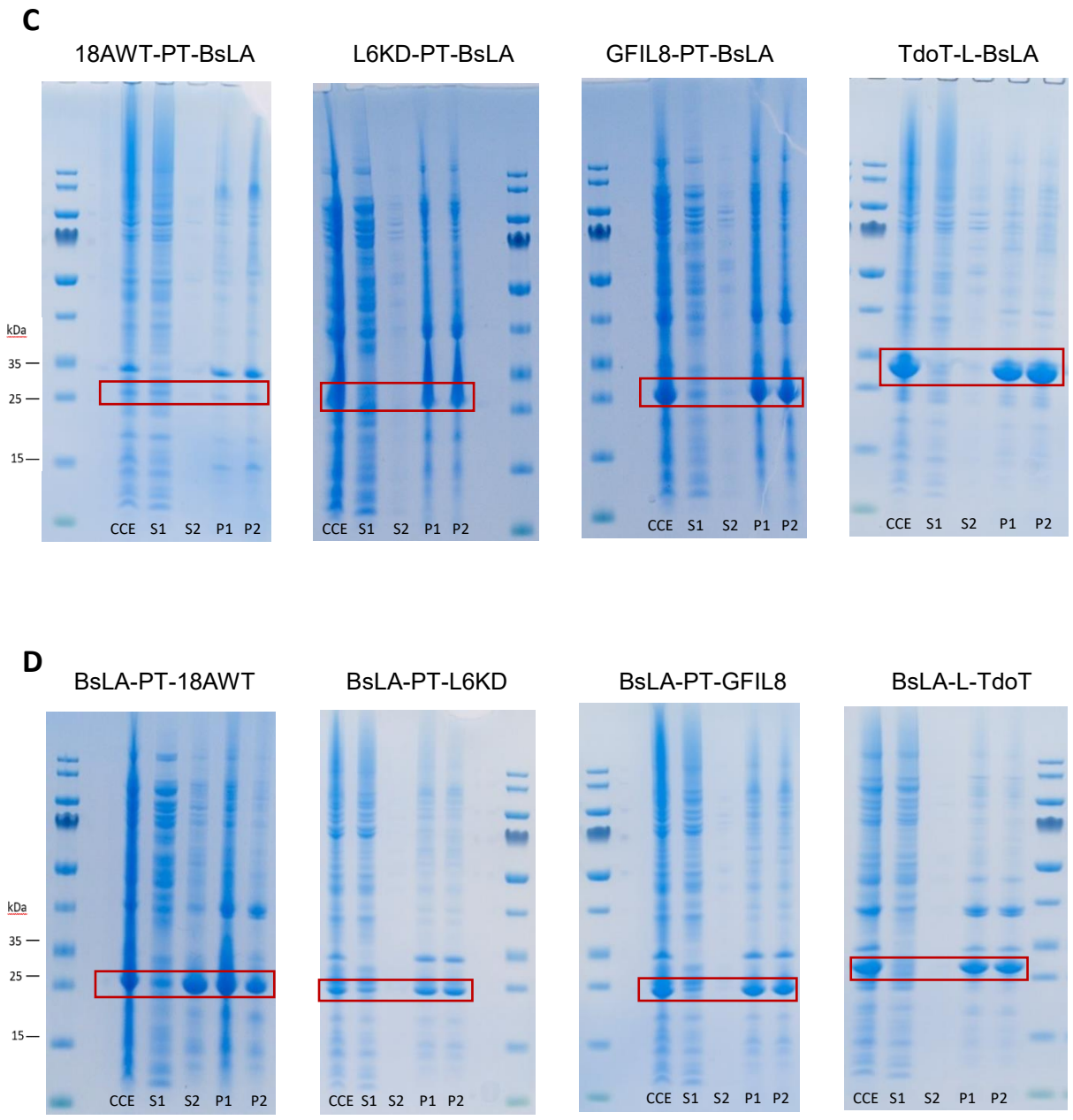

Figure S3 (continued)

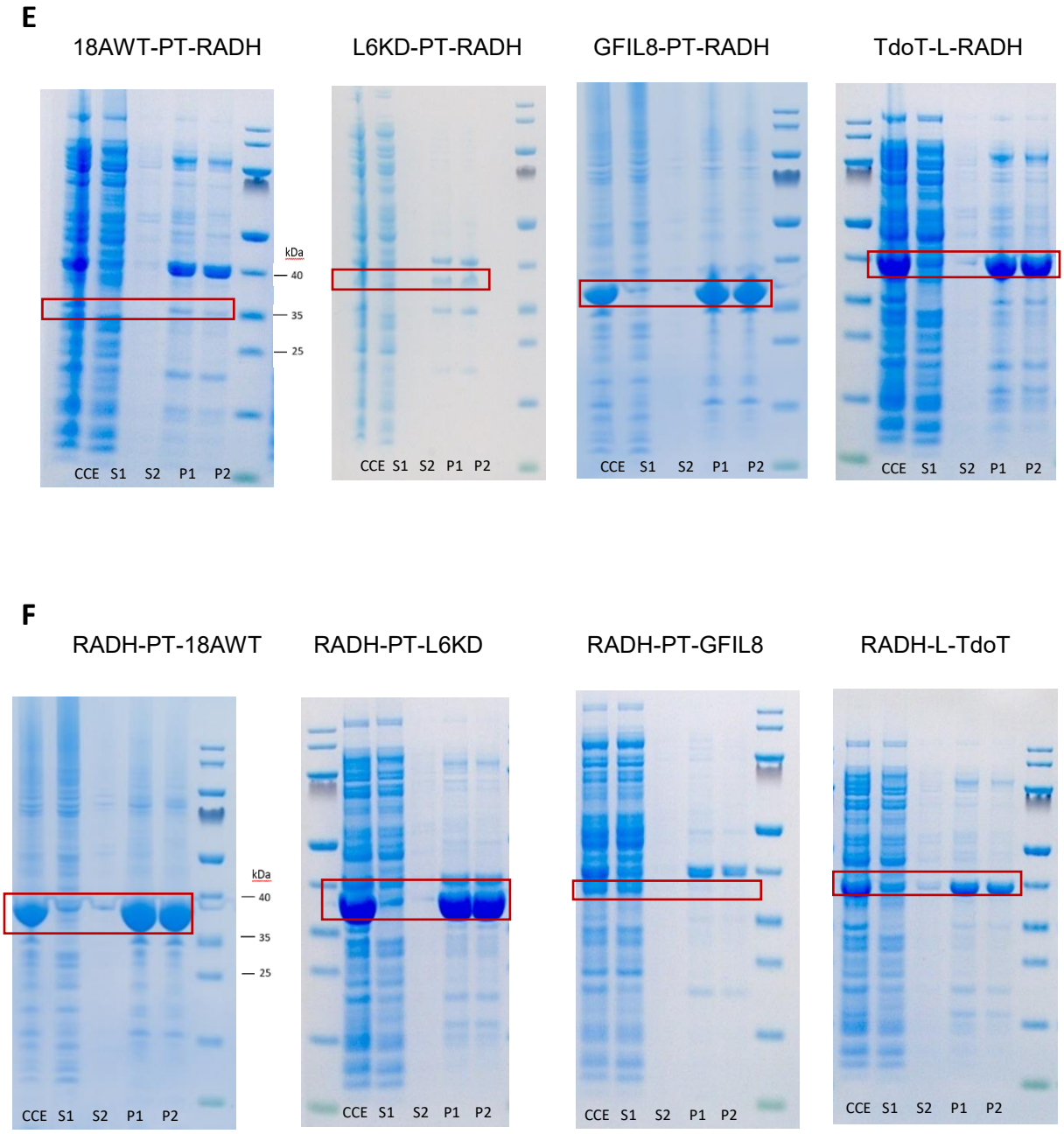

Table S3. Purity of CatIBs.

Construct	Area under the density peak		Purity (%)
	P2 lane	POI	
mCherry			
18AWT-PT-mCherry	28907.77	1992.841	6.9
L6KD-PT-mCherry	99533.852	9852.225	9.9
GFIL8-PT-mCherry	39438.285	5279.134	13.4
TdoT-mCherry	192454.591	52922.146	27.5
mCherry-PT-18AWT	183819.876	19083.083	10.4
mCherry-PT-L6KD	191419.4	7059.719	3.7
mCherry-PT-GFIL8	97060.65	1387.92	1.4
mCherry-TdoT	62569.5	1106.728	1.8
BsLA			
18AWT-PT-BsLA	98726.24	1993.506	2.0
L6KD-PT-BsLA	135301	34580.309	25.6
GFIL8-PT-BsLA	231851.4	66717.037	28.8
TdoT-L-BsLA	127935.2	49785.288	38.9
BsLA-PT-18AWT	90942.87	29822.78	32.8
BsLA-PT-L6KD	56435.6	17616.36	31.2
BsLA-PT-GFIL8	123932.4	39002.87	31.5
BsLA-L-TdoT	95264.59	30503.76	32.0
RADH			
18AWT-PT-RADH	78073.05	5316.012	6.8
L6KD-PT-RADH	87052	16316.983	18.7
GFIL8-PT-RADH	67186.7	38194.024	56.9
TdoT-L-RADH	107021.2	36667.803	34.3
RADH-PT-18AWT	88169.86	50239.26	57.0
RADH-PT-L6KD	72356.31	32409.05	44.8
RADH-PT-GFIL8	31864.95	842.263	2.6
RADH-L-TdoT	62432.33	17562.03	28.1

P2 lane: CatIB fraction (washed pellet) lane. POI: protein of interest in the P2 lane. Purity (%) for each case is calculated by converting the bands of the SDS-PAGE analyses to density peaks and applying the formula (area under the POI peak / area under the P2 lane) x 100.

Table S4. Protein content of lyophilized CatIBs, yields, and biomass specific activity yields of all constructs.

Construct	Protein content lyophilizate (%)		Yield (g lyophilizate/ 100 g wet cells)		Yield (mg protein/g wet cells)		Biomass Specific Activity Yield (U/g wet cells)	
	Mean	SE	Mean	SE	Mean	SE	Mean	SE
mCherry								
18AWT-PT-mCherry	52.7	12.4	1.9	0.1	9.9	2.2	na	na
L6KD-PT-mCherry	46.2	2.4	1.9	0.3	8.6	1.1	na	na
GFIL8-PT-mCherry	49.5	5.6	2.0	0.1	9.7	1.4	na	na
TdoT-mCherry	63.0	2.2	2.5	0.2	16.2	2.9	na	na
mCherry-PT-18AWT	31.3	10.7	1.2	0.3	3.1	0.6	na	na
mCherry-PT-L6KD	47.8	6.7	1.9	0.4	8.5	0.5	na	na
mCherry-PT-GFIL8	32.5	0.8	1.7	0.5	5.5	1.5	na	na
mCherry-TdoT	42.0	6.7	1.7	0.1	7.0	0.6	na	na
BsLA								
18AWT-PT-BsLA	38.7	3.3	4.2	0.9	20.8	5.1	38.1	2.6
L6KD-PT-BsLA	49.2	3.3	8.5	1.0	43.0	7.6	391.1	73.2
GFIL8-PT-BsLA	52.0	2.8	7.7	0.7	40.3	4.4	366.2	19.6
TdoT-L-BsLA	100[1]	2.1	6.8	0.4	67.7	3.8	188.9	5.9
BsLA-PT-18AWT	29.0	3.9	1.6	0.4	5.2	1.9	52.7	2.0
BsLA-PT-L6KD	72.4	5.7	4.4	0.6	32.7	6.7	98.0	16.9
BsLA-PT-GFIL8	59.7	2.6	7.3	0.8	44.1	6.6	420.6	17.0
BsLA-L-TdoT	53.6	6.8	3.6	0.2	19.3	2.7	168.2	28.8
BsLA (soluble)	-	-	-	-	5.4 (1)	na	248.5	11.2
RADH								
18AWT-PT-RADH	85.8	2.1	4.3	0.7	37.2	6.7	2.2	0.2
L6KD-PT-RADH	95.0	4.1	3.1	0.2	29.6	2.4	9.0	0.8
GFIL8-PT-RADH	93.2	5.4	10.9	0.8	102.2	10.2	32.2	4.9
TdoT-L-RADH	90.0 (2)	7.1	5.2 (2)	0.2	47.1 (2)	5.4	5.3 (2)	0.2
RADH-PT-18AWT	93.3	1.4	5.1	0.4	47.9	3.4	1.1	0.03
RADH-PT-L6KD	91.5	0.9	5.1	0.6	46.7	5.4	2.8	0.6
RADH-PT-GFIL8	91.5	6.0	3.2	0.3	29.4	3.6	0.3	0.04
RADH-L-TdoT	90.2	4.2	5.8	0.8	51.4	5.9	1.1	0.4
RADH (soluble)	30.5[2]	6.2[2]	0.5[2,3]	na[2]	2.8[2]	na[2]	16.2	0.11

Unless stated otherwise, the values were obtained from at least three biological replicates with three technical replicates each. For the cases where a different number of replicates were tested, the number of replicates is then indicated within parentheses. SE refers to standard error.[1]: value approximated to 100% as the predicted extinction coefficient yields a protein content slightly above 100%.[2]: values taken from MS.c. thesis 'Characterization of Catalytically Active Ralstonia sp. Alcohol Dehydrogenase Inclusion Bodies' (2018) by Selina Seide (IBG-1, Forschungszentrum Jülich). [3]: Yield expressed as per liter *E. coli* culture after lyophilization (g/L).

Table S5. Extinction coefficients and molecular weights of all constructs, as calculated by the Expasy ProtParam tool (http://web.expasy.org/protparam)[5] derived from the amino acid sequences of the constructs.

Construct	Extinction coefficient (M^{-1} cm^{-1})	Molecular weight (Da)
mCherry constructs		
18AWT-PT-mCherry	41370	31073.35
L6KD-PT-mCherry	34380	29699.82
GFIL8-PT-mCherry	34380	29638.7
TdoT-mCherry	37360	32729.1
18AWT-PT-mCherry	41370	31073.35
L6KD-PT-mCherry	34380	29699.82
GFIL8-PT-mCherry	34380	29638.7
mCherry-TdoT	37360	32695.12
BsLA constructs		
18AWT-PT-BsLA	31400	23730.13
L6KD-PT-BsLA	24410	22356.6
GFIL8-PT-BsLA	24410	22295.48
TdoT-L-BsLA	27390	28380.91
BsLA-PT-18AWT	31400	23598.94
BsLA-PT-L6KD	24410	22225.41
BsLA-PT-GFIL8	24410	22164.29
BsLA-L-TdoT	27390	26884.4
RADH constructs		
18AWT-PT-RADH	21430	31081.58
L6KD-PT-RADH	14440	29708.05
GFIL8-PT-RADH	14440	29646.93
TdoT-L-RADH	17420	34313.89
RADH-PT-18AWT	21430	30950.39
RADH-PT-L6KD	14440	29576.86
RADH-PT-GFIL8	14440	29515.73
RADH-L-TdoT	17420	34235.85

Table S6. Oligonucleotides used and constructs generated in the study. The restriction sites are underlined.

Name	Sequence (5' - 3')	Construct generated
HindIII_TdoT_fw	TATATAAAGCTTATCATTAACGAA ACTGCCGATGACATCG	-C terminal TdoT -mCherry
TdoT_Stop_XhoI_rev	GTGGTGCTCGAGTTAAATGCTCG CGAGAATGGTGGACAC	-C terminal TdoT -mCherry
HindIII_RADH_fw	TATATAAAGCTTATGTATCGTCTG CTGAATAAAACCGCAG	-N terminal 18AWT, L6KD, GFIL8 -RADH
RADH_Stop_XhoI_rev	ATATATCTCGAGTTATTAAACCTG GGTCAGACCACC	-N terminal 18AWT, L6KD, GFIL8 -RADH
NdeI_RADH_fw	TATATCATATGTATCGTCTGCTGA ATAAAACCGCAGTTATTAC	-C terminal 18AWT, L6KD, GFIL8 -RADH
RADH_HindIII_rev	TATATAAAGCTTAACCTGGGTCA GACCACCATCAACAAACAG	-C terminal 18AWT, L6KD, GFIL8 -RADH
N-tag BsLA_fw	CCCGACGCCGAAGCTTATGGCT GAACACAATCCAGTCG	-N terminal 18AWT, L6KD, GFIL8 -BsLA
N-tag BsLA_rev	GGTGGTGGTGCTCGAGCTACGT ATTCTGGCCCCCGC	-N terminal 18AWT, L6KD, GFIL8 -BsLA
NdeI_BsLA_fw	TATATACATATGGCTGAACACAA TCCAGTCGTTATGGTTCACGG	-C terminal 18AWT, L6KD, GFIL8 -BsLA
BsLA_HindIII_rev	TATATAAAGCTTCGTATTCTGGC CCCCGCCGTTCAG	-C terminal 18AWT, L6KD, GFIL8 -BsLA
BsLA_C-term TdoT_fw	CCAGAATACGAAGCTTGGCGGT GGGTCTGGAGGC	-C terminal TdoT -BsLA
RADH_C-term TdoT_fw	GACCCAGGTTAAGCTTGGCGGT GGGTCTGGAGGC	-C terminal TdoT -RADH
C-term TdoT_rev	GGTGGTGGTGCTCGAGTTAAAT GCTCGCGAGAATGGTGG	-C terminal TdoT -BsLA and RADH

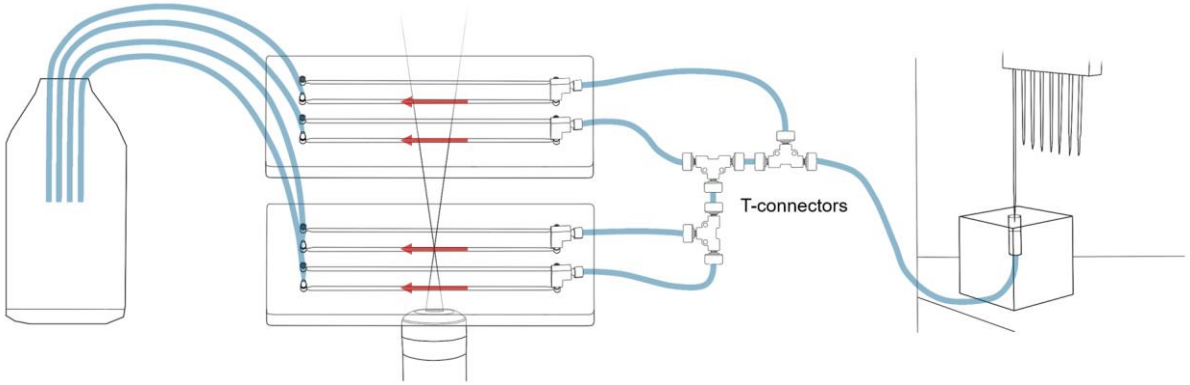

Figure S4. Scheme of the automated microscopy setup. Samples were injected into the injection station with a liquid handling system. The injection station was connected via tubing to two flow chambers. One channel of the flow chamber was focused by the microscope and a camera to take images. The other flow channels were used to lower down the pressure of the whole system. The samples were collected in a waste bottle after image acquisition.

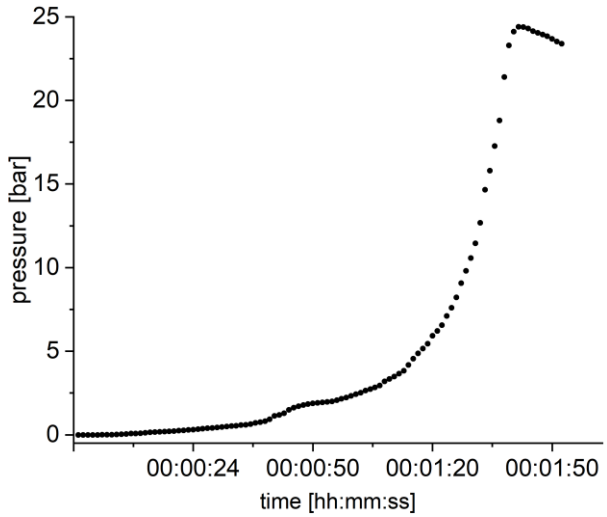

Figure S5. The initial test for packing the column was performed in the sandwich system. First, a small layer of silica was filled into the column. This was followed by rinsing with buffer from the opposite site to compact the silica. Then, the CatIBs were added and the rinsing step was repeated as far as possible due to high backpressure. Finally, the column was filled with silica and completed with another rinse step. However, this procedure was not the solution, because a very high backpressure occurred up to the pump maximum (~25 bar), which was subsequently switched off after ~1.40 min.

Table S7. Specific data on the columns used (e.g., bed height, amount of silica and CatIBs).

	Column 5 x 50 mm	**Column 5 x 150 mm**
Total bed height	2.20 cm	5.60 cm
Silica height ①	2.00 mm	2.00 mm
Amount of CatIBs ②	55.0 mg (12.1 U)	137 mg (30.3 U)
Amount of silica ②	138 mg	343 mg
CatIB / silica mixture height ②	1.90 cm	5.00 cm
Silica height ③	1.00 mm	4.00 mm

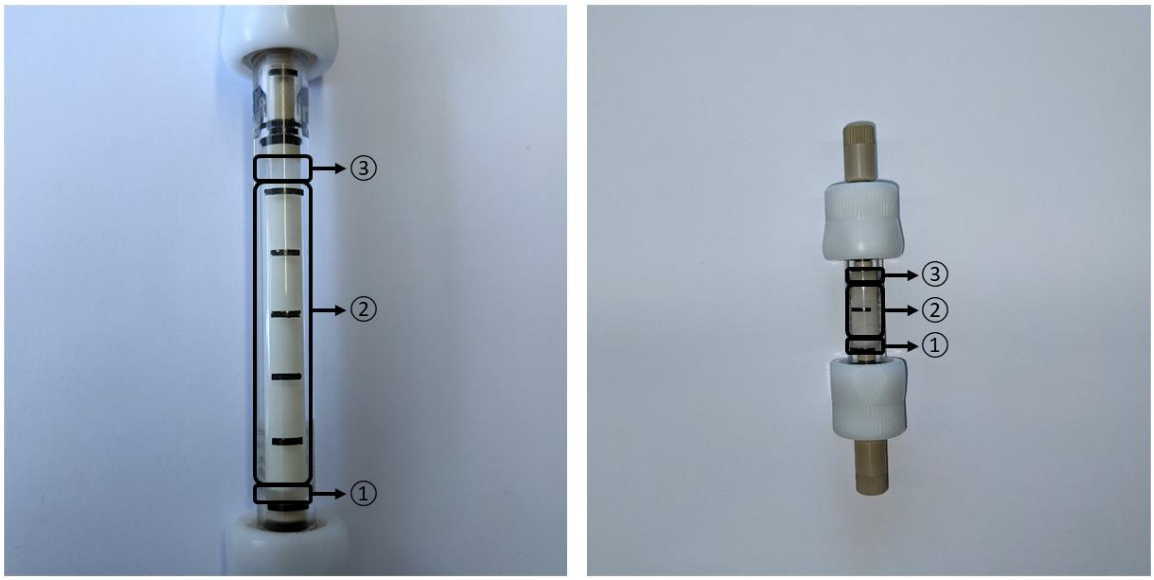

Figure S6. Pictorial representation of the two columns used. Left figure: 5 x 150 mm *Omnifit* column filled with 137 mg (30.3 U) of GFIL8-CatIBs. Right picture: 5 x 50 mm *Omnifit* column filled with 55.0 mg (12.1 U) of GFIL8-CatIBs. ① Silica layer, ② mixed CatIB / silica layer, ③ silica layer. Packing procedure is described in the experimental section.

Table S8. Enzyme catalyzed reduction of cyclohexanone (**1a**) to cyclohexanol (**2a**) in simple flow-through mode. Collection occurred after dead volume was overcome in 20 min steps. Conversion and ee were determined using GC. Flow rate was varied from 10.0 – 33.0 µL/min.

flow rate [µL/min]	**33.0**	**20.0**	**10.0**
time of collection [min]	conversion [%]	conversion [%]	conversion [%]
20	87.8	84.6	81.3
40	86.6	85.0	79.0
60	85.7	84.5	78.9
80	85.3	84.6	77.3
100	85.2	85.6	76.5
120	86.0	85.7	-

A 15.0 mM solution of cyclohexanone with 4.00 mL total volume and 7.50 vol% of 2-MeTHF was prepared. First, 50.0 mg of cyclohexanone (**1a**) were dissolved in 300 µL 2-MeTHF in vial 1. In vial 2, 53.2 mg NADPH were dissolved in TEA-buffer (50.0 mM, pH=7.50, 0.80 mM $CaCl_2$). Then, the solutions of vial 1 and vial 2 were mixed and the resulting solution was stirred continuously and filled in channel 1 of an Syrris Asia pump. As reactor, a pre-packed *Omnifit* column (5.00 mm x 50.0mm, packing as described in Methods and above) filled with CatIBs was used. Extraction was done using FLLEX-system with diisopropyl ether and the resulting product mixture was collected using an autosampler. Quick check for conversion was done using thin layer chromatography (PE:EtOAc 9:1). Exact conversion and ee were confirmed using gas chromatography. Analytical data: $\mathbf{R_f}$ = 0.15 (PE:EtOAc 9:1). **GC:** Column: CP Chirasil-DEX CB, Agilent Technologies (25 m × 0.25 mm); Retention time: t_R = 10.4 min (substrate **1a**), t_R = 13.5 min (product **1b**); Carrier gas: H_2, 0.60 bar; Solvent: MTBE; Method: 60 °C-5.00 min, 5.00 °C/min to 125 °C.

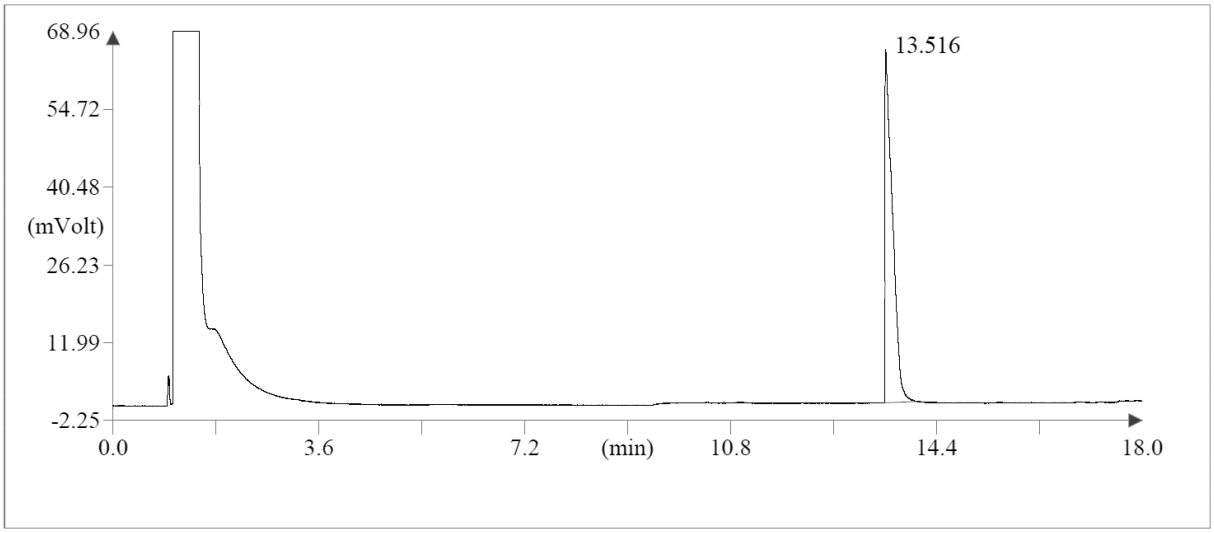

Figure S7. GC chromatogram of cyclohexanol (**2a**). For detailed method instructions see Table S7, t_R (**2a**)= 13.5 min

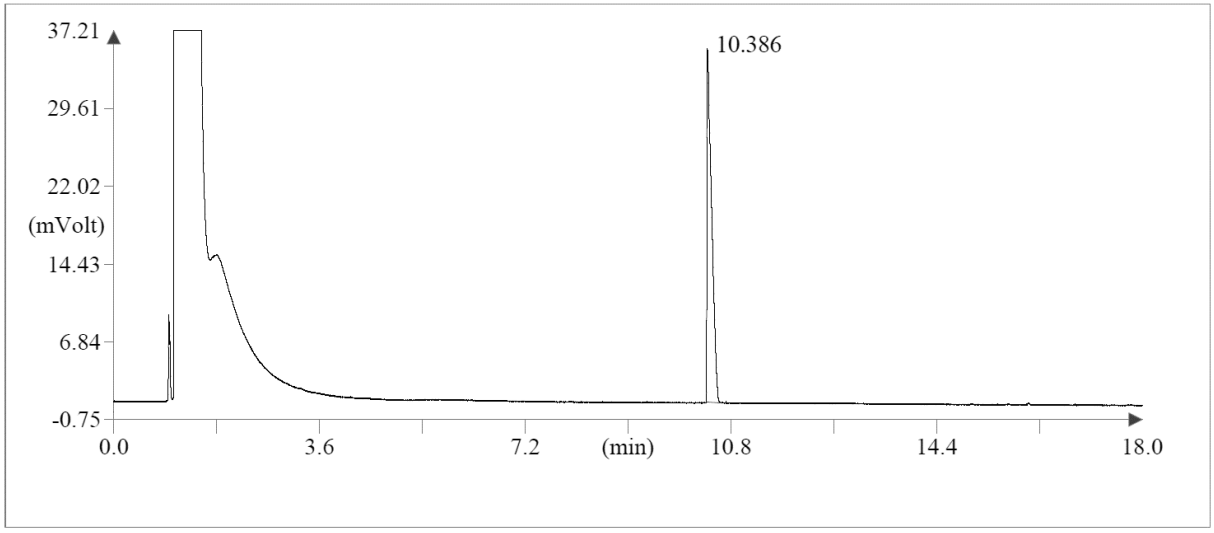

Figure S8. GC chromatogram of cyclohexanone (**1a**). For detailed method instructions see Table S7, t_R (**1a**) = 10.4 min

Table S9. Study on the acceptability of RADH-CatIBs towards 2-propanol and cyclohexanol (**2a**) as cosubstrates for batch cofactor regeneration. For more information see Methods (Batch synthesis).

cosubstrate / amount of RADH	**isopropanol / 2.20 U**		**cyclohexanol / 2.20 U**	
time of reaction control [h]	conversion [%]	ee [%]	conversion [%]	ee [%]
24	0.00	n.d.	27.7	98.2
96	0.46	n.d.	99.2	88.4

TableS10. Influence of doubling the amount of enzyme under the same reaction conditions as in **Table S8**, for more information see Methods (Batch synthesis).

cosubstrate / amount of RADH	**cyclohexanol / 4.40 U**	
time of reaction control [h]	conversion [%]	ee [%]
24	59.1	95.3
48	98.8	90.1
72	98.9	85.7

Table S11. Asymmetric reduction of *ω*-chloroacetophenone (**1b**) towards alcohol **2b** in simple flow-through mode. Collection occurred after dead volume was overcome in 20 min steps. Conversion and ee were determined using GC.

time of collection [min]	**conversion [%]**	**ee [%]**
20	99.9	94.2
40	99.9	94.3
60	99.8	93.1
80	99.8	93.5
100	99.9	92.9
120	99.9	94.0

A 15.0 mM solution of *ω*-chloroacetophenone (**1b**) with 4.00 mL total volume and 7.50 vol% of 2-MeTHF was prepared. First, 9.28 mg of ketone **1b** was dissolved in 300 µL 2-MeTHF in vial 1. In vial 2, 53.2 mg NADPH was dissolved in TEA-buffer (50.0 mM, pH=7.50, 0.80 mM $CaCl_2$). Then, the solutions of vial 1 and vial 2 were mixed and the resulting solution was stirred continuously and filled in channel 1 of an *Syrris Asia* pump. The mixed solution was then pumped at 33.0 µL/min through a pre-packed *Omnifit* column (5.00 mm x 50.0mm, see experimental section) filled with CatIBs. Extraction was done using FLLEX-system with diisopropyl ether and the resulting product mixture was collected using an autosampler. Quick check for conversion was done using thin layer chromatography (PE:EtOAc 9:1). Exact conversion and ee were confirmed using gas chromatography (for more information see Table S11)

Table S12. Screening for preliminary reactions conditions. Substrate concentrations were varied from 10.0 – 15.0 mM. Stoichiometric use of $NADP^+$ for the first three columns. The last column displays the results for 15.0 mM substrate and 2.00 mM $NADP^+$ concentration. Collection occurred after dead volume was overcome in 60 min steps. Conversion and ee were determined using GC. At this point it must be noted that the last experiment (last column) was carried out directly after the 10 mM-experiment, which is why the first conversion after 60 min (76.4%) could be faulty as it deviates significantly from the remaining values.

concentration [mM]	**10.0**		**12.5**		**15.0**		**15.0; 2.00 mM $NADP^+$**	
time of collection [min]	conversion [%]	ee [%]	conversion [%]	ee [%]	conversion [%]	ee [%]	conversion [%]	ee [%]
60	75.7	99.1	71.4	98.1	54.7	98.9	76.4	97.5
120	77.2	98.6	70.9	98.5	55.3	98.7	71.4	97.6
180	75.6	99.2	70.2	98.6	57.8	98.9	69.3	97.6
240	74.5	98.5	69.2	98.6	58.1	98.8	68.7	97.6
300	74.0	98.5	69.6	98.7	58.3	98.8	66.9	97.7
360	72.6	98.4	69.7	98.6	58.7	98.9	66.2	97.7

Basic information: Channel 1 (solution 1, aqueous): 4.00 mL total volume: 2.00/10.0/12.5/15.0 mM $NADPNa_2$ were dissolved in TEA-buffer (50.0 mM, pH=7.50, 0.80 mM $CaCl_2$). Channel 2 (solution 2, organic): The substrate was dissolved in cyclohexanol to result in 100/125/150 mM solution. However, due to the flow rate ratio between channel 1 & 2, the actual concentration in the reactor is 10.0/12.5/15.0 mM. Channel 3 (extraction, organic): Extraction was done in FLLEX with diisopropyl ether using Merck FHLP02500 PTFE membranes. **Reaction procedure:** Channels 1 & 2 of an *Syrris Asia* syringe pump were filled with prepared solutions 1 & 2. An *Omnifit* column (5.00 x 50.0 mm) with 55.0 mg / 12.1 U of catalytically active inclusion bodies (CatIBs) of RADH as catalyst was used as reactor (cartridge as described in experimental section). The flow rates were set to: Channel 1 30.0 µL/min, channel 2 3.00 µL/min and channel 3 33.0 µL/min. Product was collected with an autosampler and the aqueous layer was recycled into the initial vial. After the dead volume of the system was

overcome, product collection (in 20.0 min or 60.0 min steps) and recirculation of aqueous layer were started. Quick check for conversion was done using thin layer chromatography (PE:EtOAc 9:1). Exact conversion and ee were confirmed using gas chromatography. Analytical data: $\mathbf{R_f}$ = 0.25 (PE:EtOAc 9:1). 1H NMR (600 MHz, $CDCl_3$): δ = 7.34 – 7.29 (m, 4H), 7.28 – 7.23 (m, 1H), 4.83 (dd, *J* = 8.9, 3.4 Hz, 1H), 3.68 (dd, *J* = 11.3, 3.4 Hz, 1H), 3.58 (dd, *J* = 11.3, 8.9 Hz, 1H). ^{13}C NMR (151 MHz, $CDCl_3$): δ = 140.03 (C-2), 128.85 (C-4), 128.61 (C-5), 126.17 (C-3), 74.22 (C-1), 52.45 (C-1'). IR (ATR, Film): ũ = 3546, 3385 (OH), 1494, 1454, 1427, 1248, 1199, 1085, 1062, 1011, 916, 870, 825, 766, 721, 696, 613, 544, 521; **GC:** Column: FS Hydrodex βTBDAc, Macherey&Nagel (25 m × 0.25 mm); Retention time: t_R = 11.5 min (*R* enantiomer), 12.4 min (*S* enantiomer); Carrier gas: H_2, 0.60 bar; Solvent: MTBE; Method: 60 °C-15.0 min, 5 °C/min to 150 °C-5.00 min.

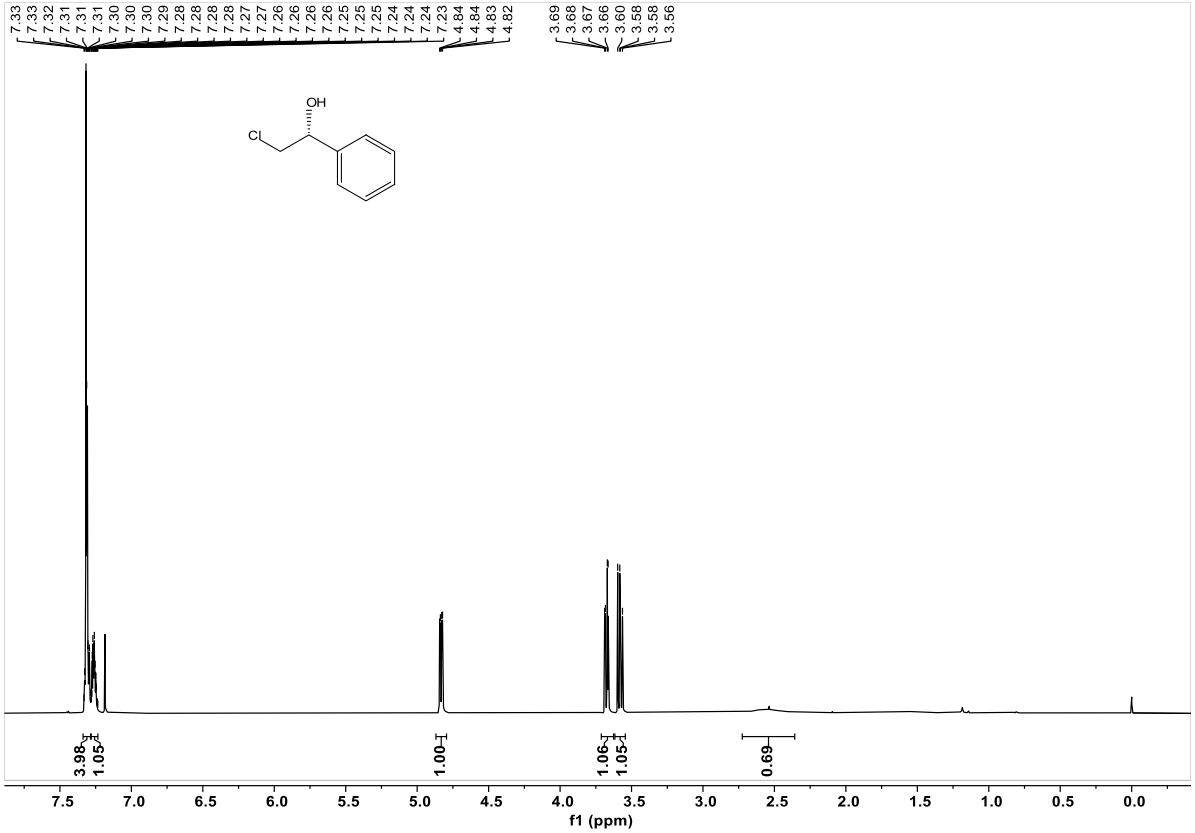

Figure S9. ^1H-NMR (600 MHz, $CDCl_3$) of alcohol **2b**.

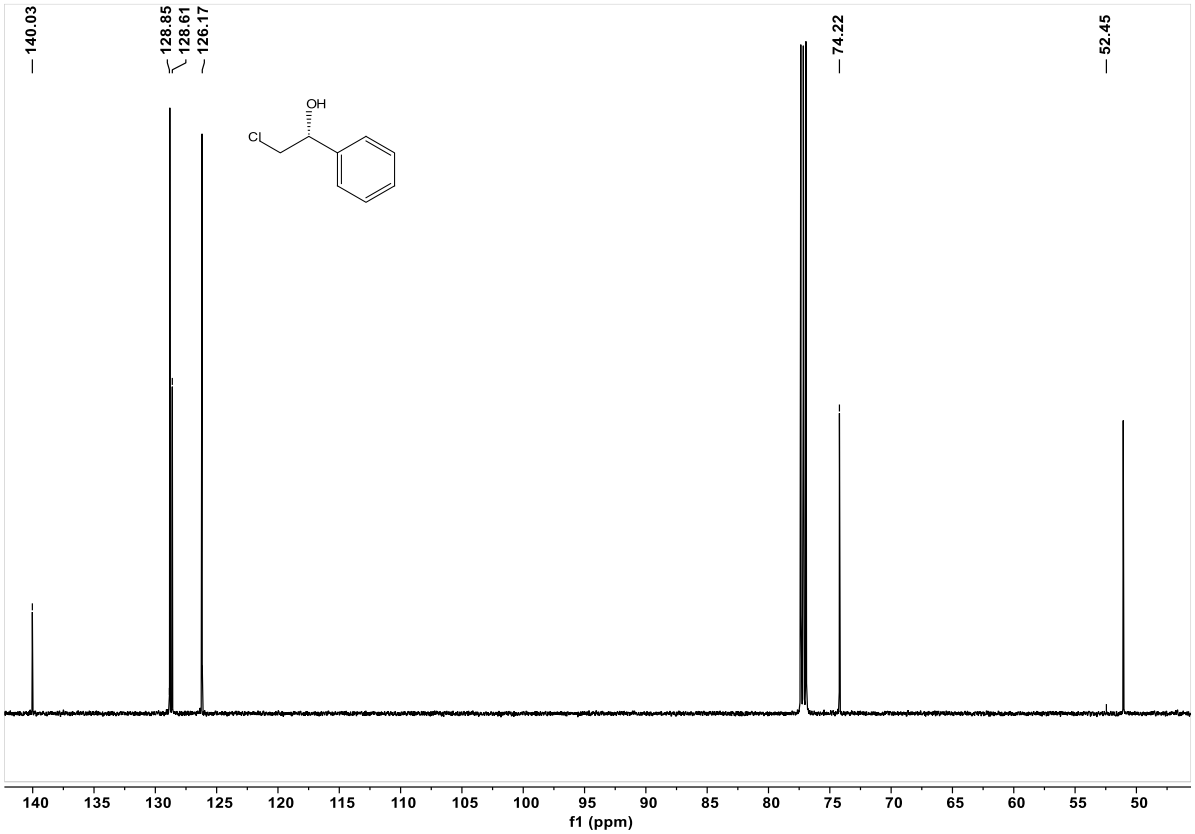

Figure S10. ^{13}C-NMR (151 MHz, $CDCl_3$) of alcohol **2b**.

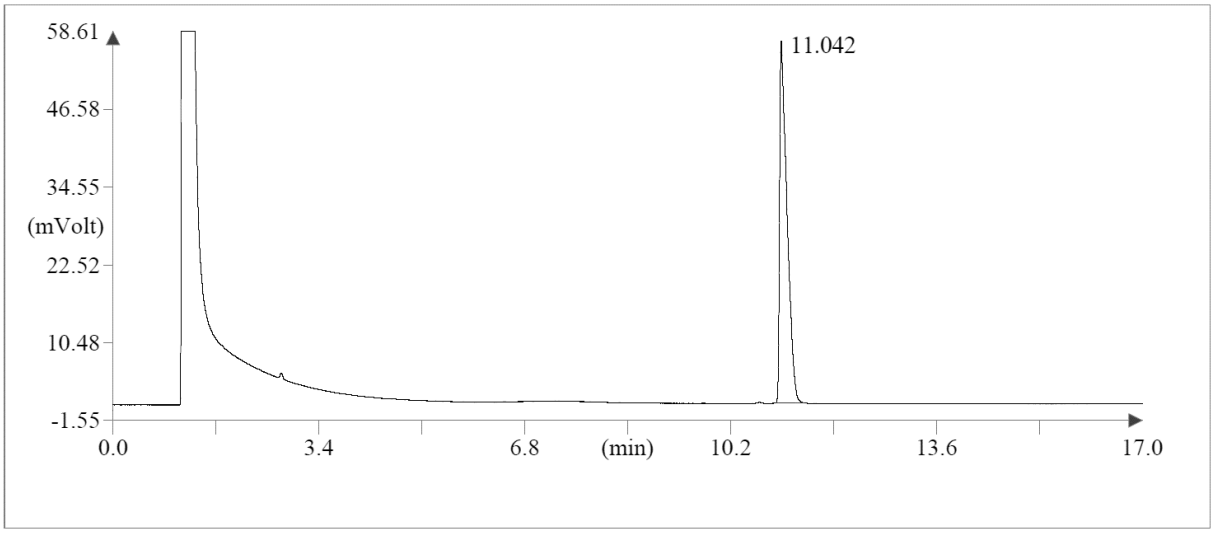

Figure S11. GC chromatogram of *ω*-chloroacetophenone (**1b**). For detailed method instructions see Table S11, t_R (**1b**) = 11.0 min

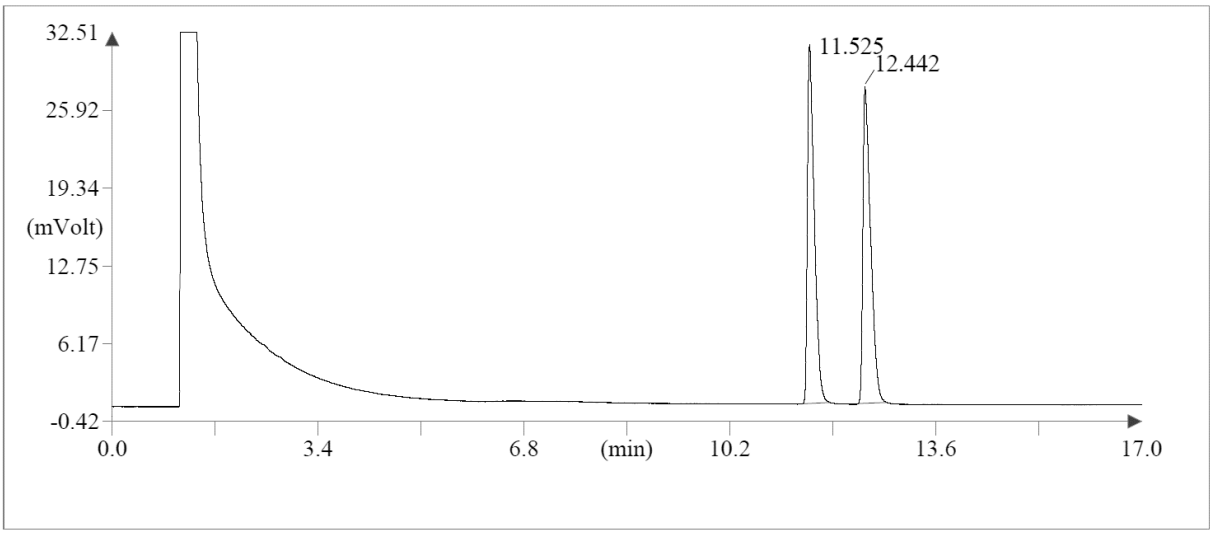

Figure S12. GC chromatogram of (*R*)-2-Chloro-1-phenylethan-1-ol (**2b**). For detailed method instructions see Table S11, t_R [(*R*)-**2b**] = 11.5 min, t_R [(*S*)-**2b**] = 12.4 min.

Supporting References

[1] Diener, M., Kopka, B., Pohl, M., Jaeger, K.-E., and Krauss, U. (2016) Fusion of a Coiled-Coil Domain Facilitates the High-Level Production of Catalytically Active Enzyme Inclusion Bodies, *ChemCatChem 8*, 142-152.

[2] Kulig, J., Frese, A., Kroutil, W., Pohl, M., and Rother, D. (2013) Biochemical characterization of an alcohol dehydrogenase from Ralstonia sp, *Biotechnol Bioeng 110*, 1838-1848.

[3] Jager, V. D., Kloss, R., Grunberger, A., Seide, S., Hahn, D., Karmainski, T., Piqueray, M., Embruch, J., Longerich, S., Mackfeld, U., Jaeger, K. E., Wiechert, W., Pohl, M., and Krauss, U. (2019) Tailoring the properties of (catalytically)-active inclusion bodies, *Microb Cell Fact 18*, 33.

[4] Jager, V. D., Lamm, R., Kloss, R., Kaganovitch, E., Grunberger, A., Pohl, M., Buchs, J., Jaeger, K. E., and Krauss, U. (2018) A Synthetic Reaction Cascade Implemented by Colocalization of Two Proteins within Catalytically Active Inclusion Bodies, *ACS Synth Biol 7*, 2282-2295.

[5] Wilkins, M. R., Gasteiger, E., Bairoch, A., Sanchez, J. C., Williams, K. L., Appel, R. D., and Hochstrasser, D. F. (1999) Protein identification and analysis tools in the ExPASy server, *Methods Mol Biol 112*, 531-552.

2.2. Publication 2. Construction and comprehensive characterization of an EcLDCc-CatIB set — varying linkers and aggregation inducing tags

Kira Küsters, Martina Pohl, Ulrich Krauss, Gizem Ölçücü, Sandor Albert, Karl-Erich Jaeger, Wolfgang Wiechert and Marco Oldiges*

*corresponding author

Microbial Cell Factories 20.49 (2021).
https://doi.org/10.1186/s12934-021-01539-w

Author Contributions: KK planned, realized and analyzed all experiments. MP provided the positive control and the DNA sequences of TDoT- and 3HAMP-Tag, and helped planning the experiments. UK helped planning the experiments. GÖ provided the DNA sequences of 18AWT-, L6KD- and GFIL8-Tag. SA did preliminary experiments on which the mentioned experiments were based on. KEJ helped to finalize the manuscript. WW helped to finalize the manuscript. MO helped to finalize the manuscript and supervised the entire project. All authors have read and approved the final manuscript.

Küsters *et al. Microb Cell Fact* (2021) 20:49
https://doi.org/10.1186/s12934-021-01539-w

Microbial Cell Factories

RESEARCH Open Access

Construction and comprehensive characterization of an *Ec*LDCc-CatIB set—varying linkers and aggregation inducing tags

Kira Küsters[1,2], Martina Pohl[1], Ulrich Krauss[1,3], Gizem Ölçücü[1,3], Sandor Albert[1,4], Karl-Erich Jaeger[1,3], Wolfgang Wiechert[1,5] and Marco Oldiges[1,2*]

Abstract

Background: In recent years, the production of inclusion bodies that retained substantial catalytic activity was demonstrated. These catalytically active inclusion bodies (CatIBs) were formed by genetic fusion of an aggregation inducing tag to a gene of interest via short linker polypeptides and overproduction of the resulting gene fusion in *Escherichia coli*. The resulting CatIBs are known for their high stability, easy and cost efficient production, and recyclability and thus provide an interesting alternative to conventionally immobilized enzymes.

Results: Here, we present the construction and characterization of a CatIB set of the lysine decarboxylase from *Escherichia coli* (*Ec*LDCc), constructed *via* Golden Gate Assembly. A total of ten *Ec*LDCc variants consisting of combinations of two linker and five aggregation inducing tag sequences were generated. A flexible Serine/Glycine (SG)- as well as a rigid Proline/Threonine (PT)-Linker were tested in combination with the artificial peptides (18AWT, L6KD and GFIL8) or the coiled-coil domains (TDoT and 3HAMP) as aggregation inducing tags. The linkers were fused to the C-terminus of the *Ec*LDCc to form a linkage between the enzyme and the aggregation inducing tags. Comprehensive morphology and enzymatic activity analyses were performed for the ten *Ec*LDCc-CatIB variants and a wild type *Ec*LDCc control to identify the CatIB variant with the highest activity for the decarboxylation of L-lysine to 1,5-diaminopentane. Interestingly, all of the CatIB variants possessed at least some activity, whilst most of the combinations with the rigid PT-Linker showed the highest conversion rates. *Ec*LDCc-PT-L6KD was identified as the best of all variants allowing a volumetric productivity of 457 g L^{-1} d^{-1} and a specific volumetric productivity of 256 g L^{-1} d^{-1} $g_{CatIB}{}^{-1}$. Noteworthy, wild type *Ec*LDCc, without specific aggregation inducing tags, also partially formed CatIBs, which, however showed lower activity compared to most of the newly constructed CatIB variants (volumetric productivity: 219 g L^{-1} d^{-1}, specific volumetric activity: 106 g L^{-1} d^{-1} $g_{CatIB}{}^{-1}$). Furthermore, we demonstrate that microscopic analysis can serve as a tool to find CatIB producing strains and thus allow for prescreening at an early stage to save time and resources.

Conclusions: Our results clearly show that the choice of linker and aggregation inducing tag has a strong influence on the morphology and the enzymatic activity of the CatIBs. Strikingly, the linker had the most pronounced influence on these characteristics.

*Correspondence: m.oldiges@fz-juelich.de
[2] Institute of Biotechnology, RWTH Aachen University, 52074 Aachen, Germany
Full list of author information is available at the end of the article

Keywords: Catalytically active inclusion bodies, Immobilization, Protein aggregates, Protein engineering, Downstream processing, Microscopic analysis, Enzymes

Background

Enzymes produced by microbial systems becoming increasingly important, e.g., for the sustainable production of platform chemicals and bio-based polymers [1–4]. Due to their advantages, like heat resistance, tensile strength and electrical insulation, polyamides are interesting for diverse applications in the electrical, automotive and textile industry as well as for consumer articles and in the medical sector [5]. One successful example of a biotechnologically produced precursor for a bio-based polyamide is 1,5-diaminopentane (DAP). Together with dicarbonic acids like sebacic acid, this C5 diamine building block is used to build up polyamides (PA). The resulting PA 5.10 (5: 1,5-diaminopentane (C5); 10: sebacic acid (C10)) shows comparable or even better material properties compared to the widely used petroleum-based polyamide PA 6 (6: caprolactam (C6)) [6]. DAP can be biotechnologically produced from L-lysine by enzymatic decarboxylation through the constitutive lysine decarboxylase (LDCc) [7] or the acid-induced variant CadA [8] from *Escherichia coli*. Both enzymes use pyridoxal 5'-phosphate (PLP) as a cofactor. Kloss and coworkers showed a workflow where *Corynebacterium glutamicum* was used to produce L-lysine from glucose. The L-lysine was then enzymatically decarboxylated to yield DAP by the native *Ec*LDCc, which was overproduced in *E. coli*, [9].

In biocatalysis such enzymatic conversions are often performed using whole cell systems or purified soluble enzymes, whereas Kloss et al. used catalytically active inclusion bodies (CatIBs) of the *Ec*LDCc to decarboxylate L-lysine to DAP [7–9]. Even though purified enzymes can be used to catalyze reactions with high activities, their application requires respective costly and laborious downstream processing and purification procedures [10–13]. Moreover, the recycling of purified enzymes from biotransformations is more difficult to achieve and usually requires application of membrane separation, membrane reactor application or particle-based immobilization strategies [14–16].

To simplify the reusability and enhance the stability, immobilization of enzymes is often used, resulting in macromolecular or heterogeneous catalysts [17–19]. Common immobilization strategies rely first on the production of the soluble enzyme in an expression host. Subsequently, purification and lastly immobilization by e.g. covalent binding, cross-linking, binding the enzyme to carrier or entrapment of the enzyme is performed [20, 21]. However, enzyme immobilization often comes at the expense of overall activity of the immobilized enzyme preparation. This could be either due to reduced activity of the enzyme or the reduced mass transfer of reaction partners within the immobilized protein matrix.

A simpler and more cost efficient strategy is the use of CatIBs. For a long time, inclusion bodies (IBs) were regarded as inactive and misfolded protein aggregates. However studies revealed that catalytically active inclusion bodies with a reasonable residual activity can be produced by fusion of an enzyme of interest with a linker, composed of a few amino acids, and an aggregation inducing tag. Two recent reviews provided a comprehensive overview over suitable linker and aggregation inducing tags that have been successfully used for CatIB formation [22, 23]. The aggregation inducing tags in this study are the coiled coil domain of the cell-surface protein tetrabrachion from *Staphylothermus marinus* (TDoT) as well as the dimeric coiled coil domain from *Pseudomonas aeruginosa* (3HAMP) [9, 24, 25]. Moreover, the aggregation inducing tag properties of three artificial peptides, a small surfactant-like L6KD peptide, an amphipathic α-helical peptide (18AWT) and a hydrophobic self-assembling peptide (GFIL8) were also analyzed [26–28]. In contrast to other enzyme formulations CatIBs possess many advantages, such as (i) simple purification, (ii) high stability, (iii) easy long-term storage, (iv) carrier-free, biodegradable and biologically produced immobilization technology, (v) reusability as well as they are considered as (vi) essentially GMO-free after separation from the producer cells [9, 22, 24, 29, 30].

However, at present, there is only limited knowledge that would allow predicting a successful combination of a target enzyme, a linker and an aggregation inducing tag. For example, CatIB formation was tested for different enzymes, such as the benzaldehyde lyase from *Pseudomonas fluorescens*, the alcohol dehydrogenases from *Ralstonia sp.* and *Lactobacillus brevis* as well as for the *Bacillus subtilis* lipase A. Here, CatIBs with varying residual activity were formed, depending on the selected aggregation inducing tag [24, 26–28]. Thus, to realize efficient CatIB formation, many different variations need to be generated and tested to find the best-performing combination of target enzyme, linker and aggregation inducing tags. So far, most of the CatIBs described in literature were generated using traditional cloning methods, which limits the fast access to a CatIB library [24–28;31–35].

One option to create such a library is Golden Gate Assembly, which relies on Type IIS restriction enzymes. These enzymes cleave the DNA outside their recognition site, allowing the generation of specific desired overhangs. The generated four-nucleotide overhang can only be ligated to the matching DNA overhang from the following fragment. Because restriction digest and ligation happen at the same time, the reaction takes place in a so-called "one-pot setup" [36]. Due to these features of the Golden Gate Assembly, three different DNA elements can be assembled in an effortless manner, thereby allowing the high-throughput generation of large CatIB libraries. This speeds up the search for the best performing CatIB-construct, while at the same time allowing the generation of large datasets useful for understanding structure/function relationships between the CatIB constituting modules. This in turn, could enable a more rational prediction of suitable elements for CatIB formation in the future.

Here, we report the generation and characterization of an *Ec*LDCc-CatIB set, generated *via* Golden Gate Assembly. A combination of two different linkers and five different aggregation inducing tags were fused to the C-terminus of the *Ec*LDCc resulting in ten different combinations. The resulting CatIB variants were analyzed comprehensively with regard to CatIB and cell morphology as well as activity of the CatIBs, proving that the linker and aggregation inducing tag revealed a strong influence on these features.

Results and discussion

Production of CatIBs and microscopic analysis

The lysine decarboxylase of *E. coli* (*Ec*LDCc; EC 4.1.1.18), was C-terminally fused with one of two linkers (a flexible SG- or a rigid PT-Linker) as well as one aggregation inducing tag out of the set of five, TDoT, 18AWT, L6KD, GFIL8 and 3HAMP [9, 26–28, 37]. *Ec*LDCc shows a decameric quaternary structure with the N-terminus being buried at the inner side of the decameric ring-like structure. Therefore, the linkers and the aggregation inducing tags were fused to the C-terminus of the *Ec*LDCc. The ten different CatIB variants were produced in *E. coli* BL21(DE3) using M9 autoinduction medium (See Additional file 1: Table S2). The formation of *Ec*LDCc-CatIBs in this host was verified using phase contrast microscopy with a 1000-fold magnification (see Methods). CatIBs appear as white refractive particles or granule-like structures at the cell poles (Fig. 1), which is typical for IBs [38].

Microscopic analyses of all strains were performed to test if the CatIB variants produce CatIBs with different morphologies, and if CatIB production, in turn, affects the morphology of the producing cells. The positive control (*Ec*LDCc-Xa-SG-TDoT, more data about this variant was published by Kloss et al. [9]) formed dense CatIBs,

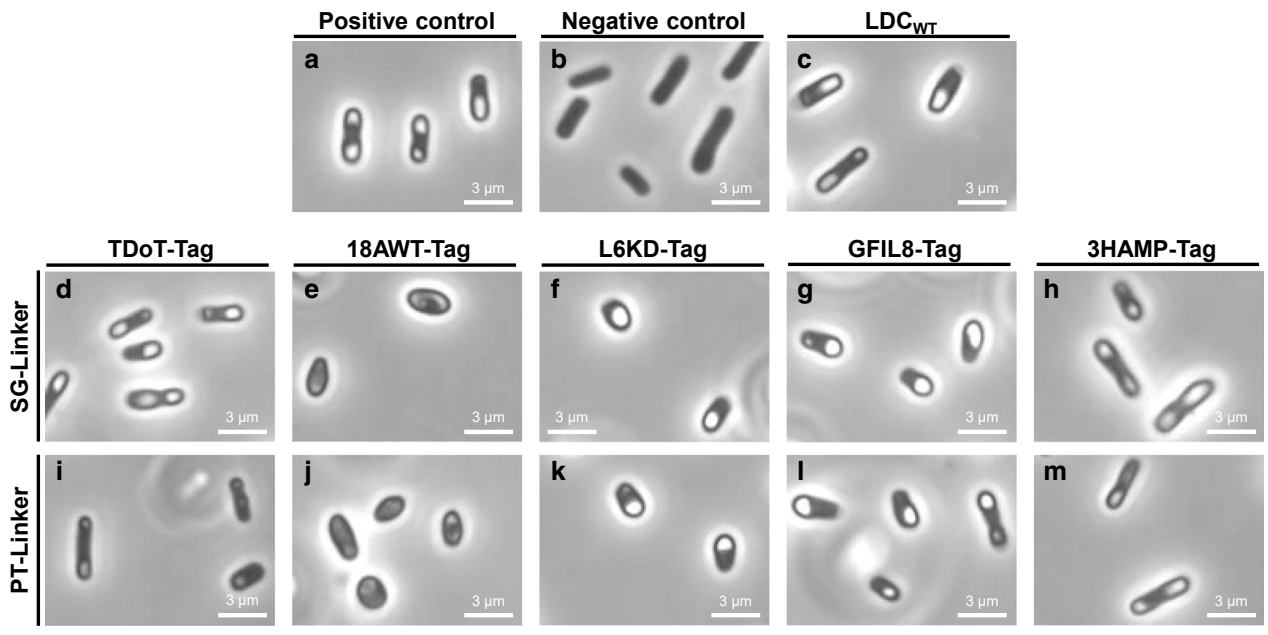

Fig. 1 Microscopic images of cells producing different *Ec*LDCc-CatIB variants and control cells at 1000-fold magnification. Cultivation was performed for 3 h at 37 °C and 69 h at 15 °C in M9-AI medium. **a** Positive control: *E. coli* BL21(DE3) with *Ec*LDCc-Xa-SG-TDoT [9], **b** Negative control: *E. coli* BL21(DE3) with pET28a, **c** wild type control: *E. coli* BL21(DE3) with *Ec*LDCc **d** *Ec*LDCc-SG-TDoT, **e** *Ec*LDCc-SG-18AWT, **f** *Ec*LDCc-SG-L6KD, **g** *Ec*LDCc-SG-GFIL8, **h** *Ec*LDCc-SG-3HAMP, **i** *Ec*LDCc-PT-TDoT, **j** *Ec*LDCc-PT-18AWT, **k** *Ec*LDCc-PT-L6KD, **l** *Ec*LDCc-PT-GFIL8, **m** *Ec*LDCc-PT-3HAMP

whereas the negative control (empty pET28a vector) did not show any detectable IBs. Contrary to expectation, the wild type *Ec*LDCc control also formed IBs, which usually is a consequence of strong gene expression and often results in complete activity loss of the enzyme [39–41].

Microscopic analysis of the *Ec*LDCc-CatIB variants revealed that different combinations of linkers and aggregation inducing tags led to different shapes of cells and IBs and morphologies. IBs were found very similar with both linkers and with the aggregation inducing tags L6KD, GFIL8, and 3HAMP. In contrast, the TDoT variant formed large and dense IBs in combination with the flexible SG-Linker only, while the respective *Ec*LDCc-PT-TDoT generated only small and diffuse IB structures and only 61 % of the cells carrying this construct produced IBs at all (Table 1). By contrast, the other CatIB producing variants showed that 71 % to 88 % of the cells produced CatIBs with a mean number of CatIBs per cell in the range of 1.18 for *Ec*LDCc-PT-L6KD up to 1.83 for *Ec*LDCc-PT-3HAMP. Strikingly, *E. coli* cells carrying constructs with the aggregation inducing tag 18AWT did not show any visible dense IBs at all. This might be because this tag is known to show a tendency to bind to the cell membrane [28], which could be responsible for the abnormal shape of the cells. Because of the absence of dense, refractive IBs, no further CatIB morphology analysis could be performed for these variants (Fig. 1). Absence of IBs in phase contrast microscopic images of the variants with aggregation inducing tag 18AWT, do not necessarily mean that there were no IBs at all. Small shaped or membrane associated IBs might had not detected, although IBs or even CatIBs could have been present. In this sense, different picture generating methods with higher precision, such as scanning electron microscopy could provide better insights.

Microscopic images were used for comprehensive image analysis to determine the size distribution of the CatIBs and their *E. coli* producer cells (Fig. 2). The cells, carrying the CatIB plasmid with the rigid PT-Linker, were smaller, except for the TDoT and 18AWT-Tag, compared to the cells with the flexible SG-Linker (Fig. 2a; Table 1). The cells producing the *Ec*LDCc-PT-TDoT variant showed the largest cells (6.14 µm^2) and the largest cell area distribution (1 µm^2 to 6.14 µm^2). The cell types producing the 18AWT variants revealed the smallest area (SG: 0.65 µm^2, PT: 0.93 µm^2) and the smallest median of the cell area distribution (SG: 2.01 µm^2, PT: 2.11 µm^2). These observations indicate that the linkers, as well as the aggregation inducing tags affect the cell morphology, i.e. size and shape.

Similar to the cell area analysis, the CatIB size analysis showed that the CatIBs seem to be smaller in combination with the PT-Linker (Fig. 2b). This time, also

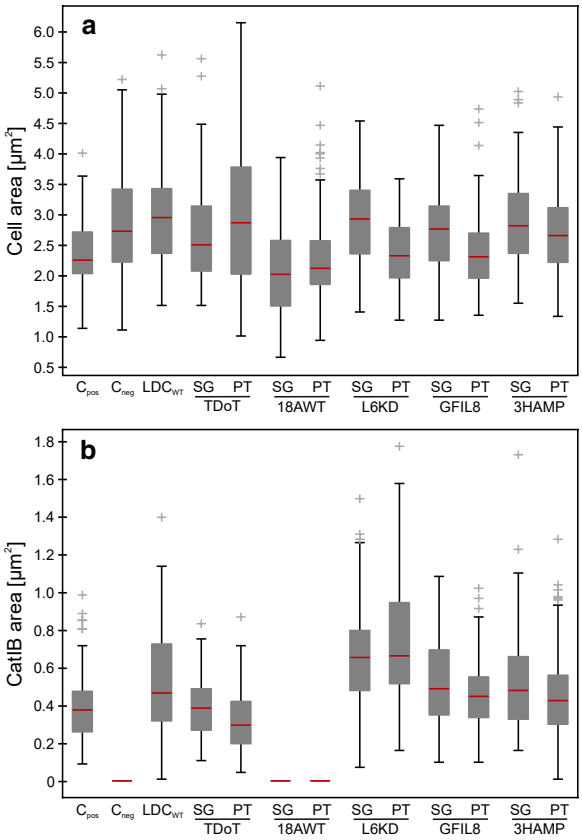

Fig. 2 Size distribution of **a** *Ec*LDCc-CatIB producer strains and **b** *Ec*LDCc-CatIBs. The median (red), the 25 and 75 % Quartiles (grey box), the 5 % and 95 % whiskers and the outliers (grey cross) of the cell or CatIB area were determined for each variant. Positive control: *E. coli* BL21(DE3) with *Ec*LDCc-Xa-SG-TDoT [9], negative control: *E. coli* BL21(DE3) with empty pET28a and wild type control: *E. coli* BL21(DE3) with pET28a::*Ec*LDCc, without any linker or aggregation inducing tag. n = 100. C_{pos} positive control, C_{neg} Negative control and LDC_{WT} wildtype *Ec*LDCc control

the TDoT variants showed the same trend. Only in combination with L6KD-Tag, the median of the distribution is similar for both linker types (PT: 0.66 µm^2 vs. SG: 0.65 µm^2) (Table 1). The TDoT-Tag combined with each one of the linkers revealed the smallest median of CatIB area and the smallest distribution of all variants (PT: 0.3 µm^2 vs. SG: 0.38 µm^2). Furthermore, *Ec*LDCc-PT-TDoT revealed the smallest CatIB area per cell area (15 %) due to large cells with small IBs. Compared to that, *Ec*LDCc-PT-L6KD showed the highest proportion of CatIB area per cell area (37 %) due to large IBs together with comparatively smaller cells. As mentioned before, no visible CatIBs were formed in combinations with 18AWT-Tag, which prohibited further morphological CatIB analysis. To conclude, the strongest influence on the CatIB area was observed for the

aggregation inducing tag, while the two linkers showed quite similar data for the same aggregation inducing tag.

Downstream processing and enzymatic activity of ten EcLDCc-CatIB variants

Besides the retained enzymatic activity of the CatIBs, a simple purification procedure, as well as a final high overall yield are important factors. In the end, the CatIB variant will be preferred that can be produced in high amounts in the cells and shows a high activity after purification. Thus, to find the best CatIB variant, not only microscopic and activity analyses, but also the CatIB purification process was included in the evaluation.

A previously established purification protocol [9] was simplified by using lysozyme instead of a high-pressure homogenizer for cell disruption, and testing the CatIBs directly after purification without lyophilization to enable the testing of many CatIB variants in parallel. Aliquots containing the same amount of purified CatIBs were prepared and half of these aliquots were used for the determination of CatIB weight and the other half was used for activity measurements. After purification, the production of *Ec*LDCc-CatIBs was verified by sodium dodecyl sulfate- (SDS) polyacrylamide gel electrophoresis (SDS-PAGE, Fig. 3). The SDS gel clearly shows respective bands of all *Ec*LDCc-CatIB variants only in the insoluble pellet fraction. Besides, the wild type *Ec*LDCc control showed a protein band in both the soluble and the pellet fraction. This is in good agreement with the microscopic images showing wild type *Ec*LDCc IB formation to some extent (Fig. 1). Variations in the apparent molecular mass of the different CatIB fusion proteins are due to different sizes of the aggregation inducing tags, with 3HAMP (172 aa) and TDoT (50 aa) being larger than the short tags L6KD (8 aa), 18AWT (18 aa) and GFIL8 (8 aa).

After CatIB purification and analysis *via* SDS-PAGE, an enzymatic activity assay was performed in 50 mM Kpi buffer (pH 7.2) using L-lysine (10 mM) as a substrate and PLP (0.1 mM) as the cofactor. First, the reproducibility of the CatIB purification procedure and the enzymatic activity assay workflow were tested. To this end, three biological replicates, as well as three analytical replicates of each sampling point were sampled from *Ec*LDCc-SG-L6KD

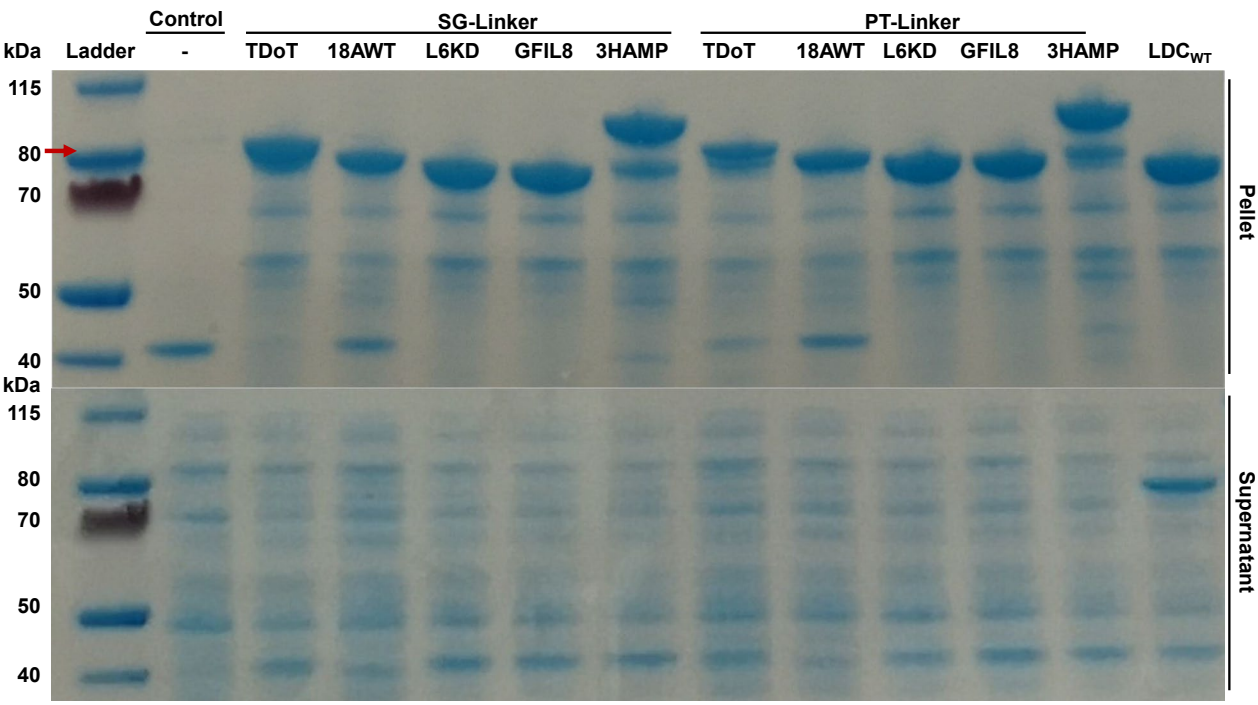

Fig. 3 Evaluation of CatIB formation by SDS-PAGE analysis. After cultivation, the optical density of the culture were normalized to $OD_{600\,nm} = 12.5$. The cells were disrupted and the crude cell extract was separated by centrifugation into the soluble protein containing supernatant and the insoluble CatIB-containing pellet fractions. The pellet fraction was washed once with Milli-Q® water. The samples were diluted 1:1 with SDS sample buffer and 15 µL of each sample was loaded onto the gel and stained with SimplyBlue™ SafeStain. The molecular mass of the wildtype *Ec*LDCc (81.88 kDa) is indicated by a red arrow. Molecular mass of negative control (empty pET28a): 0 kDa; *Ec*LDCc-SG-TDoT: 87.66 kDa; *Ec*LDCc-SG-18AWT: 84.22 kDa, *Ec*LDCc-SG-L6KD: 82.85 kDa, *Ec*LDCc-SG-GFIL8: 82.79 kDa, *Ec*LDCc-SG-3HAMP: 100.59 kDa, *Ec*LDCc-PT-TDoT: 88.48 kDa; *Ec*LDCc-PT-18AWT: 85.04 kDa, *Ec*LDCc-PT-L6KD: 83.67 kDa, *Ec*LDCc-PT-GFIL8: 83.61 kDa, *Ec*LDCc -PT-3HAMP: 101.41 kDa. Molecular weight determination of protein. Abbreviation: LDC_{WT}: wild type *Ec*LDCc control, — Negative control (empty pET28a vector)

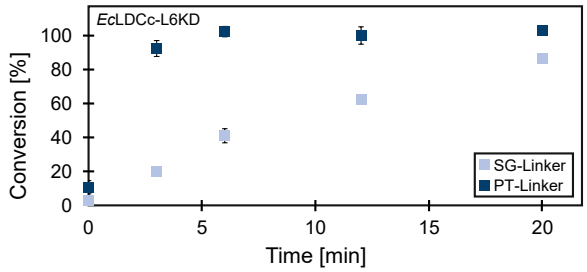

Fig. 4 DAP production with *Ec*LDCc-L6KD variants. Experimental conditions: Purified CatIBs from cells with an $OD_{600\,nm}$ = 12.5, 10 mM L-lysine, 0.1 mM PLP in 50 mM Kpi buffer (pH 7.2). Sampling times: 0, 3, 6, 12 and 20 min. n_B=3, except 3 min SG-L6KD (n_B=2), and n_A=3 (not visible, due to low standard deviation). Conversion calculated based on DAP formation from L-lysine measured by HPLC

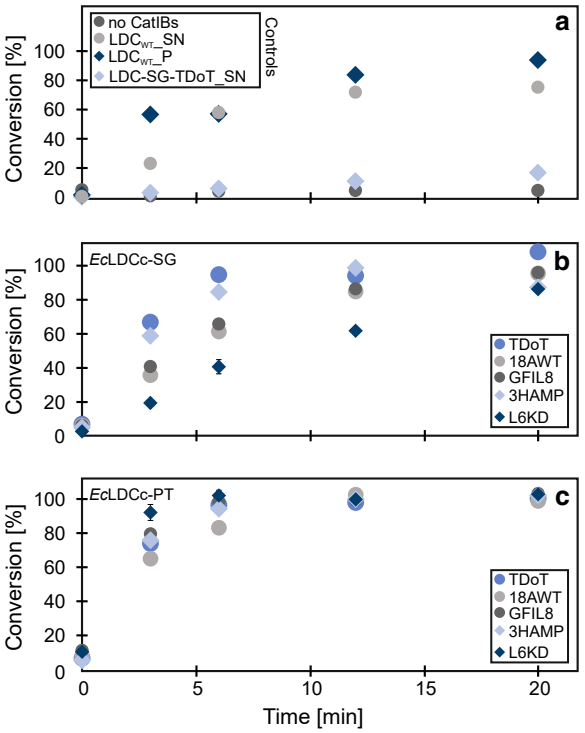

Fig. 5 DAP production with 10 *Ec*LDCc-CatIB variants—comparison of linkers. Enzymatic activity of: **a** controls with no CatIBs, supernatant and pellet fraction of wild type *Ec*LDCc and supernatant of *Ec*LDCc-SG-TDoT **b** EcLDCc-SG variants and **c** *Ec*LDCc-PT variants. Experimental conditions: Purified CatIBs from cells with an $OD_{600\,nm}$ = 12.5, 10 mM L-lysine, 0.1 mM PLP in 50 mM Kpi buffer (pH 7.2). Sampling times: 0, 3, 6, 12 and 20 min. n_A=3 (not visible, due to low standard deviation) and L6KD-Tag variants: n_B=3, except 3 min SG-L6KD (n_B=2). *P* pellet, *SN* supernatant. Conversion calculated based on DAP formation from L-lysine measured by HPLC

and *Ec*LDCc-PT-L6KD (Fig. 4). Activity of the CatIBs was determined by measurement of DAP formation from L-lysine over a time course of 20 minutes reaction time. Although both CatIB variants showed activity, L6KD in combination with the PT-Linker gave CatIBs with a much higher conversion rate (93 % after 3 min) compared to the SG-Linker variant (20 % after 3 min). The standard deviation between the different replicates was on average below 2.2 % for the analytical replicates and ≤ 5 % for most of the biological replicates, which proves high reproducibility of the experimental and analytical workflow procedures.

After having determined the reproducibility of the activity for the L6KD variants, the remaining eight CatIB constructs as well as controls were tested for their activity. As expected, the negative control, *E. coli* BL21(DE3) with an empty pET28a vector did not show any enzymatic activity (Fig. 5a; Table 1). Another control was the soluble fraction of the *Ec*LDCc-SG-TDoT CatIB producing strain. The soluble fraction showed a very low conversion of L-lysine (4 % after 3 min) meaning that a very small portion of the *Ec*LDCc was still present in the soluble fraction. Interestingly, the wild type *Ec*LDCc displayed enzymatic activity in the pellet (57 % conversion after 3 min) as well as in the supernatant fraction (24 % conversion after 3 min). Strikingly, these natural CatIBs seemed to be more active compared to the supernatant fraction of the wild type enzyme. However, the wild type *Ec*LDCc showed a smaller fraction on the SDS gel (Fig. 3), i.e., a substantial portion of the soluble protein fraction seemed to be converted into insoluble IBs during production of the recombinant protein. These natural IBs showed a higher specific volumetric productivity (specific P_v) compared to three of the SG-Linker variants (*Ec*LDCc-SG-18AWT/L6KD/GFIL8). In comparison with all PT-Linker variants, the specific P_v of these natural IBs was lower (Table 1). Nevertheless, the conversion with the wild type *Ec*LDCc reached only approx. 80 % in 20 min, which might be a result of low enzyme stability, resulting in deactivation of the enzyme.

The comparison of SG-Linker variants combined with different aggregation inducing tags revealed strongly differing activities between the five CatIB constructs (Fig. 5b; Table 1). The variant with the TDoT-Tag showed the fastest conversion rate (67 % after 3 min), followed by the 3HAMP variant (59 % after 3 min), the GFIL8 variant (41 % after 3 min), the 18AWT variant (36 % after 3 min) and the L6KD variant (20 % after 3 min). In contrast, the aggregation inducing tags in combination with the more rigid PT-Linker resulted in faster conversion (65 % to 93 % after 3 min) (Fig. 5c; Table 1). Interestingly, all CatIB variants with SG-/PT-Linker showed substantial enzyme activity. However, only two SG-Linker variants reached full conversion after 12 min, while all PT-Linker variants already reached full conversion at this time point,

demonstrating superior performance of all PT-Linker variants. Strikingly, the L6KD aggregation inducing tag revealed opposite results when using the SG- or the PT-Linker, respectively. While the combination of L6KD with PT shows fastest conversion of all variants, the construct with the SG-Linker resulted in the slowest conversion of all variants. This clearly demonstrates that for the investigated *Ec*LDCc CatIBs, the linker selection is a key factor of high relevance. The PT-Linker is expected to provide more rigidity than the SG-Linker and one may speculate that for the given example the linker rigidity might be an important structural aspect for the CatIB structure-function relationship.

A general comparison of the specific P_vs of the ten *Ec*LDCc-CatIB variants clearly illustrated that the PT-Linker led to higher specific P_vs of the variants compared to the SG-Linker combinations (Fig. 6). Only the *Ec*LDCc-SG-TDoT variant showed a higher specific P_v compared to the PT variant, namely *Ec*LDCc-PT-18AWT. Furthermore, *Ec*LDCc-SG-3HAMP just revealed a slightly lower specific P_v of *Ec*LDCc-PT-18AWT. In both linker combinations the 18AWT-Tag showed the lowest or second to lowest specific P_v, which makes 18AWT the weakest aggregation inducing tag of these CatIB variants. Although the activity of the 18AWT variants were low, the fact that they show substantial activity is a striking result, since visible IBs were absent in the microscopic pictures (Fig. 1) and no activity might be expected. Thus, it can be assumed that insoluble structures were formed, that were not visible under the microscope, due to potential association with parts of the cell membrane like mentioned before [28].

Comparison of the enzymatic activity data, i.e., conversion after 3 min, with the specific P_v of the CatIB variants led to similar results (Table 1). This gives rise to the conclusion that the applied normalization of the amount of biomass prior to purification of the different CatIBs was an effective approach to harmonize the data. Moreover, the purification efficiency seemed to be quite similar for all variants, since the optical density of the cell suspensions were normalized beforehand, and similar intensities of the protein bands were observed (Fig. 3). This indicates that there was no general distortion of the data by the purification process. There was only a small change of *Ec*LDCc-PT-3HAMP and *Ec*LDCc-PT-TDoT, with *Ec*LDCc-PT-3HAMP showing a slightly higher activity, which might be due to a slightly higher CatIB amount that was produced and purified from the cell culture. However, the most important finding can be derived from data of activity as well as specific P_v: (i) overall the PT-Linker variants showed a higher activities and specific P_v, (ii) the L6KD-Tag showed very different activity levels depending on the linker and (iii) 18AWT seemed to be the less suitable aggregation inducing tag for the tested system. Especially, the SG/PT-L6KD example showed that CatIBs that have the same morphology (Fig. 1) and the same amount of CatIBs per cell (Table 1) could provide very different enzymatic activity levels. The SG-Linker may result in less active CatIBs, since the portion of active enzyme inside the CatIBs could be less, or this

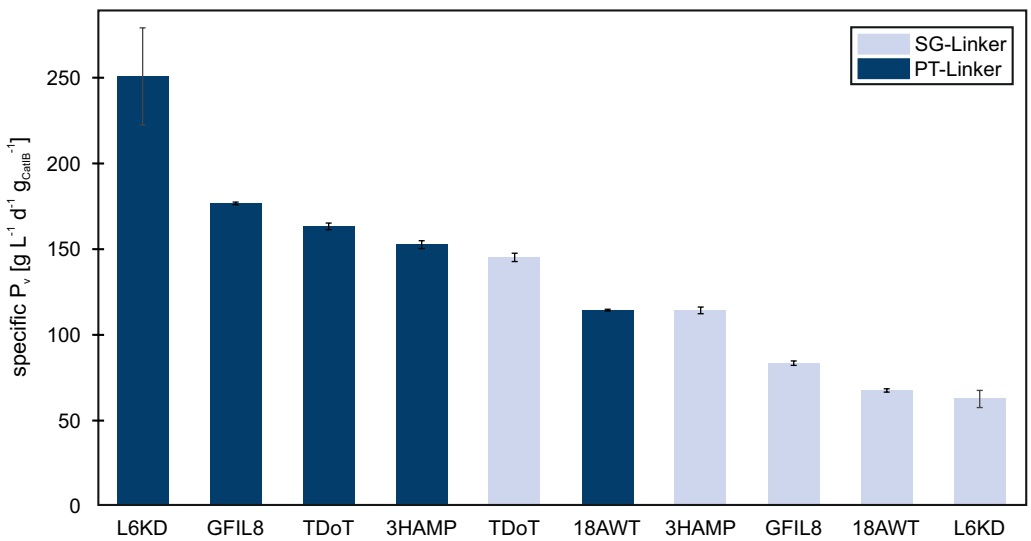

Fig. 6 Comparison of specific volumetric productivity of ten *Ec*LDCc-CatIBs. The standard deviation of the analytical replicates are shown in black for the CatIB variants n_A=3 (except PT-18AWT: n_A=2). Moreover, the standard deviation of the biological duplicate/triplicate were shown in grey (PT-L6KD-Tag: n_B=3, SG-L6KD: n_B=2)

Table 1 Morphological and enzymatic data of the CatIB variants and controls

	CatIBs visibility [Yes/No]	Cells with CatIBs [%]	Ø CatIBs per cell [-]	$Area_M$ of CatIBs [μm^2]	$Area_M$ of cells [μm^2]	CatIB area per cell area [%]	Pellet activity [Yes/No]	Conversion after 3 min [%]	P_v [$g\ L^{-1}d^{-1}$]	Specific P_v [$g\ L^{-1}d^{-1}\ g_{CatIB}^{-1}$]
$Control_{neg}$	No	0	0.00	0.00	2.72	0	No	0	0	0
LDC_{WT}	Yes	88	1.35	0.47	2.94	24	Yes	57[a] 24[b]	219[a] 87[b]	106[a]
LDC-SG-TDoT	Yes	78	1.55	0.38	2.50	23	Yes	67	258	147
LDC-PT-TDoT	Yes	61	1.43	0.30	2.86	15	Yes	74	286	165
LDC-SG-18AWT	No	0	0.00	0.00	2.01	0	Yes	36	136	67
LDC-PT-18AWT	No	0	0.00	0.00	2.11	0	Yes	65	251	116
LDC-SG-L6KD	Yes	88	1.35	0.65	2.92	31	Yes	20	105	63
LDC-PT-L6KD	Yes	88	1.18	0.66	2.32	37	Yes	93	457	256
LDC-SG-GFIL8	Yes	72	1.44	0.49	2.76	28	Yes	41	156	83
LDC-PT-GFIL8	Yes	86	1.24	0.45	2.30	24	Yes	80	308	179
LDC-SG-3HAMP	Yes	82	1.78	0.48	2.81	32	Yes	59	227	115
LDC-PT-3HAMP	Yes	71	1.83	0.43	2.65	31	Yes	76	294	155

Pellet activity as well as conversion, after 3 min, was tested by adding 10 mM L-lysine, 0.1 mM PLP and 50 mM Kpi buffer (pH 7.2) to the CatIB pellet fraction after purification. Microscopic images were taken after main cultivation (72 h) and analyzed regarding the number of cells that carry CatIBs and the amount of CatIBs in the cells with CatIBs ($n \geq 111$). Moreover, the area of cells and CatIBs were determined and the ratio of CatIB area per cell area ($n = 100$). Abbreviations: [a]Pellet fraction, [b]Supernatant fraction, SN Supernatant, $Area_M$Area of the median, $P_V$volumetric productivity

linker may have led to a CatIB conformation that suffered from transport limitation of substrate.

Enzymatic activity vs. morphology of EcLDCc-CatIB variants

After analyzing the microscopic images as well as the enzymatic activity of the variants, both data were combined to see if the CatIB morphology had an impact on the enzymatic activity. In case of the 18AWT-Tag an abnormal cell morphology was found. The cells did not form dense, refractive IBs, resulting in only low enzymatic activity, volumetric productivity and specific volumetric productivity (Table 1).

Three out of four PT-Linker CatIB variants, for example the CatIBs of *Ec*LDCc-PT-TDoT, showed smaller CatIB areas compared to the SG variants (PT-TDoT: 0.3 µm^2 vs. SG-TDoT: 0.38 µm^2). It is thus tempting to speculate that smaller IBs may retain higher enzymatic activity, possibly due to improved substrate supply to the active centers. The faster conversion rate of the PT-variants also resulted in higher P_Vs and specific P_Vs. However, in case of the TDoT variants, the enzymatic activity of both variants were in the middle range of all variants (Fig. 6). In this particular case, the size as well as the linkers seemed to have only a small impact on the enzymatic activity.

The CatIBs with the L6KD-Tags were the only ones that showed a similar size (PT: 0.66 µm^2 vs. SG: 0.65 µm^2), despite different linkers. Contrary to the above mentioned hypothesis, the similar morphologies of the L6KD-CatIBs were not reflected in their enzymatic activities, P_Vs nor specific P_Vs (Table 1). Whereas the combination of the SG-Linker with L6KD led to the lowest activity level (20 % conversion after 3 min), P_V (105 g L^{-1} d^{-1}) and specific P_V (63 g L^{-1} d^{-1} $g_{CatIB}{}^{-1}$) of all variants, the combination with the PT-Linker reached the highest activity levels (93 % after 3 min), P_V (457 g L^{-1} d^{-1}) as well as specific P_V (256 g L^{-1} d^{-1} $g_{CatIB}{}^{-1}$). Whereas the aggregation inducing tag seemed to have a stronger effect on the CatIB and cell morphology (Fig. 1), especially, the different activity levels of L6KD showed that the impact of the linker on the activity was more pronounced.

Conclusions

Although there was no clear correlation between the microscopic data and enzymatic activity, the microscopic analysis is an important tool to prove the presence of IBs in the cells. Strains which do not form dense IBs and only show little cell growth, like in case of the *Ec*LDCc-18AWT variants, can be dismissed and only the strains generating clearly visible CatIB structures need to be analyzed regarding their enzymatic activity to save time and resources.

All *Ec*LDCc-CatIB variants tested showed at least some lysine decarboxylase activity. The most productive CatIB variant was L6KD in combination with the PT-Linker, showing a superior specific P_v. However, in combination with TDoT or 3HAMP, the SG-Linker showed lower specific P_v. Moreover, it was unexpected that the wild type *Ec*LDCc control did form natural CatIBs. However, the specific P_v of the natural CatIBs was much lower compared to most of the generated set of CatIBs.

Finally, it is still challenging to determine the molecular factors which led to different activities observed for different CatIBs. The analysis of the ten *Ec*LDCc-CatIB variants revealed no clear dependency on the particle size of the IBs. A more probable hypothesis could be a combination of more than one factor. For example, for the tested ten *Ec*LDCc-CatIBs it turned out that the more rigid PT-Linker resulted in CatIBs which were more active resulting in a faster conversion rate. Besides the enzymatic activity, also mass transfer could have an impact on the conversion rate. The flexible SG-Linker possibly led to denser CatIB structures that might hinder efficient substrate diffusion to the inner part of the CatIBs or may results in incorrectly folded *Ec*LDCc.

In summary, the results of our study demonstrate that for any given target enzyme the efficiency of formation and residual activity of CatIBs cannot be predicted beforehand. Thus, a large number of linkers and aggregation inducing tags need to be tested. However, the generation and testing of large CatIB libraries is time-consuming. Hence, automation of molecular biology workflows for CatIB construction, detection and activity determination are required to identify the optimal CatIB for each target enzyme.

Methods

Reagents and chemicals

All chemicals were purchased from ROTH and Merck (Sigma-Aldrich), unless stated otherwise. Enzymes for molecular biology were purchased from New England Biolabs GmbH (Frankfurt am Main, Germany).

Construction of expression plasmids

The synthetic gene of the *Ec*LDCc, the two linkers, SG- and PT-Linker as well as the five aggregation inducing tags, TDoT-, 18AWT-, L6KD-, GFIL8- and 3HAMP-Tag, were synthesized by Synbio Technologies (Monmouth Junction, New Jersey, USA). The synthetic sequences contained the BsaI restriction and recognition sites, needed for Golden Gate Assembly. For Golden Gate Assembly, the synthetic gene encoding for *Ec*LDCc was assembled with one of the two linkers, one of the five aggregation inducing tags as well as the so-called suicide plasmid in a ratio of 1:1:1:3. The suicide plasmid functioned as

the expression plasmid backbone. It is a pET28a vector with an integrated *ccdB* gene, coding for the CcdB toxin, which is lethal for *E. coli* DH5α and *E. coli* BL21(DE3). It served as a control for accurate Golden Gate Assembly, because of zero-background cloning [42]. During Golden Gate Assembly BsaI removed the *ccdB* gene and the T4-ligase inserted the CatIB-Linker-Tag sequence. After transformation of *E. coli* DH5α with the Golden Gate Assembly mixture only strains with the successful CatIB plasmid can grow while strains carry the original vector will be killed due to the produced toxin. Moreover, 2.5 % (v/v) T4-ligase as well as 2.5 % (v/v) BsaI restriction enzyme, were added to the mixture. The Golden Gate Assembly was performed in a PCR cycler (37 °C, 5 min and 16 °C, 5 min—cycles; 65 °C, 20 min). Information about all plasmids that were used in this study are summarized in Table S1, Additional file 1. The final expression plasmids were sequenced and verified for the correct assembly (Eurofins GmbH, Hamburg, Germany). Information about construction of the positive control strain *Ec*LDCc-Xa-SG-TDoT together with experimental characterization is provided by Kloss et al. [9].

Protein production, cell disruption and protein purification

CatIB production was performed by cultivating *E. coli* BL21(DE3) carrying the respective expression plasmids in M9 autoinduction medium (See Table S2, Additional file 1). Following a modified protocol by Lamm et al. [43], 500 mL shaking flasks were used with a filling volume of 50 mL and a shaking frequency of 170 rpm (Infors HT Multitron Standard, Infors AG, Bottmingen, Swiss). The main cultivation was inoculated with an $OD_{600\,nm}$ of 0.05 of an overnight culture in LB complex medium (37 °C, 170 rpm). The incubation was performed in two phases. The first one was a growth phase at 37 °C for 3 h, followed by a second phase at15°C for 69 h to produce active *Ec*LDCc-CatIBs. The optical density of the main cultures was determined to perform a normalization of the cell cultures to $OD_{600\,nm} = 12.5$. The purification process was continued with 15 mL cell suspension with the specific optical density. The cells were harvested by centrifugation at 5000 x*g* for 10 min. Another centrifugation step (3 min at 5000 x*g*) was performed after washing the cell pellet with 10 mL of 0.9 % NaCl solution. Cell lysis was performed by adding 1.35 mL cell lysis buffer, BugBuster® HT Protein Extraction Reagent (Merck KGaA, Darmstadt, Germany) with the addition of 0.146 g L^{-1} lysozyme, to the cell pellet. The suspension was incubated at 20 °C for 20 min and 750 rpm. After cell lysis the soluble and insoluble protein fraction were separated by centrifugation at 5000 x*g* for 30 min. The pellet was washed with 10 mL Milli-Q® followed by centrifugation. 15 mL Milli-Q® was added to the CatIB pellet and 1 mL aliquots in 1.5 mL Eppis were made. A centrifugation step was performed and the Milli-Q® was discarded (10,000 x*g* for 5 min). The pellets were used for enzyme assay or for weight determination. The CatIB weight was determined via drying the pellet at 80 °C for 24 h and was then weighed. The enzymatic assay samples were stored on ice at 4 °C overnight and used for enzyme activity measurements the next day.

Sodium dodecyl sulfate-polyacrylamide gel electrophoresis (SDS-PAGE)

Sample preparation for SDS-PAGE analysis was performed by adding 2x Laemmli sample buffer to a purified CatIB-Milli-Q® suspension originated from a cell culture with a normalized $OD_{600\,nm}$ of 12.5 (See Protein production, cell disruption and protein purification) as well as to the soluble fraction. After sample incubation for 10 min at 95 °C, the samples with the insoluble fraction were centrifuged for 5 min at 11,000 x *g*. Samples were applied to a Criterion™ 4–12 % Bis-Tris protein gel, 1.0 mm, with 18 wells (Bio-Rad Laboratories GmbH, Feldkirchen, Germany) together with a protein marker (PageRuler Prestained Protein *ladder*, ThermoFisher Scientific). Gel electrophoresis was performed in NuPAGE™ MES SDS running buffer (1×) at 200 V, 500 mA and 150 W. The gel was stained with SimplyBlue™ SafeStain. The theoretical molecular mass of the enzymes were determined by using the Protein isoelectric point calculator tool (http://isoelectric.org/).

Determination of lysine decarboxylase activity

Enzyme activity was determined by adding 1 mL of 50 mM Kpi buffer (pH 7.2), 0.1 mM pyridoxalphosphat (PLP) and 10 mM L-lysine to the CatIB pellet, originated from a cell culture with a normalized $OD_{600\,nm}$ of 12.5 (See Protein production, cell disruption and protein purification and incubation). The soluble fraction, after cell lysis, was refilled to the normalized volume of 12 mL with Kpi-PLP-L-lysine ratio compared to the CatIB pellet fraction. 1 mL of the solution was used for the enzyme assay. The samples were incubated at 1000 rpm and 30 °C. Samples were taken after 0, 3, 6, 12 and 20 min and the enzyme was inactivated by adding 80 % (v/v) methanol and subsequently L-lysine and DAP concentrations were determined by HPLC to calculate conversion rate.

HPLC analysis

To determine the DAP and L-lysine concentration, an amino acid HPLC system (Agilent 1260 Infinity II, Agilent Technologies, Santa Clara, USA) was used. The system was equipped with a fluorescence detector (excitation: 230 nm; emission: 450 nm) and a C18 Kinetex Evocolumn (Phenomenex, Torrence, USA). Before

injection, the samples for the enzyme assay (See Activity assay) were diluted with 50 mM Kpi Buffer (pH 7.2) to a final dilution ratio of 1:500 (v/v), filtrated and then 1:1 (v/v) diluted with 100 µM α-aminobutyric acid (Sigma-Aldrich, St. Louis, USA) as the internal standard (Sigma-Aldrich, St. Louis; USA). For analyzing L-lysine and DAP concentrations in the samples, an amino acid quantification method, including a pre-column derivatisation step at 18 °C using 9 µL *ortho*-phthaldialdehyde (OPA, Sigma-Aldrich) and 1 µL of the sample (6 mixing iteration steps). The mobile phase A contained 2.63 g L^{-1} Na_2HPO_4, 2.08 g L^{-1} NaH_2PO_4 and 0.5 % (v/v) THF in Milli-Q® water, and the mobile phase B contained 50 % (v/v) methanol, 45 % (v/v) acetonitrile, and 5 % (v/v) Milli-Q® water. Chromatographic separation was performed with a linear gradient that was applied with a flow rate of 1 mL min^{-1} (0 % B, 0–2 min 0–38 % B, 2–6 min 38–42 % B, 6–7 min 42–70 % B, 713 min 70–100 % B, 13–17 min 100-0 % B). α-Aminobutyric acid showed an approximate retention time of 6.1 min, L-lysine of 9.6 min and DAP of 11.6 min. The DAP and L-lysine concentrations were calculated with a linear calibration curve of eight reference solutions (0.5 µM to 15 µM) after normalization with the internal standard peak area (calibration curve, See Additional file 1: Fig. S1).

Microscopic analysis

Phase-contrast microscopic analysis was performed for *E. coli* BL21(DE3) strains with CatIB formation and for control strains. Cell suspension samples from cultivation experiments were taken before CatIB purification and analyzed by microscopy. A volume of 1 µL was applied on a microscope slide and covered with a coverslip. The microscope slide was positioned upside down on the desk of an inverted Nikon Eclipse Ti2 microscope (Nikon GmbH, Düsseldorf, Germany). The sample was observed with a CFI Plan Apo Lambda 100X Oil objective (Nikon GmbH, Düsseldorf, Germany) and images were taken with a Thorlab camera DCC154M-GL (Thorlabs Inc., Newton, New Jersey, USA). Analysis of cell images were performed with Fiji ImageJ [44] to determine the areas of at least 100 inclusion bodies and cells.

Abbreviations

aa: Amino acids; CatIB: Catalytically active inclusion body ; DAP: 1,5-diaminopentane ; GOI: Gene of interest ; IB: Inclusion body; PLP: Pyridoxal-5-phosphate; P_v: Volumetric productivity ; OPA: *ortho*-phthaldialdehyde; SDS-PAGE : Sodiumdodecyl sulfate polyacrylamide gel electrophoresis.

Supplementary Information

The online version contains supplementary material available at https://doi.org/10.1186/s12934-021-01539-w.

Additional file 1. Additional tables and figure.

Acknowledgements

This work was funded by the state of North Rhine Westphalia (NRW) and the European Regional Development Fund (EFRE), Project "CLIB-Kompetenzzentrum Biotechnologie (CKB)" 34.EFRE-0300096 and 34.EFRE-0300097.

Authors' contributions

KK planned, realized and analyzed all experiments. MP provided the positive control and the DNA sequences of TDoT- and 3HAMP-Tag, and helped planning the experiments. UK helped planning the experiments. GÖ provided the DNA sequences of 18AWT-, L6KD- and GFIL8-Tag. SA did preliminary experiments on which the mentioned experiments were based on. KEJ helped to finalize the manuscript. WW helped to finalize the manuscript. MO helped to finalize the manuscript and supervised the entire project. All authors have read and approved the final manuscript.

Funding

Open Access funding enabled and organized by Projekt DEAL. This work was funded by the state of North Rhine Westphalia (NRW) and the European Regional Development Fund (EFRE), Project "CLIB-Kompetenzzentrum Biotechnologie (CKB)" 34.EFRE-0300096 and 34.EFRE-0300097.

Availability of data and materials

All data generated or analyzed during this study are included in this article and its Additional file 1.

Ethics approval and consent to participate

Not applicable.

Consent for publication

Not applicable.

Competing interests

The authors declare that they have no competing interests.

Author details

[1] Institute of Bio- and Geosciences IBG-1: Biotechnology, Forschungszentrum Jülich GmbH, 52425 Jülich, Germany. [2] Institute of Biotechnology, RWTH Aachen University, 52074 Aachen, Germany. [3] Institute of Molecular Enzyme Technology, Heinrich-Heine-Universität Düsseldorf, Forschungszentrum Jülich GmbH, 52425 Jülich, Germany. [4] Faculty of Biotechnology, University of Applied Sciences Mannheim, 68163 Mannheim, Germany. [5] Computational Systems Biotechnology (AVT.CSB), RWTH Aachen University, 52074 Aachen, Germany.

Received: 7 December 2020 Accepted: 5 February 2021
Published online: 17 February 2021

References

1. Chung H, Yanf JE, Ha JY, Chae TU, Shin JH, Gustavsson M, Lee SY. Bio-based production of monomers and polymers by metabolically engineered microorganisms. Curr Opin Biotechnol. 2015;36:73–84.
2. Kremer F, Blank LM, Jones PR, Akhtar MK. A comparison of the microbial production and combustion characteristics of three alcohol biofuels: Ethanol, 1-butanol, and 1-octanol. Front Bioeng Biotechnol. 2015;3:12.
3. Wendisch VF. Microbial production of amino acids and derived chemicals: Synthetic biology approaches to strain development. Curr Opin Biotechnol. 2014;30:51–8.
4. Erickson B, Nelson, Winters P. Perspective on opportunities in industrial biotechnology in renewable chemicals. Biotechnol J. 2012;7:176–85.
5. Winnacker M, Rieger B. Biobased polyamids: recent advances in basic and applied research. Macromol Rapid Commun. 2016;37:1391–413.
6. Thielen M. Bio-polyamides for automotive applications. Bioplastics Mag. 2010;5:10–1.
7. Kind S, Jeong WK, Schröder H, Wittmann C. Systems-wide metabolic pathway engineering in *Corynebacterium glutamicum* for bio-based production of diaminopentane. Metab Eng. 2010;2:341–51.
8. Mimitsuka T, Sawai H, Hatsu M, Yamada K. Metabolic engineering of *Corynebacterium glutamicum* for cadaverine fermentation. Biosci Biotechnol Biochem. 2007;71:2130–5.

9. Kloss R, Limberg MH, Mackfeld U, Hahn D, Grünberger A, Jäger VD, Krauss U, Oldiges M, Pohl M. Catalytically active inclusion bodies of l-lysine decarboxylase from *E. coli* for 1,5-diaminopentane production. Scientific reports. 2018;8:5856.
10. Tufvesson P, Lima-Ramos J, Nordblad M, Woodley J. Guidelines and cost analysis for catalyst production in biocatalytic processes. Org Process Res Dev. 2011;15:266–74.
11. Ray M, Mishra P, Das P, Sabat SC. Expression and purification of soluble bio-active rice plant catalase-A from recombinant *Escherichia coli*. J Biotechnol. 2012;157:12–9.
12. Zhang Y, Zborníková E, Rejman D, Gerdes K. Novel (p)ppGpp binding and metabolizing proteins of *Escherichia coli*. mBio. 2018;9:2.
13. Mathieu K, Javed W, Vallet S, Lesterlin C, Candusso MP, Ding F, Xu XN, Ebel C, Jault JM, Orelle C. Functionality of membrane proteins overexpressed and purified from *E. coli* is highly dependent upon the strain. Sci Rep. 2019;9:2654.
14. Rios GM, Belleville MP, Paolucci D, Sanchez J. Progress in enzymatic membrane reactors–a review. J Memb Sci. 2004;242:189–96.
15. Lindeque RM, Woodley JM. Reactor selection for effective continuous biocatalytic production of pharmaceuticals. Catalysts. 2019;9:262.
16. Sheldon RA, Pereira PC. Biocatalysis engineering: the big picture. Chem Soc Rev. 2017;46:2678–91.
17. Bornscheuer UT. Immobilizing enzymes: how to create more suitable biocatalysts. Angew Chem Int Ed. 2003;42:3336–7.
18. Garcia-Galan C, Berenguer-Murcia A, Fernandez-Lafuente R, Rodrigues RC. Potential of different enzyme immobilization strategies to improve enzyme performance. Adv Synth Catal. 2011;353:2885–904.
19. Datta S, Christena LR, Rajaram YRS. Enzyme immobilization: an overview on techniques and support material. 3 Biotech. 2013;3:1–9.
20. Sheldon RA, Schoevaart R, Van Langen LM. Cross-linked enzyme aggregates (CLEAs): a novel and versatile method for enzyme immobilization (a review). Biocatal Biotransfor. 2005;23:141–7.
21. Eş I, Vieira JDG, Amaral AC. Principles, techniques, and applications of biocatalyst immobilization for industrial application. Appl Microbiol Biotechnol. 2015;99:2065–82.
22. Krauss U, Jäger VD, Diener M, Pohl M, Jaeger KE. Catalytically-active inclusion bodies–carrier-free protein immobilizates for application in biotechnology and biomedicine. J Biotechnol. 2017;258:136–47.
23. Jäger VD, Lamm R, Küsters K, Ölçücü G, Oldiges M, Jaeger KE, Büchs J, Krauss U. Catalytically-active inclusion bodies for biotechnology-general concepts, optimization, and application. Appl Microbiol Biotechnol. 2020;104:7313–29.
24. Jäger VD, Kloss R, Grünberger A, Seide S, Hahn D, Karmainski T, Piqueray M, Embruch J, Longerich S, Mackfeld U, Jaeger KE, Wiechert W, Pohl M, Krauss U. Tailoring the properties of (catalytically)-active inclusion body. Microb Cell Fact. 2019;18:33.
25. Diener M, Kopka B, Pohl M, Jaeger KE, Krauss U. Fusion of a coiled-coil domain facilitates the high-level production of catalytically active enzyme inclusion bodies. Chemcatchem. 2016;8:142–52.
26. Zhou B, Ying L, Wu W, Zhang XE, Lin Z. Small surfactant-like peptides can drive soluble proteins into active aggregates. Microb Cell Fact. 2012;11:10.
27. Wang X, Zhou B, Hu W, Zhao Q, Lin Z. Formation of active inclusion bodies induced by hydrophobic self-assembling peptide GFIL8. Microb Cell Fact. 2015;14:88.
28. Lin Z, Zhou B, Wu W, Xing L, Zhao Q. Self-assembling amphipathic alpha-helical peptides induce the formation of active protein aggregates in vivo. Faraday Discuss. 2013;166:243–56.
29. Nahalka J, Nidetzky B. Fusion to a pull-down domain: a novel approach of producing *Trigonopsis variabilis* D-amino acid oxidase as insoluble enzyme aggregates. Biotechnol Bioeng. 2007;97:454–61.
30. Nahalka J. Physiological aggregation of maltodextrin phosphorylase from *Pyrococcus furiosus* and its application in a process of batch starch degradation to α-D-glucose-1-phosphate. J Ind Microbiol Biotechnol. 2008;35:219–23.
31. García-Fruitós E, González-Montalbán N, Morell M, Vera A, Ferraz RM, Arís A, Ventura S, Villaverde A. Aggregation as bacterial inclusion bodies does not imply inactivation of enzymes and fluorescent proteins. Microb Cell Fact. 2005;4:27.
32. Jiang L, Xiao W, Zhou X, Wang Q, Fan J. Comparative study of the insoluble and soluble Ulp1 protease constructs as Carrier free and dependent protein immobilizates. J Biosci Bioeng. 2019;127:23–9.
33. Wu W, Xing L, Zhou B, Lin Z. Active protein aggregates induced by terminally attached self-assembling peptide ELK16 in *Escherichia coli*. Microb Cell Fact. 2011;10:9.
34. Choi SL, Lee SJ, Ha JS, Song JJ, Rhee YH, Lee SG. Generation of catalytic protein particles in *Escherichia coli* cells using the cellulose-binding domain from *Cellulomonas fimi* as a fusion partner. Biotechnol Bioprocess Eng. 2011;16:1173–9.
35. Arie JP, Miot M, Sassoon N, Betton JM. Formation of active inclusion bodies in the periplasm of *Escherichia coli*. Mol Microbiol. 2006;62:427–37.
36. Engler C, Kandzia R, Marillonnet SA, One Pot. One step, precision cloning method with high throughput capability. PLoS ONE. 2008;3:11.
37. Kloss R, Karmainksi T, Jäger VD, Hahn D, Grünberger A, Baumgart M, Krauss U, Jaeger KE, Wiechert W, Pohl M. Tailor-made catalytically active inclusion bodies for different applications in biocatalysis. Catal Sci Technol. 2018;8:5816–26.
38. Rokney A, Shagan M, Kessel M, Smith Y, Rosenshine I, Oppenheim AB. *E. coli* transports aggregated proteins to the poles by a specific and energy-dependent process. J Mol Biol. 2009;392:589–601.
39. Rudolph R, Lilie H. In vitro folding of inclusion body proteins. FASEB J. 1995;10:49–56.
40. Kwon KS, Lee S, Yu MH. Refolding of α_1-antitrypsin expressed as inclusion bodies in *Escherichia coli*: characterization of aggregation. Biochim Biophys Acta. 1995;1247:179–84.
41. Sunitha K, Chung BH, Jang KH, Song KB, Kim CH, Rhee SK. Refolding and purification of *Zymomonas mobilis* levansucrase produced as inclusion bodies in fed-batch culture of recombinant *Escherichia coli*. Protein Expr Purif. 2000;18:388–93.
42. Miyazaki K. Lethal *ccdB* gene-based zero-background vector for construction of shotgun libraries. J Biosci Bioeng. 2010;110:372–3.
43. Lamm R, Jäger VD, Heyman B, Berg C, Gürten C, Krauss U, Jaeger K-E, Büchs J. Detailed small-scale characterization and scale-up of active YFP inclusion body production with *Escherichia coli* induced by a tetrameric coiled coil domain. J Biosci Bioeng. 2020;6:730–40.
44. Schneider CA, Rasband WS, Eliceiri KW. NIH Image to ImageJ: 25 years of image analysis. Nat Methods. 2012;9:671–5.

Publisher's note

2.2.1. Publication 2. Supporting Information

Kira Küsters, Martina Pohl, Ulrich Krauss, Gizem Ölçücü, Sandor Albert, Karl-Erich Jaeger, Wolfgang Wiechert and Marco Oldiges*

*corresponding author

Microbial Cell Factories 20.49 (2021). [185].
https://doi.org/10.1186/s12934-021-01539-w

Additional file 1

"Construction and comprehensive characterization of an *Ec*LDCc-CatIB library – varying linkers and aggregation inducing tags"

Kira Küsters[1,2], Martina Pohl[1], Ulrich Krauss[1,3], Gizem Ölçücü[1,3], Sandor Albert[1,4], Karl-Erich Jaeger[1,3], Wolfgang Wiechert[1,5], Marco Oldiges[1,2*]

Additional file Table A1: Plasmids used in this study.

Vector	Genotype
pET28a	*ColE1 lacZ'* Kan^R P_{T7} P_{lac}
pET28a::CcdB	*ColE1 lacZ'* Kan^R P_{T7} P_{lac} *ccdB*
pET28a::*Ec*LDCc::SG::TDoT	2343 bp *Ec*LDCc::SG::TDoT fragment in pET28a
pET28a::*Ec*LDCc::SG::18AWT	2247 bp *Ec*LDCc::SG::18AWT fragment in pET28a
pET28a::*Ec*LDCc::SG::L6KD	2217 bp *Ec*LDCc::SG::L6KD fragment in pET28a
pET28a::*Ec*LDCc::SG::GFIL8	2217 bp *Ec*LDCc::SG::GFIL8fragment in pET28a
pET28a::*Ec*LDCc::SG::3HAMP	2709 bp *Ec*LDCc::SG::3HAMP fragment in pET28a
pET28a::*Ec*LDCc::PT::TDoT	2355 bp *Ec*LDCc::PT::TDoT fragment in pET28a
pET28a::*Ec*LDCc::PT::18AWT	2259 bp *Ec*LDCc::PT::18AWT fragment in pET28a
pET28a::*Ec*LDCc::PT::L6KD	2229 bp *Ec*LDCc::PT::L6KD fragment in pET28a
pET28a::*Ec*LDCc::PT::GFIL8	2229 bp *Ec*LDCc::PT::GFIL8 fragment in pET28a
pET28a::*Ec*LDCc::PT::3HAMP	2721 bp *Ec*LDCc::PT::3HAMP fragment in pET28a

Additional file Table A2: Recipe of M9 Autoinduction medium – 1000 mL

Salt Stock solution (5x)	200 mL
$MgSO_4*7H_2O$ solution (246.48 g L^{-1})	1 mL
$CaCl_2*5H_2O$ solution (14.702 g L^{-1})	1 mL
Trace element solution (1000x)	1 mL
Citrate/Fe solution (7.5 g L-1 $FeSO_4*7H_2O$ 113.95 g L-1 tri-NaCitrat*$2H_2O$)	2 mL
Thiamin solution (10 g L^{-1})	1 mL
2 % (w/v) Lactose solution	100 mL
5 % (w/v) Glucose solution	10 mL
Glycerin 99%	4 mL
Kanamycin solution (50 g L^{-1})	1 mL
add Milli-Q water (final volume)	1000 mL
Salt Stock (5x)	1000 mL
$(NH_4)_2SO_4$	25 g
KH_2PO_4	15 g
Na_2HPO_4	33.9 g
NaCl	2.5 g
NH_4Cl	10 g
add Milli-Q water (final volume)	1000 mL
Trace elements (1000x)	1000 mL
$AlCl_3*6H_2O$	0.75 g
$CoCl_2*6H_2O$	0.6 g
$CuSO_4*5H_2O$	2.5 g
H_3BO_3	0.5 g
$MnSO_4*1H_2O$	17.1 g
$Na_2MoO_4*2H_2O$	3 g
$NiCl_2*6H_2O$	1.7 g
$ZnSO_4*7H_2O$	15 g
Dissolve in 100 mL Milli-Q water and 50 mL 32% HCl and add Milli-Q water to final volume	

Amino acid HPLC calibration curve

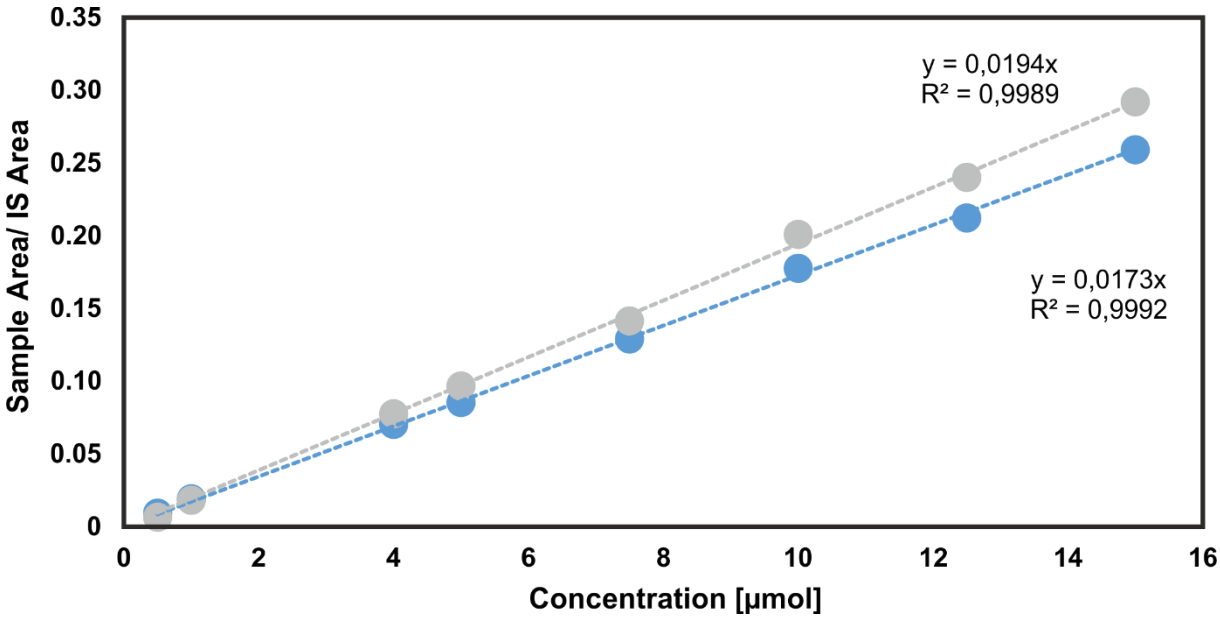

Additional file Figure A1: Calibration curve for DAP (grey) and L-lysine (blue) with the internal standard (IS) AABA (α-aminobutyric acid), HPLC analysis (See Methods in main paper).

Nucleotide sequences of *Ec*LDCc, linkers and aggregation tags

*Ec*LDCc sequence

ATGAACATCATTGCCATTATGGGACCGCATGGCGTCTTTTATAAAGATGAGCCCATCAAA
GAACTGGAGTCGGCGCTGGTGGCGCAAGGCTTTCAGATTATCTGGCCACAAAACAGCG
TTGATTTGCTGAAATTTATCGAGCATAACCCTCGAATTTGCGGCGTGATTTTTGACTGGG
ATGAGTACAGTCTCGATTTATGTAGCGATATCAATCAGCTTAATGAATATCTCCCGCTTT
ATGCCTTCATCAACACCCACTCGACGATGGATGTCAGCGTGCAGGATATGCGGATGGC
GCTCTGGTTTTTTGAATATGCGCTGGGGCAGGCGGAAGATATCGCCATTCGTATGCGTC
AGTACACCGACGAATATCTTGATAACATTACACCGCCGTTCACGAAAGCCTTGTTTACCT
ACGTCAAAGAGCGGAAGTACACCTTTTGTACGCCGGGGCATATGGGCGGCACCGCATA
TCAAAAAAGCCCGGTTGGCTGTCTGTTTTATGATTTTTTCGGCGGGAATACTCTTAAGGC
TGATGTCTCTATTTCGGTCACCGAGCTTGGTTCGTTGCTCGACCACACCGGGCCACACC
TGGAAGCGGAAGAGTACATCGCGCGGACTTTTGGCGCGGAACAGAGTTATATCGTTAC
CAACGGAACATCGACGTCGAACAAAATTGTGGGTATGTACGCCGCGCCATCCGGCAGT

ACGCTGTTGATCGACCGCAATTGTCATAAATCGCTGGCGCATCTGTTGATGATGAACGA

TGTAGTGCCAGTCTGGCTGAAACCGACGCGTAATGCGTTGGGGATTCTTGGTGGGATC

CCGCGCCGTGAATTTACTCGCGACAGCATCGAAGAGAAAGTCGCTGCTACCACGCAAG

CACAATGGCCGGTTCATGCGGTGATCACCAACTCCACCTATGATGGCTTGCTCTACAAC

ACCGACTGGATCAAACAGACGCTGGATGTCCCGTCGATTCACTTCGATTCTGCCTGGGT

GCCGTACACCCATTTTCATCCGATCTACCAGGGTAAAAGTGGTATGAGCGGCGAGCGT

GTTGCGGGAAAAGTGATCTTCGAAACGCAATCGACCCACAAAATGCTGGCGGCGTTATC

GCAGGCTTCGCTGATCCACATTAAAGGCGAGTATGACGAAGAGGCCTTTAACGAAGCCT

TTATGATGCATACCACCACCTCGCCCAGTTATCCCATTGTTGCTTCGGTTGAGACGGCG

GCGGCGATGCTGCGTGGTAATCCGGGCAAACGGCTGATTAACCGTTCAGTAGAACGAG

CTCTGCATTTTCGCAAAGAGGTCCAGCGGCTGCGGGAAGAGTCTGACGGTTGGTTTTTC

GATATCTGGCAACCGCCGCAGGTGGATGAAGCCGAATGCTGGCCCGTTGCGCCTGGC

GAACAGTGGCACGGCTTTAACGATGCGGATGCCGATCATATGTTTCTCGATCCGGTTAA

AGTCACTATTTTGACACCGGGGATGGACGAGCAGGGCAATATGAGCGAGGAGGGGATC

CCGGCGGCGCTGGTAGCAAAATTCCTCGACGAACGTGGGATCGTAGTAGAGAAAACCG

GCCCTTATAACCTGCTGTTTCTCTTTAGTATTGGCATCGATAAAACCAAAGCAATGGGAT

TATTGCGTGGGTTGACGGAATTCAAACGCTCTTACGATCTCAACCTGCGGATCAAAAAT

ATGCTACCCGATCTCTATGCAGAAGATCCCGATTTCTACCGCAATATGCGTATTCAGGAT

CTGGCACAAGGGATCCATAAGCTGATTCGTAAACACGATCTTCCCGGTTTGATGTTGCG

GGCATTCGATACTTTGCCGGAGATGATCATGACGCCACATCAGGCATGGCAACGACAAA

TTAAAGGCGAAGTAGAAACCATTGCGCTGGAACAACTGGTCGGTAGAGTATCGGCAAAT

ATGATCCTGCCTTATCCACCGGGCGTACCGCTGTTGATGCCTGGAGAAATGCTGACCAA

AGAGAGCCGCACAGTACTCGATTTTCTACTGATGCTTTGTTCCGTCGGGCAACATTACC

CCGGTTTTGAAACGGATATTCACGGCGCGAAACAGGACGAAGACGGCGTTTACCGCGT

ACGAGTCCTAAAAATGGCGGGA

SG-Linker sequence

AGCGGCGGTGGGTCTGGAGGCGGCTCAGGTGGTGGGTCG

PT-Linker sequence

CCGACCCCACCGACCACGCCAACGCCACCAACCACCCCAACCCCGACGCCG

TDoT sequence

ATCATTAACGAAACTGCCGATGACATCGTTTATCGCCTGACAGTCATTATCGATGATCGC
TACGAATCGCTGAAAAACCTGATTACCTTACGTGCAGATCGCTTGGAGATGATCATCAAT
GACAATGTGTCCACCATTCTCGCGAGCATTTAA

3HAMP sequence

ATGGGCCTGTTTAACGCCCATGCAGTTGCGCAGCAACGCGCGGATCGCATTGCGACTC
TCCTGCAGTCCTTTGCGGATGGTCAGTTGGACACCGCCGTGGGTGAAGCGCCAGCACC
TGGTTACGAACGCCTGTATGACTCGCTTCGCGCCCTTCAGCGCCAACTGCGCGAACAA
CGTGCGGAGTTACAACAGGTTGAGAGCCTGGAAGCAGGCTTGGCTGAAATGAGTCGGC
AGCATGAAGCAGGGTGGATTGACCAGACGATTCCGGCTGAACGGTTAGAGGGCCGTGC
AGCACGTATCGCCAAAGGCGTGAATGAGCTGGTTGCTGCGCACATTGCGGTGAAAATG
AAAGTCGTGAGCGTAGTCACCGCGTATGGCCAAGGGAACTTCGAACCGCTCATGGATC
GCCTGCCGGGTAAGAAAGCCCAGATCACGGAGGCCATTGATGGCGTACGTGAACGCCT
GCGTGGAGCTGCTGAAGCGACCTCTGCGCAGCTGGCCACAGCCGCCTACAATTAA

18AWT sequence

GAGTGGCTGAAAGCGTTCTACGAAAAGGTCCTGGAGAAACTGAAAGAACTGTTCTA

L6KD sequence

CTGCTGCTGCTGCTGCTGAAAGATTAA

GFIL8 sequence

GGTTTCATTCTGGGTTTCATTCTGTAA

2.3. Publication 3. Generation of Magnetic Protein Aggregates by Supramolecular Assembly of Ferritin Cages

Gizem Ölçücü, Bastian Wollenhaupt, Dietrich Kohlheyer, Karl-Erich Jaeger, Ulrich Krauss*

*corresponding author

prepared for publication in ACS Biomacromolecules

Author Contributions: U.K. conceived and designed the study. G.O. generated all constructs, prepared MPAs and CatMPAs, performed magnetic purification and imaging over permanent magnets, activity/fluorescence assays and all other experiments unless mentioned otherwise. B.W., supervised by D.K., performed the microscopic analyses. G.O. and U.K. prepared the manuscript. All authors have read and approved the final version.

Generation of Magnetic Protein Aggregates by Supramolecular Assembly of Ferritin Cages

Gizem Ölçücü[1,2], Bastian Wollenhaupt[2], Dietrich Kohlheyer[2], Karl-Erich Jaeger[1,2], Ulrich Krauss[1,2,*]

Author affiliations

[1]Institute of Molecular Enzyme Technology, Heinrich Heine University Düsseldorf, Forschungszentrum Jülich GmbH, Wilhelm Johnen Strasse, D-52425 Jülich, Germany

[2]Institute of Bio- and Geosciences IBG-1: Biotechnology, Wilhelm Johnen Strasse, Forschungszentrum Jülich GmbH, D-52425 Jülich, Germany

Corresponding author: Ulrich Krauss, Phone: +492461612939; Email: u.krauss@fz-juelich.de

Keywords: enzyme immobilization, protein-protein interactions, protein aggregates, biocatalysis, magnetic protein aggregates, MPAs, CatMPAs

Introduction

Enzyme immobilization is a vital technology to obtain reusable and stable biocatalysts with improved properties for industrial application, while remedying the shortcomings of enzymes (i.e. low tolerance to harsh process conditions, stability issues, inhibition) at the same time[1, 2]. To this end, various conventional enzyme immobilization methods exist[3-5], such as physical entrapment where the enzyme of interest is trapped within a membrane or a polymer matrix[1], surface immobilization where the enzymes are physically absorbed or covalently linked to the surface of suitable support materials[6, 7], and cross linking[8, 9] based on precipitating the proteins from the solution into aggregates (or crystals), followed by cross-linking with a bifunctional reagent. However, these strategies often suffer from various drawbacks such as lowered specific activities, leaching of the enzyme from the support material, high costs associated with carriers and immobilization onto/into such materials, along with labor intensiveness and lack of generalizability[1, 10-12]. Therefore, in recent years, a multitude of alternative, solely biologically-based, *in vivo* enzyme immobilization methods have been developed [13, 14]. These methods, relying on various principles include, amongst others, the display of target proteins on polyhydroxyalkanoate biopolymers generated *in vivo*[15, 16], trapping target proteins within biologically produced protein crystals[17], generating liquid and hydrogel-like protein condensates based on liquid-liquid phase separation principles[18, 19], or the production of catalytically-active inclusion bodies (CatIBs)[20-23]. The latter concept requires the fusion of aggregation-inducing peptides/proteins/protein domains to a target protein, resulting in the pull-down of active, correctly folded target within an inclusion body matrix formed by misfolded fusion protein species. All of the aforementioned methods can be immensely beneficial as they do not require the use of additional carrier materials and typically yield the desired enzyme immobilizate in one step, directly during heterologous overexpression of the corresponding gene fusions. Therefore, using self-aggregating/segregating proteins that retain their functionality and can be isolated with ease after cell lysis is a highly desired property for potential applications in biotechnology, prompting the need for further developments in the field.

Ferritins are a family of ubiquitous, iron-sequestering proteins which are readily exploited for wide range of biotechnological applications due to their ability to store iron, high chemical and thermal stability, self-assembling properties and biocompatibility[24-26]. Applications of ferritin includes but is not limited to serving as a contrast agent for imaging[27, 28], vessel for drug delivery through encapsulation of target molecules[29], or in synthesis of semiconductor nanoparticles[30]. Chemically-loaded magnetoferritin has previously been used for immobilization of a β-glucosidase utilizing the E-coil/K-coil protein-protein interaction[31], while,

to the best of our knowledge, no entirely biologically-based strategy for the generation of magnetic ferritin-based enzyme immobilizates has yet been presented.

To address this shortcoming, we therefore aimed at obtaining magnetic ferritin-based enzyme immobilizates by solely biological means. To this end, we utilized a previously described fusion protein based on the heavy chain of human ferritin (HuftnH) and the yellow fluorescent protein variant citrine that self-assembles into supramolecular complexes *in vivo*, showing sustained self-aggregation and sedimentation upon cell lysis [32, 33], and extended this fusion strategy to generate fully biologically produced, magnetic protein aggregates (MPAs) and catalytically-active magnetic protein aggregates (CatMPAs). Utilizing different ferritins (Figure 1) a set of MPAs were generated and characterized with regard to aggregation efficiencies and magnetic properties. The best performing fusion construct was subsequently used to generate magnetic enzyme immobilizates by relying on the SpyTag/SpyCatcher protein conjugation system[34, 35] to allow immobilization of an alcohol dehydrogenase model enzyme. The ferritin-based, CatMPAs therefore represent a novel way to immobilize enzymes *in vivo*, and can be a promising new tool for biotechnological applications in the future.

Results and Discussion

Diversification of a ferritin-based self-assembly system

To obtain biologically produced, magnetic immobilizates, we initially reconstructed a fusion protein consisting of the fluorescence reporter citrine and the heavy chain of human ferritin (Citrine-HuftnH) as first described by Bellapadrona and co-workers[32, 33]. Citrine-HuftnH had been shown to yield self-assembling supramolecular complexes, producing fluorescent particles in *E. coli*, which further aggregated and sedimented in solution upon release from the cells. Self-assembly and aggregation was postulated to be due to dimerization of citrine attached to the ferritin subunits that themselves assemble to intact ferritin cages, with the citrines mediating the formation of the supramolecular complexes (Figure 1, B). To extend on this strategy, we used a nonheme *E. coli* ferritin (EcftnA-WT), and a magnetically enhanced EcftnA H34L/ T64I[36] in addition to the HuftnH, and fused the genes encoding the human and *E. coli* ferritins to the 3' end of the gene encoding citrine (Figure 1, A). For initial assessment of the self-aggregation properties of all constructs, Citrine-HuftnH, Citrine-EcftnA-WT and Citrine-EcftnA H34L/T64I fusions were overproduced in *E. coli* BL21(DE3) and the cells were lysed to yield the crude cell extract (CCE) fractions. All CCEs visually showed self-aggregation and sedimentation when left undisturbed (Figure S1), confirming that the exchange of human ferritin with *E. coli* ferritins did not interfere with the aggregation tendency of the fusion proteins. The presence of intracellular supramolecular aggregates was further confirmed via microscopic analyses conducted on live *E. coli* BL21 (DE3) cells overproducing the citrine-

ferritin fusions, with a construct producing soluble citrine included as a negative control (Figure 2).

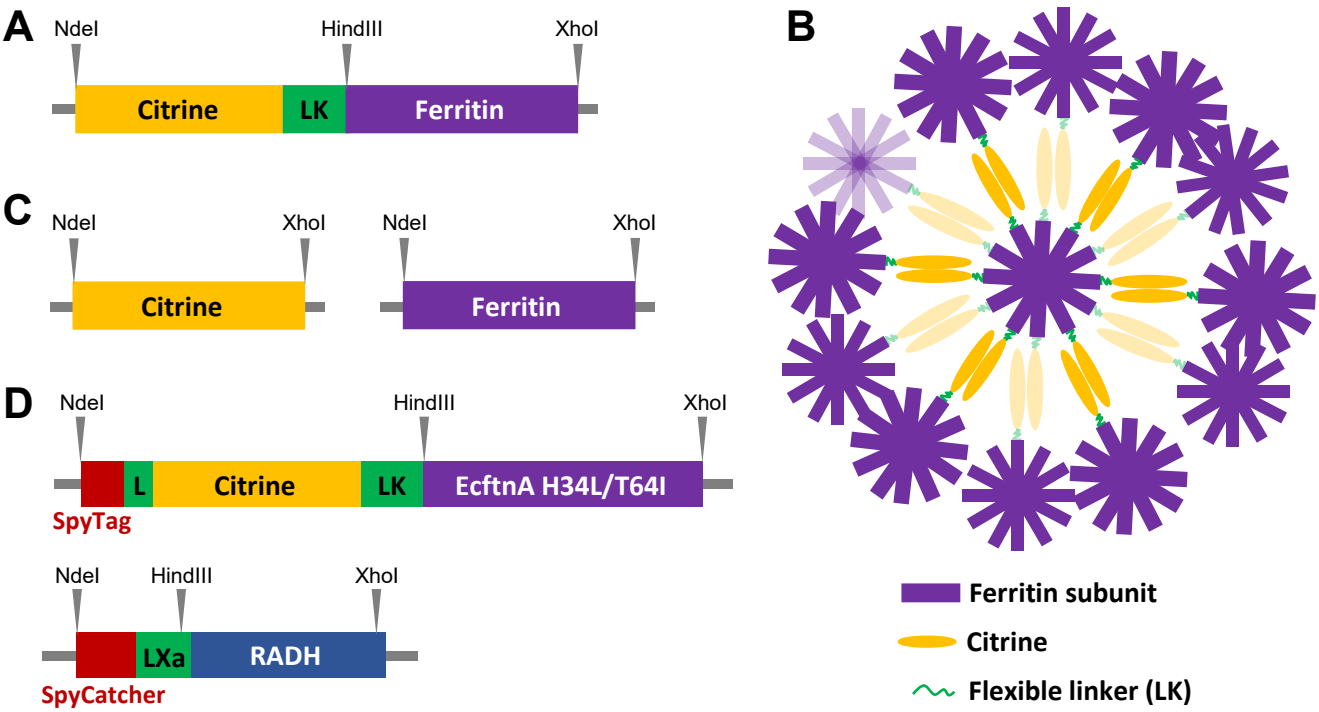

Figure 1. Overview of the constructs generated in this study, along with a cartoon diagram depicting the supramolecular assembly of citrine-ferritins. **(A)** Depiction of citrine-ferritin constructs flanked by NdeI and XhoI sites, where a 17-residue linker (LK) with the amino acid sequence GGTGGSGGSGGSGGTGG followed by the HindIII site separates the genes encoding citrine (depicted in yellow) and ferritin (depicted in purple). Ferritin refers either to the heavy chain of human ferritin (HuftnH), the nonheme ferritin from *E. coli* (EcftnA-WT) or the double mutant of the *E. coli* ferritin (EcftnA H34L/T64I). **(B)** Cartoon diagram showing the supramolecular assembly of citrine-ferritins. Ferritin subunits self-assemble to form the ferritin cage, and the citrines attached to each ferritin subunit form dimers, giving rise to the depicted supramolecular assembly. For simplicity, only half of the ferritin subunits are shown in the image. **(C)** Depiction of the soluble citrine and ferritin constructs flanked by NdeI and XhoI sites. **(D)** Deptiction of the SpyTag002/SpyCatcher002 bearing strains, abbreviated simply as SpyTag/SpyCatcher in text. The gene encoding SpyTag (depicted in red) is present at the 5' of the gene encoding Citrine-EcftnA H34L/T64I fusion for the bait construct, and the gene encoding SpyCatcher (depicted in red) is present at the 5' of the gene encoding an alcohol dehydrogenase (RADH) for the prey construct. For both SpyTag and SpyCatcher bearing constructs, a flexible $(GGGGS)_2$ linker (L) separates SpyTag/SpyCatcher from the remaining gene fusion. For the prey construct (SpyCatcher-RADH) a factor Xa cleavage site (Xa) was included at the 3' end of the $(GGGGS)_2$ linker (L). See methods for additional information and the cloning procedure, and Table S1 for the list of all constructs generated in the study.

All citrine-ferritin fusions exhibited localized signals for citrine fluorescence at a single end of the cell poles, whereas citrine control construct displayed uniform fluorescence as expected.

This observation is also in line with the relative fluorescence data (Figure 2), and the literature on the Citrine-HuftnH construct[33], where Citrine-HuftnH exhibited localized fluorescence signals. It should be noted that the aggregates produced by citrine-ferritins are visually different when compared to conventional (catalytically-active) inclusion bodies (CatIBs)[37-40], as the citrine-ferritin aggregates appear smaller in size and are predominantly present at just one cell pole, as opposed to inclusion bodies which are in general visually present at both poles. The reason for this behavior is currently unclear.

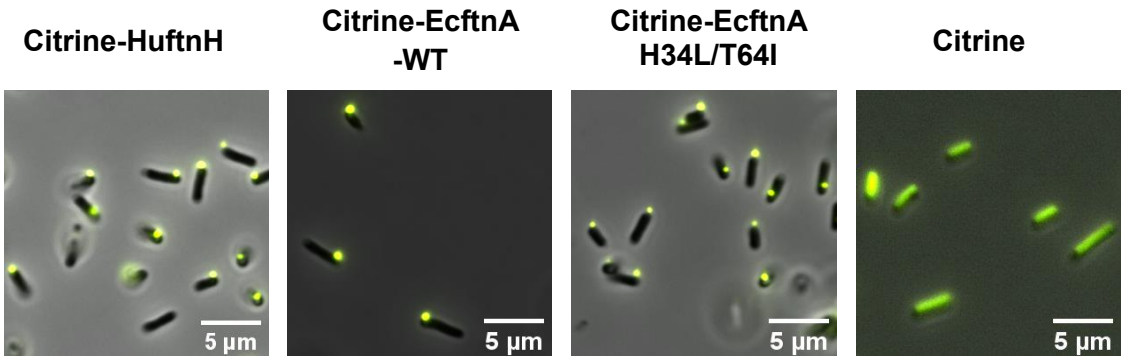

Figure 2. Fluorescence microscopy pictures of live *E. coli* BL21(DE3) cells overproducing citrine-ferritin fusions and soluble citrine. See methods section for details and cultivation conditions.

To quantify the aggregation efficiencies of all constructs, CCEs were fractionated (see Preparation of cell fractions) by centrifugation to yield the soluble supernatant (S) and the insoluble pellet fractions for all constructs. The pellets were then washed and centrifuged a second time to yield the washed pellet (P) fractions, which allowed the quantification of citrine fluorescence distributions for all constructs (Figure 3). Citrine fluorescence detected in the P fraction was then compared to the fluorescence of the CCE fraction (set to 100%) to assess the aggregation efficiencies (%) for all constructs. A construct overproducing soluble citrine was also included in the analysis as control.

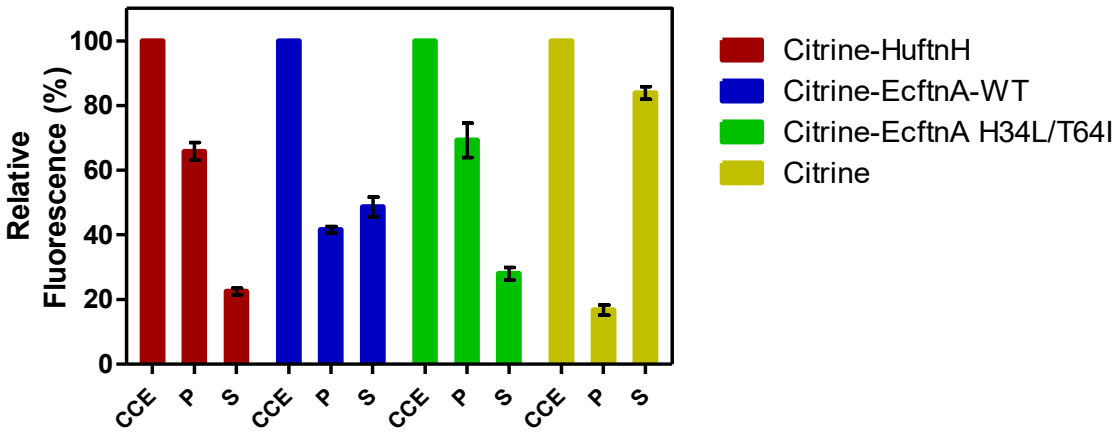

Figure 3. Relative fluorescence of cell fractions from citrine-ferritin fusions and soluble citrine control. Citrine fluorescence of the crude cell extract (CCE) fraction was set to 100% for each construct, and the fluorescence signal detected in washed pellet (P) and supernatant (S) fractions are shown relative to the fluorescence of their corresponding CCE fractions. The error bars represent standard error of the mean derived from at least three biological replicates with four technical replicates each.

As evident from Figure 3, all pellets obtained from the citrine-ferritin fusions were fluorescent and the Citrine-EcftnA H34L/T64 construct displayed the highest aggregation efficiency among the generated constructs, where 69% of the total fluorescence signal of the CCE originated from the insoluble, washed pellet fraction for this construct. Citrine-HuftnH and Citrine-EcftnA-WT constructs displayed very high aggregation efficiencies as well (66% and 42%, respectively). In contrast, the citrine construct lacking ferritins had only 17% of the citrine fluorescence in the pellet, indicating that in addition to dimerization of citrines, fusion of ferritin to the citrine is crucial for aggregation, which is in line with earlier studies conducted with the HuftnH fusion construct[32, 33]. In addition, yields of the constructs were determined, along with their protein contents (Table S4), which indicates that the ferritin-based protein aggregates possess comparable productivities (up to 4.7 g lyophilizate / 100 g wet cells, and 77% protein content depending on construct) to CatIBs with our production and handling techniques.

In conclusion, we could demonstrate that the HuftnH can be successfully exchanged with *E. coli* ferritins to obtain fluorescent aggregates, and as evidenced by the case of the EcftnA H34L/T64I mutant, the resulting fusion proteins can exhibit superior aggregation efficiencies.

Magnetic properties of MPAs and magnetic purification of the fusion proteins

After the initial characterization of citrine-ferritin fusions via live cell microscopy and fluorescence spectroscopy of the cell fractions, we moved on to investigate the magnetism of citrine-ferritin fusions. To provide an easy, visual indication on the magnetic properties of Citrine-HuftnH, Citrine-EcftnA-WT and Citrine-EcftnA H34L/T64I fusions, the fluorescent citrine-ferritin particles were tested for their response towards permanent magnets, in a similar way that was described elsewhere to test whole cell magnetism[36, 41]. To this end, cells overproducing the citrine-ferritin fusions, which were cultivated in autoinduction medium supplemented with 1 mM iron-citrate complex, were lysed (see methods for details and Fig S2 for BioLector experiment with varying iron concentrations). The crude cell extracts (CCEs) of the citrine-ferritin fusions were then transferred to mini petri dishes containing 17% (v/v) OptiPrep density gradient medium. CCE-OptiPrep suspensions were immediately placed over permanent neodymium ring magnets and were imaged up to 69 hours using a camera placed above the samples (Figure 4).

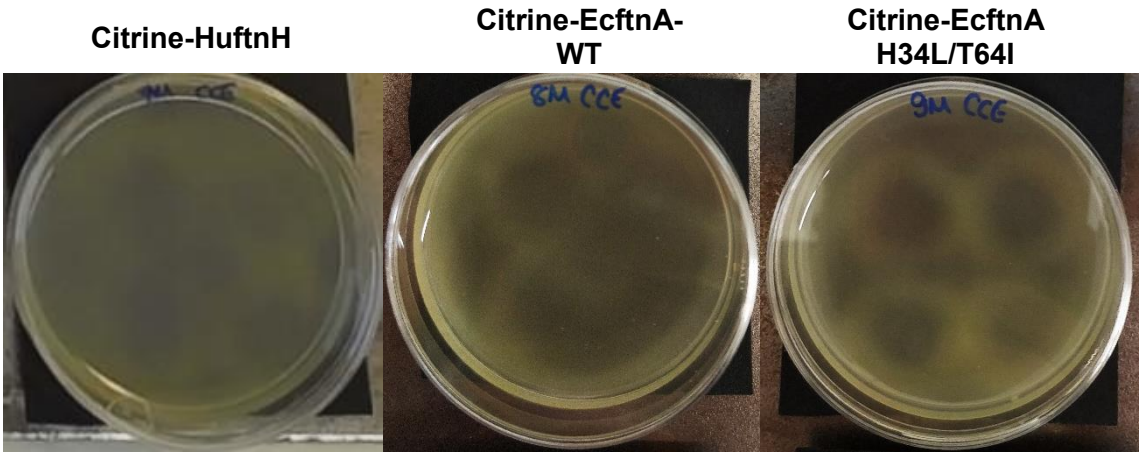

Figure 4. Crude cell extracts (CCEs) containing citrine-ferritin constructs over permanent neodymium ring magnets. The magnets were arranged in a 2x2 grid and covered with a black paper to aid visualization, onto which the mini petri dishes containing the CCE-OptiPrep density gradient medium mixture (17% Optiprep) were placed. The CCEs were left undisturbed for up to 69 hours to follow the pattern formation. The contrast of all images shown above is increased by 20%.

The attraction of citrine-ferritin particles in CCE towards the neodymium magnets underneath the suspensions gave rise to patterns of varying intensity for the tested constructs (Figure 4). Faint, albeit noticeable patterns started forming as early as six hours for the CCE of Citrine-EcftnA H34L/T64I construct, and after nine hours, faint patterns were visible for all three citrine-ferritin constructs (SI video). The imaging ensued for a total of 69 hours to ensure capturing of the entire pattern progression, which became noticeably sharper for the Citrine-EcftnA H34L/T64I construct as time progressed. As a negative control, cells overproducing HuftnH, EcftnA-WT and EcftnA H34L/T64I without the citrines were cultivated and lysed under identical conditions, and their CCEs were placed over permanent magnets as well, which showed no distinct pattern formation (Figure S3), indicating that the soluble ferritins that lack citrine do not form substantial aggregates.

In conclusion, imaging CCEs of the citrine-ferritin fusions over permanent magnets provided first insights into the magnetic properties of the corresponding MPAs, where the Citrine-EcftnA H34L/T64I construct surpassed Citrine-HuftnH and Citrine-EcftnA-WT constructs in this regard. In addition to showing superior magnetic properties, the Citrine-EcftnA H34L/T64I construct also showed the highest aggregation efficiency as judged by the fluorescence distribution data (Figure 3). Therefore, all further work was focused on this construct. The magnetic properties of the Citrine-EcftnA H34L/T64I MPAs was further exploited to purify the fusion protein using MS magnetic columns and OctoMACS separator system (Miltenyi Biotec). In brief, the CCE of Citrine-EcftnA H34L/T64I was passed through the same MS column for a total of three times and the elute was collected (nonmagnetic fraction, NM). The column was then washed twice using lysis buffer (50 mM sodium phosphate buffer, 100 mM NaCl, pH 7.0) and the wash fractions (W1 and W2) were collected. Finally, the magnetic (MG) fraction was eluted by separating the column from the OctoMACS permanent magnet, applying lysis buffer

onto the column and quickly flushing the MG fraction using a small plunger. The magnetic column purification fractions were then loaded onto an SDS-PAGE along with the cell fractions obtained via centrifugation, for assessment of purity of the Citrine-EcftnA H34L/T64I protein (Figure 5).

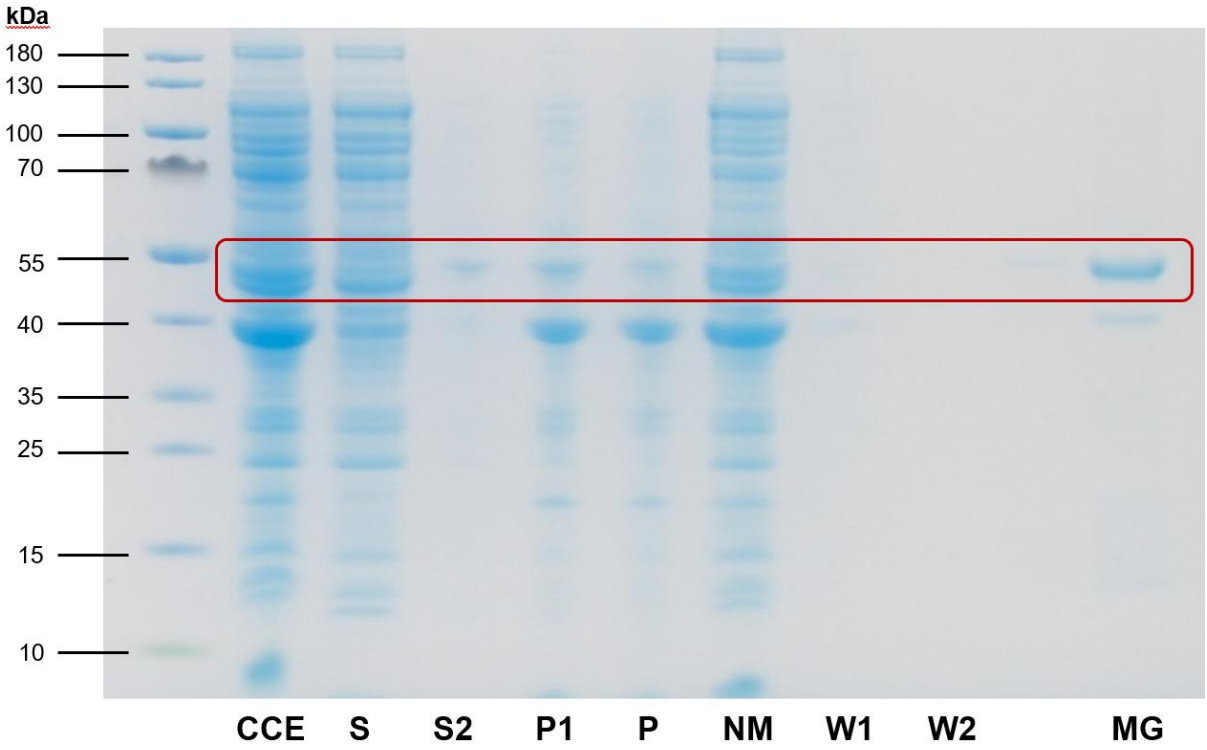

Figure 5. SDS-PAGE analysis of Citrine-EcftnA H34L/T64I cell fractions (CCE, S, S2, P1 and P) and magnetic column purification fractions (NM, W1, W2 and MG). The Citrine-EcftnA H34L/T64I fusion protein (47.8 kDa) is marked with a red rectangle for all fractions. CCE: crude cell extract, S: supernatant, S2: supernatant of wash step, P1: unwashed pellet, P: washed pellet, NM: nonmagnetic fraction, W1: first wash, W2: second wash, MG: magnetic fraction. Protein content of the S fraction was determined using Bradford assay, and the volume required to load 10 µg protein for S fraction was used as the sample volume for all remaining fractions except for MG fraction. The concentration of the MG fraction was determined separately, and the fraction was concentrated prior to loading in order to contain 20 µg protein for this fraction to assess purity of the fraction more critically (See Methods).

SDS-PAGE analysis revealed that the Citrine-EcftnA H34L/T64I fusion protein can be purified using magnetic columns, evident by the clear band present in the MG fraction (Figure 5). Furthermore, the washed pellet fraction (P) of the centrifugation approach containing MPAs contained other proteins as well (i.e. possibly chaperons and membrane proteins commonly encountered in CatIB approach[42] for such insoluble fractions), whereas the magnetically purified MPAS were of high purity. Subsequently, the wash fractions of the magnetic purification samples (W1 and W2) were clear, indicating that the columns retain the Citrine-

EcftnA H34L/T64I fusion protein rather well, and therefore using magnetic columns appears as a suitable method for purifying MPAs.

Furthermore, the citrine-specific fluorescence of the fractions obtained from the magnetic purification approach were determined, and fluorescence detected in each fraction was compared to the total fluorescence of the CCE (set to 100%). Unfortunately, the majority of the citrine fluorescence (approximately 80% of the total CCE fluorescence) originated from the nonmagnetic (NM) fraction, followed by 19% for the magnetic (MG) fraction. The wash fractions W1 and W2 displayed almost no fluorescence (4% and 0.3% when compared to CCE, respectively). As the majority of the fluorescence detected for the Citrine-EcftnA H34L/T64I construct originated from the insoluble fraction (Figure 2), this result indicates that not all of the citrine-ferritin aggregates could be purified by the magnetic purification approach. This could be due to several factors, such as, a fraction of citrine-ferritin aggregates exhibiting weaker magnetism and therefore not being retained by the column (i.e. due to unequal loading of individual ferritin cages), or conversely, the majority of the citrine-ferritin aggregates displaying magnetism and therefore being purified, but not exhibiting strong fluorescence for this fraction. Regardless, to be able to compare the two approaches quantitatively, we calculated the purification success (%) by comparing the fluorescence of the MG fraction, to the fluorescence of the washed pellet (P) fraction obtained via centrifugation (set to 100%). To this end, this quantification assumed that all citrine-ferritin aggregates that are obtained via centrifugation could in theory be purified using the columns and would display fluorescence, yielding up to 42% purification efficiency for the magnetic column purification method. Moreover, as the magnetic purification method excludes impurities (Figure 5), it can potentially make up for this loss depending on the downstream application in cases where high purity is preferable over high quantity.

Extension of the strategy to generate CatMPAs

Next, the magnetic immobilization strategy was further extended as a proof-of-concept to immobilize an alcohol dehydrogenase from *Ralstonia sp* (RADH). To this end, we used the SpyTag/SpyCatcher technology[34], which is based on the engineered CnaB2 domain from a *Streptococcus pyogenes* adhesin, where the SpyTag peptide and SpyCatcher protein arising from the split CnaB2 domain can form a spontaneous, irreversible amide bond that can be used to link two proteins together. We implemented the SpyTag/SpyCatcher system to link the insoluble, Citrine-EcftnA H34L/T64I protein fusion (bait) to soluble RADH (prey), to be able to pull RADH into the insoluble fraction. The gene encoding the faster-reacting variant of SpyTag, SpyTag002[43, 44] was fused to the 5' of the Citrine-EcftnA H34L/T64I gene fusion. Similarly, the gene encoding the engineered SpyCatcher002 variant was fused to the 5' of the

gene encoding RADH (Figure 1, C). To check if the presence of the SpyTag infers with the generation of fluorescent aggregates for the bait construct, and to confirm that the presence of the SpyTag does not result in the formation of significant amounts of RADH inclusion bodies that would shift the RADH to insoluble fraction for the prey, the live cells overproducing both constructs were evaluated by phase contrast and fluorescence microscopy (Figure 6, panels A and C). The microscopic analyses confirmed that the presence of the SpyTag did not interfere with the insoluble fluorescent particle formation for the bait, and SpyCatcher-RADH (prey) showed no particle formation as anticipated.

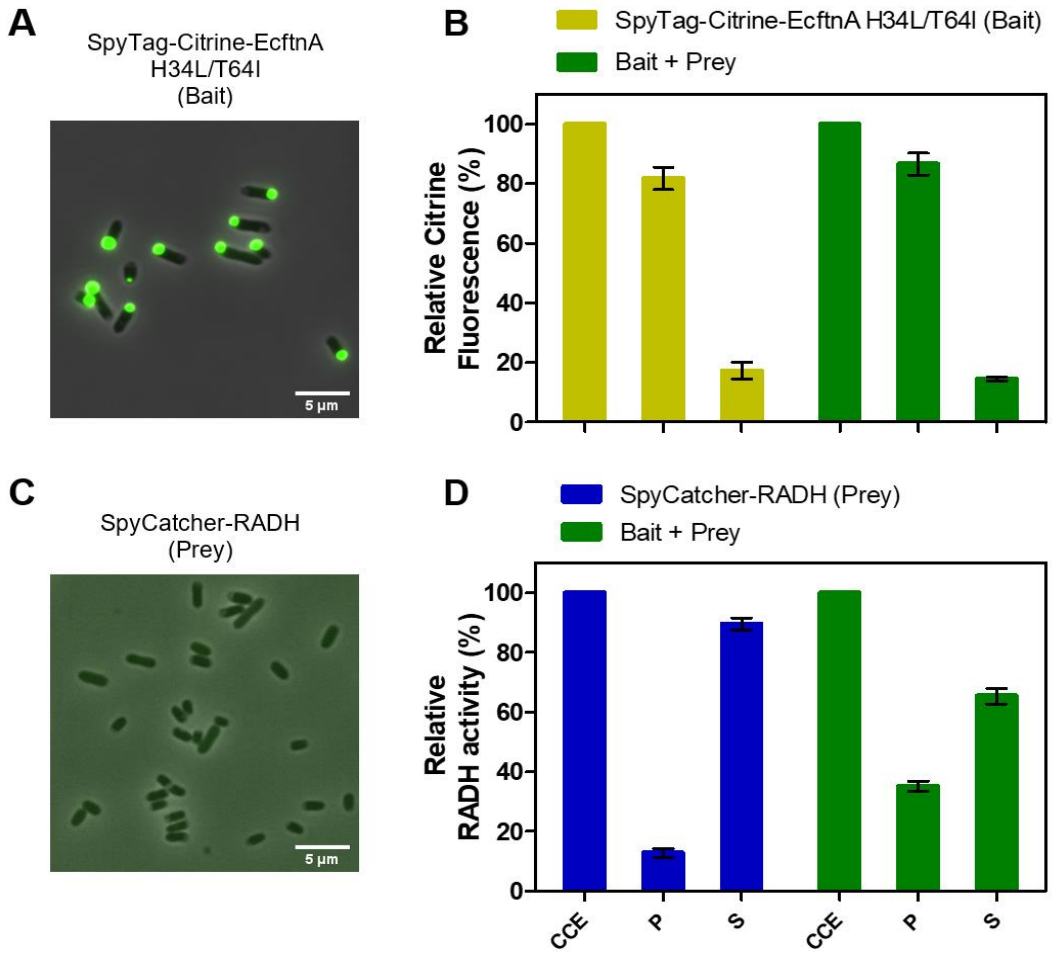

Figure 6. Microscopic analyses and relative fluorescence/activity data for bait and prey constructs. Fluorescence microscopy and phase contrast pictures of live *E. coli* BL21(DE3) cells overproducing Spytag-Citrine-EcftnA H34L/T64I (bait) is shown in (**A**), and SpyCatcher-RADH (prey) in (**C**). See methods section for cultivation conditions. Both panels show composite images obtained by the fluorescence filter and phase contrast. Relative citrine fluorescence (**B**) and relative RADH activity (**D**) of cell fractions of SpyTag-Citrine-EcftnA H34L/T64I (bait, depicted in yellow), SpyCatcher-RADH (prey, depicted in blue) along with the cell fractions of 1:1 (v/v) mixture of the two constructs (bait + prey, depicted in green). CCE: crude cell extract. P: washed pellet. S: supernatant. Error bars correspond to standard error of the mean obtained from at least three biological replicates.

To link the bait and prey constructs, the strains overproducing SpyTag-Citrine-EcftnA H34L/T64I and SpyCatcher-RADH were cultivated separately, the cells were lysed and their CCEs were mixed in 1:1 (v/v) ratio. The CCE mixture was then incubated at 25 °C for 30

minutes to allow the SpyTag/SpyCatcher interaction to take place, after which the mixed CCE was fractionated into soluble and insoluble fractions, and the fluorescence and RADH enzyme activity of the appropriate fractions were determined (for details, see Preparation of cell fractions). The unmixed CCEs of bait and prey constructs were also fractionated to obtain the soluble and insoluble cell fractions, which were tested for fluorescence for the bait construct and RADH activity for the prey (Figure 6).

For the bait construct (Figure 6, panel B, yellow bars), citrine fluorescence was detected predominantly in the insoluble fraction (82%), similar to the Citrine-EcftnA H34L/T64I construct lacking the SpyTag (Figure 2). For the prey construct, only 13% of the RADH activity could be found in the insoluble fraction (Figure 6, panel D, blue bars). Upon mixing the CCEs of bait and prey constructs, the RADH activity of the insoluble fraction could be increased to 35% of the total RADH activity of the mixture (Figure 6, panel D, green bars), corresponding to almost 3-fold activity increase in this fraction. Therefore, the RADH activity could be successfully shifted into the insoluble fraction via the SpyTag/SpyCatcher interaction using the CatMPAs. Altering bait:prey ratios and incubation times did not result in significantly higher activity in the insoluble fraction, similar to alternative bait and prey constructs tested which harbored the tags at different termini (Table S5 and S6). A different approach relying on “magnetization” of GFIL8-PT-RADH CatIBs[40] by soluble ferritin cages was likewise tested with different SpyTag/SpyCatcher constructs (Table S6), however, SpyTag-Citrine-EcftnA H34L/T64I and SpyCatcher-RADH combination presented here yielded the best results. Therefore, utilizing a bait-prey approach is a feasible way to generate CatMPAs, and testing different bait-prey constructs and combinations can be crucial for the optimal implementation of this strategy.

Conclusions

In this study, we successfully generated magnetic protein aggregates (MPAs) by the overproduction of citrine-ferritin fusions, and extended the strategy from human ferritin[33] to wild-type and magnetically enhanced *E. coli* ferritin[36] variants to obtain particles with superior aggregation efficiencies. Furthermore, we were able to demonstrate the magnetic properties displayed by citrine-ferritin fusion proteins for the first time, and further exploited this property to purify and obtain protein immobilizates of high purity. Lastly, in proof-of-concept experiments, we generated enzyme-linked magnetic aggregates utilizing the SpyTag/SpyCatcher[43, 44] technology to link citrine-ferritin to an alcohol dehydrogenase and produced catalytically-active magnetic protein aggregates (CatMPAs). As evidenced by these findings, *in vivo* produced ferritin-based aggregates are a promising, novel way of obtaining solely biologically produced, magnetic enzyme immobilizates. With our study we extend the

use of ferritin in biotechnology and further diversify the toolbox of *in vivo* immobilization methods.

Methods

Cloning

For the generation of Citrine-HuftnH[33], Citrine-EcftnA-WT and Citrine-EcftnA H34L/T64I[36] constructs, synthetic genes encoding the fusion proteins flanked by 5'-NdeI and 3'-XhoI sites were synthesized (Invitrogen GeneArt Gene Synthesis, ThermoFischer Scientific). All constructs contained a flexible linker (LK) harboring a 3'-HindIII site between the genes encoding citrine and ferritins. Additionally, since the *ecftnA* gene naturally encodes a NdeI site (nucleotides 157-162), the thymine at the position 159 was exchanged to cytosine during the design of the genes to simplify the cloning process. Therefore, all EcftnA-WT and EcftnA H34L/T64I constructs generated in this study contained this silent mutation. The plasmids harboring the synthetic genes were hydrolyzed with NdeI and XhoI restriction endonucleases, and were ligated into similarly hydrolyzed pET28a (Merck, Darmstadt, Germany) which was used as expression plasmid. A soluble citrine control strain lacking ferritin was generated via PCR by employing suitable oligonucleotide primers with 5'-NdeI and 3'-XhoI sites (Table S2), using the Citrine-HuftnH construct as template. The resulting PCR product was digested with NdeI and XhoI, and ligated into similarly hydrolyzed pET28a. For the generation of SpyTag002[43] and SpyCatcher002[43, 44] (optimized variants of SpyTag and SpyCatcher respectively, referred to as such in the manuscript) bearing strains, the genes encoding the SpyCatcher, SpyTag and a $(GGGGS)_2$ linker (L) sequence were synthesized (Invitrogen GeneArt Gene Synthesis, ThermoFischer Scientific). The bait construct SpyTag-Citrine-EcftnA H34L/T64I was generated by hydrolyzing the synthetic SpyTag-Citrine gene fusion flanked by 5'-NdeI and 3'-HindIII sites, and ligating the resulting fragment to similarly digested Citrine-EcftnA H34L/T64I containing pET28a vector, and contained the linker (L) sequence separating the gene encoding SpyTag from the gene fusion encoding citrine-ferritin. The prey construct SpyCatcher-RADH was generated by the amplification of the synthetic SpyCatcher sequence using primers with 5'-NdeI and 3'-HindIII sites (Table S2), followed by hydrolyzing the PCR product by these restriction enzymes, and ligating it to similarly hydrolyzed vector containing the RADH sequence that was generated elsewhere[40].The SpyCatcher-RADH construct hence contained a cleavage site for the Factor Xa protease followed by a HindIII site at the 3' end of the linker (L) separating the genes encoding SpyCatcher and RADH). All constructs were verified by sequencing (Seqlab GmbH, Göttingen, Germany).

Bacterial strains, media and cultivation

E. coli DH5α served as the cloning host for the generation of the constructs. For heterologous expression, *E. coli* BL21(DE3) was used. Lysogeny broth[45] served as the growth medium for the cultivation during cloning and for the precultures for heterologous overexpression of the gene fusions. Autoinduction[46] (AI) medium (12 g/l casein-hydrolysate, 24 g/l yeast extract, 2.2 g/l KH_2PO_4, 9.4 g/l K_2HPO_4, 5 g/l glycerol at pH 7.2 supplemented with 0.5 g/l glucose and 2 g/l lactose) was used as the growth medium during protein production. 50 µg/ml kanamycin was added to all growth media for plasmid maintenance. Briefly, LB precultures were used to inoculate the expression cultures with an initial OD_{600} of 0.05 and were cultivated at 37 °C for 3 hours, shaking at 130 rpm. After 3 hours, the ferritin containing strains were supplemented with iron-citrate complex to a final concentration of 1 mM iron and 5 mM citrate, using a sterile filtered stock solution of 100 mM $FeSO_4 \cdot 7H_2O$-500 mM citrate pH 7, and all expression cultures were transferred to 15 °C for 69 hours at 130 rpm. For microscopy, soluble citrine and Citrine-HuftnH/EcftnA-WT/EcftnA H34L/T64I strains were cultivated in a BioLector setup in M9-AI medium (5 g/l $(NH4)_2SO_4$, 3 g/l K_2HPO_4, 6.8 g/l Na_2HPO_4, 0.5 g/l NaCl, 2 g/l NH_4Cl, 0.2 g/l $MgSO_4 \cdot 7H_2O$, 1.5 mg/l $CaCl_2 \cdot 5H_2O$, 15 mg/l $FeSO_4$, 0.2 g/l $Na_3C_6H_5O_7 \cdot 2H_2O$, 10 mg/l thiamine, 0.75 mg/l $AlCl_3 \cdot 6H_2O$, 0.6 mg/l $CoCl_2 \cdot 6H_2O$, 2.5 mg/l $CuSO_4 \cdot 5H_2O$, 0.5 mg/l H_3Bo_3, 17.1 mg/l $MnSO_4 \cdot H_2O$, 3 mg/l $Na_2MoO_4 \cdot 2H_2O$, 1.7 mg/l $NiCl_2 \cdot 6H_2O$, 15 mg/l $ZnSO_4 \cdot 7H_2O$, 5 g/l glycerol, 0.5 g/l glucose and 2 g/l lactose) supplemented with 1 mM iron-citrate and were inoculated at a starting OD_{600} of 0.05 from LB precultures grown overnight. The initial cultivation was performed at 37 °C for 3 hours shaking at 1200 rpm, and expression took place at 15 °C for 69 hours at 1200 rpm, after which the live cells were imaged. SpyTag/SpyCatcher strains were cultivated in AI medium in shake flasks under identical conditions as described earlier in text.

Preparation of cell fractions

E. coli BL21(DE3) cells overproducing the target proteins or protein fusions were harvested (6500g, 30 min, 4 °C). Cells were resuspended 10% (w/v) in lysis buffer (50 mM sodium phosphate buffer, 100 mM NaCl, pH 7.0 for SpyTag/SpyCatcher bearing constructs, pH 8.0 for the remaining constructs). For bait and prey constructs, the lysis buffer at pH 7.0 also served as the incubation buffer for the SpyTag-SpyCatcher reaction to take place. Cells were lysed by using an Emulsiflex-C5 high pressure homogenizer (Avestin Europe GmbH, Mannheim, Germany) with internal pressure between 1000-1500 bar, 3 cycles under constant cooling. For SpyTag/SpyCatcher constructs, the freshly obtained crude cell extracts (CCEs) of bait and prey were mixed in 1:1 (v/v) ratio, vortexed for a few seconds, and then incubated at 25 °C for 30 minutes, shaking at 600 rpm. After 30 minutes, the mixed CCEs were placed on ice. To obtain the soluble and insoluble cell fractions, fresh CCE (or the CCE mixture) was diluted using lysis buffer, and half of the diluted CCE was centrifuged (7697*g*, 2 min, room

temperature) as described elsewhere[40]. The supernatant (S) was transferred to a fresh tube and the unwashed pellet (P1) was resuspended using the same volume of lysis buffer as the removed S fraction. The suspended pellet was centrifuged (7697*g*, 2 min, room temperature), and the supernatant of the wash (S2) was transferred to fresh tubes. The washed pellet was resuspended again in the same volume of lysis buffer as the removed supernatant, resulting in the washed pellet fractions (P). The obtained cell fractions (CCE, S and P) were subsequently kept on ice and were used to determine the fluorescence/RADH activity distributions of the constructs and their mixtures.

Imaging over permanent neodymium magnets

To visualize the magnetic properties of citrine-ferritin fusions, 5 ml of crude cell extracts (CCE) of constructs overproducing the citrine-ferritin fusions were mixed with 1 ml of OptiPrep Density Gradient Medium (STEMCELL Technologies Germany GmbH, Köln, Germany) and transferred to mini petri dishes, corresponding to 10% iodixanol (w/v) concentration in the mixture. The CCE-OptiPrep mixture was supplemented with 50 µg/ml kanamycin to prevent contamination during the course of imaging. Four permanent, axially magnetized N45 neodymium ring magnets (with the dimensions of 20 mm (outer diameter), 10 mm (inner diameter), 6 mm height, EarthMag GmbH, Dortmund, Germany) were arranged in a 2x2 grid and were used to assess the magnetic properties of the constructs visually. Black papers cut in a rectangular shape were placed over the neodymium magnets to aid visualization in a similar way as described elsewhere[36, 41], and the mini petri dishes containing the CCEs were placed carefully on top of the papers resting over the neodymium magnets. The samples were imaged every 10 minutes for up to 69 hours and the patterns emerging in the solution due to the attraction of the citrine-ferritin particles towards the neodymium magnets were captured using a camera (Logitech C930E Full HD-Webcam, Logitech Europe S.A., Lausanne, Switzerland) which was placed directly above the samples. The time lapse video was created using SkyStudioPro, and edited using DaVinci Resolve 17 (Blackmagic Design Pty Ltd., Melbourne, Australia).

Magnetic column purification

To magnetically purify ferritin fusion proteins, commercial MS columns were placed in an OctoMACS separator held by a MACS multistand (Miltenyi Biotec B.V. & Co. KG, Bergisch Gladbach, Germany). The crude cell extracts containing ferritin fusions were supplemented with 0.05 mg/ml DNase I to prevent clogging of the MS columns prior to application. The lysis buffer (50 mM sodium phosphate buffer, 100 mM NaCl, pH 7.0 for SpyTag/SpyCatcher constructs and pH 8.0 for the remaining constructs) was degassed to get rid of air bubbles that could likewise clog the column. 1 ml of degassed lysis buffer was used to wet the MS

column placed in an OctoMACS separator and the elute was discarded. After the equilibration step, 1 ml of CCE was passed through the MS column and collected, and the eluted CCE sample was reloaded onto the same MS column for a total of three times. The sample that eluted after the third run was collected and labelled as the NM (nonmagnetic) fraction. The column was then washed two times using 1 ml degassed lysis buffer and the elutes were collected separately as wash fractions W1 and W2. To obtain the MG (magnetic) fraction, the MS column was removed from the OctoMACS separator, loaded with 1 ml degassed lysis buffer, and the magnetic particles suspended in the column were quickly flushed out using the plunger provided in the kit and collected in a separate tube. All fractions were kept on ice until further analysis.

Fluorescence spectrophotometry

Fluorescence emission of cell fractions of the citrine-containing fusions were measured in quadruples using black Nunc 96-Well MicroWell polypropylene plates (ThermoFisher Nunc, Waltham, USA) and a TECAN infinite M1000 PRO fluorescence MTP reader (TECAN, Mänedorf, Switzerland). 100 µl of CCE, S, P cell fractions or NM, W1, W2, MG fractions in appropriate dilutions were applied in quadruples onto the microtiter plates and the fluorescence emission of the samples were quantified (λ_{ex} = 513 nm, λ_{em} = 529 nm, z-position 18.909 µm, enhancement 120, flash number 25, flash frequency 400 Hz, bandwith 5 nm). Samples were shaken (654 rpm, 2 mm amplitude) for 5-10 seconds immediately before the fluorescence measurements to ensure that the particles are suspended. All measurements were performed using at least three biological replicates.

RADH activity measurements

The cell fractions of SpyTag/SpyCatcher constructs that contained RADH, along with the respective fractions of SpyTag/SpyCatcher CCE mixtures were tested for the distribution of the RADH activity using a discontinuous photometric assay where the consumption of the NADPH was detected as described earlier[37, 40]. Briefly, RADH containing cell/magnetic purification fractions and a reaction mixture of 1400 µl containing 0.5 mM NADPH and 125 mM cyclohexanone in TEA-buffer (50 mM Triethanolamine, 0.8 mM $CaCl_2$, pH 7.5) were incubated separately at 30 °C for 5 minutes. The reaction was initiated by transferring 350 µl of the RADH containing sample onto the 1400 µl reaction mixture, immediately vortexed, and a sample of 250 µl was taken which was transferred onto 500 µl of methanol to stop the reaction. The remaining reaction mixture was quickly placed in a shaking incubator at 1000 rpm and 30 °C. The rest of the reaction mixture was then sampled every minute for a total of six times in the same manner, where the sampled reaction was stopped in methanol. After the last sampling step, the vials were centrifuged (7697*g*, 5 minutes, room temperature) and

transferred to disposable cuvettes to measure the absorption spectra (280 - 500 nm) using a Cary 60 UV-Vis Spectrophotometer (Agilent, Santa Clara, USA). All measurements were performed using at least three biological replicates.

Microscopic analyses

Live *E. coli* BL21(DE3) cells producing the citrine-ferritin constructs and soluble citrine were cultivated in M9-AI medium supplemented with 1 mM iron-citrate complex as described above. At the end of expression (69 hours), cultures were diluted appropriately in lysis buffer (50 mM sodium phosphate buffer, 100 mM NaCl, pH 8.0) and 1 µl of the cell suspension was transferred to glass slides and covered with a coverslip. The samples were then analyzed with Nikon Eclipse Ti microscope (Nikon GmbH, Düsseldorf, Germany) with a YFP filter (λ_{ex} = 500 nm, λ_{em} = 542.5 nm) and Nikon DS-Qi2 camera (Nikon GmbH, Düsseldorf, Germany). Fluorescence and camera exposure times were 200 ms for ph3 and 100 ms for the YFP filter used to detect citrine fluorescence. For bait and prey constructs bearing SpyTag or SpyCatcher, approximately 1 ml was sampled at the end of expression, centrifuged (7697g, room temperature, 1 minute), resuspended and diluted suitably using lysis buffer. The cell suspension was then transferred to polydimethylsiloxane microfluidic chips with inner chamber dimensions of 60 µm x 100 µm x 1µm, and imaged using Nikon Nikon Eclipse Ti microscope (Nikon GmbH, Düsseldorf, Germany) with a YFP filterblock (λ_{ex} 495 nm, λ_{em} 520 nm) and Andor Zyla VSC-01418 camera (Oxford Instruments plc, Oxon, UK) with exposure times of 100 ms for ph3 and YFP filters.

Determination of protein concentration and SDS-PAGE analyses

Protein concentration of the supernatant samples (S) were determined via Bradford assay[47] and bovine serum albumin standards with concentrations between 0.01 - 0.1 mg/ml. NuPAGE 4-12% Bis-TRIS protein gels in MES SDS running buffer (50 mM MES, 50 mM TRIS, 0.1% SDS, 1 mM EDTA, pH 7.3) were used for SDS-PAGE analyses. The volume required to have 10 µg of protein based on the Bradford assay for the S fraction was set as the loading volume for the remaining cell and magnetic purification fractions except for MG. For the MG fraction, the sample was applied onto polyethersulfone membrane centrifugal filters with 3 kDa cutoff (VWR International GmbH, Darmstadt, Germany) to concentrate this fraction. The concentrated MG sample was loaded onto the SDS gel to contain 20 µg of protein in order to increase sensitivity in determining any possible impurities within the fraction. Cell fractions were boiled at 100 °C for 3 minutes before loading onto the SDS gels, and each gel contained 3 µl PageRuler Prestained Protein Ladder (ThermoFisher Nunc, Waltham, USA).

Associated Content

AUTHOR INFORMATION

Corresponding Author

Ulrich Krauss. Phone: +492461612939; Email: u.krauss@fz-juelich.de

Author Contributions

U.K. conceived and designed the study. G.O. generated all constructs, prepared MPAs and CatMPAs, performed magnetic purification and imaging over permanent magnets, activity/fluorescence assays and all other experiments unless mentioned otherwise. B.W., supervised by D.K., performed the microscopic analyses. G.O. and U.K. prepared the manuscript. All authors have read and approved the final version.

Funding Sources

The research was financially supported by the CLIB Competence Centre Biotechnology (CKB) funded by the European Regional Development Fund ERDF (34.EFRE0300096 and 34.EFRE 0300097).

Acknowledgments

The authors would like to thank Kira Küsters (IBG-1 Forschungszentrum Jülich) for cultivating the citrine-ferritin and citrine control constructs in her BioLector setup, Gabriela María Fuentes Reyes (HHU, Düsseldorf) for her assistance in cloning the soluble control constructs, and Esther Knieps-Grünhagen (IMET HHU, Düsseldorf, Forschungszentrum Jülich) for her skillful technical assistance.

ABBREVIATIONS

CatIBs: catalytically-active inclusion bodies

CatMPAs: catalytically-active magnetic protein aggregates

CCE: crude cell extract

EcftnA-WT: nonheme *E. coli* ferritin, wild-type

EcftnA H34L/T64I: nonheme *E. coli* ferritin, double mutant

HuftnH: heavy chain of human ferritin

MG: magnetic fraction

MPAs: magnetic protein aggregates

NM: non-magnetic fraction

S: supernatant

S2: supernatant of wash step

P: washed pellet

P1: unwashed pellet

W1: First wash fraction of the magnetic purification method

W2: Second wash fraction of the magnetic purification method

References

[1] Sheldon, R. A., and van Pelt, S. (2013) Enzyme immobilisation in biocatalysis: why, what and how, *Chem Soc Rev 42*, 6223-6235.

[2] Datta, S., Christena, L. R., and Rajaram, Y. R. (2013) Enzyme immobilization: an overview on techniques and support materials, *3 Biotech 3*, 1-9.

[3] Liu, S. (2020) *Bioprocess Engineering Kinetics, Sustainability, and Reactor Design*, Elsevier.

[4] Mohamad, N. R., Marzuki, N. H., Buang, N. A., Huyop, F., and Wahab, R. A. (2015) An overview of technologies for immobilization of enzymes and surface analysis techniques for immobilized enzymes, *Biotechnol Biotechnol Equip 29*, 205-220.

[5] Homaei, A. A., Sariri, R., Vianello, F., and Stevanato, R. (2013) Enzyme immobilization: an update, *J Chem Biol 6*, 185-205.

[6] Barbosa, O., Ortiz, C., Berenguer-Murcia, A., Torres, R., Rodrigues, R. C., and Fernandez-Lafuente, R. (2015) Strategies for the one-step immobilization-purification of enzymes as industrial biocatalysts, *Biotechnol Adv 33*, 435-456.

[7] Bilal, M., Asgher, M., Cheng, H., Yan, Y., and Iqbal, H. M. N. (2019) Multi-point enzyme immobilization, surface chemistry, and novel platforms: a paradigm shift in biocatalyst design, *Crit Rev Biotechnol 39*, 202-219.

[8] Sheldon, R. A. (2011) Cross-Linked Enzyme Aggregates as Industrial Biocatalysts, *Organic Process Research & Development 15*, 213-223.

[9] Jegan Roy, J., and Emilia Abraham, T. (2004) Strategies in making cross-linked enzyme crystals, *Chem Rev 104*, 3705-3722.

[10] Wang, Z.-G., Wan, L.-S., Liu, Z.-M., Huang, X.-J., and Xu, Z.-K. (2009) Enzyme immobilization on electrospun polymer nanofibers: An overview, *Journal of Molecular Catalysis B: Enzymatic 56*, 189-195.

[11] Sheldon, R. A. (2007) Enzyme Immobilization: The Quest for Optimum Performance, *Advanced Synthesis & Catalysis 349*, 1289-1307.

[12] Wahab, R. A., Elias, N., Abdullah, F., and Ghoshal, S. K. (2020) On the taught new tricks of enzymes immobilization: An all-inclusive overview, *Reactive and Functional Polymers 152*.

[13] Ölçücü, G., Klaus, O., Jaeger, K.-E., Drepper, T., and Krauss, U. (2021) Emerging Solutions for in Vivo Biocatalyst Immobilization: Tailor-Made Catalysts for Industrial Biocatalysis, *ACS Sustainable Chemistry & Engineering 9*, 8919-8945.

[14] Rehm, F. B., Chen, S., and Rehm, B. H. (2016) Enzyme Engineering for In Situ Immobilization, *Molecules 21*.

[15] Wong, J. X., Ogura, K., Chen, S., and Rehm, B. H. A. (2020) Bioengineered Polyhydroxyalkanoates as Immobilized Enzyme Scaffolds for Industrial Applications, *Front Bioeng Biotechnol 8*, 156.

[16] Rasiah, I. A., and Rehm, B. H. (2009) One-step production of immobilized alpha-amylase in recombinant Escherichia coli, *Appl Environ Microbiol 75*, 2012-2016.
[17] Heater, B. S., Lee, M. M., and Chan, M. K. (2018) Direct production of a genetically-encoded immobilized biodiesel catalyst, *Sci Rep 8*, 12783.
[18] Dzuricky, M., Rogers, B. A., Shahid, A., Cremer, P. S., and Chilkoti, A. (2020) De novo engineering of intracellular condensates using artificial disordered proteins, *Nat Chem 12*, 814-825.
[19] Wei, S. P., Qian, Z. G., Hu, C. F., Pan, F., Chen, M. T., Lee, S. Y., and Xia, X. X. (2020) Formation and functionalization of membraneless compartments in Escherichia coli, *Nat Chem Biol 16*, 1143-1148.
[20] Garcia-Fruitos, E., Vazquez, E., Diez-Gil, C., Corchero, J. L., Seras-Franzoso, J., Ratera, I., Veciana, J., and Villaverde, A. (2012) Bacterial inclusion bodies: making gold from waste, *Trends Biotechnol 30*, 65-70.
[21] Jager, V. D., Lamm, R., Kusters, K., Olcucu, G., Oldiges, M., Jaeger, K. E., Buchs, J., and Krauss, U. (2020) Catalytically-active inclusion bodies for biotechnology-general concepts, optimization, and application, *Appl Microbiol Biotechnol 104*, 7313-7329.
[22] Diener, M., Kopka, B., Pohl, M., Jaeger, K.-E., and Krauss, U. (2016) Fusion of a Coiled-Coil Domain Facilitates the High-Level Production of Catalytically Active Enzyme Inclusion Bodies, *ChemCatChem 8*, 142-152.
[23] Köszagová, R. (2020) Inclusion Bodies in Biotechnology, *Journal of Microbiology, Biotechnology and Food Sciences 9*, 1191-1196.
[24] Arosio, P., Ingrassia, R., and Cavadini, P. (2009) Ferritins: a family of molecules for iron storage, antioxidation and more, *Biochim Biophys Acta 1790*, 589-599.
[25] He, D., and Marles-Wright, J. (2015) Ferritin family proteins and their use in bionanotechnology, *N Biotechnol 32*, 651-657.
[26] Truffi, M., Fiandra, L., Sorrentino, L., Monieri, M., Corsi, F., and Mazzucchelli, S. (2016) Ferritin nanocages: A biological platform for drug delivery, imaging and theranostics in cancer, *Pharmacol Res 107*, 57-65.
[27] Wang, Q., Mercogliano, C. P., and Lowe, J. (2011) A ferritin-based label for cellular electron cryotomography, *Structure 19*, 147-154.
[28] Jin, R., Lin, B., Li, D., and Ai, H. (2014) Superparamagnetic iron oxide nanoparticles for MR imaging and therapy: design considerations and clinical applications, *Curr Opin Pharmacol 18*, 18-27.
[29] Chiou, B., and Connor, J. R. (2018) Emerging and Dynamic Biomedical Uses of Ferritin, *Pharmaceuticals (Basel) 11*.
[30] Yamashita, I., Iwahori, K., and Kumagai, S. (2010) Ferritin in the field of nanodevices, *Biochim Biophys Acta 1800*, 846-857.
[31] Zhang, Y., Dong, Y., Zhou, J., Hu, Y., Li, X., and Wang, F. (2019) Peptide-Mediated Immobilization on Magnetoferritin for Enzyme Recycling, *Nanomaterials (Basel) 9*.
[32] Bellapadrona, G., and Elbaum, M. (2014) Supramolecular protein assemblies in the nucleus of human cells, *Angew Chem Int Ed Engl 53*, 1534-1537.
[33] Bellapadrona, G., Sinkar, S., Sabanay, H., Liljestrom, V., Kostiainen, M., and Elbaum, M. (2015) Supramolecular Assembly and Coalescence of Ferritin Cages Driven by Designed Protein-Protein Interactions, *Biomacromolecules 16*, 2006-2011.
[34] Zakeri, B., Fierer, J. O., Celik, E., Chittock, E. C., Schwarz-Linek, U., Moy, V. T., and Howarth, M. (2012) Peptide tag forming a rapid covalent bond to a protein, through engineering a bacterial adhesin, *Proc Natl Acad Sci U S A 109*, E690-697.
[35] Zakeri, B., and Howarth, M. (2010) Spontaneous intermolecular amide bond formation between side chains for irreversible peptide targeting, *J Am Chem Soc 132*, 4526-4527.
[36] Liu, X., Lopez, P. A., Giessen, T. W., Giles, M., Way, J. C., and Silver, P. A. (2016) Engineering Genetically-Encoded Mineralization and Magnetism via Directed Evolution, *Sci Rep 6*, 38019.

[37] Jager, V. D., Kloss, R., Grunberger, A., Seide, S., Hahn, D., Karmainski, T., Piqueray, M., Embruch, J., Longerich, S., Mackfeld, U., Jaeger, K. E., Wiechert, W., Pohl, M., and Krauss, U. (2019) Tailoring the properties of (catalytically)-active inclusion bodies, *Microb Cell Fact 18*, 33.
[38] Jager, V. D., Lamm, R., Kloss, R., Kaganovitch, E., Grunberger, A., Pohl, M., Buchs, J., Jaeger, K. E., and Krauss, U. (2018) A Synthetic Reaction Cascade Implemented by Colocalization of Two Proteins within Catalytically Active Inclusion Bodies, *ACS Synth Biol 7*, 2282-2295.
[39] Garcia-Fruitos, E., Gonzalez-Montalban, N., Morell, M., Vera, A., Ferraz, R. M., Aris, A., Ventura, S., and Villaverde, A. (2005) Aggregation as bacterial inclusion bodies does not imply inactivation of enzymes and fluorescent proteins, *Microb Cell Fact 4*, 27.
[40] Olcucu, G., Baumer, B., Kusters, K., Mollenhoff, K., Oldiges, M., Pietruszka, J., Jaeger, K. E., and Krauss, U. (2022) Catalytically Active Inclusion Bodies horizontal line Benchmarking and Application in Flow Chemistry, *ACS Synth Biol 11*, 1881-1896.
[41] Nishida, K., and Silver, P. A. (2012) Induction of biogenic magnetization and redox control by a component of the target of rapamycin complex 1 signaling pathway, *PLoS Biol 10*, e1001269.
[42] Kloss, R., Karmainski, T., Jäger, V. D., Hahn, D., Grünberger, A., Baumgart, M., Krauss, U., Jaeger, K.-E., Wiechert, W., and Pohl, M. (2018) Tailor-made catalytically active inclusion bodies for different applications in biocatalysis, *Catalysis Science & Technology 8*, 5816-5826.
[43] Keeble, A. H., Banerjee, A., Ferla, M. P., Reddington, S. C., Anuar, I., and Howarth, M. (2017) Evolving Accelerated Amidation by SpyTag/SpyCatcher to Analyze Membrane Dynamics, *Angew Chem Int Ed Engl 56*, 16521-16525.
[44] Keeble, A. H., and Howarth, M. (2019) Insider information on successful covalent protein coupling with help from SpyBank, *Methods Enzymol 617*, 443-461.
[45] Bertani, G. (1951) Studies on lysogenesis. I. The mode of phage liberation by lysogenic Escherichia coli, *J Bacteriol 62*, 293-300.
[46] Studier, F. W. (2005) Protein production by auto-induction in high density shaking cultures, *Protein Expr Purif 41*, 207-234.
[47] Bradford, M. M. (1976) A rapid and sensitive method for the quantitation of microgram quantities of protein utilizing the principle of protein-dye binding, *Anal Biochem 72*, 248-254.

2.3.1. Publication 3. Supporting Information

Gizem Ölçücü, Bastian Wollenhaupt, Dietrich Kohlheyer, Karl-Erich Jaeger, Ulrich Krauss*

*corresponding author

prepared for publication in ACS Biomacromolecules

Generation of Magnetic Protein Aggregates by Supramolecular Assembly of Ferritin Cages

Gizem Ölçücü[1,2], Bastian Wollenhaupt[2], Dietrich Kohlheyer[2], Karl-Erich Jaeger[1,2], Ulrich Krauss[1,2,*]

Author affiliations

[1]Institute of Molecular Enzyme Technology, Heinrich Heine University Düsseldorf, Forschungszentrum Jülich GmbH, Wilhelm Johnen Strasse, D-52425 Jülich, Germany

[2]Institute of Bio- and Geosciences IBG-1: Biotechnology, Wilhelm Johnen Strasse, Forschungszentrum Jülich GmbH, D-52425 Jülich, Germany

Corresponding author: Ulrich Krauss, Phone: +492461612939; Email: u.krauss@fz-juelich.de

Supporting Methods

Cloning

Control constructs containing only HuftnH/EcftnA-WT/EcftnA H34L/T64I were generated via PCR, using oligonucleotides listed in Table S2 and Citrine-HuftnH/EcftnA-WT/EcftnA H34L/T64I constructs as template for the amplification of the respective ferritin encoding genes. A 5'-NdeI site and a 3'-XhoI site were included in the oligonucleotide primers to amplify the respective ferritins with 5'-NdeI and 3'-XhoI sites, and the resulting PCR products were digested using NdeI and XhoI restriction enzymes, and ligated into similarly digested pET28a to generate the soluble HuftnH/EcftnA-WT/EcftnA H34L/T64I control constructs. The SpyTag-RADH construct was generated by using a synthetic gene containing the entire sequence of the construct and flanked by flanked by 5'-NdeI and 3'-XhoI sites, where the synthetic gene was hydrolyzed using NdeI and XhoI, and ligated to pET28a digested with the same enzymes. SpyTag-GFIL8-PT-RADH and GFIL8-PT-RADH-SpyTag constructs were generated via a modular construction strategy, using GFIL8-PT-RADH construct generated earlier[1], and a synthetic gene that contained the *radh* gene only partially. As such, the synthetic gene with SpyTag-GFIL8-PT-RADH sequence harbored a 5'-NdeI site, and contained the *radh* gene until the natural PstI site of the native *radh*. The synthetic gene was digested using NdeI and PstI, and ligated to the GFIL8-(PT)-RADH vector to obtain the complete SpyTag-GFIL8-PT-RADH construct. Similarly, the synthetic gene encoding a partial *radh* sequence (after the natural PstI site), followed by SpyTag and a 3'-XhoI site, was digested using PstI and XhoI, and ligated to GFIL8-PT-RADH, which was identically hydrolyzed to yield the complete GFIL8-PT-RADH-SpyTag. SpyCatcher-EcftnA H34L/T64I and SpyCatcher-Citrine-EcftnA H34L/T64I constructs were generated via the In-Fusion cloning kit (Clontech Laboratories, Inc., Takara Bio, Saint-Germain-en-Laye, France). Briefly, the synthetic gene containing the SpyCatcher sequence was used as a template for PCR using primers (Table S2) designed for In-Fusion cloning according to kit instructions, and ligation free cloning was performed using the PCR products and Citrine-EcftnA H34L/T64I vector either nicked using NdeI (to generate SpyCatcher-EcftnA H34L/T64I), or digested using NdeI and HindIII (to generate SpyCatcher-Citrine-EcftnA H34L/T64I). All SpyTag/SpyCatcher containing constructs included a linker (L) separating the genes encoding these tags from the genes encoding target proteins. All constructs generated in this study was verified by sequencing.

BioLector Cultivations

For Biolector (m2p-labs GmbH, Baesweiler, Germany) experiments, *E. coli* BL21(DE3) cells overproducing citrine-ferritins were initially cultivated in LB medium in shake flasks (37 °C,

130 rpm, overnight). LB precultures were used to inoculate 100 ml AI main cultures at a starting OD600 of 0.05, and were incubated at 37 °C for 3 hours, shaking at 130 rpm. After this initial growth phase, 900 µl of the AI cultures were transferred onto 100 µl AI medium with varying iron-citrate concentrations (0 mM - 100 mM) in 48-well FlowerPlates (m2p-labs GmbH, Baesweiler, Germany), giving rise to final iron-citrate concentrations ranging between 0 mM - 10 mM in the FlowerPlates. The FlowerPlates were then immediately covered with oxygen-permeable films and transferred to the Biolector, where the expression continued for 69 hours at 15 °C, shaking at 1200 rpm. The Biolector setup was used to monitor biomass as estimated by scattered light (λex 620 nm, λem 620) and citrine fluorescence using filter sets for eYFP (λex 508 nm, λem 532 nm) during the expression for the initial assessment of varying iron-citrate complex concentrations on growth and the fluorescence of live cells.

Determination of MPA yields

To determine the yields of citrine-ferritin constructs, the crude cell extracts of freshly lysed cells were centrifuged (15000*g*, 30 mins, 4 °C) and the supernatant was discarded. The pellet was then resuspended in the same volume of MilliQ water as the removed supernatant and centrifuged a second time (15000*g*, 30 mins, 4 °C). The supernatant of the wash was discarded, and the washed pellet was again resuspended in the same volume of MilliQ water, and the washed pellet suspension was frozen at -80 °C. The frozen pellet was weighed and then lyophilized (Christ ALPHA 1-3 LD Plus, Martin Christ Gefriertrocknungsanlagen GmbH, Osterode, Germany), ground into powder using mortar and pestles, and the lyophilized pellet was carefully weighed. The lyophilized samples were stored under an argon atmosphere at -20 °C. Protein content of the lyophilizates were determined[1] by dissolving the samples in 6 M guanidine-hydrochloride at 30 °C for 30 minutes, followed by centrifugation (7697*g*, 20 mins, room temperature), and the transfer of the supernatants to disposable cuvettes to measure absorbance at 280 nm (Cary 60 UV-Vis Spectrophotometer, Agilent, Santa Clara, USA). The protein contents of the lyophilized pellets were calculated using the theoretical extinction coefficients and molecular weights estimated from the amino acid sequences of the constructs using ProtParam tool[2] (see Table S3). Yields were calculated by dividing the amount of lyophilizate or protein obtained at the end of the process (in mg lyophilizate or mg protein) by the amount of wet cells that were lysed to obtain these lyophilizates (in g wet cells), see Table S4.

Supporting Results

Table S1. List of constructs generated for the study.

Construct name
Citrine-HuftnH[3]
Citrine-EcftnA-WT
Citrine-EcftnA H34L/T64I
Soluble Citrine
Soluble HuftnH
Soluble EcftnA-WT
Soluble EcftnA H34L/T64I[4]
SpyTag-GFIL8-PT-RADH
GFIL8-PT-RADH-SpyTag
SpyCatcher-EcftnA H34L/T64I
SpyCatcher-Citrine-EcftnA H34L/T64I
SpyTag-Citrine-EcftnA H34L/T64I
SpyCatcher-RADH
SpyTag-RADH

Table S2. Oligonucleotides used in the study. The restriction sites are underlined.

Name	Sequence (5' - 3')	Construct generated
NdeI_Citrine_fw	TATATACATATGGTGAGCAAGGG CGAGGAGCTGTTC	Soluble citrine
Citrine_Stop_XhoI_rev	TATATACTCGAGTTACTTGTACA GCTCGTCCATGCCG	
NdeI_HuftnH_fw	TATATACATATGACGACCGCATC CACCTCGCAGG	Soluble HuftnH
HuftnH_Stop_XhoI_rev	ATATATCTCGAGTTAGCTTTCATT ATCACTGTCTCC	
NdeI_EcftnA_fw	TATATACATATGCTGAAACCAGA AATGATTG	Soluble EcftnA-WT Soluble EcftnA H34L/T64I
EcftnA_XhoI_rev	ATATATCTCGAGTTAGTTTTGTGT GTCGAGGGTAGAG	
NdeI_SpyCatcher_R_fw	TATATACATATGGGCGCGATGGT GACCACCCTGAGCG	SpyCatcher-RADH
L_HindIII_rev	TATATAAAGCTTACGGCCTTCAA TGCTACCGCCACCGCCGCTAC	SpyCatcher-RADH
NdeI_SpyCatcher_fw	AAGGAGATATACATATGGGCGC GATGGTGACCACC	SpyCatcher-Citrine-EcftnA H34L/T64I SpyCatcher-EcftnA H34L/T64I
SpyCatcher_NdeI_rev	CCCTTGCTCACCATATGGCTACC GCCACCGCCGCTACC	SpyCatcher-Citrine-EcftnA H34L/T64I
SpyCatcher_HindIII_rev	GTTTCAGCATAAGCTTGCTACCG CCACCGCCGCTACC	SpyCatcher-EcftnA H34L+T64I

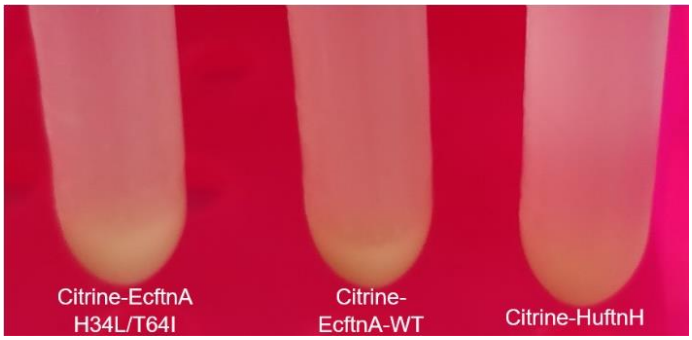

Figure S1. Self-sedimentation of crude cell extracts of citrine-ferritins in a test tube after 16 hours.

Table S3. Theoretical extinction coefficients and molecular weights of the constructs derived using the amino acid sequences and Expasy ProtParam[2] (http://web.expasy.org/protparam)

Construct name	Extinction coefficient (M^{-1} cm^{-1})	Molecular weight (Da)
Citrine-HuftnH	42540	49.6
Citrine-EcftnA-WT	47915	47.8
Citrine-EcftnA H34L/T64I	47915	47.8

Table S4. Yields and protein contents of the citrine-ferritin constructs generated in the study.

Construct name	Yield (g lyophilizate / 100 g wet cells)		Yield (mg protein / g wet cells)		Protein content of lyophilizate (%)	
	Mean	SE	Mean	SE	Mean	SE
Citrine-HuftnH	4.7	0.2	36.5	3.6	76.6	4.6
Citrine-EcftnA-WT	3.8	0.4	22.2	3.0	57.5	2.3
Citrine-EcftnA H34L/T64I	3.8	0.5	29.1	3.6	76.2	1.7

SE represents standard error of the mean derived from at least three biological replicates with three technical replicates each. Protein contents of lyophilizates were calculated using the theoretical extinction coefficients and molecular weights listed in Table S3.

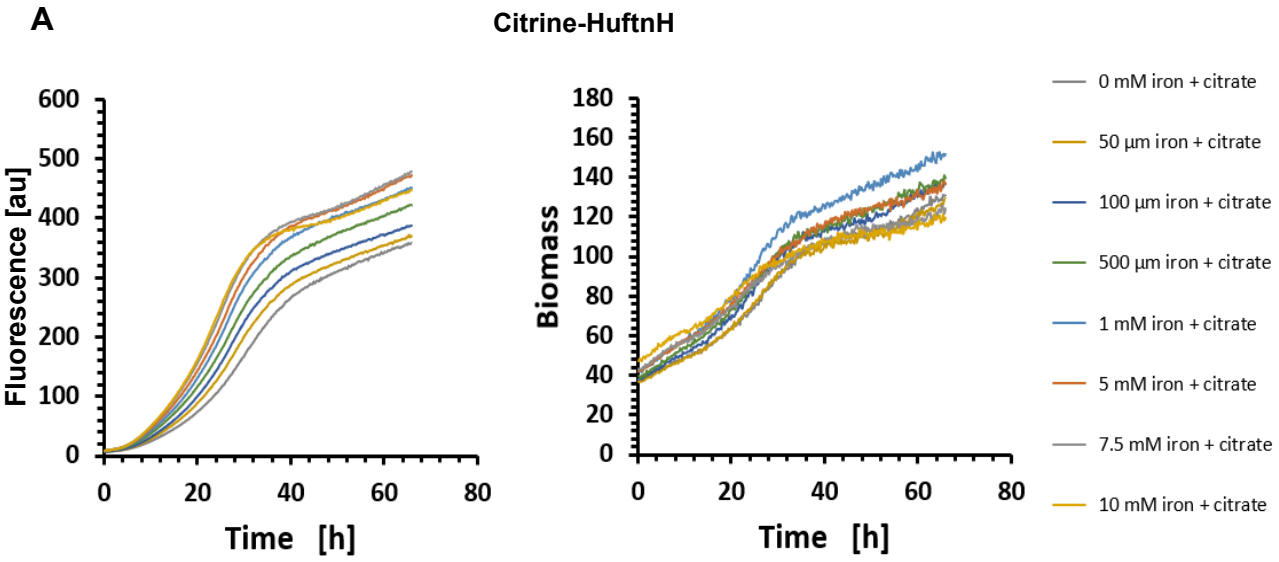

Figure S2. BioLector experiments depicting citrine fluorescence (left) and biomass (right) during expression with varying iron-citrate complex concentrations for **(A)** Citrine-HuftnH, **(B)** Citrine-EcftnA-WT and **(C)** Citrine-EcftnA H34L/T64I. Citrine-ferritins that were not supplemented with iron displayed the lowest fluorescence intensity for all three constructs, which was followed by 50 µM, 100 µM and 500 µM supplementations, indicating that iron concentration has a marked effect on the proper maturation of the citrine-ferritin fusion proteins. Supplementation of 5 mM or more of iron citrate complex had a negative impact on growth for Citrine-EcftnA-WT and Citrine-EcftnA-H34L/T64I, and the same effect was observed for supplementation of 7.5 mM or more iron for Citrine-HuftnH construct. Therefore, 1 mM was chosen as a suitable concentration for iron supplementation and was used for the cultivation of all strains.

Figure S2 (continued)

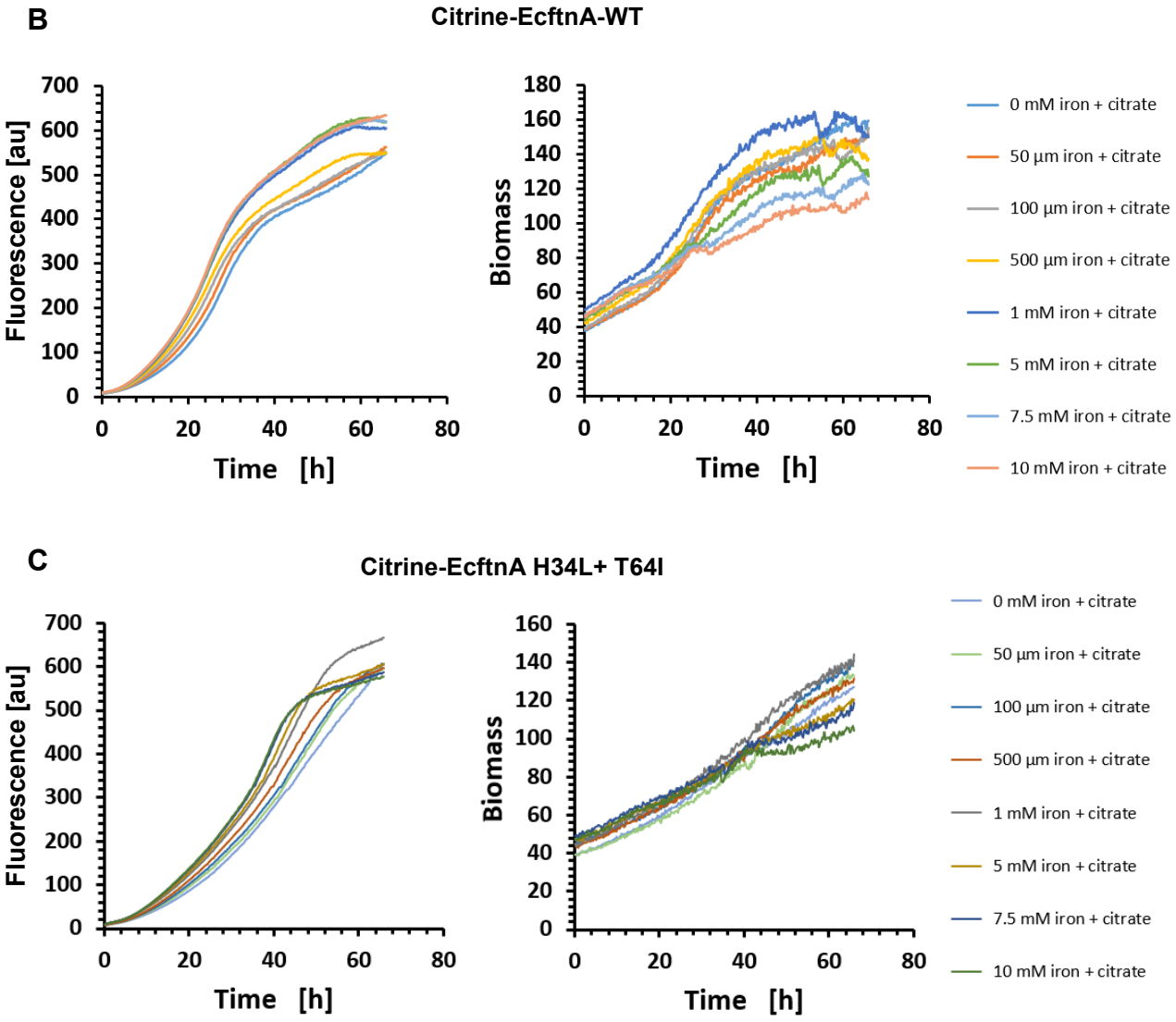

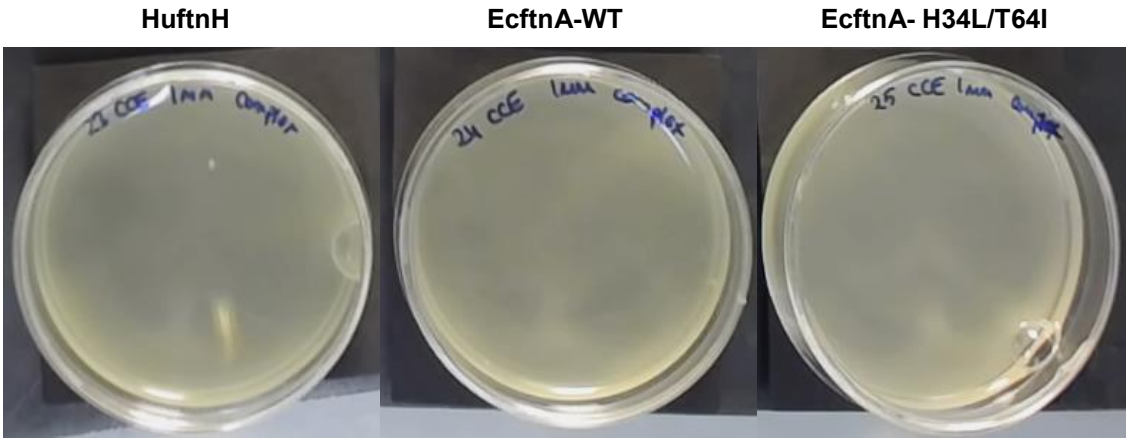

Figure S3. Crude cell extracts (CCEs) of constructs overproducing soluble ferritins. Mini petri dishes containing CCEs were placed over permanent neodymium ring magnets arranged in a 2x2 grid covered with a black paper. The CCEs were mixed with OptiPrep density gradient medium mixture (17% Optiprep) and imaged after 69 hours. The contrast of all three images were increased by 20%.

Table S5. Relative RADH activity of SpyTag-Citrine-EcftnA H34L/T64I (bait) and SpyCatcher-RADH (prey) constructs mixed and incubated under different conditions.

Mixture ratio Bait:Prey (v/v)	Incubation time (minutes)	Relative RADH Activity (%)		
		CCE	S	P
1:1	30	100	65.4	35.1
1:1	60	100	75.3	38.2
1:1	90	100	67.9	35.6
1:10	30	100	73.0	34.1
1:20	30	100	77.7	25.4
5:1	30	100	74.1	33.3
10:1	30	100	76.3	27.6

The crude cell extracts (CCEs) of bait and prey constructs were either mixed in a 1:1 ratio and incubated for different durations, or were incubated for 30 minutes but mixed in a different ratio. For all cases, after bait and prey constructs were cultivated and lysed separately, their CCEs were mixed and incubated at 25 °C, fractionated to yield soluble (S) and insoluble fractions, and the insoluble fractions were washed to obtained washed pellets (P). Each fraction was compared to the total RADH activity of the mixed CCE for each case (set to 100%).

Table S6. RADH activity distribution data and purification efficiency for all bait and prey constructs.

Names of constructs mixed (1:1 v/v)		Relative RADH Activity of bait + prey mixture (%)			Relative RADH Activity of prey (%)			Purification efficiency (%)
Bait	Prey	CCE	S	P	CCE	S	P	Bait + Prey
Spytag-Citrine-EcftnA H34L/T64I (*)	SpyCatcher-RADH	100	65.4	35.1	100	89.5	12.8	9.4 - 18.4**
SpyCatcher-Citrine-EcftnA H34L/T64I (*)	SpyTag-RADH	100	91.5	8.3	100	97.2	2.6	n.a.
SpyCatcher-EcftnA H34L/T64I	SpyTag-GFIL8-PT-RADH (*)	100	75.6	30.9	100	58.8	40.2	5.1
SpyCatcher-EcftnA H34L/T64I	GFIL8-PT-RADH-SpyTag (*)	100	73.9	24.2	100	72.7	27.7	97.4

Crude cell extracts (CCE) were fractionated to yield soluble (S) and insoluble fractions, and the insoluble fractions were washed to obtained washed pellets (P). For bait + prey, bait and prey constructs were cultivated and lysed separately, their CCEs were mixed in a 1:1 ratio (v/v) and incubated at 25 °C for 30 minutes, fractionated and washed to yield S and P fractions of the CCE mixture in the same manner. All fractions were compared to the total RADH activity of the CCE they were fractionated from (mixed CCE for bait+prey) for each case (set to 100%). For each pair, the insoluble partner is marked with an asterisk (*). Purification efficiencies were calculated using mixed CCE fractions, based on relative citrine fluorescence or relative RADH activity (**) of the magnetic fraction (MG), compared to that of the washed pellet (P2, set to 100%). For the bait-prey mixtures with a single purification efficiency value, the calculation is based on RADH activity.

Supporting References

[1] Olcucu, G., Baumer, B., Kusters, K., Mollenhoff, K., Oldiges, M., Pietruszka, J., Jaeger, K. E., and Krauss, U. (2022) Catalytically Active Inclusion Bodies horizontal line Benchmarking and Application in Flow Chemistry, *ACS Synth Biol 11*, 1881-1896.

[2] Wilkins, M. R., Gasteiger, E., Bairoch, A., Sanchez, J. C., Williams, K. L., Appel, R. D., and Hochstrasser, D. F. (1999) Protein identification and analysis tools in the ExPASy server, *Methods Mol Biol 112*, 531-552.

[3] Bellapadrona, G., Sinkar, S., Sabanay, H., Liljestrom, V., Kostiainen, M., and Elbaum, M. (2015) Supramolecular Assembly and Coalescence of Ferritin Cages Driven by Designed Protein-Protein Interactions, *Biomacromolecules 16*, 2006-2011.

[4] Liu, X., Lopez, P. A., Giessen, T. W., Giles, M., Way, J. C., and Silver, P. A. (2016) Engineering Genetically-Encoded Mineralization and Magnetism via Directed Evolution, *Sci Rep 6*, 38019.

2.4. Publication 4. Catalytically-active inclusion bodies for biotechnology — general concepts, optimization, and application

Vera D. Jäger, Robin Lamm, Kira Küsters, Gizem Ölçücü, Marco Oldiges, Karl-Erich Jaeger, Jochen Büchs and Ulrich Krauss*

*corresponding author

Applied Microbiology and Biotechnology 104.17 (2020), pp. 7313-7329. [84]. https://link.springer.com/article/10.1007/s00253-020-10760-3

Author Contributions: UK conceived the outline of this review. UK and VDJ contributed the figures. All authors contributed to literature searches and the writing of the manuscript. All authors have read and approved the final version.

Applied Microbiology and Biotechnology (2020) 104:7313–7329
https://doi.org/10.1007/s00253-020-10760-3

MINI-REVIEW

Catalytically-active inclusion bodies for biotechnology—general concepts, optimization, and application

Vera D. Jäger[1,2,3] · Robin Lamm[2,4] · Kira Küsters[5,6] · Gizem Ölçücü[1,5] · Marco Oldiges[5,6] · Karl-Erich Jaeger[1,2,5] · Jochen Büchs[2,4] · Ulrich Krauss[1,2,5]

Received: 6 May 2020 / Revised: 24 June 2020 / Accepted: 29 June 2020 / Published online: 10 July 2020

Abstract

Bacterial inclusion bodies (IBs) have long been considered as inactive, unfolded waste material produced by heterologous overexpression of recombinant genes. In industrial applications, they are occasionally used as an alternative in cases where a protein cannot be expressed in soluble form and in high enough amounts. Then, however, refolding approaches are needed to transform inactive IBs into active soluble protein. While anecdotal reports about IBs themselves showing catalytic functionality/activity (CatIB) are found throughout literature, only recently, the use of protein engineering methods has facilitated the on-demand production of CatIBs. CatIB formation is induced usually by fusing short peptide tags or aggregation-inducing protein domains to a target protein. The resulting proteinaceous particles formed by heterologous expression of the respective genes can be regarded as a biologically produced bionanomaterial or, if enzymes are used as target protein, carrier-free enzyme immobilizates. In the present contribution, we review general concepts important for CatIB production, processing, and application.

Key points

- *Catalytically active inclusion bodies (CatIBs) are promising bionanomaterials.*
- *Potential applications in biocatalysis, synthetic chemistry, and biotechnology.*
- *CatIB formation represents a generic approach for enzyme immobilization.*
- *CatIB formation efficiency depends on construct design and expression conditions.*

Keywords Catalytically active inclusion bodies · Enzyme immobilization · Protein engineering · Synthetic biology · Protein co-localization · Biocatalysis · Synthetic reaction cascades · Upstream and downstream processing

✉ Ulrich Krauss
u.krauss@fz-juelich.de

[1] Institut für Molekulare Enzymtechnologie, Heinrich-Heine-Universität Düsseldorf, Forschungszentrum Jülich GmbH, 52425 Jülich, Germany

[2] Bioeconomy Science Center (BioSC), c/o Forschungszentrum Jülich, Jülich 52425, Germany

[3] Present address: Department of Bioproducts and Biosystems, Aalto University, Kemistintie 1, Espoo 02150, Finland

[4] AVT-Chair for Biochemical Engineering, RWTH Aachen University, Aachen 52074, Germany

[5] Institute of Bio- and Geosciences IBG-1: Biotechnology, Forschungszentrum Jülich GmbH, Jülich 52425, Germany

[6] Institute of Biotechnology, RWTH Aachen University, 52074 Aachen, Germany

Introduction

Bacteria such as *Escherichia coli* often produce inclusion bodies (IBs) as consequence of the accumulation of misfolded protein due to strong overexpression of heterologous genes (Baneyx and Mujacic 2004). For a long time, IBs have thus been regarded as inactive waste or, at best, as by-products consisting solely of misfolded and aggregated proteins. Due to their purity, consisting predominately of the aggregating target protein, they have traditionally been used for refolding studies, in which they served as an easy to separate source of pure target protein (Singh et al. 2015). This long-held misconception has been challenged in recent years as more and more studies have revealed the dynamic, heterogeneous nature of bacterial IBs, which alongside of misfolded protein also contain protein species with amyloid structure as well as native-

like and correctly folded protein (Garcia-Fruitos et al. 2005; Park et al. 2012; Jäger et al. 2019a; Jäger et al. 2018; Jäger et al. 2019b; Kloss et al. 2018a, b; Lamm et al. 2020; Zhou et al. 2012; Wang et al. 2015; Jiang et al. 2019; Wu et al. 2011; Lin et al. 2013; Diener et al. 2016; Choi et al. 2011; Nahalka and Nidetzky 2007; Nahalka et al. 2008; Nahalka 2008; Nahalka and Patoprsty 2009; Koszagova et al. 2018; Huang et al. 2013; Arie et al. 2006). Thus, more and more evidence suggests that those properties are to a certain degree an inherent feature of all IBs and that all cytoplasmic proteins exist in a conformational equilibrium between soluble-folded, partially misfolded, and insoluble aggregates. This equilibrium in turn can be shifted depending on certain cellular conditions that favor either soluble production, misfolding, degradation, aggregation as IBs, or disintegration of the latter (Fig. 1a, b). Hereby, it seems reasonable to assume that conditions under which the cellular refolding and degradation machinery is outbalanced (e.g., upon conditions of strong overexpression) favor the formation of IBs. This hypothesis finds further support in recent studies, which have shown that for the same genetic construct, depending on the employed cultivation and induction conditions, either active CatIBs or classical, inactive IBs are formed (Lamm et al. 2020). Here, we refer to IBs that retain a certain degree of catalytic activity (in case of enzymes) or fluorescence (in case of fluorescent reporters) as catalytically active IBs (CatIBs). While anecdotal evidence suggests that proteins and enzymes can form CatIBs naturally (Dong et al. 2014; Garcia-Fruitos et al. 2005; Li et al. 2013; Worrall and Goss 1989; Park et al. 2012; Tokatlidis et al. 1991; Krauss et al. 2017; Nahálka et al. 2006), the majority of studies that reported successful formation of CatIBs relied on molecular biological fusion of a variety of different aggregation-inducing peptides, protein domains, or proteins (Garcia-Fruitos et al. 2005; Park et al. 2012; Jäger et al. 2018; Jäger et al. 2019a, b; Kloss et al. 2018a, b; Lamm et al. 2020; Zhou et al. 2012; Wang et al. 2015; Jiang et al. 2019; Wu et al. 2011; Lin et al. 2013; Diener et al. 2016; Choi et al. 2011; Nahalka and Nidetzky 2007; Nahalka et al. 2008; Nahalka 2008;

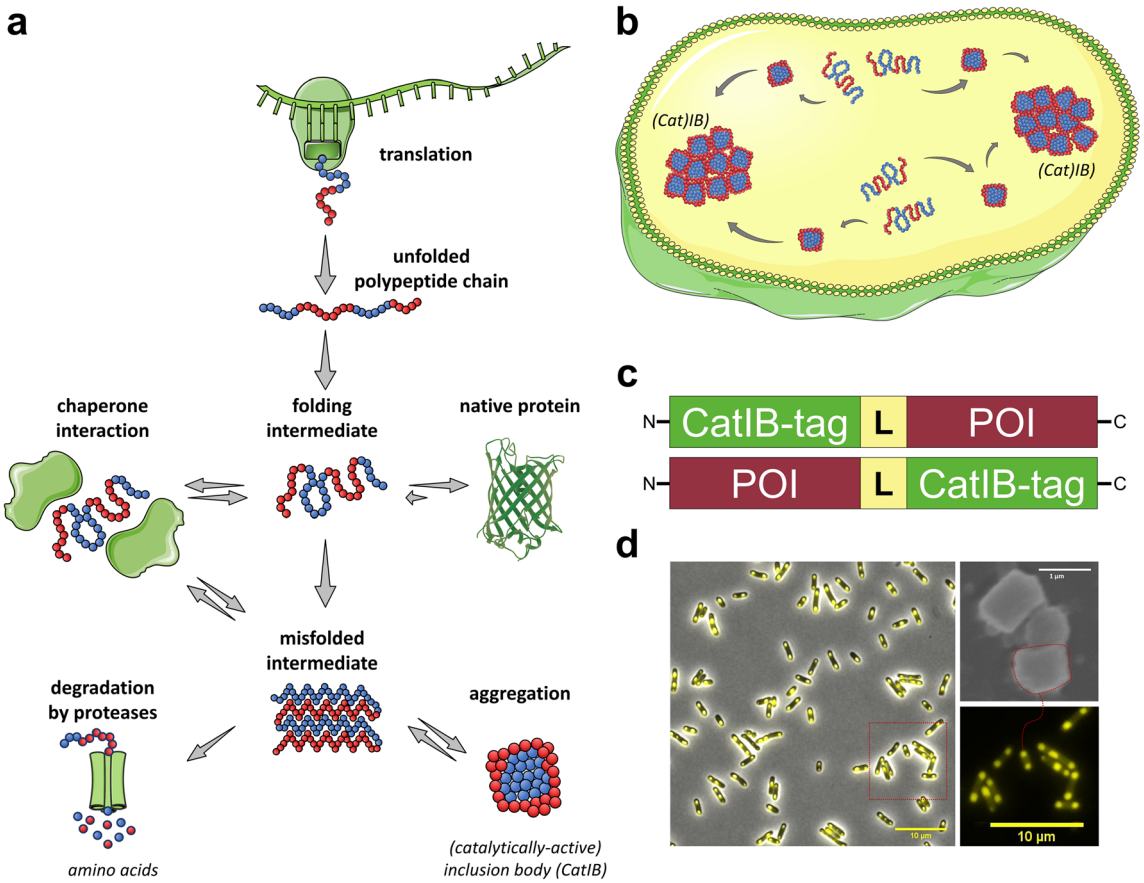

Fig. 1 (Cat)IB formation in bacteria. **a** Cellular processes leading to the formation of inclusion bodies (IBs), which are subsequently **b** deposited at the cell poles likely driven by nucleoid exclusion (Rinas et al. 2017; Kopito 2000). Structural regions that adopt a native or native-like fold are shown as red-filled circles. Aggregation-prone sequence stretches are depicted as blue-filled circles. **c** Fusion protein architectures for the induction of CatIB formation. In all cases, an aggregation-inducing CatIB-tag is fused either N- or C-terminally to a protein of interest (POI). To link both protein modules, usually linker polypeptides (L) of variable length are used. **d** Overlay of phase-contrast and fluorescence microscopy image of TDoT-L-YFP producing *E. coli* BL21(DE3) cells (Jäger et al. 2019a). The lower right panel depicts a close-up view to better visualize polar localization of the produced CatIBs. The upper right panel depicts a scanning electron microscopy image of isolated CatIB particles

Nahalka and Patoprsty 2009; Koszagova et al. 2018; Huang et al. 2013; Arie et al. 2006) (Fig. 1c). The resulting CatIBs can thus be considered as cellularly produced, insoluble bionanomaterials, or protein immobilizates (Fig. 1d) with potential application in biocatalysis, synthetic chemistry, and biomedicine (Yang et al. 2018; Jäger et al. 2018; Jäger et al. 2019b; Kloss et al. 2018a, b; Diener et al. 2016; Nahalka 2008; Nahalka and Nidetzky 2007; Nahalka and Patoprsty 2009; Nahalka et al. 2008; Ratera et al. 2014; Rueda et al. 2014; García-Fruitós et al. 2009; Vazquez et al. 2012). Since CatIBs are produced heterologously in bacteria, it is not surprising that different parameters, like fusion protein design, expression conditions, and downstream processing, strongly influence not only the general success of immobilization as CatIBs but also their properties. The latter observation also has direct consequences for biocatalytic application of CatIBs as shown recently in several studies (Jäger et al. 2019a; Kloss et al. 2018a).

With the present mini-review, we present an overview of the CatIB immobilization strategy, to provide some general guidelines for those that want to generate CatIBs for their own biocatalytic needs, at the same time paving the way towards their wider use in biotechnology. To this end, we review general aspects important for the on-demand production of CatIBs such as fusion protein design concepts, suitable molecular biological construction methods, as well upstream and downstream bioprocess parameters and selected recent applications in biotechnology.

Induction of CatIB formation—suitable tags, target proteins, and optimization strategies

The successful production of CatIBs requires the selection of an aggregation-inducing tag, which has to be fused via suitable linker polypeptides either N- or C-terminally to the target protein/enzyme. This process still requires the testing of various aggregation-inducing tags, fusions sites, and linker polypeptides because a generally applicable strategy does presently not exist. However, from recent studies, some rules can be inferred that might serve as guidelines for fusion protein design. In the following, we will provide an overview of the available aggregation-inducing tags, tested target proteins, and optimization strategies.

Aggregation-tag selection

Currently, it remains unclear which structural factors, such as polypeptide-chain composition, quaternary structure, or surface composition of the target as well as the tag, dominate the CatIB formation process. Therefore, it is advisable to always test a variety of tags as CatIB-inducing elements, which can differ in size, ranging from small artificial peptides over protein domains up to quite large aggregation-prone proteins. Table 1 summarizes well known and tested CatIB formation–inducing tags, whose structures are depicted in Fig. 2. However, before reviewing the available tags and their properties, we have to address the question: what makes a good CatIB formation–inducing tag? Here, three aspects, which are not totally independent, must be accounted for the following: (i) the CatIB formation efficiency, defined as the activity, or in case of fluorescent proteins, fluorescence, of the insoluble IBs relative to the activity/fluorescence of the crude cell extract, (ii) the yield of the CatIBs, as well as (iii) their residual activity (Jäger et al. 2019a). While the first factor is an indicator for the suitability of the tag to induce CatIB formation, in particular, the last factors are critical for application of CatIBs in biotechnology.

The class of small artificial CatIB-inducing peptide tags shows quite different structural properties: The group of Lin described small β-sheet structures (ELK16 and GFIL8) (Wang et al. 2015; Jiang et al. 2019; Wu et al. 2011) and surfactant-like tags (L6KD) (Zhou et al. 2012), as well as bigger α-helical peptides (18A and variants thereof) (Lin et al. 2013). With these tags, CatIB formation efficiencies between 61 and 120% were achieved and the produced CatIBs showed remarkably high residual activities. However, care should be taken when comparing those values to other studies, as their residual activity was mostly determined relative to the corresponding cell lysate from which they were obtained by centrifugation and not relative to the respective purified target enzyme. An interesting feature of these tags is that they can be used for mild extraction of the at least partially correct folded target from CatIBs without the need for refolding steps (Yang et al. 2018).

Another well-studied group of aggregation-inducing tags used for CatIB production are coiled coil domains. So far, a dimeric (3HAMP: derived from the oxygen sensor protein Aer2 of *Pseudomonas aeruginosa* (Airola et al. 2010)) and a tetrameric coiled coil (TDoT: tetramerization domain of the cell surface protein tetrabrachion of *Staphylothermus marinus* (Stetefeld et al. 2000)) were tested with a broad range of different target enzymes and proteins (Kloss et al. 2018a; Jäger et al. 2018; Diener et al. 2016; Jäger et al. 2019a, b; Kloss et al. 2018b; Lamm et al. 2020). Here, the CatIB formation efficiency was found to differ greatly depending on the target enzyme. In general, the tetrameric TDoT displayed a higher CatIB formation efficiency and yielded CatIBs of a higher purity. However, CatIBs that were produced using the dimeric 3HAMP coiled coil domain as CatIB-inducing tag retained higher residual activity compared to their TDoT counterparts (Jäger et al. 2019a). In addition, 3HAMP CatIBs showed a higher lipid content and a more diffuse structure (as revealed by fluorescence microscopy and scanning electron microscopy), thus indicating a less densely packed structure compared with the corresponding TDoT CatIBs. This in turn could

Table 1 Overview of different IB-inducing elements. Cases where residual activity was compared only to cell lysate are marked with *. [1]CatIB formation efficiency: defined as the activity, or in case of fluorescent proteins, fluorescence, of the insoluble IBs relative to the activity/fluorescence of the crude cell extract. [2]Residual activity compared to purified enzyme. [3]MenD: 2-succinyl-5-enol-pyruvyl-6-hydroxy-3-cyclohexene-1-carboxylate synthase. [4]Residual-specific fluorescence compared to cell lysate. [5]GalU: UDP-glucose pyrophosphorylase. [6]Volumetric activity. n.i. no information provided. n.a. not applicable

Name (origin)	**Length (no. of amino acids)**	**Tag property**	**Linker/structure**	**Target enzyme/protein**	**Target origin**	**CatIB formation efficiency (%)[1]**	**Residual activity (%)[2]**	**Ref.**
I. Artificial peptides								
L6KD	8	Amphophilic	PTPPTT PTPPTTPTPTP Unstructured	Lipase A	*B. subtilis*	80	30*	Zhou et al. (2012)
				Amadoriase II	*A. fumigatus*	61	93*	Zhou et al. (2012)
				β-xylosidase	*B. pumilus*	84	26*	Zhou et al. (2012)
				GFP	*A. victoria*	n.i.	n.a.	Zhou et al. (2012)
GFIL8	8	β-sheet	PTPPTT PTPPTTPTPTP Unstructured	Lipase A	*B. subtilis*	89	43*	Wang et al. (2015)
				Amadoriase II	*A. fumigatus*	93	54*	Wang et al. (2015)
				Ulp1 protease	*S. cerevisiae*	n.i.	40*	Jiang et al. (2019)
ELK16	16	β-sheet	PTPPTT PTPPTTPTPTP Unstructured	Amadoriase II	*A. fumigatus*	120	88*	Wu et al. (2011)
				β-xylosidase	*B. pumilus*	94	77*	Wu et al. (2011)
				GFP	*A. victoria*	n.i.	n.a.	Wu et al. (2011)
18A (and variants)	18	α-helical	PTPPTT PTPPTTPTPTP Unstructured	Lipase A	*B. subtilis*	90	150*	Lin et al. (2013)
				Amadoriase II	*A. fumigatus*	n.i.	n.i.	Lin et al. (2013)
				β-xylosidase	*B. pumilus*	n.i.	n.i.	Lin et al. (2013)
				GFP	*A. victoria*	n.i.	n.a.	Lin et al. (2013)
II. Coiled coil domains								
TDoT (*S. marinus*)	53	Tetrameric coiled coil	$(GGGS)_3$ Unstructured	Hydroxynitrile lyase	*A. thaliana*	76	11	Diener et al. (2016)
				MenD[3]	*E. coli*	90	n.i.	Diener et al. (2016)
				Lipase A	*B. subtilis*	114	n.i.	Diener et al. (2016)
				Alcohol dehydrogenase	*Ralstonia* sp.	88	2	Jäger et al. (2019a); Jäger et al. (2018)
				Alcohol dehydrogenase	*L. brevis*	5	6	Jäger et al. (2019a)
				Benzaldehyde lyase	*P. fluorescens*	88	1	Jäger et al. (2019a); Kloss et al. (2018a)
				Benzoylformate decarboxylase	*P. putida*	1	4	Jäger et al. (2019a)
				Lysine decarboxylase	*E. coli*	n.i.	n.i.	Jäger et al. (2019a); Kloss et al. (2018b)
				YFP	*A. victoria*	65	n.a.	Jäger et al. (2019a); Jäger et al. (2018)
				mCherry	*D. striata*	42	n.a.	Jäger et al. (2019a); Jäger et al. (2018)
3HAMP (*P. aeruginosa*)	172	Dimeric coiled coil	$(GGGS)_3$ Unstructured	Alcohol dehydrogenase	*Ralstonia* sp.	75	12	Jäger et al. (2019a)
				Alcohol dehydrogenase	*L. brevis*	67	1	Jäger et al. (2019a)
				Benzaldehyde lyase	*P. fluorescens*	76	18	Jäger et al. (2018)
				Benzoylformate decarboxylase	*P. putida*	61	10	Jäger et al. (2019a)
				Lysine decarboxylase	*E. coli*	n.i.	n.i.	Kloss et al. (2018b)
				YFP	*A. victoria*	6	n.a.	Jäger et al. (2019a)

Table 1 (continued)

Target (origin)	Length (no. of amino acids)	Tag property	Linker/structure	Target enzyme/protein	Target origin	CatIB formation efficiency (%)[1]	Residual activity (%)[2]	Ref.
				mCherry	*D. striata*	5	n.a.	Jäger et al. (2019a)
III. Aggregation-prone proteins (protein domains)								
Aβ42(F19D) (*Homo sapiens*)	42		n.i.	BFP	*A. victoria*	61–65	31[4]	Garcia-Fruitos et al. (2005)
CBDcell (*C. fimi*)	108	Cellulose-binding protein	n.i.	β-glucuronidase	*E. coli*	92	19	Choi et al. (2011)
				β-glycosidase	*T. caldophilus*	93	n.i.	Choi et al. (2011)
				DsRed	*D. striata*	n.i.	n.a.	Choi et al. (2011)
CBDclos (*C. cellulovorans*)	156	Cellulose-binding protein	43 amino acids with thrombin cleavage site, S-Tag™, and cloning site	D-amino acid oxidase	*T. variabilis*	> 90	42*	Nahalka and Nidetzky (2007)
				D-sialic acid aldolase	*E. coli K12*	100	100*	Nahalka et al. (2008)
				Maltodextrin phosphorylase	*P. furiosus*	83	n.i.	Nahalka et al. (2008)
				Cytidylate kinase	*E. coli*	n.i.	n.i.	Nahalka and Patoprsty (2009)
				Polyphosphate kinase PPK3	*S. pomeroyi*	n.i.	n.i.	Nahalka and Patoprsty (2009)
				GFP	*A. victoria*	n.i.	n.i.	Koszagova et al. (2018)
				GalU[5]	*E. coli*	n.i.	n.i.	Koszagova et al. (2018)
VP1 capsid protein (foot-and-mouth disease virus)	209	Virus capsid protein	n.i.	β-galactosidase	*E. coli*	36-46	166*	Garcia-Fruitos et al. (2005)
				GFP	*A. victoria*	n.i.	n.a.	Garcia-Fruitos et al. (2005)
GFP (*A. victoria*)	238	Fluorescent protein	(GGGS)5 Flexible (AAAKE)5 Rigid	Acid phosphatase	*E. aerogenes*	n.i. n.i.	48 58	Huang et al. (2013)
MalE31 (*E. coli*)	396	Maltose binding protein	RIPGG Unstructured	Alkaline phosphatase	*E. coli*	> 95	n.i.	Arie et al. (2006)
				β-lactamase	*E. coli*	> 95	n.i.	Arie et al. (2006)
PoxB (*P. polymyxa* E681)	574	Pyruvate oxidase	n.i.	GFP	*A. victoria*	n.i.	n.a.	Park et al. (2012)
				α-amylase	*B. subtilis*	77	200[6]	Park et al. (2012)

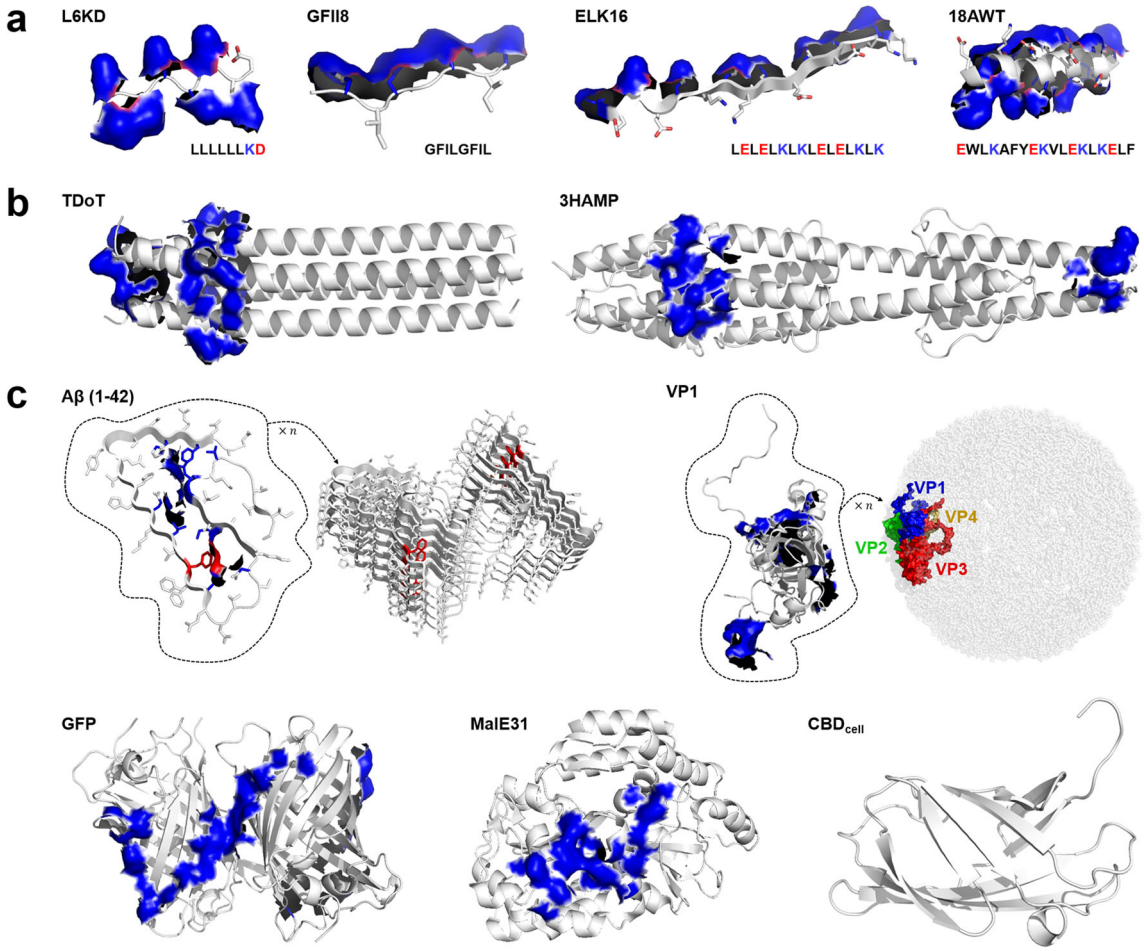

Fig. 2 Hydrophobic patch analysis of CatIB formation–inducing tags. All structures are shown in cartoon representation in gray with the Rosetta-identified hydrophobic surface patches shown as blue surfaces (Kuhlman and Baker 2000; Rohl et al. 2004). **a** Artificial peptides: L6KD, GFIL8, ELK16, and 18AWT. Structures were modelled with Yasara (Krieger and Vriend 2014, 2015) to depict their reported structure. Structures are shown in cartoon representation with residues as sticks. Carbon atoms in gray, nitrogen in blue, and oxygen in red. The amino acid sequence (in single-letter code) of each peptide tag is shown below each model, with non-polar residues in black and polar residues in red (anionic residues) and blue (cationic residues), respectively. **b** CatIB formation–inducing coiled coil domains: tetrameric TDoT and dimeric 3HAMP. **c** Aggregation-prone proteins reported to induce CatIB formation. As representative structure of Aβ42 (F19D), the structure of the wild-type Aβ42 monomer is shown (left side; circled with a dashed line) with all side chains in stick representation. F19, residing within the central hydrophobic cluster constituted by residues 17-21 (de Groot et al. 2006), is highlighted in red. In addition, the recently solved structure of the Aβ42 amyloid fibril (Gremer et al. 2017) is shown to illustrate the crossed β-pleated sheet packing of amyloids. For VP1, the foot-and-mouth disease virus (FMDV) capsid protein, the monomeric VP1 subunit (in cartoon representation; circled with a dashed line), as well as the structure of the 240-mer empty capsid constituted by VP1 (blue), VP2 (green), VP3 (red), and VP4 (yellow) of the FMDV A22 (Porta et al. 2013). PDB-IDs: TDoT: 1FE6; 3HAMP: 3LNR; Aβ1-42: 5OQV; VP1: 4IV1; GFP: 1GFL; MalE31: 1LAX; CBDcell: 1EXG. No structures are available for PoxB and CBDclos

account for their higher residual activity (Jäger et al. 2019a). Notably, the residual activities for coiled coil–induced CatIBs are generally low. However, their residual activity was determined relative to the corresponding purified, soluble enzymes (see above). Furthermore, their recyclability was shown for several targets, in both aqueous and organic-solvent-based reaction systems (Diener et al. 2016; Kloss et al. 2018b). Recently, using those domains, the co-immobilization of two target proteins/enzymes could be demonstrated (Jäger et al. 2018; Jäger et al. 2019b).

In addition to small tags and protein domains, a number of larger proteins and protein domains were tested as CatIB formation–inducing elements. Several of these were selected due to their well-known aggregation tendency, e.g., cellulose-binding domains (CBDs, (Nahalka 2008; Koszagova et al. 2018; Choi et al. 2011; Nahalka and Nidetzky 2007; Nahalka and Patoprsty 2009; Nahalka et al. 2008)). Two different CBDs have been tested for CatIB induction: the rather small 108 amino acid long CBDcell from *Cellulomonas fimi* (Choi et al. 2011), as well as the 156 amino acid long CBDclos from *Clostridium cellulovorans* (Nahalka 2008; Koszagova et al. 2018; Nahalka and Nidetzky 2007; Nahalka and Patoprsty 2009; Nahalka et al. 2008). Most of the CBD-derived CatIBs were only used for proof-of-concept

studies and IB formation efficiency, and residual activities were not determined. However, CatIBs of sialic acid aldolase fused to a CBD from *Clostridium cellulovorans* (CBDclos) showed about the same activity as the corresponding soluble protein and could be recycled 19 times without loss of activity (Nahalka et al. 2008). For higher stability and easier recycling, CBD-CatIBs were cross-linked with glutaraldehyde (Nahalka et al. 2008) or magnetized by iron oxide (Koszagova et al. 2018). Furthermore, Aβ42(F19D), a variant of the human Aβ-amyloid peptide and the VP1 capsid protein of the foot-and-mouth disease virus were selected due to their tendency to aggregate (Garcia-Fruitos et al. 2005). Both tags yielded only moderate CatIB formation efficiencies, but in case of VP1, the activity of the resulting β-galactosidase CatIBs could be increased 1.6 times compared with the cell lysate (Garcia-Fruitos et al. 2005). Interestingly, the fluorescent reporter protein GFP from *Aequorea victoria*, which is commonly used as a fusion target and known for its high solubility, can also be used as an aggregation-inducing tag. Here, fusion of GFP to an alkaline phosphatase from *Enterobacter aerogenes* resulted in CatIBs with a residual phosphatase activity of 48 to 58% (Huang et al. 2013). In addition, even larger aggregation-prone proteins have been used for CatIB formation. Those include a variant of the maltose binding protein (MalE31; 396 amino acids) of *E. coli* (Arie et al. 2006) and a pyruvate oxidase (PoxB; 574 amino acids) of *Paenibacillus polymyxa* (Park et al. 2012) that are both significantly bigger than the targets they were fused to. In contrast to most described CatIBs, MalE31-CatIBs could be found in the periplasm, which is the native location of MalE31 (Arie et al. 2006). CatIB induction is hereby likely related to the folding deficiency of the MalE31 variant. PoxB-CatIBs of an amylase showed a twofold higher volumetric activity than the soluble enzyme (Park et al. 2012).

As revealed by this overview, the presently known CatIB formation–inducing elements come in all sizes and show variable secondary, tertiary, and quaternary structures (Table 1). Therefore, it is still not possible to rationally predict the success of the CatIB formation strategy for any combination of tag, linker, and target protein/enzyme. However, first attempts to link CatIB formation and computational aggregation-propensity predictions have been made (Krauss et al. 2017). While no quantitative correlations could be found between the predicted aggregation tendency of the tag, CatIB formation efficiency, and/or CatIB residual activity, all tags were predicted computationally to show the tendency to aggregate with at least one of the employed tools (Krauss et al. 2017). In addition, from the above presented prediction of hydrophobic surface patches (Fig. 2), it becomes apparent that, with the exception of CBDcell, which appears to lack larger hydrophobic surface patches, all CatIB formation–inducing tags possess solvent exposed hydrophobic surfaces, likely contributing to aggregation and hence CatIB formation (see below).

Target-protein properties

In most proof-of-concept CatIB studies, only model enzymes or even fluorescent proteins were used as targets. Here, a commonly used enzyme was the lipase A from *B. subtilis*, a small (19 kDa), monomeric enzyme that does not require co-factors (van Pouderoyen et al. 2001), as well as the 26 kDa Ulp1 protease from *S. cerevisiae* (Jiang et al. 2019) or the 33 kDa sialic acid aldolase from *E. coli* (Nahalka et al. 2008). Inducing CatIB formation for those rather simple enzymes appears straightforward, as exemplified by relatively high CatIB formation efficiencies (Table 1). However, even larger, more complex oligomeric enzymes, such as the 98 kDa maltodextrin phosphorylase from *P. furiosus* (Nahalka 2008), the homotetrameric β-galactosidase with a total size of 540 kDa (Garcia-Fruitos et al. 2005), and the homodecameric lysine decarboxylase with a total size of 806 kDa (Jäger et al. 2019a; Kloss et al. 2018b), could successfully be produced as CatIBs. Therefore, it seems that size and oligomerization state do not have a predictable impact on the success of CatIB formation. However, it should be noted that all examples reported so far for successful CatIB formation dealt with homo-oligomeric enzymes, as hetero-oligomeric complexes of several catalytic subunits are likely difficult to properly assemble within IBs. In contrast to overall size and quaternary structure, the presence of non-covalently bound co-factors, which need to be recycled during the catalytic cycle, might play a more important role for the activity of CatIBs, since they must not only be correctly bound within the enzyme during CatIB formation but also need to be able to dissociate from and diffuse to the enzyme. However, the present data does not allow unequivocal conclusions in this regard. To this end, Jäger et al. (2019a) empirically compared the production and residual activity of different CatIBs whose production was induced by two different aggregation tags. Here, the highest residual activity was achieved with CatIBs of the only tested enzyme that did not require a co-factor (Table 1; *A. thaliana* hydroxynitrile lyase fused to TDoT), while the same tag yielded only CatIBs with lower residual activity for targets that were co-factor dependent (Table 1; alcohol dehydrogenases of *L. brevis* and *Ralstonia* sp., *P. fluorescens* benzaldehyde lyase, *P. putida* benzoylformate decarboxylase) (Diener et al. 2016; Jäger et al. 2019a; Jäger et al. 2018; Kloss et al. 2018a, b). However, the use of another CatIB formation–inducing tag yielded CatIBs of the same co-factor-dependent enzymes with much higher residual activities (see Table 1; compare TDoT and 3HAMP CatIBs (Jäger et al. 2019a)).

Thus, size, oligomerization state, and co-factor dependency do not appear to be decisive or limiting factors for CatIB formation. Given the structural diversity of the so far employed target proteins, the question arises, if there are any mutual structural features that are important for CatIB

formation. To the best of our knowledge, the only information, although limited in scope due to the small size of the dataset, again comes from Jäger et al. who showed that target enzymes possessing larger hydrophobic surface patches (Fig. 3) generally displayed higher CatIB formation efficiencies (Jäger et al. 2019a). This suggests that CatIB formation not only is driven by the aggregation-inducing tag but, at least to a certain extent, also depends on the interactions of the target proteins (and/or the tag) caused by the physical proximity of the target molecules themselves. This is illustrated by the observation that the CatIB formation efficiency observed for TDoT-CatIBs of mCherry was much reduced as compared with the corresponding YFP TDoT-CatIBs (Jäger et al. 2019a), which might be related to the fact that monomeric mCherry virtually lacks any hydrophobic surface patches compared with dimeric YFP (Fig. 3a; compare mCherry: 2H5Q; eYFP: 1YFP). Please note that a correlation between hydrophobic patch area and CatIB formation efficiency (Fig. 3b) only holds for 12 out of 18 of the here analyzed targets. For five targets, high CatIB formation efficiencies but only moderate hydrophobic patch areas are observed, while only one target (Fig. 3b; 1ZK4) shows moderately large hydrophobic patches but only low CatIB formation efficiency. While this analysis apparently does not allow for precise prediction of the CatIB formation efficiency based on structure, hydrophobic surface patches nevertheless seem to play an important role for the process.

Optimization strategies—fusion sites and linkers

From a structural perspective, several factors need to be considered when genetic fusions are designed to induce CatIB formation. First of all, a fused tag should not interfere with correct folding of the enzyme to its catalytically active form. Hence, apart from the overall monomeric structure, also the enzymes' native quaternary structure needs to be considered when designing the fusion construct. This was for example demonstrated for the lysine decarboxylase from *E. coli*, where the N-terminus is buried within the decameric structure of the enzyme, while the C-terminus is located at the protein surface. In accordance, the activity of the CatIBs derived from C-terminal fusion of TDoT was about six orders of magnitude higher than for the corresponding N-terminal fusion (Jäger et al. 2019a; Kloss et al. 2018b). Thus, in conclusion, the fusion site (N- vs C-terminal) should be carefully evaluated and if no structures are available, both sites need to be tested.

Another factor that can influence the success of CatIB formation is the presence and nature of polypeptide linkers that are employed to link the CatIB formation–inducing tag and the target enzyme. These linkers can differ greatly in size and function, e.g., flexible vs rigid linker motifs (Table 1). For GFP-induced CatIBs, the effect of the linker with regard to the aggregation propensity has been studied. Here, the exchange of the flexible $(GGGS)_5$-linker to the rigid $(AAAKE)_5$-linker improved the residual activity of the target enzyme by about 10% (Huang et al. 2013). Interestingly, this is reminiscent of a different study, where the deletion of the flexible $(GGGS)_3$-linker enhanced the CatIB formation efficiency of TDoT-mCherry CatIBs by about 30% (Jäger et al. 2019a). Other studies utilize protease cleavage sites as linkers in order to analyze CatIB fusion and target enzyme independently (Nahalka 2008; Nahalka and Nidetzky 2007; Nahalka and Patoprsty 2009; Nahalka et al. 2008; Koszagova et al. 2018). CatIBs induced by artificial peptides always contained a flexible 17 amino acid proline-threonine linker of about the same length as the aggregation tag. However, its function is not discussed in the studies (Jiang et al. 2019; Lin et al. 2013; Wang et al. 2015; Wu et al. 2011; Zhou et al. 2012).

In conclusion, the design of fusion proteins for CatIB formation is presently still a trial-and-error process and requires testing of multiple constructs, e.g., different CatIB formation–inducing tags, different fusions sites, and different linker polypeptides. Therefore, one limiting factor for the CatIB approach is the cloning strategy used for fusion construct design, which will therefore be reviewed in the following.

Towards automated fusion-protein generation—high-throughput cloning, expression, and hit identification

The construction of fusion proteins for CatIB production is usually performed by traditional cloning with classical restriction enzymes (Arie et al. 2006; Choi et al. 2011; Diener et al. 2016; Garcia-Fruitos et al. 2005; Jiang et al. 2019; Lin et al. 2013; Wang et al. 2015; Wu et al. 2011; Zhou et al. 2012); however, this is not convenient to generate an extensive CatIB library of larger numbers of variants due to numerous laborious steps. In a few cases, already more generic and concomitantly less time-consuming cloning methods like LICing and Gibson Assembly were successfully used for gene fusion generation (Heater et al. 2018; Nahalka 2008; Nahalka and Nidetzky 2007; Nahalka and Patoprsty 2009). Using modern cloning methods is a major step towards the generation and screening of a CatIB library to find the best CatIB variant in less time.

For example, Nahálka and colleagues applied ligase independent cloning (LICing) for the production of CatIBs (Nahalka 2008; Nahalka and Nidetzky 2007; Nahalka and Patoprsty 2009). The advantage of this method is that no restriction enzymes and T4 DNA ligase are needed. The linearized vector and insert are treated with T4 polymerase, due to its 3′ ➔ 5′ exonuclease activity, and only one kind of nucleotide triphosphate is added. Removing nucleotides from the 3′-end lead to single-stranded DNA tails, which are formed until the first complementary base of the added nucleotide triphosphate is reached. Due to the designed complementarity of the

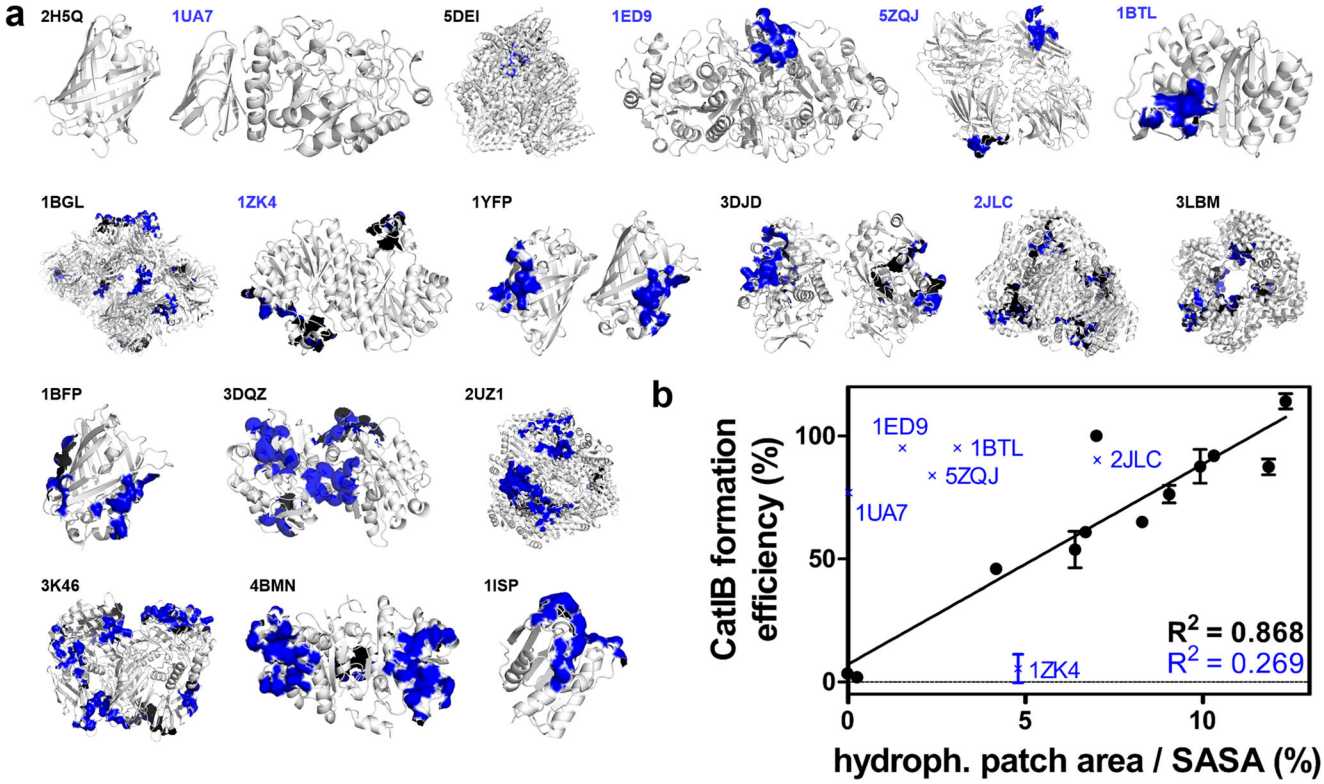

Fig. 3 Hydrophobic patch analysis of selected target proteins which were produced as CatIBs. **a** All target proteins from Table 1 for which a structure is known were analyzed for the presence of hydrophobic surface patches. All structures are shown in cartoon representation in gray with the Rosetta-identified hydrophobic surface patches shown as blue surfaces (Kuhlman and Baker 2000; Rohl et al. 2004) calculated as described in Jäger et al. (2019a). Proteins are identified by PDB-IDs (see below). **b** Correlation between CatIB formation efficiency and fraction of hydrophobic surface patches. Hydrophobic surface patches for the corresponding target protein structures were quantified by employing the hpatch tool of the Rosetta modelling suite (Kuhlman and Baker 2000; Rohl et al. 2004; Jacak et al. 2012). Surface areas were quantified using Pymol 1.7.0.0 (Schrödinger, LCC, New York, NY, USA). CatIB formation efficiency as the relative activity of the insoluble CatIB fraction (Table 1). Coefficient of determination values (R^2) is given excluding (black) and including outliers (blue). Outliers are identified by PDB ID and are depicted with blue crosses. PDB-IDs are as follows: 2H5Q: mCherry, 1UA7: *B. subtilis* α-amylase, 5DEI: *P. putida* benzoylformate decarboxylase, 1ED9: *E. coli* alkaline phosphatase, 5ZQJ: *B. pumilus* β-xylosidase, 1BTL: *E. coli* β-lactamase, 1BGL: *E. coli* β-galactosidase, 1ZK4: *L. brevis* alcohol dehydrogenase, 1YFP: yellow fluorescent protein, 3DJD: *A. fumigatus* amadoriase II, 2JLC: *E. coli* MenD, 3LBM: *E. coli* D-sialic acid aldolase, 1BFP: blue fluorescent protein, 3DQZ: *A. thaliana* hydroxynitrile lyase, 2UZI: *P. fluorescens* benzaldehyde lyase, 3K46: *E. coli* β-glucuronidase, 4BMN: *Ralstonia* sp. alcohol dehydrogenase, 1ISP: *B. subtilis* lipase A

treated vector and insert, the cohesive ends of the DNA fragments anneal to form a plasmid that can be used for transformation of bacteria (Aslanidis and Dejong 1990). An advancement of LICing is PLICing, phosphorothioate-based ligase-independent gene cloning, which was developed in 2010 by Blanusa and co-workers (Blanusa et al. 2010). In comparison to traditional LICing, the advantage is that no enzyme, no gel extraction and no purification are needed. First, the vector and the target gene are amplified via PCR with specific primers that have complementary phosphorothioate nucleotides at the 5‘-end. After amplification, the PCR products are treated with an iodine/ethanol solution, which cleaves phosphorothioate bonds, producing single-stranded DNA tails. Finally, the vector and the target gene are hybridized to generate a circular plasmid that can be used to transform competent cells. In comparison to traditional LICing, with PLICing, also large DNA fragments (>6 kb) can be formed, which could be beneficial for larger combinations of enzyme and aggregation tag. Moreover, the cleaved fragments do not have to be purified, which is a time saving benefit (Blanusa et al. 2010). In-Fusion™ assembly is a further cloning method without the use of a ligase. A seamless cloning can be achieved by using DNA fragments with the same 15 bp overlaps that can be assembled after the DNA polymerase of poxvirus with its 3′-5′ proofreading activity has removed nucleotides from the 3′ end. The complementary nucleotides can join and form a combined DNA molecule. *E. coli* will repair the remaining small gaps in the molecule after transformation (Zhu et al. 2007).

With Gibson Assembly, Heater and co-workers used another modern cloning technique (Heater et al. 2018). Their fusion constructs consisted of a GS-Linker, a Cry3Aa Tag, and the respective gene of interest. The resulting fusion protein formed solid, crystal-like particles in *Bacillus thuringiensis*, which possess a certain morphological

similarity to CatIBs, and have hence been included here. Gibson Assembly as an isothermal, single-reaction method, enabling multiple DNA fragments to be joined during a PCR if they have matching overhangs. To achieve this, three different enzymes are needed: a 5′ exonuclease, a Phusion DNA polymerase, and a *Taq* DNA ligase. First, a 5′ exonuclease generates single-stranded DNA overhangs by removing nucleotides from the 5′ ends of the double-stranded DNA fragments. Complementary single-stranded DNA overhangs can anneal, and the Phusion DNA polymerase is able to fill the gaps. Finally, the *Taq* DNA ligase can seal the nicks, and joined, double-stranded DNA molecules are generated (Gibson et al. 2009).

An additional alternative cloning technique well suited for CatIB library generation is Golden Gate cloning. It is characterized by the use of a type II restriction enzyme, which is able to cleave DNA outside of its recognition site. After restriction digestion, the recognition site is cut out of the desired fragment and a four-nucleotide overhang is generated, which can be ligated with the matching DNA overhang from the next fragment. The whole reaction can take place in a so-called one-pot setup, because ligation and restriction digest are performed at the same time (Engler et al. 2008). Thus, Golden Gate cloning could be the most efficient method for CatIB library generation, since the three different DNA elements can be assembled in an effortless manner with pipetting all elements as the only time-consuming part. However, this can be easily performed by lab automation technology, which could be seamlessly hyphenated with the next steps like the transformation of an expression host with the Golden Gate products, CatIB production, and CatIB purification and analysis. The general automation of such molecular biology workflows have been successfully demonstrated for *E. coli* (Ben Yehezkel et al. 2011; Billeci et al. 2016; Olieric et al. 2010), which is the current major producer of IBs (Carrio et al. 1998; Ventura and Villaverde 2006) as well as CatIBs in literature. The automation of all these processes would be desirable to enable fast provision of suitable CatIBs for new catalytic enzymes.

Bioprocess development for CatIB production—upstream and downstream considerations

For the development of a bioprocess to efficiently produce and isolate CatIBs, various special characteristics of CatIBs have to be considered to obtain high amounts of highly active CatIBs. Conventionally, either properly folded, active, and soluble proteins or misfolded, inactive aggregated, and insoluble IBs are produced. Since CatIBs not only consist of a scaffold of misfolded aggregated protein, but also contain active, correctly folded or native-like protein species, the characteristics of properly folded as well as aggregated insoluble proteins have to be considered for efficient CatIB production and isolation. In this section, the literature on conventional IBs and CatIBs is reviewed with respect to upstream and downstream process development.

Important process parameters for CatIB production

For upstream process development, conditions have to be selected that yield active and mostly aggregated proteins, as soluble proteins will be discarded with the soluble cell fraction during CatIB isolation. Therefore, heterologous host selection and cultivation conditions are critical to yield a high IB formation efficiency with high amounts of properly folded and therefore active proteins.

As for conventional IBs, temperature is the most studied cultivation parameter for CatIBs production. Generally, lower cultivation temperatures lead to CatIBs with higher activity (de Groot and Ventura 2006; Doglia et al. 2008; Jevsevar et al. 2005; Peternel et al. 2008; Lamm et al. 2020; Vera et al. 2007; Wang et al. 2017; Arie et al. 2006), whereby lower temperature likely results in the production of a larger fraction of properly folded protein that is incorporated within the CatIB matrix. While CatIBs with higher activities can be produced at lower cultivation temperature, different studies show that lower amounts of CatIBs or less stable CatIBs are produced under those conditions (de Groot and Ventura 2006; Peternel et al. 2008; Doglia et al. 2008). Although, a lower stability can be beneficial to obtain active, soluble proteins from conventional IBs, CatIBs with higher stability would be preferable for application as reused or immobilized biocatalysts (Krauss et al. 2017). Otherwise, the desired product can be contaminated by solubilized protein derived from disintegrating CatIBs during biocatalysis. Thus, for CatIB production, a cultivation temperature has to be chosen or empirically identified that is optimal for yielding high amounts of highly active and stable CatIBs. Here, often a compromise between yield and activity is necessary.

Another cultivation parameter that also strongly influences the production of conventional, inactive IBs is the induction strength. For conventional, inactive IBs, lower induction strength leads to less IBs and more soluble and active proteins (Jhamb and Sahoo 2012; Margreiter et al. 2008). For CatIBs, it was also shown that more active proteins are produced at lower induction strength. However, the amount of active proteins in IBs was decreased so strongly that a higher induction strength leads to an overall higher activity in CatIBs (Lamm et al. 2020). Possibly, misfolded proteins enhance the aggregation of correctly folded proteins, which leads to higher amounts of CatIBs with correctly folded protein. To identify the best induction conditions, *E. coli* Tuner rather than BL21(DE3), which is most frequently used for CatIB production, could be used as expression host to finely adjust the

induction strength by inductor dosing (e.g., isopropyl β-D-thiogalactopyranoside; IPTG). For eukaryotic proteins, the host *E. coli* Rosetta might be beneficial as it was superior for the production of a human oxidase as CatIBs compared with the BL21(DE3) host (Wang et al. 2017). For the production of food-grade or pharmaceutically relevant biologics, the need for downstream endotoxin removal can complicate the production process. Thus, the use of expression host strains that lack either endotoxic lipopolysaccharide (LPS) such as *Lactococcus lactis* (Song et al. 2017) or *E. coli* strains that contain genetically modified LPS (Mamat et al. 2015) would be favorable. Both hosts have recently been used for the production of CatIBs (Gifre-Renom et al. 2018; Cano-Garrido et al. 2016) or IBs (Viranaicken et al. 2017).

Regarding the impact of oxygen availability during cultivation, no conclusion can be drawn yet for CatIB production, as its role was hardly studied or no general trend could be observed (Lamm et al. 2020; Worrall and Goss 1989). Similarly, the impact of the growth medium on CatIB production has not been studied thoroughly. While CatIBs are mostly produced in complex media, it was shown that they can also be produced in mineral media (Lamm et al. 2020). However, as the choice of the cultivation medium and supplementations of salts, vitamins, and amino acids have a complex impact on *E. coli*'s metabolism, no general recommendations can yet be given for CatIB production (Hoffmann et al. 2004; Li et al. 2014).

Due to the solid, amorphous nature of CatIB immobilizates, diffusional limitation of educts and products to/from CatIBs during biocatalytic reactions is certainly an issue (Diener et al. 2016). Therefore, CatIB size might be an important parameter for CatIB application. As shown by Kopp et al. (2018) for conventional, inactive IBs, the size of IBs can be adjusted by nutrient feeding. This strategy might also be applicable for CatIB production to optimize the specific activity of CatIBs.

In conclusion, for CatIB production, the cultivation temperature and induction strength had the strongest impact on CatIB productivity. As both parameters strongly influence the protein synthesis rate, both parameters should be investigated simultaneously in small-scale cultivations. Therefore, the BioLector technology in combination with a high-throughput temperature profiling system could be used (Kunze et al. 2014; Samorski et al. 2005). It is important to note that with the same genetic construct CatIBs, mostly soluble proteins or conventional, inactive IBs can be produced by changing a single cultivation parameter (Lamm et al. 2020). Therefore, it might be necessary to screen the expression conditions for potential new CatIB constructs within a certain process window, e.g., by profiling expression temperature, inductor concentration, and induction time, as simulation of protein folding and aggregation with fusion proteins is at present not feasible (Krauss et al. 2017; Lamm et al. 2020; Jäger et al. 2019a; Huber et al. 2009).

Important process parameters for CatIB purification

For conventional, inactive IBs that are commonly used as starting material for protein renaturation, methods for lab and production scales have been developed (Vallejo and Rinas 2004). While low-speed centrifugation of cells is often followed by a chemical-enzymatic cell lysis step in microliter scale, at larger scales, it is followed by mechanical cell disruption. Those protocols are already applied for CatIB purification at small scales. Even for CatIB production at large scale, protocols for the isolation of conventional, inactive IBs could be applied. However, two major differences may have to be considered for CatIB purification compared with conventional IBs.

First, the stability of CatIBs might be lower as cultivation conditions are applied that promote correct protein folding. As discussed above, this might lead to a decreased CatIB stability that could lead to CatIB disintegration during purification. Those CatIB properties have also been exploited for the purification of soluble protein by solubilization under mild, non-denaturing conditions employing mild detergents at low concentration (Peternel et al. 2008). Therefore, CatIB stability should be monitored during upstream and downstream process development.

Secondly, CatIB preparations might have higher purity requirements due to their application compared with conventional, inactive IBs, which are often contaminated with bacteria by incomplete cell lysis. For small-scale purification, this requirement was already addressed by Rodriguez-Carmona et al. (2010), who developed a protocol which included cell lysis by sonication, multiple enzymatic treatment, and detergent washing steps. However, this protocol might not be economically viable for large-production processes due to high costs for multiple enzymatic purification steps (Vallejo and Rinas 2004).

Special considerations for the analysis of CatIB activities, purities, and yields

Due to the insoluble nature of the CatIBs, a few additional factors and limitations have to be considered for the optimization of the production process, i.e., compared with the production of soluble enzymes or the use of carrier immobilized enzymes (Mestrom et al. 2020; Francis and Page 2010; Zerbs et al. 2014). For CatIB production, the determination of important quality parameters such as yield, activity, and stability is complicated by the particulate nature of the CatIB material. Overall, three major aspects have to be considered when working with CatIBs.

First of all, the determination of CatIB activities is difficult, as common colorimetric/fluorometric assays for the determination of enzyme activity are usually designed for soluble enzymes thus working in optically transparent

(non-turbid) samples. Therefore, methods need to be employed that are suitable for turbid solutions, i.e., reducing the problem of light scattering and reabsorption, i.e., in fluorometry. One solution that helps to address this issue is the use of fluorescence spectrophotometers that enable measurement in a so-called front-face geometry (Eisinger and Flores 1979). Here, the excitation light is focused on the front surface of the cuvette, and fluorescence emission is recorded at an angle of, e.g., 45°, to mitigate the impact of light scattering. This technique is superior for turbid samples such as CatIBs (Jäger et al. 2019a). Alternatively, common colorimetric, absorbance-based assays can be used, when the particulate material is removed, e.g., by centrifugation, before an optical measurement is performed (Jäger et al. 2019b). This, however, complicates the measurement of initial rate velocities, as assay solutions have to be sampled rapidly after the initiation of the reaction. In addition, methods need to be established that rapidly stop the enzymatic reaction before the centrifugation step, which can be achieved by adding denaturing solutions to the assay sample (Jäger et al. 2019b). Alternatively, optical methods can be avoided altogether by, e.g., switching to high-performance liquid chromatography (HPLC)- or gas chromatography (GC)-based methods to monitor product formation or substrate consumption (Diener et al. 2016; Jäger et al. 2019a, b). Those, however, still require rapid termination and sampling as well as the removal of the particulate material. Such methods are therefore hardly adaptable for high-throughput screening purposes or process development.

Secondly, common assays for the determination of protein concentration were also developed for optically transparent (non-turbid) samples. While special adaptions of, e.g., the Bradford assay (Bradford 1976) exist for turbid samples (Gotham et al. 1988), which could be employed for CatIBs, in our hands, those methods proved error prone and less reliable. Therefore, we usually rely on the solubilization of freeze-dried CatIBs in 6M guanidinium chloride solution followed by measuring the protein absorbance at 280 nm. Please note that this method tends to be less precise, when the target protein only represents a smaller fraction of the insoluble CatIB material and fails to account for other proteinaceous impurities and nucleic acid contaminations that have been observed to be present in certain inclusion body preparations (Kloss et al. 2018a; Neerathilingam et al. 2014).

Last but not least, as with other enzyme immobilizates, also CatIBs might be prone to diffusional limitations (Diener et al. 2016; Mestrom et al. 2020), which can further complicate the determination of CatIB activities, i.e., compared with the activity of the same soluble enzyme. Due to those facts, we believe that CatIB activities in many cases have rather been underestimated (not considering other impurities and diffusional limitation).

Biotechnological potential and application of CatIBs

Last but not least, we will briefly outline the application potential for CatIBs for biocatalysis, synthetic chemistry, and biotechnology. Here, we will not focus on biomedical applications of CatIBs or IBs as this aspect has been reviewed recently (Ratera et al. 2014; Krauss et al. 2017).

The use of enzymes in biocatalysis, biotechnology, and synthetic chemistry, especially in an industrial setting, often requires harsh reaction conditions such as high temperatures, extreme basic or acidic pH values, or the use of organic solvents (Castro and Knubovets 2003; Sheldon and Brady 2018). Therefore, after (heterologous) production, enzymes are often immobilized in or on carrier materials, which in many cases results in a more stable enzyme formulation, while at the same time allowing for easier catalyst handling and recycling (Sheldon and Brady 2018, 2019; Sheldon and van Pelt 2013). At present, the immobilization process, i.e., the selection of appropriate methods and carrier materials has still to be optimized on a case to case basis for each new enzyme. Thus, apart from enzyme production and purification, immobilization represents a major cost and labor factor (Tufvesson et al. 2011) that limits the widespread industrial application of enzymes in synthetic applications. The use of CatIBs could circumvent those problems, as CatIBs essentially represent a fast and economical approach to produce enzyme/protein immobilizates.

To illustrate their utility, various CatIBs have been analyzed with regard to recyclability (Nahalka 2008; Nahalka et al. 2008; Koszagova et al. 2018; Choi et al. 2011; Jiang et al. 2019; Diener et al. 2016; Kloss et al. 2018b). For example, CBDclos-CatIBs with maltodextrin phosphorylase (Nahalka 2008), sialic acid aldolase (Nahalka et al. 2008), or UDP-glucose pyrophosphorylase (Koszagova et al. 2018) could all be recycled for 10 or more times without less than 10% activity loss. However, some of them were further immobilized by alginate (Nahalka et al. 2008) or magnetization (Koszagova et al. 2018), to allow for easier handling and separation. CBDcell-CatIBs with β-glucuronidase or β-glycosidase were both further stabilized by cross linking with glutaraldehyde, displaying no activity loss after three reaction cycles, while without cross-linking the CatIBs lost 65 and 35% of their activity, respectively (Choi et al. 2011). However, in most examples, recycling was tested in aqueous buffer systems. The influence of organic additives was tested with coiled coil–induced CatIBs: TDoT-CatIBs of the thiamine diphosphate (ThDP)-dependent enzyme MenD of *E. coli* showed about 90% activity after 8-time recycling in a buffer containing 5% methyl-*tert* butyl ether (MTBE) (Diener et al. 2016), while TDoT-CatIBs of the *A. thaliana* hydroxynitrile lyase (HNL) did not lose activity after five reaction cycles in a microaqueous system containing almost solely MTBE (Diener et al. 2016).

Another issue that was analyzed repeatedly is the stability and activity of CatIBs. Here, e.g., the stability of the benzaldehyde lyase of *P. fluorescens* (*Pf*BAL) could be considerably enhanced by the immobilization in TDoT-CatIBs (Kloss et al. 2018a). In addition, 3HAMP-CatIBs of *Pf*BAL proved useful in a biphasic system with 70% CPME, in which they showed 3 times higher activity than the corresponding soluble enzyme (Kloss et al. 2018a). GFIL8-CatIBs of the protease Ulp1 showed less leakage after 8 days of repeated recycling and storage compared to immobilizates produced by affinity binding to a cellulosic carrier via a fused cellulose-binding module CBM-tag (Jiang et al. 2019). TDoT-HNL CatIBs were significantly more stable at acidic pH values than their soluble counterpart; the half-life at pH 4.5 was with 290 min more than 100 times longer than for soluble HNL (Diener et al. 2016).

While most CatIBs studies do not go beyond mere proof of concept, e.g., illustrating the general feasibility if the fusion strategy yields CatIBs, a few examples exist where CatIBs have been used for synthetic purposes. One such example for a CatIB-based application is the biosynthesis of 1,5-diaminopentane (also known as cadaverine), a precursor for the production of bio-based polyamides. Here, CatIBs of a constitutive lysine decarboxylase (LDC) of *E. coli* were used to convert L-lysine, which was produced by whole-cell fermentation of a suitable *Corynebacterium glutamicum* strain to cadaverine (Kloss et al. 2018b). The process was tested in batch and repetitive batch mode for up to 69 h of total reaction time and could well compete with other reported approaches that used immobilized LDC in whole cells (Oh et al. 2015; Kind et al. 2014), alginate immobilizates (Bhatia et al. 2015), or cross-linked enzyme aggregates (CLEAs) (Park et al. 2017). Another recent application focused on the co-immobilization of two different enzymes within the same IB-particle in order to realize a CatIB-based synthetic reaction cascade (Jäger et al. 2018; Jäger et al. 2019b). For this purpose, an alcohol dehydrogenase from *Ralstonia* sp. (*R*ADH) and *Pf*BAL was utilized to achieve the synthesis of (1*R*,2*R*)-1-phenylpropane-1,2-diol, an enantiopure 1,2-diol, that represents a building block for different pharmaceuticals and chemicals. In the resulting recycling cascade, encompassing two enzymatic steps and co-substrate coupled recycling of the nicotine amide cofactor of the *R*ADH, CatIBs as well as Co-CatIBs greatly outperformed the soluble enzymes, which were shown to be related to an increase in stability for the (Co)CatIBs (Jäger et al. 2019b). The later example also shows that co-factor recycling is generally possible in CatIBs, although also here diffusional limitation might be a severe problem that limits productivity. Hence, further studies would be needed that address this important issue in more detail.

Last but not least, although not directly related to biocatalysis and synthetic chemistry, the use of CatIBs for mild protein extraction should be mentioned. Even though catalytic activity of the employed IB does not play a direct role here, the same aggregation-inducing tags as used for CatIB formation are used to produce IBs containing a (partially) correctly folded target protein. The use of CatIBs as protein source hereby greatly simplifies the production/purification of the target, by rendering solubilization and refolding steps obsolete (Yang et al. 2018). This technique was tested in several approaches with small artificial peptides as aggregation-inducing tags (ELK16 (Xu et al. 2016; Zhao et al. 2017; Zhao et al. 2016) and L6KD (Zhao et al. 2017)). Here, the authors genetically fused a self-cleaving Mxe GyrA intein between target and IB-inducing tag to enable autocatalytic cleavage of the tag and subsequent release of the target from the IB. With this method, they successfully produced a set of small peptides that are normally unstable and susceptible to proteolytic degradation within bacteria.

Conclusions and future perspectives

By now, a wealth of examples exists demonstrating the successful induction of CatIB formation with targets covering a broad spectrum of differently complex proteins from simple monomeric fluorescent reporter proteins to complex oligomeric co-factor–dependent enzymes. These data clearly suggest that the CatIB strategy is generically, or at least widely, applicable. Importantly, optimization strategies and a target/tag-centered rationale for the CatIB formation process have been brought forward in recent years, suggesting that the on-demand production of CatIBs for any given target protein might be within reach. From those studies, the following guidelines and future perspectives can be inferred:

- The selection of the fusion terminus for attachment of the CatIB-inducing tag needs careful consideration, e.g., with regard to accessibility based on the quaternary structure of the target protein (Jäger et al. 2019a).
- The choice of linkers (rigid vs flexible) or the lack of a linker is important for the success of the strategy and represents an important optimization strategy (Jäger et al. 2019a).
- The use of short artificial peptide tags to induce CatIB formation appears advantageous as often higher residual activities were observed (Jäger et al. 2019a; Wang et al. 2015; Wu et al. 2011; Zhou et al. 2012). However, empirical comparative studies using more complex target proteins are needed to truly assess their usefulness.
- The presence of aggregation-prone sequence motifs and of hydrophobic surface patches on tag and target might be an important factor influencing CatIB formation for certain targets (Jäger et al. 2019a; Krauss et al. 2017).
- At present, the success of the CatIB strategy for a given target protein cannot be predicted. Therefore, high-

throughput experimentation, including high-throughput cloning, e.g., relying on modern restriction enzyme free approaches, as well as automated imaging, would be needed to speed up construct generation and validation.
- More and more successful CatIB application examples and datasets that become available may allow for developing data-driven optimization algorithms or even machine learning algorithms which can lead to hypothesis generation about the structure function relationships required for successful CatIB formation. With this, even the rational design of CatIBs from scratch might become feasible in the years to come.
- For upstream process development, it is crucial to identify whether the catalytic activity is reaction- or diffusion-limited. Depending on the results, the respective bioprocess should be adjusted to produce smaller CatIBs to achieve an increase in specific CatIB activity.
- Identification of culture conditions that yield not only high amounts of correctly folded proteins (e.g., low induction strength, low temperature) but also high amounts of CatIBs (high induction strength) is instrumental for success (Lamm et al. 2020).
- Alternative purification strategies, e.g., relying on magnetization or the use of synthetic biology tools for cell lysis (Pasotti et al. 2011; Koszagova et al. 2018), could speed up CatIB isolation and purification, which would render the associated process more economic.

In conclusion, we believe that CatIBs, as novel, biologically produced enzyme immobilizates possess broad application potential in biocatalysis, synthetic chemistry, and industrial biotechnology. In particular, due to their simple and inexpensive production, CatIB-based enzyme immobilizates and the corresponding technologies contribute to the sustainable management of resources in a bioeconomic setting.

Code availability Not applicable.

Authors' contributions UK conceived the outline of this review. UK and VDJ contributed the figures. All authors contributed to literature searches and the writing of the manuscript. All authors have read and approved the final version.

Funding information Open Access funding provided by Projekt DEAL. UK, KEJ, JB, VDJ, RL, and JB received funding from the NRW Strategieprojekt Bioeconomy Science Center (No. 313/323-400-002 13). The scientific activities of the Bioeconomy Science Center were financially supported by the Ministry of Culture and Science of the State of North Rhine-Westphalia, Germany. BioSC is a research cluster of RWTH Aachen University, the universities of Düsseldorf and Bonn, and Forschungszentrum Jülich GmbH. Part of this work was funded by the European Regional Development Fund (ERDF) to support the CLIB-Kompetenzzentrum Biotechnologie (CKB)(grant 34.EFRE-0300097).

Data availability Not applicable.

Compliance with ethical standards

Conflict of interest The authors declare that they have no conflict of interest.

Ethics approval This article does not contain any studies with human participants or animals performed by any of the authors.

Consent to participate Not applicable.

Consent for publication All co-authors have given their consent to publish this manuscript.

References

Airola MV, Watts KJ, Bilwes AM, Crane BR (2010) Structure of concatenated HAMP domains provides a mechanism for signal transduction. Structure 18:436–448

Arie JP, Miot M, Sassoon N, Betton JM (2006) Formation of active inclusion bodies in the periplasm of *Escherichia coli*. Mol Microbiol 62:427–437

Aslanidis C, Dejong PJ (1990) Ligation-independent cloning of PCR products (LIC-PCR). Nucleic Acids Res 18:6069–6074

Baneyx F, Mujacic M (2004) Recombinant protein folding and misfolding in *Escherichia coli*. Nat Biotechnol 22:1399–1408

Ben Yehezkel T, Nagar S, Mackranrs D, Marx Z, Linshiz G, Shabi U, Shapiro E (2011) Computer-aided high-throughput cloning of bacteria in liquid medium. Biotechniques 50:124–127

Bhatia SK, Kim YH, Kim HJ, Seo H-M, Kim J-H, Song H-S, Sathiyanarayanan G, Park S-H, Park K, Yang Y-H (2015) Biotransformation of lysine into cadaverine using barium alginate-immobilized *Escherichia coli* overexpressing CadA. Bioprocess Biosyst Eng. 38:2315–2322

Billeci K, Suh C, Di Ioia T, Singh L, Abraham R, Baldwin A, Monteclaro S (2016) Implementation of an automated high-throughput plasmid DNA production pipeline. J Lab Autom 21:765–778

Blanusa M, Schenk A, Sadeghi H, Marienhagen J, Schwaneberg U (2010) Phosphorothioate-based ligase-independent gene cloning (PLICing): an enzyme-free and sequence-independent cloning method. Anal Biochem 406:141–146

Bradford MM (1976) A rapid and sensitive method for the quantitation of microgram quantities of protein utilizing the principle of protein-dye binding. Anal Biochem 72:248–254

Cano-Garrido O, Sanchez-Chardi A, Pares S, Giro I, Tatkiewicz WI, Ferrer-Miralles N, Ratera I, Natalello A, Cubarsi R, Veciana J, Bach A, Villaverde A, Aris A, Garcia-Fruitos E (2016) Functional

protein-based nanomaterial produced in microorganisms recognized as safe: a new platform for biotechnology. Acta Biomater 43:230–239

Carrio MM, Corchero JL, Villaverde A (1998) Dynamics of in vivo protein aggregation: building inclusion bodies in recombinant bacteria. FEMS Microbiol Lett. 169:9–15

Castro GR, Knubovets T (2003) Homogeneous biocatalysis in organic solvents and water-organic mixtures. Crit Rev Biotechnol 23:195–231

Choi SL, Lee SJ, Ha JS, Song J, Rhee YH, Lee SG (2011) Generation of catalytic protein particles in *Escherichia coli* cells using the cellulose-binding domain from *Cellulomonas fimi* as a fusion partner. Biotechnol Bioprocess Eng 16:1173–1179

de Groot NS, Ventura S (2006) Effect of temperature on protein quality in bacterial inclusion bodies. FEBS Lett 580:6471–6476

de Groot NS, Aviles FX, Vendrell J, Ventura S (2006) Mutagenesis of the central hydrophobic cluster in Aβ42 Alzheimer's peptide. FEBS J 273:658–668

Diener M, Kopka B, Pohl M, Jaeger KE, Krauss U (2016) Fusion of a coiled-coil domain facilitates the high-level production of catalytically active enzyme inclusion bodies. Chemcatchem 8:142–152

Doglia SM, Ami D, Natalello A, Gatti-Lafranconi P, Lotti M (2008) Fourier transform infrared spectroscopy analysis of the conformational quality of recombinant proteins within inclusion bodies. Biotechnol J 3:193–201

Dong Q, Yan X, Zheng M, Yang Z (2014) Characterization of an extremely thermostable but cold-adaptive β-galactosidase from the hyperthermophilic archaeon *Pyrococcus furiosus* for use as a recombinant aggregation for batch lactose degradation at high temperature. J Biosci Bioeng 117:706–710

Eisinger J, Flores J (1979) Front-face fluorometry of liquid samples. Anal Biochem 94:15–21

Engler C, Kandzia R, Marillonnet S (2008) A one pot, one step, precision cloning method with high throughput capability. PLoS One 3:e3647

Francis DM, Page R (2010) Strategies to optimize protein expression in *E. coli*, Curr. Protoc Protein Sci Chapter 5: Unit 5 24 1-29

Garcia-Fruitos E, Gonzalez-Montalban N, Morell M, Vera A, Ferraz RM, Aris A, Ventura S, Villaverde A (2005) Aggregation as bacterial inclusion bodies does not imply inactivation of enzymes and fluorescent proteins. Microb Cell Factories 4:27

García-Fruitós E, Rodríguez-Carmona E, Díez-Gil C, Ferraz RM, Vázquez E, Corchero JL, Cano-Sarabia M, Ratera I, Ventosa N, Veciana J, Villaverde A (2009) Surface cell growth engineering assisted by a novel bacterial nanomaterial. Adv Mater 21:4249–4253

Gibson DG, Young L, Chuang RY, Venter JC, Hutchison CA, Smith HO (2009) Enzymatic assembly of DNA molecules up to several hundred kilobases. Nat Methods 6:343–U41

Gifre-Renom L, Cano-Garrido O, Fabregas F, Roca-Pinilla R, Seras-Franzoso J, Ferrer-Miralles N, Villaverde A, Bach A, Devant M, Aris A, Garcia-Fruitos E (2018) A new approach to obtain pure and active proteins from *Lactococcus lactis* protein aggregates. Sci Rep 8:13917

Gotham SM, Fryer PJ, Paterson WR (1988) The measurement of insoluble proteins using a modified Bradford assay. Anal Biochem 173:353–358

Gremer L, Scholzel D, Schenk C, Reinartz E, Labahn J, Ravelli RBG, Tusche M, Lopez-Iglesias C, Hoyer W, Heise H, Willbold D, Schroder GF (2017) Fibril structure of amyloid-beta(1-42) by cryo-electron microscopy. Science 358:116–119

Heater BS, Lee MM, Chan MK (2018) Direct production of a genetically-encoded immobilized biodiesel catalyst. Sci Rep 8:12783

Hoffmann F, van den Heuvel J, Zidek N, Rinas U (2004) Minimizing inclusion body formation during recombinant protein production in *Escherichia coli* at bench and pilot plant scale. Enzym Microb Technol 34:235–241

Huang ZL, Zhang C, Chen S, Ye FC, Xing XH (2013) Active inclusion bodies of acid phosphatase PhoC: aggregation induced by GFP fusion and activities modulated by linker flexibility. Microb Cell Fact 12

Huber R, Ritter D, Hering T, Hillmer AK, Kensy F, Müller C, Wang L, Büchs J (2009) Robo-Lector - a novel platform for automated high-throughput cultivations in microtiter plates with high information content. Microb Cell Factories 8:42

Jacak R, Leaver-Fay A, Kuhlman B (2012) Computational protein design with explicit consideration of surface hydrophobic patches. Proteins 80:825–838

Jäger VD, Lamm R, Kloss R, Kaganovitch E, Grünberger A, Pohl M, Büchs J, Jaeger KE, Krauss U (2018) A synthetic reaction cascade implemented by colocalization of two proteins within catalytically active inclusion bodies. ACS Synth Biol 7:2282–2295

Jäger VD, Kloss R, Grünberger A, Seide S, Hahn D, Karmainski T, Piqueray M, Embruch J, Longerich S, Mackfeld U, Jaeger KE, Wiechert W, Pohl M, Krauss U (2019a) Tailoring the properties of (catalytically)-active inclusion bodies. Microb Cell Factories 18:33

Jäger VD, Piqueray M, Seide S, Pohl M, Wiechert W, Jaeger K-E, Krauss U (2019b) An enzymatic 2-step cofactor and co-product recycling cascade towards a chiral 1,2-diol. Part II: catalytically active inclusion bodies. Adv Synth Catal 361:2616–2626

Jevsevar S, Gaberc-Porekar V, Fonda I, Podobnik B, Grdadolnik J, Menart V (2005) Production of nonclassical inclusion bodies from which correctly folded protein can be extracted. Biotechnol Prog 21:632–639

Jhamb K, Sahoo DK (2012) Production of soluble recombinant proteins in *Escherichia coli*: effects of process conditions and chaperone co-expression on cell growth and production of xylanase. Bioresour Technol 123:135–143

Jiang L, Xiao WJ, Zhou X, Wang WY, Fan J (2019) Comparative study of the insoluble and soluble Ulp1 protease constructs as carrier free and dependent protein immobilizates. J Biosci Bioeng 127:23–29

Kind S, Neubauer S, Becker J, Yamamoto M, Volkert M, Gv A, Zelder O, Wittmann C (2014) From zero to hero - production of bio-based nylon from renewable resources using engineered *Corynebacterium glutamicum*. Metab Eng 25:113–123

Kloss R, Karmainski T, Jäger VD, Hahn D, Grünberger A, Baumgart M, Krauss U, Jaeger KE, Wiechert W, Pohl M (2018a) Tailor-made catalytically active inclusion bodies for different applications in biocatalysis. Catal Sci Technol 8:5816–5826

Kloss R, Limberg MH, Mackfeld U, Hahn D, Grünberger A, Jäger VD, Krauss U, Oldiges M, Pohl M (2018b) Catalytically active inclusion bodies of L-lysine decarboxylase from *E. coli* for 1,5-diaminopentane production. Sci Rep 8

Kopito RR (2000) Aggresomes, inclusion bodies and protein aggregation. Trends Cell Biol 10:524–530

Kopp J, Slouka C, Strohmer D, Kager J, Spadiut O, Herwig C (2018) Inclusion body bead size in *E. coli* controlled by physiological feeding. Microorganisms 6

Koszagova R, Krajcovic T, Palencarova-Talafova K, Patoprsty V, Vikartovska A, Pospiskova K, Safarik I, Nahalka J (2018) Magnetization of active inclusion bodies: comparison with centrifugation in repetitive biotransformations. Microb Cell Factories 17:139

Krauss U, Jäger VD, Diener M, Pohl M, Jaeger KE (2017) Catalytically-active inclusion bodies carrier-free protein immobilizates for application in biotechnology and biomedicine. J Biotechnol 258:136–147

Krieger E, Vriend G (2014) YASARA View - molecular graphics for all devices - from smartphones to workstations. Bioinformatics 30:2981–2982

Krieger E, Vriend G (2015) New ways to boost molecular dynamics simulations. J Comput Chem 36:996–1007

Kuhlman B, Baker D (2000) Native protein sequences are close to optimal for their structures. Proc Natl Acad Sci U S A 97:10383–10388

Kunze M, Lattermann C, Diederichs S, Kroutil W, Büchs J (2014) Minireactor-based high-throughput temperature profiling for the optimization of microbial and enzymatic processes. J Biol Eng 8:22

Lamm R, Jäger VD, Heyman B, Berg C, Cürten C, Ulrich K, Jaeger KE, Büchs J (2020) Detailed small-scale characterization and scale-up of active YFP inclusion body production with *Escherichia coli* induced by a tetrameric coiled coil domain. J Biosci Bioeng

Li S, Lin K, Pang H, Wu Y, Jianhe X (2013) Production, characterization, and application of an organic solvent-tolerant lipase present in active inclusion bodies. Appl Biochem Biotechnol 169:612–623

Li ZP, Nimtz M, Rinas U (2014) The metabolic potential of *Escherichia coli* BL21 in defined and rich medium. Microb Cell Factories 13:17

Lin ZL, Zhou BH, Wu W, Xing L, Zhao Q (2013) Self-assembling amphipathic alpha-helical peptides induce the formation of active protein aggregates in vivo. Faraday Discuss 166:243–256

Mamat U, Wilke K, Bramhill D, Schromm AB, Lindner B, Kohl TA, Corchero JL, Villaverde A, Schaffer L, Head SR, Souvignier C, Meredith TC, Woodard RW (2015) Detoxifying *Escherichia coli* for endotoxin-free production of recombinant proteins. Microb Cell Factories 14:57

Margreiter G, Messner P, Caldwell KD, Bayer K (2008) Size characterization of inclusion bodies by sedimentation field-flow fractionation. J Biotechnol 138:67–73

Mestrom L, Marsden SR, McMillan DGG, Schoevaart R, Hagedoorn PL, Hanefeld U (2020) Comparison of enzymes immobilised on immobeads and inclusion bodies: a case study of a trehalose transferase. Chemcatchem 12:3249–3256

Nahalka J (2008) Physiological aggregation of maltodextrin phosphorylase from *Pyrococcus furiosus* and its application in a process of batch starch degradation to alpha-D-glucose-1-phosphate. J Ind Microbiol Biotechnol 35:219–223

Nahalka J, Nidetzky B (2007) Fusion to a pull-down domain: a novel approach of producing *Trigonopsis variabilis* D-amino acid oxidase as insoluble enzyme aggregates. Biotechnol Bioeng 97:454–461

Nahalka J, Patoprsty V (2009) Enzymatic synthesis of sialylation substrates powered by a novel polyphosphate kinase (PPK3). Org Biomol Chem 7:1778–1780

Nahálka J, Gemeiner P, Bučko M, Wang PG (2006) Bioenergy beads: a tool for regeneration of ATP/NTP in biocatalytic synthesis. Artif Cell Blood Sub 34:515–521

Nahalka J, Vikartovska A, Hrabarova E (2008) A crosslinked inclusion body process for sialic acid synthesis. J Biotechnol 134:146–153

Neerathilingam M, Mysore S, Gandham SHA (2014) Soni-removal of nucleic acids from inclusion bodies. Biochem Biophys Res Commun 448:45–49

Oh YH, Kang KH, Kwon MJ, Choi JW, Joo JC, Lee SH, Yang YH, Song BK, Kim IK, Yoon KH, Park K, Park SJ (2015) Development of engineered *Escherichia coli* whole-cell biocatalysts for high-level conversion of L-lysine into cadaverine. J Ind Microbiol Biotechnol 42:1481–1491

Olieric N, Kuchen M, Wagen S, Sauter M, Crone S, Edmondson S, Frey D, Ostermeier C, Steinmetz MO, Jaussi R (2010) Automated seamless DNA co-transformation cloning with direct expression vectors applying positive or negative insert selection. BMC Biotechnol 10: 1–10

Park SY, Park SH, Choi SK (2012) Active inclusion body formation using *Paenibacillus polymyxa* PoxB as a fusion partner in *Escherichia coli*. Anal Biochem 426:63–65

Park SH, Soetyono F, Kim HK (2017) Cadaverine production by using cross-linked enzyme aggregate of *Escherichia coli* lysine decarboxylase. J Microbiol Biotechnol 27:289–296

Pasotti L, Zucca S, Lupotto M, Cusella De Angelis MG, Magni P (2011) Characterization of a synthetic bacterial self-destruction device for programmed cell death and for recombinant proteins release. J Biol Eng 5:8

Peternel S, Grdadolnik J, Gaberc-Porekar V, Komel R (2008) Engineering inclusion bodies for non denaturing extraction of functional proteins. Microb Cell Factories 7:34

Porta C, Kotecha A, Burman A, Jackson T, Ren J, Loureiro S, Jones IM, Fry EE, Stuart DI, Charleston B (2013) Rational engineering of recombinant picornavirus capsids to produce safe, protective vaccine antigen. PLoS Pathog 9:e1003255–e1003e55

Ratera I, Peternel S, Seras J, Garrido OC, Garcia-Fruitos E, Cubarsi R, Vazquez E, Corchero J, Rodríguez-Carmona E, Veciana J, Villaverde A (2014) Biomedical applications of bacterial inclusion bodies. In: Doglia SM, Lotti M (eds) Protein aggregation in bacteria: functional and structural properties of inclusion bodies in bacterial cells

Rinas U, Garcia-Fruitos E, Corchero JL, Vazquez E, Seras-Franzoso J, Villaverde A (2017) Bacterial inclusion bodies: discovering their better half. Trends Biochem Sci 42:726–737

Rodriguez-Carmona E, Cano-Garrido O, Seras-Franzoso J, Villaverde A, Garcia-Fruitos E (2010) Isolation of cell-free bacterial inclusion bodies. Microb Cell Factories 9:9

Rohl CA, Strauss CE, Misura KM, Baker D (2004) Protein structure prediction using Rosetta. Methods Enzymol 383:66–93

Rueda F, Cano-Garrido O, Mamat U, Wilke K, Seras-Franzoso J, Garcia-Fruitos E, Villaverde A (2014) Production of functional inclusion bodies in endotoxin-free *Escherichia coli*. Appl Microbiol Biotechnol 98:9229–9238

Samorski M, Müller-Newen G, Büchs J (2005) Quasi-continuous combined scattered light and fluorescence measurements: a novel measurement technique for shaken microtiter plates. Biotechnol Bioeng 92:61–68

Sheldon RA, Brady D (2018) The limits to biocatalysis: pushing the envelope. Chem Commun 54:6088–6104

Sheldon RA, Brady D (2019) Broadening the scope of biocatalysis in sustainable organic synthesis. ChemSusChem 12:2859–2881

Sheldon RA, van Pelt S (2013) Enzyme immobilisation in biocatalysis: why, what and how. Chem Soc Rev 42:6223–6235

Singh A, Upadhyay V, Panda AK (2015) Solubilization and refolding of inclusion body proteins. Methods Mol Biol. 1258:283–291

Song AA, In LLA, Lim SHE, Rahim RA (2017) A review on *Lactococcus lactis*: from food to factory. Microb Cell Factories 16:55

Stetefeld J, Jenny M, Schulthess T, Landwehr R, Engel J, Kammerer RA (2000) Crystal structure of a naturally occurring parallel right-handed coiled coil tetramer. Nat Struct Biol 7:772–776

Tokatlidis K, Dhurjati P, Millet J, Béguin P, Aubert J-P (1991) High activity of inclusion bodies formed in *Escherichia coli* overproducing *Clostridium thermocellum* endoglucanase D. FEBS Lett 282:205–208

Tufvesson P, Lima-Ramos J, Nordblad M, Woodley JM (2011) Guidelines and cost analysis for catalyst production in biocatalytic processes. Org Process Res Dev 15:266–274

Vallejo LF, Rinas U (2004) Strategies for the recovery of active proteins through refolding of bacterial inclusion body proteins. Microb Cell Factories 3:11–11

van Pouderoyen G, Eggert T, Jaeger KE, Dijkstra BW (2001) The crystal structure of *Bacillus subtilis* lipase: a minimal alpha/beta hydrolase fold enzyme. J Mol Biol 309:215–226

Vazquez E, Corchero JL, Burgueno JF, Seras-Franzoso J, Kosoy A, Bosser R, Mendoza R, Martinez-Lainez JM, Rinas U, Fernandez E, Ruiz-Avila L, Garcia-Fruitos E, Villaverde A (2012) Functional inclusion bodies produced in bacteria as naturally occurring nanopills for advanced cell therapies. Adv Mater 24:1742–1747

Ventura S, Villaverde A (2006) Protein quality in bacterial inclusion bodies. Trends Biotechnol 24:179–185

Vera A, Gonzalez-Montalban N, Aris A, Villaverde A (2007) The conformational quality of insoluble recombinant proteins is enhanced at low growth temperatures. Biotechnol Bioeng 96:1101–1106

Viranaicken W, Nativel B, Krejbich-Trotot P, Harrabi W, Bos S, El Kalamouni C, Roche M, Gadea G, Despres P (2017) ClearColi BL21(DE3)-based expression of Zika virus antigens illustrates a rapid method of antibody production against emerging pathogens. Biochimie 142:179–182

Wang X, Zhou BH, Hu WK, Zhao Q, Lin ZL (2015) Formation of active inclusion bodies induced by hydrophobic self-assembling peptide GFIL8. Microb Cell Fact 14

Wang W, Sun J, Xiao W, Jiang L, Wang R, Fan J (2017) Change of the N-terminal codon bias combined with tRNA supplementation outperforms the selected fusion tags for production of human D-amino acid oxidase as active inclusion bodies. Biotechnol Lett 39:1733–1740

Worrall DM, Goss NH (1989) The formation of biologically active beta-galactosidase inclusion bodies in *Escherichia coli*. Aust J Biotechnol 3:28–32

Wu W, Xing L, Zhou B, Lin Z (2011) Active protein aggregates induced by terminally attached self-assembling peptide ELK16 in *Escherichia coli*. Microb Cell Factories 10:1–8

Xu W, Zhao Q, Xing L, Lin Z (2016) Recombinant production of influenza hemagglutinin and HIV-1 GP120 antigenic peptides using a cleavable self-aggregating tag. Sci Rep 6:35430

Yang XF, Pistolozzi M, Lin ZL (2018) New trends in aggregating tags for therapeutic protein purification. Biotechnol Lett 40:745–753

Zerbs S, Giuliani S, Collart F (2014) Small-scale expression of proteins in *E. coli*. Methods Enzymol 536:117–131

Zhao Q, Xu W, Xing L, Lin Z (2016) Recombinant production of medium- to large-sized peptides in *Escherichia coli* using a cleavable self-aggregating tag. Microb Cell Factories 15:136

Zhao Q, Zhou B, Gao X, Xing L, Wang X, Lin Z (2017) A cleavable self-assembling tag strategy for preparing proteins and peptides with an authentic N-terminus. Biotechnol J 12

Zhou BH, Xing L, Wu W, Zhang XE, Lin ZL (2012) Small surfactant-like peptides can drive soluble proteins into active aggregates. Microb Cell Factories 11:10

Zhu BG, Cai GF, Hall EO, Freeman GJ (2007) In-Fusion (TM) assembly: seamless engineering of multidomain fusion proteins, modular vectors, and mutations. Biotechniques 43:356–359

2.5. Publication 5. Design, production and characterization of catalytically-active inclusion bodies

Gizem Ölçücü*, Karl-Erich Jaeger, Ulrich Krauss*

*corresponding authors

Design, Production, and Characterization of Catalytically Active Inclusion Bodies. Ed. by Julian Kopp and Oliver Spadiut. Vol. 2617. Methods in Molecular Biology. Springer US, 2023, pp. 49–74. https://link.springer.com/protocol/10.1007/978-1-0716-2930-7_4

Author Contributions: GO wrote the manuscript and prepared all figures. UK contributed to the writing of certain sub-chapters and edited the manuscript. KEJ helped with editing and proof reading. All authors have read and approved the final version.

Chapter 4

Design, Production, and Characterization of Catalytically Active Inclusion Bodies

Gizem Ölçücü, Karl-Erich Jaeger, and Ulrich Krauss

Abstract

Catalytically active inclusion bodies (CatIBs) are promising biologically produced enzyme/protein immobilizates for application in biocatalysis, synthetic chemistry, and biomedicine. CatIB formation is commonly induced by fusion of suitable aggregation-inducing tags to a given target protein. Heterologous production of the fusion protein in turn yields CatIBs. This chapter presents the methodology needed to design, produce, and characterize CatIBs.

Key words Enzyme immobilization, Biocatalysis, Enzyme aggregates, Catalytically active inclusion bodies – CatIBs, Fusion protein, Aggregation-inducing tag, Heterologous gene expression, Microscopy, Fractionation

1 Introduction

The immobilization of enzymes is a cornerstone of industrial biotechnology and has traditionally been used to stabilize enzymes in reaction systems and to allow for easy recycling and reuse of the catalyst [1–3]. More recently, numerous *in vivo* enzyme immobilization strategies have been described (reviewed in [4–7]) that combine enzyme overproduction and immobilization in one step. This allows for the solely biological production of enzyme/protein immobilizates without the need for additional carrier materials and expensive and time-consuming purification and immobilization steps. Recently, catalytically active inclusion bodies (CatIBs) have been designed and constructed as new and promising immobilizates which proved useful for applications in various fields. In contrast to conventional inclusion bodies (IBs) that consist predominately of misfolded/unfolded and hence inactive protein, CatIBs retain a certain degree of activity [8–13]. CatIB-based immobilizates have hereby been used as carrier-free enzyme immobilizates in biocatalysis and synthetic chemistry [14–24] for

Julian Kopp and Oliver Spadiut (eds.), *Inclusion Bodies: Methods and Protocols*,
Methods in Molecular Biology, vol. 2617, https://doi.org/10.1007/978-1-0716-2930-7_4,

simplified protein purification via intein self-cleavage [25, 26] as well as for biomedical applications, for example as biomaterials in tissue engineering or as drug delivery vehicles [27–29].

Generally, CatIBs are generated by molecular biological fusion of aggregation-mediating protein modules such as relatively small coiled-coil domains [14–18, 30], larger aggregation prone proteins and protein domains [20, 31, 9, 32, 33] or short synthetic peptides [19, 34, 24, 35]. These, so-called "pull-down" or CatIB tags are often fused via linker polypetides to the N- or C-terminus of a given target protein. Up to now, fusion protein design for CatIB generation is still a trial-and-error process, as rational strategies that identify the best suited tag, fusion site, and linker are still lacking. Overexpression of the corresponding gene fusions under suitable conditions in a bacterial host [36, 37] in turn results in the formation of CatIBs, likely consisting of an IB matrix of misfolded/unfolded protein and correctly folded target fusion protein deposited within the IB particles. Like IBs, CatIBs are insoluble in water and organic solvents, and can therefore easily be isolated by centrifugation of CatIB-containing crude cell extracts after cell lysis.

Qualitatively, success of CatIB formation can be followed by microscopic analysis of CatIB-producing cells, as CatIBs, like IBs, accumulate as refractile particles at the cell poles of the expression host [14, 9, 15]. Quantitatively, CatIB formation can be assessed by fractionation of crude cell extracts into soluble and insoluble (CatIB-containing) protein fractions by centrifugation. Efficacy of CatIB formation for a given construct can then be expressed as, e.g., CatIB formation efficiency, which is defined as the activity of the insoluble CatIB-containing protein fraction relative to the activity of the crude cell extract [15, 16]. Similarly, it is often necessary to determine protein content and the specific activity of CatIBs, e.g., expressed relative to the activity of the purified, soluble target enzyme [15]. Since CatIBs, as insoluble protein aggregates, yield turbid suspensions when suspended in water or buffer, the application of conventional spectrophotometric assays for protein concentration and activity determination is often not directly possible due to scattering by and sedimentation of the CatIB particles in those assays.

Since CatIBs represent promising enzyme/protein preparations for various applications in biotechnology and beyond, it is useful to present a collection of methods developed to address CatIB fusion design, production, and characterization. In the following chapters, we therefore collect various protocols needed for the generation of CatIBs for a given target protein by construction of CatIB-inducing gene fusions (Subheadings 3.1 and 3.2), production of CatIBs in *E. coli* (Subheading 3.3), their initial characterization by microscopy (Subheading 3.4) as well as the preparation of CatIB-containing cell fractions (Subheading 3.5), and the determination of CatIB formation efficiencies

(Subheadings 3.6 and 3.7). In addition, we provide protocols for the lyophilization of CatIBs (Subheading 3.8) and for a more in-depth characterization of these lyophilizates in terms of protein content (Subheading 3.9) and specific residual activity (Subheading 3.10). As specific examples, we present protocols for the characterization of CatIBs of the yellow fluorescent protein (YFP), the red fluorescent protein (mCherry), and an alcohol dehydrogenase of *Ralstonia sp.* (RADH), for which CatIBs have previously been produced and characterized [15, 16].

2 Materials

2.1 Cloning

1. CatIB gene fusion obtained by gene synthesis; consisting of CatIB-inducing tag, target gene, and optionally, a linker between these two elements, furnished with suitable 5′ and 3′ restriction endonuclease recognition sites for cloning.
2. Alternatively, if the target gene (encoding the protein for which CatIBs are to be produced) is to be cloned into an expression vector containing the CatIB-inducing tag (and, if present, the linker), PCR oligonucleotide primers for amplification of the target gene with suitable 5′ and 3′ restriction endonuclease recognition sites (*see* **Note 1**).
3. Suitable DNA template containing the target gene (genomic DNA, plasmid DNA).
4. DNA polymerase and buffer (e.g., Phusion high fidelity DNA polymerase, New England Biolabs, Massachusetts, USA).
5. Deoxynucleoside triphosphates (dNTPs).
6. PCR thermal cycler.
7. Agarose to prepare agarose gels for separation of DNA.
8. Nucleic acid stain (e.g., 0.5 μg/mL ethidium bromide or MIDORI green (Nippon genetics, Tokyo, Japan) to stain agarose gels.
9. DNA gel electrophoresis cells and power supply (e.g., Mini-Sub Cell GT Horizontal Electrophoresis System and PowerPac Basic Power Supply, Bio-Rad Laboratories GmbH, Feldkirchen, Germany).
10. DNA electrophoresis size standard.
11. DNA gel loading dye.
12. Agarose gel extraction and PCR purification kits (e.g., innuPREP Gel Extraction Kit and innuPrep PCRpure Kit, Analytik Jena, Jena, Germany).
13. Benchtop centrifuge.
14. Shaking incubator for Eppendorf tubes.

15. NanoDrop microvolume spectrophotometer (Thermofisher Scientific, Massachusetts, USA) or similar microvolume spectrophotometer that allows DNA quantification at the μL scale.
16. Suitable expression vector, e.g., for T7 RNA polymerase-dependent gene expression in *E. coli* such as pET28a (Merck KGaA, Darmstadt, Germany).
17. Restriction endonucleases (ThermoFischer Scientific, Massachusetts, USA) matching the recognition sites at 5′ and 3′ ends of the synthetic gene or PCR primers.
18. Restriction endonuclease buffer (ThermoFischer Scientific, Massachusetts, USA).
19. T4 DNA ligase and buffer (ThermoFischer Scientific, Massachusetts, USA).
20. Suitable host organism for cloning (i.e., chemically competent *E. coli* DH5α cells).
21. Lysogeny broth (LB) with the following composition: 1% tryptone, 0.5% yeast extract, 1% NaCl, and suitable antibiotic (i.e., 50 μg/mL kanamycin) depending on the vector.
22. Shaking incubator for LB cultures.
23. LB-agar (15 g/L agar-agar) plates containing a suitable antibiotic (e.g., 50 μg/mL kanamycin) depending on the vector.
24. Incubator for agar plates.
25. Plasmid preparation kit (e.g., innuPrep Plasmid Mini Kit 2.0, Analytik Jena, Jena, Germany).

2.2 Bacterial Cultivation and Expression

All solutions are prepared in ultrapure water or ddH_2O and in case of media, and media components autoclaved or sterile filtered prior to use.

1. Suitable expression strain (i.e., chemically competent *E. coli* BL21(DE3) cells).
2. Expression vector (i.e., pET28a) containing the CatIB gene fusion (*see* **Note 2**) under control of an inducible promoter (e.g., P_{T7} promoter for T7 RNA polymerase-dependent gene expression); here: pTDoT-L-YFP, pTDoT-mCherry, and pTDoT-L-RADH [15].
3. LB medium and LB-agar plates (composition *see* Subheading 2.1).
4. Suitable antibiotic (e.g., 50 μg/mL kanamycin) depending on the expression vector.
5. Incubator for agar plates.
6. Shaking incubator for LB cultures.
7. Glucose stock solution (50 g/L).

8. Concentrated lactose stock solution (200 g/L), dissolves after autoclaving.
9. Glycerol (pure).
10. Terrific Broth (TB) Medium with the following composition: 12 g/L casein-hydrolysate, 24 g/L yeast extract, 12.54 g/L K_2HPO_4, 2.31 g/L KH_2PO_4, supplemented with 5 g/L glycerol, pH 7.2.
11. Thermostated UV-VIS spectrophotometer (e.g., Cary 60 UV-Vis Spectrophotometer, Agilent, Santa Clara, USA).
12. 4x1L capacity centrifuge (e.g., ThermoFischer™ Scientific, Sorvall LYNX 4000 Superspeed Centrifuge, Massachusetts, USA).

2.3 Microscopic Analysis of CatIB Formation

All solutions are prepared in ultrapure water.

1. Freshly prepared cells containing fluorescent or nonfluorescent CatIBs (*see* **Note 3**; [15] prepared as described in Subheading 3.3).
2. Agarose to prepare agarose pads.
3. Microscope glass slides (76 × 26 mm) and cover glasses of suitable size.
4. Magnetic stirrer.
5. Microwave or hot plate stirrer.
6. Benchtop centrifuge.
7. Fluorescence microscope (e.g., inverted Nikon Eclipse Ti microscope) (Nicon GmbH, Düsseldorf, Germany) equipped with an Apo TIRF 100× Oil DIC N objective (ALA OBJ-Heater, Ala Scientific Instruments, USA), an ANDOR Zyla CMOS camera (Andor Technology plc., Belfast, UK), an Intensilight (Nicon GmbH, Düsseldorf, Germany) light source for fluorescence excitation, and fluorescence filters mCherry (excitation: 575/15 nm, dichroic mirror: 593 nm, emission: 629/56 nm) (AHF Analysentechnik, Tübingen, Germany).

2.4 Preparation of CatIBs and Cell Fractions

All solutions are prepared in ultrapure water and autoclaved prior to use.

1. *E. coli* cells containing CatIBs; either freshly prepared or stored as frozen cell pellet (*see* Subheading 3.3).
2. High-pressure homogenizer (e.g., Emulsiflex-C5 high-pressure homogenizer, Avestin Europe GmbH, Mannheim, Germany) for cell disruption.
3. Suitable lysis buffer (i.e., sodium phosphate buffer with the following composition: 50 mM Na_2HPO_4, 100 mM NaCl, pH 8.0).

4. 4x1L capacity centrifuge (e.g., ThermoFischer™ Scientific, Sorvall LYNX 4000 Superspeed Centrifuge, Massachusetts, USA).
5. Benchtop centrifuge.

2.5 Determination of CatIB Formation Efficiency for Fluorescent CatIBs

1. Cell fractions of constructs producing fluorescent CatIBs (*see* Subheading 2.3).
2. Microtiter plates for fluorescence measurements (e.g., black Nunc 96-Well MicroWell polypropylene plates, ThermoFischer Scientific, Massachusetts, USA).
3. Fluorescence microtiter plate reader (e.g., TECAN infinite M1000 PRO fluorescence MTP reader, TECAN, Männedorf, Switzerland).

2.6 Determination of CatIB Formation Efficiency for RADH CatIBs

If not stated otherwise, all solutions are prepared in ultrapure water and autoclaved prior to use.

1. Cell fractions of constructs producing RADH CatIBs (*see* Subheading 2.3).
2. TEA Buffer with the following composition: 50 mM triethanolamine, 0.8 mM $CaCl_2$, pH 7.5.
3. Methanol (*see* **Note 4**).
4. Cyclohexanone (*see* **Note 5**).
5. NADPH.
6. Temperature-controlled shaking Eppendorf tube incubator.
7. Vortex mixer.
8. Benchtop centrifuge.
9. Thermostated UV-VIS spectrophotometer (e.g., Cary 60 UV-Vis Spectrophotometer, Agilent, Santa Clara, USA).

It is highly recommended to have a multichannel pipette with adjustable-spacing, and a multichannel pipette reservoir.

2.7 Preparation of Lyophilized CatIBs

1. Ultrapure water.
2. Glass beakers.
3. Parafilm.
4. Lyophilizer (e.g., Christ ALPHA 1–3 LD Plus, Martin Christ Gefriertrocknungsanlagen GmbH, Osterode, Germany).
5. Mortar and pestle with glazed surface.
6. Spatulas.
7. Glass vials for storing CatIBs.
8. Argon.

2.8 Determination of the Protein Content of Lyophilized CatIBs

All solutions are prepared in ultrapure water.

1. Lyophilized CatIBs.
2. High precision laboratory scale (Sartorius Secura125-1S Semi-Micro Balance 120 g × 0.01 mg).
3. 6 M Guanidine-hydrochloride solution.
4. Temperature controlled shaking Eppendorf tube incubator.
5. Vortex mixer.
6. Benchtop centrifuge.
7. Thermostated UV-VIS spectrophotometer (e.g., Cary 60 UV-Vis Spectrophotometer, Agilent, Santa Clara, USA).

2.9 Determination of Residual Activity Using Lyophilized RADH CatIBs

In addition to the materials needed for the determination of the CatIB formation efficiency for RADH CatIBs (*see* Subheading 2.6), the following materials are needed.

1. Lyophilized CatIBs (prepared as described in Subheading 3.8).
2. High precision laboratory scale (e.g., Sartorius Secura125-1S Semi-Micro Balance 120 g × 0.01 mg).

3 Methods

3.1 Selection of CatIB-Inducing Tags

The design of gene fusions consisting of a CatIB-inducing "pull-down" tag, linker, and target protein, to enable CatIB production, is still a trial-and-error process, due to the lack of rational strategies to select the best suited tag, fusion site, and linker. Only few general guidelines have emerged empirically in the last years. Generally, the presence of hydrophobic surface patches on the target protein and tag surface seems to be needed for CatIB formation [15, 13]. Along those lines, highly soluble, monomeric targets such as the fluorescent reporter protein mCherry [15, 16] seem to be more difficult to immobilize following the CatIB strategy. Both N- and C-terminal tag fusions seem to be possible in most cases; however, target protein structures (if available) should be considered when selecting the fusion site, since buried termini might prohibit fusion at a specific terminus [15]. Likewise, the presence and structure of the employed linker polypeptides can have a marked impact on CatIB formation. No general rules for linker selection can be derived since both flexible and rigid linkers have been employed successfully [19]. The following steps are recommended for the design of CatIB-producing gene fusions.

1. Obtain the pdb file for your target protein (if available) from the protein data bank (e.g., at https://www.rcsb.org/) [38] (*see* **Note 6**).

2. Verify that the crystal structure of your target protein represents the native biological quaternary structure by using the "Protein interfaces, surfaces and assemblies" service PISA at the European Bioinformatics Institute http://www.ebi.ac.uk/pdbe/prot_int/pistart.html [39]. If needed, analyze alternative oligomeric assemblies alongside the obtained structure as described in the following steps.
3. Analyze the surface hydrophobicity of your target protein structure, e.g., by using online tools such as Aggrescan3D [40], the hydrophobic cluster computation tool available online as part of the ProteinTools suite of programs [41] or the hpatch tool [42] of the Rosetta protein design software [43, 44].
4. Check protein structures (and if needed alternative oligomeric assemblies) for buried and hence not accessible termini. This can be achieved using most molecule viewers such as Chimera and Pymol [45, 46].
5. Based on **step 4**, identify a suited fusion terminus. If both termini appear suitable, both fusion sites should be tested. Surface hydrophobicity determined in **step 3** only provides a first hint, if CatIB formation might be feasible.
6. Select a suitable CatIB-formation inducing "pulldown" tag (see [13, 4] for a comprehensive overview).
7. Select a suitable linker (*see* Subheading 3.2 for details).

3.2 Cloning

CatIB gene fusions can be obtained by various means. The simplest, arguably also the most expensive way, is to design the complete gene fusion in silico and order the synthetic gene containing all elements needed for CatIB formation. We recommend to design the synthetic construct to include unique restriction enzyme recognition sites to flank each element. Such modular constructs allow the generation of additional constructs by simply exchanging the target gene, CatIB-inducing tag or linker, thereby saving a lot of time and effort in future experiments, e.g., when CatIBs of other targets need to be produced. Alternatively, all elements needed for construction of the CatIB gene fusion can be PCR amplified containing 5′- and 3′-restriction endonuclease recognition sites and ligated in a suitable manner to yield the desired gene fusion, or by employing alternative methods (*see* **Note 7**). The following protocol describes the steps needed to obtain CatIB gene fusions by gene synthesis and to clone them into a suitable expression vector, or alternatively, PCR amplification of a target gene to be cloned into a suitable expression vector that contains the CatIB-inducing elements, in order to generate the same expression construct:

1. Design the CatIB gene fusion by including the gene encoding the CatIB-inducing tag (*see* Subheading 3.1) at either 5′- or

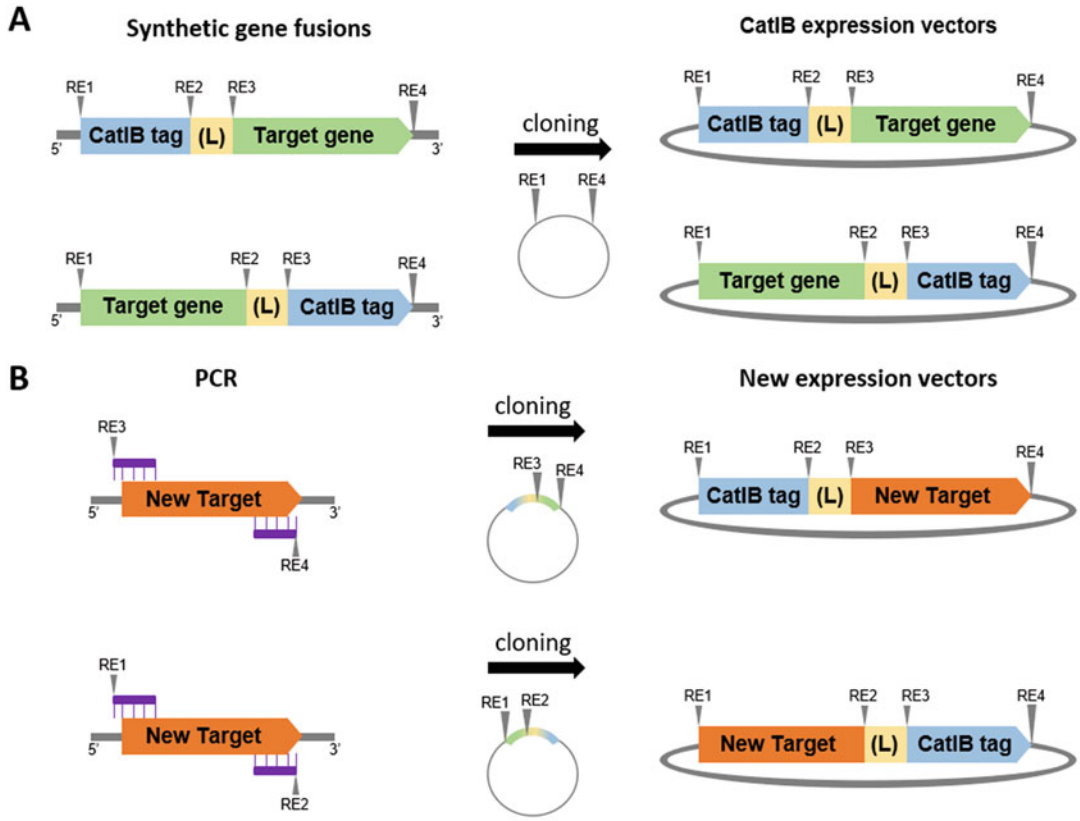

Fig. 1 Design principles for generating CatIB gene fusions. Panel **a** depicts the cloning of CatIB gene fusions obtained by gene synthesis into an expression vector. Synthetic gene fusions (left) contain DNA fragments that encode a CatIB-inducing tag, linker (L), and a target protein in either orientation (N- vs. C-terminal fusion), with restriction enzyme recognition sites (RE) flanking each element. Panel **b** depicts the modular construction strategy in which a new target gene can be cloned into existing CatIB expression vectors. Primers (depicted in purple) that anneal to a new target gene are designed to include matching restriction enzyme recognition sites that allow their cloning into suitable CatIB expression vectors. As each element in these constructs is flanked by a unique restriction enzyme recognition site, virtually each element, including the CatIB-inducing tag and linker, can be exchanged using the same principle

3′-end of the target gene (*see* **Note 8**). In most cases, it is advisable to add a linker between the CatIB-inducing tag and the target (*see* **Note 9**). Figure 1 illustrates the design principles for generating CatIB gene fusions.

2. Obtain the designed CatIB gene fusion by gene synthesis. Usually, synthetic genes are provided in synthesis vectors from which they can be released by digestion with restriction endonucleases. If the gene fusion is ordered directly cloned into a suitable expression vector, skip to Subheading 3.3, otherwise proceed with **step 4**. If CatIB gene fusions are not obtained by gene synthesis, amplify the isolated target gene (for which CatIBs are to be obtained) by using PCR primers

with suitable restriction endonuclease recognition sites to allow cloning of the target gene and proceed to **step 3** (*see* **Note 7**).

3. If the target gene is amplified via PCR, purify gene fragment (s) by using a PCR purification kit.
4. Perform a restriction digestion of the synthesis vector containing the CatIB gene fusion from **step 2** or digest the purified PCR product obtained in **step 3**.
5. Similarly digest the expression vector or the expression vector containing the CatIB-inducing tag using suitable restriction enzymes.
6. Separate digested CatIB gene fusion, the digested target gene fragment as well as the respective expression vector (with or without CatIB-inducing tag) by agarose gel electrophoresis. Purify respective fragments using a gel extraction kit.
7. Ligate the gene fragments and the expression vector using T4 DNA ligase according to manufacturer's instructions. Overnight ligation at 20 °C or lower is generally recommended.
8. Inactivate the ligase by incubation of the mixture for 10 min at 65 °C and transform competent *E. coli* DH5α cells using 15 μL of the ligation mixture.
9. Spread transformation mixture onto LB-agar plates containing the appropriate antibiotic, and cultivate the plates overnight at 37 °C.
10. Pick a single colony from the transformation plate and inoculate a 5 mL LB medium in a 50 mL shake flask (10% filling volume) supplemented with the appropriate antibiotic. Picking several colonies to inoculate more LB cultures is highly recommended to speed up the screening process. Cultivate the cells overnight at 37 °C, shaking at 130 rpm.
11. Isolate plasmid DNA by using a plasmid preparation kit according to manufacturer's instructions.
12. Sequence the plasmid to ensure correct insertion of the CatIB gene fusion or proper fusion of CatIB-inducing tag, target gene, and if included, the linker.

3.3 Cultivation and Expression

The following procedure uses pET28a as the expression vector, and employs autoinduction (AI) medium [47]. The medium contains glucose, glycerol, and lactose as carbon sources. After the preferred carbon source, glucose, is used up by the microorganisms, cells switch to utilize lactose and glycerol. The lactose, present in the media, induces the heterologous protein production via the T7 system (P_{lacUV5}-dependent expression of T7 RNA polymerase controlling the P_{T7}-dependent expression of the target gene fusion). Presence of multiple carbon sources prevents the cells from producing the recombinant proteins until preferential

substrates are depleted [48, 49], and adjusting the concentration of these substrates appropriately eliminates the necessity of measuring cell density periodically, therefore simplifying the expression procedure. Importantly, expression at low temperatures has been shown crucial for CatIB formation [37]; therefore, this method uses expression at 15 °C for CatIB-producing constructs. The following steps describe a standardized expression method, which we has successfully used for CatIB production:

1. Transform *E. coli* BL21(DE3) cells using 100 ng of plasmid DNA containing the CatIB gene fusion under control of a suitable promoter (e.g., pET28a-based expression plasmids prepared as described in Subheading 3.2.) (*see* **Note 10**).
2. Plate transformed cells onto LB-agar supplemented with a suitable antibiotic (i.e., 50 μg/mL kanamycin), and cultivate overnight at 37 °C.
3. Pick a single colony from the transformation plate and inoculate a 10 mL LB preculture in a 100 mL flask (10% filling volume) containing 50 μg/mL kanamycin. Cultivate overnight at 37 °C, shaking at 130 rpm.
4. In a 1 L flask, prepare 100 mL of fresh AI medium using TB medium, glycerol, and lactose stocks. AI medium composition: 12 g/L casein-hydrolysate, 24 g/L yeast extract, 12.54 g/L K_2HPO_4, 2.31 g/L KH_2PO_4, 5 g/L glycerol, pH 7.2, supplemented with 0.5 g/L glucose, 2 g/L lactose, and 50 μg/mL kanamycin.
5. Measure the OD_{600} of the LB preculture, and inoculate the AI medium with a starting OD_{600} of 0.05. Transfer the AI culture to 37 °C, 130 rpm for 3 h.
6. After 3 h, transfer the culture to 15 °C,130 rpm, and cultivate the cells up to additional 69 h (for detailed expression studies see, [37]).
7. Harvest the cells by centrifugation; 30 min, 6750 ×*g*, 4 °C.
8. Store the pellet at −20 °C until use.

3.4 Microscopic Analysis of CatIB Formation

Microscopy can be used as a quick method to verify CatIB formation, since CatIBs, like conventional inclusion bodies, form dense refractile particles at the cell poles, which can be detected in phase-contrast images, or, if fluorescent reporter proteins such as mCherry or YFP are used as target, in the corresponding fluorescence microscopic images [30, 15, 16]. Different setups for the microscopic analysis of living cells are possible. In the following, we will describe a simple method for immobilizing living cells on agarose pads for microscopic analysis:

1. Prepare a 1% (w/v) agarose solution in MilliQ water. Boil the solution for a few minutes in a microwave to completely

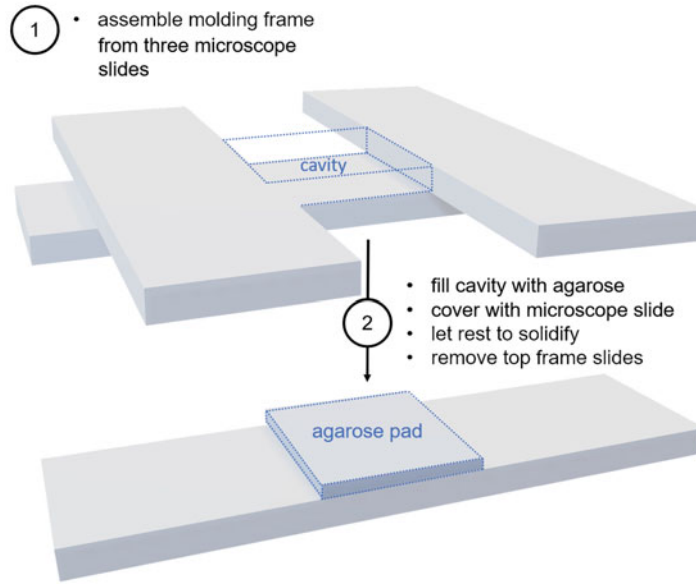

Fig. 2 Preparation of a simple molding frame for casting agarose pads for the microscopic analysis of living cells producing CatIBs. Three microscope slides are arranged as shown in (1) yielding a cavity into which the liquid agarose is poured (2). The frame is subsequently covered with another microscope slide (not shown) and kept undisturbed for 15 min for the agarose to solidify. Subsequently, the top slide and the frame are removed to yield a microscopy slide with agarose pad covering

dissolve the agarose. Afterwards, the solution can be kept warm on a hot plate stirring heater until further use.

2. Prepare a simple molding frame by using three microscope glass slides arranged as shown in Fig. 2.
3. Fill the frame with 750–1000 μL of liquid agarose and cover it with another microscope slide as a lid to produce an agarose pad of even thickness (Fig. 2) (*see* **Note 11**).
4. Let the agarose solidify by letting the frame stand undisturbed for 15 min.
5. Carefully remove the "lid" slide and disassemble the frame.
6. Pre-prepared microscopy slide with agarose pads can be stored at 4 °C in a sealable container filled with moist tissue paper to avoid drying out. Avoid direct long-term exposure to bright sunlight and heat to minimize dry-out.
7. Prepare a fresh *E. coli* culture with potential CatIB-producing cells, e.g., obtained as described in Subheading 3.3, **steps 1–6**.
8. Remove a 1 mL aliquot from the expression culture and centrifuge for 2 min at 15,800 ×*g* using a benchtop centrifuge.
9. Resuspend the resulting cell pellet in a suitable buffer (e.g., 50 mM sodium phosphate buffer, 100 mM NaCl, pH 8) to an

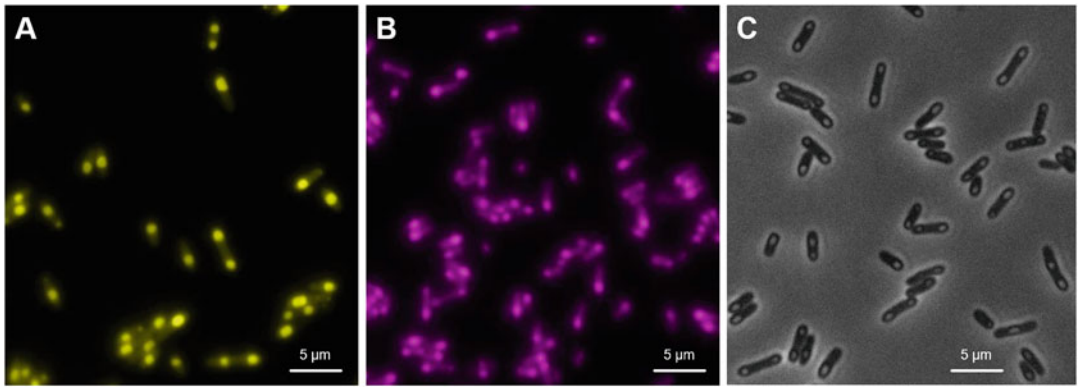

Fig. 3 Exemplary fluorescence and phase-contrast images of YFP (**a**), mCherry (**b**), and RADH CatIB (c) producing cells, respectively. CatIBs can be detected as dense refractile particles (showing fluorescence in **a** and **b**) at the cell poles

OD_{600} of approx. 10 and resuspend by carefully pipetting the suspension up and down.

10. Carefully pipette 1.5 µL on top of the agarose pad of a prepared microscope slide and cover the pad with a cover glass.
11. Place microscope slide into the microscope setup for imaging. For phase contrast and fluorescence imaging, follow the instructions of the microscope manufacturer. Details about suitable light sources and filter sets for YFP and mCherry can be found in the Materials Subheading 2.3. Exemplary fluorescence and phase-contrast images of YFP-, mCherry-, and RADH-CatIB-producing cells are shown in Fig. 3.

3.5 Preparation of CatIBs and Cell Fractions

Cell fractions should be kept on ice at all times. Depending on the requirements of the protein/enzyme assay, the volume of cell fractions (**step 4** and following steps) can be increased or decreased as necessary. However, it is important to always keep a 1:1 ratio when removing or resuspending fractions to ensure no cell fraction is being diluted differently compared to others. The following protocol (illustrated in Fig. 4) describes the steps needed to obtain CatIB fractions that can be analyzed by various means (*see* Subheadings 3.6 and 3.7):

1. Resuspend cell pellet (10% w/v) in a suitable lysis buffer (i.e., 50 mM Na_2HPO_4, 100 mM NaCl, pH 8.0). Transfer the suspension on ice.
2. Disrupt the cells using a high-pressure cell homogenizer, ensuring that the sample is kept cool during the process.
3. Using the crude cell extract (CCE), perform the appropriate protein/enzyme assay (*see* Subheadings 3.6 and 3.7 for examples) to determine the appropriate dilution factor for the assay (*see* **Note 12**).

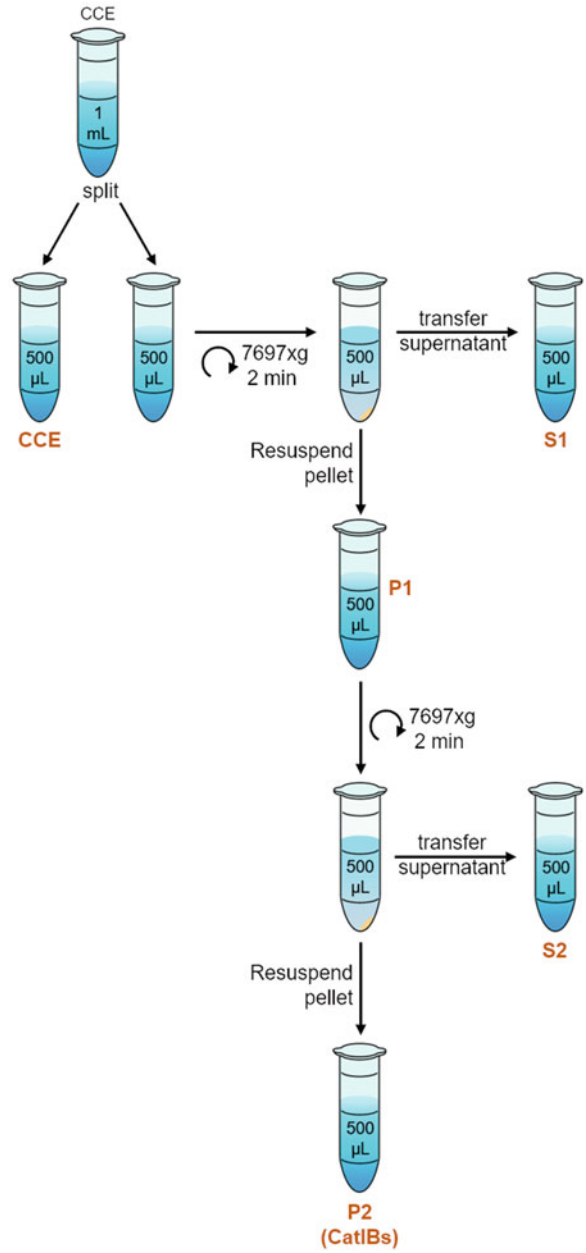

Fig. 4 Schematic illustration of the CatIB preparation procedure. Abbreviations: CCE: crude cell extract, S1: supernatant, P1: pellet (unwashed); sample not retained for analysis, S2: supernatant of the wash, P2: washed pellet (CatIB fraction)

4. Using the determined dilution factor, pipette the required volume of the CCE into a fresh tube and dilute the sample appropriately using lysis buffer, with the final volume of 1 mL in the tube.
5. Transfer half of the diluted CCE (500 μL) into a fresh tube, and centrifuge (7697*xg*, 2 min, room temperature).
6. Pipette 500 μL of the resulting supernatant into a fresh tube (S1 fraction, supernatant).
7. Resuspend the pellet using 500 μL (1:1 ratio) lysis buffer (P1 fraction, unwashed pellet; sample not retained for analysis).
8. Centrifuge the resuspended pellet sample (7697 ×*g*, 2 min, room temperature).
9. Transfer the resulting supernatant into a fresh tube (S2 fraction, supernatant of the wash).
10. Resuspend the pellet again in 500 μL lysis buffer (P2 fraction, washed pellet). The washed pellet fraction is the CatIB fraction to be used for the determination of the CatIB formation efficiency.

3.6 Determination of CatIB Formation Efficiency for Fluorescent CatIBs

Fluorescent CatIBs can be generated by fusing a CatIB-inducing tag to the appropriate terminus of the gene encoding a protein such as mCherry or YFP [15, 16]. Overproduction of such a protein fusion in a suitable host will cause the target protein to be deposited into inclusion bodies that display fluorescence, which can be easily detected by microscopy (*see* Subheading 3.4). To quantify the success of CatIB formation for a fluorescent target protein, soluble and insoluble cell fractions are obtained from the fluorescent CatIB-producing construct (*see* Subheading 3.5). The fluorescence of the resulting soluble and insoluble fractions can then be compared to the total fluorescence of the crude cell extract. The fluorescence detected in the washed pellet fraction (P2, CatIB fraction) compared to that of the crude cell extract hereby gives the CatIB-formation efficiency. In the following, we will use YFP and mCherry CatIBs as examples to show how to derive fluorescence distribution of cell fractions and the corresponding CatIB-formation efficiencies.

1. Pipette 100 μL of the CCE, S1, and P2 fractions in a suitable dilution into the wells of a fluorescence microtiter plate (*see* **Note 13**).
2. For mCherry CatIBs, measure the fluorescence of each fraction using λ_{ex}: 587 nm, λ_{em}: 610 nm. For YFP CatIBs, use λ_{ex}: 513 nm, λ_{em}: 527 nm (*see* **Note 14**).
3. To determine the relative fluorescence of a fraction (x), the following equation is used:

$$\text{Rel.fluorescence fraction } (x)\ [\%] = \frac{\text{Fluorescence fraction } (x)\ [\text{AU}]}{\text{Fluorescence fraction (CCE)}\ [\text{AU}]}\ x\ 100 \quad (1)$$

4. Relative fluorescence of the CatIB fraction (P2) compared to CCE (set to 100%) is defined as the CatIB-formation efficiency (%):

$$\text{CatIB} - \text{formation efficiency}\ [\%] = \frac{\text{Fluorescence fraction (P2)}\ [\text{AU}]}{\text{Fluorescence fraction (CCE)}\ [\text{AU}]}\ x\ 100 \quad (2)$$

3.7 Determination of CatIB Formation Efficiency for RADH CatIBs

Similar to fluorescent proteins, enzymes can be localized in CatIBs by fusion of the target gene to the gene fragment encoding a CatIB-inducing tag, followed by overexpression in a host organism. Since CatIB preparations are generally turbid, the direct use of continuous spectrophotometric assays is difficult due to the scattering of CatIB samples and sedimentation of larger CatIB particles during the measurement. For illustrative purposes, we here use the alcohol dehydrogenase from *Ralstonia sp.* (RADH) (*see* **Note 15**) as an example and describe a discontinuous assay for quantifying RADH activity by monitoring the consumption of the cofactor NADPH, with cyclohexanone as a substrate [15, 16]. The reaction is stopped at various time points by taking samples and diluting them in methanol, and the NADPH concentration at each time point is quantified spectrophotometrically.

1. For each assay sample (e.g., crude cell extract (CCE), supernatant (S1), and washed pellet (P2); *see* **Note 16**), prepare six Eppendorf tubes and label the tubes from 0 to 5 for each sampling point. One additional tube is needed to prepare the blank.
2. Pipette 500 μL of methanol to each of the six Eppendorf tubes (*see* **Note 17**).
3. Prepare the reaction master-mix (volume depending on the number of assays to be conducted) with the following composition: 0.5 mM NADPH (*see* **Note 18**), 125 mM cyclohexanone in TEA buffer.
4. Pipette 1.4 mL of the reaction master-mix into a fresh tube, and place it into the shaking incubator at 1000 rpm, 30 °C. Incubate for 5 min. (*see* **Note 19**).
5. To allow temperature equilibration of the sample, incubate 500 μL of the appropriately diluted cell fraction (i.e., CCE) at the shaking incubator at 1000 rpm, 30 °C for 5 min (*see* **Note 19**).

6. Start the assay by pipetting 350 μL of the diluted cell fraction (i.e., CCE, S1, S2, P2) onto the tube containing 1.4 mL of reaction mixture, vortex well, and immediately note the starting time of the assay.
7. Immediately pipette 250 μL of the reaction mixture onto the methanol containing tube labeled "0", vortex, and note the time the sample was taken in seconds.
8. Place the reaction mixture back onto the incubator at 1000 rpm, 30 °C. Incubate for 1 min.
9. Pipette 250 μL of sample from the reaction mixture onto tube "1", vortex and note the time the sample was taken in seconds. Place the reaction mixture back onto the incubator.
10. Repeat sampling 250 μL from the reaction mixture every minute and noting the sampling times until all six tubes (0–5) contain the reaction mixture sampled at different time points.
11. Centrifuge the tubes 0–5 for 5 min at room temperature at 7697 ×*g*.
12. Pipette 250 μL TEA buffer onto the 500 μL of methanol containing tube set aside for blank in **step 1**. Vortex.
13. Set the spectrophotometer to scan mode starting from 500 nm to 280 nm. Measure the blank sample.
14. Measure the absorption spectra of samples 0–5. Figure 5 shows a set of typical assay spectra as well as the plot used to determine the volumetric activity of the RADH in U/mL.
15. Determine the concentration of NADPH for each tube (0–5) using Beer-Lambert law [50]:

$$c_{\mathrm{NADPH}}[\mathrm{mM}] = \frac{\mathrm{Abs}_{340\mathrm{nm}}}{\varepsilon_{\mathrm{NADPH},340\mathrm{nm}} \times l} \tag{3}$$

where c_{NADPH} = concentration of NADPH [mM], $\mathrm{Abs}_{340\mathrm{nm}}$ = Absorption of NADPH at 340 nm, $\varepsilon_{\mathrm{NADPH,\ 340nm}}$ = extinction coefficient of NADPH [mM^{-1} cm^{-1}], l = length of light path [cm].

16. Activity of RADH [U/mL] for the tested fractions can then be calculated by plotting NADPH concentration (C) against time (t) in minutes, where the slope of the curve will give the rate (R) of NADPH consumption

$$c_{\mathrm{NADPH}}\ [\mathrm{mM}] = -\,R\ t[\,\mathrm{min}\,] + b \tag{4}$$

where R = slope of the line, b = y intercept of the line. Minus sign is due to the consumption of the cofactor over time (*see* **Note 20**).

The volumetric activity (in U/mL) can then be derived by dividing R by the total reaction volume (here 1.75 mL).

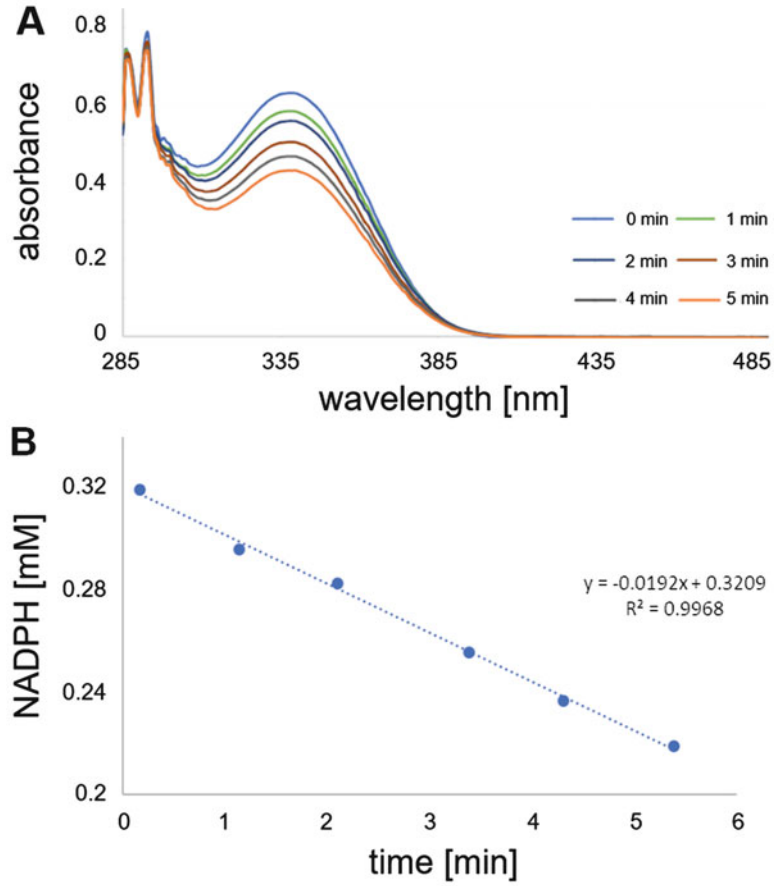

Fig. 5 Set of typical assay spectra illustrating the consumption of NADPH due to conversion of cyclohexanone by RADH. (**a**) Example assay spectra where the measured absorbance values are plotted for six different time points. (**b**) The plot showing NADPH concentration [mM] over time [min] for six time points. From this plot, the slope R is used to determine the activity of the RADH CatIBs (*see* Subheadings 3.7 and 3.10)

1 U is defined as the amount of enzyme that catalyzes the consumption of 1 mM NADPH per minute under the given reaction conditions.

17. To determine the activity distribution of a fraction (x), the following formula is used:

$$\text{Rel.activity fraction } (x)\ [\%] = \frac{\text{Activity fraction } (x)[\text{U/mL}]}{\text{Activity fraction (CCE) [U/mL]}}\ x\ 100 \qquad (5)$$

18. Relative activity of the CatIB fraction (P2) compared to CCE (set to 100%) will be equal to CatIB formation efficiency (%):

$$\text{CatIB formation efficiency } [\%] = \frac{\text{Activity fraction (P2)}[\text{U/mL}]}{\text{Activity fraction (CCE) } [\text{U/mL}]} \, x\, 100 \quad (6)$$

3.8 Preparation of Lyophilized CatIBs

As described in Subheading 3.5, CatIBs can be easily recovered from the crude cell extract by centrifugation and used for catalysis in their wet form. Here, we describe a procedure to prepare CatIBs in powder form which is suitable for long-term storage. This simple procedure is based on centrifugation to obtain the CatIB containing pellet fraction, followed by washing and freeze-drying steps. Since the steps to obtain lyophilized CatIBs involve working with cell fractions that mimic those described in Subheading 3.5, saving a small volume (i.e., 100 μL) of the fractions from the following process is advisable, as this would enable SDS-PAGE analyses which can provide hints regarding expression levels and purity. It is likewise recommended to record the wet and dry weights of the CatIBs during the below described process since it would allow yield calculations if desired.

1. Add a known amount of CCE (e.g., derived from 25 g wet cells) to the centrifugation tube.
2. Centrifuge the tube for 30 min, 15,000 ×*g*, 4 °C.
3. Discard the supernatant (S1), and freeze the pellet for at least 1 h for easier resuspension.
4. Resuspend the pellet in ultrapure water (1:1 w/w).
5. Centrifuge for 30 min, 15,000 ×*g*, 4 °C.
6. Discard supernatant (S2), and freeze pellet (P2) for easier resuspension.
7. Resuspend the pellet (P2) with the same amount of ultrapure water as the weight of CCE in **step 1**.
8. Pour the P2 suspension in a beaker of known weight.
9. Cover the top of the beaker with parafilm, puncture small holes to the parafilm (can be done using a white pipette tip), and freeze overnight at −80 °C.
10. Lyophilize CatIBs for 72 h and record the dry weight.
11. Carefully transfer the lyophilized CatIBs into a mortar with a glazed surface (important for recovering CatIBs afterwards).
12. Grind CatIBs into a fine powder using a glazed pestle, and transfer CatIBs carefully into glass vials.
13. Overlay the CatIBs very slowly with argon, and cover the cap with parafilm. Note that the argon atmosphere prevents rehydration of CatIBs. Lyophilized CatIBs can be stored at −20 °C.

3.9 Determination of the Protein Content of CatIBs

The determination of CatIB protein concentrations is complicated by the turbid nature of the samples, which does not allow direct quantification by spectroscopic or colorimetric means. Protein content of the lyophilized CatIBs can be determined by the measuring the absorbance of the denatured/solubilized protein in solution. This is achieved by denaturing/solubilizing the lyophilized CatIBs in 6 M guanidine-hydrochloride and measuring the absorbance of the resulting optically clear solution at 280 nm (*see* **Note 21**).

The theoretical molar extinction coefficient corresponding to the CatIB protein fusion can then be used to determine the concentration of the sample via Beer-Lambert law [50], and to calculate the protein content of CatIBs.

1. Determine the theoretical molar extinction coefficient $\varepsilon_{\text{protein, 280nm}}$ and the molecular weight [g/mol] of the CatIB forming fusion protein based on sequence (e.g., using the ProtParam tool (http://web.expasy.org/protparam) [51].
2. Weigh 4 mg lyophilized CatIBs in a reaction tube.
3. Add 400 μL of ultrapure water to resuspend the CatIBs. Gently pipette up and down, and vortex for a few minutes until there are no visible clumps in the sample. (*see* **Notes 21** and **22**).
4. Transfer 100 μL of the CatIB suspension into a new reaction tube. Repeat until there are four tubes, corresponding to four technical replicates, containing 100 μL of the suspension each.
5. Add 900 μL of 6 M guanidine-hydrochloride onto each of the four tubes, leading to a final lyophilizate concentration of 1 mg/mL for CatIBs in each tube.
6. Incubate all samples in a shaking incubator for 30 min, at 30 °C, and 1000 rpm.
7. Centrifuge the samples for 20 min at room temperature at 7697 ×*g*.
8. Measure the absorbance of the samples at 280 nm.
9. Determine the protein concentration of CatIBs using Beer-Lambert law:

$$c_{\text{protein}}[\text{mM}] = \frac{\text{Abs}_{280\text{nm}}}{\varepsilon_{\text{protein,280nm}} \times l} \tag{7}$$

c_{protein} = protein concentration [mM], $\text{Abs}_{280\text{nm}}$ = Absorption at 280 nm, $\varepsilon_{\text{protein, 280nm}}$ = theoretical molar extinction coefficient of the target protein [mM^{-1} cm^{-1}], l = length of light path [cm]. Express the protein concentration in [mg/ml] using the theoretical molecular weight determined in **step 1**.

10. The protein content of CatIBs can then be calculated by the following equation, using the concentration of CatIBs

calculated in **step 9**, and the lyophilizate concentration of the CatIB suspension in **step 5**:

$$\text{Protein content CatIBs [\%]} = \frac{\text{Protein concentration CatIBs } \left[\frac{\text{mg}}{\text{mL}}\right]}{\text{Lyophilizate concentration } \left[\frac{\text{mg}}{\text{mL}}\right]} \; x \; 100\% \qquad (8)$$

3.10 Determination of Residual Activity Using Lyophilized RADH CatIBs

The activity of lyophilized CatIBs can be measured in a similar way as described for cell fractions (*see* Subheading 3.7). Here, we describe the RADH activity assay for lyophilized CatIBs, and define the specific activity of the lyophilizate as residual activity [U/mg] expressed relative to the activity of a soluble purified RADH. It is necessary to determine the protein concentration of the lyophilized CatIBs (*see* Subheading 3.9) in order to derive the residual activity of the CatIBs.

1. Weigh 1 mg lyophilized CatIBs in a reaction tube.
2. Resuspend the CatIBs using 1 mL of a suitable buffer (i.e., sodium phosphate buffer with the following composition: 50 mM Na_2HPO_4, 100 mM NaCl, pH 8.0) yielding a CatIB lyophilizate concentration of 1 mg/mL.
3. For each sample, prepare six tubes where the reaction will be stopped using methanol, and label the tubes from 0 to 5 for each sample. One additional tube is needed to prepare the blank.
4. Pipette 500 μL of methanol to each tube.
5. Carry out **steps 3–16** of Subheading 3.7.
6. Activity of CatIBs can be calculated from the volumetric activity (*see* Subheading 3.7, **step 16**) as specific activity (in U/mg CatIB lyophilizate; Eq. 9), or alternatively, by taking the protein content of CatIBs into account (as U/mg protein; Eq. 10):

$$\text{Specific activity [U/mg CatIB lyophilizate]} = \frac{\text{Volumetric Activity [U/mL]}}{\text{Lyophilizate concentration [mg/mL]}} \qquad (9)$$

By multiplying the calculated protein content of CatIBs (in %) (*see* Subheading 3.9) by the CatIB lyophilizate concentration (in mg/mL), the protein concentration in the assay [mg protein/mL] can be calculated, which can then be used to derive the specific activity of the lyophilized CatIBs (in U/mg protein) according to:

$$\text{Specific activity [U/mg protein]} = \frac{\text{Volumetric Activity [U/mL]}}{\text{Protein in assay [mg protein/mL]}} \quad (10)$$

7. When the activity of the soluble, purified RADH is determined (in U/mg protein) with the same enzyme assay using purified enzyme in a known concentration, it is possible to compare the activity of lyophilized RADH-CatIBs directly to that of the soluble, purified RADH, yielding the residual activity of the CatIB preparation as follows:

$$\text{Residual activity [\%]} = \frac{\text{Specific activity CatIBs [U/mg protein]}}{\text{Specific activity soluble RADH [U/mg protein]}} \, x\, 100 \quad (11)$$

4 Notes

1. The gene encoding the target protein can also be obtained by gene synthesis. The synthetic gene needs to be furnished with suitable 5′- and 3′-restriction endonuclease recognition sequences to allow cloning into an expression vector containing the CatIB-inducing tag (and if used linker).
2. CatIB-producing gene fusions are prepared by fusion of a gene coding for a CatIB-inducing tag to either the 5′- or 3′-end of a target gene. The resulting fusion proteins carry the CatIB formation inducing tag at either the N- or C-terminus.
3. e.g., *E. coli* BL21(DE3) cell with pTDoT-mCherry plasmid, pTDoT-L-YFP or pTDoT-L-RADH [15].
4. Methanol should always be handled under a fume hood.
5. Cyclohexanone is hygroscopic, therefore bottles containing cyclohexanone should be overlaid with argon after each use and stored in air-tight bottles.
6. If no crystal or nuclear magnetic resonance (NMR) structure of the target protein is available, a homology model based on the amino acid sequence of the target and a template structure, i.e., of a homologous protein can be generated manually or by automated means using suitable web services [52]. Please note that, a higher sequence identity between target and homologous structure usually results in better models.
7. CatIB gene fusions can also be generated by other means, e.g., using Overlap-Extension PCR [53], Golden Gate Assembly, which relies on Type IIS restriction enzymes [54, 19] or related methods.

8. The crystal structure of the target protein may indicate that the N- and/or C-termini are not accessible or buried within an oligomer interface. If this does not apply, it is recommended to test both fusion sites to identify which construct would yield better expression levels, higher activity of the target protein, and high CatIB formation efficiencies (*see* Subheadings 3.6 and 3.7).
9. Including a linker between the genes encoding the CatIB-inducing tag and target gene is advisable in most cases. Variable linker elements can be used and we have so far successfully applied flexible serine/glycine (SG)- as well as a rigid proline/threonine (PT)-linkers [19]. Sequences are as follows: SG: 5′- AGC GGC GGT GGG TCT GGA GGC GGC TCA GGT GGT GGG TCG-3′ coding for SGGGSGGGSGGGS and PT: 5′- CCG ACC CCA CCG ACC ACG CCA ACG CCA CCA ACC ACC CCA ACC CCG ACG CCG-3′ coding for PTPPTTPTPPTTPTPTP.
10. For the examples used in later protocols of the chapter, pTDoT-mCherry and pTDoT-L-RADH [15] should be used as expression plasmids.
11. Gently press the top slide down on the molding frame to remove air bubbles. Lifting the lid and repeating the procedure might also help with removing trapped air.
12. Note that diluting the CCE directly and using the diluted CCE for fractionation as described in the next steps is important, as this approach ensures that no dilution errors of variable degree are being introduced to each fraction, which would be the case if they were to be diluted separately.
13. It is recommended to measure technical replicates in triplicates or quadruples for each fraction, as for CCE and P2 fractions that contain proteins in insoluble form, homogeneity between the technical replicates is often challenging to achieve.
14. It is important to shake the microtiter plate directly prior to the measurement to ensure suspension of cell fractions. When using the Tecan m1000 microplate reader, an in-built shaker (settings: 654 rpm, amplitude 2 mm, 10 s) allows proper mixing prior the measurement.
15. RADH is a tetrameric enzyme that preferentially uses aromatic and cyclic aliphatic compounds as substrates, with exceptionally high stereoselectivity [55].
16. It is advisable to measure at least three technical replicates per sample (crude cell extract (CCE), supernatant (S1, S2), and washed pellet (P2)); only CCE, S1, and P2 needed to determine CatIB formation efficiencies. Also measuring S2 and P1 might help to close the mass balance, e.g., if CatIBs become

solubilized during the preparation process, S2 fractions might contain also target activity. Since all of the P1 sample is used to obtain P2 in our protocol, sampling volumes need to be adapted, if the P1 sample is to be measured as well (*see* Subheadings 3.5 and 3.6).

17. Note that, to quantify three cell fractions (crude cell extract, supernatant, and washed pellet) with three technical replicates each and include one blank measurement, it is necessary to prepare 55 tubes, each containing 500 µL of methanol. Therefore, pouring methanol into a multichannel pipette reservoir and using a multichannel pipette for pipetting methanol is highly recommended.
18. NADPH stocks should be prepared freshly and kept on ice.
19. Depending on the temperature optima and the temperature stability of the analyzed enzyme, other temperatures for the reaction may be used.
20. Note that for accuracy, the actual time points (in seconds) when the samples were taken should be considered in the calculation. If the NADPH is consumed too fast, the cell fraction can be diluted further before repeating the assay. When volumetric [U/mL] or specific activities [U/mg] are calculated, this dilution factor has to be taken into account. Alternatively, the incubation time and sampling time points can be shortened (**steps 8–10**). Conversely, if the NADPH consumption is too slow, the assay time can be extended (i.e., to 10 min where the reaction mixture is sampled once every 2 min instead of every minute in **steps 8–10**).
21. When working with insoluble samples such as CatIBs in powder form, it is recommended to use at least four technical replicates to account for the resuspension and homogeneity issues arising from such samples. It should be noted that this method does not account for the impurities of the CatIB fraction (other proteins, nucleic acids, etc.), which can lead to an overestimation of the concentration of the target protein within CatIBs. By extension, the overestimation of the protein content can lead to an underestimation of specific activity (*see* Subheading 3.10) of CatIBs [U/mg].
22. If only the direct determination of protein concentrations is attempted, the CatIB lyophilizates can be directly suspended in 6 M guanidine-hydrochloride.

Acknowledgments

The research was financially supported by the CLIB Competence Center Biotechnology (CKB) funded by the European Regional Development Fund ERDF (34.EFRE 0300096 and 34.EFRE 0300097).

References

1. Guisan JM (2013) New opportunities for immobilization of enzymes. Methods Mol Biol 1051:1–13
2. Homaei AA, Sariri R, Vianello F et al (2013) Enzyme immobilization: an update. J Chem Biol 6:185–205
3. Sheldon RA, Van Pelt S (2013) Enzyme immobilisation in biocatalysis: why, what and how. Chem Soc Rev 42:6223–6235
4. Ölçücü G, Klaus O, Jaeger KE et al (2021) Emerging solutions for in vivo biocatalysts immobilization: tailor-made catalysts for industrial biocatalysis. ACS Sustain Chem Eng 9:8919–8945
5. Rehm FB, Chen S, Rehm BH (2016) Enzyme engineering for in situ immobilization. Molecules 21:1370
6. Schmidt-Dannert S, Zhang G, Johnston T et al (2018) Building a toolbox of protein scaffolds for future immobilization of biocatalysts. Appl Microbiol Biotechnol 102:8373–8388
7. Steinmann B, Christmann A, Heiseler T et al (2010) In vivo enzyme immobilization by inclusion body display. Appl Environ Microbiol 76:5563–5569
8. De Marco A, Ferrer-Miralles N, Garcia-Fruitos E et al (2019) Bacterial inclusion bodies are industrially exploitable amyloids. FEMS Microbiol Rev 43:53–72
9. Garcia-Fruitos E, Gonzalez-Montalban N, Morell M et al (2005) Aggregation as bacterial inclusion bodies does not imply inactivation of enzymes and fluorescent proteins. Microb Cell Factories 4:27
10. Garcia-Fruitos E, Vazquez E, Diez-Gil C et al (2012) Bacterial inclusion bodies: making gold from waste. Trends Biotechnol 30:65–70
11. Rinas U, Garcia-Fruitos E, Corchero JL et al (2017) Bacterial inclusion bodies: discovering their better half. Trends Biochem Sci 42:726–737
12. Jäger VD, Lamm R, Küsters K et al (2020) Catalytically-active inclusion bodies for biotechnology-general concepts, optimization, and application. Appl Microbiol Biotechnol 104:7313–7329
13. Krauss U, Jäger VD, Diener M et al (2017) Catalytically-active inclusion bodies carrier-free protein immobilizates for application in biotechnology and biomedicine. J Biotechnol 258:136–147
14. Diener M, Kopka B, Pohl M et al (2016) Fusion of a coiled-coil domain facilitates the high-level production of catalytically active enzyme inclusion bodies. ChemCatChem 8: 142–152
15. Jäger VD, Kloss R, Grünberger A et al (2019) Tailoring the properties of (catalytically)-active inclusion bodies. Microb Cell Factories 18:33
16. Jäger VD, Lamm R, Kloss R et al (2018) A synthetic reaction cascade implemented by colocalization of two proteins within catalytically active inclusion bodies. ACS Synth Biol 7: 2282–2295
17. Kloss R, Karmainski T, Jäger VD et al (2018) Tailor-made catalytically active inclusion bodies for different applications in biocatalysis. Cat Sci Technol 8:5816–5826
18. Kloss R, Limberg MH, Mackfeld U et al (2018) Catalytically active inclusion bodies of L-lysine decarboxylase from *E. coli* for 1,5-diaminopentane production. Sci Rep 8: 5856
19. Küsters K, Pohl M, Krauss U et al (2021) Construction and comprehensive characterization of an EcLDCc-CatIB set-varying linkers and aggregation inducing tags. Microb Cell Factories 20:49
20. Arie JP, Miot M, Sassoon N et al (2006) Formation of active inclusion bodies in the periplasm of *Escherichia coli*. Mol Microbiol 62: 427–437
21. Huang Z, Zhang C, Chen S et al (2013) Active inclusion bodies of acid phosphatase PhoC: aggregation induced by GFP fusion and activities modulated by linker flexibility. Microb Cell Factories 12:25
22. Köszagová R, Krajcovic T, Palencarova-Talafova K et al (2018) Magnetization of active inclusion bodies: comparison with centrifugation in repetitive biotransformations. Microb Cell Factories 17:139
23. Wang R, Li J, Dang D et al (2020) Bacterial production of maize and human serine racemases as partially active inclusion bodies for d-serine synthesis. Enzym Microb Technol 137:109547
24. Wang X, Zhou BH, Hu WK et al (2015) Formation of active inclusion bodies induced by hydrophobic self-assembling peptide GFIL8. Microb Cell Fact 14:88
25. Du J, Rehm BHA (2017) Purification of target proteins from intracellular inclusions mediated by intein cleavable polyhydroxyalkanoate synthase fusions. Microb Cell Factories 16:184
26. Xing L, Wu W, Zhou B et al (2011) Streamlined protein expression and purification using cleavable self-aggregating tags. Microb Cell Factories 10:42
27. Villaverde A, Garcia-Fruitos E, Rinas U et al (2012) Packaging protein drugs as bacterial

inclusion bodies for therapeutic applications. Microb Cell Factories 11:76

28. García-Fruitós E, Rodríguez-Carmona E, Díez-Gil C et al (2009) Surface cell growth engineering assisted by a novel bacterial nanomaterial. Adv Mat 21:4249–4253
29. García-Fruitós E, Seras-Franzoso J, Vazquez E et al (2010) Tunable geometry of bacterial inclusion bodies as substrate materials for tissue engineering. Nanotechnology 21:205101
30. Gil-Garcia M, Navarro S, Ventura S (2020) Coiled-coil inspired functional inclusion bodies. Microb Cell Factories 19:117
31. Choi SL, Lee SJ, Ha JS et al (2011) Generation of catalytic protein particles in *Escherichia coli* cells using the cellulose-binding domain from *Cellulomonas fimi* as a fusion partner. Biotechnol Bioproc E 16:1173–1179
32. Nahalka J, Nidetzky B (2007) Fusion to a pull-down domain: a novel approach of producing *Trigonopsis variabilis* D-amino acid oxidase as insoluble enzyme aggregates. Biotechnol Bioeng 97:454–461
33. Park SY, Park SH, Choi SK (2012) Active inclusion body formation using *Paenibacillus polymyxa* PoxB as a fusion partner in *Escherichia coli*. Anal Biochem 426:63–65
34. Lin ZL, Zhou BH, Wu W et al (2013) Self-assembling amphipathic alpha-helical peptides induce the formation of active protein aggregates *in vivo*. Faraday Discuss 166:243–256
35. Zhou BH, Xing L, Wu W et al (2012) Small surfactant-like peptides can drive soluble proteins into active aggregates. Microb Cell Factories 11:10
36. Gifre-Renom L, Cano-Garrido O, Fabregas F et al (2018) A new approach to obtain pure and active proteins from Lactococcus lactis protein aggregates. Sci Rep 8:13917
37. Lamm R, Jager VD, Heyman B et al (2020) Detailed small-scale characterization and scale-up of active YFP inclusion body production with Escherichia coli induced by a tetrameric coiled coil domain. J Biosci Bioeng 129:730–740
38. Berman HM, Westbrook J, Feng Z et al (2000) The protein data bank. Nucleic Acids Res 28: 235–242
39. Krissinel E, Henrick K (2007) Inference of macromolecular assemblies from crystalline state. J Mol Biol 372:774–797
40. Kuriata A, Iglesias V, Pujols J et al (2019) Aggrescan3D (A3D) 2.0: prediction and engineering of protein solubility. Nucleic Acids Res 47:W300–W307
41. Ferruz N, Schmidt S, Hocker B (2021) ProteinTools: a toolkit to analyze protein structures. Nucleic Acids Res 49:W559–W566
42. Jacak R, Leaver-Fay A, Kuhlman B (2012) Computational protein design with explicit consideration of surface hydrophobic patches. Proteins 80:825–838
43. Kuhlman B, Baker D (2000) Native protein sequences are close to optimal for their structures. Proc Natl Acad Sci U S A 97:10383–10388
44. Rohl CA, Strauss CE, Misura KM et al (2004) Protein structure prediction using Rosetta. Methods Enzymol 383:66–93
45. Pettersen EF, Goddard TD, Huang CC et al (2004) UCSF chimera--a visualization system for exploratory research and analysis. J Comput Chem 25:1605–1612
46. Schrödinger L, Delano W (2020) PyMOL [Internet]. Available from: http://www.pymol.org/pymol
47. Studier FW (2005) Protein production by auto-induction in high density shaking cultures. Protein Expr Purif 41:207–234
48. Fox BG, Blommel PG (2009) Autoinduction of protein expression. Curr Protoc Protein Sci Chapter 5:Unit 5.23
49. Blommel PG, Becker KJ, Duvnjak P et al (2007) Enhanced bacterial protein expression during auto-induction obtained by alteration of lac repressor dosage and medium composition. Biotechnol Prog 23:585–598
50. Swinehart DF (1962) The Beer-Lambert Law. J Chem Educ 39:333
51. Gasteiger E, Hoogland C, Gattiker A et al (2005) Protein identification and analysis tools on the ExPASy server. In: Walker JM (ed) The proteomics protocols handbook. Humana Press, Totowa, New Jersey, USA, pp 571–607
52. Hameduh T, Haddad Y, Adam V et al (2020) Homology modeling in the time of collective and artificial intelligence. Comput Struct Biotechnol J 18:3494–3506
53. Lu Y, Xiao S, Yuan M et al (2018) Using overlap-extension PCR technique to fusing genes for constructing recombinant plasmids. J Basic Microbiol 58:273–276
54. Engler C, Kandzia R, Marillonnet S (2008) A one pot, one step, precision cloning method with high throughput capability. PLoS One 3: e3647
55. Kulig J, Frese A, Kroutil W et al (2013) Biochemical characterization of an alcohol dehydrogenase from *Ralstonia* sp. Biotechnol Bioeng 110:1838–1848

2.6. Publication 6. Emerging Solutions for in vivo Biocatalyst Immobilization: Tailor-Made Catalysts for Industrial Biocatalysis

Gizem Ölçücü, Oliver Klaus, Karl-Erich Jaeger, Thomas Drepper*, and Ulrich Krauss*

*corresponding authors

ACS Sustainable Chemistry & Engineering. 9 (2021), pp. 8919-8945. Reprinted with permission from [103]. `https://pubs.acs.org/doi/abs/10.1021/acssuschemeng.1c02045`

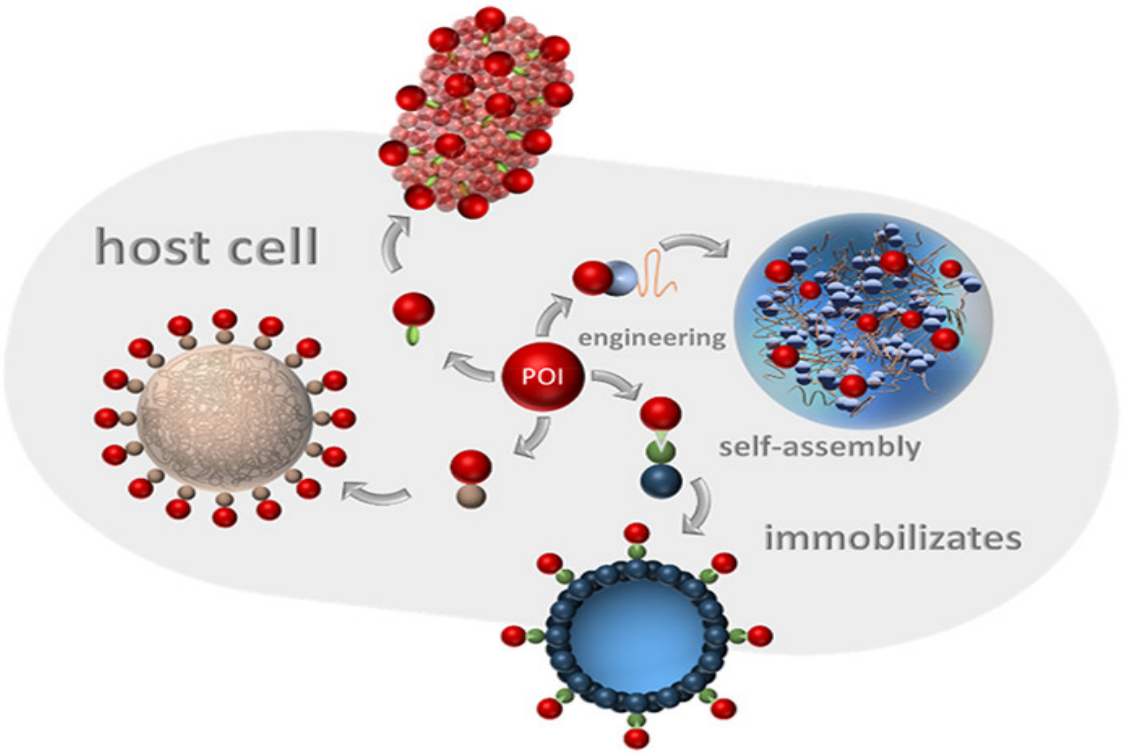

Author Contributions: U.K. concieved the outline of the review. G.Ö. wrote the section "Display/entrapment of proteins on/within inclusion bodies and protein crystals" and all its sub-chapters, U.K. wrote the section "Designed synthetic organelles-liquid protein condensates as immobilizates?" all its sub-chapters, and T.D. and O.K. wrote the section "Polyhydroxyalkanoate-based systems and virus-like particles" all its sub-chapters. All authors contributed to literature searches and the writing of the introduction and conclusions. G.Ö. and O.K. contributed equally. All authors have read and approved the final version.

ACS Sustainable Chemistry & Engineering

pubs.acs.org/journal/ascecg

Perspective

Emerging Solutions for *in Vivo* Biocatalyst Immobilization: Tailor-Made Catalysts for Industrial Biocatalysis

Gizem Ölçücü,[§] Oliver Klaus,[§] Karl-Erich Jaeger, Thomas Drepper,* and Ulrich Krauss*

Cite This: *ACS Sustainable Chem. Eng.* 2021, 9, 8919–8945

Read Online

ACCESS | Metrics & More | Article Recommendations | Supporting Information

ABSTRACT: In industry, enzymes are often immobilized to generate more stable enzyme preparations that are easier to store, handle, and recycle for repetitive use. Traditionally, enzymes are bound to inorganic carrier materials, which requires case-to-case optimization and incurs additional labor and costs. Therefore, with the advent of rational protein design strategies as part of bottom-up synthetic biology approaches, numerous immobilization methods have been developed that enable the one-step production and immobilization of enzymes onto biogenic carrier materials often directly within the production host, which we here refer to as *in vivo* immobilization. As a result, nano- to micro-meter-sized functionalized biomaterials, or biologically produced enzyme immobilizates, are obtained that can directly be used for synthetic purposes. In this Perspective, we provide an overview over established and recently emerging *in vivo* enzyme immobilization methods, with special emphasis on their applicability for (industrial) biocatalysis. For each approach, we present fundamental working principles as well as advantages and limitations guiding future research avenues toward sustainable applications in the bioindustry.

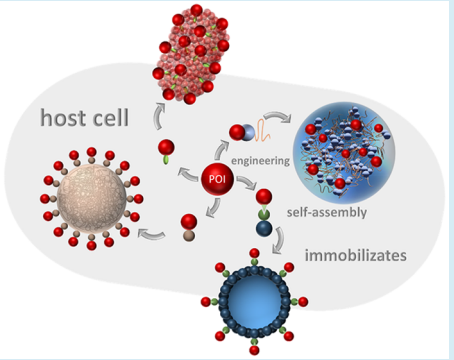

KEYWORDS: *Biocatalysis, Bioeconomy, Sustainable chemistry, Protein engineering, Synthetic biology, Enzyme immobilization*

INTRODUCTION

Industrial biocatalysis is part of a multibillion dollar industry,[1] concerned with the industrial-scale production of valuable chemical compounds such as fine chemicals, agrochemicals, and pharmaceuticals. The employed biocatalysts are enzymes, which carry out chemical reactions with exquisite efficiency and chemo-, regio-, and stereoselectivity, often not achievable with conventional chemical catalysts.[1,2] As biologically produced macromolecules, enzymes are a renewable resource and, in addition, can be regarded as sustainable and biodegradable catalysts, i.e., in contrast to rare earth or transition metal catalysts used in chemical asymmetric catalysis.[1,3] This is all the more true if the microorganism used to produce an enzyme is grown on inexpensive renewable resources, e.g., in the framework of third-generation biorefineries.[4] Likewise, enzymes as cellular constituents have evolved to optimize the biological function of their respective host organism and are generally most active and stable in an aqueous environment, at physiological temperature and pH. In contrast, industrial processes are often performed under harsh conditions, at elevated temperatures, at extreme pH values, and in the presence of organic solvents, to enable high substrate loads and product yields.[5−7] Under those conditions, however, enzymes are often unstable. While modern protein engineering methods allow the tailoring of enzymes to meet specific process requirements, the custom engineering of such tailored biocatalysts is still a time- and labor-intensive process.[1] Traditionally, enzymes have therefore been immobilized in or on inorganic and organic carrier materials, respectively, to improve their stability, while at the same time allowing easier handling and recycling in industrial settings.[8−11] This, however, increases process costs as additional materials and preparation steps are needed.[12] Furthermore, immobilization commonly results in reduced enzymatic activities as compared to the free enzymes,[13] which can be due to (partial) denaturation as a consequence of carrier attachment or diffusional limitation.[13,14] Finally, there are no truly generic immobilization techniques that work for every enzyme, so that time-consuming case-to-case optimization is needed as part of process development. Thus, in addition to the engineering of improved enzyme variants, generic, cheap, and easy to perform immobilization methods are urgently needed to further promote the use of enzymes in industrial biocatalysis, in the framework of fostering a sustainable bioeconomy.

To meet these shortcomings, a multitude of *in vivo* enzyme immobilization methods have been developed in recent years to engineer the production of solely biologically produced

Received: March 24, 2021
Revised: June 7, 2021
Published: June 28, 2021

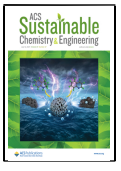

https://doi.org/10.1021/acssuschemeng.1c02045
ACS Sustainable Chem. Eng. 2021, 9, 8919–8945

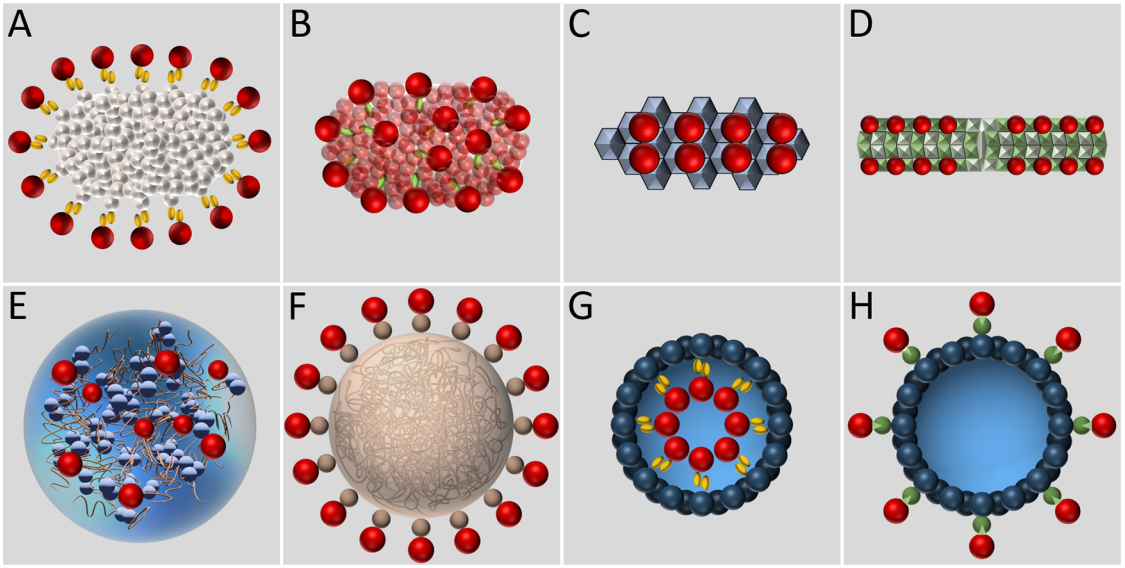

Figure 1. *In vivo* protein immobilization strategies of increasing complexity. The figure summarizes all protein immobilization principles that were considered in this Perspective. Immobilized target proteins are shown in red. (A) Inclusion body (IB) display. (B) Catalytically active inclusion bodies (CatIBs). (C) Cry3Aa crystal-based protein entrapment. (D) Forizymes. (E) Protein condensates formed by liquid−liquid phase separation (LLPS). (F) Polyhydroxyalkanoate (PHA) granule-based protein immobilization. (G) Protein encapsulation using viruslike particles (VLPs). (H) VLP-based protein display. For a better understanding, simplified schematic structures are shown, which are not drawn to scale. See Figures 2−4 for details. All abbreviations used in this Perspective are summarized in Table S1 in the Supporting Information.

enzyme immobilizates for applications in life sciences, biocatalysis, synthetic chemistry, and biomedicine.[14−24] In general, the target enzymes are engineered, e.g., by fusing them to other protein modules, which intrinsically facilitate self-assembly of the recombinant fusion protein into nano- or micro-meter-sized supramolecular structures inside (microbial) cells. This renders such *in vivo* enzyme immobilization methods very cost-effective as they enable the production of immobilized biocatalysts in one step. The insoluble nature of the resulting biocatalyst immobilizates at the same time enables efficient preparation and downstream processing, e.g., recycling from the reaction system, by centrifugation and/or filtration.

In summary, a plethora of *in vivo* methods have been developed, where different protein modules, such as aggregation or crystallization promoting tags,[17,24−27] intrinsically disordered proteins or parts thereof,[28−32] or affinity and protein−protein interaction tags, are fused to target proteins[23,33] in order to facilitate their (i) aggregation,[26,34] (ii) self-assembly,[15,35] (iii) crystal entrapment,[18,27] (iv) liquid−liquid phase separation (LLPS),[36] or (v) sequestration to cellular carrier materials[19,20,37,38] (Figure 1).

Due to the diverse nature of the different immobilization strategies, e.g., with regard to both the carrier (biogenic proteinaceous and nonproteinaceous) and the method of immobilization (surface binding/attachment, particle/crystal entrapment, or encapsulation/sequestration in compartments), it is very difficult to define decisive criteria under which the different strategies and systems can be grouped. Therefore, in the following, the different *in vivo* immobilization methods will be presented in order of increasing architectural/structural complexity of the enzyme immobilizates and the involved building principles (Figure 1). For each approach, we present fundamental working principles to illustrate the necessary engineering effort, highlight application examples to showcase applicability for biocatalysis, and summarize applicable production hosts, which are an important issue for biocatalyst production. Finally, we develop a concise overview of potential advantages and limitations for future industrial applications and research avenues.

DISPLAY/ENTRAPMENT OF PROTEINS ON/WITHIN INCLUSION BODIES AND PROTEIN CRYSTALS

The group of *in vivo* immobilizates, which we consider as architecturally "less" complex, includes systems that feature protein-based "carrier" materials such as conventional, inactive inclusion bodies (IBs) as the carrier for IB-display approaches,[16,39] catalytically active IBs (CatIBs),[17,25,26,40] as well as related systems that rely on target protein sequestration/encapsulation within *in vivo* produced protein crystals or compartments formed by the Cry3Aa protein of *Bacillus thuringiensis*,[18,27] plant-derived forizymes,[21] and liquid-protein condensates.[22,30,41] All abbreviations used throughout this Perspective are summarized in Table S1 of the Supporting Information.

Enzyme Immobilization by Inclusion Body Display. Bacterial IBs are dense, insoluble, submicrometer particles that form due to cellular stress, where the misfolded and partially unfolded recombinant proteins aggregate to form IBs.[42,43] In most cases, IB formation occurs due strong overexpression of recombinant genes, which puts a high load on the cell's protein quality control machinery. This is especially the case when the recombinant protein is, e.g., a large mono- or oligomer that requires assistance by chaperones and foldases to attain its native conformation. In those cases the target proteins are incorrectly folded and/or targeted within the cell (e.g., membrane proteins), or the host is unable to provide posttranslational modifications needed for native function/folding of the target. More generally, the availability of chaperones to assist the proper folding of the protein can be low due the folding/degradation machinery being titered out,

https://doi.org/10.1021/acssuschemeng.1c02045
ACS Sustainable Chem. Eng. 2021, 9, 8919−8945

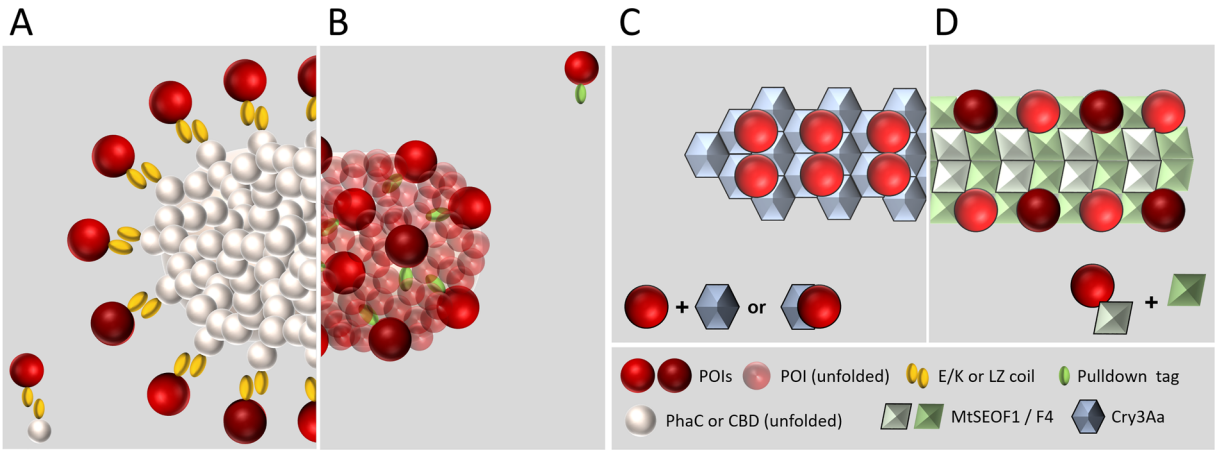

Figure 2. Inclusion body (IB) display, catalytically active IBs (CatIBs), and crystal-based immobilizates. Engineered fusion proteins required for POI immobilization as well as the resulting immobilizates are shown. Details are given in the text. (A) IB display; protein of interest (POI) linked to the surface of IBs formed by the polyhydroxybutyrate synthase PhaC or a cellulose binding domain (CBD) via E/K or LZ heterodimeric coiled coils. (B) CatIB formation is induced by the fusion of different "pull-down" tags (Table 1) to a POI. (C) POIs entrapped in crystals formed by the Cry3Aa protein of *Bacillus thuringiensis* resulting from either coexpression of Cry3Aa and a POI or fusion of a POI to Cry3Aa. (D) The POI assembled into plant-derived forisome-like crystalline structures is achieved by fusion of a POI to one forisome subunit, which is coexpressed with the same or another forisome subunit protein (e.g., POI-MtSEO-F1/MtSEO-F4).

which results in protein aggregation and deposition into IBs. IBs are formed in the cytoplasm and are typically located at the cell poles;[44] however, they can be also located in the periplasm of Gram-negative bacteria, as shown for a folding-defective variant of the maltose binding protein (MalE31), translocated to the periplasm via the Sec-secretion apparatus.[45] In addition, their presence has also been shown in yeasts[46] and mammalian cells, where they are known as aggresomes.[47] IB formation is possibly initiated from a single molecule (or a few molecules) serving as a nucleation site(s) or, rather, where smaller aggregates of proteins associate to form larger aggregates.[43] Further, the composition of IBs can vary depending on several factors such as culture conditions and the properties of the recombinant protein, and some IBs have been shown to contain amyloid-like, fibril structures, pointing toward a rather complex structure.[43,48]

Despite containing high amounts of almost pure (80−95%) target protein in a stable form that is essentially protected against proteolytic degradation,[42] IBs are generally viewed as an undesired consequence of heterologous expression as enzymes located in IBs typically lack activity (unlike enzymes that are immobilized in CatIBs, see the next section). As such, IBs are usually either discarded as waste or used for refolding studies where they are solubilized by applying denaturing agents such as urea in high concentrations, followed by slowly removing the denaturing agent from the solution to facilitate refolding of the solubilized proteins.[49]

For immobilization purposes, IBs have been used as a biological scaffold material for the immobilization of proteins of interest (POIs) (Figure 2A), which was exemplified by the aggregation of a galactose oxidase (GOase, from *Fusarium* spp.) within IBs formed by high-level expression of the polyhydroxybutyrate (PHB) synthase (PhaC) of *Cupriavidus necator* in *Escherichia coli*.[50] IB display was achieved by fusing the gene encoding the engineered, negatively charged, α-helical coil (E coil) to *phaC*, along with the fusion of the gene encoding positively charged, lysine-rich coil (K coil) to that of GOase. When coproduced in the same cell, the E coil and K coil form a heterodimer, resulting in the localization of GOase to the PhaC IBs. The loading capacity of the PhaC-IBs for GOase was estimated to exceed 200 mg of wet IBs/g, albeit with a 35% decrease in GOase activity, when compared to the activity detected in cells expressing only GOase.

In 2016, the same principle was successfully implemented using a modified PhaC-IB strategy to coimmobilize an alcohol dehydrogenase from *Rhodococcus erythropolis* and a formate dehydrogenase from *Candida boidinii*, where the formate dehydrogenase was used to regenerate NADH required by the alcohol dehydrogenase.[51] Both POIs were tagged with a K coil and cultivated as separate strains to produce the corresponding enzymes in a soluble form, using *E. coli* as a host organism. A strain producing E coil-tagged PhaC IBs was cultivated separately, and colocalization of K coil tagged alcohol dehydrogenase and formate dehydrogenase to the E coil tagged PhaC particles was achieved by mixing the appropriate fractions of the crude cell extracts together after cell lysis. In this way, an enzyme cascade was established on the surface of the PhaC IBs catalyzing the conversion of 4-chloroacetophenone to (*S*)-4-chloro-α-methylbenzyl alcohol with a 99.7% conversion rate and 99% ee, in addition to requiring NAD^+ only in catalytic amounts. The approach was also tested in a biphasic system to account for the low water solubility of the substrate, where the enzyme decorated PhaC IBs were reported to localize to the water/*n*-heptane phase boundary and catalyzed the reaction, albeit with a lowered conversion rate (67% after 72 h).

It is likewise possible to use leucine zippers (LZs) in a bait−prey strategy to localize a POI to IBs, making use of the dimerization of antiparallel LZ bait and prey domains. For instance, the cellulose binding domain (CBD) from *Cellulomonas fimi*, which was shown to form IBs when overproduced in *E. coli*,[52] was fused to a bait-LZ tag, which successfully localized the prey-LZ tagged, soluble monomeric red fluorescent protein 1 to CBD IBs.[16] Notably, an artificial 1-butanol production pathway requiring four different enzymes, namely, 3-hydroxybutyryl-CoA dehydrogenase, crotonase, and butylaldehyde/butanol dehydrogenase from *Clostridium acetobutylicum* and butyryl-CoA dehydrogenase from *Treponema*

https://doi.org/10.1021/acssuschemeng.1c02045
ACS Sustainable Chem. Eng. 2021, 9, 8919−8945

denticola, has been established using LZ-mediated IB display.[39] It is worthwhile to underline that the use of E coil/K coil tagged PhaC IBs and LZ tagged CBD IBs in the above presented cases is different from the direct production of CatIBs (see the following section). Despite relying on the targeted formation of functional IBs, IB display approaches only employ the nonfunctional IB material as a scaffold onto which soluble enzymes are displayed.

Catalytically Active Inclusion Bodies (CatIBs)—Biologically Produced Enzyme Immobilizates. As outlined above, IBs are dense, insoluble aggregates of recombinant proteins that typically lack activity. However, IBs possessing catalytic activity had been reported as early as 1989, where β-galactosidase IBs were shown to be active.[53] The importance of this discovery bas been brought into more light in recent years, with the emergence of unconventional, active IBs, lately also called catalytically active inclusion bodies (CatIBs), as a targeted strategy to naturally produce novel, carrier-free enzyme immobilizates.[34,40,54−56] Unlike the more common approach employing conventional (inactive) IBs, the CatIB strategy relies on the production of the POI in a correctly folded, functional form, which is incorporated into IBs formed by the fusion protein.[40] The strategy relies on the use of aggregation-prone or aggregation-inducing tags (also called "pull-down" tags; for details see below), whose genes are fused to the gene encoding the POI at the 5′ or 3′ end, with or without linker sequences separating the tag and POI. When overproduced in the host cells, the POI folds, at least partially, into its functional conformation, while the tag provides the driving force for aggregation of the fusion protein, thereby localizing it into CatIBs (Figure 2B). Making use of the higher density pertaining to IBs, CatIBs can be easily obtained via centrifugation after cell lysis.[49] Therefore, the power of the CatIB method lies in the utilization of biologically produced enzyme immobilizates that can be directly used for biocatalysis without tedious, time-consuming, and expensive chromatographic purification and further immobilization steps. Like most immobilizates, where the substrates/products have to cross a physical barrier, CatIBs are prone to diffusional limitation,[17] which, however, was not addressed explicitly for many of the systems.

"Pull-down" tag systems available to induce CatIB formation have been reviewed extensively in recent years.[26,40] In brief, tags range from short peptides of 8−20 amino acids in length, coiled-coil tags of intermediate size (53−172 amino acids), larger aggregation-prone protein domains of up to a few hundred amino acids, to full-length proteins of more than 500 amino acids in size. Since the last published compilation of the available systems reviewed by Jäger et al. (2020) has seen a few additions, we include here a table that provides an overview over all available "pull-down" tags for CatIB formation (Table 1). Along the same lines, strategies to improve CatIB formation have also been summarized in recent reviews and are thus not covered here in detail. In summary, several factors are known that influence both CatIB formation efficiency (fraction of active POI within the insoluble IB) as well as the residual activity of the CatIBs relative to the soluble purified enzyme. In particular, the presence and nature of linker polypeptides between the tag and POI and the site of tag fusion (N- vs C-terminal), but also expression parameters such as induction strength and temperature, proved to be important.[25,40,57−59] However, systematic studies that comparatively address the properties of CatIBs produced by different means (i.e., tag and linker combinations) using the same host strain and plasmid construct as well as identical production conditions are direly needed to provide better insights into future applications of the CatIB strategy.

To illustrate the application potential of the CatIB strategy, we will, in the following paragraphs, summarize the repertoire of target proteins that have been successfully immobilized (see also Table 1). From the first discovery of β-galactosidase IBs displaying catalytic activity in the late 1980s[53] to present day, numerous POIs ranging from simple, monomeric reporter proteins to complex, cofactor requiring multimeric enzymes have been successfully immobilized within CatIBs. For instance, monomeric red fluorescent protein mCherry[25,60] and yellow fluorescent protein mYFP from *Aequorea victoria*,[25,60] weakly dimeric blue and green fluorescent proteins BFP and GFP from *A. victoria*,[24,61−65] along with DsRed from *Discosoma* sp.[52] have been aggregated in CatIBs in a functional form.

Similarly, CatIBs containing the monomeric enzymes Amadoriase II[24,62,63,67] and β-glycosidase from *Thermus caldophilus*[52] as well as the industrially relevant enzyme lipase A from *Bacillus subtilis*[17,24,62,67] have been produced. The clinically relevant, yet unstable and difficult to produce enzyme hyaluronidase from *Apis mellifera* was successfully generated as natural CatIBs (not requiring the fusion of a "pull-down" tag) in *E. coli* in a fed batch cultivation mode by the careful modification of the process parameters.[76] The resulting hyaluronidase CatIBs were used to generate hyaluronan oligosaccharides, which can be employed to stimulate angiogenesis and tumor suppression.

Dimeric enzymes that have been immobilized in CatIBs include an alkaline phosphatase from *E. coli*,[45] a β-xylosidase from *Bacillus pumilus*,[62,63] the hydroxynitrile lyase (AtHNL) from *Arabidopsis thaliana*, and the thiamine-diphosphate dependent enzyme MenD (2-succinyl-5-enol-pyruvyl-6-hydroxy-3-cyclohexene-1-carboxylate synthase) from *E. coli*, which is a promising biocatalyst for the production of functionalized α-hydroxy ketones.[17] AtHNL CatIBs were employed for the production of various chiral cyanohydrins with very high conversion rates and excellent ee values (96−99% ee), demonstrating the high stability and recyclability of CatIBs in an organic solvent-based reaction system. In addition, AtHNL CatIBs displayed a higher stability at low pH values compared to the native enzyme. Dimeric serine racemases from maize and human sources, which are dependent on pyridoxal 5′-phosphate (PLP) as a cofactor, have been recently added to the growing list of POIs that were incorporated within CatIBs.[78] It is worthwhile to note that, in the case of human and maize serine racemase CatIBs, from the two functions of these enzymes, namely, the reversible racemization of L-serine to D-serine, and the dehydration of both enantiomers to produce pyruvate and ammonia, only the first function has been retained, therefore generating CatIBs with altered substrate specificity.

More complex targets were also immobilized via the CatIB strategy. These include the tetrameric sialic acid aldolase[74] involved in the production of sialic acid Neu5Ac, which is a precursor for the synthesis of anti-influenza drugs, in addition to being a food additive,[79] and β-glucuronidase from *E. coli*.[52] Additionally, NADPH-dependent, tetrameric alcohol dehydrogenases from *Ralstonia* sp. (RADH) and *Lactobacillus brevis* (LbADH), and ThDP-dependent, tetrameric enzymes benzaldehyde lyase from *Pseudomonas fluorescens* (PfBAL)[25,69] and

https://doi.org/10.1021/acssuschemeng.1c02045
ACS Sustainable Chem. Eng. 2021, 9, 8919−8945

Table 1. Overview of Different CatIB Formation-Inducing "Pull-Down" Tags[a]

name (origin)	length (no. of amino acids)	tag property	linker/*structure*	target enzyme/ protein	target origin	CatIB-formation efficiency[b] [%]	residual activity[c] [%]	ref
			(I) Artificial Peptides					
L6KD (and variants)	8	amphiphilic	PTPPTTPTPPTTPTPTP *unstructured*	lipase A	*Bacillus subtilis*	80	30*	24
			PTPPTTPTPPTTPTPTP *unstructured*	amadoriase II	*Aspergillus fumigatus*	61	93*	24
			PTPPTTPTPPTTPTPTP *unstructured*	β-xylosidase	*Bacillus pumilus*	84	26*	24
			PTPPTTPTPPTTPTPTP *unstructured*	GFP	*Aequorea victoria*	n.i.[d]	n.a.[e]	24
			PTPPTTPTPPTTPTPTP *unstructured*	lysine decarboxylase	*Escherichia coli*	n.i.	n.i.	59
			$(GGGS)_3$ *unstructured*	lysine decarboxylase	*E. coli*	n.i.	n.i.	59
			n.i.	tyrosine phenol-lyase	*Citrobacter freundii*	up to 41	n.i.	66
GFIL8 (and variants)	8	β-sheet	PTPPTTPTPPTTPTPTP *unstructured*	lipase A	*B. subtilis*	89	43*	67
			PTPPTTPTPPTTPTPTP *unstructured*	amadoriase II	*A. fumigatus*	93	54*	67
			PTPPTTPTPPTTPTPTP *unstructured*	Ulp1 protease	*Saccharomyces cerevisiae*	n.i.	40*	68
			PTPPTTPTPPTTPTPTP *unstructured*	lysine decarboxylase	*E. coli*	n.i.	n.i.	59
			$(GGGS)_3$ *unstructured*	lysine decarboxylase	*E. coli*	n.i.	n.i.	59
			n.i.	tyrosine phenol-lyase	*C. freundii*	98	n.i.	66
ELK16 (and variants)	16	β-sheet	PTPPTTPTPPTTPTPTP *unstructured*	amadoriase II	*A. fumigatus*	120	88*	63
			PTPPTTPTPPTTPTPTP *unstructured*	β-xylosidase	*B. pumilus*	94	77*	63
			PTPPTTPTPPTTPTPTP *unstructured*	GFP	*A. victoria*	n.i.	n.a.	63
			n.i.	tyrosine phenol-lyase	*C. freundii*	up to 49	n.i.	66
18A (and variants)	18	α-helical	PTPPTTPTPPTTPTPTP *unstructured*	lipase A	*B. subtilis*	90	150*	62
			PTPPTTPTPPTTPTPTP *unstructured*	amadoriase II	*A. fumigatus*	n.i.	n.i.	62
			PTPPTTPTPPTTPTPTP *unstructured*	β-xylosidase	*B. pumilus*	n.i.	n.i.	62
			PTPPTTPTPPTTPTPTP *unstructured*	GFP	*A. victoria*	n.i.	n.a.	62
			PTPPTTPTPPTTPTPTP *unstructured*	lysine decarboxylase	*E. coli*	n.i.	n.i.	59
			$(GGGS)_3$ *unstructured*	lysine decarboxylase	*E. coli*	n.i.	n.i.	59
			n.i.	tyrosine phenol-lyase	*C. freundii*	87	n.i.	66
ELP10	10	random coil/β-turn spiral[f]	n.i.	tyrosine phenol-lyase	*C. freundii*	51	n.i.	66
ELP20	20	random coil/β-turn spiral[f]	n.i.	tyrosine phenol-lyase	*C. freundii*	>20	n.i.	66
			(II) Coiled-Coil Domains/Proteins					
TDoT (*Staphylothermus marinus*)	53	tetrameric coiled coil	$(GGGS)_3$ *unstructured*	hydroxynitrile lyase	*Arabidopsis thaliana*	76	11	17
			$(GGGS)_3$ *unstructured*	MenD[g]	*E. coli*	90	n.i.	17
			$(GGGS)_3$ *unstructured*	lipase A	*B. subtilis*	114	n.i.	17
			$(GGGS)_3$ *unstructured*	alcohol dehydrogenase	*Ralstonia* sp.	88	2	25, 60
			$(GGGS)_3$ *unstructured*	alcohol dehydrogenase	*Lactobacillus brevis*	5	6	25
			$(GGGS)_3$ *unstructured*	benzaldehyde lyase	*Pseudomonas fluorescens*	88	1	25, 69
			$(GGGS)_3$ *unstructured*	benzoylformate decarboxylase	*Pseudomonas putida*	1	4	25

https://doi.org/10.1021/acssuschemeng.1c02045
ACS Sustainable Chem. Eng. 2021, 9, 8919−8945

Table 1. continued

name (origin)	length (no. of amino acids)	tag property	linker/*structure*	target enzyme/ protein	target origin	CatIB-formation efficiency[b] [%]	residual activity[c] [%]	ref
			(II) Coiled-Coil Domains/Proteins					
			$(GGGS)_3$ *unstructured*	lysine decarboxylase	*E. coli*	n.i.	n.i.	25, 59, 70
			$(GGGS)_3$ *unstructured*	YFP	*A. victoria*	65	n.a.	25, 60
			$(GGGS)_3$ *unstructured*	mCherry	*Discosoma* sp.	42	n.a.	25, 60
			PTPPTTPTPPTTPTPTP *unstructured*	lysine decarboxylase	*E. coli*	n.i.	n.i.	59
Jun	62	leucine zippers	SGGGSGGS *unstructured*	EGFP	*A. victoria*	53[h]	n.a.	71
Fos	93	leucine zippers	SGGGSGGS *unstructured*	EGFP	*A. victoria*	74[i]	n.a.	71
ZapB (*E. coli*)	81	dimeric coiled coil protein	SIPGA	GFP	*A. victoria*	95	n.a.	72
				mCherry	*Discosoma* sp.	55	n.a.	72
3HAMP (*Pseudomonas aeruginosa*)	172	dimeric coiled coil	$(GGGS)_3$ *unstructured*	alcohol dehyrogenase	*Ralstonia* sp.	75	12	25
			$(GGGS)_3$ *unstructured*	alcohol dehyrogenase	*L. brevis*	67	1	25
			$(GGGS)_3$ *unstructured*	benzaldehyde lyase	*P. fluorescens*	76	18	60
			$(GGGS)_3$ *unstructured*	benzoylformate decarboxylase	*P. putida*	61	10	25
			$(GGGS)_3$ *unstructured*	lysine decarboxylase	*E. coli*	n.i.	n.i.	59, 70
			$(GGGS)_3$ *unstructured*	YFP	*A. victoria*	6	n.a.	25
			$(GGGS)_3$ *unstructured*	mCherry	*Discosoma* sp.	5	n.a.	25
			PTPPTTPTPPTTPTPTP *unstructured*	lysine decarboxylase	*E. coli*	n.i.	n.i.	59
			(III) Aggregation-Prone Proteins (Protein Domains)					
Aβ42(F19D) (*Homo sapiens*)	42	amyloid peptide	n.i.	BFP	*A. victoria*	61−65	31[j]	61
CBDcell (*Cellulomonas fimi*)	108	cellulose binding protein	n.i.	β-glucuronidase	*E. coli*	92	19	52
				β-glycosidase	*Thermus caldophilus*	93	n.i.	52
				DsRed	*Discosoma* sp.	n.i.	n.a.	52
CBDclos (*Clostridium cellulovorans*)	156	cellulose binding protein	43 amino acids with thrombin cleavage site, S-Tag, and cloning site	D-amino acid oxidase	*Trigonopsis variabilis*	>90	42*	73
				D-sialic acid aldolase	*E. coli K12*	100	100*	74
				maltodextrin phosphorylase	*Pyrococcus furiosus*	83	n.i.	74
				cytidylate kinase	*E. coli*	n.i.	n.i.	75
				polyphosphate kinase PPK3	*Silicibacter pomeroyi*	n.i.	n.i.	75
				GFP	*A. victoria*	n.i.	n.i.	65
				GalU[k]	*E. coli*	n.i.	n.i.	65
VP1 capsid protein (foot-and-mouth disease virus)	209	virus capsid protein	n.i.	β-galactosidase	*E. coli*	36−46	166*	61
				GFP	*A. victoria*	n.i.	n.a.	61
GFP (*A. victoria*)	238	fluorescent protein	$(GGGS)_5$ *flexible*	acid phosphatase	*Enterobacter aerogenes*	n.i.	48	58
			$(AAAKE)_5$ *rigid*	acid phosphatase	*Enterobacter aerogenes*	n.i.	58	58

https://doi.org/10.1021/acssuschemeng.1c02045
ACS Sustainable Chem. Eng. 2021, 9, 8919−8945

Table 1. continued

name (origin)	length (no. of amino acids)	tag property	linker/*structure*	target enzyme/protein	target origin	CatIB-formation efficiency[b] [%]	residual activity[c] [%]	ref
(III) Aggregation-Prone Proteins (Protein Domains)								
MalE31 (*E. coli*)	396	maltose binding protein	RIPGG *unstructured*	alkaline phosphatase	*E. coli*	>95	n.i.	45
				β-lactamase	*E. coli*	>95	n.i.	45
PoxB (*Paenibacillus polymyxa E681*)	574	pyruvate oxidase	n.i.	GFP	*A. victoria*	n.i.	n.a.	64
				α-amylase	*B. subtilis*	77	200[l]	64

[a]Cases where residual activity was compared only to cell lysate are marked with an asterisk (*). Details, like sequences, names, and originating organisms for all listed "pull-down" tags, can be found in refs 26 and 40. [b]CatIB-formation efficiency: defined as the activity, or in the case of fluorescent proteins, fluorescence, of the insoluble IBs relative to the activity/fluorescence of the crude cell extract. [c]Residual activity compared to purified enzyme. [d]n.i.: No information provided. [e]n.a.: Not applicable. [f]Tag property information obtained from ref 77. [g]MenD: 2-succinyl-5-enol-pyruvyl-6-hydroxy-3-cyclohexene-1-carboxylate synthase. [h]Construct containing both leucine zippers. [i]Coproduction of leucine zippers. [j]Residual specific fluorescence compared to cell lysate. [k]GalU: UDP-glucose pyrophosphorylase. [l]Volumetric activity.

benzoylformate decarboxylase from *Pseudomonas putida* (PpBFD),[25] have been similarly immobilized in the past. Particularly noteworthy is the successful implementation of a two-step cascade reaction, which was realized using CatIBs with colocalized PfBAL and RADH, where PfBAL converted benzaldehyde and acetaldehyde to (*R*)-2-hydroxy-1-phenyl-propanone, which was further converted by RADH to benzyl alcohol and (1*R*, 2*R*)-1-phenylpropane-1,2-diol, a precursor of the calcium channel blocker diltiazem.[60] Recently, the tetrameric, PLP-dependent tyrosine phenol-lyase, which can be employed to produce enantiomerically pure *α*-deuterated (*S*)-amino acids, such as the dopamine precursor L-dihydroxyphenylalanine, has been immobilized using C-terminal fusions of nine different artificial peptide tags.[66] Notably, two of those constructs (bearing GFIL16 and 18AWT tags) yielded CatIBs with improved thermostability and half-lives, reaching 87−98% of the activity detected in the supernatant of the soluble enzyme, respectively. To the best of our knowledge, the most complex oligomeric POI that was immobilized with the CatIB strategy is the PLP-dependent, decameric L-lysine decarboxylase from *E. coli*, using TdoT and 3HAMP as tags.[25,70] The enzyme is of high industrial relevance due to its ability to produce 1,5-diaminopentane (cadaverine), which is a building block for biobased polyamides. Recently, a number of small, artificial peptide tags have also been employed for the immobilization of L-lysine decarboxylase in CatIBs as well.[59]

Enzyme Immobilization by Cry3Aa Crystal Entrapment. The Cry family of proteins, produced by the Gram-positive soil bacterium *B. thuringiensis*, comprises highly valued toxins due to their insecticidal use.[80] Cry proteins have been classified in over 70 subgroups based on their sequence identities, and in general, each class exhibits selective toxicity against specific insect orders. For instance, the Cry1 class proteins exhibit specific toxicity to larvae of Lepidoptera species; Cry2 proteins are effective against Lepidoptera and Diptera species, and Cry3 class proteins are active against Coleoptera species.[80,81] Historically, Cry formulations have been used in agriculture for pest control, and since the 1990s, genetically modified crops that heterologously produce Cry proteins have been conferred with a resistance toward certain insects.[82] Moreover, an interesting characteristic of the Cry proteins is their ability to form crystals as inclusions within their natural host, which is thought to facilitate the invasion of the insect gut tissues.[80]

Apart from their common employment as an insecticide, a novel use of Cry crystals was demonstrated in 2015, where the ability of the Cry3Aa protein to form natural crystals was exploited to deliver several POIs to macrophages and mice in a functional form.[83] The genes encoding fluorescent reporter proteins GFP and mCherry, along with the firefly luciferase as model POIs, have been fused to the *cry3Aa* gene, which facilitates the entrapment of the respective POI within the intracellularly formed Cry3Aa crystals (Figure 2C). The isolated crystals, obtained via density gradient centrifugation, were shown to exhibit GFP- and mCherry-specific fluorescence, confirming the proper folding of these POIs within the crystals. Notably, the crystals were reported to retain their fluorescence for several weeks, pointing toward high stability of the POIs within the crystalline matrix.

Cry3Aa crystal entrapment was utilized for enzyme immobilization. Here, the monomeric enzymes peptide deformylase from *Borrelia burgdorferi* along with the lipase A

https://doi.org/10.1021/acssuschemeng.1c02045
ACS Sustainable Chem. Eng. 2021, 9, 8919−8945

and a *para*-nitrobenzyl esterase PnbA from *B. subtilis* were immobilized within Cry3Aa crystals, where they displayed very high activities.[27] Notably, the immobilized *para*-nitrobenzyl esterase completely retained its activity, whereas the lipase A and the peptide deformylase showed approximately 84% and 48% of the activities when compared to their purified soluble counterparts, respectively. An additional construct lacking 19 residues from the C-terminus of Cry3Aa and carrying a flexible GGGS linker between the lipase and Cry3Aa was generated in an attempt to improve substrate accessibility to the enzyme, through providing a better orientation toward the large channels of the Cry3Aa crystals. Utilizing this approach, the authors reported that the activity of immobilized lipase A within the modified Cry3Aa crystals was boosted by more than 2-fold. The authors, moreover, noted that all constructs had similar K_m values and concluded that, for Cry3Aa-based immobilizates, unlike for other immobilization strategies, internal diffusion and mass transfer limitations are not an issue. In addition, improved thermostability, tolerance to organic solvents, and recyclability have been demonstrated for the modified Cry3Aa immobilized lipase, and fatty acid methyl ester (FAME) biodiesel was produced with high conversion rates (over 80% after 10 cycles). *Proteus mirabilis* lipase (PML) and its mutant Dieselzyme 4 (DLZM4) with high methanol tolerance have been likewise immobilized using the self-crystallizing Cry3Aa protein in *B. thuringiensis*.[84] However, these fusions resulted in a 20-fold activity reduction for PML and an almost complete loss of activity for DLZM4 when compared to the purified native enzymes. According to the authors, the exact reason for the observed reduction in activity remains unclear but could be because fusion to Cry3Aa does not orient PML in an optimal position for catalysis. To counter this, the authors used a directed evolution approach, and *E. coli* colonies were screened resulting in the identification of a Cry3Aa-PML double mutant (Cry3Aa-PML^{VG}) with improved activity. Additionally, despite the positive effect of Cry3Aa immobilization on thermostability, Cry3Aa-PML incubated in methanol showed a 2-fold lower activity compared to soluble PML, indicating that tolerance toward organic solvents could not be improved in this case. Interestingly, the K_m values for both immobilized Cry3Aa-PML and Cry3Aa-PML^{VG} were only about 2-fold higher compared to their soluble counterparts, suggesting that the lower activity was not due to significantly limited substrate diffusion. In a follow-up study, it was demonstrated that enzymes can be entrapped within the Cry3Aa crystals when coproduced, without the need of generating Cry3Aa fusions[18] (Figure 2C). The previously identified double mutant PML^{VG} was entrapped within the crystals via coproduction, and washing the crystals with buffers at pH values between 4 and 9, or high concentrations of sodium chloride, did not result in substantial release of the enzyme. Furthermore, the strategy has found use in bioremediation, where a metallothionein from *Synechococcus elongatus* was fused to Cry3Aa.[85] Here, the *smtA* gene encoding the metallothionein was cloned in up to six tandem repeats for the fusion to Cry3Aa, which generated crystals with similar sizes and morphologies and bound chromium and cadmium with efficiencies positively correlating with the *smtA* copy number. Notably, when nine copies of SmtA were fused to Cry3Aa, the yield was low, and the resulting crystals were less stable, pointing toward the limitation of the approach for incorporating large POIs.

Forizymes—Scaffolding of Enzymes by Using Plant Mechanoprotein Complexes. Forisomes are mechanoprotein complexes found exclusively in the phloem of legumes.[86] When the phloem is wounded, forisomes undergo a reversible conformational change and assume a dispersed, pluglike state in an adenosine triphosphate (ATP)-independent manner, allowing them to plug the sieve tubes and therefore prevent the loss of photoassimilates.[86,87] When the sieve elements regenerate, forisomes revert to their condensed, spindlelike shape. This process is triggered by the influx of calcium ions caused by wounding of the phloem; however, other divalent ions and pH change are also shown to trigger the conformational change of forisomes *ex vivo*.[88] The size of forisomes is between approximately 10 × 1 and 55 × 5 μm depending on the plant species, and the conformational change can confer an up to 9-fold increase in volume *in vitro*.[86,87,89]

From the four genes encoding forisome subunits, MtSEO-F1−4 (SEO-F1−4: sieve element occlusion by forisome) from *Medicago truncatula*, expressing only *mtSEO-F1* or *mtSEO-F4* was shown to be sufficient in generating functional forisome bodies in yeast and plant systems.[88,90] This finding paved the way for the production of functional artificial forisomes (hereinafter referred as forizymes), where heterologously expressed forisomes were used to produce several POIs in an active form in *Saccharomyces cerevisiae*.[21] The blue fluorescent protein cerulean, enhanced yellow fluorescent protein (eYFP), dimeric glucose-6-phosphate dehydrogenase (G6PDH), and hexokinase 2 (HXK2) containing forizymes were generated via the fusion of the corresponding genes to forisome subunits MtSEO-F1 and MtSEO-F4. Fusions of eYFP to forisome subunits showed that the generation of functional forizymes is highly dependent on the fusion site. Moreover, a simple fusion of the POI to MtSEO-F1 or MtSEO-F4 subunit was not enough to trigger forizyme formation in all cases except one. Instead, a heteromeric combination approach based on the coproduction of the forisome subunit together with the POI-MtSEO-F1/MtSEO-F4 fusion was required (Figure 2D). Interestingly, C-terminal fusions of eYFP to either forisome subunit generated fluorescent IBs rather than forizymes, which were similarly observed in C-terminal fusions in heteromeric combinations. Furthermore, the activity of the G6PDH forizymes was measured at different Ca^{2+} concentrations, and the resulting conformational change was shown to have no significant effect on the enzyme activity. This demonstration highlights the suitability of forizyme-based immobilizates for the immobilization of divalent-metal-utilizing/containing enzymes, yet further studies are needed to ascertain this issue. A positive effect of the approach on stability was also reported, where 80% of the original G6PDH activity could be detected after 10 reaction cycles. Notably, the HXK2 forizymes generated in a similar manner displayed activities within the same range of the literature values as reported in the study. For colocalization analyses, the authors built constructs bearing eYFP and cerulean as fluorescent reporters fused to genes encoding G6PDH and HXK2 enzymes, respectively, with each fusion additionally containing a forisome subunit. A cascade reaction was realized using G6PDH and HXK2 forizymes coproduced in yeast cells. To this end, fusion proteins consisting of G6PDH and HXK2 fused to MtSEO-F1 were coproduced with MtSEO-F1, yielding colocalization of the enzymes in approximately 51% of the forizymes. In addition, the reaction rate of the bifunctional forizymes was 1.3-fold higher, when compared to the mixtures of forizymes of

https://doi.org/10.1021/acssuschemeng.1c02045
ACS Sustainable Chem. Eng. 2021, 9, 8919−8945

Table 2. Overview of Different Systems Used for Liquid−Liquid Phase Separation (LLPS) to Form Biomolecular Condensates[a]

*[name of system]*LLPS-inducing tag	architecture	LLPS by	condensate morphology	*in vivo* production *[host/cell line]*	reversibility	target recruitment by	ref
[−/−]; SH3, PRM	$(SH3)_{1-5}$	multivalent interaction	liquidlike, maturation into gel	yes, *[HeLa]*	reversible, but sol−gel hardening observed *in vitro*	fusion to droplet forming domain fusion $(SH3)_5$ and $(PRM)_5$	29
[REPS]; RGG	$(RGG)_{1-3}$; RGG-[TEV/Th]-RGG; MBP-[HRV 3C]-$(RGG)_2$	multivalent interaction of IDPs; droplet disassembly by proteolytic cleavage; droplet assembly by proteolytic cleavage of MBP	liquidlike	yes, *[HEK293, HeLa, and U2OS]*	reversible assembly and dissassembly	fusion of synthetic coiled-coil peptides (SYNZIPs) to droplet forming domain fusion and POI recruitment via SYNZIP interaction	31
[iPOLYMER]; FKBP, FRB	$(FKBP)_{1-5}$ = $(YF)_{1-5}$ and $(FRB)_{1-5}$ = $(CR)_{1-5}$	multivalent interaction	hydrogel-like	yes, *[COS-7]*	irreversible	fusion to droplet forming domain fusion (e.g., $(YF)_{1-5}$ or sequestration to RNA granula formed by via TIA-1 fused to CR_5)	30
[iPOLYMER-Li; iLID, SspB	$(iLID)_6$ and $(SspB)_6$	light-triggered multivalent interaction	likely liquidlike	yes, *[COS-7]*	reversible	fusion to droplet forming domain fusion (e.g., $(iLID)_6$ or $(SspB)_6$)	30
[optoDroplets]; FUS_N, $HNRNPA1_C$; $DDX4_N$	FUS_N-Cry-2; $HNRNPA1_C$-Cry-2; DDX4-Cry-2	light-triggered multivalent interaction of IDPs	mostly liquidlike, partially gel-like	yes, *[NIH 3T3]*	mostly reversible	fusion to droplet forming domain fusion (e.g., FUS_N-Cry-2)	32
[optoClusters]; FUS_N; $HNRNPA1_C$; $DDX4_N$	FUS_N-Cry-2Olig	light-triggered multivalent interaction of IDPs	mostly gel-like clusters	yes, *[Saccharomyces cerevisiae]*	mostly irreversible	fusion to droplet forming domain fusion (e.g., FUS_N-Cry-2Olig)	32, 102
[PixELLs]; FUS_N	FUS_N-PixE and FUS_N-PixD	light-triggered dissociation of multivalent IDP interactions	liquidlike	yes, *[NIH 3T3, Saccharomyces cerevisiae]*	reversible	fusion to droplet forming domain fusion (e.g., FUS_N-PixD or FUS_N-PixE)	102, 103
[Corelets]; IDRs: FUS_N; $DDX4_N$; $HNRNPA1_C$; TDP-43_C; PGL-1	iLID-FTH1 and IDP-SspB	light-triggered multivalent interaction of IDPs	liquidlike	yes, [U2OS, HEK293, *Caenorhabditis elegans, S. cerevisiae]*	reversible	fusion of POI to FTH1-iLID and/or SspB-IDR module	28
[−/−]; MaSp1-I16	$(MaSp1\text{-}I16)_{16}$	multivalent interaction of IDPs	liquidlike	yes, *Escherichia coli*	reversible *in vitro*	fusion to droplet forming domain fusion (e.g., $(MaSp1\text{-}I16)_{16}$	22
[−/−]; artificial IDRs (A-IDPs)	$(GRGDSPYS)_{20-80}$	multivalent interaction of IDPs	liquidlike	yes, *[HEK293, E. coli]*	reversible	fusion to droplet forming domain fusion	41

[a]Abbreviations: REPS, RGG-based, enzyme-triggered, phase-separating systems; SH3, SRC homology 3 domain; PRM, proline-rich-motif ligand of SH3; RGG domain, domain of the LAF1 deadbox DDX3 RNA helicase containing closely spaced Arg-Gly-Gly (RGG) repeats; [TEV/Th], tobacco etch virus or thrombin protease cleavage site; HRV 3C, human rhinovirus protease 3C; iPOLYMER, intracellular production of ligand-yielded multivalent enhancers; FKBP, FK506 binding protein; FRB, rapamycin binding protein; $(YF)_{1-5}$, constructs containing 1−5 copies of FKBP; $(CR)_{1-5}$, constructs containing 1−5 copies of FRB; TIA-1, stress granule forming protein that binds to Poly-A containing RNAs; iPOLYMER-Li, intracellular production of light-yielded multivalent enhancers with light inducibility; iLID, optogenetic construct derived from a light, oxygen, voltage (LOV) sensory domain of *Avena sativa* Phototropin-2 fused with SsrA peptide; SspB, protein binding partner of the SsrA peptide; FUS_N, $HNRNPA1_C$; $DDX4_N$, N- or C-terminal intrinsically disordered protein regions (IDRs) of intrinsically disordered proteins (IDPs) of the fused in sarcoma protein (FUS), Heterogeneous nuclear ribonucleoprotein A1 (HNRNPA1), and the ATP-dependent RNA helicase, Deadbox Helicase 4 (DDX4); TDP-43_C, IDR of TAR DNA binding protein 4; PGL-1, RNA-binding IDP of *C. elegans* germ granules; FTH1, human ferritin heavy chain; MaSp1-I16, IDP consisting of 16 repeats of the major ampullate spidroin 1 protein of *Nephila clavipes*; GRGDSPYS, parent motif of artificial IDRs inspired by the *Drosophila melanogaster* Rec-1 resilin.

https://doi.org/10.1021/acssuschemeng.1c02045
ACS Sustainable Chem. Eng. 2021, 9, 8919−8945

corresponding individual enzymes, as well as their soluble forms.

DESIGNED SYNTHETIC ORGANELLES—LIQUID PROTEIN CONDENSATES AS IMMOBILIZATES?

Compartmentalization, the formation of intracellular compartments or organelles for separating and orchestrating biochemical reaction pathways, is an essential feature of biological systems. Classically, organelles are membrane-separated compartments such as the nucleus, mitochondria, chloroplasts, and the Golgi apparatus. However, recent studies have shown that eukaryotic cells also contain various compartments that lack such a separating membrane structure. These so-called membraneless organelles, also called biomolecular condensates, liquid protein condensates, or coacervates, are widespread in eukaryotes.[91−93] They were first identified in the form of the P granules in *Caenorhabditis elegans* embryos.[94] Other naturally present membraneless organelles are nucleoli,[95] heterochromatin,[96] stress granules,[97] Balbiani bodies in *Xenopus* oocytes, the centrosome of *C. elegans* embryos,[93] and membrane receptor signaling clusters such as the nephrin−Nck−N-WASP signaling pathway,[98] to name just a few. They are formed by liquid−liquid phase separation (LLPS), a physical phenomenon that can be described as the coexistence of a dense phase that resembles liquid droplets with a dilute phase.[99] Cellular condensates or membraneless organelles are hereby formed by a dense phase of macromolecules such as proteins and DNA/RNA that form submicrometer[36] liquidlike droplets within the dilute cytoplasm.[99] In turn, due to the liquidlike properties of LLPS protein condensates, diffusional limitation is likely much less of an issue as for the aforementioned encapsulation-based systems, where the substrate/product has to cross a liquid/solid phase boundary. This is exemplified by the observation that even POIs can be recruited to the respective condensates after they have formed (see below).

Mechanistically, one factor that is instrumental for LLPS is multivalency, a tendency of certain types of molecules to undergo inter- or intramolecular interactions to form higher-order oligomers or polymers. Those in turn have a lower solubility as compared to the dilute phase and hence tend to demix, thereby forming a separate phase from the surrounding solution.[100] In the case of folded proteins, the presence of multiple interaction sites or interacting domains, implicated in homo- or hetero-oligomerization, promotes LLPS. Similarly, for intrinsically disordered proteins (IDPs) or protein domains, multivalent weak interactions between those regions seem to drive LLPS.[100]

Sequence determinants or structure−function relationships for LLPS formation are far from understood; however, our understanding of the basic principles of LLPS now facilitates the design of synthetic membraneless organelles.[36] Please note that the (natural) building principles of membraneless organelles and their properties, biological role, and function have been expertly reviewed before (see, e.g., refs 93, 99, and 101 and references therein). Therefore, in the present Perspective we will solely focus on designed synthetic membraneless organelles and their application potential for (industrial) biocatalysis and biotechnology. All strategies for the generation of membraneless organelles/biomolecular condensates described in this Perspective are summarized in Table 2.

From Initial Approaches to Enzymatically and Chemically Triggered LLPS. In an early study, the artificial generation of membraneless organelles by LLPS was demonstrated utilizing signaling and interaction domains of multivalent signaling proteins.[101] The system presented by Li et al. hereby relied on the interaction between the SRC homology 3 (SH3) domain and its proline-rich-motif (PRM) ligand.[29] To capitalize on multivalent interactions between those molecules, they generated two types of engineered proteins consisting of 1−5 SH3 ($SH3_1$−$SH3_5$) or PRM (PRM_1−PRM_5) domains (Figure 3A). When purified proteins of higher valency ($SH3_4$ + PRM_4) were mixed together at high concentration, liquid−liquid demixing was observed resulting in the formation of spherical droplets. In addition, different experimental approaches, including dynamic light scattering, photobleaching experiments, and cryoelectron microscopy studies, suggested that the macroscopically detectable LLPS is coupled to a molecular sol−gel transition within the droplet.[29] This phenomenon is nowadays known as maturation or hardening, in some cases also reported to occur *in vivo*, with the hardened condensates likely being gels, glasses, or two-phase solids.[101,104]

Moreover, LLPS was also observed *in vivo* in HeLa cells, where the coexpression of mCherry-$SH3_5$ and EGFP-PRM_5 fusions resulted in the formation of cytoplasmic puncta showing both mCherry and EGFP fluorescence. Similarly, the authors utilized multivalent interactions of components of the nephrin−NCK−N−WASP signaling system to trigger LLPS. This study clearly demonstrated that LLPS can be engineered to yield membraneless organelles *in vivo*, which moreover can be "loaded" with cargo proteins, as demonstrated by Li et al. for the colocalization (or coimmobilization) of EGFP and mCherry. Moreover, the observation of hardened states of the condensates could be beneficial for using them as enzyme immobilizates in biocatalysis, as gels or glasses would be much more easily recoverable from the reaction system.

LLPS Droplet Assembly/Disassembly Triggered by Proteolytic Cleavage. Another artificial LLPS system, which was developed more recently, employed several strategies to make LLPS enzymatically inducible. Schuster and co-workers utilized the RGG domain (containing closely spaced Arg−Gly−Gly repeats) of the *C. elegans* LAF1 deadbox DDX3 family RNA helicase, which is found in P granules.[31] The RGG domain, located at the N-terminus of LAF1, is an IDP that shows an upper critical solution temperature (UCST): it is soluble at higher temperatures, with LLPS occurring only when the temperature is lowered below the UCST. The systems abbreviated by the authors as REPS (RGG-based, enzyme-triggered, phase-separating systems) utilized 1−3 RGG domains as single, tandem, and triple constructs. Depending on the number of RGG domains, different phase-separating properties were observed, with constructs containing a larger number of RGG domains showing an improved tendency for LLPS and an increase of the UCST (RGG: below 15 to <50 °C for RGG−RGG−RGG). To trigger droplet disassembly at a physiological temperature, the authors utilized a tandem RGG−RGG construct that contained a tobacco etch virus (TEV) or thrombin protease cleavage site between the two RGG domains (Figure 3B). While the tandem RGG−RGG construct shows LLPS at a physiological temperature for tissue culture (>15 and <40 °C), proteolytic cleavage to yield single RGG domains lowers the UCST, so that the droplets disassemble. Similarly, triggered droplet assembly was achieved

https://doi.org/10.1021/acssuschemeng.1c02045
ACS Sustainable Chem. Eng. 2021, 9, 8919−8945

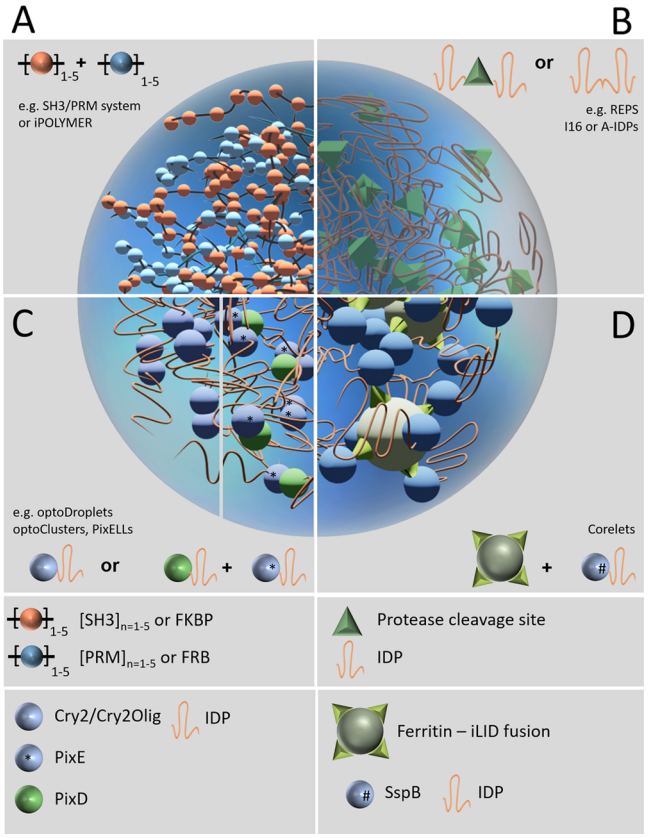

Figure 3. Liquid protein condensates as immobilizates. (A) Liquid−liquid phase separation (LLPS) due to multivalent interactions of proteins containing, e.g., multiple repeats of the SRC homology 3 domain (SH3) and its proline-rich motif (PRM) ligand (SH3/PRM system) or the FK506 binding protein (FKBP) and the rapamycin binding protein (FRB) (iPOLYMER strategy). Protein of interest (POI) recruitment by fusion to droplet/hydrogel-forming multivalent domain fusions. (B) LLPS due to fusion of multiple intrinsically disordered proteins (IDPs) such as the RGG domain of the *C. elegans* deadbox DDX3 helicase LAF1, 16 repeats of the major ampullate spidroin 1 protein of *Nephila claviceps* (I16), or artificial intrinsically disordered protein regions (A-IDPs). POI recruitment via fusion of synthetic coiled-coil peptides (SYNZIPs) that interact with the correspondingly tagged droplet forming IDP-fusions or by direct fusion to the IDPs. (C) optoDroplets/optoClusters and PixELLs: light-triggered LLPS by utilizing the light-dependent homo-/hetero-oligomerization tendency of photoreceptor proteins such as cryptochromes (Cry-2/Cry-2Olig) and blue-light using flavin adenine dinucleotide (BLUF) proteins (PixE/D) fused to IDPs such as the N-terminal intrinsically disordered region (IDR) of the fused in sarcoma (FUS_N) protein, C-terminal IDR of the heterogeneous nuclear ribonucleoprotein A1 (HNRNPA1), or the N-terminal IDR of the deadbox helicase DDX4. POI recruitment by fusion of POIs to droplet/hydrogel-forming multivalent domain fusions. (D) Corelets: light-driven LLPS by utilizing the human ferritin heavy chain fused with the optogenetic tool iLID, derived from a light, oxygen, voltage (LOV) sensory domain of *Avena sativa* Phototropin-2, which upon illumination interacts with an SspB-IDP fusion, triggering LLPS. IDPs used for the Corelet strategy include FUS_N, HNRNPA1, and DDX4. POI recruitment by fusion of POIs to ferritin-iLID and/or the SspB-IDR module.

by fusing the maltose binding protein (MBP) to a tandem RGG−RGG construct, with MBP serving as a solubility enhancing tag. To allow enzyme-triggered LLPS, a cleavage site for the human rhinovirus protease 3C (HRV 3C) was inserted between MBP and RGG−RGG. While the MBP−RGG−RGG construct remained soluble at 25 °C, proteolytic cleavage of the MBP solubility enhancer yielded LLPS droplets at 25 °C. In addition, the authors demonstrated the recruitment of soluble cargo proteins to the RGG−RGG membraneless organelles by using the SYNZIP coiled-coil system,[105] which utilizes two coiled coils SYNZIP 1 and 2 (SZ1 and SZ2) to facilitate coiled-coil-mediated protein−protein interactions between the RGG−RGG compartment and the cargo protein (Figure 3B). To this end, SZ1−RGG−RGG fusion constructs were used alongside SZ2−cargo fusion constructs with either the red fluorescent protein (RFP) or the green fluorescent protein (GFP) serving as cargo model proteins. The systems were shown to work in various mammalian cells, clearly demonstrating intracellular LLPS and cargo recruitment.

Chemically Triggered Hydrogel-Formation Utilizing LLPS. The next step forward yielded the so-called iPOLYMER technique (intracellular production of ligand-yielded multivalent enhancers), which realized the chemically triggered formation of LLPS hydrogels.[30] The iPOLYMER system (Figure 3A) utilized a chemically inducible dimerizer technique, which relies on the interaction between the FK506 binding protein (FKBP) and the rapamycin binding protein (FRB), which interact upon the addition of rapamycin.[106] The authors generated fusion proteins consisting of up to five copies (n = 1−5) of FKBP (YF_1−YF_5) or FRB (CR_1−CR_5) linked via short linker polypeptides, with or without an N-terminal nuclear export signal. For easy detection of polymerization, yellow fluorescent protein (YFP) and cyan fluorescent protein (CFP) reporters were utilized, reporting simultaneously on polymerization and colocalization. The corresponding cells were shown to exhibit diffuse fluorescence signals that rapidly turned into puncta upon rapamycin addition. Depending on the valency of interactions (1−5 copies of FKBP/FRB), increased puncta formation was observed. Ultrastructural analyses by correlative electron microscopy revealed fibrillogranular structures that morphologically resembled stress granules. Further *in vitro* studies corroborated the formation of irreversible hydrogel-like materials that formed structurally stable, optically translucent materials that are able to retain water and act as a molecular sieve allowing the efficient diffusion of small molecules. Last but not least, the authors also showed the possibility of recruiting a target protein to iPOLYMER hydrogels. They fused the RNA recognition motif of TIA-1, a stress granule forming protein that binds to Poly-A containing RNAs,[107] to CR_5 and coexpressed YF_5. After the addition of rapamycin, the formed puncta were shown to contain PABP-1, which most likely binds to the Poly-A containing RNAs sequestered to the condensates via the RNA recognition motif of TIA-1 fused to CR_5. This indicates that the functionalized iPOLYMER puncta sequester Poly-A RNAs similarly to native stress granules and that, in principle, target proteins can be sequestered to iPOLYMER hydrogels by utilizing specific interaction modules. This, for example, might facilitate target recruitment via, e.g., the above-described SYNZIP coiled-coil system. The hydrogel-like properties along with the potential for target protein recruitment render the formed hydrogels an attractive platform for applications in biocatalysis, although transfer of the system to yeast or *E. coli* cells would be desirable from an application as well as sustainability perspective.

https://doi.org/10.1021/acssuschemeng.1c02045
ACS Sustainable Chem. Eng. 2021, 9, 8919−8945

Overcoming Irreversibility—Light-Driven LLPS Droplet Formation. All until-now presented approaches, relying on either simple gene expression (SH3/PRM approach) or enzymatically (REPS) and chemically triggered (iPOLYMER) LLPS, are intrinsically irreversible, e.g., forming LLPS droplets under specific conditions (temperature, salt concentration), i.e., when concentrations above a critical concentration are reached. However, for the dynamic control of, e.g., metabolic processes by scavenging or scaffolding within LLPS droplets, reversible droplet assembly/disassembly is necessary. To this end, a number of light-driven, so-called optogenetic, techniques have been developed. All of the following presented systems thereby combine light-triggered protein−protein interactions with IDP-driven LLPS to allow for reversible intracellular droplet formation. While being advantageous from a metabolic engineering perspective, reversible LLPS seems less applicable for the production of *in vivo* enzyme immobilizates for biocatalytic applications.

The optoDroplets approach (Figure 3C) utilizes intrinsically disordered regions (IDRs) from proteins known to drive LLPS in living cells, fused to the *A. thaliana* cryptochrome 2 (Cry-2) photoreceptor protein, which tends to reversibly form oligomeric clusters upon blue-light illumination.[32] IDRs that were employed are the N-terminal IDR of the fused in sarcoma protein (FUS_N), the C-terminal IDR of the heterogeneous nuclear ribonucleoprotein A1 ($HNRNPA1_C$), and the N-terminal IDR of the deadbox DDX4 helicase. In addition to Cry-2, Cry-2Olig, which shows enhanced clustering, was used to drive LLPS (optoClusters[102]) (Figure 3C). Target recruitment is possible, as shown by the fusion of mCherry to the opto-IDR construct. In all cases, the use of the resulting fusion proteins allowed the intracellular formation of LLPS droplets under blue-light illumination, which in most cases fully disassembled in the dark. Only cyclic activation with high-light intensities yielded irreversible cluster formation for optoFUS. The use of the Cry-2Olig instead of Cry-2 yielded irreversible, gel-like aggregates, even under low-light activation in a single activation cycle. Interestingly, the formation of those gel-like aggregates was initially reversible, but aging processes led to the formation of irreversible aggregates. Thus, from a biocatalytic application perspective, the use of Cry-2Olig-based optoClusters seems better suited, although prokaryotic production would be desirable. Subsequently, based on the optoDroplet approach, the PixELL (Pix evaporates from liquidlike droplets in light) system (Figure 3C) was developed, which shows an inverted response (light-driven droplet dissociation) and relies on the blue light using flavin adenine dinucleotide (BLUF) photoreceptor PixE/PixD, which forms heterodimers in the dark and dissociates upon blue-light illumination.[102] All three systems were later adapted for use in yeast (*S. cerevisiae*) and used to enable light-based control of metabolic flux (see the Application of Synthetic Organelles in Metabolic Engineering and Biocatalysis section).

The later developed Corelet system (Figure 3D)[28] uses human ferritin heavy chain, a 24-mer iron storage protein that forms a spherical protein core of 12 nm in diameter, as an oligomerization hub. Each ferritin monomer is fused with the light, oxygen, voltage (LOV) domain-based optogenetic tool iLID. iLID is based on the *Avena sativa* LOV2 domain (AsLOV2) in which seven residues of the *E. coli* SsrA peptide have been incorporated within the C-terminal Jα helix (with which it shares sequence similarity).[108] Upon illumination with blue light, the SsrA-bearing Jα helix dissociates from the AsLOV2 core domain allowing for interaction with the SsrA partner protein SspB. Fusion of an IDR (FUS_N, $DDX4_N$, $HNRNPA1_C$, TAR DNA binding protein $TDP\text{-}43_C$, PGL-1) to SspB thereby facilitates light-driven LLPS droplet formation (Figure 3D). Moreover, the fusion of additional proteins to the ferritin-iLID and/or the SspB-IDP module allows for target recruitment to the LLPS droplets (exemplarily shown for EGFP and mCherry). The system, which was shown to be fully reversible over 15 cycles of activation, was also shown to work in cultured mammalian cells, in yeast (*S. cerevisiae*) and *C. elegans*, as well as in both the cytoplasm and nucleus.[28]

Similarly to the Corelet strategy, an adaptation of the above-described iPOLYMER system, coined iPOLYMER-Li (intracellular production of light-yielded multivalent enhancers),[30] utilized fusion proteins containing six iLID domains alongside a fusion protein consisting of six SspB repeats separated by short linkers. This allowed the formation of cytosolic polymer networks upon illumination, which moreover reversibly dissociated in the dark. Target recruitment was demonstrated by fusion of mCherry and YFP.[30]

LLPS in Prokaryotes—Designing Membraneless Organelles in *Escherichia coli*. While all of the above-described systems were developed for use in mammalian cells or, at best, were adapted to drive LLPS in yeast, the development of *E. coli*-produced synthetic LLPS organelles is highly desirable from a biocatalytic application and sustainability perspective. Only very recently, two studies could demonstrate that indeed IDR/IDP-driven LLPS is possible in *E. coli* using natural and artificial IDR/IDPs as fusion modules to drive POI recruitment to LLPS droplets. Both strategies rely on constructs that are architecturally similar to the RGG-based REPs system (Figure 3B) but utilize different IDPs for LLPS.[22,41] The first study, by Wei et al.,[22] showed that, e.g., the expression of a protein module consisting of 16 repeats of the consensus sequence of the major ampullate spidroin 1 protein of *Nephila clavipes* (MaSp1-I16; abbreviated as I16 by the authors) alone is sufficient to induce the formation of cellular compartments, while fusion of GFP allowed tracking in living cells, also demonstrating target recruitment. Likewise, the coexpression of two similarly tagged fluorescent proteins (GFP and mCherry) verified colocalization of the two proteins within those compartments. Finally, the authors showed that their strategy can be used for assembling a synthetic reaction cascade to produce 1,3-diaminopropane (DAP) by the coexpression of two I16-tagged enzymes (for details, see the Application of Synthetic Organelles in Metabolic Engineering and Biocatalysis section). In a second study,[41] LLPS was realized in *E. coli* by using a subset of artificial IDRs (designated by the authors as A-IDPs), inspired by the *Drosophila melanogaster* Rec-1 resilin containing multiple repeats of the parent motif $(GRGDSPYS)_x$ (with x being the number of repeats, between 20 and 80) as well as variants thereof containing rational amino acid substitutions. For a set of those variants, robust LLPS was shown in mammalian cells and in *E. coli*. Selective colocalization was demonstrated for two A-IDPs with similar phase-behavior utilizing superfolder GFP (sfGFP) and red fluorescent protein mRuby3 tagged constructs. Moreover, the authors also demonstrated that small molecules and even protein fragments (demonstrated for split GFP) can penetrate the intracellularly formed compartments opening up the possibility to generate functionalized A-IDP droplets, which was also demonstrated in proof of principle experiments using β-galactosidase[41] (see also the Application

https://doi.org/10.1021/acssuschemeng.1c02045
ACS Sustainable Chem. Eng. 2021, 9, 8919−8945

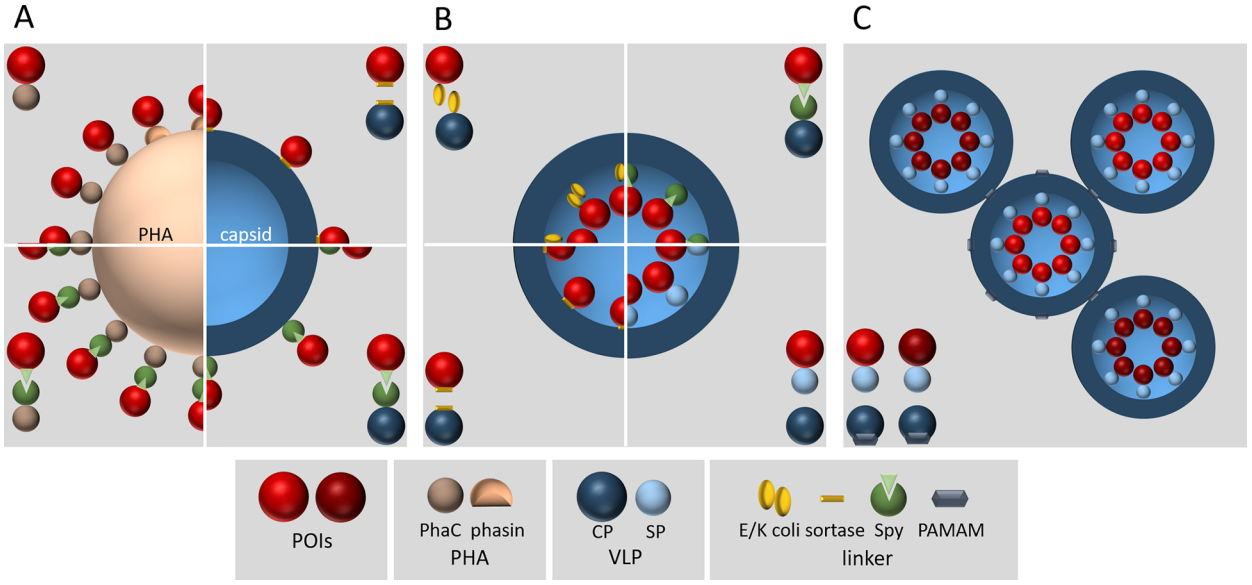

Figure 4. Polyhydroxyalkanoate (PHA) immobilizates and viruslike particles (VLPs). Engineered proteins required for respective POI immobilization as well as the resulting immobilizates are shown. Details are given in the text. (A) Carrier-based POI display. (top left) POI is covalently linked to a polyhydroxybutyrate (PHB) granule via PhaC or phasins. (bottom left) POI is covalently linked to PHB granule via the PhaC-SpyCatcher and POI-Spy tag. (top right) P22-VLP: POI is linked to capsid protein (CP) by the sortase SrtA (the yellow boxes symbolize the sorting signal peptide and the glycine-containing motif, respectively). (bottom right) T4- and B19-VLP: POI is linked to CP via the SpyCatcher/Tag system. (B) Carrier-based POI encapsulation. (top left) CCMV-VLP: POI is noncovalently linked to CP via E/K coil. (bottom left) CCMV-VLP: POI is linked to CP via SrtA. (top right) MS2-VLP: POI linked to CP via SpyCatcher/Tag. (bottom right) P22-VLP: POI covalently linked to truncated scaffolding protein (SP). (C) P22 super lattice. VLPs encapsulating different POIs were noncovalently interlinked by positively charged PAMAM dendrimers.

of Synthetic Organelles in Metabolic Engineering and Biocatalysis section). This underscores the liquidlike nature of those condensates, yet again highlighting that substrate diffusion is not a limiting factor.

Application of Synthetic Organelles in Metabolic Engineering and Biocatalysis. The ability to assemble and disassemble synthetic membraneless organelles within cells shows great potential for metabolic engineering. It could enable the on-demand compartmentalization of metabolic enzymes facilitating dynamic control of metabolic flux. The potential was demonstrated in a proof of concept study in which optogenetic clustering/LLPS tools were used in yeast to control the flux through the deoxyviolacein pathway.[103] Zhao and co-workers utilized the optoCluster and PixELL system to light-dependently enhance or suppress the metabolic flux through the deoxyviolacein pathway or control the flux through a two-enzyme metabolic branch point.[103] Similarly, first attempts were made to use the *E. coli* LLPS system, relying on enzyme fusions with the IDR I16 (*vide supra*), to realize the *de novo* synthesis of 1,3-diaminopropane within membraneless organelles.[22] The authors tagged both the L-2,4-diaminobutyrate:α-ketoglutarate 4-aminotransferase (Dat) and the L-2,4-diaminobutyrate decarboxylase (Ddc) with the I16 IDR, to facilitate the formation of membraneless organelles in *E. coli*. The corresponding cells, in turn, were utilized for the conversion of aspartate β-semialdehyde to 1,3-diaminopropane. However, the corresponding experiments did not show a clear advantage of the LLPS coimmobilized enzymes over the use of soluble expressed Dat and Ddc.[22] Second, the A-IDP approach (*vide supra*) was used to generate functionalized LLPS condensates in *E. coli* by recruiting the β-galactosidase enzyme to the droplets.[41] This was achieved by capitalizing on the widely used β-galactosidase (LacZ) blue−white screening system, in which the α peptide (αp) complements the mutated enzyme LacZΔM15, by interaction with it, to create a functional β-galactosidase enzyme. αp was therefore fused to an A-IDP−mRuby3 fragment, while inactive LacZΔM15 was coexpressed in *E. coli*. Using a fluorescein-based β-galactosidase substrate, the authors demonstrated an up to 7.5-fold increase in catalytic turnover for the droplet recruited enzyme compared to the soluble control without the A-IDP module. Based on the quantification of fluorescence production at various substrate concentrations, the authors reasoned that, while the Michaelis−Menten constant (K_m) of the enzyme for the substrate remained essentially unchanged, the colocalization of the enzyme and substrate within the droplets facilitated a better turnover by an increase in the turnover number K_{cat}.[41]

POLYHYDROXYALKANOATE-BASED SYSTEMS AND VIRUSLIKE PARTICLES

In addition to the strategies described in the first two parts of this Perspective, *in vivo* protein immobilization has also been achieved by attaching POIs via suited anchor proteins to natural and artificial cellular compartments offering a higher structural complexity.[19,20,109] To this end, (i) biological, often naturally occurring, membrane-separated compartments such as liposomes,[20] membrane vesicles,[110] and polymersomes;[111] or (ii) bacterial, membrane-free microcompartments such as carboxysomes,[38] metabolosomes,[19] magnetosomes,[37] bacterial bioplastic inclusions,[112,113] and viruslike particles[114−116] were rationally designed for target protein encapsulation or display. Given the diversity of nanocompartments, a comprehensive review of all available systems would exceed the scope of the present contribution. Therefore, we here describe some examples in more detail, whose applicability for *in vivo* enzyme immobilization could already be demonstrated.

https://doi.org/10.1021/acssuschemeng.1c02045
ACS Sustainable Chem. Eng. 2021, 9, 8919−8945

Polyhydroxyalkanoate Granule-Based POI Immobilization. Polyhydroxyalkanoates are linear polyesters composed of (*R*)-3-hydroxy fatty acids linked by ester bonds. Under conditions of carbon excess, they are naturally produced by various Gram-positive and Gram-negative bacteria as energy storage compounds.[33,117] Depending on the chain length of the fatty acid monomers, polyhydroxyalkanoates (PHAs) are categorized into three main classes: short- (3−5 carbon atoms), medium- (6−14 carbon atoms), and long-chain-length PHAs with more than 14 carbon atoms.[118,119] The biosynthesis of polyhydroxybutyrate (PHB), one of the PHA members that is most frequently used for POI immobilization, is catalyzed by three enzymes, starting with the β-ketothiolase PhaA condensing two acetyl-CoA subunits to form acetoacetyl-CoA. Acetoacetyl-CoA is subsequently reduced to D-3-hydroxybutyryl-CoA by the acetoacetyl-CoA reductase PhaB, and finally, the polymerization reaction is catalyzed by the PHB synthase PhaC.[120−122] PHAs have been widely evaluated as an environmentally friendly surrogate for petroleum-based plastics as the bioplastic can be sustainably synthesized in natural producers or engineered bacteria and exhibits beneficial properties including good biocompatibility, high biodegradability, and nontoxicity.[123] Under appropriate growth conditions, synthesized PHA makes up up to 90% of the cell dry weight and accumulates in the cytoplasm as spherical particles with a size of 100−500 nm.[124,125] Besides the hydrophobic PHA core, the granules are surrounded by a protein layer.[126,127] This layer is composed of different PHA-associated proteins including PhaC, different phasins (e.g., PhaP or PhaF), a depolymerase, and other regulatory and structural proteins.[127−129] Based on this observation, PHA granules were further used to develop a versatile *in vivo* protein immobilization and display technology.[112,113,130−135] In most cases, accordingly engineered *E. coli* strains, harboring the essential PHB biosynthesis genes, are applied for POI *in vivo* immobilization. For this purpose, the synthase PhaC can be employed as a versatile anchor protein, because it tolerates POI fusions at its N- and C-termini. The recombinant PhaC proteins remain covalently attached to the nascent PHB chain thereby forming an amphiphilic molecule capable of self-assembling into a POI-decorated PHB sphere.[113,130,136] In addition, phasins like PhaF are applicable as alternative anchor proteins that are able to guide a POI to the PHB core via hydrophobic interactions (Figure 4A).[137] Depending on the chosen anchor protein, the distribution of POIs as well as the stability of POI−PHB conjugates can differ remarkably.[138,139] POI-decorated PHB inclusions can be easily isolated from cell extracts by centrifugation.[140−142] A linker located between the POI and the respective PHB anchor protein, harboring, e.g., a protease cleavage or intein site, can be used for subsequent (auto)catalytic POI release from the PHB carrier.[132,136,143]

Proof of concept demonstrations for the applicability of *in vitro* or *in vivo* PHB-immobilized enzymes were reported, e.g., for the production of food ingredients, commodity and fine chemicals, as well as bioremediation (e.g., reviewed in ref 112). For example, a bacterial laccase-like multicopper oxidase (CueO), suitable for the degradation of harmful synthetic dyes, was fused to PhaF, a phasin derived from *P. putida* and expressed in *E. coli*.[135] After purification of the recombinant protein, CueO-PhaF was attached *in vitro* to commercially available PHB granules resulting in enzyme immobilizates with an improved catalytic performance in comparison to unfused CueO. Here, the catalytic activity of the POI-immobilizate was up to 40-fold higher leading to a significantly increased decolorization efficiency.[135] The authors assumed that this effect is due to a preferential accumulation of some of the tested dyes at the PHB surface thereby leading to an increased substrate support.[135] In contrast to the *in vitro* assembly approach, a P450-BM3 monooxygenase was tethered to PHB granules *in vivo* via a phasin fusion using *E. coli* as the production host.[141] Here, the POI−PHB complex was assembled in one step and subsequently purified, and the enzyme activity was compared to the unfused P450-BM3. In this case, POI immobilization led to a higher stability against elevated temperatures, low pH, and increased concentrations of urea and ions. Furthermore, the simplified purification procedure of P450-BM3-PHB conducted by centrifugation enabled the use of this enzyme immobilizate to convert 7-ethoxycoumarin to the antioxidant 7-hydroxycoumarin at the preparative reactor-scale.[141] Besides the examples described above, many more enzymes were *in vivo* immobilized using PHA-based approaches (e.g., recently summarized in ref 112). For example, noncovalent PHA immobilization mediated by PhaF or PhaP was applied for the β-galactosidase from *E. coli*,[144] the D-hydantoinase D-HDT from *Agrobacterium radiobacter*,[145] the lysine decarboxylase CadA from *E. coli*,[146] or the tetrameric organophosphorus anhydride hydrolase from *Pseudoalteromonas* sp.[138] Furthermore, there are also numerous applications where the POI was covalently bound to the PHB surface via PhaC,[112] including the α-amylase from *Bacillus licheniformis*,[131] the lipase B from *Candida antarctica*,[147] the lipase M37 from *Photobacterium lipolyticum*,[142] the hexavalent chromium reductase NemA from *E. coli*,[148] the *N*-acetylglucosamine 2-epimerase Sir1975 from *Synechocystis* sp. PCC6803,[149] the carbonic anhydrase from *Desulfovibrio vulgaris*,[150] the alkaline polygalacturonate lyase from *B. subtilis*,[151] the tyrosinase from *Verrucomicrobium spinosum*,[152] or the D-tagatose-3-epimerase DTW from *Pseudomonas cichorii*.[153] In recent studies, the PhaC-mediated POI immobilization platform was further improved by combining it with the SpyTag/SpyCatcher chemistry (Figure 4A), which enables better control over PHB decoration.[23,154] In this context, the authors demonstrated that the Spy-tagged POIs can be covalently bound to the SpyCatcher-PhaC-coated PHB particles *in vitro* and *in vivo* (see below).

Taken together, PHA granules represent a promising alternative carrier material suitable for efficient enzyme scaffolding. In many cases, enzyme immobilization on PHA surfaces led to an improved tolerance against elevated temperature, low pH, or different solvents[138,145] as well as to higher catalytic performance and recyclability. PHA thus expands the large group of natural biopolymers, which also includes, e.g., chitosan, cellulose, alginate, and agarose, that are basically suitable for the immobilization of enzymes (for example, recently reviewed by ref 155). However, in contrast to immobilization strategies with these biopolymeric carrier materials, the POI can be easily immobilized to biogenic PHA granules *in vitro* and *in vivo*, using different surface proteins as anchor molecules. *In vitro* functionalization of PHA granules has some advantages, including the maintenance of tight control over particle size and density of immobilized enzymes, but requires a more tedious process. In contrast, the *in vivo* production of POI-decorated PHA nanobeads can be directly implemented in bacterial cells thereby enabling their use as artificial cellular compartments in whole-cell biocatalysis. In addition, it is a low-cost, one-step production process for

https://doi.org/10.1021/acssuschemeng.1c02045
ACS Sustainable Chem. Eng. 2021, 9, 8919−8945

enzymatic active biopolymers making the *in vivo* approach convenient, efficient, and ecofriendly. However, *in vivo* formation of functionalized PHA particles intrinsically results in only limited control over POI surface coverage and particle sizes, which may restrict their applicability for flow-chemical bioprocesses. Furthermore, PHA particles tend to aggregate, and their nonporous character can further lead to high back-pressure in such processes. To overcome these limitations, Rehm and co-workers recently applied a porous alginate hydrogel as a matrix for embedding enzyme-coated PHB particles.[156]

Using Viruslike Particles as POI Encapsulating and Displaying Scaffolds. Viruslike particles (VLPs) are multiprotein complexes with a size of ∼20−200 nm that resemble the structural organization of corresponding virus envelopes. In general, they consist of one or more viral capsid proteins (CPs), which can be easily synthesized *in vivo* via heterologous gene expression using different microbial hosts such as *E. coli*, *S. cerevisiae*, and *Pichia pastoris* (e.g., refs 157−159). The CPs exhibit the intrinsic property for self-assembly, and due to the lack of genetic material, the resulting VLPs are nonreplicating and noninfectious. Different VLPs were established by employing CPs from the cowpea chlorotic mottle virus (CCMV), the cowpea mosaic virus (CPMV), the parvovirus B19, as well as the bacteriophages P22, Qβ, and MS2.[112,116,159] The broad variety of structurally diverse virus capsids thus provides a molecular platform allowing the application of the genetically modifiable CPs as building blocks for generating functionalized VLPs (e.g., reviewed in refs 114, 115, 160, and 161). In the past decade, the generation of various genetically engineered VLPs was described, and these have been applied in the biomedical sector as new vaccines or drug delivery systems. Furthermore, VLPs gained increasing interest as versatile proteinaceous carrier materials that can be modularly engineered to form biocatalytically active nanomaterials. As spherical VLPs can be seen as macromolecular shells, the POIs can principally be directed to either the interior or exterior of the virus capsid. To achieve this goal, different strategies were described that are applicable for either noncovalent or covalent linkage of the POIs and the envelope of the VLP.

VLP-Mediated POI Encapsulation. In the following section, we mainly describe the application of two different VLP systems that are based on the small RNA plant virus CCMV or the *Salmonella typhimurium* bacteriophage P22 and that have been extensively studied for either *in vitro* or *in vivo* enzyme encapsulation. The CCMV-based VLP was the first virus shell system that was evaluated for POI encapsulation since its CP can be easily expressed in *E. coli*. *In vitro* VLP assembly and disassembly can be reversibly triggered by shifting the pH value, which facilitates the passive packaging of cargo molecules. Furthermore, the N-terminus of the CCMV CP is located in the shell interior, which therefore intrinsically provides a suitable site for POI attachment and subsequent directed encapsulation (e.g., reviewed in ref 114). Directed noncovalent CCMV-mediated POI encapsulation, for instance, involves the heterodimerization of suitable coiled-coil domains such as the E and K coil domains[162] that can be genetically fused to the respective VLP CP and POI thereby conferring them the ability to stably bind to each other (Figure 4B). In a pioneering work, Cornelissen and co-workers used the CCMV CP for the E/K coil-mediated encapsulation of EGFP.[163] By fusing the K coil to the N-terminus of the CP and the E coil to the C-terminus of EGFP, their heterodimerization could be facilitated by the formation of a leucine zipperlike E-K coiled-coil structure. Subsequent *in vitro* VLP self-assembly experiments revealed that up to 15 EGFP molecules were encapsulated in the interior of a CCMV capsid. This technology was further applied for the packing of the lipase CalB from *Candida antarctica*.[164] The authors could demonstrate that CCMV-encapsulated CalB exhibits increased overall reaction rates as compared to the unmodified, soluble lipase, which is presumably caused by an increased efficiency of enzyme−substrate complex formation. However, the noncovalent VLP-mediated encapsulation of POIs can be accompanied by a variable or limited POI packaging density.[114] This observation led to the development of alternative encapsulation strategies relying on covalent POI tethering, generally resulting in an improved control over site-selectivity and VLP loading efficiency. In principle, the simplest way to obtain covalent POI encapsulation is the generation of a recombinant fusion protein consisting of a CP and a POI domain. This strategy was applied, for example, for the packaging of the fluorescent marker protein TFP in CCMV-based VLPs to avoid a dissociation of the E−K coiled-coil-based heterodimers.[165] A more sophisticated strategy to achieve the covalent encapsulation was recently developed employing the sortase SrtA-catalyzed formation of peptide bonds between POIs and capsid proteins (Figure 4B).[166−170] To this end, SrtA first recognizes the sorting signal peptide (LPXTG) that can be fused, for example, to the C-terminus of POIs followed by its enzymatic cleavage. In a second catalytic reaction, the truncated signal peptide is covalently linked to a glycine-containing motif, which is fused to the N-terminus of the VLP capsid protein. The applicability was, e.g., demonstrated by using the lipase CalB as a cargo protein. It could be shown that the encapsulation in this artificial compartment affected neither enzyme activity nor substrate diffusion and additionally exerted POI protection against proteases.[167] In a similar approach, GFP, the T4 lysozyme, and a heparin binding peptide were covalently encapsulated by SrtA in CCMV capsids.[168,170,171] In addition to SrtA-mediated covalent linkage, sequestration of PLP-dependent tryptophanase TnaA and monooxygenase PMO to the interior surface of the SpyTag-MS2 capsid (Figure 4B) could be achieved by using the SpyCatcher/SpyTag system (see below).

In contrast to the CCMV VLP, formation of the bacteriophage P22 additionally relies on the assistance of a scaffolding protein (SP), which directs the CP into the procapsid structure and is subsequently located inside the VLP shell (typically ∼100−300 copies per P22 VLP).[172] Remarkably, only the last 18 amino acid residues of the respective C-terminus are needed for proper P22 shell formation. Therefore, POIs can be genetically fused to the N-terminus of the truncated SP, which in turn allows the utilization of the engineered SP as a vehicle to obtain P22 VLP encapsulated POIs. Basically, coexpression of the POI-SP fusion protein and the P22 capsid protein in the heterologous expression host *E. coli* enables the formation of POI-containing VLPs *in vivo* (Figure 4B).[173,174] Because of the robustness of the *in vivo* P22 VLP assembly, this approach can also be applied for POIs that are very large (fusion proteins with sizes ≤180 kDa have been reported so far) or rather tend to aggregation or degradation.[175,176] Moreover, sequential expression of POI-SP and CP enables the synthesis of cofactor-containing enzymes. Here, POI folding and/or cofactor loading is performed before VLP encapsulation.[177,178] The applicability of P22 VLP-based POI

https://doi.org/10.1021/acssuschemeng.1c02045
ACS Sustainable Chem. Eng. 2021, 9, 8919−8945

packaging was demonstrated for various enzymes with increasing structural complexity including the monomeric alcohol dehydrogenase AdhD,[179,180] the α-galactosidase GalA,[175] the homodimeric FAD-binding NADH oxidase NOX,[181] and the homotetrameric β-glucosidase CelB from *Pyrococcus furiosus*[182,183] as well as the heme-containing P450 monooxygenase CYPBM3 (variant 21B3) from *Bacillus megaterium*,[178,184] the homodimeric, bifunctional glutathione synthase GshF from *Pasteurella multocida*,[185] and the heterodimeric [NiFe]-hydrogenase 1 (EcHyd-1) from *E. coli*.[177] The P22 VLP technology could be further used to implement multienzyme reaction cascades either via directed coencapsulation of various enzymes, whose catalytic activities are interconnected in a respective cascade reaction, or by the assembly of VLPs carrying different POIs into three-dimensional arrays (see below). For example, CelB was fused to the glucokinase GLUK and galactokinase GALK with flexible linkers to hydrolyze the disaccharide lactose into the monosaccharides galactose and glucose, which could subsequently be phosphorylated to form galactose-1-P and glucose-6-P.[176]

It can be assumed that enzyme encapsulation in P22 VLPs, which function as bacterial microcompartments, can lead to decreased enzymatic activities due to lower diffusion rates of the substrate, cofactor, or product molecules. However, so far there is no evidence that the P22 shell hampers those processes suggesting free diffusion of small molecules across the VLP wall.[180] Furthermore, colocalization of functionally coupled enzymes within the crowded interior space of VLPs may even enhance pathway kinetics via so-called diffusion channeling of intermediates.[172]

VLP-Based POI Display. Although the VLP-based POI display is mainly applied for biomedical applications as a technology platform for the generation of immunotherapeutic nanomaterials (e.g., reviewed by ref 115), some reports also describe the POI-decoration of capsid surfaces for biotechnological approaches (e.g., reviewed in ref 161). In that case, VLPs can be rationally designed to offer new catalytic or functional surface activities. In addition, functionalized surfaces can be applied for creating new VLP-based materials offering a higher three-dimensional complexity. As described for POI encapsulation, the surface display of target proteins can also be achieved by their noncovalent attachment or directed covalent linkage via SpyCatcher/SpyTag systems (see below).

In a recent approach, the encapsulation and surface display of POIs were combined to form biocatalytically active superlattices. First, the group of T. Douglas could demonstrate that the C-terminus of the P22 CP is exposed to the exterior of the VLP capsid thereby allowing the generation of surface modified P22 VLP variants.[186] Based on these findings, a strategy was developed that is based on sortase-catalyzed ligation to obtain a covalent linkage of a POI and P22 CP.[187] To this end, the authors genetically fused the above-mentioned LPXTG tag to the C-terminus of the CP and subsequently displayed GFP, offering a polyglycine peptide at its N-terminus, on the capsid surface (Figure 4A). Furthermore, by exposing the K or E coil on the capsid surface, the differently decorated virus shells could be transformed into building blocks capable of self-assembling into extended network structures.[186] This strategy was finally employed to assemble two different P22 VLPs encapsulating either the ketoisovalerate decarboxylase (KivD) or the alcohol dehydrogenase A (AdhA), which catalyze the synthesis of isobutanol from α-ketoisovalerate in a coupled two-step reaction.[188] The VLPs further display small negatively charged peptides on the capsid surfaces. Spontaneous self-assembly of the two VLP species into three-dimensional higher-order structures was subsequently facilitated by positively charged polyamidoamine (PAMAM) dendrimers (Figure 4C). Importantly, the resulting bifunctional PP2 VLP arrays could easily be recovered to enable their reuse and exhibited improved catalytic conversion *in vitro*. This result demonstrated that P22 VLP-based superlattices form porous structures allowing efficient diffusion of the substrate and product molecules.

Taken together, VLPs constitute a versatile POI immobilization platform for targeted encapsulation, scaffolding, and display of POIs *in vitro* and *in vivo* thereby providing tailor-made macromolecular assemblies where sequential biocatalytic reactions can be conducted in a concerted multienzyme reaction. Furthermore, recent advances in understanding and engineering these nanomaterials enabled the creation of new and highly functionalized synthetic nanobiological devices.

SpyCatcher SpyTag System—Covalent Functionalization of Carrier-Free and Carrier-Bound Immobilizates. Many Gram-positive bacteria including *Streptococcus pyogenes* (Spy) naturally express surface proteins that are able to spontaneously form intramolecular isopeptide bonds during folding.[189,190] One of these proteins is the fibronectin-binding adhesin FbaB,[191,192] which was shown to generate an isopeptide bond between Lys31 and Asp117 of the fibronectin binding domain CnaB2.[192] By splitting this domain into a short peptide designated as SpyTag (13 residues, contains the reactive aspartate) and the so-called SpyCatcher protein (138 residues harboring the reactive lysine), a new and powerful genetically encoded click-chemistry tool was developed that is suitable for a fast and specific covalent POI coupling with high affinity that can be applied *in vitro* and *in vivo*.[193,194] To this end, the SpyTag is fused to the N- or C-terminus of a POI or can even be inserted into internal positions.[193] To further improve this technology, the binding efficiency of both partners was enhanced by protein engineering approaches including truncations of the SpyCatcher and amino acid substitutions at selected positions of SpyCatcher and SpyTag.[195,196] For example, the amino acid sequence of the SpyCatcher002 variant starts with GAMVD instead of GAMVT, which leads to the faster formation of the covalent bond with SpyTag.[197] The removal of 23 N-terminal residues of the SpyCatcher protein (SpyCatcherΔN1) additionally enhances the ability to interact with the surface of VLPs.[195,198] Finally, SpyTag002 reacts faster with any SpyCatcher variant in comparison to SpyTag.[197] Recently, an orthologous system, without cross-reactivity to the SpyTag/SpyCatcher system, has been developed from the *Streptococcus pneumoniae* surface protein RrgA, D4 domain, which forms an isopeptide bond between Lys742 and Asp854.[199] The system consists of a so-called SnoopTag with residues 734−745 and SnoopCatcher with residues 749−860 of the D4 domain, and furthermore, mutations (G842T and D848G) were inserted to improve stability.[199] This system is also suitable for covalent binding of a POI to a reaction partner or a surface for enzyme immobilization.[200−202] To obtain a comprehensive overview of the available Spy systems and applications published so far, the group of Mark Howarth developed the SpyBank database offering more than 600 entries (https://www2.bioch.ox.ac.uk/howarth/info.htm; status, March 2021) with useful informa-

https://doi.org/10.1021/acssuschemeng.1c02045
ACS Sustainable Chem. Eng. 2021, 9, 8919−8945

tion including the applied expression host and Spy system configuration in the respective experiments.[196]

The Spy-technology has been frequently used to link one or more POIs to various macromolecular carriers. For example, PHA granules and VLPs were applied as matrices as briefly described above (Figure 4A,B). As already mentioned, PHB granules constitute a promising biopolymeric-based carrier material for the generation POI scaffolds. The group of Bernd Rehm recently applied a combination of the Spy system and PHB technology for biomedical and biotechnological applications.[23,154] Therefore, PHB granules were heterologously produced in *E. coli*, using the PHB synthase PhaC as an anchor to immobilize the SpyCatcher protein on the granule surface. The SpyCatcher-decorated nanobeads were subsequently applied *in vitro* for functionalization with Spy-tagged POIs like GFP, an α-amylase (BLA), and an organophosphohydrolase (OpdA), thereby enhancing the POI's functionality, stability, and reusability (Figure 4A). Furthermore, by mixing two or three POIs, tunable coimmobilization could be achieved.[23] In a following step, the system was transferred to an *in vivo* assembly process in *E. coli*, where the SpyCatcher-PHB particles and the Spy-tagged POIs were produced in the same host cell.[154]

In addition to PHA granules, VLPs represent a promising immobilization platform for biocatalytic approaches. It is therefore appealing to likewise combine this technology with the Spy and Snoop systems. To reconstitute the two-step indigo biosynthetic pathway inside MS2 VLPs, the PLP-dependent tryptophanase TnaA and monooxygenase PMO were fused to SpyCatcher and covalently linked to the interior surface of the SpyTag-MS2 capsid (Figure 4B).[203] Remarkably, an improved conversion of L-tryptophan to indigo could be demonstrated *in vitro* as well as in living *E. coli* cells. *In vitro* studies additionally revealed that MS2 packaging of these enzymes resulted in an increased storage stability. In an analogous SpyCatcher/Tag-based approach, VLPs could also successfully be coated with POIs (Figure 4A). For example, the T4 phage capsid was used as a scaffold to immobilize an amylase, maltase, and glucokinase via *in vitro* assembly. These three enzymes are part of a four-enzyme pathway, converting maltoheptaose and 6-phosphogluconolactone.[204] The enzymes were linked to the SpyTag, and the outer capsid protein Hoc was fused to SpyCatcher.[205] By detecting the formation of the byproduct NADH, it could be demonstrated that the virus capsid-based immobilization of the enzyme cascade resulted in an 18-times higher activity as compared to the respective enzymes in solution. Furthermore, Bustos-Jaimes and coworkers described the generation of a POI nanocarrier based on the parvovirus B19 VLP, whose shell is composed of the structural protein V2. POIs such as the lipase BplA from *B. pumilus* and α-glucosidase Ima1p from *S. cerevisiae* were either genetically inserted into V2 or covalently attached to its N-terminus via the SpyCatcher/SpyTag system resulting in enzyme-displaying B19 VLPs after *in vitro* self-assembly.[206,207] In the latter case, the displayed enzymes exhibited a higher temperature optimum and increased activity. The Catcher/Tag technology was further applied to generate an enzyme complex consisting of the three enzymes isopentenyl diphosphate isomerase (Idi), farnesyl pyrophosphate (FPP) synthase (IspA), and amorpha-4,11-diene synthase (ADS) by using the *Tobacco mosaic virus* (TMV)-based VLP as a protein scaffold.[202] To this end, either the SpyTag or the SnoopTag were fused to the respective CP, and Idi- and ADS-SnoopCatcher and IspA-SpyCatcher fusions were created. The enzyme-decorated VLP was assembled in a one-step approach using *E. coli* as a heterologous production host. Remarkably, amorpha-4,11-diene only accumulated in the VLP-immobilization approach, whereas no signal was detectable when unfused enzyme variants were used.[202]

Similar to VLPs, the ethanolamine utilization bacterial microcompartment proteins are able to form hexamers which, in turn, self-assemble into large protein filaments, when overexpressed in *E. coli*.[208,209] To use this microbial microcompartment for POI immobilization, the EutM protein from *Salmonella enterica* was fused to SpyCatcher and subsequently used as an *in vitro* scaffolding system for multienzyme cascades.[210] As a proof of concept, a two-step enzyme system consisting of an alcohol dehydrogenase and an amine dehydrogenase for chiral amine synthesis was tested *in vitro*. The ADH oxidizes an alcohol to a ketone intermediate, which is further reduced by the AmDH into a chiral amine. Each of the catalytic enzymes were combined with SpyTag to build a scaffold complex with SpyCatcher-tagged EutM domains. In comparison to unfused variants, the immobilized enzymes were stabilized and able to convert the substrate more efficiently.[210] In a following step, eight EutM homologues with a different scaffold structure were fused to the SpyCatcher domain allowing the generation of a multitude of possible hybrid scaffolds.[211,212]

For the functionalization of a bacterial biofilm consisting of *E. coli* cells, a chitinase, an exo-β-D-glucosaminidase, and a deacetylase suitable for conversion of α-chitin to glucosamine were immobilized on extracellular amyloid fiber structures consisting of CsgA curli proteins.[200,213] In many Enterobacteriaceae, CsgA monomers assemble after secretion into amyloid fibers which, in turn, are promising alternative scaffolds for Spy-assisted POI immobilization. In this case, the catalytic enzymes were combined with SpyTag or SpyCatcher as well as SnoopTag or SnoopCatcher in a distinct manner. After heterologous expression, POIs are secreted by the production host *E. coli* resulting in a spontaneous assembly of the functionalized amyloid structures. This approach led to a 2-times higher activity and tolerance toward nonphysiological temperature and pH values during production of glucosamine from α-chitin in comparison to unfused variants.[200]

In contrast to applications in which biopolymeric and proteinaceous carriers serve as a framework for enzyme immobilization, all-enzyme hydrogels represent an alternative where the biocatalytically active POI itself forms the matrix.[214−216] For example, a stereoselective alcohol dehydrogenase carrying a SpyCatcher domain and a cofactor-regenerating glucose 1-dehydrogenase fused to the SpyTag were used to reduce prochiral ketones.[214] Both enzymes form homotetramers, so that ultimately, each enzyme complex contains four SpyTag or SpyCatcher domains, respectively, capable of forming a hydrogel by latticelike interconnections of the recombinant POIs. For this approach, the proteins were overexpressed in *E. coli* and subsequently purified. After *in vitro* self-assembly, the POI-hydrogel was applied in continuous flow biocatalysis to produce chiral (*R*)-configured alcohols. This application led to conversion rates of up to 99% and offered a possibility to counteract the limitations of biocatalytic flow chemistry processes, since higher enzyme concentrations can be used, and at the same time, no carrier materials increase the pressure in the reaction cell.[214,217,218]

https://doi.org/10.1021/acssuschemeng.1c02045
ACS Sustainable Chem. Eng. 2021, 9, 8919−8945

Table 3. Comparison of POI *in Vivo* Immobilization Strategies Suitable for Biocatalytic Applications

immobilization system	Engineering effort	Heterologous production host	Size of *in vivo* immobilizates	applicability for biocatalysis[a]	pros/advantages	cons/limitations
IB display	very low to low	bacteria (*E. coli*) transferrable to other pro- and eukaryotic hosts	500 nm – 1 μm	yes (but limited) yes	▪ simplest strategy for *in vivo* POI immobilization ▪ high density allowing easy separation and purification	▪ only a few cases of rational POI targeting to IBs have been reported ▪ high proportion of POI offers reduced activity or is inactive ▪ no control over scaffolding process
CatIBs	low extended toolbox available	bacteria (*E. coli*) transferrable to other hosts	500 nm – 1 μm	yes yes	▪ high POI purities (80-95%) ▪ low effort/costs for purification ▪ web tools for evaluating the aggregation tendencies available	▪ POIs in lyophilized CatIB preparations displayed activities below 15% ▪ non-porous character can lead to high back-pressure in continuous flow processes and can cause limited substrate/product diffusion
Cry3aA entrapment	low	*B. thuringiensis*	< 1 μm	no yes	▪ direct isolation of immobilizates without further purification steps ▪ immobilized enzymes with high activities	▪ only small monomeric enzymes have been successfully immobilized ▪ cascade reactions with multiple enzymes might not be feasible ▪ the crystalline nature of the immobilizates might result in limited substrate/product diffusion
Forizymes	intermediate (co-expression of F4 is needed)	yeast plant cells	10 – 55 μm	yes yes	▪ large size allows e.g. filtration of immobilizates ▪ cascade reaction has been realized	▪ approach is so far restricted to eukaryotic expression hosts ▪ large forisome subunits needs to be fused to the POI ▪ likely prone to diffusional limitation due to crystalline nature
LLPS	low to intermediate (depending on the used system co-expression of multiple constructs needed)	mammalian cells, recently *E. coli*	< 1 μm	yes yes	▪ liquid- or gel-like nature enables easy substrate diffusion and on-demand recruitment of multiple enzymes at specific time points ▪ liquid-like environment does not impair proper protein folding	▪ LLPS droplets are not stable and dissociate below a certain critical concentration ▪ irreversible aging processes resulting in the formation of gels or glasses ▪ *E. coli* is not established as host for most systems
Polyhydroxy-alkanoate granules	intermediate (requires co-expression of *phaA* and *phaB*) extended toolbox available	bacteria (*E. coli*) transferrable to other prokaryotic hosts	100 – 500 nm	yes yes	▪ non-proteinaceous carrier material ▪ low effort/costs for purification ▪ orientation of POI is determined by the used PhaC fusion (N- or C-terminal) ▪ suitable for POI co-immobilization in combination with Spy/Snoop technology	▪ potential competition of PHA biosynthesis and POI-catalyzed reactions e.g., when the precursor acetyl-CoA is needed ▪ PHA particles tend to aggregate and their non-porous character can lead to high back-pressure in continuous flow processes
Virus-like particles	low to intermediate (depending on the used system, co-expression of a scaffolding protein might be needed) extended toolbox available	bacteria (*E. coli*) transferrable to other pro- and eukaryotic hosts including yeast	20 – 200 nm	yes yes	▪ can be used for POI encapsulation and POI-display ▪ homogeneous orientation and density of immobilized POIs ▪ highly monodisperse in shape and size ▪ especially suited for POI co-immobilization in combination with Spy/Snoop technology ▪ can increase sequential enzymatic conversions via diffusional channeling ▪ creation of super lattices possible (e.g. P22)	▪ genetic fusion of POI and CP can lead to misfolding and loss of activity thereby affecting VLP ▪ endogenous assembly behavior of some CPs (e.g. instability of CCMV capsid at physiological pH) hinders *in vivo* POI immobilization without further CP modifications ▪ relative small size of VLPs can limit the POI scaffolding process and complicate its isolation

[a]Applicable for *in vivo* co-immobilization (blue) and biotransformation (green).

https://doi.org/10.1021/acssuschemeng.1c02045
ACS Sustainable Chem. Eng. 2021, 9, 8919−8945

GENERAL CONCLUSIONS

The constantly growing toolbox for *in vivo* immobilization provides us with a plethora of different methods. In general, immobilization increases the operational stability (e.g., with respect to temperature, pH, ionic strength, organic solvents) as well as the shelf life of the immobilized POI and allows enzyme recycling for repetitive use. In addition, scaffolding of multiple enzymes brings them into close proximity to each other, thus providing the possibility for better substrate or intermediate channeling, e.g., allowing for cascade use. In comparison to other chemical immobilization strategies, the here described *in vivo* immobilization methods further benefit from their easy, environmentally friendly, cost-efficient, one-step production, by using sustainable feedstocks or industrial waste streams. In addition, the resulting enzyme immobilizates are nontoxic, biocompatible, and biodegradable thereby allowing their implementation into circular bioeconomy processes. However, as often is the case for emerging technologies, lab-scale applications have been shown for many of the described *in vivo* immobilization systems, but systematic studies that compare their efficacy and scalability are still missing. For many systems (forizymes, Cry3Aa immobilizates, LLPS systems), only a limited number of proof-of-concept studies are available. Thus, properties such as stability, recyclability, and even residual activity compared to the soluble, purified POI often remain undercharacterized or were simply not tested yet. A summary of advantages as well as limitations of the immobilization strategies considered in this Perspective are presented in Table 3.

In principle, only minor engineering efforts are needed for *in vivo* enzyme immobilization. In all cases, proper incorporation or display of POIs inside or on the surface of the respective biogenic carrier materials includes the genetic fusion of the POI with a protein domain that causes the self-assembly into respective immobilizate structures. For forizymes, liquid protein condensates, PHA, and VLPs, coexpression of the POI-anchor protein fusion with proteins or enzymes that are required to provide the polymeric immobilization matrix is needed. For most of the here described *in vivo* systems, engineering of fusion proteins is still a trial-and-error approach, and construct optimization might be necessary to obtain efficiently self-immobilizing catalysts. Some systems (i.e., CatIBs, PHA, and VLPs) already offer a modular immobilization toolbox allowing the comparative evaluation of different "pull down" tags, PHA anchors, or VLP capsids, whose application can result in remarkable differences of the particle properties (e.g., size, porosity, POI density, and activity). The *in vivo* production of POI immobilizates can be performed in either a narrow or a broad range of different host organisms. In most cases, the standard bacterial expression host *E. coli* is readily applicable, whereas the formation of forizymes requires yeast or plant cells. Cry3Aa immobilizates are commonly produced in *B. thuringiensis*, the natural host of the Cry3Aa protein. Liquid protein condensates are most often produced in mammalian cells, but yeast production and lately also the production in *E. coli* were shown to be feasible. Remarkably, some of the systems including CatIBs, PHA, and VLPs can be applied in various pro- and eukaryotic expression hosts including Gram-positive and Gram-negative bacteria as well as yeasts, thereby allowing the adaptation of the expression protocol to specific POI requirements, e.g., the absence of toxic LPS for biomedical applications or posttranslational modification of POIs with eukaryotic origin. Notably, the production of POI immobilizates beyond the laboratory scale requires well-established production hosts like *E. coli* or *S. cerevisiae* for which a wide range of different expression systems already exist. Depending on the respective application, the size of the POI immobilizates also matters, which can differ significantly ranging from ∼20 nm to 50 μm permitting isolation by simple centrifugation (e.g., CatIBs and PHAs) or alternatively requiring ultracentrifugation or size exclusion chromatography (e.g., some VLPs, forizymes). For *in vivo* POI coimmobilization, the presented VLP systems in combination with a "click-chemistry-like" Spy/Snoop-tag technology are particularly useful because a uniform orientation, coherent composition, and density of the immobilized POIs can be achieved. Like most enzyme immobilizates, also the here described *in vivo* generated immobilizates might suffer from suboptimal substrate turnover resulting from diffusional limitation, as they, like all immobilizates, require that substrates or products are crossing a physical barrier like a phase boundary (liquid/solid, liquid/gel, liquid/liquid) to reach the enzyme or be released from it after turnover. This, however, is in principal not the case for technologies that rely on POI-surface display such as IB display, most PHA-based strategies, and respective VLP-based protein display technologies. In those cases though, the immobilized enzymes might be more prone to inactivation by components of the reaction system as they are immobilized only on the surface of the "carrier". In contrast, most strategies that rely on POI encapsulation within microcompartment-like structures such as CatIBs-, Cry3aA-, and forisome-based immobilizates are likely to experience more severe diffusional limitation, although this issue has not been addressed empirically in all cases. In turn, due to the liquidlike properties of LLPS protein condensates, probably with the exception of those forming hydrogels, diffusional limitation should be much less of an issue as for the aforementioned encapsulation-based systems, where the substrate/product has to cross a liquid/solid phase boundary.

For future applications, expandability of the spatial structure and function, e.g., allowing the generation of multifunctionalized biomaterial, will be key. For most of the here presented immobilization systems, such expandability is limited; however, LLPS, CatIBs, PHA, and VLP systems might open up new avenues to design liquid, gel-like, or rigid supramolecular assemblies that may enable completely new biocatalytic applications.

ASSOCIATED CONTENT

Supporting Information

The Supporting Information is available free of charge at https://pubs.acs.org/doi/10.1021/acssuschemeng.1c02045.

A table of abbreviations used in the manuscript (PDF)

AUTHOR INFORMATION

Corresponding Authors

Thomas Drepper − *Institute of Molecular Enzyme Technology, Heinrich Heine University Düsseldorf, D-52425 Jülich, Germany*; Phone: ++49 2461-61-4173; Email: t.drepper@fz-juelich.de

Ulrich Krauss − *Institute of Molecular Enzyme Technology, Heinrich Heine University Düsseldorf, D-52425 Jülich, Germany; Institute of Bio- and Geosciences IBG-1: Biotechnology, Forschungszentrum Jülich GmbH, D-52425*

Jülich, Germany; orcid.org/0000-0003-2219-7388; Phone: ++49 2461-61-2939; Email: u.krauss@fz-juelich.de

Authors

Gizem Ölçücü − *Institute of Molecular Enzyme Technology, Heinrich Heine University Düsseldorf, D-52425 Jülich, Germany; Institute of Bio- and Geosciences IBG-1: Biotechnology, Forschungszentrum Jülich GmbH, D-52425 Jülich, Germany*

Oliver Klaus − *Institute of Molecular Enzyme Technology, Heinrich Heine University Düsseldorf, D-52425 Jülich, Germany*

Karl-Erich Jaeger − *Institute of Molecular Enzyme Technology, Heinrich Heine University Düsseldorf, D-52425 Jülich, Germany; Institute of Bio- and Geosciences IBG-1: Biotechnology, Forschungszentrum Jülich GmbH, D-52425 Jülich, Germany*

Complete contact information is available at: https://pubs.acs.org/10.1021/acssuschemeng.1c02045

Author Contributions

[§]G.Ö. and O.K. contributed equally.

Notes

The authors declare no competing financial interest.

Biographies

Gizem Ölçücü studied bioengineering at Montana State University, USA, and Istanbul Technical University, Turkey. She obtained her B.Sc. degrees from the bioengineering dual diploma program in 2012. In 2016, she obtained her M.Sc. degree on molecular life sciences from Friedrich Schiller University Jena, Germany. Since 2018, she has been pursuing her Ph.D. at the Institute of Molecular Enzyme Technology of the Heinrich-Heine-University Düsseldorf located at Forschungszentrum Jülich, Germany. She is interested in protein engineering and *in vivo* enzyme immobilization strategies, and her current research, within the "CLIB Competence Centre Biotechnology", is focused on catalytically active inclusion bodies and ferritin-based immobilizates for biotechnological applications.

Oliver Klaus studied biology at the Heinrich-Heine-University Düsseldorf (HHU), Germany. He finished his B.Sc. degree in 2015 and his M.Sc. degree in 2017. Since 2018, he performed his doctoral studies at the HHU Institute of Molecular Enzyme Technology, located at the Forschungszentrum Jülich, Germany. He is interested in the production of secondary metabolites in phototrophic bacteria and immobilization of biotechnologically relevant enzymes on polyhydroxybutyrate granules. His work is a part of the "CLIB Competence Centre Biotechnology" project and funded by the European Regional Development Fund.

Prof. Dr. Karl-Erich Jaeger studied biology and chemistry and obtained a Ph.D. in microbiology at Ruhr-University Bochum, Germany. From 1988 to 1989, he worked as a postdoc with Prof. Dr. Robert E.W. Hancock at the Department of Microbiology, University of British Columbia, Vancouver, B.C., Canada. In 2002, he became full professor at Heinrich-Heine-University Düsseldorf and director of the Institute of Molecular Enzyme Technology at Forschungszentrum Jülich. In 2013, the Forschungszentrum Jülich GmbH of the German Helmholtz Association additionally appointed him as director at the Institute of Bio- and Geosciences IBG-1: Biotechnology. Karl-Erich Jaeger published more than 200 research papers and 17 patent applications; he is an editorial board member of several scientific journals and serves as vice-president of the Cluster of Industrial Biotechnology—CLIB. His research interests are focused on bacterial enzymes and proteins, their identification, expression, biochemical and structural characterization, and biotechnological applications.

Dr. Thomas Drepper studied biology and received his diploma and Ph.D. from the Ruhr-Universität Bochum Bochum, Germany. Since 2004, he is head of the "Bacterial Photobiotechnology" group at the Institute of Molecular Enzyme Technology, Heinrich-Heine-University Düsseldorf, located at the Forschungszentrum Jülich, Germany. He published more than 70 peer-reviewed articles with an h index of 32 and more than 3000 citations (Google scholar). His current research focuses lie in synthetic biology, optogenetics, and natural product synthesis in phototrophic and nonphototrophic bacteria.

Dr. Ulrich Krauss studied applied natural sciences at the TU Bergakademie Freiberg, Germany, and obtained his Ph.D. in 2008 from the Heinrich-Heine-University Düsseldorf, Germany. From 2008 to 2010, he worked as a postdoc with Prof. Dr. Karl-Erich Jaeger and Prof. Dr. Wolfgang Gärtner at the Institute of Molecular Enzyme Technology, Heinrich-Heine-University Düsseldorf, Germany, and the Max-Planck Institute for Bioinorganic Chemistry (now MPI Chemical Energy Conversion), Mülheim an der Ruhr, Germany. Since 2009, he is heading the group "Molecular Biophotonics" at the Institute of Molecular Enzyme Technology, Heinrich-Heine-University Düsseldorf located at the Forschungszentrum Jülich, Germany. He published more than 40 peer-reviewed articles with an h index of 22 and more than 1700 citations (Google scholar). His research is focused on enzymes and photoreceptors covering the fields of photochemistry, photobiology, and optogenetics as well as biocatalysis, synthetic biology, and structural biochemistry.

■ ACKNOWLEDGMENTS

The research was financially supported by the CLIB Competence Centre Biotechnology (CKB) funded by the European Regional Development Fund ERDF (34.EFRE 0300096 and 34.EFRE 0300097).

■ REFERENCES

(1) Badenhorst, C. P. S.; Bornscheuer, U. T. Getting Momentum: From Biocatalysis to Advanced Synthetic Biology. *Trends Biochem. Sci.* **2018**, *43* (3), 180−198.
(2) Nestl, B. M.; Nebel, B. A.; Hauer, B. Recent progress in industrial biocatalysis. *Curr. Opin. Chem. Biol.* **2011**, *15* (2), 187−193.
(3) Truppo, M. D. Biocatalysis in the Pharmaceutical Industry: The Need for Speed. *ACS Med. Chem. Lett.* **2017**, *8* (5), 476−480.
(4) Liu, Z.; Wang, K.; Chen, Y.; Tan, T.; Nielsen, J. Third-generation biorefineries as the means to produce fuels and chemicals from CO_2. *Nat. Catal* **2020**, *3*, 274−288.
(5) Castro, G. R.; Knubovets, T. Homogeneous biocatalysis in organic solvents and water-organic mixtures. *Crit. Rev. Biotechnol.* **2003**, *23* (3), 195−231.
(6) Khmelnitsky, Y. L.; Rich, J. O. Biocatalysis in nonaqueous solvents. *Curr. Opin. Chem. Biol.* **1999**, *3* (1), 47−53.
(7) Sheldon, R. A. Biocatalysis and Biomass Conversion in Alternative Reaction Media. *Chem. - Eur. J.* **2016**, *22* (37), 12984−12999.
(8) Balcao, V. M.; Vila, M. M. Structural and functional stabilization of protein entities: state-of-the-art. *Adv. Drug Delivery Rev.* **2015**, *93*, 25−41.
(9) Guisan, J. M. New opportunities for immobilization of enzymes. *Methods Mol. Biol.* **2013**, *1051*, 1−13.
(10) Liese, A.; Hilterhaus, L. Evaluation of immobilized enzymes for industrial applications. *Chem. Soc. Rev.* **2013**, *42* (15), 6236−6249.
(11) Sheldon, R. A. Characteristic features and biotechnological applications of cross-linked enzyme aggregates (CLEAs). *Appl. Microbiol. Biotechnol.* **2011**, *92* (3), 467−477.
(12) Tufvesson, P.; Lima-Ramos, J.; Nordblad, M.; Woodley, J. M. Guidelines and cost analysis for catalyst production in biocatalytic processes. *Org. Process Res. Dev.* **2011**, *15*, 266−274.
(13) Homaei, A. A.; Sariri, R.; Vianello, F.; Stevanato, R. Enzyme immobilization: an update. *J. Chem. Biol.* **2013**, *6* (4), 185−205.
(14) Kress, J.; Zanaletti, R.; Amour, A.; Ladlow, M.; Frey, J. G.; Bradley, M. Enzyme accessibility and solid supports: which molecular weight enzymes can be used on solid supports? An investigation using confocal Raman microscopy. *Chem. - Eur. J.* **2002**, *8* (16), 3769−72.
(15) Bellapadrona, G.; Sinkar, S.; Sabanay, H.; Liljestrom, V.; Kostiainen, M.; Elbaum, M. Supramolecular Assembly and Coalescence of Ferritin Cages Driven by Designed Protein-Protein Interactions. *Biomacromolecules* **2015**, *16* (7), 2006−2011.
(16) Choi, S. L.; Lee, S. J.; Yeom, S. J.; Kim, H. J.; Rhee, Y. H.; Jung, H. C.; Lee, S. G. Controlled localization of functionally active proteins to inclusion bodies using leucine zippers. *PLoS One* **2014**, *9* (6), No. e97093.
(17) Diener, M.; Kopka, B.; Pohl, M.; Jaeger, K. E.; Krauss, U. Fusion of a coiled-coil domain facilitates the high-level production of catalytically active enzyme inclusion bodies. *ChemCatChem* **2016**, *8* (1), 142−152.
(18) Heater, B. S.; Yang, Z.; Lee, M. M.; Chan, M. K. In Vivo Enzyme Entrapment in a Protein Crystal. *J. Am. Chem. Soc.* **2020**, *142* (22), 9879−9883.
(19) Huber, I.; Palmer, D. J.; Ludwig, K. N.; Brown, I. R.; Warren, M. J.; Frunzke, J. Construction of Recombinant Pdu Metabolosome Shells for Small Molecule Production in *Corynebacterium glutamicum*. *ACS Synth. Biol.* **2017**, *6* (11), 2145−2156.
(20) Noireaux, V.; Libchaber, A. A vesicle bioreactor as a step toward an artificial cell assembly. *Proc. Natl. Acad. Sci. U. S. A.* **2004**, *101* (51), 17669−17674.
(21) Visser, F.; Muller, B.; Rose, J.; Prufer, D.; Noll, G. A. Forizymes - functionalised artificial forisomes as a platform for the production and immobilisation of single enzymes and multi-enzyme complexes. *Sci. Rep.* **2016**, *6*, 30839.
(22) Wei, S. P.; Qian, Z. G.; Hu, C. F.; Pan, F.; Chen, M. T.; Lee, S. Y.; Xia, X. X. Formation and functionalization of membraneless compartments in *Escherichia coli*. *Nat. Chem. Biol.* **2020**, *16* (10), 1143−1148.

https://doi.org/10.1021/acssuschemeng.1c02045
ACS Sustainable Chem. Eng. 2021, 9, 8919−8945

(23) Wong, J. X.; Rehm, B. H. A. Design of Modular Polyhydroxyalkanoate Scaffolds for Protein Immobilization by Directed Ligation. *Biomacromolecules* **2018**, *19* (10), 4098−4112.
(24) Zhou, B. H.; Xing, L.; Wu, W.; Zhang, X. E.; Lin, Z. L. Small surfactant-like peptides can drive soluble proteins into active aggregates. *Microb. Cell Fact.* **2012**, *11*, 10.
(25) Jäger, V. D.; Kloss, R.; Grünberger, A.; Seide, S.; Hahn, D.; Karmainski, T.; Piqueray, M.; Embruch, J.; Longerich, S.; Mackfeld, U.; Jaeger, K. E.; Wiechert, W.; Pohl, M.; Krauss, U. Tailoring the properties of (catalytically)-active inclusion bodies. *Microb. Cell Fact.* **2019**, *18*, 18.
(26) Krauss, U.; Jäger, V. D.; Diener, M.; Pohl, M.; Jaeger, K. E. Catalytically-active inclusion bodies carrier-free protein immobilizates for application in biotechnology and biomedicine. *J. Biotechnol.* **2017**, *258*, 136−147.
(27) Heater, B. S.; Lee, M. M.; Chan, M. K. Direct production of a genetically-encoded immobilized biodiesel catalyst. *Sci. Rep.* **2018**, *8* (1), 12783.
(28) Bracha, D.; Walls, M. T.; Wei, M. T.; Zhu, L.; Kurian, M.; Avalos, J. L.; Toettcher, J. E.; Brangwynne, C. P. Mapping Local and Global Liquid Phase Behavior in Living Cells Using Photo-Oligomerizable Seeds. *Cell* **2018**, *175* (6), 1467−1480.
(29) Li, P.; Banjade, S.; Cheng, H. C.; Kim, S.; Chen, B.; Guo, L.; Llaguno, M.; Hollingsworth, J. V.; King, D. S.; Banani, S. F.; Russo, P. S.; Jiang, Q. X.; Nixon, B. T.; Rosen, M. K. Phase transitions in the assembly of multivalent signalling proteins. *Nature* **2012**, *483* (7389), 336−340.
(30) Nakamura, H.; Lee, A. A.; Afshar, A. S.; Watanabe, S.; Rho, E.; Razavi, S.; Suarez, A.; Lin, Y. C.; Tanigawa, M.; Huang, B.; DeRose, R.; Bobb, D.; Hong, W.; Gabelli, S. B.; Goutsias, J.; Inoue, T. Intracellular production of hydrogels and synthetic RNA granules by multivalent molecular interactions. *Nat. Mater.* **2018**, *17* (1), 79−89.
(31) Schuster, B. S.; Reed, E. H.; Parthasarathy, R.; Jahnke, C. N.; Caldwell, R. M.; Bermudez, J. G.; Ramage, H.; Good, M. C.; Hammer, D. A. Controllable protein phase separation and modular recruitment to form responsive membraneless organelles. *Nat. Commun.* **2018**, *9* (1), 2985.
(32) Shin, Y.; Berry, J.; Pannucci, N.; Haataja, M. P.; Toettcher, J. E.; Brangwynne, C. P. Spatiotemporal Control of Intracellular Phase Transitions Using Light-Activated optoDroplets. *Cell* **2017**, *168* (1−2), 159−171.
(33) Rehm, F. B.; Chen, S.; Rehm, B. H. Enzyme Engineering for In Situ Immobilization. *Molecules* **2016**, *21* (10), 1370.
(34) Garcia-Fruitos, E.; Vazquez, E.; Diez-Gil, C.; Corchero, J. L.; Seras-Franzoso, J.; Ratera, I.; Veciana, J.; Villaverde, A. Bacterial inclusion bodies: making gold from waste. *Trends Biotechnol.* **2012**, *30* (2), 65−70.
(35) Li, H.; Zheng, G.; Zhu, S. Construction of an organelle-like nanodevice via supramolecular self-assembly for robust biocatalysts. *Microb. Cell Fact.* **2018**, *17* (1), 26.
(36) Bracha, D.; Walls, M. T.; Brangwynne, C. P. Probing and engineering liquid-phase organelles. *Nat. Biotechnol.* **2019**, *37* (12), 1435−1445.
(37) Ginet, N.; Pardoux, R.; Adryanczyk, G.; Garcia, D.; Brutesco, C.; Pignol, D. Single-step production of a recyclable nanobiocatalyst for organophosphate pesticides biodegradation using functionalized bacterial magnetosomes. *PLoS One* **2011**, *6* (6), No. e21442.
(38) Menon, B. B.; Dou, Z.; Heinhorst, S.; Shively, J. M.; Cannon, G. C. *Halothiobacillus neapolitanus* carboxysomes sequester heterologous and chimeric RubisCO species. *PLoS One* **2008**, *3* (10), No. e3570.
(39) Han, G. H.; Seong, W.; Fu, Y.; Yoon, P. K.; Kim, S. K.; Yeom, S. J.; Lee, D. H.; Lee, S. G. Leucine zipper-mediated targeting of multi-enzyme cascade reactions to inclusion bodies in *Escherichia coli* for enhanced production of 1-butanol. *Metab. Eng.* **2017**, *40*, 41−49.
(40) Jäger, V. D.; Lamm, R.; Küsters, K.; Ölcücü, G.; Oldiges, M.; Jaeger, K. E.; Büchs, J.; Krauss, U. Catalytically-active inclusion bodies for biotechnology-general concepts, optimization, and application. *Appl. Microbiol. Biotechnol.* **2020**, *104* (17), 7313−7329.
(41) Dzuricky, M.; Rogers, B. A.; Shahid, A.; Cremer, P. S.; Chilkoti, A. De novo engineering of intracellular condensates using artificial disordered proteins. *Nat. Chem.* **2020**, *12* (9), 814−825.
(42) Baneyx, F.; Mujacic, M. Recombinant protein folding and misfolding in *Escherichia coli*. *Nat. Biotechnol.* **2004**, *22* (11), 1399−1408.
(43) Rinas, U.; Garcia-Fruitos, E.; Corchero, J. L.; Vazquez, E.; Seras-Franzoso, J.; Villaverde, A. Bacterial Inclusion Bodies: Discovering Their Better Half. *Trends Biochem. Sci.* **2017**, *42* (9), 726−737.
(44) Rokney, A.; Shagan, M.; Kessel, M.; Smith, Y.; Rosenshine, I.; Oppenheim, A. B. E. coli transports aggregated proteins to the poles by a specific and energy-dependent process. *J. Mol. Biol.* **2009**, *392* (3), 589−601.
(45) Arie, J. P.; Miot, M.; Sassoon, N.; Betton, J. M. Formation of active inclusion bodies in the periplasm of *Escherichia coli*. *Mol. Microbiol.* **2006**, *62* (2), 427−437.
(46) Cousens, L. S.; Shuster, J. R.; Gallegos, C.; Ku, L.; Stempien, M. M.; Urdea, M. S.; Sanchez-Pescador, R.; Taylor, A.; Tekamp-Olson, P. High level expression of proinsulin in the yeast, *Saccharomyces cerevisiae*. *Gene* **1987**, *61* (3), 265−275.
(47) Kopito, R. R. Aggresomes, inclusion bodies and protein aggregation. *Trends Cell Biol.* **2000**, *10* (12), 524−530.
(48) Wang, L. Towards revealing the structure of bacterial inclusion bodies. *Prion* **2009**, *3* (3), 139−145.
(49) Singh, S. M.; Panda, A. K. Solubilization and refolding of bacterial inclusion body proteins. *J. Biosci Bioeng* **2005**, *99* (4), 303−310.
(50) Steinmann, B.; Christmann, A.; Heiseler, T.; Fritz, J.; Kolmar, H. In vivo enzyme immobilization by inclusion body display. *Appl. Environ. Microbiol.* **2010**, *76* (16), 5563−5569.
(51) Spieler, V.; Valldorf, B.; Maass, F.; Kleinschek, A.; Huttenhain, S. H.; Kolmar, H. Coupled reactions on bioparticles: Stereoselective reduction with cofactor regeneration on PhaC inclusion bodies. *Biotechnol. J.* **2016**, *11* (7), 890−898.
(52) Choi, S. L.; Lee, S. J.; Ha, J. S.; Song, J.; Rhee, Y. H.; Lee, S. G. Generation of catalytic protein particles in *Escherichia coli* cells using the cellulose-binding domain from *Cellulomonas fimi* as a fusion partner. *Biotechnol. Bioprocess Eng.* **2011**, *16* (6), 1173−1179.
(53) Worrall, D. M.; Goss, N. H. The formation of biologically active beta-galactosidase inclusion bodies in *Escherichia coli*. *Aust J. Biotechnol* **1989**, *3* (1), 28−32.
(54) de Marco, A.; Ferrer-Miralles, N.; Garcia-Fruitos, E.; Mitraki, A.; Peternel, S.; Rinas, U.; Trujillo-Roldan, M. A.; Valdez-Cruz, N. A.; Vazquez, E.; Villaverde, A. Bacterial inclusion bodies are industrially exploitable amyloids. *FEMS Microbiol Rev.* **2019**, *43* (1), 53−72.
(55) Köszagová, R. Inclusion Bodies in Biotechnology. *J. Microbiol., Biotechnol. Food Sci.* **2020**, *9* (6), 1191−1196.
(56) Slouka, C.; Kopp, J.; Spadiut, O.; Herwig, C. Perspectives of inclusion bodies for bio-based products: curse or blessing? *Appl. Microbiol. Biotechnol.* **2019**, *103* (3), 1143−1153.
(57) Chen, X.; Zaro, J. L.; Shen, W. C. Fusion protein linkers: property, design and functionality. *Adv. Drug Delivery Rev.* **2013**, *65* (10), 1357−1369.
(58) Huang, Z.; Zhang, C.; Chen, S.; Ye, F.; Xing, X. H. Active inclusion bodies of acid phosphatase PhoC: aggregation induced by GFP fusion and activities modulated by linker flexibility. *Microb. Cell Fact.* **2013**, *12*, 25.
(59) Kusters, K.; Pohl, M.; Krauss, U.; Olcucu, G.; Albert, S.; Jaeger, K. E.; Wiechert, W.; Oldiges, M. Construction and comprehensive characterization of an EcLDCc-CatIB set-varying linkers and aggregation inducing tags. *Microb. Cell Fact.* **2021**, *20* (1), 49.
(60) Jäger, V. D.; Lamm, R.; Kloss, R.; Kaganovitch, E.; Grünberger, A.; Pohl, M.; Büchs, J.; Jaeger, K. E.; Krauss, U. A synthetic reaction cascade implemented by colocalization of two proteins within catalytically active inclusion bodies. *ACS Synth. Biol.* **2018**, *7* (9), 2282−2295.
(61) Garcia-Fruitos, E.; Gonzalez-Montalban, N.; Morell, M.; Vera, A.; Ferraz, R. M.; Aris, A.; Ventura, S.; Villaverde, A. Aggregation as

bacterial inclusion bodies does not imply inactivation of enzymes and fluorescent proteins. *Microb. Cell Fact.* **2005**, *4*, 27.
(62) Lin, Z. L.; Zhou, B. H.; Wu, W.; Xing, L.; Zhao, Q. Self-assembling amphipathic alpha-helical peptides induce the formation of active protein aggregates *in vivo*. *Faraday Discuss.* **2013**, *166*, 243–256.
(63) Wu, W.; Xing, L.; Zhou, B.; Lin, Z. Active protein aggregates induced by terminally attached self-assembling peptide ELK16 in *Escherichia coli*. *Microb. Cell Fact.* **2011**, *10* (9), 9.
(64) Park, S. Y.; Park, S. H.; Choi, S. K. Active inclusion body formation using *Paenibacillus polymyxa* PoxB as a fusion partner in *Escherichia coli*. *Anal. Biochem.* **2012**, *426* (1), 63–65.
(65) Köszagová, R.; Krajcovic, T.; Palencarova-Talafova, K.; Patoprsty, V.; Vikartovska, A.; Pospiskova, K.; Safarik, I.; Nahalka, J. Magnetization of active inclusion bodies: comparison with centrifugation in repetitive biotransformations. *Microb. Cell Fact.* **2018**, *17*, 17.
(66) Han, H.; Zeng, W.; Zhang, G.; Zhou, J. Active tyrosine phenol-lyase aggregates induced by terminally attached functional peptides in *Escherichia coli*. *J. Ind. Microbiol. Biotechnol.* **2020**, *47* (8), 563–571.
(67) Wang, X.; Zhou, B. H.; Hu, W. K.; Zhao, Q.; Lin, Z. L. Formation of active inclusion bodies induced by hydrophobic self-assembling peptide GFIL8. *Microb. Cell Fact.* **2015**, *14*, 14.
(68) Jiang, L.; Xiao, W. J.; Zhou, X.; Wang, W. Y.; Fan, J. Comparative study of the insoluble and soluble Ulp1 protease constructs as carrier free and dependent protein immobilizates. *J. Biosci Bioeng* **2019**, *127* (1), 23–29.
(69) Kloss, R.; Karmainski, T.; Jäger, V. D.; Hahn, D.; Grünberger, A.; Baumgart, M.; Krauss, U.; Jaeger, K. E.; Wiechert, W.; Pohl, M. Tailor-made catalytically active inclusion bodies for different applications in biocatalysis. *Catal. Sci. Technol.* **2018**, *8* (22), 5816–5826.
(70) Kloss, R.; Limberg, M. H.; Mackfeld, U.; Hahn, D.; Grünberger, A.; Jäger, V. D.; Krauss, U.; Oldiges, M.; Pohl, M. Catalytically active inclusion bodies of L-lysine decarboxylase from *E. coli* for 1,5-diaminopentane production. *Sci. Rep.* **2018**, *8*, 8.
(71) Roca-Pinilla, R.; Fortuna, S.; Natalello, A.; Sanchez-Chardi, A.; Ami, D.; Aris, A.; Garcia-Fruitos, E. Exploring the use of leucine zippers for the generation of a new class of inclusion bodies for pharma and biotechnological applications. *Microb. Cell Fact.* **2020**, *19* (1), 175.
(72) Gil-Garcia, M.; Navarro, S.; Ventura, S. Coiled-coil inspired functional inclusion bodies. *Microb. Cell Fact.* **2020**, *19* (1), 117.
(73) Nahalka, J.; Nidetzky, B. Fusion to a pull-down domain: A novel approach of producing *Trigonopsis variabilis* D-amino acid oxidase as insoluble enzyme aggregates. *Biotechnol. Bioeng.* **2007**, *97* (3), 454–461.
(74) Nahalka, J.; Vikartovska, A.; Hrabarova, E. A crosslinked inclusion body process for sialic acid synthesis. *J. Biotechnol.* **2008**, *134* (1–2), 146–153.
(75) Nahalka, J.; Patoprsty, V. Enzymatic synthesis of sialylation substrates powered by a novel polyphosphate kinase (PPK3). *Org. Biomol. Chem.* **2009**, *7* (9), 1778–1780.
(76) Schwaighofer, A.; Ablasser, S.; Lux, L.; Kopp, J.; Herwig, C.; Spadiut, O.; Lendl, B.; Slouka, C. Production of Active Recombinant Hyaluronidase Inclusion Bodies from *Apis mellifera* in E. coli Bl21(DE3) and characterization by FT-IR Spectroscopy. *Int. J. Mol. Sci.* **2020**, *21* (11), 3881.
(77) Pastuszka, M. K.; MacKay, J. A. Engineering structure and function using thermoresponsive biopolymers. *WIREs Nanomed Nanobiotechnol.* **2016**, *8* (1), 123–138.
(78) Wang, R.; Li, J.; Dang, D.; Hu, J.; Hu, Y.; Fan, J. Bacterial production of maize and human serine racemases as partially active inclusion bodies for d-serine synthesis. *Enzyme Microb. Technol.* **2020**, *137*, 109547.
(79) Ji, W.; Sun, W.; Feng, J.; Song, T.; Zhang, D.; Ouyang, P.; Gu, Z.; Xie, J. , Characterization of a novel N-acetylneuraminic acid lyase favoring industrial N-acetylneuraminic acid synthesis. *Sci. Rep.* **2015**, *5*, 5.
(80) Latham, J. R.; Love, M.; Hilbeck, A. The distinct properties of natural and GM cry insecticidal proteins. *Biotechnol. Genet. Eng. Rev.* **2017**, *33* (1), 62–96.
(81) Park, H.-W.; Ge, B.; Bauer, L. S.; Federici, B. A. Optimization of Cry3A Yields in *Bacillus thuringiensis* by Use of Sporulation-Dependent Promoters in Combination with the STAB-SD mRNA Sequence. *Appl. Environ. Microbiol.* **1998**, *64* (10), 3932–3938.
(82) Hammond, B. G.; Koch, M. S. A Review of the Food Safety of Bt Crops. In *Bacillus thuringiensis Biotechnology*; Sansinenea, E., Ed.; Springer: Dordrecht, 2012; pp 305–325.
(83) Nair, M. S.; Lee, M. M.; Bonnegarde-Bernard, A.; Wallace, J. A.; Dean, D. H.; Ostrowski, M. C.; Burry, R. W.; Boyaka, P. N.; Chan, M. K. Cry protein crystals: a novel platform for protein delivery. *PLoS One* **2015**, *10* (6), No. e0127669.
(84) Heater, B. S.; Chan, W. S.; Lee, M. M.; Chan, M. K. Directed evolution of a genetically encoded immobilized lipase for the efficient production of biodiesel from waste cooking oil. *Biotechnol. Biofuels* **2019**, *12*, 165.
(85) Sun, Q.; Cheng, S. W.; Cheung, K.; Lee, M. M.; Chan, M. K. Cry Protein Crystal-Immobilized Metallothioneins for Bioremediation of Heavy Metals from Water. *Crystals* **2019**, *9* (6), 287.
(86) Noll, G. A.; Müller, B.; Ernst, A. M.; Rüping, B.; Twyman, R. M.; Prüfer, D. Native and artificial forisomes: functions and applications. *Appl. Microbiol. Biotechnol.* **2011**, *89* (6), 1675–1682.
(87) Müller, B.; Groscurth, S.; Menzel, M.; Rüping, B. A.; Twyman, R. M. D.; Prüfer, D.; Noll, G. A. Molecular and ultrastructural analysis of forisome subunits reveals the principles of forisome assembly. *Ann. Bot.* **2014**, *113* (7), 1121–1137.
(88) Müller, B.; Noll, G. A.; Ernst, A. M.; Rüping, B.; Groscurth, S.; Twyman, R. M.; Kawchuk, L. M.; Prüfer, D. Recombinant artificial forisomes provide ample quantities of smart biomaterials for use in technical devices. *Appl. Microbiol. Biotechnol.* **2010**, *88* (3), 689–698.
(89) Knoblauch, M.; Stubenrauch, M.; van Bel, A. J.; Peters, W. S. Forisome performance in artificial sieve tubes. *Plant, Cell Environ.* **2012**, *35* (8), 1419–1427.
(90) Groscurth, S.; Müller, B.; Schwan, S.; Menzel, M.; Diekstall, F.; Senft, M.; Kendall, A.; Kommor, B. A.; Neumann, U.; Kalischuk, M.; Kawchuk, L. M.; Krzyzanek, V.; Heilmann, A.; Stubbs, G.; Twyman, R. M.; Prüfer, D.; Noll, G. A. Artificial Forisomes Are Ideal Models of Forisome Assembly and Activity That Allow the Development of Technical Devices. *Biomacromolecules* **2012**, *13* (10), 3076–3086.
(91) Hyman, A. A.; Weber, C. A.; Julicher, F. Liquid-liquid phase separation in biology. *Annu. Rev. Cell Dev. Biol.* **2014**, *30*, 39–58.
(92) Brangwynne, C. P.; Eckmann, C. R.; Courson, D. S.; Rybarska, A.; Hoege, C.; Gharakhani, J.; Julicher, F.; Hyman, A. A. Germline P granules are liquid droplets that localize by controlled dissolution/condensation. *Science* **2009**, *324* (5935), 1729–1732.
(93) Alberti, S. The wisdom of crowds: regulating cell function through condensed states of living matter. *J. Cell Sci.* **2017**, *130* (17), 2789–2796.
(94) Marnik, E. A.; Updike, D. L. Membraneless organelles: P granules in *Caenorhabditis elegans*. *Traffic* **2019**, *20* (6), 373–379.
(95) Latonen, L. Phase-to-Phase With Nucleoli - Stress Responses, Protein Aggregation and Novel Roles of RNA. *Front. Cell. Neurosci.* **2019**, *13*, 151.
(96) Gibson, B. A.; Doolittle, L. K.; Schneider, M. W. G.; Jensen, L. E.; Gamarra, N.; Henry, L.; Gerlich, D. W.; Redding, S.; Rosen, M. K. Organization of Chromatin by Intrinsic and Regulated Phase Separation. *Cell* **2019**, *179* (2), 470–484.
(97) Molliex, A.; Temirov, J.; Lee, J.; Coughlin, M.; Kanagaraj, A. P.; Kim, H. J.; Mittag, T.; Taylor, J. P. Phase separation by low complexity domains promotes stress granule assembly and drives pathological fibrillization. *Cell* **2015**, *163* (1), 123–133.
(98) Case, L. B.; Zhang, X.; Ditlev, J. A.; Rosen, M. K. Stoichiometry controls activity of phase-separated clusters of actin signaling proteins. *Science* **2019**, *363* (6431), 1093–1097.
(99) Alberti, S.; Gladfelter, A.; Mittag, T. Considerations and Challenges in Studying Liquid-Liquid Phase Separation and Biomolecular Condensates. *Cell* **2019**, *176* (3), 419–434.

https://doi.org/10.1021/acssuschemeng.1c02045
ACS Sustainable Chem. Eng. 2021, 9, 8919–8945

(100) Feng, Z.; Chen, X.; Wu, X.; Zhang, M. Formation of biological condensates via phase separation: Characteristics, analytical methods, and physiological implications. *J. Biol. Chem.* **2019**, *294* (40), 14823−14835.
(101) Banani, S. F.; Lee, H. O.; Hyman, A. A.; Rosen, M. K. Biomolecular condensates: organizers of cellular biochemistry. *Nat. Rev. Mol. Cell Biol.* **2017**, *18* (5), 285−298.
(102) Dine, E.; Gil, A. A.; Uribe, G.; Brangwynne, C. P.; Toettcher, J. E. Protein Phase Separation Provides Long-Term Memory of Transient Spatial Stimuli. *Cell Syst* **2018**, *6* (6), 655−663.
(103) Zhao, E. M.; Suek, N.; Wilson, M. Z.; Dine, E.; Pannucci, N. L.; Gitai, Z.; Avalos, J. L.; Toettcher, J. E. Light-based control of metabolic flux through assembly of synthetic organelles. *Nat. Chem. Biol.* **2019**, *15* (6), 589−597.
(104) Zhang, H. The glassiness of hardening protein droplets. *Science* **2020**, *370* (6522), 1271−1272.
(105) Thompson, K. E.; Bashor, C. J.; Lim, W. A.; Keating, A. E. SYNZIP protein interaction toolbox: in vitro and in vivo specifications of heterospecific coiled-coil interaction domains. *ACS Synth. Biol.* **2012**, *1* (4), 118−129.
(106) Banaszynski, L. A.; Liu, C. W.; Wandless, T. J. Characterization of the FKBP.rapamycin.FRB ternary complex. *J. Am. Chem. Soc.* **2005**, *127* (13), 4715−4721.
(107) Waris, S.; Wilce, M. C.; Wilce, J. A. RNA recognition and stress granule formation by TIA proteins. *Int. J. Mol. Sci.* **2014**, *15* (12), 23377−23388.
(108) Guntas, G.; Hallett, R. A.; Zimmerman, S. P.; Williams, T.; Yumerefendi, H.; Bear, J. E.; Kuhlman, B. Engineering an improved light-induced dimer (iLID) for controlling the localization and activity of signaling proteins. *Proc. Natl. Acad. Sci. U. S. A.* **2015**, *112* (1), 112−117.
(109) Chowdhury, C.; Sinha, S.; Chun, S.; Yeates, T. O.; Bobik, T. A. Diverse bacterial microcompartment organelles. *Microbiol. Mol. Biol. Rev.* **2014**, *78* (3), 438−68.
(110) Turner, K. B.; Dean, S. N.; Walper, S. A. Bacterial bioreactors: Outer membrane vesicles for enzyme encapsulation. *Methods Enzymol.* **2019**, *617*, 187−216.
(111) De Hoog, H. P.; Arends, I. W.; Rowan, A. E.; Cornelissen, J. J.; Nolte, R. J. A hydrogel-based enzyme-loaded polymersome reactor. *Nanoscale* **2010**, *2* (5), 709−716.
(112) Wong, J. X.; Ogura, K.; Chen, S.; Rehm, B. H. A. Bioengineered Polyhydroxyalkanoates as Immobilized Enzyme Scaffolds for Industrial Applications. *Front. Bioeng. Biotechnol.* **2020**, *8*, 156.
(113) Hooks, D. O.; Venning-Slater, M.; Du, J.; Rehm, B. H. Polyhydroyxalkanoate synthase fusions as a strategy for oriented enzyme immobilisation. *Molecules* **2014**, *19* (6), 8629−8643.
(114) Wilkerson, J. W.; Yang, S. O.; Funk, P. J.; Stanley, S. K.; Bundy, B. C. Nanoreactors: Strategies to encapsulate enzyme biocatalysts in virus-like particles. *New Biotechnol.* **2018**, *44*, 59−63.
(115) Charlton Hume, H. K.; Vidigal, J.; Carrondo, M. J. T.; Middelberg, A. P. J.; Roldao, A.; Lua, L. H. L. Synthetic biology for bioengineering virus-like particle vaccines. *Biotechnol. Bioeng.* **2019**, *116* (4), 919−935.
(116) Ren, H.; Zhu, S.; Zheng, G. Nanoreactor Design Based on Self-Assembling Protein Nanocages. *Int. J. Mol. Sci.* **2019**, *20* (3), 592.
(117) Schlegel, H. G.; Gottschalk, G.; Von Bartha, R. Formation and utilization of poly-beta-hydroxybutyric acid by Knallgas bacteria (Hydrogenomonas). *Nature* **1961**, *191*, 463−465.
(118) Steinbüchel, A.; Valentin, H. E. Diversity of bacterial polyhydroxyalkanoic acids. *FEMS Microbiol. Lett.* **1995**, *128* (3), 219−228.
(119) Park, S. J.; Kim, T. W.; Kim, M. K.; Lee, S. Y.; Lim, S. C. Advanced bacterial polyhydroxyalkanoates: towards a versatile and sustainable platform for unnatural tailor-made polyesters. *Biotechnol. Adv.* **2012**, *30* (6), 1196−1206.
(120) Merrick, J. M.; Doudoroff, M. Enzymatic synthesis of poly-beta-hydroxybutyric acid in bacteria. *Nature* **1961**, *189*, 890−892.
(121) Peoples, O. P.; Sinskey, A. J. Poly-beta-hydroxybutyrate (PHB) biosynthesis in *Alcaligenes eutrophus* H16. Identification and characterization of the PHB polymerase gene (phbC). *J. Biol. Chem.* **1989**, *264* (26), 15298−15303.
(122) Jendrossek, D.; Pfeiffer, D. New insights in the formation of polyhydroxyalkanoate granules (carbonosomes) and novel functions of poly(3-hydroxybutyrate). *Environ. Microbiol.* **2014**, *16* (8), 2357−2373.
(123) Chen, G. Q. A microbial polyhydroxyalkanoates (PHA) based bio- and materials industry. *Chem. Soc. Rev.* **2009**, *38* (8), 2434−2446.
(124) Madison, L. L.; Huisman, G. W. Metabolic engineering of poly(3-hydroxyalkanoates): from DNA to plastic. *Microbiol. Mol. Biol. Rev.* **1999**, *63* (1), 21−53.
(125) Moradali, M. F.; Rehm, B. H. A. Bacterial biopolymers: from pathogenesis to advanced materials. *Nat. Rev. Microbiol.* **2020**, *18* (4), 195−210.
(126) Barnard, G. N.; Sanders, J. K. The poly-beta-hydroxybutyrate granule in vivo. A new insight based on NMR spectroscopy of whole cells. *J. Biol. Chem.* **1989**, *264* (6), 3286−3291.
(127) Gerngross, T. U.; Reilly, P.; Stubbe, J.; Sinskey, A. J.; Peoples, O. P. Immunocytochemical analysis of poly-beta-hydroxybutyrate (PHB) synthase in *Alcaligenes eutrophus* H16: localization of the synthase enzyme at the surface of PHB granules. *J. Bacteriol.* **1993**, *175* (16), 5289−5293.
(128) Prieto, M. A.; Buhler, B.; Jung, K.; Witholt, B.; Kessler, B. PhaF, a polyhydroxyalkanoate-granule-associated protein of *Pseudomonas oleovorans* GPo1 involved in the regulatory expression system for pha genes. *J. Bacteriol.* **1999**, *181* (3), 858−68.
(129) Potter, M.; Steinbuchel, A. Poly(3-hydroxybutyrate) granule-associated proteins: impacts on poly(3-hydroxybutyrate) synthesis and degradation. *Biomacromolecules* **2005**, *6* (2), 552−560.
(130) Peters, V.; Rehm, B. H. In vivo monitoring of PHA granule formation using GFP-labeled PHA synthases. *FEMS Microbiol. Lett.* **2005**, *248* (1), 93−100.
(131) Rasiah, I. A.; Rehm, B. H. One-step production of immobilized alpha-amylase in recombinant *Escherichia coli*. *Appl. Environ. Microbiol.* **2009**, *75* (7), 2012−2006.
(132) Geng, Y.; Wang, S.; Qi, Q. Expression of active recombinant human tissue-type plasminogen activator by using in vivo polyhydroxybutyrate granule display. *Appl. Environ. Microbiol.* **2010**, *76* (21), 7226−7230.
(133) Hafizi, A.; Malboobi, M. A.; Jalali-Javaran, M.; Maliga, P.; Alizadeh, H. Covalent-display of an active chimeric-recombinant tissue plasminogen activator on polyhydroxybutyrate granules surface. *Biotechnol. Lett.* **2017**, *39* (11), 1683−1688.
(134) Stenger, B.; Gerber, A.; Bernhardt, R.; Hannemann, F. Functionalized poly(3-hydroxybutyric acid) bodies as new in vitro biocatalysts. *Biochim. Biophys. Acta, Proteins Proteomics* **2018**, *1866* (1), 52−59.
(135) Bello-Gil, D.; Roig-Molina, E.; Fonseca, J.; Sarmiento-Ferrandez, M. D.; Ferrandiz, M.; Franco, E.; Mira, E.; Maestro, B.; Sanz, J. M. An enzymatic system for decolorization of wastewater dyes using immobilized CueO laccase-like multicopper oxidase on poly-3-hydroxybutyrate. *Microb. Biotechnol.* **2018**, *11* (5), 881−892.
(136) Du, J.; Rehm, B. H. A. Purification of target proteins from intracellular inclusions mediated by intein cleavable polyhydroxyalkanoate synthase fusions. *Microb. Cell Fact.* **2017**, *16* (1), 184.
(137) Tarazona, N. A.; Machatschek, R.; Schulz, B.; Prieto, M. A.; Lendlein, A. Molecular Insights into the Physical Adsorption of Amphiphilic Protein PhaF onto Copolyester Surfaces. *Biomacromolecules* **2019**, *20* (9), 3242−3252.
(138) Li, R.; Yang, J.; Xiao, Y.; Long, L. In vivo immobilization of an organophosphorus hydrolyzing enzyme on bacterial polyhydroxyalkanoate nano-granules. *Microb. Cell Fact.* **2019**, *18* (1), 166.
(139) Dinjaski, N.; Prieto, M. A. Smart polyhydroxyalkanoate nanobeads by protein based functionalization. *Nanomedicine* **2015**, *11* (4), 885−899.
(140) Gerngross, T. U.; Snell, K. D.; Peoples, O. P.; Sinskey, A. J.; Csuhai, E.; Masamune, S.; Stubbe, J. Overexpression and purification

of the soluble polyhydroxyalkanoate synthase from *Alcaligenes eutrophus*: evidence for a required posttranslational modification for catalytic activity. *Biochemistry* **1994**, *33* (31), 9311−9320.
(141) Lee, J. H.; Nam, D. H.; Lee, S. H.; Park, J. H.; Park, S. J.; Lee, S. H.; Park, C. B.; Jeong, K. J. New platform for cytochrome p450 reaction combining in situ immobilization on biopolymer. *Bioconjugate Chem.* **2014**, *25* (12), 2101−4.
(142) Yang, T. H.; Kwon, M. A.; Lee, J. Y.; Choi, J. E.; Oh, J. Y.; Song, J. K. In situ immobilized lipase on the surface of intracellular polyhydroxybutyrate granules: preparation, characterization, and its promising use for the synthesis of fatty acid alkyl esters. *Appl. Biochem. Biotechnol.* **2015**, *177* (7), 1553−1564.
(143) Banki, M. R.; Gerngross, T. U.; Wood, D. W. Novel and economical purification of recombinant proteins: intein-mediated protein purification using in vivo polyhydroxybutyrate (PHB) matrix association. *Protein Sci.* **2005**, *14* (6), 1387−1395.
(144) Moldes, C.; Garcia, P.; Garcia, J. L.; Prieto, M. A. In vivo immobilization of fusion proteins on bioplastics by the novel tag BioF. *Appl. Environ. Microbiol.* **2004**, *70* (6), 3205−3212.
(145) Chen, S. Y.; Chien, Y. W.; Chao, Y. P. In vivo immobilization of D-hydantoinase in *Escherichia coli*. *J. Biosci Bioeng* **2014**, *118* (1), 78−81.
(146) Seo, H. M.; Kim, J. H.; Jeon, J. M.; Song, H. S.; Bhatia, S. K.; Sathiyanarayanan, G.; Park, K.; Kim, K. J.; Lee, S. H.; Kim, H. J.; Yang, Y. H. In situ immobilization of lysine decarboxylase on a biopolymer by fusion with phasin: Immobilization of CadA on intracellular PHA. *Process Biochem.* **2016**, *51* (10), 1413.
(147) Jahns, A. C.; Rehm, B. H. Immobilization of active lipase B from *Candida antarctica* on the surface of polyhydroxyalkanoate inclusions. *Biotechnol. Lett.* **2015**, *37* (4), 831−835.
(148) Robins, K. J.; Hooks, D. O.; Rehm, B. H.; Ackerley, D. F. *Escherichia coli* NemA is an efficient chromate reductase that can be biologically immobilized to provide a cell free system for remediation of hexavalent chromium. *PLoS One* **2013**, *8* (3), No. e59200.
(149) Hooks, D. O.; Blatchford, P. A.; Rehm, B. H. Bioengineering of bacterial polymer inclusions catalyzing the synthesis of N-acetylneuraminic acid. *Appl. Environ. Microbiol.* **2013**, *79* (9), 3116−3121.
(150) Hooks, D. O.; Rehm, B. H. Surface display of highly-stable *Desulfovibrio vulgaris* carbonic anhydrase on polyester beads for CO2 capture. *Biotechnol. Lett.* **2015**, *37* (7), 1415−20.
(151) Ran, G.; Tan, D.; Dai, W.; Zhu, X.; Zhao, J.; Ma, Q.; Lu, X. Immobilization of alkaline polygalacturonate lyase from *Bacillus subtilis* on the surface of bacterial polyhydroxyalkanoate nano-granules. *Appl. Microbiol. Biotechnol.* **2017**, *101* (8), 3247−3258.
(152) Tan, D.; Zhao, J. P.; Ran, G. Q.; Zhu, X. L.; Ding, Y.; Lu, X. Y. Highly efficient biocatalytic synthesis of L-DOPA using in situ immobilized Verrucomicrobium spinosum tyrosinase on polyhydroxyalkanoate nano-granules. *Appl. Microbiol. Biotechnol.* **2019**, *103* (14), 5663−5678.
(153) Ran, G.; Tan, D.; Zhao, J.; Fan, F.; Zhang, Q.; Wu, X.; Fan, P.; Fang, X.; Lu, X. Functionalized polyhydroxyalkanoate nano-beads as a stable biocatalyst for cost-effective production of the rare sugar d-allulose. *Bioresour. Technol.* **2019**, *289*, 121673.
(154) Wong, J. X.; Gonzalez-Miro, M.; Sutherland-Smith, A. J.; Rehm, B. H. A. Covalent Functionalization of Bioengineered Polyhydroxyalkanoate Spheres Directed by Specific Protein-Protein Interactions. *Front. Bioeng. Biotechnol.* **2020**, *8*, 44.
(155) Bilal, M.; Iqbal, H. M. N. Naturally-derived biopolymers: Potential platforms for enzyme immobilization. *Int. J. Biol. Macromol.* **2019**, *130*, 462−482.
(156) Ogura, K.; Rehm, B. H. A. Self-Assembly: Alginate Encapsulation of Bioengineered Protein-Coated Polyhydroxybutyrate Particles: A New Platform for Multifunctional Composite Materials. *Adv. Funct. Mater.* **2019**, *29* (37), 1970256.
(157) Roldao, A.; Mellado, M. C.; Castilho, L. R.; Carrondo, M. J.; Alves, P. M. Virus-like particles in vaccine development. *Expert Rev. Vaccines* **2010**, *9* (10), 1149−1176.
(158) Shirbaghaee, Z.; Bolhassani, A. Different applications of virus-like particles in biology and medicine: Vaccination and delivery systems. *Biopolymers* **2016**, *105* (3), 113−132.
(159) Diaz, D.; Care, A.; Sunna, A. Bioengineering Strategies for Protein-Based Nanoparticles. *Genes* **2018**, *9* (7), 370.
(160) Douglas, T.; Young, M. Viruses: making friends with old foes. *Science* **2006**, *312* (5775), 873−875.
(161) Aumiller, W. M.; Uchida, M.; Douglas, T. Protein cage assembly across multiple length scales. *Chem. Soc. Rev.* **2018**, *47* (10), 3433−3469.
(162) Litowski, J. R.; Hodges, R. S. Designing heterodimeric two-stranded alpha-helical coiled-coils. Effects of hydrophobicity and alpha-helical propensity on protein folding, stability, and specificity. *J. Biol. Chem.* **2002**, *277* (40), 37272−37279.
(163) Minten, I. J.; Hendriks, L. J.; Nolte, R. J.; Cornelissen, J. J. Controlled encapsulation of multiple proteins in virus capsids. *J. Am. Chem. Soc.* **2009**, *131* (49), 17771−17773.
(164) Minten, I. J.; Claessen, V. I.; Blank, K.; Rowan, A. E.; Nolte, R. J. M.; Cornelissen, J. J. L. M. Catalytic capsids: the art of confinement. *Chem. Sci.* **2011**, *2*, 358−362.
(165) Rurup, W. F.; Verbij, F.; Koay, M. S.; Blum, C.; Subramaniam, V.; Cornelissen, J. J. Predicting the loading of virus-like particles with fluorescent proteins. *Biomacromolecules* **2014**, *15* (2), 558−563.
(166) Clancy, K. W.; Melvin, J. A.; McCafferty, D. G. Sortase transpeptidases: Insights into mechanism, substrate specificity, and inhibition. *Biopolymers* **2010**, *94* (4), 385−396.
(167) Schoonen, L.; Nolte, R. J.; van Hest, J. C. Highly efficient enzyme encapsulation in a protein nanocage: towards enzyme catalysis in a cellular nanocompartment mimic. *Nanoscale* **2016**, *8* (30), 14467−14472.
(168) Schoonen, L.; Pille, J.; Borrmann, A.; Nolte, R. J.; van Hest, J. C. Sortase A-Mediated N-Terminal Modification of Cowpea Chlorotic Mottle Virus for Highly Efficient Cargo Loading. *Bioconjugate Chem.* **2015**, *26* (12), 2429−2434.
(169) Schoonen, L.; van Hest, J. C. M. Modification of CCMV Nanocages for Enzyme Encapsulation. *Methods Mol. Biol.* **2018**, *1798*, 69−83.
(170) Valimaki, S.; Liu, Q.; Schoonen, L.; Vervoort, D. F. M.; Nonappa Linko, V.; Nolte, R. J. M.; van Hest, J. C. M.; Kostiainen, M. A. Engineered protein cages for selective heparin encapsulation. *J. Mater. Chem. B* **2021**, *9* (5), 1272−1276.
(171) Schoonen, L.; Maassen, S.; Nolte, R. J. M.; van Hest, J. C. M. Stabilization of a Virus-Like Particle and Its Application as a Nanoreactor at Physiological Conditions. *Biomacromolecules* **2017**, *18* (11), 3492−3497.
(172) Schwarz, B.; Uchida, M.; Douglas, T. Biomedical and Catalytic Opportunities of Virus-Like Particles in Nanotechnology. *Adv. Virus Res.* **2017**, *97*, 1−60.
(173) Patterson, D. P. Encapsulation of Active Enzymes within Bacteriophage P22 Virus-Like Particles. *Methods Mol. Biol.* **2018**, *1798*, 11−24.
(174) McCoy, K.; Douglas, T. In Vivo Packaging of Protein Cargo Inside of Virus-Like Particle P22. *Methods Mol. Biol.* **2018**, *1776*, 295−302.
(175) Patterson, D. P.; LaFrance, B.; Douglas, T. Rescuing recombinant proteins by sequestration into the P22 VLP. *Chem. Commun. (Cambridge, U. K.)* **2013**, *49* (88), 10412−4.
(176) Patterson, D. P.; Schwarz, B.; Waters, R. S.; Gedeon, T.; Douglas, T. Encapsulation of an enzyme cascade within the bacteriophage P22 virus-like particle. *ACS Chem. Biol.* **2014**, *9* (2), 359−365.
(177) Jordan, P. C.; Patterson, D. P.; Saboda, K. N.; Edwards, E. J.; Miettinen, H. M.; Basu, G.; Thielges, M. C.; Douglas, T. Self-assembling biomolecular catalysts for hydrogen production. *Nat. Chem.* **2016**, *8* (2), 179−185.
(178) Sanchez-Sanchez, L.; Tapia-Moreno, A.; Juarez-Moreno, K.; Patterson, D. P.; Cadena-Nava, R. D.; Douglas, T.; Vazquez-Duhalt, R. Design of a VLP-nanovehicle for CYP450 enzymatic activity delivery. *J. Nanobiotechnol.* **2015**, *13*, 66.

https://doi.org/10.1021/acssuschemeng.1c02045
ACS Sustainable Chem. Eng. 2021, 9, 8919−8945

(179) Patterson, D.; Edwards, E.; Douglas, T. Hybrid Nanoreactors: Coupling Enzymes and Small-Molecule Catalysts within Virus-Like Particles. *Isr. J. Chem.* **2015**, *55* (1), 96−101.
(180) Patterson, D. P.; Prevelige, P. E.; Douglas, T. Nanoreactors by programmed enzyme encapsulation inside the capsid of the bacteriophage P22. *ACS Nano* **2012**, *6* (6), 5000−5009.
(181) Patterson, D. P.; McCoy, K.; Fijen, C.; Douglas, T. Constructing catalytic antimicrobial nanoparticles by encapsulation of hydrogen peroxide producing enzyme inside the P22 VLP. *J. Mater. Chem. B* **2014**, *2* (36), 5948−5951.
(182) Patterson, D. P.; Schwarz, B.; El-Boubbou, K.; van der Oost, J.; Prevelige, P. E.; Douglas, T. Virus-like particle nanoreactors: programmed encapsulation of the thermostable CelB glycosidase inside the P22 capsid. *Soft Matter* **2012**, *8* (39), 10158−10166.
(183) Waghwani, H. K.; Uchida, M.; Fu, C. Y.; LaFrance, B.; Sharma, J.; McCoy, K.; Douglas, T. Virus-Like Particles (VLPs) as a Platform for Hierarchical Compartmentalization. *Biomacromolecules* **2020**, *21* (6), 2060−2072.
(184) Gonzalez-Davis, O.; Chauhan, K.; Zapian-Merino, S. J.; Vazquez-Duhalt, R. Bi-enzymatic virus-like bionanoreactors for the transformation of endocrine disruptor compounds. *Int. J. Biol. Macromol.* **2020**, *146*, 415−421.
(185) Wang, Y.; Uchida, M.; Waghwani, H. K.; Douglas, T. Synthetic Virus-like Particles for Glutathione Biosynthesis. *ACS Synth. Biol.* **2020**, *9* (12), 3298−3310.
(186) Servid, A.; Jordan, P.; O'Neil, A.; Prevelige, P.; Douglas, T. Location of the bacteriophage P22 coat protein C-terminus provides opportunities for the design of capsid-based materials. *Biomacromolecules* **2013**, *14* (9), 2989−95.
(187) Patterson, D.; Schwarz, B.; Avera, J.; Western, B.; Hicks, M.; Krugler, P.; Terra, M.; Uchida, M.; McCoy, K.; Douglas, T. Sortase-Mediated Ligation as a Modular Approach for the Covalent Attachment of Proteins to the Exterior of the Bacteriophage P22 Virus-like Particle. *Bioconjugate Chem.* **2017**, *28* (8), 2114−2124.
(188) Uchida, M.; McCoy, K.; Fukuto, M.; Yang, L.; Yoshimura, H.; Miettinen, H. M.; LaFrance, B.; Patterson, D. P.; Schwarz, B.; Karty, J. A.; Prevelige, P. E., Jr.; Lee, B.; Douglas, T. Modular Self-Assembly of Protein Cage Lattices for Multistep Catalysis. *ACS Nano* **2018**, *12* (2), 942−953.
(189) Kang, H. J.; Baker, E. N. Intramolecular isopeptide bonds: protein crosslinks built for stress? *Trends Biochem. Sci.* **2011**, *36* (4), 229−237.
(190) Kang, H. J.; Coulibaly, F.; Clow, F.; Proft, T.; Baker, E. N. Stabilizing isopeptide bonds revealed in gram-positive bacterial pilus structure. *Science* **2007**, *318* (5856), 1625−1628.
(191) Terao, Y.; Kawabata, S.; Nakata, M.; Nakagawa, I.; Hamada, S. Molecular characterization of a novel fibronectin-binding protein of *Streptococcus pyogenes* strains isolated from toxic shock-like syndrome patients. *J. Biol. Chem.* **2002**, *277* (49), 47428−35.
(192) Hagan, R. M.; Bjornsson, R.; McMahon, S. A.; Schomburg, B.; Braithwaite, V.; Buhl, M.; Naismith, J. H.; Schwarz-Linek, U. NMR spectroscopic and theoretical analysis of a spontaneously formed Lys-Asp isopeptide bond. *Angew. Chem., Int. Ed.* **2010**, *49* (45), 8421−8425.
(193) Zakeri, B.; Fierer, J. O.; Celik, E.; Chittock, E. C.; Schwarz-Linek, U.; Moy, V. T.; Howarth, M. Peptide tag forming a rapid covalent bond to a protein, through engineering a bacterial adhesin. *Proc. Natl. Acad. Sci. U. S. A.* **2012**, *109* (12), E690−7.
(194) Hatlem, D.; Trunk, T.; Linke, D.; Leo, J. C. Catching a SPY: Using the SpyCatcher-SpyTag and Related Systems for Labeling and Localizing Bacterial Proteins. *Int. J. Mol. Sci.* **2019**, *20* (9), 2129.
(195) Li, L.; Fierer, J. O.; Rapoport, T. A.; Howarth, M. Structural analysis and optimization of the covalent association between SpyCatcher and a peptide Tag. *J. Mol. Biol.* **2014**, *426* (2), 309−317.
(196) Keeble, A. H.; Howarth, M. Insider information on successful covalent protein coupling with help from SpyBank. *Methods Enzymol.* **2019**, *617*, 443−461.
(197) Keeble, A. H.; Banerjee, A.; Ferla, M. P.; Reddington, S. C.; Anuar, I.; Howarth, M. Evolving Accelerated Amidation by SpyTag/SpyCatcher to Analyze Membrane Dynamics. *Angew. Chem., Int. Ed.* **2017**, *56* (52), 16521−16525.
(198) Brune, K. D.; Leneghan, D. B.; Brian, I. J.; Ishizuka, A. S.; Bachmann, M. F.; Draper, S. J.; Biswas, S.; Howarth, M. Plug-and-Display: decoration of Virus-Like Particles via isopeptide bonds for modular immunization. *Sci. Rep.* **2016**, *6*, 19234.
(199) Veggiani, G.; Nakamura, T.; Brenner, M. D.; Gayet, R. V.; Yan, J.; Robinson, C. V.; Howarth, M. Programmable polyproteams built using twin peptide superglues. *Proc. Natl. Acad. Sci. U. S. A.* **2016**, *113* (5), 1202−1207.
(200) Bao, J.; Liu, N.; Zhu, L.; Xu, Q.; Huang, H.; Jiang, L. Programming a Biofilm-Mediated Multienzyme-Assembly-Cascade System for the Biocatalytic Production of Glucosamine from Chitin. *J. Agric. Food Chem.* **2018**, *66* (30), 8061−8068.
(201) Qu, J.; Cao, S.; Wei, Q.; Zhang, H.; Wang, R.; Kang, W.; Ma, T.; Zhang, L.; Liu, T.; Wing-Ngor Au, S.; Sun, F.; Xia, J. Synthetic Multienzyme Complexes, Catalytic Nanomachineries for Cascade Biosynthesis In Vivo. *ACS Nano* **2019**, *13* (9), 9895−9906.
(202) Wei, Q.; He, S.; Qu, J.; Xia, J. Synthetic Multienzyme Complexes Assembled on Virus-like Particles for Cascade Biosynthesis In Cellulo. *Bioconjugate Chem.* **2020**, *31* (10), 2413−2420.
(203) Giessen, T. W.; Silver, P. A. A Catalytic Nanoreactor Based on in Vivo Encapsulation of Multiple Enzymes in an Engineered Protein Nanocompartment. *ChemBioChem* **2016**, *17* (20), 1931−1935.
(204) Klein, W. P.; Thomsen, R. P.; Turner, K. B.; Walper, S. A.; Vranish, J.; Kjems, J.; Ancona, M. G.; Medintz, I. L. Enhanced Catalysis from Multienzyme Cascades Assembled on a DNA Origami Triangle. *ACS Nano* **2019**, *13* (12), 13677−13689.
(205) Liu, J. L.; Zabetakis, D.; Breger, J. C.; Anderson, G. P.; Goldman, E. R. Multi-Enzyme Assembly on T4 Phage Scaffold. *Front. Bioeng. Biotechnol.* **2020**, *8*, 571.
(206) Cayetano-Cruz, M.; Coffeen, C. F.; Valadez-Garcia, J.; Montiel, C.; Bustos-Jaimes, I. Decoration of virus-like particles with an enzymatic activity of biomedical interest. *Virus Res.* **2018**, *255*, 1−9.
(207) Bustos-Jaimes, I.; Soto-Roman, R. A.; Gutierrez-Landa, I. A.; Valadez-Garcia, J.; Segovia-Trinidad, C. L. Construction of protein-functionalized virus-like particles of parvovirus B19. *J. Biotechnol.* **2017**, *263*, 55−63.
(208) Takenoya, M.; Nikolakakis, K.; Sagermann, M. Crystallographic insights into the pore structures and mechanisms of the EutL and EutM shell proteins of the ethanolamine-utilizing microcompartment of *Escherichia coli*. *J. Bacteriol.* **2010**, *192* (22), 6056−63.
(209) Choudhary, S.; Quin, M. B.; Sanders, M. A.; Johnson, E. T.; Schmidt-Dannert, C. Engineered protein nano-compartments for targeted enzyme localization. *PLoS One* **2012**, *7* (3), No. e33342.
(210) Zhang, G.; Quin, M. B.; Schmidt-Dannert, C. Self-Assembling Protein Scaffold System for Easy in Vitro Coimmobilization of Biocatalytic Cascade Enzymes. *ACS Catal.* **2018**, *8* (6), 5611−5620.
(211) Schmidt-Dannert, S.; Zhang, G.; Johnston, T.; Quin, M. B.; Schmidt-Dannert, C. Building a toolbox of protein scaffolds for future immobilization of biocatalysts. *Appl. Microbiol. Biotechnol.* **2018**, *102* (19), 8373−8388.
(212) Zhang, G.; Johnston, T.; Quin, M. B.; Schmidt-Dannert, C. Developing a Protein Scaffolding System for Rapid Enzyme Immobilization and Optimization of Enzyme Functions for Biocatalysis. *ACS Synth. Biol.* **2019**, *8* (8), 1867−1876.
(213) Nguyen, P. Q.; Botyanszki, Z.; Tay, P. K.; Joshi, N. S. Programmable biofilm-based materials from engineered curli nanofibres. *Nat. Commun.* **2014**, *5*, 4945.
(214) Peschke, T.; Bitterwolf, P.; Gallus, S.; Hu, Y.; Oelschlaeger, C.; Willenbacher, N.; Rabe, K. S.; Niemeyer, C. M. Self-Assembling All-Enzyme Hydrogels for Flow Biocatalysis. *Angew. Chem., Int. Ed.* **2018**, *57* (52), 17028−17032.
(215) Yin, L.; Guo, X.; Liu, L.; Zhang, Y.; Feng, Y. Self-Assembled Multimeric-Enzyme Nanoreactor for Robust and Efficient Biocatalysis. *ACS Biomater. Sci. Eng.* **2018**, *4* (6), 2095−2099.
(216) Hammer, J. A.; Ruta, A.; Therien, A. M.; West, J. L. Cell-Compatible, Site-Specific Covalent Modification of Hydrogel

Scaffolds Enables User-Defined Control over Cell-Material Interactions. *Biomacromolecules* **2019**, *20* (7), 2486−2493.
(217) Bitterwolf, P.; Gallus, S.; Peschke, T.; Mittmann, E.; Oelschlaeger, C.; Willenbacher, N.; Rabe, K. S.; Niemeyer, C. M. Valency engineering of monomeric enzymes for self-assembling biocatalytic hydrogels. *Chem. Sci.* **2019**, *10* (42), 9752−9757.
(218) Mittmann, E.; Gallus, S.; Bitterwolf, P.; Oelschlaeger, C.; Willenbacher, N.; Niemeyer, C. M.; Rabe, K. S. A Phenolic Acid Decarboxylase-Based All-Enzyme Hydrogel for Flow Reactor Technology. *Micromachines (Basel)* **2019**, *10* (12), 795.

https://doi.org/10.1021/acssuschemeng.1c02045
ACS Sustainable Chem. Eng. 2021, 9, 8919−8945

2.6.1. Publication 6. Supporting Information

Gizem Ölçücü, Oliver Klaus, Karl-Erich Jaeger, Thomas Drepper*, and Ulrich Krauss*

*corresponding authors

ACS Sustainable Chemistry & Engineering. 9 (2021), pp. 8919-8945. Reprinted with permission from [103]. `https://pubs.acs.org/doi/abs/10.1021/acssuschemeng.1c02045`

Table S1: Abbreviations used in the manuscript in alphabetical order.

LLPS	Liquid-liquid phase separation
AdhA	alcohol dehydrogenase A
AdhD	monomeric alcohol dehydrogenase
ADS	amorpha-4,11-diene synthase
A-IDPs	Artificial IDRs
AmDH	amine dehydrogenase
AsLOV2	LOV2 domain from *Avena sativa*
AtHNL	Hydroxynitrile lyase from *Arabidopsis thaliana*
BFP	Blue fluorescent protein
BLA	α-amylase
BlpA	lipase from *Bacillus pumilus*
Bt	*Bacillus thuringiensis*
CadA	lysine decarboxylase
CalB	lipase from *Candida antarctica*
CatIBs	Catalytically-active inclusion bodies
CBD	Cellulose binding domain
CCMV	Cowpea Chlorotic Mottle Virus
CelB	homotetrameric b-glucosidase
CFP	Cyan fluorescent protein
CnaB2	fibronectin-binding domain
CP	capsid protein
CPMV	Cowpea mosaic virus
CsgA	curli protein monomer
CueO	bacterial laccase-like multicopper oxidase
Cry1-3	Cry family of proteins *B. thuringiensis*, toxins used as insecticides
Cry-2	Cryptochrome-2 photoreceptor
Cry-2Olig	E490G variant of Cry-2, showing enhanced clustering
CYPBM3	*B. megaterium* P450 monooxygenase
DAP	1,3-diaminopropane
Dat	L-2,4-diaminobutyrate:α-ketoglutarate 4-aminotransferase
Ddc	L-2,4-diaminobutyrate decarboxylase
DDX4/3	ATP-dependent RNA helicase, Deadbox Helicase 4 or 3
D-HDT	D-hydantoinase
DLZM4	Dieselzyme 4
DTW	D-tagatose-3-epimerase
E coil	Artificial, negatively charged, α-helical coil
EcHyd-1	heterodimeric [NiFe]-hydrogenase 1
eGFP	Enhanced green fluorescent protein
EutM	ethanolamine utilization bacterial microcompartment protein
eYFP	Enhanced yellow fluorescent protein
FAME	Fatty acid methyl ester
FbaB	fibronectin-binding adhesin
FKBP	FK506 binding protein
FRB	Rapamycin binding protein
FUS	fused in sarcoma protein

FUS_N	N-terminal intrinsically disordered region of FUS
G6PDH	Glucose-6-phosphate dehydrogenase
GalA	α-galactosidase
GALK	galactosidase
GFP	Green fluorescent protein
GLUK	glucokinase
GOase	Galactose oxidase
GshF	homodimeric, bifunctional glutathione full synthase
HEK cells	Human embryonic kidney cells
HNRNPA1	Heterogeneous nuclear ribonucleoprotein A1
$HNRNPA1_C$	C-terminal intrinsically disordered region of HNRNPA1
Hoc	outer capsid protein
HRV 3C	3C protease derived from human Rhinovirus type 14
HXK2	Hexokinase 2
IBs	Inclusion bodies
Idi	isopentenyl diphosphate isomerase
IDPs	Intrinsically disordered proteins
IDRs	Intrinsically disordered regions
Ima1p	α-glucosidase
iPOLYMER	Intracellular Production Of Ligand-Yielded Multivalent Enhancers
iPOLYMER-Li	Intracellular Production of Light-Yielded Multivalent Enhancers
IspA	farnesyl pyrophosphate (FPP) synthase
K coil	Artificial, positively charged, lysine-rich coil
KivD	ketoisovalerate decarboxylase
LacZ	β-galactosidase
LbADH	Alcohol dehydrogenase from *Lactobacillus brevis*
LOV	Light, oxygen, voltage domain
LZ	Leucine zipper
MaSp1-I16	Major ampullate spidroin 1 protein from *Nephila claviceps*
MBP	Maltose binding protein
MenD	2-succinyl-5-enol-pyruvyl-6-hydroxy-3-cyclohexene-1-carboxylate synthase
MS2	bacteriophage
MtSEO-F-4	*Medicago truncatula* sieve element occlusion by forisome
NADPH	Nicotinamide adenine dinucleotide phosphate
NemA	hexavalent chromium reductase
nephrin-NCK-N-WASP	Signalling complex of the actin-regulatory pathway, which forms clusters due to LLPS
NOX	homodimeric FAD-binding NADH oxidase
OpdA	organophosphohydrolase
optoDDX4	Optgenetic construct containing the N-terminal intrinsically disordered region of DDX4
optoFUS	Optgenetic construct containing the N-terminal intrinsically disordered region of FUS
optoHNRNPA1	Optgenetic construct containing the C-terminal intrinsically disordered region of RNA binding protein HNRNPA1
P22	bacteriophage

P450-BM3	monooxygenase
PAMAM	positively charged polyamidoamine
PfBAL	Benzaldehyde lyase from *Pseudomonas fluorescens*
PHA	polyhydroxyalkanoate
PhaA	β-ketothiolase
PhaB	acetoacetyl-CoA reductase
PhaC	Polyhydroxybutyrate synthase
PhaC	PHA synthase
PhaP/PhaF	phasin (PHA-associated protein)
PhaZ	PHA depolymerase
PHB	Polyhydroxybutyrate
PixE/PixD	Photoreceptor system of the sensors of blue-light using flavin adenine dinucleotide (BLUF) family
PixELL	Pix Evaporates from Liquid-like droplets in Light
PLP	Pyridoxal 5′-phosphate
PML	Lipase from *Proteus mirabilis*
PML^{VG}	Double mutant of *Proteus mirabilis* lipase
PMO	monooxygenase
POI	Protein of interest
PpBFD	Benzoylformate decarboxylase from *Pseudomonas putida*
PRM	Proline-rich-motif
Qb	bacteriophage
RADH	Alcohol dehydrogenase from *Ralstonia sp.*
REPS	RGG-based, enzyme-triggered, phase-separating systems
RFP	Red fluorescent protein
RGG	intrinsically disordered protein domain, containing closely spaced Arg-Gly-Gly repeats, from the N-terminus of LAF1 RNA helicase from *C. elegans*
SEO-F1-4	Sieve element occlusion by forisome
sfGFP	Superfolder green fluorescent protein
SH3	SRC homology 3
Sir1975	N-acetylglucosamine 2-epimerase
SP	scaffolding protein
Spy	
SrtA	sortase
SZ1-2	SYNZIP coiled-coil 1-2
$TDP43_C$	C-terminal intrinsically disordered region of the TAR DNA-binding protein 43
TFP	teal fluorescent marker protein
TIA-1	RNA binding protein that promotes the assembly of stress granules
TnaA	PLP-dependent tryptophanase
UCST	Upper critical solution temperature
VLP	virus-like particle
YFP	Yellow fluorescent protein
αp	Alpha peptide

2.7. Publication 7. Carrier-Free Enzyme Immobilizates for Flow Chemistry

Gizem Ölçücü, Ulrich Krauss*, Karl-Erich Jaeger and Jörg Pietruszka

*corresponding author

Chemie Ingenieur Technik. 95 (2023), pp. 531-542.

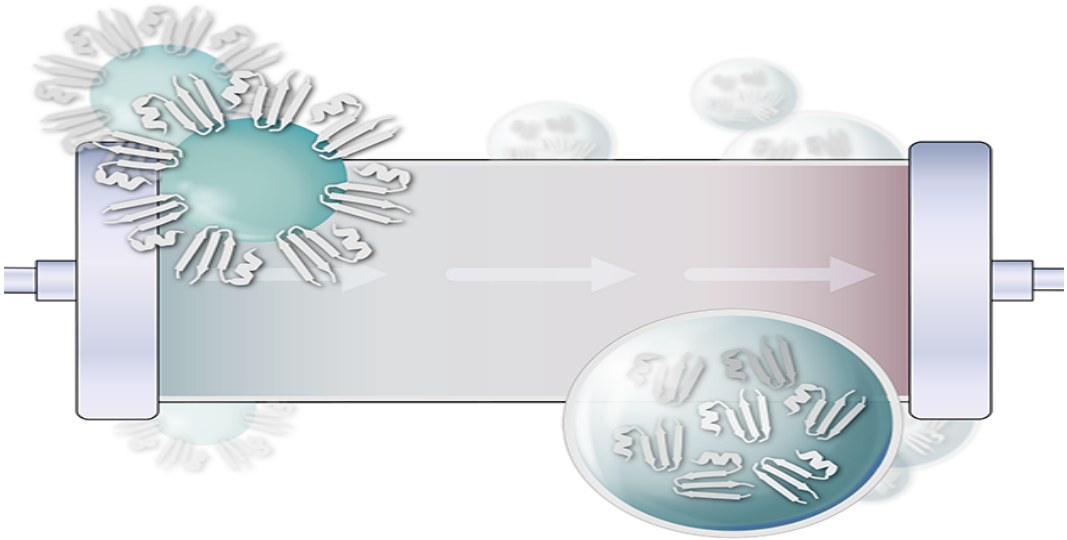

Author Contributions: UK and JP conceived the outline of the review. UK, GO and JP wrote the manuscript, and UK prepared all figures. KEJ helped with editing and proof reading. All authors have read and approved the final version.

Carrier-Free Enzyme Immobilizates for Flow Chemistry

Gizem Ölçücü, Ulrich Krauss*, Karl-Erich Jaeger, and Jörg Pietruszka

DOI: 10.1002/cite.202200167

For the development of efficient and green industrial processes, the combination of biocatalysis and flow chemistry holds great promises. Flow chemical utilization of biocatalysts, essentially made possible by the immobilization (or retention) of enzymes in flow reactors, has attracted increased academic attention during recent years. In the present review we present an overview of immobilization strategies suitable for flow chemistry, particularly focusing on recently developed carrier-free immobilization methods, highlighting advances in the field and presenting future trends.

Keywords: biocatalysis, enzyme immobilization, flow chemistry

Received: August 15, 2022; *revised:* December 20, 2022; *accepted:* February 01, 2023

1 Introduction

Over the past decades, advancements in molecular biology, microbiology, chemistry, engineering, and biotechnology have paved the way for the utilization of enzymes in various sectors such as food, feed, pharmaceutical, textile, and cosmetic industries. Enzymes, often outperforming conventional transition metal catalysts with regard to chemo-, stereo- and regioselectivity [1–3], are renewable biomaterials that possess lower toxicity and represent a reduced environmental burden, due to generally lower waste generation and energy consumption associated with their production [3–5]. In addition, microorganisms overproducing the corresponding enzymes can be grown on renewable feedstocks, rendering enzyme production even more sustainable [5–7]. Nonetheless, enzymes are still underutilized in the chemical industry due their often low tolerance towards harsh reaction conditions, and the costs that are associated with their production and purification on a larger industrial scale [8]. Hence, the realization of sustainable industrial bioprocesses requires the development of highly stable enzyme preparations, obtained in a resource efficient way that can be conveniently recycled from a batch reaction system or used in continuous flow processes. In this regard, protein engineering methods have successfully been used to improve, e.g., enzyme stability to meet specific process requirements. However, such engineering campaigns, often relying on directed evolution, remain a time- and labor-intensive endeavor [9, 10]. Similarly, enzyme immobilization, traditionally defined as the confinement of active enzyme molecules onto/within a material, allowing for catalyst stabilization and easy reuse, can likewise fulfill a key role in realizing the full (industrial) potential of enzymes. Importantly, the development of novel immobilization concepts that forgo the use of carrier-materials [5, 11, 12] and the use of immobilized enzymes in flow synthesis represents a promising approach that can foster broader acceptance of enzymes in synthetic chemistry and industry, thereby contributing to the sustainable management of resources in next-generation bioeconomic processes. Machine assisted processes provide a number of opportunities for organic synthesis in flow. While improved safety during operation or the utilization of intermediates with limited stability were early selling points, the potential of automation and process intensification are increasingly recognized. With new equipment and enabling technologies becoming available, the advantages, e.g., for self-optimization protocols and the ability to collect data in real-time to profile the reactions, are meanwhile widely accepted to aid with the synthesis of active pharmaceutical ingredients. With respect to the increasingly popular home office options in today's working environments, the possibility to control reactions remotely has become an attractive tool. In addition, cloud sharing of process data within collaborative R&D projects has become feasible [13–15].

[1,2]Gizem Ölçücü https://orcid.org/0000-0001-5126-4530, [1,2]Dr. Ulrich Krauss https://orcid.org/0000-0003-2219-7388 (u.krauss@fz-juelich.de)*, [1,2]Prof. Dr. Karl-Erich Jaeger https://orcid.org/0000-0002-6036-0708, [2,3]Prof. Dr. Jörg Pietruszka https://orcid.org/0000-0002-9819-889X

[1]Institute of Molecular Enzyme Technology, Heinrich Heine University Düsseldorf, Forschungszentrum Jülich GmbH, Wilhelm Johnen Straße, 52425 Jülich, Germany.

[2]Institute of Bio- and Geosciences IBG-1: Biotechnology, Forschungszentrum Jülich GmbH, Wilhelm Johnen Straße, 52425 Jülich, Germany.

[3]Institute of Biorganic Chemistry, Heinrich Heine University Düsseldorf, Forschungszentrum Jülich GmbH, Wilhelm Johnen Straße, 52425 Jülich, Germany.

In conclusion, the combination of biocatalysis and flow chemistry, i.e., by using carrier-free enzyme immobilizates, represents a promising and rapidly growing field of research [16, 17]. In the present contribution, we present an overview of selected immobilization strategies suitable for flow chemical applications, particularly focusing on recently developed carrier-free immobilization methods.

2 Enzyme Immobilization

Immobilization methods can be grouped based on various principles [5, 11, 12, 18–25]. On the coarsest level, a subdivision into carrier-based and carrier-free techniques is possible (Fig. 1, Tab. 1). Please note that this grouping does not always enable a clear-cut distinction, since also carrier-free immobilizates are sometimes used embedded in classical carrier materials [26], or some *in vivo* methods rely on self-immobilization, with the carrier constituted by the target protein itself [11, 27]. Carrier-based methods hereby rely on either the binding or encapsulation/entrapment of enzymes in/on suitable carrier materials [5, 25], while carrier-free methods are often based on *in vitro* or *in vivo* bioconjugation (self-assembly or cross-linking) and often combine enzyme overproduction and immobilization in one step [5, 11, 12].

Traditional, carrier-based methods employ different inorganic and organic carrier materials such as magnetic nanoparticles, synthetic polymers, alginate beads, nanofibers, resins, silica materials, cellulose and hydrogels amongst others [28–34]. Carrier binding can be realized via covalent-attachment, ionic binding, adsorption, affinity binding, metal-link/chelation as well as entrapment and encapsulation in hydrogels [2, 4, 21, 24]. Please note that a detailed review of traditional immobilization methods, relying on carrier binding and entrapment/encapsulation is beyond the scope of the present contribution. Excellent reviews that cover these topics have, however, been presented in recent years (see exemplarily [5, 20, 25, 29]). In addition to these conventional strategies, carrier-free methods include *in vitro* approaches such as the preparation of cross-linked enzyme aggregates and crystals (CLEAs and CLECs) [35, 36], which have been around for many years, as well as more recent *in vivo* methods that rely on enzyme overproduction and immobilization in one step.

The latter *in vivo* produced carrier-free immobilizates can be obtained by various means, but generally rely on the "self-immobilization" of the target protein in a proteinaceous matrix that can either be formed by the target protein fused with an aggregation (catalytically-active inclusion bodies, CatIBs) [11, 27, 53] or a crystallization (Cry3Aa-based protein crystals) [11, 47, 54–56] mediating pull-down tag. Furthermore, *in vivo* immobilization is possible by utilizing additional proteins or macromolecular protein assemblies onto or within which the target is displayed or entrapped (virus-like particles, VLPs; forizymes) [11, 48, 57–59]. More detailed information about these methods, in particular with focus to their applicability in flow chemistry, are provide in the sections 2.1.1–2.1.3. As with all techniques, carrier-based and carrier-free methods possess certain advantages and drawbacks which are summarized in Tab. 1. Hereby, in particular factors like leakage of the enzyme from the carrier, binding affinity, generic applicability, site-specific immobilization, carrier costs, enzyme loading, activity loss due to immobilization, stability of the immobilizate and mass transfer limitation play an important role for selecting the best-suited immobilizate. For the immobilization for flow chemical application additional parameters are important, which are outlined in the following chapters.

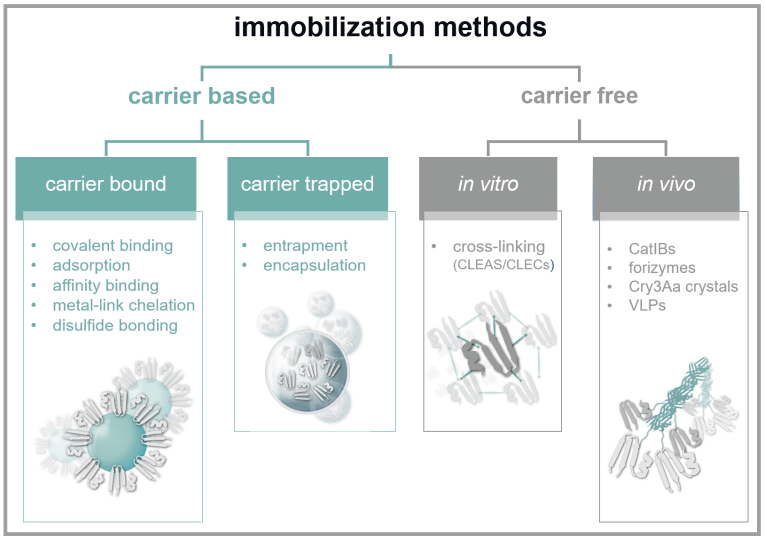

Figure 1. Immobilization methods grouped based on the distinction between carrier-free and carrier-based methods. For details see text.

2.1 Enzyme Immobilization and Use in Flow Chemistry

Biocatalysis in continuous flow utilizes some of the key advantages that have been recognized for flow chemistry. Process intensification that is based on the automation of highly controlled process parameters is one of the key benefits, but also aspects such as improved total turnover numbers (TTN), shorter reaction times, improved catalyst stability, and the possibility to overcome compatibility issues in (chemoenzymatic) cascades should be considered. Furthermore, the concept is often associated with green and sustainable principles in synthesis [17, 60–63].

While various setup configurations for biocatalytic reactions in continuous flow processes are feasible, conceptually two groups of flow

Table 1. General advantages and drawbacks of selected immobilization methods.

Immobilization method	Example[1)]	Advantages	Disadvantages	Reference
undirected covalent binding[2)]	production of β-lactam antibiotics (Penicillin G amidase), decomposition of H_2O_2 (catalase)	no leakage, simple, selective application	low activity, matrix or enzyme regeneration not possible, low enzyme loading	[29, 37, 4, 38]
adsorption	transesterification, herbicide production (lipase), L-amino acid synthesis (aminoacylase)	simple, low cost, matrix or enzyme regeneration possible	high leakage, nonspecific adsorption issues	[29, 37]
affinity binding (covalent and non-covalent)[3)]	amination of alcohols (alcohol dehydrogenase and amine dehydrogenase, co-immobilization)	very high selectivity, site specific immobilization	high cost of carrier	[39, 24]
metal-link chelation	flavor synthesis (lipase)	simple, low activity loss	low reproducibility	[40]
entrapment	hydrolysis of lactose in milk (β-galactosidase)	widely applicable, minimal activity loss	high leakage, mass transfer limitations	[41, 42]
encapsulation	carbon capture (carbonic anhydrase)	high enzyme loading, low leakage	mass transfer limitations	[4, 43]
CLEAs/CLECs	resolution of amino acid esters, amines and peptide synthesis (alcalase), trans-esterification (lipase)	widely applicable, low leakage, no carrier	optimization required based on target, variable loss of activity, CLECs: high costs, crystallization unpredictable	[36]
CatIBs	drug precursor synthesis (alcohol dehydrogenase and benzaldehyde lyase, co-immobilization), cadaverin synthesis (lysine decarboxylase)	simple, cheap, no carrier, no additional immobilization steps	optimization required based on target, variable loss of activity	[44-46]
Cry3Aa crystals	biodiesel production (lipase)	very stable immobilizate, high activity	likely limited to smaller (monomeric enzymes), potential mass transfer limitations	[47]
forizymes, magnetosomes	NADPH synthesis (glucose-6-phosphate dehydrogenase, hexokinase, co-immobilization), magnetosomes: proof of concept conversion of *p*-coumaric acid by phenolic acid decarboxylase	stable immobilizates, highly active, large size enables simple reuse	complex architecture, coexpression of multiple proteins needed, likely production in *E. coli* not possible	[48, 49]
virus-like particles	reduction of ketones (alcohol dehydrogenase)	Monodisperse in size and shape, suitable for encapsulation and surface display of targets	small size of particles hinders simple preparation and reuse	[50]

1) These are arbitrarily selected, not necessarily representative, examples. 2) This refers to the undirected covalent carrier attachment via specific amino acid types; in contrast to site-directed covalent attachment via bioconjugation, i.e., in case of 3), e.g., HaloTag and SpyTag/SpyCatcher systems [51, 52].

reactors are in use, namely those utilizing free enzymes and systems working with immobilized biocatalysts. Even when focusing only on immobilized enzymes, several configurations have to be considered rendering the choice for the best variant difficult. While packed-bed reactors are operationally simple, surface-immobilized enzymes might be advantageous when high pressure drops prove problematic. Other materials, e.g., membranes, monolith materials [16, 64, 65] or agarose-based hydrogels have been used [66]. Besides these conceptual challenges, practical questions such as the cost of the carrier, the site of immobilization (on the surface or within a carrier), the problem of enzyme and cofactor leaching, and the mode of cofactor recycling need to be considered. In the end, in order to find the most economical and sustainable solution for a given problem, all parameters need to be addressed.

While carrier-free, nano-sized enzyme aggregates/immobilizates (see above) are of interest for flow processes, certain limitations result from the small size of the corresponding enzyme preparation. The separation of the immobilizate from small molecule products is trivial but retaining the catalyst in a packed-bed reaction remains challenging. Several solutions have been established in the last years and some representative examples will be presented in

the following chapters. Here, we focus on methods and approaches for the carrier-free immobilization of enzymes that appear suitable or have already been used for flow chemical application.

2.1.1 Cross-Linked Enzyme Aggregates and Cross-Linked Enzyme Crystals

Cross-linked enzyme crystals (CLECs) and cross-linked enzyme aggregates (CLEAs) as an extension of the CLEC strategy, have been first developed in the 1990s and since then have been used for the immobilization of a multitude of different enzymes. CLECs are obtained by batch crystallization of enzymes, and subsequent cross-linking of the crystals via free amino groups of the enzyme by using glutaraldehyde [67]. Generally, enzyme crystals with a size of 1–100 µm [21, 67] can be generated, with the size controllable by the conditions used during crystallization (e.g., temperature, pH, mixing speed). The method was shown to be widely applicable for a variety of enzymes and was commercialized soon after its development [35]. However, the time consuming and unpredictable nature of the crystallization process, the requirement for enzyme purification and hence high costs (Tab. 1), prompted the development of the conceptionally much simpler CLEA approach. CLEAs can be generated by precipitation of the enzyme using polyethylene glycol or ammonium sulfate [36, 68], followed by cross-linking by glutaraldehyde. This yields particles with sizes between 5–50 µm [69], which are insoluble in water and can be retained via centrifugation or filtration [2, 5, 36]. While the preparation of CLECs requires purified enzymes, CLEAs can also be prepared from the crude cell extracts. Due to the unspecific nature of the cross-linking process, targeting free amino groups of lysine residues, for certain target, a variable or complete loss of activity has been observed, which is sometimes attributed to the cross-linking of active-site residues [35]. CLEA formation can be optimized by opting for different cross-linkers or by modifying process parameters like pH, temperature, precipitants, and the enzyme to cross-linker ratio [36]. Despite that, often case-to-case optimization is needed to obtain active CLEAs, the process has been widely used for the immobilization of various enzymes [35, 36]. CLEAs are suitable for use with organic solvents, can show high operational stability and often retain relatively high activities [69]. Importantly, CLEAs, albeit in form of a composite material, have recently been used for flow synthesis [70]. Here, the design of a compartmentalized template CLEAs (*c*-CLEAs) enable application of the corresponding CLEAs in flow. Cross-linking was carried out in the nano-cavity of a bowl-shaped polymer vehicle (so-called stomatocytes). Since the enzyme was preorganized in high concentration in the cavity, a relatively low amount of cross-linker (glutaraldehyde or genipin) was employed. Overall, improved residual activity of the biocatalysts, either the lipase B from *Candida antarctica* (CalB), the porcine liver esterase (PLE) as well as mixtures of a glucose oxidase (GOx) and horseradish peroxidase (HRP), were observed. Compared to non-cross-linked enzymes, a drastically reduced leaching of the enzyme was reported [70]. Apart from the above-described *in vitro* strategies for the production of carrier-free immobilizates, various *in vivo* methods have been described in recent years, some of which were already used to generate enzyme immobilizates for flow chemistry.

2.1.2 Natural Enzyme Crystals, Complex Macromolecular Assemblies and All-Enzyme Hydrogels

One example for such an *in vivo* method, which yields crystalline enzyme immobilizates, likely similar to CLECs, are *in vivo* produced enzyme crystals, which have been used as a protein delivery platform as well as for immobilization [47, 54, 55, 71]. The method utilizes the *Bacillus thuringiensis* Cry3Aa protein, which naturally forms protein crystals [71], as fusion partner to allow target immobilization [54]. So far, the approach has been used for the immobilization of the green fluorescent protein (GFP), the red-fluorescent protein mCherry, a peptide deformylase, *Bacillus subtilis* lipase A and dieselzyme 4 (a mutant of *Proteus mirabilis* lipase) [47, 54, 71]. When combined with SpyTag/SpyCatcher technology (Fig. 2a) co-immobilization of multiple enzymes of the menaquinone biosynthesis pathway was recently shown to be possible using the Cry3Aa approach (Fig. 2b) [56]. With an average size of about 1 µm, rod-shaped Cry3Aa crystals [56] are likely too small for direct utilization in flow chemistry. However, when suitable methods for their retention in flow bioreactors can be found (see below), their generally high stability renders them promising catalysts for continuous flow application.

Another recent *in vivo* immobilization strategy utilizes plant mechanoprotein complexes (called forisomes), which are giant fusiform protein complexes constituted by monomeric sieve element occlusion (SEO) proteins, which are exclusively found in sieve elements of legumes [72]. Molecular biological fusion of some SEO-protein-encoding genes to a target gene, allowed the production of functionalized forisomes in *Saccharomyces cerevisiae*, which were coined forizymes by the authors [48]. To the best of our knowledge, the method has so far only been used for the immobilization of yellow and blue fluorescent proteins, a glucose-6-phosphate dehydrogenase, and a hexokinase [48].

Although not much is known about the mechanic stability of forizyme immobilizates, their rather large size (10 × 1 µm to 55 × 5 µm) [48] should allow easy preparation and easier retention in flow bioreactors. Virus-like particles (VLPs) are protein complexes formed from viral capsid proteins that self-assemble into spherical particles, which in turn can be used for target protein entrapment or surface display. Since VLPs are only constituted by the capsid proteins of the virus, VLPs, lacking genetic material, are nonin-

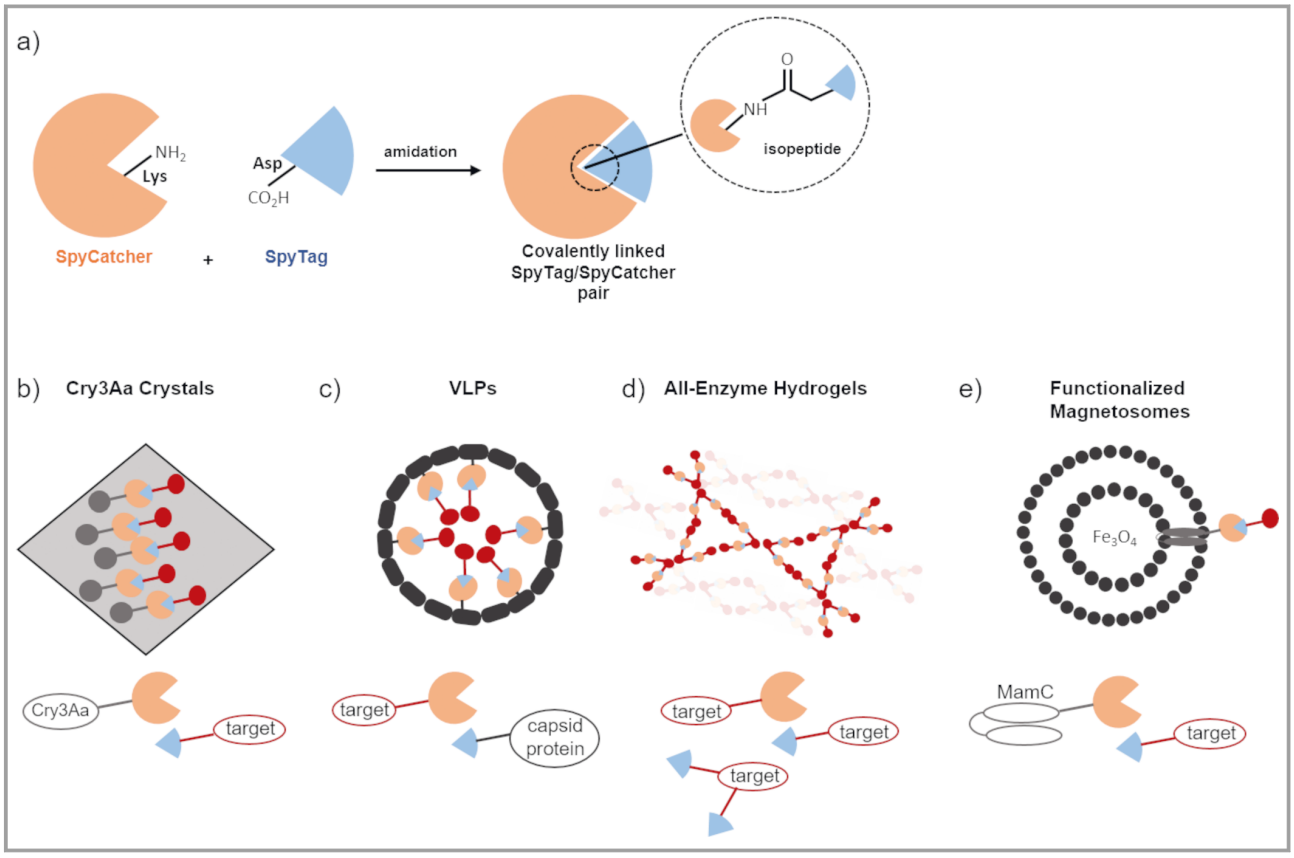

Figure 2. Illustration of the SpyTag/SpyCatcher technology (a) and selected examples in which the method has been used for enzyme immobilization (b–e). a) The SpyTag/SpyCatcher system, which was engineered by splitting the CnaB2 domain of the fibronectin-binding protein FbaB from *Streptococcus pyogenes*, into a 13 residue SpyTag and the 116 residue SpyCatcher part [51, 73], can spontaneously form an isopeptide bond, when the two modules are mixed together, thereby covalently linking SpyTag and SpyCatcher. Using this strategy, enzymes can be immobilized in Cry3Aa protein crystals (b), in virus-like particles (c), all-enzyme hydrogels (d) and functionalized magnetosomes (e). For details see text.

fectious and nonreplicating. A variety of strategies have been developed for the immobilization of proteins using the VLP approach (recently reviewed in [11]). Prominent examples include the use of the cowpea chlorotic mottle virus (CCMV) capsid [74, 75] and the capsid of the *Salmonella typhimurium* bacteriophage P22 [58]. Target immobilization is possible either by direct molecular biological fusion to the capsid or scaffolding proteins [76] that constitute the VLP, by utilizing protein-protein interaction tags (such as the E and K coil system) [74, 75], by sortase-catalyzed covalent-linking [77] or by employing the SpyTag/SpyCatcher system (Fig. 2c) [78] for covalent immobilization of the target. With a size between 20 and 200 nm [79], VLPs are too small for direct use in flow bioreactors; however, gold-containing CCMV-based VLPs have been immobilized in microfluidic flow reactor channels and used for the reduction of nitroarenes in a proof-of-principle study [80].

While the aforementioned strategies have in most cases not directly been used for the immobilization of enzymes in flow chemistry, a set of methods already has been used for that purpose. Those include the use of SpyTag/SpyCatcher based all-enzyme hydrogels [81–85] and functionalized magnetosomes [49].

The formation of all-enzyme hydrogels often uses multivalent enzymes, e.g., possessing a tetrameric quaternary structure, which are covalently crosslinked via attached SpyTag/SpyCatcher Modules (Fig. 2d) [81]. The SpyTag/SpyCatcher system is derived by splitting the CnaB2 domain of the fibronectin-binding protein FbaB from *Streptococcus pyogenes*, yielding the 13 residue SpyTag and the 116 residue SpyCatcher module [51, 73]. When mixed together, the two modules spontaneously reconstitute to form an isopeptide bond resulting in a covalent linkage of SpyTag and SpyCatcher. If the two modules are fused to two target proteins, the two targets become covalently linked (Fig. 2a). Attachment of SpyTag and SpyCatcher to multivalent targets in turn yields higher-order architectures such as nanometer sized protein clusters that can form free standing hydrogels under further desiccation, which have been used in flow biocatalysis [81]. Initially targeted and relying on oligomeric enzymes [81, 82], the strategy was recently extended to work also with monomeric targets [83]. For flow applica-

tion, the 'all-enzyme-hydrogel' approach relies on the fact that upon SpyTag/SpyCatcher-driven self-assembly a homogeneous structure on the micrometer length scale is formed. Since the pore size (< 200 nm) is in the range of microfiltration membranes, the gels are suitable for flow reactions [81]. This was shown first for a combination of an alcohol dehydrogenase from *Lactobacillus brevis* (LbADH) and a glucose-1-dehydrogenase (GDH) for cofactor-regeneration. Later this was extended to other alcohol dehydrogenases also in comparison with an alternative flow setup showing for this application superior space-time yields (STY) [83, 84]. Furthermore, the gel itself serves as compartment entrapping the cofactor thus providing an economical solution for cofactor-regeneration in flow. The concept is not limited to dehydrogenases, but is also applicable, e.g., for phenolic acid decarboxylase (PAD) in the flow production of 4-hydroxystyrene from *p*-coumaric acid [82].

A more complex system, also relying on the SpyTag/SpyCatcher system, was very recently used for the immobilization of enzymes for flow biocatalysis. Mittmann et al. [49] generated functionalized magnetosomes (Fig. 2e) in *Magnetospirillum gryphiswaldense*, a magnetotactic bacterium that can contain up to 40 so-called magnetosomes per cell. Magnetosomes are naturally produced nanoparticles that consist of a cuboctahedral magnetite (Fe_3O_4) core surrounded by a proteinaceous phospholipid bilayer [86, 87]. The latter, in turn, was functionalized using the SpyTag/SpyCatcher system. Here, the SpyCatcher module was fused to magnetosome protein MamC, which tightly associates with the magnetosome membrane thereby displaying the SpyCatcher module on the magnetosome surface. Target proteins, fused with the SpyTag can in turn be covalently linked to the SpyCatcher-functionalized magnetosome. Proof-of-concept studies in flow have been conducted using phenolic acid decarboxylase (PAD) as model enzyme, where the particles could be retained by means of a magnet and stable substrate conversion could be observed over 60 h [49].

2.1.3 Catalytically Active Inclusion Bodies

Traditionally, inclusion bodies (IBs) were conceived as inactive cellular waste, accumulating, e.g., in the cytoplasm of a microbial host due to strong overexpression of heterologous genes. This view perceives IBs as inactive protein aggregates constituted of unfolded target protein [88], useful only as relatively pure source of protein for refolding studies aimed at obtaining the target in its native soluble form [89]. Despite this long-held assumption, IBs can retain a variable degree of activity, which was documented already since the 1980s [90]. As a consequence, the on-demand generation and production of catalytically active inclusion bodies (CatIBs) has emerged in recent years as a promising method for *in vivo* enzyme immobilization [27, 45, 91–93]. CatIB production is hereby achieved via the molecular biological fusion of an aggregation inducing element, a so-called CatIB-tag, to either the 5' or 3' end of a target gene (Fig. 3a), which, upon overexpression of the gene fusion in, e.g., *E. coli*, results in the pull-down of the active fusion protein into an IB matrix constituted of unfolded, or partially folded fusion protein. Tag selection and fusion protein design is still a trial-and-error process. However, in recent years, several parameters were identified, that can aid successful CatIB formation. Those include the presence of hydrophobic surface patches on CatIB-tag and target [94, 45] as well as the choice of the proper fusion terminus [26]. Often, CatIB-formation inducing tag and target are separated by addition of a linker that connects

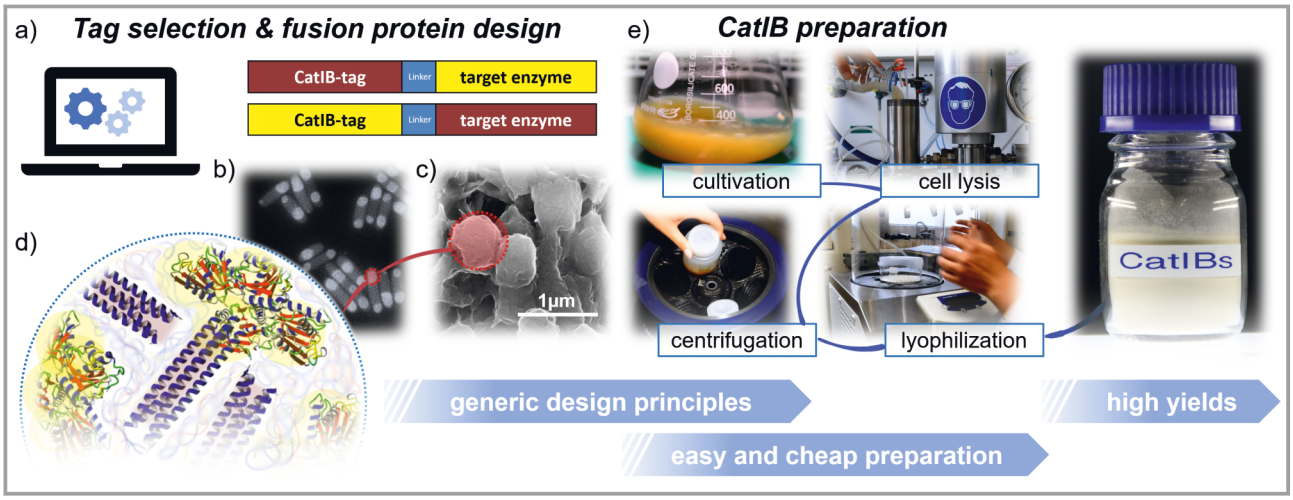

Figure 3. Illustration of the CatIB strategy. a–d) Rational, computer-aided tag selection and fusion protein design. Molecular biological fusion of a so-called CatIB tag to a target enzyme (a) yields CatIBs, visible as refractile particles in microscopic analyses of growing *E. coli* cells (b). Scanning electron microscopy shows water insoluble, proteinaceous CatIBs as sub-micrometer sized particles (c), likely constituted by a matrix of unfolded fusion protein interspersed with correctly folded, and hence active, fusion protein (d). CatIB production is straightforward only requiring heterologous expression of fusions in *E. coli*, cell lysis, centrifugation and washing steps; wet CatIBs can be lyophilized to obtain dry CatIB powder that can be stored for extended time periods [103] (e). To illustrate CatIB yields, a 100 mL glass bottle is shown on the right side containing lyophilized CatIBs prepared from a 5 L *E. coli* culture (right side of panel e).

the two modules and has been shown to impact CatIB formation efficiency and immobilizate activity [44, 95].

Due to their heterogenous nature, the structures of IBs and CatIBs are difficult to access, but studies using different spectroscopic methods have shown that their internal structure also depends on the aggregation inducing tags and can possess or be devoid of amyloid-like structures [96], and can contain a variable degree of unfolded polypeptides alongside natively folded protein [97–99]. Like IBs, CatIBs can easily be obtained by simple heterologous production in, e.g., *E.coli*, cell lysis and subsequent centrifugation and washing steps, yielding relatively pure (up to 90 % target protein) preparations (Fig. 3). The latter property, along with their activity and physical characteristics as dense particles insoluble in water and organic solvents, renders on-demand produced CatIBs an attractive form of *in vivo* carrier-free enzyme immobilizate for application in biocatalysis and flow chemistry. As with all immobilization strategies, optimization may be required, mostly carried out at the construct design level. As already outlined above, the optimal choice of the aggregation inducing tag [26, 94], fusion terminus [26] and linker [95] is critical for obtaining highly active CatIBs. Maintaining a lower temperature during expression, as well as using strong inducers or autoinduction likewise favors the formation of CatIBs with higher activity and yields [100]. In addition to optimal performance characteristics, like activity, stability and yield, it is critical that an immobilization strategy is generically applicable. Both aspects have extensively been reviewed previously [11, 45]. Although the CatIB size, ranging from 50–800 nm, is too small for direct application in flow bioreactors, certain tricks have recently facilitated their use in continuous flow synthesis [26]. Physical entrapment was achieved by utilizing silica, which proved to be inert towards the alcohol dehydrogenase used (from *Ralstonia sp.* – RADH). The conversion was shown to be stable and without loss of enantioselectivity for 280 h; after 120 h of continuous production, 92 % product was isolated in 98 % *ee* corresponding to a STY of 3.55 $g\,L^{-1}h^{-1}$ [26]. For the cofactor recycling, a closed-loop setup was applied that had previously been established for a carrier-based system [101].

3 Future Trends in Flow Chemistry with Biocatalysts

The small size of standard flow chemical reactors renders 3D printing techniques ideal for both rapid prototyping of flow synthesis reaction vessels [103–105] as well as the printing of carrier materials and enzymes [107–108] that facilitate enzyme immobilization [64, 109]. 3D printing, or additive manufacturing, hereby offers unlimited design possibilities and is suitable for a wide range of materials such as various kinds of polymers, metal alloys or even wood-containing filaments. Thus, when suitable polymer materials, such as low-melting point, biodegradable filaments such polycaprolactone (PCL) are combined with suitable enzyme preparations, polymer-enzyme composites can be obtained [110]. A recent study used PCL, which melts at approx. 60 °C, mixed with powdered Amano lipase to yield defined composite films of ~400 to ~500 µm by extrusion-based 3D printing. The films were subsequently analyzed for lipase-promoted hydrolysis, with the goal of producing materials that can be formed by thermoplastic processing while featuring more rapid degradation than by unassisted hydrolysis [110]. In addition, also the controlled release of small molecules (mimicked by a dye) from the material was shown [110]. Albeit, to the best of our knowledge not utilized for biocatalysis, this approach might be readily extendable to printing *in vivo* carrier-free enzyme immobilizates, such as CatIBs, which can be prepared in powdered lyophilized form and represent very stable immobilizates that should withstand moderately high extrusion temperatures as the ones needed for printing PCL filaments.

An exciting field of research covers the extension of flow methods to novel (bio)catalysts and reaction types. For example, the integration of photo(bio)catalytic reactions driven by conventional photocatalysts or enzyme-coupled photocatalysts [111, 112] of naturally occurring photoenzymes [113] into continuous flow processes could further increase the potential applications of flow chemistry [64]. While conventional photocatalytic routes are carried out since many years in continuous flow mode, and certain applications using whole cell systems, e.g., relying of phototrophic organisms have been described [114–116], the use of isolated enzymes is, to the best of our knowledge, restricted to using a photocatalytic nicotinamide adenine dinucleotide (NADH) regeneration system for a conventional biocatalyst in flow [117]. *Bona fide* photoenzymes, thus, still need to see application in continuous flow synthesis. To this end, promising photoenzymes include the recently discovered family of fatty acid photodecarboxylases, which convert free fatty acids to alkanes and alkanes [118, 119], as well as a recently described light-dependent flavoprotein monooxygenase, which is involved in the biosynthesis of 2-alkyl-4-hydroxyquinoline N-oxides in the opportunistic pathogen *Pseudomonas aeruginosa* [120]. For the integration of photo(bio)catalysis in flow synthesis, scalability is certainly an issue for application, due to limited light penetration depths and hence increased requirements for reaction vessels design as well as choice and integration of light sources [64, 121]. However, due to the availability of improved technology on both the reactor and light-source side, the scalability of photochemical reactions in flow has changed tremendously in recent years. For conventional photocatalysts, i.e., the continuous synthesis of cyclobutene by [2+2]-photocycloaddition of ethylene has been scaled to > 5 $kg\,d^{-1}$ [122]. In addition, rapid prototyping methods, including 3D-printing, could contribute to the rapid screening of suitable reactor geometries. Similarly, the choice of catalyst preparation appears more critical for the integration of photocatalytic reactions into flow synthesis than for

conventional catalysts, since carrier materials that are employed should be transparent and scatter the light only minimally, to enable efficient catalysis. While conventional photocatalysts are already available on production scale, photobiocatalysis in flow chemistry certainly is still in its infancy.

Last but not least, with the digitalization of many industrial sectors, digital approaches like computer-aided synthesis planning (CASP) and reaction optimization, have already seen first applications in the flow chemistry field [123–125]. While, CASP is challenging in itself for batch reactions, it becomes even more challenging when aimed at identifying synthetic routes suitable for flow application. Along those lines, Plehiers et al. have recently presented different machine learning models to assess whether a specific reaction would benefit from operation in continues flow mode [124]. Similarly, process optimization using machine learning approaches has also been extended to optimizing reactions in flow mode [123, 125].

4 Conclusions

As outlined above, *in vivo* carrier-free enzyme immobilizates can be produced in a sustainable, resource-efficient manner. Continuous flow chemistry offers outstanding properties such as small size and reagent volume requirements, improved mixing and environmental control. It is thus obvious that both techniques appear as an ideal merger for the production of fine chemicals such as active pharmaceutical ingredients. Identification and synthesis planning can greatly be facilitated by applying flow chemical approaches contributing to process acceleration and hence to the reduction of drug development costs and times [124]. It can thus be expected that both "biocatalyst preparation/immobilization" and "flow chemistry" will receive increased attention in academia in the coming years.

The Authors thank Dr. Irene Küberl (Institute of Bioorganic Chemistry) for her help with generating the Figures of the manuscript. The research was financially supported by the CLIB Competence Centre Biotechnology (CKB) funded by the European Regional Development Fund ERDF (34.EFRE 0300096 and 34.EFRE 0300097). Open access funding enabled and organized by Projekt DEAL.

Gizem Ölçücü studied bioengineering at Montana State University, USA, and Istanbul Technical University, Turkey. She obtained her B.Sc. degrees from the bioengineering dual diploma program in 2012. In 2016, she obtained her M.Sc. degree on molecular life sciences from Friedrich Schiller University Jena, Germany. Since 2018, she has been pursuing her Ph.D. at the Institute of Molecular Enzyme Technology of the Heinrich-Heine-University Düsseldorf located at Forschungszentrum Jülich, Germany. She is interested in protein engineering and *in vivo* enzyme immobilization strategies, and her current research, within the "CLIB Competence Centre Biotechnology", is focused on catalytically active inclusion bodies and ferritin-based immobilizates for biotechnological applications.

Ulrich Krauss studied applied natural sciences at the TU Bergakademie Freiberg, Germany, and obtained his Ph.D. in 2008 from the Heinrich-Heine-University Düsseldorf, Germany. From 2008 to 2010, he worked as a postdoc with Prof. Dr. Karl-Erich Jaeger and Prof. Dr. Wolfgang Gärtner at the Institute of Molecular Enzyme Technology, Heinrich-Heine-University Düsseldorf, Germany, and the Max-Planck Institute for Bioinorganic Chemistry (now MPI Chemical Energy Conversion), Mülheim an der Ruhr, Germany. Since 2009, he is heading the group "Molecular Biophotonics" at the Institute of Molecular Enzyme Technology, Heinrich-Heine-University Düsseldorf located at the Forschungszentrum Jülich, Germany. His research is focused on enzymes and photoreceptors covering the fields of photochemistry, photobiology, and optogenetics as well as biocatalysis, synthetic biology, and structural biochemistry.

Karl-Erich Jaeger studied biology and chemistry and obtained a Ph.D. in microbiology at Ruhr-University Bochum, Germany. From 1988 to 1989, he worked as a postdoc with Prof. Dr. Robert E.W. Hancock at the Department of Microbiology, University of British Columbia, Vancouver, B.C., Canada. In 2002, he became full professor at Heinrich Heine University Düsseldorf and director of the Institute of Molecular Enzyme Technology at Forschungszentrum Jülich. In 2013, the Forschungszentrum Jülich GmbH of the German Helmholtz Association additionally appointed him as director at the Institute of Bio- and Geosciences IBG-1: Biotechnology. Karl-Erich Jaeger is an editorial board member of several scientific journals and serves as vice-president of the Cluster of Industrial Biotechnology–CLIB. His research interests are focused on bacterial enzymes and proteins, their identification, expression, biochemical and structural characterization, and biotechnological applications.

Jörg Pietruszka studied chemistry at the University of Hamburg where he obtained his doctoral degree in 1993 (Prof. Dr. W. A. König). After a postdoctoral stay with Professor Dr. S. V. Ley (Cambridge, UK), he moved to the University of Stuttgart where he finished his Habilitation in 2001. Since 2004 he holds the position as a full professor of bioorganic chemistry at the Heinrich Heine University Düsseldorf; he was appointed as director at the Institute for Bio- and Geosciences IBG-1: Biotechnology at the Forschungszentrum Jülich in 2013. Jörg Pietruszka serves in the management boards of BioRiver and the Bioeconomy Science Centre (BioSC). His research interests include the development of new chemoenzymatic methods and their application in the synthesis of natural products.

Abbreviations

CalB	lipase B of *C. antarctica*
CatIBs	catalytically-active inclusion bodies
CCMV	cowpea chlorotic mottle virus
CLEAS	cross-linked enzyme aggregates
CLECs	cross-linked enzyme crystals
Cry3Aa	*B. thuringensis* Cry3Aa protein forming intracellular protein crystals
GDH	glucose dehydrogenase
GOx	glucose oxidase
HRP	horseradish peroxidase
IBs	inclusion bodies
LbADH	alcohol dehydrogenase of *L. brevis*
MamC	magnetosome protein MamC of *M. gyphiswaldense*
NADH	nicotinamide adenine dinucleotide
NADPH	Nicotinamide adenine dinucleotide phosphate
P22	*S. typhimurium* bacteriophage P22
PAD	phenolic acid decarboxylase
PCL	polycaprolactone
PLE	porcine liver esterase
RADH	alcohol dehydrogenase of *Ralstonia sp.*
SEO	sieve element occlusion
SpyTag	13 residue fragment of the CnaB2 domain of the fibronectin-binding protein FbaB from *S. pyogenes*
SpyCatcher	116 residue fragment of the CnaB2 domain of the fibronectin-binding protein FbaB from *S. pyogenes*
STY	space time yield
TTN	total turnover number
VLPs	virus-like particles

References

[1] C. Bernal, K. Rodríguez, R. Martínez, *Biotechnol. Adv.* **2018**, *36*, 1470–1480. DOI: https://doi.org/10.1016/j.biotechadv.2018.06.002

[2] M. Bilal, Y. Zhao, S. Noreen, S. Z. H. Shah, R. N. Bharagava, H. M. N. Iqbal, *Biocatal. Biotransform.* **2019**, *37*, 159–182. DOI: https://doi.org/10.1080/10242422.2018.1564744

[3] S. I. Shoda, H. Uyama, J. I. Kadokawa, S. Kimura, S. Kobayashi, *Chem. Rev.* **2016**, *116*, 2307–2413. DOI: https://doi.org/10.1021/acs.chemrev.5b00472

[4] J. Chapman, A. E. Ismail, C. Z. Dinu, *Catalysts* **2018**, *8*, 238. DOI: https://doi.org/10.3390/catal8060238

[5] R. A. Sheldon, A. Basso, D. Brady, *Chem. Soc. Rev.* **2021**, *50*, 5850–5862. DOI: https://doi.org/10.1039/d1cs00015b

[6] J. L. Adrio, A. L. Demain, *Biomolecules* **2014**, *4*, 117–139. DOI: https://doi.org/10.3390/biom4010117

[7] R. Hatti-Kaul, U. Törnvall, L. Gustafsson, P. Börjesson, *Trends Biotechnol.* **2007**, *25*, 119–124. DOI: https://doi.org/10.1016/J.TIBTECH.2007.01.001

[8] R. Singh, M. Kumar, A. Mittal, P. K. Mehta, *3 Biotech* **2016**, *6*, 174. DOI: https://doi.org/10.1007/s13205-016-0485-8

[9] C. P. S. Badenhorst, U. T. Bornscheuer, *Trends Biochem. Sci.* **2018**, *43*, 180–198. DOI: https://doi.org/10.1016/j.tibs.2018.01.003

[10] S. Wu, R. Snajdrova, J. C. Moore, K. Baldenius, U. T. Bornscheuer, *Angew. Chem., Int. Ed.* **2021**, *60*, 88–119. DOI: https://doi.org/10.1002/anie.202006648

[11] G. Ölçücü, O. Klaus, K. E. Jaeger, T. Drepper, U. Krauss, *ACS Sustain. Chem. Eng.* **2021**, *9*, 8919–8945.

[12] F. B. Rehm, S. Chen, B. H. Rehm, *Molecules* **2016**, *21*, 1370. DOI: https://doi.org/10.3390/molecules21101370

[13] D. E. Fitzpatrick, S. V. Ley, *Tetrahedron* **2018**, *74*, 3087–3100. DOI: https://doi.org/10.1016/j.tet.2017.08.050

[14] P. Müller, A. D. Clayton, J. Manson, S. Riley, O. S. May, N. Govan, S. Notman, S. V. Ley, T. W. Chamberlain, R. A. Bourne, *React. Chem. Eng.* **2022**, *7*, 987–993. DOI: https://doi.org/10.1039/d1re00549a

[15] M. B. Plutschack, B. Pieber, K. Gilmore, P. H. Seeberger, *Chem. Rev.* **2017**, *117*, 11796–11893. DOI: https://doi.org/10.1021/acs.chemrev.7b00183

[16] A. I. Benitez-Mateos, M. L. Contente, D. R. Padrosa, F. Paradisi, *React. Chem. Eng.* **2021**, *6*, 599–611. DOI: https://doi.org/10.1039/d0re00483a

[17] M. Santi, L. Sancineto, V. Nascimento, J. Braun Azeredo, E. V. M. Orozco, L. H. Andrade, H. Groger, C. Santi, *Int. J. Mol. Sci.* **2021**, *22*, 990. DOI: https://doi.org/10.3390/ijms22030990

[18] M. Bilal, H. M. N. Iqbal, *Int. J. Biol. Macromol.* **2019**, *130*, 462–482. DOI: https://doi.org/10.1016/j.ijbiomac.2019.02.152

[19] S. Datta, L. R. Christena, Y. R. Rajaram, *3 Biotech.* **2013**, *3*, 1–9. DOI: https://doi.org/10.1007/s13205-012-0071-7

[20] H. J. Federsel, T. S. Moody, S. J. C. Taylor, *Molecules* **2021**, *26 (9)*, 2822. DOI: https://doi.org/10.3390/molecules26092822

[21] A. A. Homaei, R. Sariri, F. Vianello, R. Stevanato, *J. Chem. Biol.* **2013**, *6*, 185–205. DOI: https://doi.org/10.1007/s12154-013-0102-9

[22] T. Jesionowski, J. Zdarta, B. Krajewska, *Adsorption* **2014**, *20*, 801–821. DOI: https://doi.org/10.1007/s10450-014-9623-y

[23] R. A. Sheldon, *Adv. Synth. Catal.* **2007**, *349*, 1289–1307. DOI: https://doi.org/10.1002/adsc.200700082

[24] A. Taheri-Kafrani, S. Kharazmi, M. Nasrollahzadeh, A. Soozanipour, F. Ejeian, P. Etedali, H. A. Mansouri-Tehrani, A. Razmjou, S. M. G. Yek, R. S. Varma, *Crit. Rev. Food Sci. Nutr.* **2021**, *61*, 3160–3196. DOI: https://doi.org/10.1080/10408398.2020.1793726

[25] J. Zdarta, A. S. Meyer, T. Jesionowski, M. Pinelo, *Catalysts* **2018**, *8*, 92. DOI: https://doi.org/10.3390/catal8020092

[26] G. Ölçücü, B. Baumer, K. Küsters, K. Möllenhoff, M. Oldiges, J. Pietruszka, K. E. Jaeger, U. Krauss, *ACS Synth. Biol.* **2022**, *11*, 1881–1896. DOI: https://doi.org/10.1021/acssynbio.2c00035

[27] U. Krauss, V. D. Jäger, M. Diener, M. Pohl, K. E. Jaeger, *J. Biotechnol.* **2017**, *258*, 136–147.

[28] E. Barouni, T. Petsi, D. Kolliopoulos, D. Vasileiou, P. Panas, A. Bekatorou, M. Kanellaki, A. A. Koutinas, *Food Chem.* **2016**, *200*, 76–82. DOI: https://doi.org/10.1016/J.FOODCHEM.2016.01.009

[29] A. Basso, S. Serban, *Mol. Catal.* **2019**, *479*, 110607–110607. DOI: https://doi.org/10.1016/J.MCAT.2019.110607

[30] M. Bilal, M. Asgher, H. M. N. Iqbal, H. Hu, X. Zhang, *Catal. Lett.* **2016**, *146*, 2221–2228. DOI: https://doi.org/10.1007/s10562-016-1848-9

[31] M. F. Canbolat, H. B. Savas, F. Gultekin, *J. Appl. Polym. Sci.* **2017**, *134*. DOI: https://doi.org/10.1002/app.44404

[32] M. R. Mehrasbi, J. Mohammadi, M. Peyda, M. Mohammadi, *Renewable Energy* **2017**, *101*, 593–602. DOI: https://doi.org/10.1016/J.RENENE.2016.09.022

[33] A. Pal, F. Khanum, *Process Biochem.* **2011**, *46*, 1315–1322. DOI: https://doi.org/10.1016/J.PROCBIO.2011.02.024

[34] H. Xue, Z. Shen, C. Li, *Biosens. Bioelectron.* **2005**, *20*, 2330–2334. DOI: https://doi.org/10.1016/J.BIOS.2004.07.018

[35] R. A. Sheldon, *Biochem. Soc. Trans.* **2007**, *35*, 1583–1587. DOI: https://doi.org/10.1042/BST0351583

[36] R. A. Sheldon, *Org. Process Res. Dev.* **2011**, *15*, 213–223. DOI: https://doi.org/10.1021/op100289f

[37] A. Basso, S. Serban, Overview of Immobilized Enzymes' Applications in Pharmaceutical, Chemical, and Food Industry, in *Immobilization of Enzymes and Cells*, Humana Press, New York **2020**.

[38] Y. Li, J. Quan, C. Branford-White, G. R. Williams, J. X. Wu, L. M. Zhu, *J. Mol. Catal., B* **2012**, *76*, 15–22. DOI: https://doi.org/10.1016/j.molcatb.2011.12.003

[39] W. Böhmer, T. Knaus, F. G. Mutti, *ChemCatChem* **2018**, *10*, 731–735. DOI: https://doi.org/10.1002/cctc.201701366

[40] A. Sadighi, S. F. Motevalizadeh, M. Hosseini, A. Ramazani, L. Gorgannezhad, H. Nadri, B. Deiham, M. R. Ganjali, A. Shafiee, M. A. Faramarzi, M. Khoobi, *Appl. Biochem. Biotechnol.* **2017**, *182*, 1371–1389. DOI: https://doi.org/10.1007/s12010-017-2404-9

[41] K. Ohmiya, C. Terao, S. Shimizu, T. Kobayashi, *Agric. Biol. Chem.* **1975**, *39*, 491–498. DOI: https://doi.org/10.1080/00021369.1975.10861617

[42] H. T. Imam, P. C. Marr, A. C. Marr, *Green Chem* **2021**, *23*, 4980–5005. DOI: https://doi.org/10.1039/d1gc01852c

[43] M. Yan, Z. X. Liu, D. N. Lu, Z. Liu, *Biomacromolecules* **2007**, *8*, 560–565. DOI: https://doi.org/10.1021/bm060746a

[44] V. D. Jäger, R. Lamm, R. Kloß, E. Kaganovitch, A. Grünberger, M. Pohl, J. Büchs, K. E. Jaeger, U. Krauss, *ACS Synth. Biol.* **2018**, *7*, 2282–2295. DOI: https://doi.org/10.1021/acssynbio.8b00274

[45] V. D. Jäger, R. Lamm, K. Küsters, G. Ölçücü, M. Oldiges, K. E. Jaeger, J. Büchs, U. Krauss, *Appl. Microbiol. Biotechnol.* **2020**, *104*, 7313–7329.

[46] R. Kloss, M. H. Limberg, U. Mackfeld, D. Hahn, A. Grünberger, V. D. Jäger, U. Krauss, M. Oldiges, M. Pohl, *Sci. Rep.* **2018**, *8*, 5856. DOI: https://doi.org/10.1038/s41598-018-24070-2

[47] B. S. Heater, W. S. Chan, M. M. Lee, M. K. Chan, *Biotechnol. Biofuels* **2019**, *12*, 165. DOI: https://doi.org/10.1186/s13068-019-1509-5

[48] F. Visser, B. Müller, J. Rose, D. Prüfer, G. A. Noll, *Sci. Rep.* **2016**, *6*. DOI: https://doi.org/10.1038/srep30839

[49] E. Mittmann, F. Mickoleit, D. S. Maier, S. Y. Stabler, M. A. Klein, C. M. Niemeyer, K. S. Rabe, D. Schuler, *ACS Appl. Mater. Interfaces* **2022**, *14*, 22138–22150. DOI: https://doi.org/10.1021/acsami.2c03337

[50] D. P. Patterson, P. E. Prevelige, T. Douglas, *ACS Nano* **2012**, *6*, 5000–5009. DOI: https://doi.org/10.1021/nn300545z

[51] S. C. Reddington, M. Howarth, *Curr. Opin. Chem. Biol.* **2015**, *29*, 94–99. DOI: https://doi.org/10.1016/j.cbpa.2015.10.002

[52] G. V. Los, L. P. Encell, M. G. Mcdougall, D. D. Hartzell, N. Karassina, C. Zimprich, M. G. Wood, R. Learish, R. F. Ohana, M. Urh, D. Simpson, J. Mendez, K. Zimmerman, P. Otto, G. Vidugiris, J. Zhu, A. Darzins, D. H. Klaubert, R. F. Bulleit, K. V. Wood, *ACS Chem. Biol.* **2008**, *3*, 373–382. DOI: https://doi.org/10.1021/cb800025k

[53] M. Diener, B. Kopka, M. Pohl, K. E. Jaeger, U. Krauss, *ChemCatChem* **2016**, *8*, 142–152. DOI: https://doi.org/10.1002/cctc.201501001

[54] B. S. Heater, M. M. Lee, M. K. Chan, *Sci. Rep.* **2018**, *8*, 12783. DOI: https://doi.org/10.1038/s41598-018-31213-y

[55] B. S. Heater, Z. Yang, M. M. Lee, M. K. Chan, *J. Am. Chem. Soc.* **2020**, *142*, 9879–9883. DOI: https://doi.org/10.1021/JACS.9B13462

[56] Q. Sun, B. S. Heater, T. L. Li, W. Ye, Z. Guo, M. K. Chan, *Bioconjug. Chem.* **2022**, *33*, 386–396. DOI: https://doi.org/10.1021/acs.bioconjchem.2c00003

[57] I. Bustos-Jaimes, R. A. Soto-Román, I. A. Gutiérrez-Landa, J. Valadez-García, C. L. Segovia-Trinidad, *J. Biotechnol.* **2017**, *263*, 55–63. DOI: https://doi.org/10.1016/J.JBIOTEC.2017.09.014

[58] K. Mccoy, T. Douglas, In vivo packaging of protein cargo inside of virus-like particle P22, *in Virus-Derived Nanoparticles for Advanced Technologies* (Eds: C. Wege, G. Lomonossoff), Humana Press, New York **2018**, 295–302.

[59] D. P. Patterson, B. Schwarz, R. S. Waters, T. Gedeon, T. Douglas, *ACS Chem. Biol.* **2014**, *9*, 359–365. DOI: https://doi.org/10.1021/cb4006529

[60] J. Britton, S. Majumdar, G. A. Weiss, *Chem. Soc. Rev.* **2018**, *47*, 5891–5918. DOI: https://doi.org/10.1039/c7cs00906b

[61] J. Coloma, Y. Guiavarc'h, P. L. Hagedoorn, U. Hanefeld, *Chem. Commun.* **2021**, *57*, 11416–11428. DOI: https://doi.org/10.1039/d1cc04315c

[62] S. C. Cosgrove, A. P. Mattey, *Chem.-Eur. J.* **2022**, *28*, e202103607. DOI: https://doi.org/10.1002/chem.202103607

[63] R. A. Sheldon, J. M. Woodley, *Chem. Rev.* **2018**, *118*, 801–838. DOI: https://doi.org/10.1021/acs.chemrev.7b00203

[64] P. De Santis, L. E. Meyer, S. Kara, *React. Chem. Eng.* **2020**, *5*, 2155–2184. DOI: https://doi.org/10.1039/d0re00335b

[65] L. Tamborini, P. Fernandes, F. Paradisi, F. Molinari, *Trends Biotechnol.* **2018**, *36*, 73–88. DOI: https://doi.org/10.1016/j.tibtech.2017.09.005

[66] F. Croci, J. Vilim, T. Adamopoulou, V. Tseliou, P. J. Schoenmakers, T. Knaus, F. G. Mutti, *ChemBioChem* **2022**, *23*, e202200549. DOI: https://doi.org/10.1002/cbic.202200549

[67] A. L. Margolin, *Trends Biotechnol.* **1996**, *14*, 223–230. DOI: https://doi.org/10.1016/0167-779910031-7

[68] E. M. Papamichael, P.-Y. Stergiou, *Enzyme immobilization strategies and bioprocessing applications*, Elsevier, Amsterdam **2020**.

[69] R. A. Sheldon, *Appl. Microbiol. Biotechnol.* **2011**, *92*, 467–477. DOI: https://doi.org/10.1007/s00253-011-3554-2

[70] M. T. De Martino, F. Tonin, N. A. Yewdall, M. Abdelghani, D. S. Williams, U. Hanefeld, F. Rutjes, L. Abdelmohsen, J. C. M. Van Hest, *Chem. Sci.* **2020**, *11*, 2765–2769. DOI: https://doi.org/10.1039/c9sc05420k

[71] M. S. Nair, M. M. Lee, A. Bonnegarde-Bernard, J. A. Wallace, D. H. Dean, M. C. Ostrowski, R. W. Burry, P. N. Boyaka, M. K. Chan, *PLoS ONE* **2015**, *10*.

[72] M. K. Paulmann, M. R. Zimmermann, L. Wegner, A. J. E. Van Bel, G. Kunert, A. C. U. Furch, *Int. J. Mol. Sci.* **2021**, *22*, 492. DOI: https://doi.org/10.3390/ijms22020492

[73] B. Zakeri, J. O. Fierer, E. Celik, E. C. Chittock, U. Schwarz-Linek, V. T. Moy, M. Howarth, *Proc. Natl. Acad. Sci. U. S. A.* **2012**, *109*, E690–697. DOI: https://doi.org/10.1073/pnas.1115485109

[74] I. J. Minten, V. I. Claessen, K. Blank, A. E. Rowan, R. J. M. Nolte, J. J. L. M. Cornelissen, *Chem. Sci.* **2011**, *2*, 358–362. DOI: https://doi.org/10.1039/c0sc00407c

[75] I. J. Minten, L. J. A. Hendriks, R. J. M. Nolte, J. J. L. M. Cornelissen, *J. Am. Chem. Soc.* **2009**, *131*, 17771–17773. DOI: https://doi.org/10.1021/ja907843s

[76] D. P. Patterson, Encapsulation of Active Enzymes within Bacteriophage P22 Virus-Like Particles, in *Protein Scaffolds – Design, Synthesis, and Applications* (Ed: A. Udit), Humana Press, New York **2018**, 11–24.

[77] L. Schoonen, J. C. M. Van Hest, Modification of CCMV Nanocages for Enzyme Encapsulation, in *Protein Scaffolds – Design, Synthesis, and Applications* (Ed: A. Udit), Humana Press, New York **2018**, 69–83.

[78] T. W. Giessen, P. A. Silver, *ChemBioChem* **2016**, *17*, 1931–1935. DOI: https://doi.org/10.1002/cbic.201600431

[79] C. Qian, X. Liu, Q. Xu, Z. Wang, J. Chen, T. Li, Q. Zheng, H. Yu, Y. Gu, S. Li, N. Xia, *Vaccines (Basel)* **2020**, *8*, 139. DOI: https://doi.org/10.3390/vaccines8010139

[80] A. Liu, L. Yang, C. H. Traulsen, J. Cornelissen, *Chem. Commun.* **2017**, *53*, 7632–7634. DOI: https://doi.org/10.1039/c7cc03024j

[81] T. Peschke, P. Bitterwolf, S. Gallus, Y. Hu, C. Oelschlaeger, N. Willenbacher, K. S. Rabe, C. M. Niemeyer, *Angew. Chem., Int. Ed.* **2018**, *57*, 17028–17032. DOI: https://doi.org/10.1002/anie.201810331

[82] E. Mittmann, S. Gallus, P. Bitterwolf, C. Oelschlaeger, N. Willenbacher, C. M. Niemeyer, K. S. Rabe, *Micromachines (Basel)* **2019**, *10*, 795. DOI: https://doi.org/10.3390/mi10120795

[83] P. Bitterwolf, S. Gallus, T. Peschke, E. Mittmann, C. Oelschlaeger, N. Willenbacher, K. S. Rabe, C. M. Niemeyer, *Chem. Sci.* **2019**, *10*, 9752–9757. DOI: https://doi.org/10.1039/c9sc04074a

[84] T. Peschke, P. Bitterwolf, S. Hansen, J. Gasmi, K. S. Rabe, C. M. Niemeyer, *Catalysts* **2019**, *9*, 164. DOI: https://doi.org/10.3390/catal9020164

[85] J. Meyer, L. E. Meyer, S. Kara, *Eng. Life Sci.* **2022**, *22*, 165–177. DOI: https://doi.org/10.1002/elsc.202100087

[86] S. E. Greene, A. Komeili, *Curr. Opin. Cell. Biol.* **2012**, *24*, 490–495. DOI: https://doi.org/10.1016/j.ceb.2012.05.008

[87] R. Uebe, D. Schüler, *Nat. Rev. Microbiol.* **2016**, *14*, 621–637. DOI: https://doi.org/10.1038/nrmicro.2016.99

[88] U. Rinas, E. Garcia-Fruitós, J. L. Corchero, E. Vázquez, J. Seras-Franzoso, A. Villaverde, *Trends Biochem. Sci.* **2017**, *42*, 726–737. DOI: https://doi.org/10.1016/j.tibs.2017.01.005

[89] I. Palmer, P. T. Wingfield, *Curr. Protoc. Protein Sci.* **2012**, *70 (1)*, 2.6.1–28.3.17. DOI: https://doi.org/10.1002/0471140864.ps0603s70

[90] D. M. Worrall, N. H. Goss, *Aust. J. Biotechnol.* **1989**, *3*, 28–32.

[91] R. Köszagová, J. Nahálka, *J. Microbiol. Biotechnol. Food Sci.* **2020**, *9*, 1191–1196.

[92] A. D. Marco, N. Ferrer-Miralles, E. Garcia-Fruitós, A. Mitraki, S. Peternel, U. Rinas, M. A. Trujillo-Roldán, N. A. Valdez-Cruz, E. Vázquez, A. Villaverde, *FEMS Microbiol. Rev.* **2019**, *43*, 53–72. DOI: https://doi.org/10.1093/femsrefuy038

[93] C. Slouka, J. Kopp, O. Spadiut, C. Herwig, *Appl. Microbiol. Biotechnol.* **2019**, *103*, 1143–1153. DOI: https://doi.org/10.1007/s00253-018-9569-1

[94] V. D. Jäger, R. Kloss, A. Grünberger, S. Seide, D. Hahn, T. Karmainski, M. Piqueray, J. Embruch, S. Longerich, U. Mackfeld, K. E. Jaeger, W. Wiechert, M. Pohl, U. Krauss, *Microb. Cell Factories* **2019**, *18*, 33. DOI: https://doi.org/10.1186/s12934-019-1081-5

[95] K. Küsters, M. Pohl, U. Krauss, G. Ölçücü, S. Albert, K. E. Jaeger, W. Wiechert, M. Oldiges, *Microb. Cell Factories* **2021**, *20*, 49. DOI: https://doi.org/10.1186/s12934-021-01539-w

[96] M. Gil-Garcia, S. Ventura, *Front. Bioeng. Biotechnol.* **2021**, *9*. DOI: https://doi.org/10.3389/fbioe.2021.734068

[97] C. Capitini, S. Conti, M. Perni, F. Guidi, R. Cascella, A. D. Poli, A. Penco, A. Relini, C. Cecchi, F. Chiti, *PLoS ONE* **2014**, *9*. DOI: https://doi.org/10.1371/journal.pone.0086720

[98] L. Wang, *Prion* **2009**, *3*, 139–145. DOI: https://doi.org/10.4161/pri.3.3.9922

[99] J. Curtis-Fisk, R. M. Spencer, D. P. Weliky, *J. Am. Chem. Soc.* **2008**, *130*, 12568. DOI: https://doi.org/10.1021/ja8039426

[100] R. Lamm, V. D. Jäger, B. Heyman, C. Berg, C. Curten, U. Krauss, K. E. Jaeger, J. Büchs, *J. Biosci. Bioeng.* **2020**, *129*, 730–740. DOI: https://doi.org/10.1016/j.jbiosc.2020.02.003

[101] B. Baumer, T. Classen, M. Pohl, J. Pietruszka, *Adv. Synth. Catal.* **2020**, *362*, 2894–2901. DOI: https://doi.org/10.1002/adsc.202000058
[102] K. Küsters, R. Saborowski, C. Wagner, R. Hamel, J. D. Sporing, W. Wiechert, M. Oldiges, *Microb. Cell Factories* **2022**, *21*, 108. DOI: https://doi.org/10.1186/s12934-022-01816-2
[103] M. J. J. Harding, S. Brady, H. O'connor, R. Lopez-Rodriguez, M. D. D. Edwards, T. Tracy, D. Dowling, G. Gibson, K. P. P. Girard, S. Ferguson, *React. Chem. Eng.* **2020**, *5*, 728–735. DOI: https://doi.org/10.1039/c9re00408d
[104] E. Peris, O. Okafor, E. Kulcinskaja, R. Goodridge, S. V. Luis, E. Garcia-Verdugo, E. O'reilly, V. Sans, *Green Chem.* **2017**, *19*, 5345–5349. DOI: https://doi.org/10.1039/c7gc02421e
[105] C. R. Sagandira, M. Siyawamwaya, P. Watts, *Arab. J. Chem.* **2020**, *13*, 7886–7908. DOI: https://doi.org/10.1016/j.arabjc.2020.09.020
[106] F. D. Belgrano, O. Diegel, N. Pereira, R. Hatti-Kaul, *Bioresour. Technol.* **2018**, *249*, 777–782. DOI: https://doi.org/10.1016/j.biortech.2017.10.087
[107] C. Fee, S. Nawada, S. Dimartino, *J. Chromatogr. A* **2014**, *1333*, 18–24. DOI: https://doi.org/10.1016/j.chroma.2014.01.043
[108] M. Peng, E. Mittmann, L. Wenger, J. Hubbuch, M. K. M. Engqvist, C. M. Niemeyer, K. S. Rabe, *Chem.-Eur. J.* **2019**, *25*, 15998–16001. DOI: https://doi.org/10.1002/chem.201904206
[109] Y. Shao, Z. Liao, B. Gao, B. He, *ACS Omega* **2022**, *7*, 11530–11543. DOI: https://doi.org/10.1021/acsomega.2c00357
[110] A. F. Greene, A. Vaidya, C. Collet, K. R. Wade, M. Patel, M. Gaugler, M. West, M. Petcu, K. Parker, *Biomacromolecules* **2021**, *22*, 1999–2009. DOI: https://doi.org/10.1021/acs.biomac.1c00105
[111] F. Feyza Ozgen, M. E. Runda, B. O. Burek, P. Wied, J. Z. Bloh, R. Kourist, S. Schmidt, *Angew. Chem., Int. Ed.* **2020**, *59*, 3982–3987. DOI: https://doi.org/10.1002/anie.201914519
[112] S. Kochius, Y. Ni, S. Kara, S. Gargiulo, J. Schrader, D. Holtmann, F. Hollmann, *Chempluschem* **2014**, *79*, 1554–1557. DOI: https://doi.org/10.1002/cplu.201402152
[113] L. O. Björn, *Photochem. Photobiol.* **2018**, *94*, 459–465. DOI: https://doi.org/10.1111/php.12892
[114] Y. K. Dasan, M. K. Lam, S. Yusup, J. W. Lim, P. L. Show, I. S. Tan, K. T. Lee, *J CO2 Util.* **2020**, *41*, 101226. DOI: https://doi.org/10.1016/j.jcou.2020.101226
[115] K. Köninger, Á. Gómez Baraibar, C. Mügge, C. E. Paul, F. Hollmann, M. M. Nowaczyk, R. Kourist, *Angew. Chem., Int. Ed.* **2016**, *55*, 5582–5585. DOI: https://doi.org/10.1002/anie.201601200
[116] F. F. Özgen, M. E. Runda, S. Schmidt, *ChemBioChem* **2021**, *22*, 790–806. DOI: https://doi.org/10.1002/cbic.202000587
[117] F. J. Gu, Y. Z. Wang, Z. H. Meng, W. F. Liu, L. Y. Qiu, *Catal. Commun.* **2020**, *136*, 105903. DOI: https://doi.org/10.1016/j.catcom.2019.105903
[118] V. A. Aleksenko, D. Anand, A. Remeeva, V. V. Nazarenko, V. Gordeliy, K. E. Jaeger, U. Krauss, I. Gushchin, *Catalysts* **2020**, *10*, 1072. DOI: https://doi.org/10.3390/catal10091072
[119] D. Sorigue, B. Legeret, S. Cuine, S. Blangy, S. Moulin, E. Billon, P. Richaud, S. Brugiere, Y. Coute, D. Nurizzo, P. Muller, K. Brettel, D. Pignol, P. Arnoux, Y. Li-Beisson, G. Peltier, F. Beisson, *Science* **2017**, *357*, 903–907. DOI: https://doi.org/10.1126/science.aan6349
[120] S. Ernst, S. Rovida, A. Mattevi, S. Fetzner, S. L. Drees, *Nat. Commun.* **2020**, *11*, 2600. DOI: https://doi.org/10.1038/s41467-020-16450-y
[121] K. Donnelly, M. Baumann, *J Flow Chem* **2021**, *11*, 223–241. DOI: https://doi.org/10.1007/s41981-021-00168-z
[122] M. G. Beaver, E. X. Zhang, Z. Q. Liu, S. Y. Zheng, B. Wang, J. P. Lu, J. Tao, M. Gonzalez, S. Jones, J. S. Tedrow, *Org. Process Res. Dev.* **2020**, *24*, 2139–2146. DOI: https://doi.org/10.1021/acs.oprd.0c00185
[123] A. M. Schweidtmann, A. D. Clayton, N. Holmes, E. Bradford, R. A. Bourne, A. A. Lapkin, *Chem. Eng. J.* **2018**, *352*, 277–282. DOI: https://doi.org/10.1016/j.cej.2018.07.031
[124] P. P. Plehiers, C. W. Coley, H. Gao, F. H. Vermeire, M. R. Dobbelaere, C. V. Stevens, K. M. Van Geem, W. H. Green, *Front. Chem. Eng.* **2020**, *2*, 5. DOI: https://doi.org/10.3389/fceng.2020.00005
[125] M. I. Jeraal, S. Sung, A. A. Lapkin, *Chem.: Methods* **2021**, *1*, 71–77. DOI: https://doi.org/10.1002/cmtd.202000044

3. Discussion

The overarching aim of this PhD thesis was the extension of the available toolbox of recent *in vivo* enzyme immobilization strategies, which combine enzyme production and immobilization in one step, thereby forgoing expensive protein purification and immobilization steps. To this end, different fusion strategies were investigated in an attempt to rationalize catalytically-active inclusion body (CatIB) formation, where a commonly employed CatIB tag of coiled-coil nature (TdoT), and short, artificial peptide tags (18AWT, L6KD and GFIL8) were fused both N- and C- terminally to the red fluorescent reporter protein mCherry from *Discosoma striata*, and two industrially relevant enzymes, Lipase A from *B. subtilis* (BsLA) and alcohol dehydrogenase from *Ralstonia sp.* (RADH). The resulting CatIBs were assayed under identical conditions in a benchmarking fashion to allow a direct comparison of their biotechnologically relevant properties, and the best performing CatIBs were used in flow applications for the first time (**Section 2.1**). Furthermore, this benchmarking study aimed towards improving the shortcomings of previous constructs generated by the TdoT tag [108, 109, 117], such as low residual activities and CatIB stabilities, as well as investigating the CatIB formation capabilities of the short tags with difficult-to-immobilize targets such as mCherry. Moreover, the same rationale was extended to determine the role of flexible vs. rigid intra-domain linkers present between either of the five CatIB tags (TdoT, 3HAMP, 18AWT, L6KD, and GFIL8) and the lysine decarboxylase from *E. coli* (EcLDC) as target for immobilization (**Section 2.2**, main work of Kira Küsters, IBG-1, FZJ). In addition, a novel method was established to generate magnetic protein aggregates (MPAs) based on the fusion of ferritin to a target protein, which aimed towards addressing purity issues resulting from the CatIB preparation procedure and providing a simplified alternative for purification via exploiting the magnetism of the MPAs due to the superparamagnetism of iron-loaded ferritin (**Section 2.3**). Additionally, MPAs were shown to be useful in immobilizing enzymes via a bait-prey strategy using the SpyTag/SpyCatcher interaction.

Due to the growing popularity of CatIBs and the wealth of knowledge originating from various research groups that use different strategies and focus on different CatIB tags and targets, an overview over the state of the art was urgently required to disseminate all relevant information in the field, rendering the strategy more accessible for the wider research and industrial community. Therefore, a review paper (**Section 2.4**) was prepared that summarizes available CatIB tags and so far employed targets, highlighting general strategies that have been shown to work under different conditions, as well as achievements, limitations, and considerations for future research. As already men-

tioned, multiple groups that conduct research on CatIBs use a variety of conditions for cultivation, expression, and characterization, and even consider immobilization success based on different parameters. This fact made it imperative to provide an up-to-date collection of methods suitable for the generation, production, and characterization of CatIBs to serve as an up-to-date laboratory manual (**Section 2.5**). The presented book chapter illustrates the entire process of CatIB generation from rational design principles to step-by-step preparation and handling of CatIBs. Moreover, as the interest in enzyme immobilization is rapidly growing, and new and promising *in vivo* enzyme immobilization methods have been emerging, the current knowledge in the field regarding such *in vivo* methods, including advantages, disadvantages, and common pitfalls was reviewed in a comprehensive manner (**Section 2.6**). Finally, various carrier-free enzyme immobilizates including CatIBs were critically reviewed from the perspective of flow chemistry application (**Section 2.7**).

In the following discussion sections, firstly the parameters that have been deemed important for the generation of CatIBs (**Section 2.4, Section 2.5** and **Section 2.6**) will be briefly summarized and critically discussed to provide a methodological basis for the work that will be discussed later, as well as putting the employed design strategies (**Section 2.1**, **Section 2.2** and **Section 2.3**) into a broader perspective. To this end, the design parameters that are imperative for the successful employment of the CatIB method, which encompasses properties of the target protein, the CatIB tag, and linker selection will be discussed first (**Section 3.1**). Conventional cloning methods that are commonly employed to generate CatIBs, as well as newer approaches that are more suitable for automation (**Section 3.1.2**), and expression conditions that are vital to obtaining CatIBs will be summarized (**Section 3.1.3**). Furthermore, from the perspective of characterization of CatIBs, limitations of certain conventional methods which are suitable for the characterization of soluble proteins will be discussed, and the modifications applied to such methods to render them applicable for analysis of CatIBs will be summarized (**Section 3.1.4**). Moreover, methods used in the determination of immobilization success for CatIBs such as automated microscopy, as well as specifically defined parameters that are important for their critical analysis, such as CatIB formation efficiency, residual activity, yields and biomass specific activity yields (**Section 3.1.5**) will be discussed in detail, as these parameters were used to critically evaluate different CatIB producers that were benchmarked as part of this PhD thesis (**Section 2.1**).

In **Section 3.2**, the industrially relevant properties of the CatIB constructs such as activities and yields, which could be improved by genetic design are critically discussed and evaluated from a broader perspective. In the following section (**Section 3.3**), design

parameters that affect specifically CatIB formation efficiency, as well as strategies that could help to immobilize difficult targets via the approach are discussed. The discussion of the CatIBs section will be extended to flow chemistry applications (**Section 3.4**), as demonstrated for the first time within this work, and covered by the recent review (**Section 2.7**). Finally, the newly generated, magnetic *in vivo* produced immobilizates (MPAs) will be discussed in detail, and the advantages, limitations, and possible future iterations of the approach will be covered (**Section 3.5**).

3.1. General strategies for the production and characterization of CatIBs

The successful immobilization of a given protein via the CatIB approach relies on many different parameters. Factors that have been deemed crucial for the implementation of the CatIB approach are, fusion construct design, choice of cloning methods, expression conditions, adaptation of characterization methods, and lastly, how the immobilization success is quantified. Therefore, the above-mentioned concepts covered as results in **Section 2.4, Section 2.5** and **Section 2.6** and the corresponding parameters to judge CatIB-formation success will be briefly summarized and discussed.

3.1.1. Fusion construct design principles for successful CatIB formation

The genetic constructs facilitating the pull-down of the target protein into CatIBs generally consist of genes encoding the target, a CatIB tag, and a linker sandwiched between these two elements. Despite the rather large toolbox of CatIB tags that were shown to generate CatIBs for different targets, whether or not a certain tag would result in successful immobilization when used in combination with a given target can not be determined with certainty. Therefore, the strategy to generate CatIBs is still regarded as a "trial and error" process, where the optimal tag, fusion terminus, and the employed linker needs to be identified experimentally in order to obtain the best performing CatIB immobilizate. However, this does not mean that the process to generate CatIBs can not be predicted, or rationalized at all; in fact, there are numerous considerations that can aid the design process to ultimately help determine the best possible path when generating CatIBs (**Figure 3.1**). Similarly, these considerations can also guide the optimization of existing CatIB constructs to facilitate the tailoring of CatIB properties.

Since it is advisable to not temper with a terminus that is buried within the protein

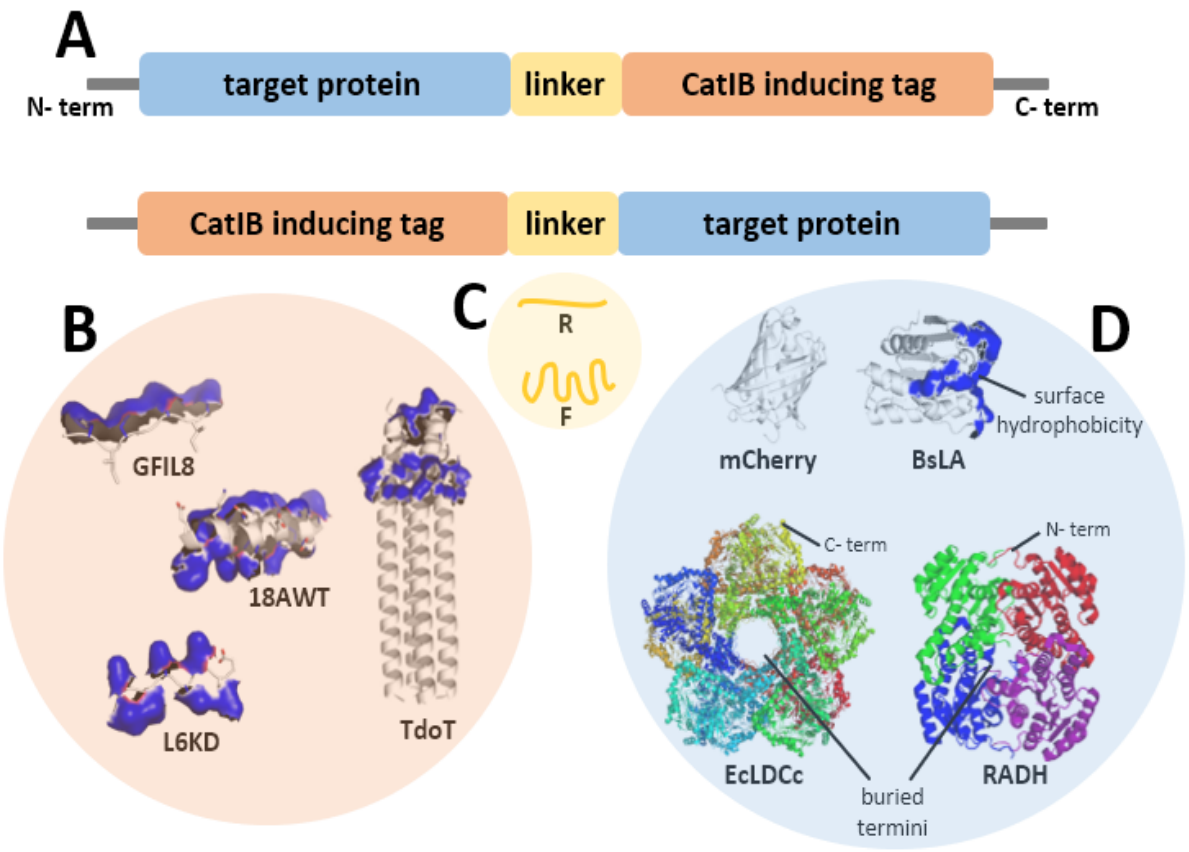

Figure 3.1. Illustration of design parameters and properties of relevant elements involved in successful CatIB construct design.

(A) The choice of CatIB tag, exemplified by GFIL8, 18AWT, L6KD, and TdoT tags, and its fusion site (N- or C-terminal), **(B)** the 3D structure, oligomeric state, surface hydrophobicity of the employed tag, **(C)** rigid (R) or flexible (F) nature of the linker, and **(D)** structure, oligomeric state, surface hydrophobicity and eventually buried termini of the target proteins are illustrated. Depicted proteins are mCherry (PDB ID: 2H5Q), BsLA (PDB ID: 1ISP), RADH (PDB ID: 4BMN) and EcLDC (PDB ID: 5FKZ). The tag and protein structures showing surface hydrophobicity are adapted from [84].

structure, the first and foremost parameter to consider when designing a CatIB construct is the native 3D structure of the target protein(**Figure 3.1, D**). To this end, the protein data bank (PDB [188]) and structure visualization tools such as PyMol [189] are invaluable tools for ruling out a given terminus from fusion with the CatIB tag. Moreover, since protein crystal structures do not always reflect the correct or native quaternary structure of the crystallized protein [190], it is imperative to consider quaternary structure information alongside structural information. X-ray crystallography hereby commonly yields

atomic coordinates of the asymmetric unit (ASU) with the crystal being constituted by an "infinite" lattice of ASUs. But, the quaternary structure of a given protein may be formed from one or more ASUs. The difficulty with protein oligomer structures identified by crystallography therefore lies in discriminating non-native protein contacts, which form due to crystal packing, from biologically relevant protein contacts in their native environment. Similarly, since PDB files obtained from the protein data bank only contain atomic coordinates of the ASU, but the native quaternary structure might be present in the crystal built from symmetry-related molecules, tools like the Proteins, Interfaces, Structures and Assemblies (PISA [191]) can be used to infer alternative biological assemblies. Moreover, since flexible termini in the crystal do not yield electron density in X-ray spectroscopy, the completeness of the protein sequence covered in the crystal should always be validated. For proteins whose structure is not solved, or when both termini appear to accommodate a fusion, two constructs should be designed that harbor the tag at either terminus to increase the chances of a desirable outcome. Here, our benchmarking study has shown that the fusion of the same tag to different termini (**Figure 3.1, A**) can have a profound impact on the activity of CatIBs, as was shown with N- versus C-terminal fusions of the GFIL8 tag to obtain RADH CatIBs, where fusion at the optimal terminus yielded CatIBs with a striking 32-fold higher activity (see **Section 2.1** and **Section 3.2**). Therefore, it is imperative to ensure that the best fusion site is identified when generating CatIBs.

When it comes to the choice of the CatIB tag itself, analyzing the properties of the target protein might provide a hint for determining a promising tag candidate. For instance, proteins that possess a larger hydrophobic surface (**Figure 3.1, B**) can be considered rather facile targets, whereas those displaying less surface hydrophobicity can be considered highly soluble targets that are more difficult to pull-down. The hydrophobic patches of an immobilization target can be analyzed via tools such as AGGRESCAN [192] or TANGO [193]. Furthermore, these tools can be applied to derive the aggregation tendencies of the CatIB tags as well, however, care must be taken here as there are indications that for certain tags such as coiled-coil proteins or protein domains, the driving force of CatIB formation depends on the coiled-coiled propensity rather than the aggregation tendency of the tag, and this property can be analyzed with various tools such as PSIPRED [194, 195] or GOR [196]. Moreover, the polarity of a tag can be analyzed as well, which might have a negative impact on the aggregation tendency [141]. However, this parameter was also shown to be less important when the nature of CatIB formation is driven by a coiled-coil tag. Therefore, coiled-coil tags that have already been used to generate CatIBs of numerous targets, such as TdoT, can be regarded as a good

starting point, especially when difficult-to-immobilize proteins serve as targets where the shorter CatIB tags were shown to work only sub-optimally (**Section 2.1**, see **Section 3.3**). Likewise, widely used tags that were generally shown to yield CatIBs with high efficiencies and activities such as L6KD, GFIL8, 18AWT, or cellulose binding domains can prove useful [112, 113, 114, 124].

Last but not least, the choice of the linker (**Figure 3.1, C**) is an important parameter to consider when designing a CatIB construct. There are indications that the presence of a rigid linker (such as a proline-threonine, PT-linker or alanine-lysine-glutamic acid, AAAKE-linker) yields a better outcome (i.e CatIBs with increased activities) [107] when compared to those bearing flexible linkers (such as glycine-serine, GS-linker, see **Section 2.3** and **Section 3.2**). Finally, not including a linker at all has also been shown to improve CatIB formation for certain targets, previously exemplified by the generation of CatIBs displaying higher fluorescence when a flexible linker was removed from the mCherry and YFP constructs [108]. In summary, the parameters described above can aid the successful design of CatIBs constructs, yielding CatIBs displaying desired properties. So far, a comprehensive study simultaneously optimizing all of these parameters in a high-throughput fashion is still lacking, but several studies, also part of this PhD thesis (**Section 2.1**), have addressed them separately for optimizing the biotechnologically relevant properties of the resulting CatIB immobilizates.

3.1.2. Cloning methods for generation of CatIBs

When generating CatIB constructs, a modular design of the genetic elements and boundaries that allow the facile exchange of the CatIB tag, linker, and target gene are extremely helpful. At the moment, this is achieved simply by including unique restriction enzyme recognition sites between each element (**Figure 3.2**), which can be digested with corresponding restriction endonucleases, thereby allowing facile creation of constructs via conventional cloning methods. The entire CatIB construct can be synthesized commercially and cloned into suitable expression vectors, which can be later used to generate additional constructs for initial testing, as well as optimization of the existing ones. This strategy was utilized in combination with In-Fusion cloning (see below) to generate CatIB constructs used in this work (**Section 2.1**).

In addition to conventional cloning methods relying on the hydrolysis of DNA by restriction endonucleases and directed cloning by employing T4 DNA ligase, a few studies that utilize restriction enzyme-free/ligation-free cloning methods for generating CatIB constructs exist [122, 123, 124]. As part of the PhD thesis presented here,

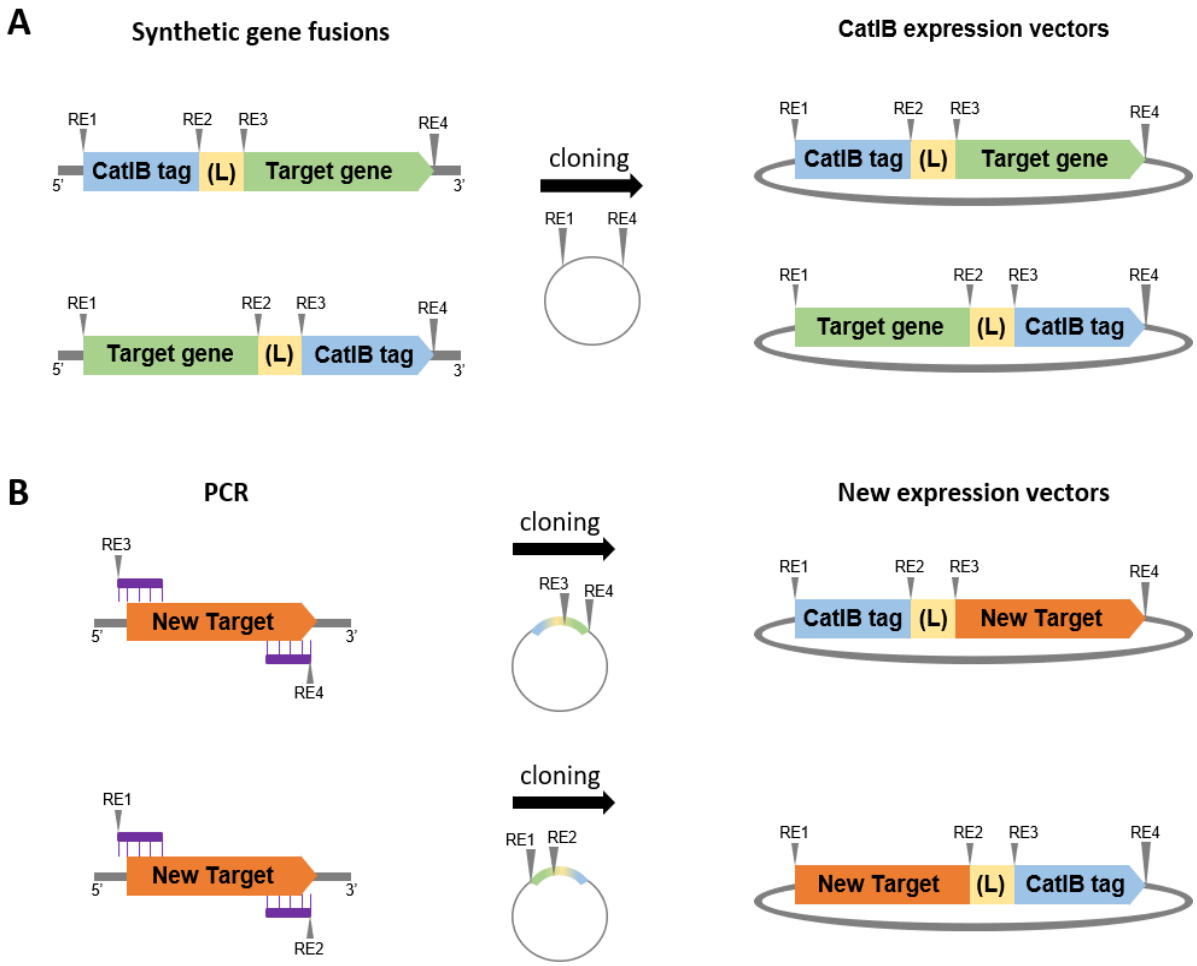

Figure 3.2. Modular construction of CatIB constructs.

Restriction enzyme recognition sites (RE) are present between a gene that encodes a CatIB tag, a linker (L), and the target gene, as well as flanking the entire construct. **(A)** Constructs that contain the CatIB tag at 5' as well as 3' end (left, expressing fusions with the N-terminal and C-terminal tags, respectively) can be cloned into a suitable expression vector to generate CatIB expression vectors (right). **(B)** CatIB expression vectors in (A) can then be digested to remove the old immobilization target and insert the new target which is e.g. amplified via PCR to generate new expression vectors. Though not depicted, new CatIB tags and linkers can be cloned into CatIB expression vectors using the same principle. Reproduced from [186] with permission from Springer Nature.

two non-conventional cloning methods that are suitable for automation have been used, which will be described briefly. In-Fusion cloning is a highly efficient, ligation-free cloning method that allows the seamless, scar-free generation of constructs, not resulting in the insertion of additional bases [197]. Developed by Clonetech (now TakaraBio), In-Fusion cloning relies on the vaccinia virus DNA polymerase that can join DNA fragments bear-

ing complementary base pairs [198]. To this end, 15-20 base pairs that are complementary to the 5' and 3' ends of the vector at the desired insertion site are included at both ends of the insert. The enzymes in the In-Fusion enzyme mixture digest 3' ends of the linearized DNA, creating 5' overhangs that are then annealed. In addition to not leaving a scar, the method is also extremely fast, as the reaction takes only 15 minutes to complete and the resulting construct can be directly used for transformation. Therefore, the In-Fusion cloning method was implemented in this thesis as an alternative method for the facile generation of CatIB expression constructs (**Section 2.1**, see methods for further details).

Similarly, Golden Gate cloning can be used to assemble CatIB tag, linker, and the target gene seamlessly [199]. The method relies on type IIs restriction enzymes that cleave DNA at a site that is distant from their recognition site, therefore effectively removing their recognition site from the final construct. Furthermore, the method allows the easy and simultaneous assembly of multiple DNA fragments, due to the generation of four-nucleotide overhangs that can only ligate to that of the complementary fragment. As such, Golden Gate cloning is a powerful method, and was implemented to generate EcLDC constructs bearing different linker and CatIB tag combinations (see **Section 2.3**). Other cloning methods such as Gibson assembly, which can be useful when assembling multiple elements, as well as additional methods that forego the need for ligation such as TOPO cloning, might prove useful as well [200].

As outlined above, when attempting CatIB immobilization of new target proteins, optimizing existing CatIB constructs by the linker and CatIB tag variations, as well as exploring new CatIB tags, it is often necessary to generate multiple constructs to ensure success. This can lead to the necessity of generating a large number of constructs, especially when multiple options are explored for each element of the CatIB fusion construct, making the cloning process highly time consuming and laborious. Therefore, the implementation of automated workflows for the generation of CatIB constructs would be highly desirable. Depending on the choice of cloning method, some of the steps that are necessary to follow, such as PCR, gel electrophoresis, restriction digestion, ligation, transformation, colony picking, and cultivation, are already automated using robotic liquid and plate handling stations, which are also available commercially [201]. Additionally, the use of seamless cloning methods such as In-Fusion already forgoes the ligation step and are therefore especially suited for automation. Moreover, an alternative strategy that is likewise suited for automation relies on a process called "co-transformation cloning", where the expression plasmid containing the desired gene is constructed *in vivo* via recombination, without additional *in vitro* steps [202]. In this method, the vec-

tor backbone and the insert are amplified by PCR and contain matching ends that are up to 20 base pairs long, which are therefore suitable to be joined inside transformed *E. coli* cells. The method allows for easy positive and negative selection via the specifically engineered vectors, where positive selection is achieved by the complementation of a defective antibiotic resistance gene present in the engineered vector backbone, in the presence of the correctly orientated insert. Negative selection is performed by the employment of a different vector backbone, where the lack of insert results in the retainment of the toxic *ccdB* gene instead. In this case, the gene encoding the CcdB protein targets the A subunit of DNA gyrase, resulting in DNA breakage and subsequent cell death [203]. Very recently, using a similar approach, Golden Gate cloning was combined with a suicide vector containing the toxic *ccdB* gene for negative selection to generate glucose dehydrogenase CatIBs [204]. In conclusion, the implementation of suitable methods to achieve fully automated cloning for the generation of CatIBs would prove an invaluable tool for the future.

3.1.3. Expression conditions for successful CatIBs production

Apart from the construct design, different cultivation conditions can also have a profound impact on CatIB production. The important cultivation parameters for successful CatIB production have been established rather well across many different research groups. The temperature during expression is one of the most important factors, as low temperatures favor the formation of CatIBs rather than conventional, inactive IBs [205, 206, 207], leading to an overall higher activity or increased fluorescence for the immobilized target (**Section 2.4**). Though there are studies that use 37 °C as expression temperature [111, 115], expression is more commonly performed at lower temperatures, typically between 15-30 °C to ensure generation of CatIBs with enhanced activities [113, 112, 114, 104, 107, 117]. Another equally important parameter for CatIB formation is the induction strength, where strong inducers promote higher CatIB yields, albeit at the expense of activity. Regardless, isopropyl β-D-1-thiogalactopyranoside (IPTG) is commonly used as a strong inducer of T7-lac based expression, as it was shown that low induction strength can result in extremely low amounts of protein within CatIBs, rendering strong inducers more beneficial [205]. Along these lines, autoinduction for T7-lac based expression that contains optimized concentrations of glycerol, lactose and glucose allows the production of CatIBs without the need for measuring the optical density periodically and is therefore especially suited for automation of the process. While *E. coli* is the most commonly used host for CatIB production, and was also employed within the

experimental part of this thesis (**Section 2.1** and **Section 2.2**), production of CatIBs was shown in yeast as well [208]. Along the same lines, while T7-lac based expression and induction with IPTG or autoinduction media comprise the most common way of CatIB production, other expression systems such as lac-trp hybrids were used in the past [115]. Nevertheless, using *E. coli* as an expression host, and strong inducers while maintaining a low temperature during expression comprise the most widely utilized expression strategy for ensuring CatIB formation. Further empirical studies would be needed to test CatIB formation in different hosts and or optimize the production process.

3.1.4. Adaptation of characterization methods for analyzing CatIB formation and CatIB properties

Being insoluble particles, biotechnologically relevant properties of CatIBs such as stability, activity, and yield typically need special methods to be suitably evaluated. Many methods that allow the characterization of soluble proteins with ease, such as spectrophotometric analyses, or dynamic light scattering (DLS), are in general not directly applicable to CatIBs. Size determination methods using DLS usually fail for CatIBs, due to their heterogeneous size distribution. This does not mean that CatIBs can not be analyzed via conventional methods. For instance, as an alternative to DLS, instruments relying on laser diffraction can be very beneficial for CatIBs. To address issues due to the turbidity of CatIB samples in i.e. activity assays, a simple centrifugation step can be implemented after a discontinuous activity assay to remove the CatIB particles that might otherwise pose an obstacle to the analysis of the sample via spectrophotometry. For efficient colorimetric assays that do not require copious amounts of CatIBs, such as a typical esterase/lipase activity assay for a lipase using a model substrate like para-nitrophenyl butyrate (*p*-NPB), directly using the CatIB containing reaction mixture for a continuous measurement is possible (as shown for BsLA CatIBs, **Section 2.1**). Moreover, CatIBs can pose a challenge for flow applications due to their rather small particle size, which can be remedied by directly mixing CatIBs with appropriate materials (such as silica) to ensure their retention, and this technique allowed their use in flow chemistry applications in both flow-through and closed-loop modes (**Section 2.1**, also see **Section 3.4**).

Furthermore, the insoluble nature of CatIBs represents an additional difficulty in terms of reproducibility, as homogeneity is often difficult to achieve within technical replicates of a given CatIB sample. Therefore, when working with CatIBs, it is recommended to increase the number of technical replicates to reduce the room for error. Also, proper mixing is indispensable for the handling of CatIB suspension. Similarly, CatIB

fractions should always be handled very carefully and thoroughly suspended to ensure no visible clumps remain that might complicate analyses and have a negative impact on reproducibility. Finally, when measuring protein concentration of CatIBs, a conventional assay such as Bradford, which is suitable for optically clear samples [209] is not feasible. However, CatIBs can be solubilized using a strong base such as a solution of 6M guanidine-hydrochloride, followed by centrifugation to obtain solubilized CatIB proteins, which can be used to determine the protein concentration based on absorbance at 280 nm. It should be noted that, despite being rather pure, CatIB preparations can also contain other proteins, such as membrane proteins OmpA, OmpB, and IB associated chaperones IbpA and IbpB [119] that localize to the insoluble fraction. This likely results in the overestimation of the protein content of CatIBs measured via the above-described approach, leading to an underestimation of specific activities as a consequence.

3.1.5. Quantifying CatIB formation efficiency, activity and yield

To quantify the immobilization success and the suitability of CatIBs for a given application, there are certain analyses that can be conducted. Microscopy can serve as a simple, yet very useful tool to obtain insights into (Cat)IB formation. As stated previously, CatIBs appear as refractive particles at the cell poles. Therefore, living cells overexpressing a CatIB fusion construct can be screened via phase-contrast microscopy to reveal the presence of (Cat)IBs and can be used to determine the percentage of cells that exhibit CatIBs (**Section 2.2**). Furthermore, automated microscopy [210] can be especially powerful as it enables rapid and facile pre-screening of CatIB constructs, and this approach was applied to screen RADH and BsLA constructs bearing coiled-coil tags and artificial peptides (**Section 2.1**). However, care must be taken as it is not possible to distinguish between conventional IBs from CatIBs via microscopic analyses, and despite revealing their presence, microscopy does not offer any hints on the stability of (Cat)IBs. Therefore, the activity of the target protein in the CatIB fraction must always be determined to ensure that the strategy actually yields active immobilizates, and stability analyses should ideally also be conducted.

Despite allowing a high throughput visual analysis of a given CatIB construct, analysis of the automated microscopy pictures can be a difficult and laborious process. For instance, **Figure 3.3** depicting RADH CatIBs bearing the N-terminal GFIL8 tag show the same *E. coli* cells imaged approximately four seconds apart. Here, cells, clearly showing the presence of (Cat)IBs in panel **(A)** are marked with red and blue arrows, while the very same cells in panel **(B)** appear blurry, and instead, the cells marked with yellow arrows

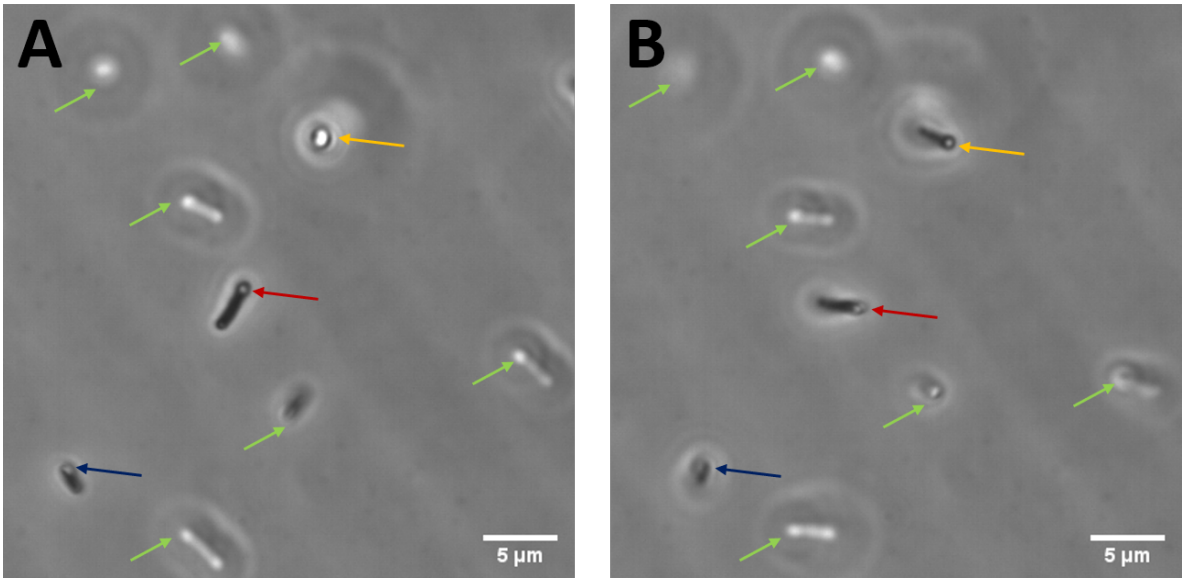

Figure 3.3. Automated microscopy pictures depicting live *E. coli* cells producing GFIL8-RADH CatIBs.

Panels **(A)** and **(B)** show the same cells analyzed via automated microscopy, where the image in panel **(B)** was obtained approximately four seconds after the image shown in panel **(A)**. The red, yellow, and blue arrows that are colored the same in both panels point towards the same cells that produce GFIL8-RADH CatIBs. Green arrows point toward cells that are not in focus.

clearly show (Cat)IB presence, though this was not detected in panel **(A)**. This effect is an unavoidable consequence of imaging unfixed, living cells, where the cells can rotate or move across the frame due to the flow rate of the automated injection station (flow chamber dimensions; height: 20 µm, length: 58.5 mm, width: 800 µm, for further details, see methods section of **Section 2.1**) therefore resulting in cells that are going in and out of focus. Additionally, cells that are completely out of focus (indicated with green arrows) make the analysis of the images difficult at times by obstructing the clear view of other cells. During a single imaging session via automated microscopy, the setup is able to produce 500 individual images. When combined with the technical replicates needed for a single CatIB construct, one needs to manually analyze up to 2,000 images for the presence or absence of IBs. In this sense, automating image analysis, i.e. via deep learning algorithms, would prove immensely time-efficient and helpful. Overall, microscopic studies only yield qualitative information, e.g. whether or not a construct is yielding IBs. Thus, a more quantitative assessment of CatIB formation is needed that incorporates both the efficacy of the CatIB formation process and also considers that not all of the proteins incorporated into IBs are necessarily active. Along those lines,

CatIB formation efficiencies and CatIB residual activities have proven useful parameters for the characterization of CatIBs, both of which will be described in the following.

CatIB formation efficiency (%) is a parameter that refers to the ability of a certain tag at a given terminus to "shift" or "pull" the target protein into the insoluble (CatIB) fraction. As such, calculating CatIB formation efficiency requires fractionation of the crude cell extract (CCE) to yield soluble and insoluble fractions, where the latter contains CatIBs (**Figure 3.4**). It is determined by measuring the volumetric activity (U/ml, where U is the enzyme unit expressed as µmol/min), or fluorescence, of a target protein in the CatIB fraction (P2, washed pellet), and expressing this value relative to the activity or fluorescence of the CCE **Equation 3.1**.

$$CatIB\ formation\ efficiency\ [\%] = \frac{Activity\ of\ P2\ [\frac{U}{ml}]}{Activity\ of\ CCE\ [\frac{U}{ml}]} \times 100 \tag{3.1}$$

Since the process of obtaining the CatIB fraction involves only centrifugation and resuspension steps, CatIB formation efficiency is a parameter that is simple to determine, yet offers important insights into the usefulness of a CatIB construct by describing the amount of active protein in CatIBs relative to the total activity/fluorescence displayed by the same construct. Additionally, activity assays can be performed on other cell fractions such as the supernatant of the washing step (S2), which can provide first hints towards the stability of CatIBs (i.e. as in **Section 2.1.1**).

As CatIBs are typically lyophilized for long term storage, the activity of the freeze-dried CatIBs represents another crucial parameter for industrial application. Therefore, CatIB residual activity is defined as the specific activity of the freeze-dried CatIBs of a target enzyme, compared to the activity of the same enzyme that is purified from its soluble form. As such, it is derived from the specific activity of lyophilized CatIBs (in U/mg protein) relative to the corresponding activity of the soluble, purified enzyme produced without the CatIB tag **Equation 3.2**. Please note that this parameter does not consider a potential loss or reduction of activity due to the lyophilization process.

$$Residual\ activity\ [\%] = \frac{Activity\ of\ lyophilized\ CatIBs\ [\frac{U}{mg\ protein}]}{Activity\ of\ soluble\ enzyme\ [\frac{U}{mg\ protein}]} \times 100 \tag{3.2}$$

Lastly, the stability and yield of CatIBs are crucial parameters for application. The first parameter can be determined simply by, for instance, suspending a defined amount of lyophilized CatIBs in a suitable buffer, followed by incubation for a period of time at a constant temperature, where the suspension is periodically sampled and assayed for

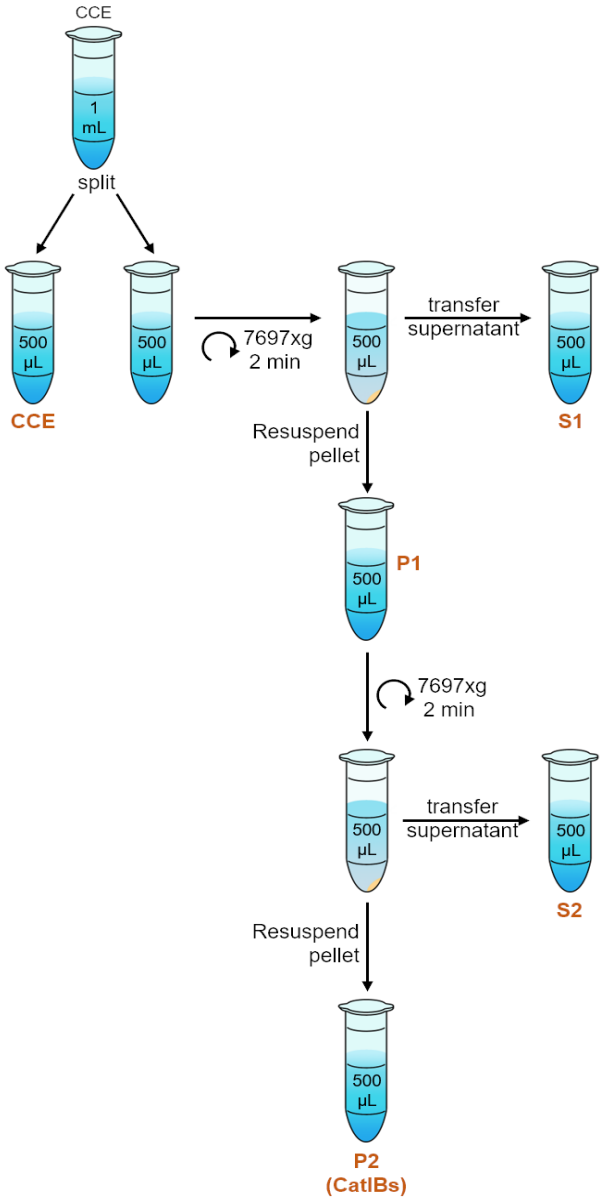

Figure 3.4. Cell fractionation process for obtaining CatIBs.

Crude cell extract (CCE) of a CatIB producer is centrifuged, resulting in the supernatant and pellet fractions, where the latter fraction contains CatIBs. The pellet is resuspended in a suitable buffer as depicted in order to obtain the washed pellet fraction (P2) containing CatIBs. S1: supernatant. P1: unwashed pellet. S2: supernatant of the wash step. P2: washed pellet (CatIB fraction). All fractions are resuspended in the same volume of the appropriate buffer as the buffer removed upon centrifugation, therefore keeping a 1:1 ratio between the fractions at all times (see **Section 2.1** Methods for details). Reproduced from [186] with permission from Springer Nature.

activity. The stability of 16 RADH and BsLA CatIBs bearing coiled-coil and synthetic peptide tags at varying termini were analyzed, together with the corresponding soluble enzymes (**Section 2.1**), revealing the remarkable stability displayed by the immobilizates

over several days, which will be discussed in further detail in **Section 3.2**. Lastly, the CatIB yield for a given construct can be calculated by weighing the amount of net CatIBs obtained after the lyophilization process, and expressing the obtained amount relative to the initial wet cell weight that was used to produce the respective lyophilizate. The CatIB yield can be also expressed in terms of the amount of protein obtained from the lyophilizate relative to the cells cultivated, or further expressed as biomass specific activity yield (**Section 2.1**) to incorporate the amount of activity displayed by the amount of lyophilizate obtained (see **Section 3.2**). This parameter is obtained by multiplying the CatIB yield for a given CatIB construct (expressed as mg lyophilizate/g wet cells) by its specific activity (U/mg lyophilizate). This assessment therefore considers different expression levels and could prove to be an easy way to critically compare different CatIB constructs, and is calculated by **Equation 3.3**:

$$Biomass\ specific\ activity\ yield\ [\frac{U}{g\ wet\ cells}] = \frac{Activity\ of\ lyop.\ CatIBs\ [\frac{U}{mg\ CatIBs}]}{Yield\ of\ CatIBs\ [\frac{mg\ CatIBs}{g\ wet\ cells}]} \tag{3.3}$$

3.2. Improvement of CatIB properties by genetic design

The concepts outlined in the previous section, namely, residual activity, stability, yield, and biomass specific activity yield, allow a comprehensive and critical assessment of CatIBs of reporter proteins and enzymes. Genetic fusions to obtain such CatIBs can be tailored to yield immobilizates displaying superior residual activity and stability, which was previously shown via linker iterations [107]. However, despite the large number of studies on CatIBs, the CatIB tags which are the driving force of CatIB formation, have been rarely fused to both termini to allow a direct assessment of the impact of the genetic design on desirable CatIB properties [108, 109, 112, 113, 114, 115, 116, 123, 124, 132, 138]. For instance, the large coiled-coil TdoT tag (53 residues, 5.7 kDa) has been tested solely in N-terminal fusions (with the exception of EcLDC [108]), whereas the short, synthetic peptide tags 18AWT, L6KD and GFIL8 (8-18 residues, 0.9-2.3 kDa) have only been employed in C-terminal fusions [112, 113, 114].

To fill this gap, the benchmarking study presented as part of this thesis investigated general strategies to improve industrially relevant properties of CatIBs (**Section 2.1**). As target proteins mCherry, BsLA, and RADH were employed, which were previously im-

mobilized as CatIBs with the N-terminally fused TdoT tag [108, 109, 117]. Here, the existing CatIB toolbox was extended by generating C-terminal TdoT fusions of all targets, as well as N- and C- terminal fusions of 18AWT, L6KD and GFIL8 tags. Overall, 24 CatIB constructs were generated and the resulting CatIBs were analyzed to provide a comprehensive assessment on how genetic design affects the properties of CatIBs. The genetic design approach, pursued within this thesis, was aimed towards improving the low residual activity of N-terminal TdoT-tagged RADH CatIBs (2% of soluble, purified RADH[117]), as well as quantifying the residual activity and other relevant properties (such as stability) of similarly tagged BsLA CatIBs which were not reported previously [109]. The effect of genetic design on successful CatIB formation (exemplified by CatIB formation efficiency of mCherry, BsLA and RADH constructs) on the other hand, will be discussed in more detail in the upcoming chapter (**Section 3.3**).

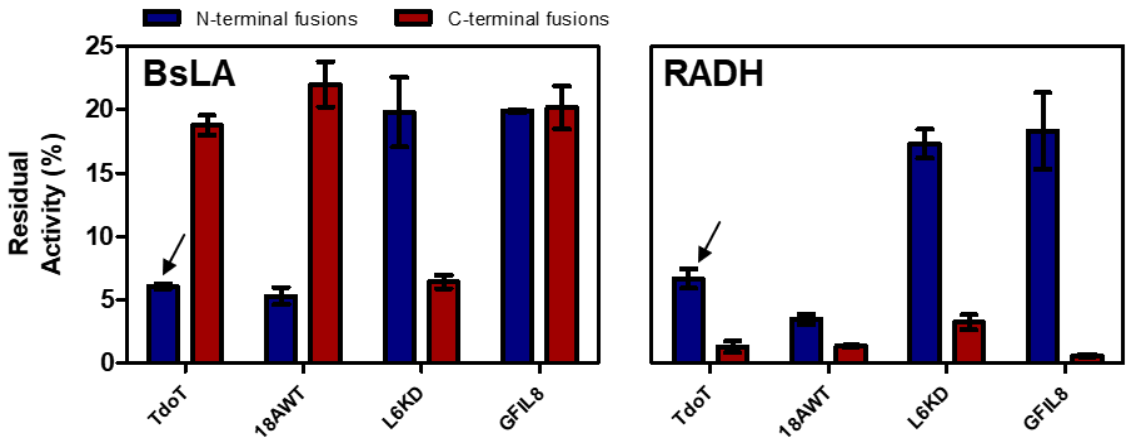

Figure 3.5. Residual activities of BsLA and RADH CatIBs bearing four different CatIB inducing tags at different termini.

Residual activity (%) refers to the activity of lyophilized CatIBs [U/mg protein] relative to the activity of the corresponding soluble, purified enzyme [U/mg protein] set to 100%, as defined in **Equation 3.2**. The first bars in both BsLA (left) and RADH (right) datasets are marked with arrows, which indicate the N-terminal TdoT bearing CatIB constructs which were generated in previous studies by [109] and [117], respectively. The residual activity values depicted for these constructs were derived from the experiments conducted as part of this PhD thesis, as published in and adapted from [184]. Adapted with permission from [184]. Copyright © 2022 American Chemical Society. The numerical values for the residual activity (%) depicted in this figure are further listed in **Table 3.1**.

The residual activity of BsLA and RADH CatIBs could be improved drastically by utilizing the optimal CatIB tag at the optimal terminus (**Section 2.1**, **Figure 3.5**). For

BsLA, while the fusion terminus did not affect the activity of the CatIBs generated by the GFIL8 tag and both fusions yielded high residual activities (approximately 20%), it had a large impact on the activity of CatIBs generated by the remaining tags, and a more than 3-fold difference in activity was observed for opposing fusions of 18AWT, L6KD and TdoT tags (**Figure 3.5** and **Table 3.1**, see below). N-terminal fusion of the L6KD tag, as well as C-terminal fusions of 18AWT and TdoT tags all yielded CatIBs that displayed over 18% residual activity. The N-terminal TdoT-BsLA construct generated earlier [109] was characterized, yielding a residual activity of 6.1% when compared to soluble purified BsLA (**Figure 3.5**, left panel, marked with an arrow). This rather low activity could be improved in this thesis by about 3-fold by the fusion of the TdoT tag to the C-terminus. Furthermore, C-terminal tag fusions in general yielded higher residual activities, corresponding to a mean difference of 16% between N- and C-terminal fusions. In terms of yields, however, N-terminally fused tags yielded higher amounts of CatIBs (25.7% mean difference between termini), in line with the higher CatIB formation efficiencies of N-terminal fusions (**Section 2.1.1**). These findings point towards the importance of testing different tags and fusion termini for improving the activities of CatIBs.

The importance of the genetic design for producing highly active CatIBs is also exemplified by the here presented characterization of different RADH CatIBs, where CatIBs produced by N-terminally fused tags outperformed C-terminal fusions for all tags (**Figure 3.5**, right panel). Remarkably, the GFIL8 tag, when fused to the N-terminus yielded CatIBs with more than 32-fold higher activity when compared to the fusion of the same tag to the C-terminus, corresponding to 18% of the activity displayed by the soluble, purified RADH. N-terminal fusions of all tags for RADH were highly stable, and these constructs retained 87-96% of their initial activity over 5 days, outperforming the soluble RADH, which retained only 31% of its initial activity (**Section 2.1**) under the same conditions. Contrarily, the unsuitability of C-terminal fusions could be established for RADH, despite the high CatIB formation efficiencies obtained for C-terminal fusions with some of the CatIB tags (**Section 2.1**). Upon lyophilization, RADH CatIBs generated by C-terminal tag fusion showed very low residual activities (0.6-3.2% of purified soluble RADH, **Figure 3.5** and **Table 3.1**, see below), as well as mediocre stabilities (11-47% activity retention over 5 days, **Section 2.1**).

Regardless, for both target enzymes, the fusion of L6KD or GFIL8 tags at the optimal terminus yielded CatIBs with higher activities in general, which could indicate that the shorter peptide tags having less of a negative impact on proper folding and therefore the activity of the enzyme. This effect appeared less relevant however when the CatIB tag is present at its optimal terminus, which was exemplified by C-terminal TdoT bearing

Table 3.1. Properties of several lipase and alcohol dehydrogenase (ADH) enzymes immobilized via different carrier-free methods.

Target	Tag	Tag terminus	Residual activity (%)
CatIBs			
BsLA	TdoT	N	6.1
	TdoT	C	18.8
	18AWT	N	5.3
	18AWT	C	22.0
	L6KD	N	19.8
	L6KD	C	6.4
	GFIL8	N	19.9
	GFIL8	C	20.2
RADH	TdoT	N	6.7
	TdoT	C	1.3
	3HAMP [108]	N	12
	18AWT	N	3.5
	18AWT	C	1.4
	L6KD	N	17.3
	L6KD	C	3.2
	GFIL8	N	18.3
	GFIL8	C	0.6
LbADH [108]	TdoT	N	1
	3HAMP	N	5.8
Cry3Aa crystals			
BsLA[156]	Cry3Aa/ Cry3Aa*	N	83.7 - 221
PML [155]	Cry3Aa/ Cry3Aa*	N	2.4-5
DLZM4 [155]	Cry3Aa/ Cry3Aa*	N	0.1
PML^{VG} [155, 211]	none (co-production)	-	< 8.5
PHA granules			
CalB [212]	PhaC	N	< 4
VLP entrapment			
CalB [213]	CCMV capsid	C	77
PalB [214]	CCMV capsid, E/K-coil	C	200 - 500
BplA [215]	B19V VP2 capsid	N	< 4.9
ADHD [216]	SP	C	< 18
ADHA [217]	SP	C	approx. 100

Unless referenced, all values for CatIBs originate from this work. LbADH: *L. brevis* ADH. PML: *P. mirabilis* lipase. DLZM4 and PML^{VG}: mutants of PML. CalB: *C. antarctica* lipase B. PalB: *P. antarctica* lipase B. BplA: *B. pumilus* lipase A. ADHD: *P. furiosus* ADH. ADHA: *L. lactis* ADH. Cry3Aa*: Truncated Cry3Aa. CCMV: Cowpea chlorotic mottle virus. B19V: Parvovirus B19. SP: scaffolding protein involved in capsid assembly and localization.

BsLA CatIBs performing similarly to CatIBs with small peptide tags in terms of residual activity. Importantly, when biomass specific activity yields are considered, N-terminal L6KD, N- and C- terminal GFIL8 CatIBs of BsLA, as well as N-terminal GFIL8 CatIBs of RADH all outperformed soluble, purified enzymes by almost 2-fold (**Section 2.1**), indicating that optimally fused GFIL8 and L6KD tags can be quite useful for generating CatIBs with desirable properties.

Moreover, while many lipases and alcohol dehydrogenases had been immobilized using a wide range of carrier-free approaches (**Table 3.1**), most studies utilized lipases or alcohol dehydrogenases of different origins. Therefore, a direct comparison of the immobilization efficiencies or residual activities of these enzymes from different organisms to the RADH and BsLA CatIBs generated in this PhD thesis would not be feasible. However, BsLA, which was extensively immobilized as CatIBs, was also entrapped within unmodified and modified Cry3Aa crystals in *E. coli* [156] (also see **Table 3.2** below). While BsLA entrapped within unmodified Cry3Aa suffered an activity loss (16.7% activity reduction), the fusion of the Cry3Aa variant lacking 19 amino acids from its C-terminus (Cry3Aa*) to BsLA yielded immobilizates that outperformed soluble BsLA by more than 2-fold. Apart from high activity, Cry3Aa* entrapped BsLA also showed high stabilities, as demonstrated in various organic solvents and at different pH values. Here, the immobilized enzyme retained high conversions (93%) after 9 reaction cycles. Similarly, BsLA CatIBs also showed high stabilities (tested in sodium phosphate buffer over 5 days), where they retained 81-88% of their initial activity (**Section 2.1**). In contrast, the activity of the soluble BsLA was reduced to only 23% of its initial value within the same time frame. This result is in line with previous studies involving MenD, AtHNL, RADH and PfBAL CatIBs [109, 218], indicating that the CatIB approach confers additional benefits (such as stability) to the enzyme.

Furthermore, Cry3Aa immobilizates yielded more than 4-fold enzyme (per liter of cell culture), when compared to the amount of soluble enzyme obtained via purification in the same study **Table 3.2**. To allow a direct comparison of BsLA CatIBs to Cry3Aa-BsLA constructs reported by Heater *et al*., it was necessary to calculate biomass specific activity yields of BsLA CatIBs as activity per liter of culture. When compared to soluble BsLA, N-terminal L6KD bearing BsLA CatIBs had over 8-fold higher yield, and this construct, as well as BsLA constructs bearing the GFIL8 tag at either terminus had a much higher biomass specific activity yield when compared to the soluble BsLA purified in the CatIB study (approximately 2-fold). It is worthwhile to note here that, in the study of Heater *et al*., the purification efficiency of soluble BsLA appears to be quite low (only 5.5 mg BsLA per liter of culture), whereas BsLA purified as part of this PhD thesis **(Sec-**

Table 3.2. Activity, yield, and biomass specific activity yields of BsLA CatIBs and Cry3Aa immobilizates.

Construct	Activity (U/mg protein)	Yield (mg protein/L)	Activity yield (U/L)
CatIBs			
Soluble BsLA	45.8	94.3	4324.7
N-terminal tag fusions			
18AWT	2.4	493.9	1199.2
L6KD	9.1	796.1	7229.6
GFIL8	9.1	657.5	5996.3
TdoT	2.8	1446.7	4014.2
C-terminal tag fusions			
18AWT	10.1	128.9	1300.0
L6KD	2.9	573.0	1681.8
GFIL8	9.2	786.6	7272.1
TdoT	8.6	397.6	3422.4
Cry3Aa crystals			
Soluble BsLA	44.3	5.5	243.7
C-terminal tag fusions			
Cry3Aa	37.1	24.5	908.95
Cry3Aa*	98.1	26.3	2580.0

All values for BsLA CatIBs and free lipase are derived from this original work. The activity and yield of Cry3Aa immobilizates and the soluble BsLA from the work of Heater *et al.* were taken directly from [156]. Biomass specific activity yields of Cry3Aa immobilizates and the soluble enzyme were calculated based on this data, by multiplying activity (in U/mg protein) by the yield (mg protein/L), in the same way as CatIBs. Cry3Aa* stands for the engineered Cry3Aa construct lacking 19 residues from its C-terminus. 1 unit (U) was defined as the amount of enzyme that leads to the release of 1 mmol *p*-nitrophenolate per minute at 25 °C, using p-nitrophenyl butyrate as substrate (for CatIBs), and p-nitrophenyl acetate as substrate for Cry3Aa crystals.

tion 2.1 and **Table 3.2**) was produced with a much higher yield (94.3 mg/L expression culture). Therefore, the biomass specific activity yield of soluble BsLA is much higher (approximately 18-fold) in the CatIB study when compared to the biomass specific activity yield of soluble BsLA by Heater *et al.*, resulting in a less pronounced improvement of activity yields for CatIB constructs when they are compared to their corresponding soluble enzyme. Despite this, the best performing BsLA CatIBs (N-terminal L6KD and C-terminal GFIL8 bearing BsLA CatIBs) still possess almost 3-fold higher biomass specific

activity yields when compared to BsLA entrapped within optimized Cry3Aa* crystals. In terms of applicability, Cry3Aa crystal entrapment method has been so far limited to small monomeric proteins and was not tested with complex targets, and was deemed unsuitable for co-immobilization [155, 156, 211, 154]. Still, more studies are necessary to evaluate the overall usefulness of the approach.

The work of Kira Küsters (**Section 2.2**), which is also part of this thesis, where five CatIB inducing tags (18AWT, L6KD, GFIL8, TdoT, and 3HAMP) were fused C-terminally to EcLDC together with either flexible (SG linker) or rigid (PT linker) also provided insights into how the genetic design affects the activity of CatIBs. In general, constructs bearing the rigid PT linker displayed higher conversion rates when compared to their SG linker bearing counterparts. This effect was especially pronounced for the L6KD tagged EcLDC construct, where the variant bearing the rigid PT linker displayed the highest conversion rate (93% after 3 minutes), whereas the corresponding flexible SG linker bearing construct displayed the lowest conversion rate (20% after 3 minutes) among all tested constructs (**Section 2.2**). This finding indicates that the choice of the linker is a highly important parameter to consider when generating CatIBs, and is in line with previous studies demonstrating that the activity of CatIBs can be improved by replacing flexible linkers by rigid ones [107].

Along the same lines, it should be highlighted here that in the benchmarking study (**Section 2.1**) discussed in detail above, CatIB constructs bearing any of the synthetic tags all contained the rigid PT linker. Among such BsLA and RADH constructs, when L6KD and GFIL8 tags were present at the optimal terminus, the resulting CatIBs displayed enhanced activity and stability, in addition to outperforming the soluble enzymes in terms of biomass specific activity yields. These findings are in line with the study on EcLDC CatIBs bearing varying linkers (**Section 2.2**), where the PT linker harboring L6KD and GFIL8 constructs showed the highest conversion rates (93% and 80% after 3 minutes, respectively) as well as the highest volumetric productivities (256 and 179 gram per liter per day, respectively). A new study further analyzing the effect of linkers in terms of activity for various glucose dehydrogenase CatIBs is likewise in agreement with this finding, as the positive impact of the PT linker on CatIBs could be demonstrated [204]. Taken together, optimally fused, rigid linker bearing L6KD and GFIL8 constructs seem to produce CatIBs with superior performance, therefore CatIB constructs harboring these elements can prove to be valuable additions to the CatIB toolbox for immobilizing more industrially relevant enzymes. However, more systematic studies directed towards the above-mentioned synthetic CatIB tags and the PT linker are needed to disentangle the positive influence of these elements on desirable CatIB properties.

3.3. Rationalizing CatIB formation

The above-described benchmarking studies using mCherry, BsLA and RADH as immobilization targets (**Section 2.1**), aimed to shed light on the design parameters that play a role for obtaining highly active and stable CatIBs, as well as on the CatIB formation process in general. Additionally, the study was directed towards improving the rather low CatIB formation efficiencies reported previously for mCherry CatIBs (4% - 32% depending on the linker [108]). To this end, the propensity of 18AWT, L6KD, GFIL8, and TdoT tags for CatIB formation was evaluated for three target proteins via fusion to both termini. While the short peptide tags 18AWT, L6KD and GFIL8 (8-18 residues, 0.9-2.3 kDa) were sufficient in generating CatIBs for BsLA and RADH, they appeared to be limited in their ability to pull difficult targets into the insoluble fraction, which is exemplified by the observation that these short CatIB-tags did not yield stable mCherry CatIBs. All short peptides yielded low CatIB formation efficiencies for mCherry (< 8.5%, **Table 3.3**), indicating that larger tags, such as TdoT (53 residues, 5.7 kDa), may be more beneficial for immobilizing highly soluble targets. This observation is in line with a study where the short LHS1 tag (10 residues, 1 kDa) generated turbo GFP CatIBs with an efficiency of 40%, whereas a lengthier tag (LHS2, 32 residues, 3.4 kDa) could immobilize the highly soluble target with more than 90% efficiency [126]. In fact, the highest immobilization efficiency for mCherry with the CatIB method was achieved by employing a full-length protein as pull-down tag [141] (ZapB, 82 residues, 9.6 kDa), yielding approximately 55% CatIB formation efficiency (**Table 3.3**).

Furthermore, mCherry CatIBs with the larger 3HAMP tag (172 residues, 18.7 kDa), which contained a flexible $(GGGS)_3$ linker, had been previously shown to have a slightly higher CatIB formation efficiency (5.5%) when compared to TdoT CatIBs bearing the same linker (3.5%, see table **Table 3.3**) [108]. Since the CatIB formation efficiency of TdoT-mCherry CatIBs had been improved drastically upon deletion of the flexible linker (up to 32%, [108]), it might be worthwhile to apply the same strategy to 3HAMP-mCherry CatIBs as well. In this regard, linker deletions could be likewise extended to 18AWT, L6KD and GFIL8 CatIBs of mCherry in the future, which could improve the rather low CatIB formation efficiencies obtained with these tags.

Despite the increasing number of novel methods that rely on *in vivo* immobilization, for studies employing mCherry, BsLA and RADH, immmobilization efficiencies with such techniques are under-reported. Nevertheless, LLPS-based immobilization methods where various intrinsically disordered proteins or domains were employed could successfully immobilize mCherry [160, 219, 161, 220], (**Table 3.3**). Cry3Aa crystal en-

Table 3.3. Immobilization of mCherry via various carrier-free methods.

Method	Tag and linker	Tag terminus	Immobilization efficiency (%)
CatIBs	TdoT (no linker)	N	22.2 - 32 [108]
	TdoT (GS linker) [108]	N	3.5
	TdoT (no linker)	C	6.3
	3HAMP (GS linker) [108]	N	5.5
	18AWT (PT linker)	N	8.4
	18AWT (PT linker)	C	1.8
	L6KD (PT linker)	N	8.4
	L6KD (PT linker)	C	3.5
	GFIL8 (PT linker)	N	5.7
	GFIL8 (PT linker)	C	1.6
	ZapB (SIPGA linker) [141]	N	approx. 55
Cry3Aa crystals	Cry3Aa [154]	N	n.d.
LLPS	$SH3_5$ + PRM5 co-expression [160]	C	n.d.
	RRM, $iLID_{x6}$ + co-expression with $SspB_{x6}$ [219]	N and C	n.d.
	I16/II16/R32 [161]	N	n.d.
	IDR, Cry2 [220]	N and C	n.d.

Unless referenced, all values for CatIBs originate from this work. LLPS: Liquid-liquid phase separation. $SH3_5$: 5 tandem repeats of SRC homology 3 domain. PRM: proline-rich motif. RRM: RNA recognition motif. $iLID_{x6}$: 6 tandem repeats of the improved light-inducible dimer. $SspB^{x6}$: binding partner of iLID. I16: major ampullate spidroin 1. II16: major ampullate spidroin 2. R32: resilin-like protein. IDR: intrinsically disordered region, referring to N-terminal IDR of fused in sarcoma protein (FUSN), N-terminal IDR of deadbox DDX4 helicase, and C-terminal IDR of the heterogeneous nuclear ribonucleoprotein A1 (HNRNPA1C). Cry2: photolyase homology region of *A. thaliana*. nd: not determined.

trapment of mCherry was likewise achieved and while no entrapment efficiency was reported, the remarkable stability of mCherry crystals was described, as evidenced by the retention of fluorescence over several weeks [154]. In spite of the low number of studies employing Cry3Aa crystals for immobilization, the high stability of mCherry crystals could indicate the suitability of this method towards difficult targets such as mCherry, where the soluble nature of the target proved problematic for immobilization via the CatIB method, evidenced by solubilization and subsequent loss of CatIBs during washing steps (**Section 2.1.1**).

In addition to the tag size, first hints towards the importance of alternating fu-

sion termini for CatIB tags could be obtained from the studies conducted with mCherry CatIBs, as N-terminal fusions of all tested tags yielded visible CatIBs when live *E. coli* cells overproducing CatIB tag-mCherry fusions were analyzed microscopically, whereas C-terminal fusions did not promote CatIB formation except for the 18AWT fusion which contained CatIBs in a fraction of the observed cells (**Section 2.1**). This observation was also supported by fluorescence spectroscopic assays, where the insoluble fractions of constructs harboring N-terminal tags displayed up to 4-fold more mCherry fluorescence when compared to those of C-terminal tag bearing constructs (**Table 3.3**). A similar conclusion could be derived for BsLA CatIBs, where each tag was able to pull the target into the insoluble fraction more efficiently when present at the N-terminus, corresponding to a range of 10-28% increase in CatIB formation efficiencies as opposed to C-terminal fusions (**Section 2.1**). For RADH, the presence of the tags at opposing termini had a profound effect on CatIB formation efficiency for some constructs. For instance, when the GFIL8 tag was present at the N-terminus, it yielded the highest CatIB formation efficiency (76.4%) among all tested constructs, whereas when the tag was fused to the C-terminus it yielded the lowest efficiency (15.8%). Similarly, the 18AWT tag yielded a 36% increase in pull-down efficiency when present at the C-terminus, with less significant differences observed with opposing termini for the remaining tags.

Moreover, more insights on how intradomain linkers affect CatIB properties could be drawn via employing rigid PT linkers or flexible SG linkers together with 18AWT, L6KD, GFIL8, TdoT and 3HAMP tags with EcLDC as the target (**Section 2.2**). Though the morphology and activity of CatIBs did not show a clear correlation, the choice of linker appeared to affect the morphology and the size of resulting CatIBs. While CatIB formation efficiencies in terms of the activity of EcLDC in the CatIB fraction relative to the activity of its corresponding crude cell extract were not reported, the percentage of cells that possessed visible EcLDC CatIBs were included in the study. Here, with the exception of the 18AWT tag bearing either flexible or rigid linkers, all remaining tags with either linker generated CatIBs with over > 60% of the cells visually presenting CatIBs. However, as the EcLDC construct lacking CatIB inducing tags and linkers also produced CatIBs with rather high efficiencies (88% cells with visible structures), it is not feasible to claim that any of the tags (with the exception of the negative impact of 18AWT tag) contribute to CatIB formation. Regardless, when taken together with the findings of our above-discussed benchmarking study (**Section 2.1**), it appears that despite the indication of larger tags being more suited to immobilize difficult targets, there is no generally applicable rule toward predicting which fusion termini or tag with certain linkers produces better results overall. Moreover, rigid linkers that generally have

a positive influence on activity might produce variable results in terms of CatIB formation efficiencies, and the latter parameter can be indicative of yields. Therefore, it is still imperative to test both fusion termini as well as different tag combinations for each target, and automated cloning and testing can aid tremendously in this effort.

3.4. CatIBs in flow chemistry applications

The benchmarking study that generated, evaluated, and ranked mCherry, BsLA and RADH CatIBs (**Section 2.1**), highlighted the superior properties of RADH CatIBs produced by an N-terminally fused GFIL8 tag. This construct possessed high stability and high residual activity and could be obtained easily in large amounts. These properties resulted in a high biomass specific activity yield for GFIL8-RADH CatIBs, which surpassed that of the soluble RADH, opening up the possibility of using GFIL8-RADH CatIBs for proof-of-concept flow applications. To this end, lyophilized GFIL8-RADH CatIBs were used in simple flow and closed-loop cofactor regeneration modes. Apart from the optimization of the column packing process, CatIBs could be used directly for flow catalysis.

To render them applicable for flow catalysis, the lyophilized GFIL8-RADH CatIBs were mixed with silica in a ratio of 1:2.5% (w/w, CatIBs:silica), which prevented their unintended compression within the column. The GFIL8-RADH CatIBs catalyzed the reduction of cyclohexanone to cyclohexanol, as well as the asymmetric reduction of ω-chloroacetophenone to (*R*)-2-chloro-1-phenylethan-1-ol in simple-flow through mode for the first time. Here, the substrates for RADH CatIBs were supplied into the system via a mixture of 2-methyltetrahydrofuran and triethanolamine buffer (7.5% v/v, with a flow rate of 33 µl/min, see methods of **Section 2.1** for details). GFIL8-RADH CatIBs catalyzed the reduction of both ketones to the corresponding alcohols, with full conversion and an enantiomeric excess (*ee*) of 99% over 120 minutes for the reduction of ω-chloroacetophenone, and a turnover of 86% over 120 minutes for that of cyclohexanone, where the resulting alcohols were extracted via phase separation using a flow liquid-liquid extraction (FLLEX) system with diisopropyl ether as solvent.

Upon proving the applicability of CatIBs in flow, they were subsequently used in closed-loop cofactor regeneration mode, where the GFIL8-RADH CatIBs catalyzed the reduction of ω-chloroacetophenone while oxidizing cyclohexanol to regenerate NADPH as necessary for the reduction at the same time. The aqueous layer containing the cofactor was recycled back into the reactor after phase extraction. In this mode, a yield of

Table 3.4. Examples of immobilized enzymes in continuous flow.

Enzyme	Origin	STY (g L^{-1} h^{-1})	Stability
Covalent binding			
Ketoreductase, GDH	*P. glucozyma*, *B. megaterium* [221]	0.2	several weeks
Ketoreductase	P1-A04* [222]	4-4.7	n.a.
HbHNL, MeHNL [223]	*H. brasiliensis*, *M. esculenta*	613-1229	n.a.
ω-transaminase [224]	*Arthrobacter sp.*, ATA-117*	8-20[a]	> 4 days
Adsorption			
LDH, FDH [225]	*Leporidae sp.**, FDH102*	22.9	> 1 day
ADH, hydrogenase, dehydrogenase, NAD^+ reductase [226]	ADH 105*, *E. coli*, *B. subtilis*, *R. eutropha*	n.a.	n.a.
Entrapment/Encapsulation			
ω-transaminase [227]	ATA-WT*	n.a.	21 days
Lipase [228]	*C. antarctica*	n.a.	> 4 days
Lipase, ADH, GDH [229]	*C. antarctica*, EVO200*, *B. cepacia*	n.a.	1 day
Affinity binding			
ω-transaminase [230]	*Arthrobacter sp.*, *C. violaceum*	1.9	n.a.
Ketoreductase, GDH [231]	*S. cerevisiae*, *B. subtilis*	13.3	n.a.
RedAms, NdRedAm [232]	*N. fumigatus*	8.1	12 hours
ADH, Gre2p, GDH [233]	*L. brevis*, *S. cerevisiae*, *B. subtilis*	n.d.	> 14 days
BFD, ADH [234]	*P. putida*, *L. brevis*	38	3-14 days[b]
ADH [235]	*L. brevis*	n.d.	> 5 days
ADH [236]	*L. brevis*	121	> 5 days
CatIBs			
ADH **(Section 2.1)**	*Ralstonia sp.*	3.6	> 11 days

In cases where several co-immobilized enzymes are listed, the origin or space time yield (STY) of the enzymes are given in the same order (if provided in the original study). GDH: Glucose dehydrogenase. HbHNL, MeHNL: hydroxynitrile lyases. LDH: Lactate dehydrogenase. FDH: Formate dehydrogenase. ADH: Alcohol dehydrogenase. RedAms, NdRedAm: Fungal reductive aminases. Gre2p: Methylglyoxal reductase. BFD: Benzoylformate decarboxylase. The asterisk (*) denotes commercial enzymes. [a]: space time yield with the unit of µmol h^{-1} mg^{-1}, [b]: for PFD and ADH, respectively. The examples given in the table were collected using [237] and [238].

92% and an *ee* value of 98% was obtained after 5 days of continuous operation, where the conversion decreased to 78% after an additional continuous production cycle over 6 days using the same CatIBs in the reactor. Therefore, the remarkable stability of GFIL8-RADH CatIBs within the flow setup could be demonstrated for the first time, indicating that CatIBs can prove to be useful biocatalysts for flow applications.

While RADH was never used in any immobilized form in flow before, **Table 3.4** lists various industrially relevant enzymes previously used in immobilized form in continuous flow applications (as also reviewed part of this thesis, see **Section 2.7**), such as several ω-transaminases for amino acid synthesis [221, 222, 231], or co-immobilization cases such as the utilization of immobilized lipase, ADH, and glucose dehydrogenase (GDH) for fragrance synthesis [229], where the latter enzyme was used for cofactor regeneration. In terms of stability, RADH CatIBs performed well when compared to other immobilizates used in continuous flow applications, despite the rather low space time yield (STY) of 3.6 g L^{-1} h^{-1} after 120 hours of simultaneous conversion of ω-chloroacetophenone and cyclohexanol. Furthermore, as immobilization invariably results in some degree of activity loss, parameters such as high stability and yields might play a more important role in terms of application potential. For instance, two different ω-transaminases used for continuous amine production retained only 25-30% of their original activity upon covalent immobilization, though the stability of the enzymes was enhanced [239, 224]. Similarly, ketoreductase and GDH (from *Pichia glucozyma* and *Bacillus megaterium*, respectively) lost up to 60% of their activity upon immobilization [221], and HaloTag immobilized benzoylformate decarboxylase (BFD) and ADH lost 35-65% of their activity, respectively [234]. While CatIBs may suffer from a similar degree of activity loss comparable to that of covalent attachment, the superior physical properties such as high stability exhibited by the immobilizates, as well as their exemption from possible issues encountered during other immobilization methods (i.e. low loading yields onto the carrier, additional preparation steps, etc.) can render them useful alternatives for flow application.

3.5. Generation of MPAs as novel immobilizates

As part of this PhD thesis, a novel *in vivo* protein immobilization method generating magnetic protein aggregates (MPAs, see **Section 2.3**, and **Figure 3.6**) was developed. The method was further expanded and utilized to immobilize alcohol dehydrogenase from *Ralstonia sp*., generating catalytically-active magnetic protein aggregates (CatMPAs), as a proof of concept for enzyme immobilization. To this end, the superparamagnetic properties of iron-loaded ferritin (as described in **Section 1.2.2.4**), and a fusion protein consisting of ferritin and a yellow fluorescent protein variant (citrine), first described by Bellapadrona *et al.* [181, 182], were utilized. The fusion protein containing citrine and the H-chain of human ferritin (HuFtnH) was previously shown to display self aggregation properties, as well as fluorescence in the insoluble fraction upon release from the cells, which could be obtained via centrifugation similar to CatIBs (see **Figure 3.7, A**). Therefore, the identical construct was generated and expressed in *E. coli*, and in addition, the HuFtnH was exchanged by two other ferritin variants; ferritin A from *E. coli* (EcftnA), and EcftnA H34L+T64I [240] in order to investigate the aggregation propensities and magnetic properties of fusions generated by *E. coli* ferritins (**Figure 3.6**).

All citrine-ferritin fusions were tested for self aggregation, evaluated in terms of the percentage of active protein in the insoluble fractions judged via citrine fluorescence, and investigated for their magnetic properties by evaluating their attraction to permanent neodymium magnets. Though defined in **Section 3.1.4** as CatIB formation efficiency (%), the quantification of the fluorescence of insoluble protein in the MPAs compared to the total fluorescence of the CCE (defined here as aggregation efficiency), was calculated in the same manner according to **Equation 3.1**. High aggregation efficiencies and evident magnetic properties could be demonstrated for all citrine-ferritin constructs, where the citrine-EcftnA H34L+T64I possessed the highest aggregation efficiency (69%, see **Figure 3.8**, green bars) as well as the highest attraction to permanent magnets evidenced by its crude cell extract (CCE) forming the sharpest pattern over permanent magnets (**Section 2.3** and **Figure 3.8**, see methods for details). Making use of the magnetic properties of the fusion protein, direct purification from the CCE using commercial magnetic columns was possible (**Figure 3.7**, **B**), where the target protein could be obtained with very high purity. The yields and protein contents of the MPAs were also comparable to those of CatIBs, where up to 4.7 grams of lyophilized MPAs could be obtained per 100 grams of wet cells, and the immobilizates contained up to 77% protein (**Section 2.3.1**).

Furthermore, additional constructs were generated in order to immobilize RADH

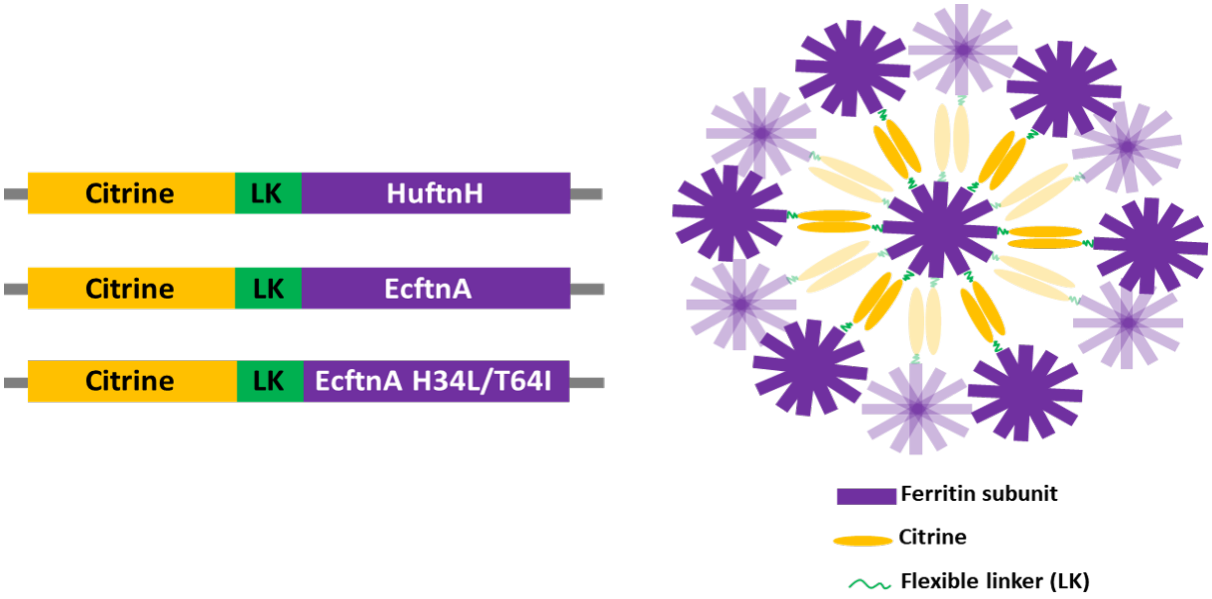

Figure 3.6. Depiction of constructs generating magnetic protein aggregates (MPAs) and cartoon diagram showing the supramolecular assembly of MPAs.

Constructs generating MPAs consist of the fusion of citrine to any of the ferritins (H-chain of human ferritin (HuFtnH)[181, 182]), ferritin A from *E. coli* (EcftnA), or a double mutant of EcftnA (EcftnA H34L+T64I)), separated by a flexible glycine-serine linker (LK), which forms the supramolecular assembly depicted at the right side of the image. Modified from **Section 2.3**.

via a bait-prey strategy to generate CatMPAs (**Figure 3.9**). Here, the CnaB2 domain of the *Streptococcus pyogenes* adhesin FbaB, which was split and engineered (giving rise to the improved SpyTag002 and SpyCatcher002 pair with faster reactivity [128, 241]), was used for the covalent, post-translational linkage of the two proteins. Several constructs either carrying a SpyTag or SpyCatcher tag genetically fused to either insoluble citrine-ferritins and soluble RADH, or soluble ferritin (without citrine) and insoluble RADH (i.e. GFIL8-RADH CatIBs described in **Section 2.1**, and depicted in **Figure 3.9**) were generated. Each SpyTag/SpyCatcher tag bearing construct was cultivated separately, cells lysed and the CCEs were mixed in a 1:1 ratio to link SpyTag and SpyCatcher harboring proteins together. The most promising (Cat)MPAs were produced by combining the constructs generated by the fusion of SpyTag-citrine-ferritin, and SpyCatcher-RADH ((**Figure 3.9**, topmost bait and prey constructs marked with an asterisk). Upon mixing the CCEs of the above-mentioned pair, the activity of RADH in the insoluble fraction could be increased by nearly 3-fold (from 13% to 35%, **Figure 3.10**). Therefore, the ability of insoluble citrine-ferritins to pull down and immobilize soluble RADH via the SpyTag/SpyCatcher interaction could be shown, which gave rise to RADH CatMPAs.

MPAs present a promising alternative to obtain magnetic protein immobilizates

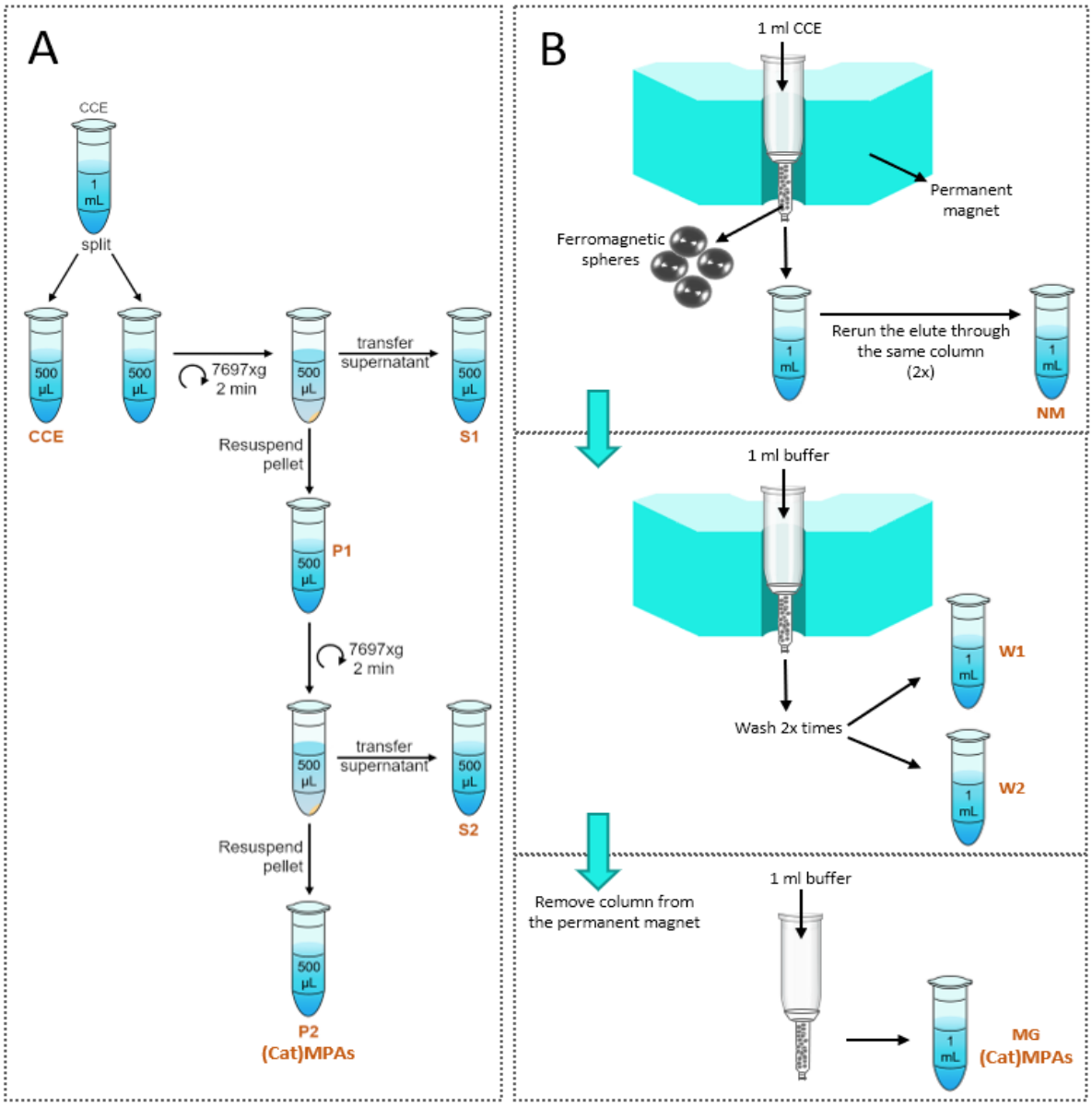

Figure 3.7. Cell fractionation and magnetic column purification processes for obtaining MPAs.

(A) Cell fractionation. **(B)** Magnetic column purification. CCE: crude cell extract. S1: supernatant. P1: unwashed pellet. S2: supernatant of the wash step. P2: washed pellet, (catalytically-active) magnetic protein aggregates (Cat)MPAs. NM: non-magnetic fraction, W1, W2: 1st and 2nd wash fractions. MG: Magnetic fraction containing MPAs. For CatMPAs, the starting material for both procedures is the CCE mixture containing the CCEs of suitable SpyTag and SpyCatcher constructs (1:1 v/v), as well as unmixed CCEs from both constructs. Panel **(A)** was adapted from [186] and reproduced with permission from Springer Nature.

without the need for *ex-vivo* magnetization or attachment to magnetic carrier materials,

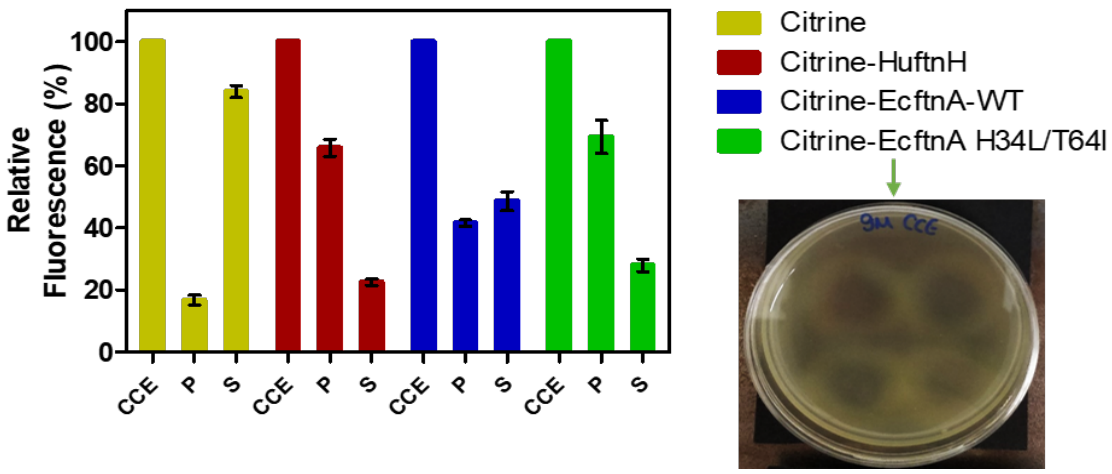

Figure 3.8. Relative citrine fluorescence of cell fractions of soluble citrine, MPA constructs and attraction of citrine-EcftnA H34L+T64I CCE to permanent magnets.

Citrine fluorescence of the crude cell extract (CCE) fractions was set to 100% for each construct, and the fluorescence signal of the washed pellet (P) and supernatant (S) fractions are depicted relative to the fluorescence of their corresponding CCE fractions. The relative fluorescence of the P fraction is defined as the aggregation efficiency (%). The image on the bottom right corner corresponds to the CCE of citrine-EcftnA H34L+T64I MPAs imaged 69 hours after placement over permanent neodymium ring magnets arranged in a 2x2 grid. Adapted from **Section 2.3**.

however, the approach currently has several shortcomings that need to be addressed in order to render it more applicable for enzyme immobilization. Though RADH CatMPAs could be obtained by the post-translational linkage of insoluble citrine-ferritin fusion to soluble RADH, the purification of this rather large protein aggregate proved to be challenging. The magnetic columns that were used to purify the unlinked citrine-ferritin had a purification efficiency of 42% (based on the fluorescence of the magnetic fraction (MG) compared to that of the washed pellet fraction (P2) set to 100%, see **Figure 3.7** and methods for details). However, this efficiency decreased significantly when the CatMPAs were purified with the magnetic columns. The SpyTag-citrine-ferritin covalently linked to SpyCatcher-RADH via the Spy-pair had only 9.4-18.4% purification efficiency (judged by citrine fluorescence and RADH activity of the magnetic fraction in comparison to the fluorescence and RADH activity of the P2 fraction of the mixed CCEs, respectively (**Table 3.5**). This finding further points towards an interesting property displayed by the CatMPAs obtained via SpyTag/SpyCatcher tag approach. As the purification efficiencies calculated by the relative fluorescence of citrine and relative activity of RADH in the magnetic fraction relative to the washed pellet differ by almost 10%, the amount of active protein in the magnetic fraction must be different for each

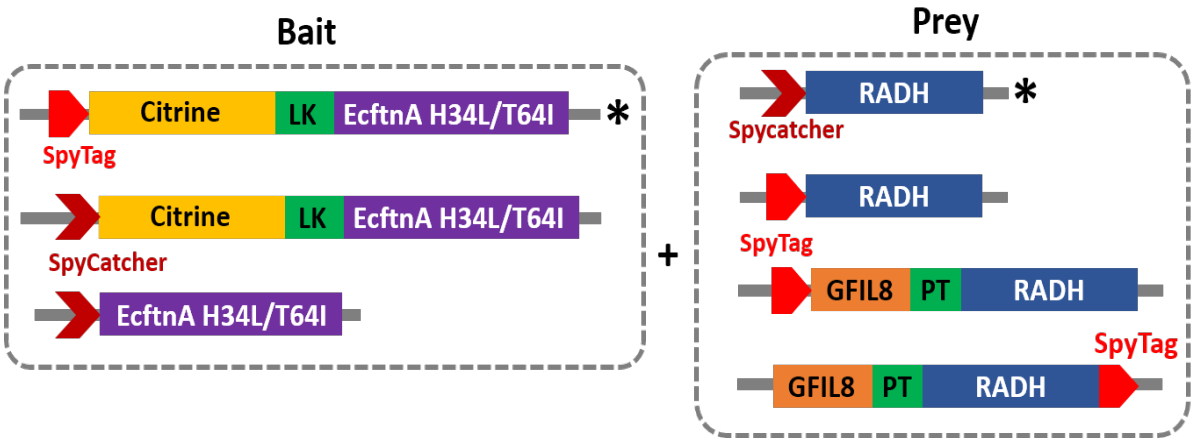

Figure 3.9. Bait and prey constructs used to generate catalytically-active magnetic protein aggregates (CatMPAs).

CCEs of bait and prey constructs each containing either the SpyTag or the SpyCatcher tag ([128, 241]) were used to post-translationally link the ferritin containing fusion proteins to RADH containing fusion proteins, giving rise to CatMPAs. The best performing bait and prey pairs are depicted on top of their respective sections and are marked with an asterisk (*). Adapted from **Section 2.3**.

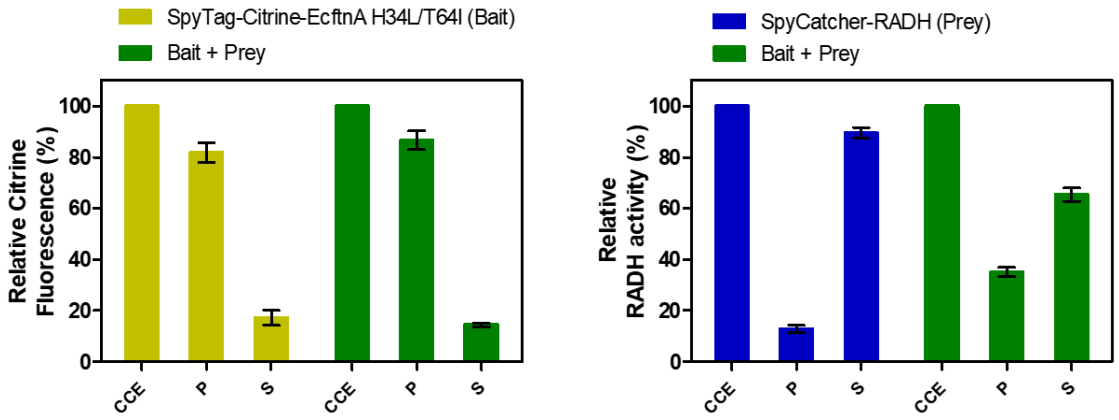

Figure 3.10. Fluorescence and activity distribution of CatMPAs and the individual bait and prey constructs used to generate CatMPAs.

Relative citrine fluorescence and relative RADH activity of cell fractions of the best performing CatMPA pair (SpyTag-Citrine-EcftnA H34L/T64I and SpyCatcher-RADH). SpyTag-Citrine-EcftnA H34L/T64I (bait, depicted in yellow), SpyCatcher-RADH (prey, depicted in blue) along with the cell fractions of 1:1 (v/v) mixture of the two constructs (bait + prey, depicted in green). CCE: crude cell extract. P: washed pellet. S: supernatant. Adapted from **Section 2.3**.

target. This might be due to, for instance, unequal iron loading of ferritin cages, or rather, CatMPAs consisting of the linked citrine-ferritin-RADH that can be purified more efficiently by the magnetic column (i.e. containing high amounts of properly folded ferritin that can take up iron effectively) conversely containing a higher amount of misfolded and hence non-fluorescent citrine. In this case, the purification efficiency of 18% would be the more accurate estimate for the purification efficiency of CatMPAs.

Table 3.5. Activity distribution data for alternative constructs generating CatMPAs.

Bait construct	Prey construct	Activity of P2 for prey (%)	Activity of P2 for bait + prey (%)	Purification efficiency (%)
Spytag-Citrine-EcftnA H34L/T64I (*)	SpyCatcher-RADH	12.8	35.1	9.4 - 18.4**
SpyCatcher-Citrine-EcftnA H34L/T64I (*)	SpyTag-RADH	2.6	8.3	n.a.
SpyCatcher-EcftnA H34L/T64I	SpyTag-GFIL8-PT-RADH (*)	40.2	30.9	5.1
SpyCatcher-EcftnA H34L/T64I	GFIL8-PT-RADH-SpyTag (*)	27.7	24.2	97.4

For all cases, bait, and prey constructs were cultivated and lysed separately, and their CCEs were mixed in a 1:1 ratio (v/v) and incubated at 25 °C for 30 minutes, fractionated to yield soluble and insoluble fractions, and the insoluble fractions were washed to obtained washed pellets (P2, CatMPAs). Activity for each case is given as relative RADH activity of the P2 fraction, compared to the total RADH activity of the CCE it was fractionated from (set to 100%). For each pair, the insoluble partner is marked with an asterisk (*). Purification efficiency was calculated based on relative citrine fluorescence and relative RADH activity of the magnetic fraction (MG), compared to that of the washed pellet (P2), respectively (**). For the bait-prey mixtures containing a single purification efficiency (%) value, relative RADH activity is reported. Adapted from **Section 2.3.1**.

Moreover, additional construct pairs were evaluated within the bait-prey strategy in order to generate CatMPAs (**Section 2.3.1**, depicted in **Figure 3.9**). Replacing the N-terminal SpyTag with SpyCatcher abolished the ability of the citrine-ferritin construct to generate MPAs (**Table 3.5**), possibly due to the larger SpyCatcher tag impairing with the dimerization of citrines, which is the driving force of aggregation ([182], see below). Further, the combined CatIBs and MPAs approach utilizing two insoluble GFIL8-RADH constructs that bore the SpyTag at either terminus to allow linkage to the SpyCatcher-ferritin were tested. Here, the presence of the SpyTag at the N-terminus impaired CatIB formation, similar to the lack of aggregate formation for the SpyCatcher bearing citrine-ferritin construct, implicating that the presence of the smaller SpyTag is not tolerated in

close proximity of the CatIB-inducing tag as well. Fusion of the SpyTag to the C-terminus of GFIL8-RADH lead to a decrease in RADH activity and immobilization efficiency (28%). However, magnetization and subsequent purification of the linked ferritin-GFIL8-RADH protein produced a very high purification yield (over 97%, see **Table 3.5**). This finding indicates that magnetization of CatIBs via linkage to soluble ferritin cages is feasible. However, exploring various CatIB producers that tolerate the attachment of bait-prey tags would help minimize the negative impact of these tag fusions and increase the efficiency of the method in the future.

In addition to genetic design, there are several optimization strategies that could be pursued in order to improve the purification efficiency of CatMPAs. For instance, *in vitro* iron loading could be implemented as an extra step upon cell lysis, before mixing of the CCEs to obtain more magnetic protein fusions. This can be achieved either quickly by adding a solution of ferrous iron to the solution containing ferritin at pH 8.5 under an inert atmosphere and in the presence of H_2O_2 at 60-65°C, or under the slow oxidation by air at the same temperature [242, 243]. The high stability of ferritin makes this harsh *ex vivo* mineralization process possible, however, it would likely be unsuitable for fusion partners of ferritin. Despite the indication of the SpyTag and SpyCatcher tags conferring improved thermostability on some proteins upon the linkage of the Spy-pairs [244, 245], the effect is less clear on unlinked proteins containing SpyTag or SpyCatcher tag, and therefore the possible denaturation of the proteins during the iron loading process needs to be investigated beforehand. Here, utilizing a construct containing soluble ferritin (i.e. without citrine) for *in vitro* iron loading, and combining it with a suitable, insoluble protein producing construct such as CatIBs might be the better strategy.

A simple and better alternative to the iron loading procedure could be using specially developed *E. coli* strains for increased iron uptake. For instance, an *E. coli* K-12 based strain suitable for gene knockouts such as BW25113 has already been tailored to include further knockouts for iron accumulation [240] by removal of the genes encoding metal cation exporters (*fiEf*, *rcnA*, *zntA*) and the ferric uptake regulator (*fur*). Fur is the transcriptional regulator of various iron transport genes including *feo* in *E. coli*, where the ferrous iron uptake directly depends on the presence of Feo, as its deletion was shown to completely abolish the ability of cells to uptake ferrous iron [246, 247]. For EcftnA H34L+T64I overproducing *E. coli* cells where the genes of all above-mentioned metal cation exporters and *fur* were knocked out, it was shown that cells can sequester iron efficiently up to a concentration of 2 mM, and high iron sequestering ability also positively correlated with retention in magnetic columns [240]. Therefore, using a suitable knockout strain for citrine-ferritin fusions would be a benign and viable strategy for

improving the magnetism of MPAs and CatMPAs.

Furthermore, it might be possible to generate CatMPAs directly via a much simpler approach, which can be envisioned through the postulated mechanism of aggregation for the fusion of citrine and ferritin. The aggregation propensity of the citrine-ferritin fusion was attributed to the self-assembly of ferritin subunits and dimerization of citrines that results in the formation of a supramolecular assembly [181, 182]. Moreover, the dimerization of citrines was shown to be the driving force of aggregation which was evidenced by the A206K substitution for citrine. This residue exchange introduces a positive charge into the hydrophobic patch of citrine at the dimerization interface and effectively removes the dimerization potential of the protein, where it was shown to result in the elimination of the aggregation propensity for citrine-ferritin. This finding presents an interesting possibility to generate CatMPAs without employing bait-prey strategies, as it could be possible to replace citrine with an oligomeric target enzyme to directly produce self-aggregating, magnetic enzyme immobilizates.

For targets that can be fused to the N-terminus of ferritin, the above-mentioned strategy might prove to be the simplest means of obtaining CatMPAs, whereas the viability of C-terminal fusions for *E. coli* ferritins should be investigated beforehand. The C-terminus of ferritin is involved in the control of iron flux through the ferroxidase center [168]. However, there are studies that indicate that the C-terminus of HuFtnH including the E-helix (**Figure 1.7**) not being essential for proper folding of ferritin monomers nor the assembly of the 24meric protein, and HuFtnH was shown to accommodate C-terminal fusions of proteins and retain its magnetic properties [180, 248]. Interestingly, the fusion of proteins or peptides to the C-terminus of ferritin does not impair protein function but instead results in alternative configurations of the ferritin cage, where the position of the E-helix differs in two possible ways. In case the target has a suitable size that allows the incorporation of 24 target peptides or protein subunits inside the ferritin cavity, this results in the "flip" conformation where the E-helix points inside the cavity, where the target protein is surrounded by the ferritin cage. Otherwise, it results in the "flop" conformation where the E-helix is protruding outside of the cage, resulting in a ferritin cage decorated by the target protein [249, 248]. Therefore, it might be worthwhile to attempt C-terminal fusions of immobilization targets to *E. coli* ferritins to assess their suitability for the direct production of CatMPAs. For target enzymes that can be fused to the N-terminus of ferritin without any issues (such as EcLDC that was shown to accommodate C-terminal fusions), the direct CatMPAs approach would likely be suitable and could be tested without any further considerations. In conclusion, the fusion of oligomeric targets directly to ferritin might present a unique opportunity to obtain

CatMPAs in one step, without employing SpyTag or SpyCatcher tags.

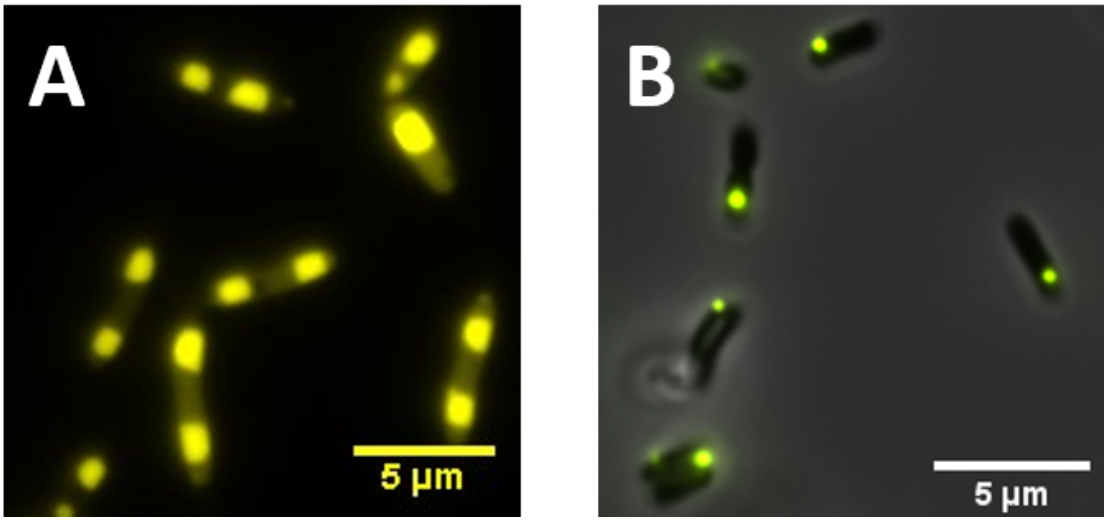

Figure 3.11. Live *E. coli* cells producing CatIBs or MPAs.

(A) TdoT-YFP CatIBs (image used with permission from Vera D. Jäger). **(B)** MPAs of Citrine-EcftnA H34L + T64I.

Due to certain visible properties of MPAs observed during microscopic analyses, it may be worthwhile to conduct detailed morphological analyses to shed some light on their nature. Microscopic analyses performed on all citrine-ferritins fusions revealed the presence of localized fluorescent signals originating at a single cell pole for MPAs, that despite resembling fluorescent CatIBs to a degree, possessed some visible differences. CatIBs usually exhibit fluorescence of the target protein at both cell poles and appear relatively large in comparison to the cytoplasmic space [108, 111, 115, 134] (see **Figure 3.11, A**), however, fluorescent MPAs generated by either ferritin fusion appear visually smaller, and only a single cell pole exhibits citrine fluorescence (**Figure 3.11, B**). This finding is in line with the study by Bellapadrona *et al*. who investigated the Citrine-HuFtnH fusion [182], where cells exhibited fluorescence at a single pole and transmission electron microscopy (TEM) analyses revealed the particles to be of non-crystalline nature with a size smaller than 500 nm in *E. coli*. This indicates that MPAs likely possess a different morphology compared to CatIBs, and may hint that they might instead share similarities to membraneless organelles generated via LLPS, as their generation was shown to be possible in *E. coli*, synthetically [250]. It would likewise be interesting to decipher whether MPAs contain amyloid-like fibrils similar to CatIBs generated by certain tags such as ELK16 or L6KD [112, 134]. Since the amyloid-like nature of CatIBs is a disadvantage for certain applications (i.e. for biomedicine where the release of potential toxic β-sheet species might be of concern [251]), MPAs could offer a better alternative.

As ferritin is highly biocompatible and therefore already widely used for biomedical applications such as photothermal therapy, diagnostics, and drug delivery [252], MPAs can prove promising for applications in biomedicine as well.

Another advantage of the MPAs is their principal suitability for flow applications. Unlike enzymes immobilized onto magnetic carriers (such as magnetic CLEAs), MPAs can be used directly without further modifications, and be fixed in place by using magnetically stabilized fluidized bed reactors where a weak external magnetic field is applied axially, relative to the direction of flow [253, 254]. Such reactors have been already used jointly with enzymes immobilized onto magnetic carriers for continuous operation, such as lipases immobilized onto magnetized chitosan microspheres to produce biodiesel [255], laccases immobilized on mesoporous silica for degradation of phenolic compounds [256], and whole yeast cells immobilized in magnetic particles for ethanol fermentation [257]. Along the same lines, microfluidic magnetic oscillation reactors (μMORE [258]) could be utilized to the same end and can be useful for the characterization of new CatMPAs consisting of different industrially relevant targets. Further, due to the suitability of magnetic nanoparticles in terms of recoverability by standard commercial equipment [45], MPAs can simplify downstream applications. In conclusion, MPAs as fully biologically-produced protein immobilizates that are suitable for magnetic separation techniques can be useful for biotechnology, including flow applications and biomedicine.

3.6. Summary and Outlook

In this PhD thesis, a detailed characterization of 24 CatIB constructs generated by the fusion of four CatIB tags with various lengths and properties, to two industrially relevant enzymes and a fluorescent reporter protein was conducted (**Section 2.1**). Various analyses on the resulting 18AWT, L6KD, GFIL8, and TdoT CatIBs revealed that CatIB formation efficiency, yield, residual activity, and stability highly depend on the fusion terminus and the CatIB tag, as well as the target protein. For the highly soluble fluorescent protein mCherry, a positive influence of the larger TdoT tag, as well as utilization of the optimal fusion terminus on CatIB formation efficiency could be demonstrated (discussed in **Section 3.3**). For BsLA and RADH, a positive influence of the shorter GFIL8 and L6KD tags fused to the optimal terminus was demonstrated in terms of CatIB formation efficiency, stability and residual activity, where the latter could be improved drastically compared to the previously commonly utilized TdoT CatIBs [109, 117, 108].

Being a fully *in vivo* method that does not require laborious and expensive purification or immobilization steps, the rather low residual activity of CatIBs had been the main limitation of these immobilizates. This drawback was shown to be in part remediable at the design level, through the utilization of suitable CatIB tags for each target. Furthermore, through investigating biomass specific activity yields that incorporate activities and yields of CatIBs in a simple way, multiple BsLA and RADH CatIBs were shown to outperform their soluble enzyme counterparts (discussed in **Section 3.2**) and therefore show enhanced potential for application. A positive effect of the CatIB immobilization on enzyme stability could be demonstrated as well, which allowed the proof-of-concept application of GFIL8-RADH CatIBs for batch and continuous flow applications for the first time (discussed in **Section 3.4**). The investigations on linker rigidity and properties of EcLDC CatIBs (**Section 2.2**) provided further hints on important design parameters to obtain highly active CatIBs, pointing towards the better suitability of rigid linkers.

The superior properties of CatIBs generated by GFIL8 and L6KD tags described above, which is also supported by works of other groups studying these tags [112, 114, 138, 132], identify short, synthetic peptide tags as promising candidates to generate CatIBs of enzymes that had been so far not tested, whereas coiled-coil tags such as TdoT or ZapB [141] might still be better candidates for difficult-to-immobilize targets. On a broader scale, as the general applicability of a certain CatIB tag that can generate superior CatIBs for all enzyme targets appear to be unlikely, indicated by the differences in relevant properties of CatIBs where the same tags were fused to different enzymes or termini, or harbored different linkers (**Section 2.1**, **Section 2.2**, [108, 109, 113, 114, 113]), implementation of automated workflows to facilitate time-efficient characterization of various CatIB constructs might be crucial to generate CatIBs of different targets at an enhanced rate in the future. While automated microscopy can be a highly useful tool for an initial screen of (Cat)IB formation at a qualitative level and at a rapid pace, activity and stability analyses need to be conducted on the constructs that appear promising, to ensure the activity of the immobilizate and its actual potential for further application (discussed in **Section 3.1.5**).

MPAs based on the self-aggregating fusion of iron storage protein ferritin and the yellow fluorescent protein citrine were generated as an alternative method to obtain *in vivo* produced immobilizates with magnetic properties that can be easily separated and purified (**Section 2.3**). In this regard, 17 constructs were generated and characterized, and MPAs could be obtained in comparable yields and remarkable purities i.e. compared to CatIBs, which can therefore complement the CatIB strategy for applications where the latter possess shortcomings. Use of MPAs could be especially suitable for biomedi-

cal applications, due to their high purity and the bio-compatibility of ferritin (discussed in **Section 3.5**). Moreover, due to their magnetism, MPAs can be used in reactors utilizing magnetic fields and therefore can be especially suitable to flow applications. The current shortcomings of CatMPAs generated via a bait-prey approach could potentially be overcome via simpler molecular biological fusions where the target gene is directly fused to the gene encoding the ferritin, making the application much easier and more efficient. Furthermore, utilization of strategies such as the employment of suitable iron accumulation strains, could confer increased magnetic properties to MPAs and improve their purification efficiencies.

Last but not least, three review papers that provide a comprehensive and up to date overview about the CatIBs immobilization approach in terms of design parameters, relevant properties (**Section 2.4**), flow applications (**Section 2.7**), as well as other *in vivo* immobilization methods (**Section 2.6**), and a book chapter to serve as a laboratory manual for CatIBs (**Section 2.5**) have been written as part of this thesis.

Taken together, this PhD thesis offers improvements to the existing CatIB method by highlighting suitable CatIB tags for target proteins with different limitations and challenges in order to generate immobilizates with enhanced performance parameters, as well as demonstrating their suitability for flow applications. Further, it offers a new method for enzyme immobilization and provides hints towards optimizations for two different, fully biological immobilization methods. Due to the importance of utilizing green biocatalysts within optimized immobilization protocols, expanding the scope of current enzyme immobilization methods as well as establishing new ones could offer countless benefits from environmental, industrial, and economical standpoints.

4. References

[1] Barcelos, Mayara C.S., Lupki, Fernanda B., Campolina, Gabriela A., Nelson, David Lee, and Molina, Gustavo. “The colors of biotechnology: General overview and developments of white, green and blue areas”. *FEMS Microbiology Letters* 365.21 (2018).

[2] Liu, Li, Wang, Jiajing, Rosenberg, Danny, Zhao, Hao, Lengyel, György, and Nadel, Dani. “Fermented beverage and food storage in 13,000 y-old stone mortars at Raqefet Cave, Israel: Investigating Natufian ritual feasting”. *Journal of Archaeological Science: Reports* 21 (2018), pp. 783–793.

[3] McGovern, Patrick E., Zhang, Juzhong, Tang, Jigen, Zhang, Zhiqing, Hall, Gretchen R, Moreau, Robert A, ez, Alberto Nuñ, Butrym, Eric D, Richards, Michael P, Wang, Chen shan, Cheng, Guangsheng, Zhao, Zhijun, and Wang, Changsui. “Fermented beverages of pre- and proto- historic China”. *Proceedings of the National Academy of Sciences* 101.51 (2004), pp. 17593–17598.

[4] Boethius, Adam. “Something rotten in Scandinavia: The world’s earliest evidence of fermentation”. *Journal of Archaeological Science* 66 (2016), pp. 169–180.

[5] Evershed, Richard P., Payne, Sebastian, Sherratt, Andrew G., Copley, Mark S., Coolidge, Jennifer, Urem-K., Duska, Kotsakis, Kostas, Özdoğan, Mehmet, Özdoğan, Asli E., Nieuwenhuyse, Olivier, Akkermans, Peter M.M.G., Bailey, Douglass, Andeescu, Radian Romus, Campbell, Stuart, Farid, Shahina, Hodder, Ian, Yalman, Nurcan, Özbaşaran, Mihriban, Biçakci, Erhan, Garfinkel, Yossef, Levy, Thomas, and Burton, Margie M. “Earliest date for milk use in the Near East and southeastern Europe linked to cattle herding”. *Nature* 455.7212 (2008), pp. 528–531.

[6] Salque, Mélanie, Bogucki, Peter I., Pyzel, Joanna, Sobkowiak-Tabaka, Iwona, Grygiel, Ryszard, Szmyt, Marzena, and Evershed, Richard P. “Earliest evidence for cheese making in the sixth millennium BC in northern Europe”. *Nature* 493.7433 (2013), pp. 522–525.

[7] Garnier, Nicolas and Valamoti, Soultana Maria. “Prehistoric wine-making at Dikili Tash (Northern Greece): Integrating residue analysis and archaeobotany”. *Journal of Archaeological Science* 74 (2016), pp. 195–206.

[8] Arranz-Otaegui, Amaia, Carretero, Lara Gonzalez, Ramsey, Monica N., Fuller, Dorian Q., and Richter, Tobias. “Archaeobotanical evidence reveals the origins of bread 14,400 years ago in northeastern Jordan”. *Proceedings of the National Academy of Sciences of the United States of America* 115.31 (2018), pp. 7925–7930.

[9] Samuel, Delwen. “Investigation of Ancient Egyptian Baking and Brewing Methods by Correlative Microscopy”. *Science* 273.5274 (1996), pp. 488–490.

[10] Regulski, Ilona. “The Origins and Early Development of Writing in Egypt” (2016).

[11] Hurley, Thomas D. and Edenberg, Howard J. “Genes Encoding Enzymes Involved in Ethanol Metabolism”. *Alcohol research* 34.3 (2012), pp. 339–44.

[12] Carrigan, Matthew A., Uryasev, Oleg, Frye, Carole B., Eckman, Blair L., Myers, Candace R., Hurley, Thomas D., and Benner, Steven A. “Hominids adapted to metabolize ethanol long before human-directed fermentation”. *Proceedings of the National Academy of Sciences of the United States of America* 112.2 (2015), pp. 458–463.

[13] Peters, Anna, Krumbholz, Petra, Jäger, Elisabeth, Heintz-Buschart, Anna, Çakir, Mehmet Volkan, Rothemund, Sven, Gaudl, Alexander, Ceglarek, Uta, Schöneberg, Torsten, and Stäubert, Claudia. “Metabolites of lactic acid bacteria present in fermented foods are highly potent agonists of human hydroxycarboxylic acid receptor 3”. *PLoS Genetics* 15.5 (2019).

[14] Christopher, Jon A., Raso, Stephen W., Ziegler, Miriam M., and Baldwin, Thomas O. *Molecular biology and biotechnology: a comprehensive desk reference*. Ed. by Robert A Meyers. John Wiley & Sons, 1995, pp. 295–301.

[15] Dixon, Malcolm. *The chemistry of life: eight lectures on the history of biochemistry*. Ed. by Joseph Needham. Cambridge University Press, 1970, pp. 15–38.

[16] Armstrong, E. F. “Enzymes: A Discovery and its Consequences”. *Nature* (1933).

[17] Heckmann, Christian M. and Paradisi, Francesca. “Looking Back: A Short History of the Discovery of Enzymes and How They Became Powerful Chemical Tools”. *ChemCatChem* 12.24 (2020), pp. 6082–6102.

[18] Bhatia, Saurabh. *Introduction to enzymes and their applications*. IOP Publishing, 2018.

[19] Gest, Howard. “The discovery of microorganisms by Robert Hooke and Antoni van Leeuwenhoek, fellows of the Royal Society”. *Notes and Records of the Royal Society* 58.2 (2004), pp. 187–201.

[20] Barnett, James A. “A history of research on yeasts 1: Work by chemists and biologists 1789-1850”. *Yeast* 14.16 (1998), pp. 1439–1451.

[21] Barnett, James A. “A history of research on yeasts 2: Louis Pasteur and his contemporaries, 1850-1880”. *Yeast* 16.8 (2000), pp. 755–771.

[22] Wisniak, Jaime. “The History of Catalysis. From the Beginning to Nobel Prizes”. *Educacion Quimica* 21.1 (2010), pp. 60–69.

[23] Bornscheuer, U. T. and Bucholz, K. “Highlights in biocatalysis - Historical landmarks and current trends”. *Engineering in Life Sciences* 5.4 (2005), pp. 309–323.

[24] Barnett, James A. and Lichtenthaler, Frieder W. “A history of research on yeasts 3: Emil Fischer Eduard Buchner and their contemporaries, 1880-1900”. *Yeast* 18.4 (2001), pp. 363–388.

[25] Avery, Oswald T., Macleod, Colin M., and Maclyn, McCarty. “Studies on the chemical nature of the substance inducing transformation of pneumococcal types : Induction of transformation by a desoxyribonucleic acid fraction isolated from Pneumococcus type III”. *Journal of Experimental Medicine* 1.79 (1944), pp. 137–58.

[26] Dahm, Ralf. “Friedrich Miescher and the discovery of DNA”. *Developmental Biology* 278.2 (2005), pp. 274–288.

[27] Brooks-Bartlett, Jonathan C. and Garman, Elspeth F. “The nobel science: One hundred years of crystallography”. *Interdisciplinary Science Reviews* 40.3 (2015), pp. 244–264.

[28] Koshland, Daniel E. “Application of a theory of enzyme specificity to protein synthesis”. *Proceedings of the National Academy of Sciences of the United States of America* 44 (1958), pp. 98–104.

[29] Robinson, Peter K. “Enzymes: principles and biotechnological applications”. *Essays in Biochemistry* 59 (2015), pp. 1–41.

[30] Hsiao, H. Y., Walter, J. F., Anderson, D. M., and Hamilton, B. K. “Enzymatic production of amino acids”. *Biotechnology and Genetic Engineering Reviews* 6.1 (1988), pp. 179–220.

[31] F., Sanger and R., Coulson A. “A rapid method for determining sequences in DNA by primed synthesis with DNA polymerase”. *Journal of Molecular Biology* 94.3 (1975), pp. 441–8.

[32] F, Sanger, S., Nicklen, and AR., Coulson. “DNA sequencing with chain-terminating inhibitors”. *Proceedings of the National Academy of Sciences of the United States of America* 74.12 (1977), pp. 5463–7.

[33] Quianzon, Celeste C. and Cheikh, Issam. “History of insulin”. *Journal of Community Hospital Internal Medicine Perspectives* 2.2 (2012).

[34] Kleppe, K., Ohtsuka, E., Kleppe, R., Molineux, I., and Khorana, H. “Studies on polynucleotides. XCVI. Repair replications of short synthetic DNA’s as catalyzed by DNA polymerases”. *Journal of Molecular Biology* 56.2 (1971), pp. 341–61.

[35] Mullis, K., Faloona, F., Scharf, S., Saiki, R., Horn, G., and Erlich, H. “Specific enzymatic amplification of DNA *in vitro*: the polymerase chain reaction”. *Cold Spring Harbor Symposia on Quantitative Biology* 51.1 (1986), pp. 263–73.

[36] Bornscheuer, U., G., Huisman, Kazlauskas, R., Lutz, S., Moore, JC., and Robins, K. “Engineering the third wave of biocatalysis”. *Nature* 485 (2012), pp. 185–194.

[37] Zhang, Shangjie, Guo, Feng, Yan, Wei, Dai, Zhongxue, Dong, Weiliang, Zhou, Jie, Zhang, Wenming, Xin, Fengxue, and Jiang, Min. “Recent Advances of CRISPR/Cas9-Based Genetic Engineering and Transcriptional Regulation in Industrial Biology”. *Frontiers in Bioengineering and Biotechnology* 7 (2020).

[38] Fasim, Aneesa, More, Veena S., and More, Sunil S. “Large-scale production of enzymes for biotechnology uses”. *Current Opinion in Biotechnology* 69 (2021), pp. 68–76.

[39] BBC. *Global Markets for Enzymes in Industrial Applications*. Vol. BIO030L. BCC Publishing, 2021.

[40] Zhu, D., Wu, Q., and Wang, N. “Industrial Enzymes”. *Comprehensive Biotechnology, Second Edition* 3 (2011), pp. 3–13.

[41] Basso, Alessandra and Serban, Simona. “Industrial applications of immobilized enzymes—A review”. *Molecular Catalysis* 479 (2019), p. 110607.

[42] Adrio, Jose L. and Demain, Arnold L. “Microbial enzymes: tools for biotechnological processes”. *Biomolecules* 4.1 (2014), pp. 117–139.

[43] Adrio, Jose-Luis and Demain, Arnold L. “Recombinant organisms for production of industrial products”. *Bioengineered Bugs* (2010).

[44] Hauer, Bernhard, Branneby, Cecilia Kvarnström, Hult, Karl, Magnusson, Anders, and Hamberg, Anders. “Enzymatically catalyzed method of preparing mono-acylated polyols”. Pat. 2014.

[45] Sheldon, Roger A., Basso, Alessandra, and Brady, Dean. “New frontiers in enzyme immobilisation: Robust biocatalysts for a circular bio-based economy”. *Chemical Society Reviews* 50.10 (2021), pp. 5850–5862.

[46] Chapman, Jordan, Ismail, Ahmed E., and Dinu, Cerasela Zoica. “Industrial applications of enzymes: Recent advances, techniques, and outlooks”. *Catalysts* 8.6 (2018).

[47] Shoda, Shin Ichiro, Uyama, Hiroshi, Kadokawa, Jun Ichi, Kimura, Shunsaku, and Kobayashi, Shiro. “Enzymes as green catalysts for precision macromolecular synthesis”. *Chemical Reviews* 116.4 (2016), pp. 2307–2413.

[48] Hatti-Kaul, Rajni, Törnvall, Ulrika, Gustafsson, Linda, and Börjesson, Pål. “Industrial biotechnology for the production of bio-based chemicals – a cradle-to-grave perspective”. *Trends in Biotechnology* 25.3 (2007), pp. 119–124.

[49] Bernal, Claudia, Rodríguez, Karen, and Martínez, Ronny. “Integrating enzyme immobilization and protein engineering: An alternative path for the development of novel and improved industrial biocatalysts”. *Biotechnology Advances* 36.5 (2018), pp. 1470–1480.

[50] Bilal, Muhammad, Zhao, Yuping, Noreen, Sadia, Shah, Syed Zakir Hussain, Bharagava, Ram Naresh, and Iqbal, Hafiz M.N. “Modifying bio-catalytic properties of enzymes for efficient biocatalysis: a review from immobilization strategies viewpoint”. *Biocatalysis and Biotransformation* 37.3 (2019), pp. 159–182.

[51] Yang, Haiquan, Li, Jianghua, Du, Guocheng, and Liu, Long. “Microbial Production and Molecular Engineering of Industrial Enzymes: Challenges and Strategies”. *Biotechnology of Microbial Enzymes: Production, Biocatalysis and Industrial Applications* (2017), pp. 151–165.

[52] Wu, Shuke, Snajdrova, Radka, Moore, Jeffrey C., Baldenius, Kai, and Bornscheuer, Uwe T. “Biocatalysis: Enzymatic Synthesis for Industrial Applications”. *Angewandte Chemie - International Edition* 60.1 (2021), pp. 88–119.

[53] Cosimo, Robert Di, Auliffe, Joseph Mc, Poulose, Ayrookaran J., and Bohlmann, Gregory. “Industrial use of immobilized enzymes”. *Chemical Society Reviews* 42.15 (2013), pp. 6437–6474.

[54] Taheri-Kafrani, Asghar, Kharazmi, Sara, Nasrollahzadeh, Mahmoud, Soozanipour, Asieh, Ejeian, Fatemeh, Etedali, Parisa, Mansouri-Tehrani, Hajar Alsadat, Razmjou, Amir, Yek, Samaneh Mahmoudi Gom, and Varma, Rajender S. “Recent developments in enzyme immobilization technology for high-throughput processing in food industries”. *Critical Reviews in Food Science and Nutrition* 61.19 (2021), pp. 3160–3196.

[55] Ren, Sizhu, Li, Conghai, Jiao, Xiaobo, Jia, Shiru, Jiang, Yanjun, Bilal, Muhammad, and Cui, Jiandong. “Recent progress in multienzymes co-immobilization and multienzyme system applications”. *Chemical Engineering Journal* 373 (2019), pp. 1254–1278.

[56] Arana-Peña, Sara, Carballares, Diego, Morellon-Sterlling, Roberto, Berenguer-Murcia, Ángel, Alcántara, Andrés R., Rodrigues, Rafael C., and Fernandez-Lafuente, Roberto. “Enzyme co-immobilization: Always the biocatalyst designers’ choice…or not?” *Biotechnology Advances* 51 (2021).

[57] Zdarta, Jakub, Meyer, Anne S., Jesionowski, Teofil, and Pinelo, Manuel. “A general overview of support materials for enzyme immobilization: Characteristics, properties, practical utility”. *Catalysts* 8.2 (2018).

[58] Papamichael, Emmanuel M. and Stergiou, Panagiota-Yiolanda. *Enzyme immobilization strategies and bioprocessing applications*. Elsevier, 2020, pp. 217–241.

[59] Mehrasbi, Mohammad Reza, Mohammadi, Javad, Peyda, Mazyar, and Mohammadi, Mehdi. “Covalent immobilization of *Candida antarctica* lipase on core-shell magnetic nanoparticles for production of biodiesel from waste cooking oil”. *Renewable Energy* 101 (2017), pp. 593–602.

[60] Vineh, Monireh Besharati, Saboury, Ali A., Poostchi, Amir A., Rashidi, Ali M., and Parivar, Kazem. “Stability and activity improvement of horseradish peroxidase by covalent immobilization on functionalized reduced graphene oxide and biodegradation of high phenol concentration”. *International Journal of Biological Macromolecules* 106 (2018), pp. 1314–1322.

[61] Wan, Ling Shu, Ke, Bei Bei, and Xu, Zhi Kang. “Electrospun nanofibrous membranes filled with carbon nanotubes for redox enzyme immobilization”. *Enzyme and Microbial Technology* 42.4 (2008), pp. 332–339.

[62] Pal, Ajay and Khanum, Farhath. “Covalent immobilization of xylanase on glutaraldehyde activated alginate beads using response surface methodology: Characterization of immobilized enzyme”. *Process Biochemistry* 46.6 (2011), pp. 1315–1322.

[63] Guisan, Jose M., Bolivar, Juan M., López-Gallego, Fernando, and Rocha-Martín, Javier. *Immobilization of Enzymes and Cells*. Vol. 4. Humana Press Inc., 2020, pp. 1064–3745.

[64] Reshmi, R., Sanjay, G., and Sugunan, S. “Immobilization of α-amylase on zirconia: A heterogeneous biocatalyst for starch hydrolysis”. *Catalysis Communications* 8.3 (2007), pp. 393–399.

[65] Canbolat, M. Fatih, Savas, Hasan Basri, and Gultekin, Fatih. “Improved catalytic activity by catalase immobilization using γ-cyclodextrin and electrospun PCL nanofibers”. *Journal of Applied Polymer Science* 134.4 (2017).

[66] Zhang, Baohua, Weng, Yanqing, Xu, Hong, and Mao, Zhiping. “Enzyme immobilization for biodiesel production”. *Applied Microbiology and Biotechnology* 93.1 (2012), pp. 61–70.

[67] Martín, María C., López, Olivia V., Ciolino, Andrés E., Morata, Vilma I., Villar, Marcelo A., and Ninago, Mario D. “Immobilization of enological pectinase in cal-

cium alginate hydrogels: A potential biocatalyst for winemaking". *Biocatalysis and Agricultural Biotechnology* 18 (2019), p. 101091.

[68] Barouni, Eleftheria, Petsi, Theano, Kolliopoulos, Dionysios, Vasileiou, Dimitrios, Panas, Panagiotis, Bekatorou, Argyro, Kanellaki, Maria, and Koutinas, Athanasios A. "Immobilized rennin in TC/SG composite in cheese production". *Food Chemistry* 200 (2016), pp. 76–82.

[69] Mukhopadhyay, Arka, Dasgupta, Anjan Kr., and Chakrabarti, Krishanu. "Enhanced functionality and stabilization of a cold active laccase using nanotechnology based activation-immobilization". *Bioresource Technology* 179 (2015), pp. 573–584.

[70] Bilal, Muhammad, Asgher, Muhammad, Iqbal, Hafiz M.N., Hu, Hongbo, and Zhang, Xuehong. "Gelatin-Immobilized Manganese Peroxidase with Novel Catalytic Characteristics and Its Industrial Exploitation for Fruit Juice Clarification Purposes". *Catalysis Letters* 146.11 (2016), pp. 2221–2228.

[71] Xue, Huaiguo, Shen, Zhiquan, and Li, Chunmei. "Improved selectivity and stability of glucose biosensor based on *in situ* electropolymerized polyaniline–polyacrylonitrile composite film". *Biosensors and Bioelectronics* 20.11 (2005), pp. 2330–2334.

[72] Weltz, James S., Kienle, Daniel F., Schwartz, Daniel K., and Kaar, Joel L. "Reduced Enzyme Dynamics upon Multipoint Covalent Immobilization Leads to Stability-Activity Trade-off". *Journal of the American Chemical Society* 142.7 (2020), pp. 3463–3471.

[73] Wu, Jeffrey Chun Yu, Hutchings, Christopher Hayden, Lindsay, Mark Jeffrey, Werner, Christopher James, and Bundy, Bradley Charles. "Enhanced Enzyme Stability Through Site-Directed Covalent Immobilization". *Journal of Biotechnology* 193 (2015), pp. 83–90.

[74] Liu, Dong Mei, Chen, Juan, and Shi, Yan Ping. "Advances on methods and easy separated support materials for enzymes immobilization". *TrAC - Trends in Analytical Chemistry* 102 (2018), pp. 332–342.

[75] Liu, Dong Mei and Dong, Chen. "Recent advances in nano-carrier immobilized enzymes and their applications". *Process Biochemistry* 92 (2020), pp. 464–475.

[76] Jesionowski, Teofil, Zdarta, Jakub, and Krajewska, Barbara. "Enzyme immobilization by adsorption: A review". *Adsorption* 20.5-6 (2014), pp. 801–821.

[77] Bilal, Muhammad, Zhao, Yuping, Rasheed, Tahir, and Iqbal, Hafiz M.N. "Magnetic nanoparticles as versatile carriers for enzymes immobilization: A review". *International Journal of Biological Macromolecules* 120 (2018), pp. 2530–2544.

[78] Brena, Beatriz, González-Pombo, Paula, and Batista-Viera, Francisco. *Immobilization of enzymes: A literature survey*. Ed. by J.M. Guisan. Vol. 1051. Humana Press Inc., 2013, pp. 15–31.

[79] Döbber, Johannes and Pohl, Martina. "HaloTag™: Evaluation of a covalent one-step immobilization for biocatalysis". *Journal of Biotechnology* 241 (2017), pp. 170–174.

[80] England, Christopher G., Luo, Haiming, and Cai, Weibo. "HaloTag Technology: A Versatile Platform for Biomedical Applications". *Bioconjugate Chemistry* 26.6 (2015), pp. 975–986.

[81] Ovsejevi, Karen, Manta, Carmen, and Batista-Viera, Francisco. *Reversible covalent immobilization of enzymes via disulfide bonds*. Ed. by J.M. Guisan. Vol. 1051. Humana Press Inc., 2013, pp. 89–116.

[82] Homaei, Ahmad Abolpour, Sariri, Reyhaneh, Vianello, Fabio, and Stevanato, Roberto. "Enzyme immobilization: An update". *Journal of Chemical Biology* 6.4 (2013), pp. 185–205.

[83] Thangaraj, Baskar and Solomon, Pravin Raj. "Immobilization of Lipases – A Review. Part I: Enzyme Immobilization". *ChemBioEng Reviews* 6.5 (2019), pp. 157–166.

[84] Jäger, Vera D., Lamm, Robin, Küsters, Kira, Ölçücü, Gizem, Oldiges, Marco, Jaeger, Karl-Erich, Büchs, Jochen, and Krauss, Ulrich. "Catalytically-active inclusion bodies for biotechnology - general concepts, optimization, and application". *Applied Microbiology and Biotechnology* 104.17 (2020), pp. 7313–7329.

[85] Sheldon, Roger A. "Cross-linked enzyme aggregates as industrial biocatalysts". *Organic Process Research and Development* 15.1 (2011), pp. 213–223.

[86] Li, Shaofen. *Fundamentals of Biochemical Reaction Engineering*. Elsevier, 2017, pp. 491–539.

[87] Liu, Shijie. *Enzymes*. Elsevier, 2017, pp. 297–373.

[88] Cacicedo, Maximiliano L., Manzo, Ricardo M., Municoy, Sofía, Bonazza, Horacio L., Islan, German A., Desimone, Martín, Bellino, Martin, Mammarella, Enrique J., and Castro, Guillermo R. "Immobilized Enzymes and Their Applications". *Biomass, Biofuels, Biochemicals: Advances in Enzyme Technology* (2019), pp. 169–200.

[89] Margolin, Alexey L. "Novel crystalline catalysts". *Trends in Biotechnology* 14.7 (1996), pp. 223–230.

[90] Sheldon, R A. "Cross-linked enzyme aggregates (CLEAs): stable and recyclable biocatalysts". *Biochemical Society Transactions* (2007), pp. 1583–7.

[91] Winter, Karel De, Soetaert, Wim, and Desmet, Tom. “An imprinted cross-linked enzyme aggregate (iCLEA) of sucrose phosphorylase: Combining improved stability with altered specificity”. *International Journal of Molecular Sciences* 13.9 (2012), pp. 11333–11342.

[92] López-Serrano, P., Cao, L., Rantwijk, F. Van, and Sheldon, R. A. “Cross-linked enzyme aggregates with enhanced activity: application to lipases”. *Biotechnology Letters* 24 (2002), pp. 1379–1383.

[93] Brady, Dean, Jordaan, Justin, Simpson, Clinton, Chetty, Avashnee, Arumugam, Cherise, and Moolman, Francis S. “Spherezymes: A novel structured self-immobilisation enzyme technology”. *BMC Biotechnology* 8 (2008).

[94] Mbanjwa, Mesuli B., Land, Kevin J., Windvoel, Thobile, Papala, Prince M., Fourie, Louis, Korvink, Jan G., Visser, Daniel, and Brady, Dean. “Production of self-immobilised enzyme microspheres using microfluidics”. *Process Biochemistry* 69 (2018), pp. 75–81.

[95] Krauss, Ulrich, Jäger, Vera D., Diener, Martin, Pohl, Martina, and Jaeger, Karl-Erich. “Catalytically-active inclusion bodies - Carrier-free protein immobilizates for application in biotechnology and biomedicine”. *Journal of Biotechnology* 258 (2017), pp. 136–147.

[96] Marco, Ario De, Ferrer-Miralles, Neus, Garcia-Fruitós, Elena, Mitraki, Anna, Peternel, Spela, Rinas, Ursula, Trujillo-Roldán, Mauricio A., Valdez-Cruz, Norma A., Vázquez, Esther, and Villaverde, Antonio. “Bacterial inclusion bodies are industrially exploitable amyloids”. *FEMS Microbiology Reviews* 43.1 (2019), pp. 53–72.

[97] Köszagová, Romana and Nahálka, Jozef. “Inclusion bodies in biotechnology”. *Journal of Microbiology, Biotechnology and Food Sciences* 9.6 (2020), pp. 1191–1196.

[98] Slouka, Christoph, Kopp, Julian, Spadiut, Oliver, and Herwig, Christoph. “Perspectives of inclusion bodies for bio-based products: curse or blessing?” *Applied Microbiology and Biotechnology* 103.3 (2019), pp. 1143–1153.

[99] Rinas, Ursula, Garcia-Fruitós, Elena, Corchero, José Luis, Vázquez, Esther, Seras-Franzoso, Joaquin, and Villaverde, Antonio. “Bacterial Inclusion Bodies: Discovering Their Better Half”. *Trends in Biochemical Sciences* 42.9 (2017), pp. 726–737.

[100] Worrall, D.M. and Goss, N.H. “The formation of biologically active beta-galactosidase inclusion bodies in *Escherichia coli*.” *Australian Journal of Biotechnology* 3.1 (1989), pp. 28–32.

[101] Baneyx, François and Mujacic, Mirna. “Recombinant protein folding and misfolding in *Escherichia coli*”. *Nature Biotechnology* 22.11 (2004), pp. 1399–1407.

[102] Carrió, M. Mar, Cubarsi, Rafael, and Villaverde, Antonio. “Fine architecture of bacterial inclusion bodies”. *FEBS Letters* 1.471 (2000), pp. 7–11.

[103] Ölçücü, Gizem, Klaus, Oliver, Jaeger, Karl-Erich, Drepper, Thomas, and Krauss, Ulrich. “Emerging Solutions for *in vivo* Biocatalyst Immobilization: Tailor-Made Catalysts for Industrial Biocatalysis”. *ACS Sustainable Chemistry and Engineering* 9.27 (2021), pp. 8919–8945.

[104] Arié, Jean Philippe, Miot, Marika, Sassoon, Nathalie, and Betton, Jean Michel. “Formation of active inclusion bodies in the periplasm of *Escherichia coli*”. *Molecular Microbiology* 62.2 (2006), pp. 427–437.

[105] Capitini, Claudia, Conti, Simona, Perni, Michele, Guidi, Francesca, Cascella, Roberta, Poli, Angela De, Penco, Amanda, Relini, Annalisa, Cecchi, Cristina, and Chiti, Fabrizio. “TDP-43 inclusion bodies formed in bacteria are structurally amorphous, non-amyloid and inherently toxic to neuroblastoma cells”. *PLoS ONE* 9.1 (2014).

[106] Wang, Lei. “Towards revealing the structure of bacterial inclusion bodies.” *Prion* 3.3 (2009), pp. 139–145.

[107] Huang, Ziliang, Zhang, Chong, Chen, Shuo, Ye, Fengchun, and Xing, Xin Hui. “Active inclusion bodies of acid phosphatase PhoC: Aggregation induced by GFP fusion and activities modulated by linker flexibility”. *Microbial Cell Factories* 12.1 (2013).

[108] Jäger, V. D., Kloss, R., Grünberger, A., Seide, S., Hahn, D., Karmainski, T., Piqueray, M., Embruch, J., Longerich, S., Mackfeld, U., Jaeger, K.-E., Wiechert, W., Pohl, M., and Krauss, U. “Tailoring the properties of (catalytically)-active inclusion bodies”. *Microbial Cell Factories* 18.1 (2019).

[109] Diener, Martin, Kopka, Benita, Pohl, Martina, Jaeger, Karl-Erich, and Krauss, Ulrich. “Fusion of a Coiled-Coil Domain Facilitates the High-Level Production of Catalytically Active Enzyme Inclusion Bodies”. *ChemCatChem* 8.1 (2016), pp. 142–152.

[110] Kloss, Ramona, Limberg, Michael H., Mackfeld, Ursula, Hahn, Doris, Grünberger, Alexander, Jäger, Vera D., Krauss, Ulrich, Oldiges, Marco, and Pohl, Martina. “Catalytically active inclusion bodies of L-lysine decarboxylase from *E. coli* for 1,5-diaminopentane production”. *Scientific Reports* 8.1 (2018).

[111] Choi, Su Lim, Lee, Sang Jun, Ha, Jae Seok, Song, Jae Jun, Rhee, Young Ha, and Lee, Seung Goo. “Generation of catalytic protein particles in *Escherichia coli* cells using the cellulose-binding domain from *Cellulomonas fimi* as a fusion partner”. *Biotechnology and Bioprocess Engineering* 16.6 (2011), pp. 1173–1179.

[112] Zhou, Bihong, Xing, Lei, Wu, Wei, Zhang, Xian En, and Lin, Zhanglin. “Small surfactant-like peptides can drive soluble proteins into active aggregates”. *Microbial Cell Factories* 11 (2012).

[113] Lin, Zhanglin, Zhou, Bihong, Wu, Wei, Xing, Lei, and Zhao, Qing. “Self-assembling amphipathic alpha-helical peptides induce the formation of active protein aggregates *in vivo*”. *Faraday Discussions* 166 (2013), pp. 243–256.

[114] Wang, Xu, Zhou, Bihong, Hu, Weike, Zhao, Qing, and Lin, Zhanglin. “Formation of active inclusion bodies induced by hydrophobic self-assembling peptide GFIL8”. *Microbial Cell Factories* 14.1 (2015).

[115] García-Fruitós, Elena, González-Montalbán, Nuria, Morell, Montse, Vera, Andrea, Ferraz, Rosa María, Arís, Anna, Ventura, Salvador, and Villaverde, Antonio. “Aggregation as bacterial inclusion bodies does not imply inactivation of enzymes and fluorescent proteins”. *Microbial Cell Factories* 4.27 (2005).

[116] Köszagová, Romana, Krajčovič, Tomas, Palencarova-Talafova, Klaudia, Patoprsty, Vladimir, Vikartovská, Alica, Pospiskova, Kristyna, Safarik, Ivo, and Nahálka, Jozef. “Magnetization of active inclusion bodies: Comparison with centrifugation in repetitive biotransformations”. *Microbial Cell Factories* 17.139 (2018).

[117] Jäger, Vera D., Lamm, Robin, Kloß, Ramona, Kaganovitch, Eugen, Grünberger, Alexander, Pohl, Martina, Büchs, Jochen, Jaeger, Karl-Erich, and Krauss, Ulrich. “A Synthetic Reaction Cascade Implemented by Colocalization of Two Proteins within Catalytically Active Inclusion Bodies”. *ACS Synthetic Biology* 7.9 (2018), pp. 2282–2295.

[118] García-Fruitós, Elena, Vázquez, Esther, Díez-Gil, César, Corchero, José Luis, Seras-Franzoso, Joaquin, Ratera, Imma, Veciana, Jaume, and Villaverde, Antonio. “Bacterial inclusion bodies: Making gold from waste”. *Trends in Biotechnology* 30.2 (2012), pp. 65–70.

[119] Kloss, Ramona, Karmainski, Tobias, Jäger, Vera D., Hahn, Doris, Grünberger, Alexander, Baumgart, Meike, Krauss, Ulrich, Jaeger, Karl-Erich, Wiechert, Wolfgang, and Pohl, Martina. “Tailor-made catalytically active inclusion bodies for different applications in biocatalysis”. *Catalysis Science and Technology* 8.22 (2018), pp. 5816–5826.

[120] Pei, Xiaolin, Wang, Jiapao, Zheng, Haoteng, Xiao, Qinjie, Wang, Anming, and Su, Weike. “Catalytically active inclusion bodies (CatIBs) induced by terminally attached self-assembling coiled-coil domains: To enhance the stability of (*R*)-hydroxynitrile lyase”. *Enzyme and Microbial Technology* 153 (2022).

[121] Murphy, M. Paul and Levine, Harry. “Alzheimer’s disease and the amyloid-β peptide”. *Journal of Alzheimer’s Disease* 19.1 (2010), pp. 311–323.

[122] Nahálka, Jozef and Pätoprstý, Vladimír. “Enzymatic synthesis of sialylation substrates powered by a novel polyphosphate kinase (PPK3)”. *Organic and Biomolecular Chemistry* 7.9 (2009), pp. 1778–1780.

[123] Nahálka, Jozef and Nidetzky, Bernd. “Fusion to a pull-down domain: A novel approach of producing *Trigonopsis variabilis* D-amino acid oxidase as insoluble enzyme aggregates”. *Biotechnology and Bioengineering* 97.3 (2007), pp. 454–461.

[124] Nahálka, Jozef, Vikartovská, Alica, and Hrabárová, Eva. “A crosslinked inclusion body process for sialic acid synthesis”. *Journal of Biotechnology* 134.1-2 (2008), pp. 146–153.

[125] Roca-Pinilla, Ramon, Fortuna, Sara, Natalello, Antonino, Sánchez-Chardi, Alejandro, Ami, Diletta, Arís, Anna, and Garcia-Fruitós, Elena. “Exploring the use of leucine zippers for the generation of a new class of inclusion bodies for pharma and biotechnological applications”. *Microbial Cell Factories* 19.1 (2020).

[126] Hrabárová, Eva, Belkova, Martina, Köszagová, Romana, and Nahálka, Jozef. “Pull-Down Into Active Inclusion Bodies and Their Application in the Detection of (Poly)-Phosphates and Metal-Ions”. *Frontiers in Bioengineering and Biotechnology* 10 (2022).

[127] Dong, Wenge, Sun, Hongxu, Chen, Qiwei, Hou, Liangyu, Chang, Yanhong, and Luo, Hui. “SpyTag/Catcher chemistry induces the formation of active inclusion bodies in *E. coli*”. *International Journal of Biological Macromolecules* 199 (2022), pp. 358–371.

[128] Keeble, Anthony H. and Howarth, Mark. *Insider information on successful covalent protein coupling with help from SpyBank*. Vol. 617. Academic Press Inc., 2019, pp. 443–461.

[129] Maltzahn, Geoffrey Von, Vauthey, Sylvain, Santoso, Steve, and Zhang, Shuguang. “Positively Charged Surfactant-like Peptides Self-assemble into Nanostructures”. *Langmuir* 19 (2003), pp. 4332–4337.

[130] Jumper, John, Evans, Richard, Pritzel, Alexander, Green, Tim, Figurnov, Michael, Ronneberger, Olaf, Tunyasuvunakool, Kathryn, Bates, Russ, Žídek, Augustin, Potapenko, Anna, Bridgland, Alex, Meyer, Clemens, Kohl, Simon A A, Ballard, Andrew J, Cowie, Andrew, Romera-Paredes, Bernardino, Nikolov, Stanislav, Jain, Rishub, Adler, Jonas, Back, Trevor, Petersen, Stig, Reiman, David, Clancy, Ellen, Zielinski, Michal, Steinegger, Martin, Pacholska, Michalina, Berghammer, Tamas, Bodenstein, Sebastian, Silver, David, Vinyals, Oriol, Senior, Andrew W, Kavukcuoglu, Koray, Kohli, Push-

meet, and Hassabis, Demis. “Highly accurate protein structure prediction with AlphaFold”. *Nature* 596.7873 (2021), pp. 583–589.

[131] Smith, Jonathan D. “Apolipoprotein E4: An allele associated with many diseases”. *Annals of Medicine* 32.2 (2000), pp. 118–127.

[132] Jiang, Li, Xiao, Wenjun, Zhou, Xuan, Wang, Weiyu, and Fan, Jun. “Comparative study of the insoluble and soluble Ulp1 protease constructs as Carrier free and dependent protein immobilizates”. *Journal of Bioscience and Bioengineering* 127.1 (2019), pp. 23–29.

[133] Naskar, Jishu, Palui, Goutam, and Banerjee, Arindam. “Tetrapeptide-based hydrogels: For encapsulation and slow release of an anticancer drug at physiological ph”. *Journal of Physical Chemistry B* 113.35 (2009), pp. 11787–11792.

[134] Wu, Wei, Xing, Lei, Zhou, Bihong, and Lin, Zhanglin. “Active protein aggregates induced by terminally attached self-assembling peptide ELK16 in *Escherichia coli*”. *Microbial Cell Factories* 10 (2011).

[135] Zhang, Shuguang, Lockshin, Curtis, Herbert, Alan, Winter’, Edward, and Rich, Alexander. “Zuotin, a putative Z-DNA binding protein in *Saccharomyces cerevisiae*”. *The EMBO Journal* 1.10 (1992), pp. 3787–3796.

[136] Jun, S., Hong, Y., Imamura, H., Ha, B. Y., Bechhoefer, J., and Chen, P. “Self-Assembly of the Ionic Peptide EAK16: The Effect of Charge Distributions on Self-Assembly”. *Biophysical Journal* 87.2 (2004), pp. 1249–1259.

[137] Trabbic-Carlson, K., Meyer, D. E., Liu, L., Piervincenzi, R., Nath, N., LaBean, T., and Chilkoti, A. “Effect of protein fusion on the transition temperature of an environmentally responsive elastin-like polypeptide: A role for surface hydrophobicity?” *Protein Engineering, Design and Selection* 17.1 (2004), pp. 57–66.

[138] Han, Hongmei, Zeng, Weizhu, Zhang, Guoqiang, and Zhou, Jingwen. “Active tyrosine phenol-lyase aggregates induced by terminally attached functional peptides in *Escherichia coli*”. *Journal of Industrial Microbiology and Biotechnology* 47.8 (2020), pp. 563–571.

[139] Xing, Lei, Wu, Wei, Zhou, Bihong, and Lin, Zhanglin. “Streamlined protein expression and purification using cleavable self-aggregating tags”. *Microbial Cell Factories* 10 (2011).

[140] Park, Soo Young, Park, Seung Hwan, and Choi, Soo Keun. “Active inclusion body formation using *Paenibacillus polymyxa* PoxB as a fusion partner in *Escherichia coli*”. *Analytical Biochemistry* 426.1 (2012), pp. 63–65.

[141] Gil-Garcia, Marcos, Navarro, Susanna, and Ventura, Salvador. “Coiled-coil inspired functional inclusion bodies”. *Microbial Cell Factories* 19.1 (2020).

[142] Choi, Su Lim, Lee, Sang Jun, Yeom, Soo Jin, Kim, Hyun Ju, Rhee, Young Ha, Jung, Heung Chae, and Lee, Seung Goo. "Controlled localization of functionally active proteins to inclusion bodies using leucine zippers". *PLoS ONE* 9.6 (2014).

[143] Tripet, Brian, Yu, Lei, Bautista, Daisy L, Wong, Wah Y, Irvin, Randall T, and Hodges, Robert S. "Engineering a *de novo* designed coiled-coil heterodimerization domain for the rapid detection, purification and characterization of recombinantly expressed peptides and proteins". *Protein Eng* 9 (1996), pp. 1029–1042.

[144] Steinmann, Björn, Christmann, Andreas, Heiseler, Tim, Fritz, Janine, and Kolmar, Harald. "*In vivo* enzyme immobilization by inclusion body display". *Applied and Environmental Microbiology* 76.16 (2010), pp. 5563–5569.

[145] Spieler, Valerie, Valldorf, Bernhard, Maaß, Franziska, Kleinschek, Alexander, Hüttenhain, Stefan H., and Kolmar, Harald. "Coupled reactions on bioparticles: Stereoselective reduction with cofactor regeneration on PhaC inclusion bodies". *Biotechnology Journal* 11.7 (2016), pp. 890–898.

[146] Grage, Katrin, Jahns, Anika C., Parlane, Natalie, Palanisamy, Rajasekaran, Rasiah, Indira A., Atwood, Jane A., and Rehm, Bernd H.A. "Bacterial polyhydroxyalkanoate granules: Biogenesis, structure, and potential use as nano-/micro-beads in biotechnological and biomedical applications". *Biomacromolecules* 10.4 (2009), pp. 660–669.

[147] Peters, Verena and Rehm, Bernd H.A. "*in vivo* monitoring of PHA granule formation using GFP-labeled PHA synthases". *FEMS Microbiology Letters* 248.1 (2005), pp. 93–100.

[148] Du, Jinping and Rehm, Bernd H.A. "Purification of target proteins from intracellular inclusions mediated by intein cleavable polyhydroxyalkanoate synthase fusions". *Microbial Cell Factories* 16.1 (2017).

[149] Lee, Jae Hyung, Nam, Dong Heon, Lee, Sahng Ha, Park, Jong Hyun, Park, Si Jae, Lee, Seung Hwan, Park, Chan Beum, and Jeong, Ki Jun. "New platform for cytochrome P450 reaction combining *in situ* immobilization on biopolymer". *Bioconjugate Chemistry* 25.12 (2014), pp. 2101–2104.

[150] Moldes, Cristina, García, Pedro, García, José L., and Prieto, María A. "*In vivo* immobilization of fusion proteins on bioplastics by the novel tag BioF". *Applied and Environmental Microbiology* 70.6 (2004), pp. 3205–3212.

[151] Seo, Hyung Min, Kim, Jung Ho, Jeon, Jong Min, Song, Hun Suk, Bhatia, Shashi Kant, Sathiyanarayanan, Ganesan, Park, Kyungmoon, Kim, Kwang Jin, Lee, Sang Hyun, Kim, Hyung Joo, and Yang, Yung Hun. "*In situ* immobilization of lysine de-

carboxylase on a biopolymer by fusion with phasin: Immobilization of CadA on intracellular PHA". *Process Biochemistry* 51.10 (2016), pp. 1413–1419.

[152] Noll, Gundula A., Müller, Boje, Ernst, Antonia M., Rüping, Boris, Twyman, Richard M., and Prüfer, Dirk. "Native and artificial forisomes: Functions and applications". *Applied Microbiology and Biotechnology* 89.6 (2011), pp. 1675–1682.

[153] Visser, Franziska, Müller, Boje, Rose, Judith, Prüfer, Dirk, and Noll, Gundula A. "Forizymes-functionalised artificial forisomes as a platform for the production and immobilisation of single enzymes and multi-enzyme complexes". *Scientific Reports* 6 (2016).

[154] Nair, Manoj S., Lee, Marianne M., Bonnegarde-Bernard, Astrid, Wallace, Julie A., Dean, Donald H., Ostrowski, Michael C., Burry, Richard W., Boyaka, Prosper N., and Chan, Michael K. "Cry protein crystals: A novel platform for protein delivery". *PLoS ONE* 10.6 (2015).

[155] Heater, Bradley S., Chan, Wai Shan, Lee, Marianne M., and Chan, Michael K. "Directed evolution of a genetically encoded immobilized lipase for the efficient production of biodiesel from waste cooking oil". *Biotechnology for Biofuels* 12.1 (2019).

[156] Heater, Bradley S., Lee, Marianne M., and Chan, Michael K. "Direct production of a genetically-encoded immobilized biodiesel catalyst". *Scientific Reports* 8.1 (2018).

[157] Sun, Qian, Heater, Bradley S., Li, Tin Lok, Ye, Weijian, Guo, Zhihong, and Chan, Michael K. "Cry3Aa*SpyCatcher Fusion Crystals Produced in Bacteria as Scaffolds for Multienzyme Coimmobilization". *Bioconjugate Chemistry* 33.2 (2022), pp. 386–396.

[158] McCoy, Kimberly and Douglas, Trevor. *In vivo packaging of protein cargo inside of virus-like particle P22*. Vol. 1776. Humana Press Inc., 2018, pp. 295–302.

[159] Patterson, Dustin P., Schwarz, Benjamin, Waters, Ryan S., Gedeon, Tomas, and Douglas, Trevor. "Encapsulation of an enzyme cascade within the bacteriophage P22 virus-like particle". *ACS Chemical Biology* 9.2 (2014), pp. 359–365.

[160] Li, Pilong, Banjade, Sudeep, Cheng, Hui Chun, Kim, Soyeon, Chen, Baoyu, Guo, Liang, Llaguno, Marc, Hollingsworth, Javoris V., King, David S., Banani, Salman F., Russo, Paul S., Jiang, Qiu Xing, Nixon, B. Tracy, and Rosen, Michael K. "Phase transitions in the assembly of multivalent signalling proteins". *Nature* 483.7389 (2012), pp. 336–340.

[161] Wei, Shao Peng, Qian, Zhi Gang, Hu, Chun Fei, Pan, Fang, Chen, Meng Ting, Lee, Sang Yup, and Xia, Xiao Xia. "Formation and functionalization of membraneless

compartments in *Escherichia coli*". *Nature Chemical Biology* 16.10 (2020), pp. 1143–1148.

[162] He, Didi and Marles-Wright, Jon. "Ferritin family proteins and their use in bionanotechnology". *New Biotechnology* 32.6 (2015), pp. 651–657.

[163] Ford, G. C., Harrison, P. M., Rice, D. W., Smith, J. M., Treffry, A., White, J. L., and Yariv, J. "Ferritin: design and formation of an iron-storage molecule." *Philosophical transactions of the Royal Society of London. Biological sciences* 304.1121 (1984), pp. 551–565.

[164] Andrews, Simon C., Robinson, Andrea K., and Rodríguez-Quiñones, Francisco. "Bacterial iron homeostasis". *FEMS Microbiology Reviews* 27.2-3 (2003), pp. 215–237.

[165] Arosio, Paolo and Levi, Sonia. "Cytosolic and mitochondrial ferritins in the regulation of cellular iron homeostasis and oxidative damage". *Biochimica et Biophysica Acta - General Subjects* 1800.8 (2010), pp. 783–792.

[166] Yoshimura, Hideyuki. "Protein-assisted nanoparticle synthesis". *Colloids and Surfaces A: Physicochemical and Engineering Aspects* 282-283 (2006), pp. 464–470.

[167] Crichton, Robert R. and Declercq, Jean Paul. "X-ray structures of ferritins and related proteins". *Biochimica et Biophysica Acta - General Subjects* 1800.8 (2010), pp. 706–718.

[168] Bradley, Justin M., Moore, Geoffrey R., and Brun, Nick E. Le. "Diversity of Fe2+ entry and oxidation in ferritins". *Current Opinion in Chemical Biology* 37 (2017), pp. 122–128.

[169] Pourciau, Christine, Pannuri, Archana, Potts, Anastasia, Yakhnin, Helen, Babitzke, Paul, and Romeo, Tony. "Regulation of Iron Storage by CsrA Supports Exponential Growth of *Escherichia coli*". *ASM Journals* 10.4 (2019).

[170] Abdul-tehrani, Hossein, Hudson, Aaron J, Chang, Yung sheng, Timms, Andrew R, Hawkins, Chris, Williams, John M, Harrison, Pauline M, Guest, John R, and Andrews, Simon C. "Ferritin Mutants of *Escherichia coli* Are Iron Deficient and Growth Impaired, and fur Mutants are Iron Deficient". *Journal of Bacteriology* 181.5 (1999), pp. 1415–1428.

[171] Bolaji, Naimah. "Characterization of the SUF FE-S Pathway In *Escherichia coli*". University of South Carolina, 2017.

[172] Velayudhan, Jyoti, Castor, Margaret, Richardson, Anthony, Main-Hester, Kara L., and Fang, Ferric C. "The role of ferritins in the physiology of *Salmonella enterica* sv. Typhimurium: A unique role for ferritin B in iron-sulphur cluster repair and virulence". *Molecular Microbiology* 63.5 (2007), pp. 1495–1507.

[173] Yao, Huili, Soldano, Anabel, Fontenot, Leo, Donnarumma, Fabrizio, Lovell, Scott, Chandler, Josephine R., and Rivera, Mario. "*Pseudomonas aeruginosa* Bacterioferritin Is Assembled from FtnA and BfrB Subunits with the Relative Proportions Dependent on the Environmental Oxygen Availability". *Biomolecules* 12.3 (2022), p. 366.

[174] Mohanty, Abhinav, Parida, Akankshika, Raut, Rohit Kumar, and Behera, Rabindra K. "Ferritin: A Promising Nanoreactor and Nanocarrier for Bionanotechnology". *ACS Bio & Med Chem Au* (2022).

[175] Jutz, Günther, Rijn, Patrick Van, Miranda, Barbara Santos, and Böker, Alexander. "Ferritin: A versatile building block for bionanotechnology". *Chemical Reviews* 115.4 (2015), pp. 1653–1701.

[176] Zang, Jiachen, Zheng, Bowen, Zhang, Xiuqing, Arosio, Paolo, and Zhao, Guanghua. "Design and site-directed compartmentalization of gold nanoclusters within the intrasubunit interfaces of ferritin nanocage". *Journal of Nanobiotechnology* 17.1 (2019).

[177] Yamashita, Ichiro, Iwahori, Kenji, and Kumagai, Shinya. "Ferritin in the field of nanodevices". *Biochimica et Biophysica Acta - General Subjects* 1800.8 (2010), pp. 846–857.

[178] Kanekiyo, Masaru, Wei, Chih Jen, Yassine, Hadi M., McTamney, Patrick M., Boyington, Jeffrey C., Whittle, James R.R., Rao, Srinivas S., Kong, Wing Pui, Wang, Lingshu, and Nabel, Gary J. "Self-assembling influenza nanoparticle vaccines elicit broadly neutralizing H1N1 antibodies". *Nature* 499.7456 (2013), pp. 102–106.

[179] Tetter, Stephan and Hilvert, Donald. "Enzyme Encapsulation by a Ferritin Cage". *Angewandte Chemie* 129.47 (2017), pp. 15129–15132.

[180] Zhang, Yu, Dong, Yixin, Zhou, Jinhua, Hu, Ying'Ao, Li, Xun, and Wang, Fei. "Peptide-mediated immobilization on magnetoferritin for enzyme recycling". *Nanomaterials* 9.11 (2019).

[181] Bellapadrona, Giuliano and Elbaum, Michael. "Supramolecular protein assemblies in the nucleus of human cells". *Angewandte Chemie - International Edition* 53.6 (2014), pp. 1534–1537.

[182] Bellapadrona, Giuliano, Sinkar, Shwetali, Sabanay, Helena, Liljeström, Ville, Kostiainen, Mauri, and Elbaum, Michael. "Supramolecular assembly and coalescence of ferritin cages driven by designed protein-protein interactions". *Biomacromolecules* 16.7 (2015), pp. 2006–2011.

[183] Xue, Le, Deng, Dawei, and Sun, Jianfei. “Magnetoferritin: Process, prospects, and their biomedical applications”. *International Journal of Molecular Sciences* 20.10 (2019).

[184] Ölçücü, Gizem, Baumer, Benedikt, Küsters, Kira, Möllenhoff, Kathrin, Oldiges, Marco, Pietruszka, Jörg, Jaeger, Karl-Erich, and Krauss, Ulrich. “Catalytically Active Inclusion Bodies-Benchmarking and Application in Flow Chemistry”. *ACS Synthetic Biology* (2022), pp. 1881–1896.

[185] Küsters, Kira, Pohl, Martina, Krauss, Ulrich, Ölçücü, Gizem, Albert, Sandor, Jaeger, Karl-Erich, Wiechert, Wolfgang, and Oldiges, Marco. “Construction and comprehensive characterization of an EcLDCc-CatIB set—varying linkers and aggregation inducing tags”. *Microbial Cell Factories* 20.1 (2021).

[186] Ölçücü, Gizem, Jaeger, Karl-Erich, and Krauss, Ulrich. *Design, Production, and Characterization of Catalytically Active Inclusion Bodies*. Ed. by Julian Kopp and Oliver Spadiut. Vol. 2617. Springer US, 2023, pp. 49–74.

[187] Ölçücü, Gizem, Krauss, Ulrich, Jaeger, Karl-Erich, and Pietruszka, Jörg. “Carrier-Free Enzyme Immobilizates for Flow Chemistry”. *Chemie-Ingenieur-Technik* 95 (2023), pp. 531–542.

[188] Berman, Helen M., Westbrook, John, Feng, Zukang, Gilliland, Gary, Bhat, T. N., Weissig, Helge, Shindyalov, Ilya N., and Bourne, Philip E. “The Protein Data Bank”. *Nucleic Acids Research* 28.1 (2000).

[189] Schrödinger, LLC and DeLano, Warren. *PyMOL*. Version 2.4.0. 2020.

[190] Dey, Sucharita and Levy, Emmanuel D. *Inferring and using protein quaternary structure information from crystallographic data*. Vol. 1764. Humana Press Inc., 2018, pp. 357–375.

[191] Krissinel, Evgeny and Henrick, Kim. “Inference of Macromolecular Assemblies from Crystalline State”. *Journal of Molecular Biology* 372.3 (2007), pp. 774–797.

[192] Conchillo-Solé, Oscar, Groot, Natalia S. de, Avilés, Francesc X., Vendrell, Josep, Daura, Xavier, and Ventura, Salvador. “AGGRESCAN: A server for the prediction and evaluation of "hot spots" of aggregation in polypeptides”. *BMC Bioinformatics* 8 (2007).

[193] Fernandez-Escamilla, Ana Maria, Rousseau, Frederic, Schymkowitz, Joost, and Serrano, Luis. “Prediction of sequence-dependent and mutational effects on the aggregation of peptides and proteins”. *Nature Biotechnology* 22.10 (2004), pp. 1302–1306.

[194] Jones, David T. “Protein secondary structure prediction based on position-specific scoring matrices”. *Journal of Molecular Biology* 292.2 (1999), pp. 195–202.

[195] Buchan, Daniel W. A. and Jones, David T. “The PSIPRED Protein Analysis Workbench: 20 years on”. *Nucleic Acids Research* 47.W1 (2019), pp. 402–407.

[196] Garnier, J., Osguthorpe, D. J., and Robson, B. “Analysis of the accuracy and implications of simple methods for predicting the secondary structure of globular proteins”. *Journal of Molecular Biology* 120.1 (1978), pp. 97–120.

[197] Berrow, Nick S., Alderton, David, and Owens, Raymond J. *Methods in Molecular Biology: High Throughput Protein Expression and Purification*. Ed. by Sharon A. Doyle. Vol. 498. Humana Press, 2009.

[198] Park, Jaehong, Throop, Andrea L., and LaBaer, Joshua. “Site-specific recombinational cloning using gateway and in-fusion cloning schemes”. *Current Protocols in Molecular Biology* 2015 (2015), pp. 3201–3223.

[199] Engler, Carola, Kandzia, Romy, and Marillonnet, Sylvestre. “A one pot, one step, precision cloning method with high throughput capability”. *PLoS ONE* 3.11 (2008).

[200] Shuman, S. “Novel approach to molecular cloning and polynucleotide synthesis using vaccinia DNA topoisomerase.” *Journal of Biological Chemistry* 269.51 (1994), pp. 32678–32684.

[201] Klock, Heath E., White, Aprilfawn, Koesema, Eric, and Lesley, Scott A. “Methods and results for semi-automated cloning using integrated robotics”. *Journal of Structural and Functional Genomics* 6.2-3 (2005), pp. 89–94.

[202] Olieric, Natacha, Kuchen, Melanie, Wagen, Sandro, Sauter, Marion, Crone, Stephanie, Edmondson, Sonia, Frey, Daniel, Ostermeier, Christian, Steinmetz, Michel O, and Jaussi, Rolf. “Automated seamless DNA co-transformation cloning with direct expression vectors applying positive or negative insert selection”. *BMC Biotechnology* 10.56 (2010).

[203] Dao-Thi, Minh Hoa, Melderen, Laurence Van, Genst, Erwin De, Buts, Lieven, Ranquin, An, Wyns, Lode, and Loris, Remy. “Crystallization of CcdB in complex with a GyrA fragment”. *Acta Crystallographica Section D: Biological Crystallography* 60.6 (2004), pp. 1132–1134.

[204] Küsters, Kira, Saborowski, Ronja, Wagner, Christian, Hamel, Rebecca, Spöring, Jan-Dirk, Wiechert, Wolfgang, and Oldiges, Marco. “Construction and characterization of BsGDH-CatIB variants and application as robust and highly active redox cofactor regeneration module for biocatalysis”. *Microbial Cell Factories* 21.1 (2022).

[205] Lamm, Robin, Jäger, Vera D., Heyman, Benedikt, Berg, Christoph, Cürten, Christin, Krauss, Ulrich, Jaeger, Karl-Erich, and Büchs, Jochen. “Detailed small-scale characterization and scale-up of active YFP inclusion body production with *Escherichia*

coli induced by a tetrameric coiled coil domain". *Journal of Bioscience and Bioengineering* 129.6 (2020), pp. 730–740.

[206] Doglia, Silvia Maria, Ami, Diletta, Natalello, Antonino, Gatti-Lafranconi, Pietro, and Lotti, Marina. "Fourier transform infrared spectroscopy analysis of the conformational quality of recombinant proteins within inclusion bodies". *Biotechnology Journal* 3.2 (2008), pp. 193–201.

[207] Groot, Natalia Sánchez de and Ventura, Salvador. "Effect of temperature on protein quality in bacterial inclusion bodies". *FEBS Letters* 580.27 (2006), pp. 6471–6476.

[208] Rueda, Fabián, Gasser, Brigitte, Sánchez-Chardi, Alejandro, Roldán, Mònica, Villegas, Sandra, Puxbaum, Verena, Ferrer-Miralles, Neus, Unzueta, Ugutz, Vázquez, Esther, Garcia-Fruitós, Elena, Mattanovich, Diethard, and Villaverde, Antonio. "Functional inclusion bodies produced in the yeast *Pichia pastoris*". *Microbial Cell Factories* 15.1 (2016).

[209] Bradford, Marion M. "A rapid and sensitive method for the quantitation of microgram quantities of protein utilizing the principle of protein-dye binding". *Analytical Biochemistry* 72.1-2 (1976), pp. 248–254.

[210] Jansen, Roman, Küsters, Kira, Morschett, Holger, Wiechert, Wolfgang, and Oldiges, Marco. "A fully automated pipeline for the dynamic at-line morphology analysis of microscale *Aspergillus* cultivation". *Fungal Biology and Biotechnology* 8.1 (2021).

[211] Heater, Bradley S., Yang, Zaofeng, Lee, Marianne M., and Chan, Michael K. "*in vivo* Enzyme Entrapment in a Protein Crystal". *Journal of the American Chemical Society* 142.22 (2020), pp. 9879–9883.

[212] Jahns, Anika C. and Rehm, Bernd H. A. "Immobilization of active lipase B from *Candida antarctica* on the surface of polyhydroxyalkanoate inclusions". *Biotechnology Letters* 37.4 (2015), pp. 831–835.

[213] Schoonen, Lise, Nolte, Roeland J.M., and Hest, Jan C.M. Van. "Highly efficient enzyme encapsulation in a protein nanocage: Towards enzyme catalysis in a cellular nanocompartment mimic". *Nanoscale* 8.30 (2016), pp. 14467–14472.

[214] Minten, Inge J., Claessen, Victor I., Blank, Kerstin, Rowan, Alan E., Nolte, Roeland J.M., and Cornelissen, Jeroen J.L.M. "Catalytic capsids: The art of confinement". *Chemical Science* 2.2 (2011), pp. 358–362.

[215] Bustos-Jaimes, Ismael, Soto-Román, Ricardo Arturo, Gutiérrez-Landa, Isabel Alejandra, Valadez-García, Josefina, and Segovia-Trinidad, Carla Lizbeth. "Construction of protein-functionalized virus-like particles of parvovirus B19". *Journal of Biotechnology* 263 (2017), pp. 55–63.

[216] Patterson, Dustin P., Prevelige, Peter E., and Douglas, Trevor. “Nanoreactors by programmed enzyme encapsulation inside the capsid of the bacteriophage P22”. *ACS Nano* 6.6 (2012), pp. 5000–5009.

[217] Uchida, Masaki, McCoy, Kimberly, Fukuto, Masafumi, Yang, Lin, Yoshimura, Hideyuki, Miettinen, Heini M., LaFrance, Ben, Patterson, Dustin P., Schwarz, Benjamin, Karty, Jonathan A., Prevelige, Peter E., Lee, Byeongdu, and Douglas, Trevor. “Modular Self-Assembly of Protein Cage Lattices for Multistep Catalysis”. *ACS Nano* 12.2 (2018), pp. 942–953.

[218] Jäger, Vera D., Piqueray, Maja, Seide, Selina, Pohl, Martina, Wiechert, Wolfgang, Jaeger, Karl-Erich, and Krauss, Ulrich. “An Enzymatic 2-Step Cofactor and Co-Product Recycling Cascade towards a Chiral 1,2-Diol. Part II: Catalytically Active Inclusion Bodies”. *Advanced Synthesis and Catalysis* 361.11 (2019), pp. 2616–2626.

[219] Nakamura, Hideki, Lee, Albert A., Afshar, Ali Sobhi, Watanabe, Shigeki, Rho, Elmer, Razavi, Shiva, Suarez, Allister, Lin, Yu Chun, Tanigawa, Makoto, Huang, Brian, DeRose, Robert, Bobb, Diana, Hong, William, Gabelli, Sandra B., Goutsias, John, and Inoue, Takanari. “Intracellular production of hydrogels and synthetic RNA granules by multivalent molecular interactions”. *Nature Materials* 17.1 (2018), pp. 79–88.

[220] Shin, Yongdae, Berry, Joel, Pannucci, Nicole, Haataja, Mikko P., Toettcher, Jared E., and Brangwynne, Clifford P. “Spatiotemporal Control of Intracellular Phase Transitions Using Light-Activated optoDroplets”. *Cell* 168.1-2 (2017), pp. 159–171.

[221] Dall’oglio, Federica, Contente, Martina Letizia, Conti, Paola, Molinari, Francesco, Monfredi, Danila, Pinto, Andrea, Romano, Diego, Ubiali, Daniela, Tamborini, Lucia, and Serra, Immacolata. “Flow-based stereoselective reduction of ketones using an immobilized ketoreductase/glucose dehydrogenase mixed bed system”. *Catalysis Communications* 93 (2017), pp. 29–32.

[222] Benítez-Mateos, Ana I., Sebastian, Eneko San, Ríos-Lombardía, Nicolás, Morís, Francisco, González-Sabín, Javier, and López-Gallego, Fernando. “Asymmetric Reduction of Prochiral Ketones by Using Self-Sufficient Heterogeneous Biocatalysts Based on NADPH-Dependent Ketoreductases”. *Chemistry - A European Journal* 23.66 (2017), pp. 16843–16852.

[223] Helm, Michelle P. Van Der, Bracco, Paula, Busch, Hanna, Szymańska, Katarzyna, Jarzbski, Andrzej B., and Hanefeld, Ulf. “Hydroxynitrile lyases covalently immo-

bilized in continuous flow microreactors". *Catalysis Science and Technology* 9.5 (2019), pp. 1189–1200.

[224] Peris, Edgar, Okafor, Obinna, Kulcinskaja, Evelina, Goodridge, Ruth, Luis, Santiago V, Garcia-Verdugo, Eduardo, O'Reilly, Elaine, and Sans, Victor. "Tuneable 3D printed bioreactors for transaminations under continuous-flow". *Green Chemistry* 19.22 (2017), pp. 5345–5349.

[225] Poznansky, Barnabas, Thompson, Lisa A, Warren, Sarah A, Reeve, Holly A, and Vincent, Kylie A. "Carbon as a Simple Support for Redox Biocatalysis in Continuous Flow". *Organic Process Research and Development* 24.10 (2020), pp. 2281–2287.

[226] Zor, Ceren, Reeve, Holly A., Quinson, Jonathan, Thompson, Lisa A., Lonsdale, Thomas H., Dillon, Frank, Grobert, Nicole, and Vincent, Kylie A. "H2-Driven biocatalytic hydrogenation in continuous flow using enzyme-modified carbon nanotube columns". *Chemical Communications* 53.71 (2017), pp. 9839–9841.

[227] Bajić, Marijan, Plazl, Igor, Stloukal, Radek, and Plazl, Polona Žnidaršič. "Development of a miniaturized packed bed reactor with ω-transaminase immobilized in LentiKats®". *Process Biochemistry* 52 (2017), pp. 63–72.

[228] Alotaibi, Mohammed, Manayil, Jinesh C, Greenway, Gillian M, Haswell, Stephen J, Kelly, Stephen M, Lee, Adam F, Wilson, Karen, and Kyriakou, Georgios. "Lipase immobilised on silica monoliths as continuous-flow microreactors for triglyceride transesterification". *Reaction Chemistry and Engineering* 3.1 (2018), pp. 68–74.

[229] Tentori, Francesca, Brenna, Elisabetta, Crotti, Michele, Pedrocchi-fantoni, Giuseppe, Ghezzi, Maria Chiara, and Tessaro, Davide. "Continuous-flow biocatalytic process for the synthesis of the best stereoisomers of the commercial fragrances leather cyclohexanol (4-isopropylcyclohexanol) and woody acetate (4-(tert-butyl) cyclohexyl acetate)". *Catalysts* 10.1 (2020).

[230] Böhmer, Wesley, Volkov, Alexey, Cassimjee, Karim Engelmark, and Mutti, Francesco G. "Continuous Flow Bioamination of Ketones in Organic Solvents at Controlled Water Activity using Immobilized ω-Transaminases". *Advanced Synthesis and Catalysis* (2020).

[231] Bitterwolf, Patrick, Gallus, Sabrina, Peschke, Theo, Mittmann, Esther, Oelschlaeger, Claude, Willenbacher, Norbert, Rabe, Kersten S, and Niemeyer, Christof M. "Valency engineering of monomeric enzymes for self-assembling biocatalytic hydrogels". *Chemical Science* 10.42 (2019), pp. 9752–9757.

[232] Mangas-Sanchez, Juan, Sharma, Mahima, Cosgrove, Sebastian C, Ramsden, Jeremy I, Marshall, James R, Thorpe, Thomas W, Palmer, Ryan B, Grogan, Gideon, and

Turner, Nicholas J. “Asymmetric synthesis of primary amines catalyzed by thermotolerant fungal reductive aminases”. *Chemical Science* 11.19 (2020), pp. 5052–5057.

[233] Peschke, Theo, Skoupi, Marc, Burgahn, Teresa, Gallus, Sabrina, Ahmed, Ishtiaq, Rabe, Kersten S, and Niemeyer, Christof M. “Self-Immobilizing Fusion Enzymes for Compartmentalized Biocatalysis”. *ACS Catalysis* 7.11 (2017), pp. 7866–7872.

[234] Döbber, J, Gerlach, T, Offermann, H, Rother, D, and Pohl, M. “Closing the gap for efficient immobilization of biocatalysts in continuous processes: HaloTag™ fusion enzymes for a continuous enzymatic cascade towards a vicinal chiral diol”. *Green Chemistry* 20.2 (2018), pp. 544–552.

[235] Döbber, J., Pohl, M., Ley, S. V., and Musio, B. “Rapid, selective and stable HaloTag-Lb ADH immobilization directly from crude cell extract for the continuous biocatalytic production of chiral alcohols and epoxides”. *Reaction Chemistry and Engineering* 3.1 (2018), pp. 8–12.

[236] Baumer, Benedikt, Classen, Thomas, Pohl, Martina, and Pietruszka, Jörg. “Efficient Nicotinamide Adenine Dinucleotide Phosphate [NADP(H)] Recycling in Closed-Loop Continuous Flow Biocatalysis”. *Advanced Synthesis and Catalysis* 362.14 (2020), pp. 2894–2901.

[237] Santis, Piera De, Meyer, Lars Erik, and Kara, Selin. “The rise of continuous flow biocatalysis-fundamentals, very recent developments and future perspectives”. *Reaction Chemistry and Engineering* 5.12 (2020), pp. 2155–2184.

[238] Thompson, Matthew P., Peñafiel, Itziar, Cosgrove, Sebastian C., and Turner, Nicholas J. “Biocatalysis Using Immobilized Enzymes in Continuous Flow for the Synthesis of Fine Chemicals”. *Organic Process Research and Development* 23.1 (2019), pp. 9–18.

[239] Planchestainer, Matteo, Contente, Martina Letizia, Cassidy, Jennifer, Molinari, Francesco, Tamborini, Lucia, and Paradisi, Francesca. “Continuous flow biocatalysis: production and in-line purification of amines by immobilised transaminase from *Halomonas elongata*”. *Green Chemistry* 19.2 (2017), pp. 372–375.

[240] Liu, Xueliang, Lopez, Paola A., Giessen, Tobias W., Giles, Michael, Way, Jeffrey C., and Silver, Pamela A. “Engineering Genetically-Encoded Mineralization and Magnetism via Directed Evolution”. *Scientific Reports* 6 (2016).

[241] Keeble, A. H., Banerjee, A., Ferla, M. P., Reddington, S. C., Anuar, Inak, and Howarth, M. “Evolving Accelerated Amidation by SpyTag/SpyCatcher to Analyze Membrane Dynamics”. *Angewandte Chemie - International Edition* 56.52 (2017), pp. 16521–16525.

[242] Xue, Le, Deng, Dawei, and Sun, Jianfei. “Magnetoferritin: Process, prospects, and their biomedical applications”. *International Journal of Molecular Sciences* 20.10 (2019).

[243] Cai, Yao, Huang, Jinjin, Xu, Huangtao, Zhang, Tongwei, Cao, Changqian, and Pan, Yongxin. “Synthesis, characterization and application of magnetoferritin nanoparticle by using human H chain ferritin expressed by *Pichia pastoris*”. *Nanotechnology* 31.48 (2020).

[244] Si, Meng, Xu, Qing, Jiang, Ling, and Huang, He. “Spytag/spycatcher cyclization enhances the thermostability of firefly luciferase”. *PLoS ONE* 11.9 (2016).

[245] Wang, Yida, Tian, Junwei, Xiao, Ying, Wang, Yue, Sun, Hongxu, Chang, Yanhong, and Luo, Hui. “SpyTag/SpyCatcher cyclization enhances the thermostability and organic solvent tolerance of L-phenylalanine aldolase”. *Biotechnology Letters* 41.8-9 (2019), pp. 987–994.

[246] Lau, Cheryl K.Y., Krewulak, Karla D., and Vogel, Hans J. “Bacterial ferrous iron transport: The Feo system”. *FEMS Microbiology Reviews* 40.2 (2016), pp. 273–298.

[247] Hantke, Klaus. “Ferrous iron transport mutants in *Escherichia coli* K12”. *FEMS Microbiology Letters* 44.1 (1987), pp. 53–57.

[248] Kim, Seong Eun, Ahn, Keum Young, Park, Jin Seung, Kim, Kyung Rim, Lee, Kyung Eun, Han, Sung Sik, and Lee, Jeewon. “Fluorescent ferritin nanoparticles and application to the aptamer sensor”. *Analytical Chemistry* 83.15 (2011), pp. 5834–5843.

[249] Luzzago, A. and Cesareni, G. “Isolation of point mutations that affect the folding of the H chain of human ferritin in *E. coli*”. *The EMBO Journal* 8.2 (1989), pp. 569–576.

[250] Wei, Shao Peng, Qian, Zhi Gang, Hu, Chun Fei, Pan, Fang, Chen, Meng Ting, Lee, Sang Yup, and Xia, Xiao Xia. “Formation and functionalization of membraneless compartments in *Escherichia coli*”. *Nature Chemical Biology* 16.10 (2020), pp. 1143–1148.

[251] Gil-Garcia, Marcos and Ventura, Salvador. “Multifunctional antibody-conjugated coiled-coil protein nanoparticles for selective cell targeting”. *Acta Biomaterialia* 131 (2021), pp. 472–482.

[252] Truffi, Marta, Fiandra, Luisa, Sorrentino, Luca, Monieri, Matteo, Corsi, Fabio, and Mazzucchelli, Serena. “Ferritin nanocages: A biological platform for drug delivery, imaging and theranostics in cancer”. *Pharmacological Research* 107 (2016), pp. 57–65.

[253] Webb, Colin, Kang, Hong Ku, Moffat, Gillian, Williams, Richard A., Estévez, Angel M., Cuéllar, Jorge, Jaraiz, Eladio, and Galan, Miguel Angel. "The magnetically stabilized fluidized bed bioreactor: a tool for improved mass transfer in immobilized enzyme systems?" *The Chemical Engineering Journal and the Biochemical Engineering Journal* 61.3 (1996), pp. 241–246.

[254] Sheldon, Roger A. and Pereira, Pedro C. "Biocatalysis engineering: The big picture". *Chemical Society Reviews* 46.10 (2017), pp. 2678–2691.

[255] Zhou, Gui Xiong, Chen, Guan Yi, and Yan, Bei Bei. "Biodiesel production in a magnetically-stabilized, fluidized bed reactor with an immobilized lipase in magnetic chitosan microspheres". *Biotechnology Letters* 36.1 (2014), pp. 63–68.

[256] Wang, Feng, Hu, Yiru, Guo, Chen, Huang, Wei, and Liu, Chun Zhao. "Enhanced phenol degradation in coking wastewater by immobilized laccase on magnetic mesoporous silica nanoparticles in a magnetically stabilized fluidized bed". *Bioresource Technology* 110 (2012), pp. 120–124.

[257] Liu, Chun Zhao, Wang, Feng, and Ou-Yang, Fan. "Ethanol fermentation in a magnetically fluidized bed reactor with immobilized *Saccharomyces cerevisiae* in magnetic particles". *Bioresource Technology* 100.2 (2009), pp. 878–882.

[258] Jussen, Daniel, Soltner, Helmut, Stute, Birgit, Wiechert, Wolfgang, Lieres, Eric von, and Pohl, Martina. "µMORE: A microfluidic magnetic oscillation reactor for accelerated parameter optimization in biocatalysis". *Journal of Biotechnology* 231 (2016), pp. 174–182.

VIII. Acknowledgments

First and foremost, I would like to thank my supervisor Prof. Karl-Erich Jaeger for giving me the opportunity to pursue my PhD in IMET, as well as for providing me with an engaging topic to work on.

I would like to offer my thanks to Prof. Martina Pohl for her readily acceptance for being my co-supervisor, and the helpful course she offered in my first year, which served as a great knowledge refresher and made me see the common lab equipment that one does not think about often in a completely new light.

I would like to offer my sincerest gratitude to my daily supervisor Dr. Ulrich Krauss, who welcomed me into his team, initiating my PhD journey. I am grateful for his kind demeanor, calm attitude, and bright ideas. He showed me that group meetings can be a relaxed and fun environment, made working in IMET an enjoyable experience, and made the roadblocks I encountered along the course of my PhD much more tolerable. I am thankful for his support and gentle push toward new collaborations and projects, which allowed me to play around with a variety of ideas and gain invaluable experience along the way.

I would also like to thank the members of our working group, especially Esther Knieps-Grünhagen and Maja Piqueray, for creating a fun lab environment and for their eager assistance at all times.

I would like to thank my collaboration partners, especially to fellow PhDs Kira Küsters, Benedikt Baumer and Bastian Wollenhaupt, to whom working together was an enjoyable experience and whose efforts led to interesting insights.

I would also like to thank all my friends who supported me in the course of this PhD and beyond. A special thanks goes to Vera D. Jäger, who showed me the ropes when I first came to the institute, and who I am truly happy to call my friend. It was super fun to work with her, and from our numerous dates and countless 'just one cigarette's to everything in between, her presence made IMET brighter. She also made my job a lot easier in convincing people that "CatIBs are awesome!"

I am grateful to Annika Vaksmaa for her friendship and support which helped me immensely across more than just one PhD, and whose undying passion for her field serves as a great source of inspiration to me.

A special thanks goes to my dear friend Buşra Başaran, who stood by me with her ever cheerful demeanor as we cruised through life, always in parallel but never quite in the same place, for all these years.

I would like to offer my biggest thanks to my family for their continuous support. A very special thanks goes to my love, my fiancé, Daniel Niesel. I am very lucky to have this incredibly warm, gentle, brilliant person that he is in my life. I am forever thankful to him for averting the crises during the crazy time that was my PhD, and always reassuring and guiding me along my path. I know that it was his continuous support that kept me sane, and I also know, I can just call him Daniel ;)

I am thankful to my guardian angel Canan Cenk, for always being there for me and putting a smile on my face when I'm down, and making my smile even wider when all is well.

I am grateful to my grandmother, who initiated my journey as a lifelong student, and who is no doubt one of the biggest reasons to why I pursued higher education in the first place.

Last but not least, I am sincerely grateful to my parents for their support and unwavering belief in my success no matter what I do. I thank my father for always cheering me on and being ever so proud of me, and my mother for being the coolest role model a girl could imagine, as well as being a friend to me. Their trust in me has always been a strong motivator in all my pursuits; everywhere they have already led, and wherever they may still lead.

– THE END –

IX. Declaration

I declare under oath that I have produced my thesis independently and without any undue assistance by third parties under consideration of the 'Principles for the Safeguarding of Good Scientific Practice at Heinrich Heine University Düsseldorf'. I hereby declare that I have not submitted this dissertation to any other institution and that I do not hold another doctoral degree or made any failed attempts to obtain one.

Date, Place	Gizem Ölçücü